

AD-A260 135



TIC

ECTE

JAN 29 1993

S

B

D

USAFETAC/TN--91/002
Revised

2



SWANEA

(SOUTHWEST ASIA--NORTHEAST AFRICA)

A CLIMATOLOGICAL STUDY

VOLUME II--THE MIDDLE EAST PENINSULA

by

1st Lt Michael J. Vojtesak
Capt Kevin P. Martin
TSgt Gregory Myles
Michael T. Gilford

Revised by TSgt Kenneth R. Gibson

FEBRUARY 1991

Revised September 1992

APPROVED FOR PUBLIC RELEASE;
DISTRIBUTION IS UNLIMITED

93-01690

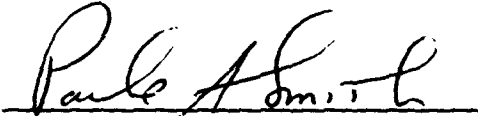


276pgs

USAF
Environmental Technical Applications Center
Scott Air Force Base, Illinois 62225-5116

REVIEW AND APPROVAL STATEMENT

USAFETAC/TN-91/002, SWANEA (Southwest Asia--Northeast Africa)--A Climatological Study, Volume II--The Middle East Peninsula, February 1991 (Revised September 1992), has been reviewed and is approved for public release. There is no objection to unlimited distribution of this document to the public at large, or by the Defense Technical Information Center (DTIC) to the National Technical Information Service (NTIS).

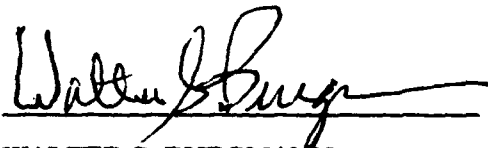


PARKE A. SMITH, Major, USAF
Chief, Operations



KENNETH R. WALTERS, SR.
Chief, Readiness Support

FOR THE COMMANDER



WALTER S. BURGMANN
Scientific and Technical Information
Program Manager

REPORT DOCUMENTATION PAGE

2. Report Date: September 1992
3. Report Type and Dates Covered: Technical Note
4. Title and Subtitle: SWANEA (Southwest Asia--Northeast Africa)--A Climatological Study, Volume II--The Middle East Peninsula
6. Authors: Original by: 1st Lt Michael J. Vojtesak, Capt Kevin P. Martin, TSgt Gregory Myles, Michael T. Gilford, Revised by: TSgt Kenneth R. Gibson
7. Performing Organization Name and Address: USAF Environmental Technical Applications Center (USAFETAC/DOJ), Scott AFB, IL 62225-5116
8. Performing Organization Report Number: USAFETAC/TN--91/002
(Revised September 1992)
11. Supplementary Notes: Revised in September 1992; supersedes AD-A232776.
12. Distribution/Availability Statement: Approved for Public Release; distribution is unlimited.
13. Abstract: This report (the second in a four-volume series) is a climatological study of the Middle East Peninsula, an area that includes the Red Sea Coastal Plains, the Arabian Desert, the Fertile Crescent, and the Persian Gulf Coastal Plains. It was revised in September 1992 to include additional information acquired during the conduct of the August 1990-March 1991 Persian Gulf War. After describing the general geography of land areas in the Middle East Peninsula, the study discusses major meteorological features of the entire study area. Each major subregion (based on "climatic commonality") is then broken into its own geography and general weather sections. Finally, each of the four so-called "seasons" in each of these subregions is discussed in detail.
14. Subject Terms: CLIMATOLOGY, METEOROLOGY, WEATHER, GEOGRAPHY, AFRICA, MIDDLE EAST, PERSIAN GULF
15. Number of Pages: 263
17. Security Classification of Report: Unclassified
18. Security Classification of this Page: Unclassified
19. Security Classification of Abstract: Unclassified
20. Limitation of Abstract: UL

DTIC QUALITY INSPECTED 3

Standard Form 398

Accession For	
NTIS GRA&I	<input checked="" type="checkbox"/>
DTIC TAB	<input type="checkbox"/>
Unannounced	<input type="checkbox"/>
Justification	
By	
Distribution/	
Availability Codes	
Dist	Avail and/or Special
A-1	

PREFACE

This revision of USAFETAC/TN--91/002 (SWANEA (Southwest Asia--Northeast Africa)--A Climatological Study, Volume II--The Middle East Peninsula) was prepared by the United States Air Force Environmental Applications Center, Readiness Support Branch (USAFETAC/DOJ), in response to a support assistance request (SAR) from The Air Combat Command Directorate of Weather, Langley AFB, VA. The revision, written under USAFETAC project 910840, includes meteorological lessons learned during the 1990-91 Persian Gulf War and incorporates additional information acquired from this region during the conduct of Operations DESERT SHIELD and DESERT STORM. This project would not have been possible without the dedicated support of the many people and agencies we have listed below. We sincerely hope we've not omitted anyone.

Thanks first to the authors of the original report: 1st Lt Michael J. Vojtesak, Capt Kevin P. Martin, TSgt Gregory Myles, and Michael T. Gilford; their efforts made this revision relatively easy.

Thanks to Mr Kenneth R. Walters Sr, Maj Kathleen M. Traxler, Mr Michael T. Gilford, Capt Richard D. Arnold, and TSgt Richard C. Bonam (USAFETAC/DOJ) for their hard work, assistance, guidance, and encouragement.

Thanks to the members of the DESERT STORM Forecast Unit; Capt John Murphy, Capt Jeff Johnson, Capt Tom Coe, Lt Dave Wood, MSgt Neal Roll, TSgt Joel Hart, TSgt Dan Rozich, TSgt Tony Taylor, SSgt Jon Adams, SSgt Craig Balsoma, SSgt John Cerone, SSgt Joseph Federico, SSgt Jeff Isom, and SSgt Robert Steenburgh.

Thanks to Capt Gary Grigorian, Lt Frank Hinson, Lt Tina Smith, Lt Bridgette Tobin, MSgt George Strunk, TSgt Ron Kellerman, for the excellent terminal forecast reference notebooks.

Thanks to Lt Col Gerald Riley and Lt Col Kenneth A. Nash for helping to obtain data necessary for this study.

Thanks to MSgt Brian Folk, TSgt Bobby Dempsey, and SSgt Colin McCoy for the hours spent with the author "on the steps, cussin' and discussin' the weather."

Finally, all the authors owe sincere gratitude to the Technical Publishing Team of the AWS Technical Library (USAFETAC/DOL), Mr George M. Horn and Sgt Corinne M. Kawa. Without their patience, cooperation, and creativity, this project would not have been possible.

CONTENTS

Chapter 1	INTRODUCTION	
	Area of Interest	1-1
	Geography	1-2
	Study Content	1-4
	Climatological Regimes	1-5
	Conventions	1-6
	Data Sources	1-6
	Related References	1-6
Chapter 2	MAJOR METEOROLOGICAL FEATURES OF THE MIDDLE EAST PENINSULA	
	Semipermanent Climatic Controls	2-3
	Synoptic Disturbances	2-44
	Regional Winds	2-73
	Mesoscale and Local Effects	2-79
Chapter 3	RED SEA COASTAL PLAINS	
	Situation and Relief	3-2
	The Southwest Monsoon	3-5
	The Southwest-to-Northeast Monsoon Transition	3-12
	The Northeast Monsoon	3-18
	The Northeast-to-Southwest Monsoon Transition	3-27
Chapter 4	THE FERTILE CRESCENT	
	Situation and Relief	4-2
	Winter	4-7
	Spring	4-19
	Summer	4-26
	Fall	4-32
Chapter 5	THE ARABIAN DESERT	
	Situation and Relief	5-2
	The Southwest Monsoon	5-6
	The Southwest-to-Northeast Monsoon Transition	5-14
	The Northeast Monsoon	5-19
	The Northeast-to-Southwest Monsoon Transition	5-27
Chapter 6	THE PERSIAN GULF COASTAL PLAINS	
	Situation and Relief	6-2
	The Southwest Monsoon	6-6
	The Southwest-to-Northeast Monsoon Transition	6-17
	The Northeast Monsoon	6-24
	The Northeast-to-Southwest Monsoon Transition	6-31
	BIBLIOGRAPHY	BIB-1

FIGURES

Figure 1-1.	The Southwest Asia-Northeast Africa (SWANEA) Region	1-1
Figure 1-2.	The Middle East Peninsula and its Four "Zones of Climatic Commonality"	1-2
Figure 1-3.	Major Topographic and Geopolitical Features of the Middle East Peninsula . . .	1-3
Figure 1-4.	The Monsoon Climate with Respect to the Middle East Peninsula	1-5
Figure 2-1a.	Mean January-February Sea-Surface Temperatures ($^{\circ}$ F)	2-3
Figure 2-1b.	Mean April Sea-Surface Temperatures ($^{\circ}$ F)	2-4
Figure 2-1c.	Mean July-August Sea-Surface Temperatures ($^{\circ}$ F)	2-4
Figure 2-1d.	Mean October Sea-Surface Temperatures ($^{\circ}$ F)	2-5
Figure 2-2a.	January Sea-Surface Currents	2-6
Figure 2-2b.	July Sea-Surface Currents	2-6
Figure 2-3.	Southwest Monsoon Circulation Over Southern Asia and the Indian Ocean (from Hamilton, 1987)	2-7
Figure 2-4a.	Mean May 200-mb Flow Showing the Tibetan Anticyclone	2-8
Figure 2-4b.	Mean June 200-mb Flow Showing the Tibetan Anticyclone	2-8
Figure 2-4c.	Mean July 200-mb Flow Showing the Tibetan Anticyclone	2-9
Figure 2-5.	Mean July 200-mb Zonal Flow Showing the Tropical Easterly Jet (TEJ)	2-10
Figure 2-6a.	Mean April Position of the Mascarene High	2-11
Figure 2-6b.	Mean July Position of the Mascarene High	2-11
Figure 2-6c.	Mean August Position of the Mascarene High	2-12
Figure 2-6d.	Mean October Position of the Mascarene High	2-12
Figure 2-7.	Successive Positions of the 20-Knot Isotach at 3,000 Feet (915 meters) AGL Between April and July (from Findlater, 1971)	2-13
Figure 2-8.	Movement of the Somali Jet Core, 13-14 August 1966 (from Findlater, 1969) .	2-14
Figure 2-9a.	850-mb Streamline Chart (1200Z) for 23 May 1979 <i>Prior to Onset Vortex</i> . . .	2-15
Figure 2-9b.	850-mb Streamline Chart (1200Z) for 17 June 1979 <i>During Onset Vortex</i> . . .	2-16
Figure 2-9c.	850-mb Streamline Chart (1200Z) for 27 June 1979 <i>After Onset Vortex</i>	2-16
Figure 2-10.	Mean July Surface Positions of Azores High, Saharan Low, and Pakistani Low	2-17
Figure 2-11.	Mean July Gradient-Level Flow Showing the Position of the Saudi Arabian Heat Low	2-18
Figure 2-12.	Mean Surface Monsoon Trough Positions: April through November	2-19
Figure 2-13a.	METEOSAT IR Imagery (14 June 1979, 1155Z) of Subtropical Africa and the Middle East Peninsula (from NEPRF, 1980)	2-20
Figure 2-13b.	Enlarged View of the Inset in Photo Above	2-20
Figure 2-14a.	Mean June Positions for the 3,000-Foot Monsoon Trough (NET) and the Southern Equatorial Trough (SET) (from Findlater, 1971)	2-21
Figure 2-14b.	Mean July Positions for the 3,000-Foot Monsoon Trough (NET) and the Southern Equatorial Trough (SET) (from Findlater, 1971)	2-22
Figure 2-14c.	Mean August Positions for the 3,000-Foot Monsoon Trough (NET) and the Southern Equatorial Trough (SET) (from Findlater, 1971)	2-23
Figure 2-15.	Location of the Low-Level Persian Gulf Jet During the Southwest Monsoon (Jun-Sep)	2-24
Figure 2-16.	Low-Level Vertical Wind Profile of Persian Gulf Jet Over Bahrain	2-24
Figure 2-17a.	Mean January Surface Positions of Pressure Cells	2-25
Figure 2-17b.	Mean October Surface Positions of Pressure Cells	2-26
Figure 2-17c.	Mean April Surface Positions of Pressure Cells	2-27
Figure 2-18.	Typical January Surface Streamline Flow Pattern Showing the Saudi Arabian High	2-29
Figure 2-19.	Satellite View of Red Sea Convergence Zone (from NEPRF, 1980)	2-30

Figure 2-20.	RSCZ Positions: October--April	2-31
Figure 2-21.	Cross-Section View of Stratocumulus Cloud Cover Distributions Along the RSCZ (from Pedgley, 1966)	2-32
Figure 2-22a.	Mean January Upper-Air Flow Pattern, 850 mb	2-33
Figure 2-22b.	Mean January Upper-Air Flow Pattern, 700 mb	2-33
Figure 2-22c.	Mean January Upper-Air Flow Pattern, 500 mb	2-34
Figure 2-22d.	Mean January Upper-Air Flow Pattern, 300 mb	2-34
Figure 2-22e.	Mean January Upper-Air Flow Pattern, 200 mb	2-35
Figure 2-23a.	Mean April Upper-Air Flow Pattern, 850 mb	2-35
Figure 2-23b.	Mean April Upper-Air Flow Pattern, 700 mb	2-36
Figure 2-23c.	Mean April Upper-Air Flow Pattern, 500 mb	2-36
Figure 2-23d.	Mean April Upper-Air Flow Pattern, 300 mb	2-37
Figure 2-23e.	Mean April Upper-Air Flow Pattern, 200 mb	2-37
Figure 2-24a.	Mean July Upper-Air Flow Pattern, 850 mb	2-38
Figure 2-24b.	Mean July Upper-Air Flow Pattern, 700 mb	2-38
Figure 2-24c.	Mean July Upper-Air Flow Pattern, 500 mb	2-39
Figure 2-24d.	Mean July Upper-Air Flow Pattern, 300 mb	2-39
Figure 2-24e.	Mean July Upper-Air Flow Pattern, 200 mb	2-40
Figure 2-25a.	Mean October Upper-Air Flow Pattern, 850 mb	2-40
Figure 2-25b.	Mean October Upper-Air Flow Pattern, 700 mb	2-41
Figure 2-25c.	Mean October Upper-Air Flow Pattern, 500 mb	2-41
Figure 2-25d.	Mean October Upper-Air Flow Pattern, 300 mb	2-42
Figure 2-25e.	Mean October Upper-Air Flow Pattern, 200 mb	2-42
Figure 2-26.	Mean January and July Positions of the Subtropical Ridge	2-43
Figure 2-27.	Mean January and July Positions of the Polar Jet (PJ) and Subtropical Jet (STJ)	2-44
Figure 2-28.	Vertical Cross-Section of the Subtropical Jet Along 45° E (5 January 1978, 0000Z)	2-45
Figure 2-29a.	Typical Jet Positions During Formation of Atlas Low	2-46
Figure 2-29b.	Typical Jet Positions During Formation of Cyprus Low	2-46
Figure 2-30a.	Primary (solid arrow) and Secondary (dashed arrow) Mid-Latitude Storm Tracks, December, January and February	2-47
Figure 2-30b.	Primary (solid arrow) and Secondary (dashed arrow) Mid-Latitude Storm Tracks, March, April, and May	2-47
Figure 2-30c.	Primary (solid arrow) and Secondary (dashed arrow) Mid-Latitude Storm Tracks, November	2-47
Figure 2-30d.	Primary Storm Track during Operation DESERT STORM, January-March 1991	2-48
Figure 2-31.	Mid-Latitude Cyclogenesis Regions	2-48
Figure 2-32.	Mediterranean-Generated Cyclonic Activity and Trailing Cold Front Entering the Gulf of Aden	2-49
Figure 2-33a.	Synoptic Surface Chart (7 Apr 1954, 0000Z), Atlas Low	2-50
Figure 2-33b.	500-mb Flow (7 April 1954, 0300Z), Atlas Low	2-51
Figure 2-33c.	Synoptic Surface Chart (8 April 1954, 0000Z), Atlas Low	2-52
Figure 2-33d.	500-mb Flow (8 April 1954, 0300Z), Atlas Low	2-53
Figure 2-33e.	Synoptic Surface Chart (9 April 1954, 0000Z), Atlas Low	2-54
Figure 2-34a.	Synoptic Surface Chart (16 April 1964, 1200Z/1500L) Showing an Eastward-Tracking Atlas Low	2-55
Figure 2-34b.	Synoptic Surface Chart (17 April 1964, 1200Z/1500L) Showing Secondary Low Formation Along the Active Cold Front	2-55
Figure 2-35.	Surface Circulation Causing the Development of the Cyprus Low	2-56
Figure 2-36a.	Synoptic Surface Chart (16 November 1953, 0000Z), Cyprus Low	2-57

Figure 2-36b.	Synoptic Surface Chart (17 November 1953, 0000Z), Cyprus Low	2-58
Figure 2-36c.	Synoptic Surface Chart (18 November 1953, 0000Z), Cyprus Low	2-59
Figure 2-36d.	500-mb Flow (18 November 1953, 0300Z), Cyprus Low	2-60
Figure 2-37a.	Synoptic Surface Chart (19 August 1949, 0000Z), Black Sea Low	2-61
Figure 2-37b.	Synoptic Surface Chart (20 August 1949, 0000Z), Black Sea Low	2-62
Figure 2-37c.	500-mb Flow (18 August 1949, 0300Z), Black Sea Low	2-63
Figure 2-37d.	500-mb Flow (20 August 1949, 0300Z), Black Sea Low	2-64
Figure 2-38.	Low-Level Southwesterly Flow Across the Red Sea	2-65
Figure 2-39.	Locations Affected by the Omani Convergence Zone (OCZ) (from Pedgley, 1970)	2-66
Figure 2-40a.	Schematic Patterns of Wind Flow Below 3,000 Feet/915 meters (1000L) Over Oman, January (from Pedgley, 1970)	2-66
Figure 2-40b.	Schematic Patterns of Wind Flow Below 3,000 Feet/915 meters (1000 LST) Over Oman, April (from Pedgley, 1970)	2-66
Figure 2-41.	Desert Front During October from an Incursion of Mediterranean Air	2-68
Figure 2-42.	Desert Front during October from a Northward Surge of the Monsoonal Trough	2-69
Figure 2-43a.	May Tropical Cyclone Tracks, 1891-1960 (from Indian Meteorological Department, 1964)	2-70
Figure 2-43b.	October Tropical Cyclone Tracks, 1891-1960 (from Indian Meteorological Department, 1964)	2-71
Figure 2-43c.	November Tropical Cyclone Tracks, 1891-1960 (from Indian Meteorological Department, 1964)	2-71
Figure 2-44.	Vertical Cross-Section of a Subtropical Cyclone (from Ramage, 1974)	2-72
Figure 2-45.	Areas Affected by Etesian Winds	2-73
Figure 2-46.	Active Storm Track for Sharav Conditions	2-74
Figure 2-47a.	Typical Low Pressure System Storm Track Producing Khamsin Conditions	2-75
Figure 2-47b.	Typical Northeast-Moving Storm Track Producing Widespread Dust	2-76
Figure 2-48.	Khamsin-Type Conditions Associated With a Rare Eastward-Moving Atlas Low	2-77
Figure 2-49.	Primary Duststorm Source Areas	2-79
Figure 2-50a.	Typical Daytime Mountain/Valley Circulation (from Flohn, 1969)	2-82
Figure 2-50b.	Typical Nighttime Mountain/Valley Circulation (from Flohn, 1969)	2-82
Figure 2-51a.	Mountain/Valley Circulation--SUNRISE	2-83
Figure 2-51b.	Mountain/Valley Circulation--LATE MORNING	2-83
Figure 2-51c.	Mountain/Valley Circulation--MIDDAY	2-83
Figure 2-51d.	Mountain/Valley Circulation--LATE AFTERNOON	2-83
Figure 2-51e.	Mountain/Valley Circulation--SUNSET	2-83
Figure 2-51f.	Mountain/Valley Circulation--LATE EVENING	2-83
Figure 2-51g.	Mountain/Valley Circulation--MIDNIGHT	2-83
Figure 2-51h.	Mountain/Valley Circulation--PRE-DAWN	2-84
Figure 2-52.	Fully Developed Lee Wave System (from Wallace and Hobbs, 1977)	2-85
Figure 2-53.	Downburst Inversion Sequence	2-86
Figure 2-54.	Three Dimension View of Longitudinal Vortices in the Boundary Layer (from Hanna, 1969)	2-87
Figure 2-55.	Cross-Sectional View of Dune and Cloud Formation Mechanism (from Hanna, 1969)	2-87
Figure 2-56.	The "Common" Daytime Sea Breeze (A) and Nighttime Land Breeze (B).	2-88
Figure 2-57a.	Gradient Flow With Offshore Wind Component Slopes Gently Over Dense, Cooler Marine Boundary Layer	2-88
Figure 2-57b.	Increased Compacting Tightens Pressure Gradient Along Land/Sea Interface	2-88
Figure 2-57c.	Maximum Compacting of the Marine Boundary Layer	2-88

Figure 2-57d.	Frontal Sea Breeze Accelerates Towards Shore	2-88
Figure 2-57e.	Sea Breeze "Front" Reaches the Coast	2-89
Figure 2-57f.	Land/Sea Breeze Mechanism in Full Swing	2-89
Figure 2-58.	WBGT Heat Stress Index Activity Guidelines	2-90
Figure 2-59a.	Average Maximum WBGT--January	2-91
Figure 2-59b.	Average Maximum WBGT--April	2-92
Figure 2-59c.	Average Maximum WBGT--July	2-93
Figure 2-59d.	Average Maximum WBGT--October	2-94
Figure 3-1a.	The Red Sea Coastal Plains	3-2
Figure 3-1b.	Climatological Summaries for Selected Stations in the Red Sea Coastal Plains ..	3-3
Figure 3-2.	Mean Southwest Monsoon Cloudiness (Isolines) and Frequencies of Ceilings Below 3,000 Feet (915 meters), Red Sea Coastal Plains	3-6
Figure 3-3.	Southwest Monsoon Frequencies of Visibilities Below 3 Miles, Red Sea Coastal Plains	3-7
Figure 3-4.	Mean Southwest Monsoon Surface Wind Speed (kts) and Prevailing Direction, Red Sea Coastal Plains	3-8
Figure 3-5a.	Mean Annual Wind Direction, Gizan, Saudi Arabia	3-9
Figure 3-5b.	Mean Annual Wind Direction, Al Wejh, Saudi Arabia	3-9
Figure 3-6.	Mean Southwest Monsoon Monthly/Maximum 24-hour Precipitation, Red Sea Coastal Plains	3-10
Figure 3-7.	Mean Southwest Monsoon Daily Maximum/Minimum Temperatures (° F), Red Sea Coastal Plains	3-11
Figure 3-8.	Mean SW-NE Monsoon Transition Cloudiness (Isolines) and Frequencies of Ceilings Below 3,000 Feet (915 meters), Red Sea Coastal Plains	3-13
Figure 3-9.	SW-NE Monsoon Transition Frequencies of Visibilities Below 3 Miles, Red Sea Coastal Plains	3-14
Figure 3-10.	Mean SW-NE Monsoon Transition Wind Speed (kts) and Prevailing Direction, Red Sea Coastal Plains	3-15
Figure 3-11.	Mean SW-NE Monsoon Transition Monthly/Maximum 24-hour Precipitation, Red Sea Coastal Plains	3-16
Figure 3-12.	Mean SW-NE Monsoon Transition Daily Maximum/Minimum Temperatures (° F), Red Sea Coastal Plains	3-17
Figure 3-13.	Mean Northeast Monsoon Cloudiness (Isolines) and Frequencies of Ceilings Below 3,000 Feet (915 meters), Red Sea Coastal Plain	3-19
Figure 3-14.	Mean Northeast Monsoon Frequencies of Visibilities Below 3 Miles, Red Sea Coastal Plains	3-20
Figure 3-15.	Mean Northeast Monsoon Surface Wind Speed (kts) and Prevailing Direction, Red Sea Coastal Plains	3-21
Figure 3-16.	Mean Wind Speeds (30,000-45,000 Feet/9,1-13,7 km) MSL at Al Wejh, Saudi Arabia	3-21
Figure 3-17.	Mean Northeast Monsoon Monthly/Maximum 24-hour Precipitation, Red Sea Coastal Plains	3-22
Figure 3-18a.	500-mb Contour Chart Over an Intense Surface Low With No Precipitation ..	3-23
Figure 3-18b.	Surface Chart Depicting Cyprus Low Position Beneath a Shallow Mid-Level Trough With No Precipitation	3-23
Figure 3-19a.	500-mb Contour Chart Over an Intense Surface Low That Produced Significant Rainfall In The Northern Red Sea Coastal Plains	3-24
Figure 3-19b.	Surface Chart Depicting Cyprus Low Position Beneath a Deep Mid-Level Trough That Produced Significant Rainfall	3-24
Figure 3-20.	A Normal (A) and Reversed (B) Slope of the Upper-Level Wind Flow Pattern ..	3-25
Figure 3-21.	Mean Northeast Monsoon Daily Maximum/Minimum Temperatures (° F), Red Sea Coastal Plains	3-26

Figure 3-22.	Mean SW-NE Monsoon Transition Cloudiness (Isolines) and Frequencies of Ceilings Below 3,000 feet (915 meters), Red Sea Coastal Plains	3-27
Figure 3-23.	Mean NE-SW Monsoon Transition Frequencies of Visibilities Below 3 Miles, Red Sea Coastal Plains	3-28
Figure 3-24.	Mean NE-SW Monsoon Transition Wind Speed (kts) and Prevailing Direction, Red Sea Coastal Plains	3-29
Figure 3-25.	Mean NE-SW Monsoon Transition Monthly/Maximum 24-hour Precipitation, Red Sea Coastal Plains	3-30
Figure 3-26.	Mean NE-SW Monsoon Transition Daily Maximum/Minimum Temperatures (° F), Red Sea Coastal Plains	3-31
Figure 4-1a.	The Fertile Crescent	4-2
Figure 4-1b.	Climatological Summaries for Selected Stations in the Fertile Crescent	4-3
Figure 4-2.	The Fertile Crescent's Important Rivers, Streams, and Lakes	4-5
Figure 4-3.	Mean Winter Cloudiness (Isolines) and Frequencies of Ceilings Below 3,000 Feet (915 meters), Fertile Crescent	4-8
Figure 4-4.	Mean Winter Frequencies of Visibilities Below 3 Miles, Fertile Crescent	4-9
Figure 4-5.	Mean Winter Surface Wind Speed (kts) and Prevailing Direction, Fertile Crescent	4-10
Figure 4-6a.	Mean Annual Wind Direction, Baghdad, Iraq	4-11
Figure 4-6b.	Mean Annual Wind Direction, Aleppo, Syria	4-11
Figure 4-6c.	Mean Annual Wind Direction, Damascus, Syria	4-12
Figure 4-7.	Mean Monthly (Winter) 39,000-Foot (11,900-meter) MSL Wind Speeds (kts), Fertile Crescent Upper-Air Data Network	4-12
Figure 4-8.	Mean Winter Monthly/Maximum 24-hour Precipitation, Fertile Crescent	4-14
Figure 4-9.	Mean Winter Frequencies of Thunderstorms, Fertile Crescent	4-15
Figure 4-10a.	500-mb Contour Chart Over a Cyprus Low With No Severe Thunderstorms Or Heavy Precipitation	4-16
Figure 4-10b.	Surface Chart Depicting Cyprus Low Position Beneath a Weak Mid-Level Trough With No Severe Thunderstorms or Heavy Precipitation	4-16
Figure 4-10c.	500-mb Contour Chart Over an Intense Cyprus Low With Severe Thunderstorms and Heavy Precipitation	4-17
Figure 4-10d.	Surface Chart Depicting Cyprus Low Position Beneath a Strong Mid-Level Trough With Severe Thunderstorms and Heavy Precipitation	4-17
Figure 4-11.	Mean Winter Daily Maximum/Minimum Temperature (° F), Fertile Crescent	4-18
Figure 4-12.	Mean Spring Cloudiness (Isolines) and Frequencies of Ceilings Below 3,000 Feet (915 meters), Fertile Crescent	4-20
Figure 4-13.	Mean Spring Frequencies of Visibilities Below 3 Miles, Fertile Crescent	4-21
Figure 4-14.	Mean Spring Surface Wind Speed (kts) and Prevailing Direction, Fertile Crescent	4-22
Figure 4-15.	Mean Spring Monthly/Maximum 24-hour Precipitation, Fertile Crescent	4-23
Figure 4-16.	Mean Spring Frequencies of Thunderstorms, Fertile Crescent	4-24
Figure 4-17.	Mean Spring Daily Maximum/Minimum Temperatures (° F), Fertile Crescent	4-25
Figure 4-18.	Mean Summer Cloudiness (Isolines) and Frequencies of Ceilings Below 3,000 Feet (915 meters), Fertile Crescent	4-27
Figure 4-19.	Mean Summer Frequencies of Visibilities Below 3 Miles, Fertile Crescent	4-28
Figure 4-20.	Mean Summer Surface Wind Speed (kts) and Prevailing Direction, Fertile Crescent	4-29
Figure 4-21.	Mean Monthly (Summer) 39,000-Foot (11,900-meter) MSL Wind Speeds (kts), Fertile Crescent Upper-Air Network	4-30
Figure 4-22.	Mean Summer Daily Maximum/Minimum Temperatures (° F), Fertile Crescent	4-31

Figure 4-23.	Mean Fall Cloudiness (Isolines) and Frequencies of Ceilings Below 3,000 Feet (915 meters), Fertile Crescent	4-33
Figure 4-24.	Fall Frequencies of Visibilities Below 3 Miles, Fertile Crescent	4-34
Figure 4-25.	Mean Fall Surface Wind Speeds (kts) and Prevailing Direction, Fertile Crescent	4-35
Figure 4-26.	Mean Fall Monthly/Maximum 24-hour Precipitation, Fertile Crescent	4-36
Figure 4-27.	Mean Fall Frequencies of Thunderstorms, Fertile Crescent	4-37
Figure 4-28.	Mean Fall Daily Maximum/Minimum Temperatures (° F), Fertile Crescent	4-38
Figure 5-1a.	The Arabian Desert	5-2
Figure 5-1b.	Climatological Summaries for Selected Stations in the Arabian Desert	5-3
Figure 5-2.	Mean Southwest Monsoon Cloudiness (Isolines) and Frequencies of Ceilings Below 3,000 Feet (915 meters), Arabian Desert	5-7
Figure 5-3.	Southwest Monsoon Frequencies of Visibilities Below 3 Miles, Arabian Desert	5-8
Figure 5-4.	Mean Southwest Monsoon Surface Wind Speeds (kts) and Prevailing Direction, Arabian Desert	5-9
Figure 5-5a.	Mean Annual Wind Direction, Tabuk, Saudi Arabia	5-10
Figure 5-5b.	Mean Annual Wind Direction, Hafr-al-Batin, Saudi Arabia	5-10
Figure 5-5c.	Mean Annual Wind Direction, Riyadh, Saudi Arabia	5-11
Figure 5-6.	Mean Southwest Monsoon Monthly/Maximum 24-hour Precipitation, Arabian Desert	5-12
Figure 5-7.	Mean Southwest Monsoon Daily Maximum/Minimum Temperatures (° F), Arabian Desert	5-13
Figure 5-8.	Mean SW-NE Monsoon Transition Cloudiness (Isolines) and Frequencies of Ceiling Below 3,000 Feet (915 meters), Arabian Desert	5-14
Figure 5-9.	SW-NE Monsoon Transition Frequencies of Visibilities Below 3 Miles, Arabian Desert	5-15
Figure 5-10.	Mean SW-NE Monsoon Transition Surface Wind Speeds (kts) and Prevailing Direction, Arabian Desert	5-16
Figure 5-11.	Mean SW-NE Monsoon Transition Monthly/Maximum 24-hour Precipitation, Arabian Desert	5-17
Figure 5-12.	Mean SW-NE Monsoon Transition Daily Maximum/Minimum Temperatures (° F), Arabian Desert	5-18
Figure 5-13.	Mean Northeast Monsoon Cloudiness (Isolines) and Frequencies of Ceilings Below 3,000 Feet (915 meters), Arabian Desert	5-20
Figure 5-14.	Northeast Monsoon Frequencies of Visibilities Below 3 Miles, Arabian Desert	5-21
Figure 5-15.	Mean Northeast Monsoon Surface Wind Speeds (kts) and Prevailing Direction, Arabian Desert	5-22
Figure 5-16.	Mean Monthly (Northeast Monsoon) 39,000-Foot (11.9-km) MSL Wind Speed (kts), Upper-Air Network, Arabian Desert	5-22
Figure 5-17.	Mean Northeast Monsoon Monthly/Maximum 24-hour Precipitation, Arabian Desert	5-24
Figure 5-18.	Mean Northeast Monsoon Frequencies of Thunderstorms, Arabian Desert	5-25
Figure 5-19.	Mean Northeast Monsoon Daily Maximum/Minimum Temperatures (° F), Arabian Desert	5-26
Figure 5-20.	Mean NE-SW Monsoon Transition Cloudiness (Isolines) and Frequencies of Ceiling Below 3,000 Feet (915 meters), Arabian Desert	5-28
Figure 5-21.	NE-SW Monsoon Transition Frequencies of Visibilities Below 3 Miles, Arabian Desert	5-29
Figure 5-22.	Mean NE-SW Monsoon Transition Surface Wind Speeds (kts) and Prevailing Direction, Arabian Desert	5-30

Figure 5-23.	Mean NE-SW Monsoon Transition Monthly/Maximum 24-hour Precipitation, Arabian Desert	5-32
Figure 5-24.	Mean NE-SW Monsoon Transition Frequencies of Thunderstorms, Arabian Desert	5-33
Figure 5-25.	Mean NE-SW Monsoon Transition Daily Maximum/Minimum Temperatures (F), Arabian Desert	5-34
Figure 6-1a.	The Persian Gulf Coastal Plains	6-2
Figure 6-1b.	Climatological Summaries for Dhahran and Kuwait International	6-3
Figure 6-2.	Mean Southwest Monsoon Cloudiness (Isolines) and Frequencies of Ceiling Below 3,000 Feet (915 meters), Persian Gulf Coastal Plains	6-7
Figure 6-3.	DMSP LS Low Enhancement Photo of Stratus Deck Near Salalah, Oman on 30 June 2979 (0750Z)	6-8
Figure 6-4.	Southwest Monsoon Frequencies of Visibilities Below 3 Miles, Persian Gulf Coastal Plains	6-10
Figure 6-5.	Mean Southwest Monsoon Surface Wind Speeds (kts) and Prevailing Direction, Persian Gulf Coastal Plains	6-11
Figure 6-6a.	Mean Annual Wind Direction, Salalah, Oman	6-12
Figure 6-6b.	Mean Annual Wind Direction, Seeb IAP (Muscat, Oman)	6-12
Figure 6-6c.	Mean Annual Wind Direction, Kuwait IAP, Kuwait	6-13
Figure 6-6d.	Mean Annual Wind Direction, Jiwani, Pakistan	6-13
Figure 6-7.	Mean Southwest Monsoon Monthly/Maximum 24-hour Precipitation, Persian Gulf Coastal Plains	6-14
Figure 6-8.	A Tropical Disturbance Over the Northwest India-Central Pakistan Area Which May Produce Heavy 24-hour Rainfall Along the Makran Coast	6-15
Figure 6-9.	Mean Southwest Monsoon Daily Maximum/Minimum Temperatures (° F), Persian Gulf Coastal Plains	6-16
Figure 6-10.	Mean SW-NE Monsoon Transition Cloudiness (Isolines) and Frequencies of Ceilings Below 3,000 Feet (915 meters), Persian Gulf Coastal Plains	6-18
Figure 6-11.	SW-NE Monsoon Transition Frequencies of Visibilities Below 3 Miles, Persian Gulf Coastal Plains	6-19
Figure 6-12.	Mean SW-NE Monsoon Transition Surface Wind Speeds (kts) and Prevailing Direction, Persian Gulf Coastal Plains	6-20
Figure 6-13.	Mean SW-NE Monsoon Transition Monthly/Maximum 24-hour Precipitation, Persian Gulf Coastal Plains	6-22
Figure 6-14.	Mean SW-NE Monsoon Transition Daily Maximum/Minimum Temperatures (° F), Persian Gulf Coastal Plains	6-23
Figure 6-15.	Mean Northeast Monsoon Cloudiness (Isolines) and Frequencies of Ceilings Below 3,000 Feet (915 meters), Persian Gulf Coastal Plains	6-25
Figure 6-16.	Northeast Monsoon Frequencies of Visibilities Below 3 Miles, Persian Gulf Coastal Plains	6-26
Figure 6-17.	Mean Northeast Monsoon Surface Wind Speeds (kts) and Prevailing Direction, Persian Gulf Coastal Plains	6-27
Figure 6-18.	Mean Northeast Monsoon Wind Speeds at 39,000 Feet (11.9 km) MSL (kts), Persian Gulf Coastal Plains	6-28
Figure 6-19.	Mean Northeast Monsoon Monthly/Maximum 24-hour Precipitation, Persian Gulf Coastal Plains	6-29
Figure 6-20.	Mean Northeast Monsoon Daily Maximum/Minimum Temperatures (° F), Persian Gulf Coastal Plains	6-30
Figure 6-21.	Mean NE-SW Monsoon Transition Cloudiness (Isolines) and Frequencies of Ceiling Below 3,000 Feet (915 meters), Persian Gulf Coastal Plains	6-32
Figure 6-22.	NE-SW Monsoon Transition Frequencies of Visibilities Below 3 Miles, Persian Gulf Coastal Plains	6-34

Figure 6-23.	Mean NE-SW Monsoon Transition Surface Wind Speeds (kts) and Prevailing Direction, Persian Gulf Coastal Plains	6-35
Figure 6-24.	Mean NE-SW Monsoon Transition Monthly/Maximum 24-hour Precipitation, Persian Gulf Coastal Plain	6-36
Figure 6-25.	Mean NE-SW Monsoon Transition Daily Maximum/Minimum Temperatures (° F), Persian Gulf Coastal Plains	6-37

Chapter 1

INTRODUCTION

AREA OF INTEREST. This revised study incorporates a number of meteorological "lessons learned," along with other additional information acquired during Operations DESERT SHIELD and DESERT STORM. It is the second of four volumes that cover the entire "SWANEA" (Southwest Asia-Northeast Africa) region shown in Figure 1-1. This volume describes the geography, climatology, and meteorology of the Middle East Peninsula, an area that includes

Saudi Arabia, Oman, United Arab Emirates, Bahrain, Qatar, Kuwait, and Iraq along with small portions of Egypt, Sudan, Ethiopia, Djibouti, Yemen-Sana, Pakistan, Iran, Turkey, Syria, and Jordan. For this study, the Middle East Peninsula has been divided into four zones of "climatic commonality": the Red Sea Coastal Plains, The Fertile Crescent, the Arabian Desert, and the Persian Gulf Coastal Plains. These zones are shown in Figure 1-2.

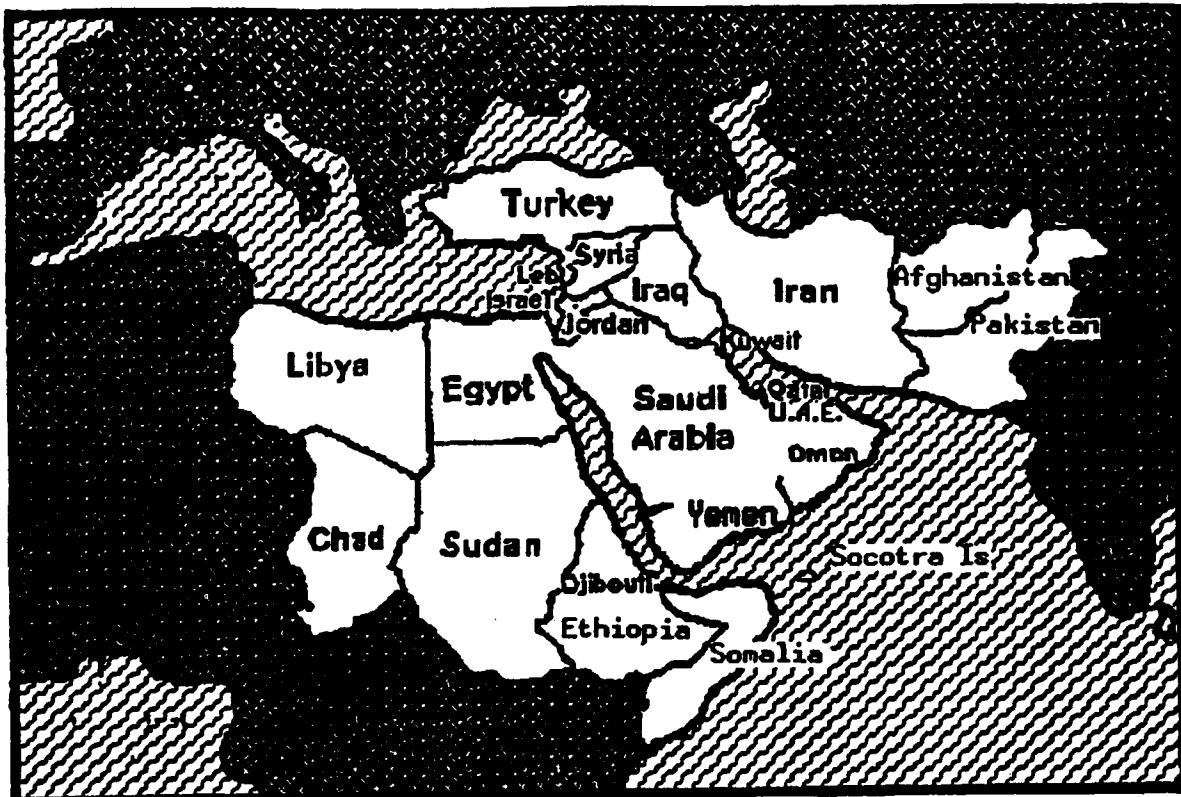


Figure 1-1. The Southwest Asia-Northeast Africa (SWANEA) Region.

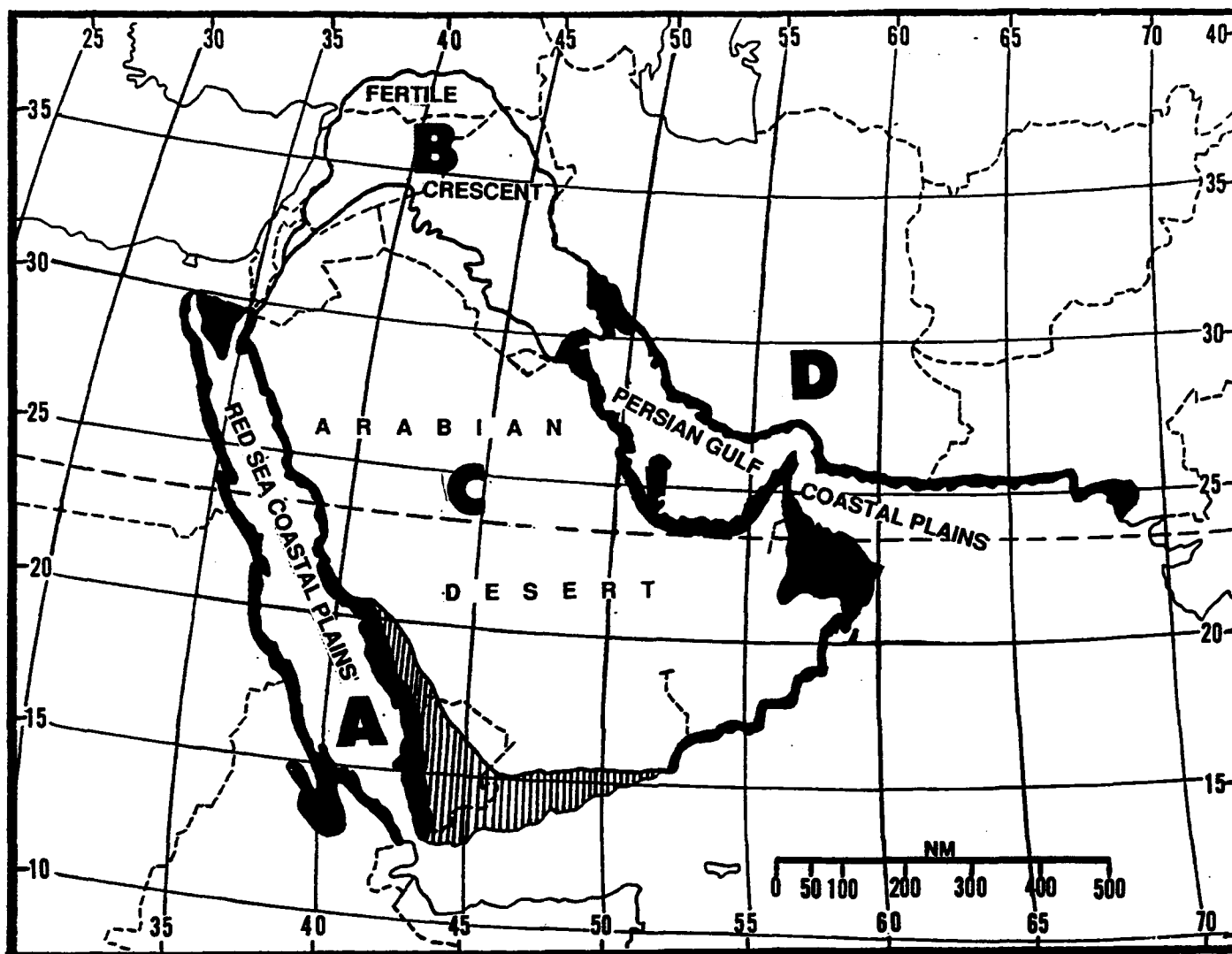


Figure 1-2. The Middle East Peninsula and its Four "Zones of Climatic Commonality" (A - The Red Sea Coastal Plains, B - The Fertile Crescent, C - The Arabian Desert, and D - The Persian Gulf Coastal Plains).

GEOGRAPHY. The Middle East Peninsula extends from the southern Red Sea to south-central Turkey, and from the northern Gulf of Suez to Pakistan's Hab River Delta. The study area is dominated by the large Arabian Peninsula, but excludes the Yemen Highlands and the northern coastline of the Gulf of Aden. It includes portions of southeastern Turkey that

lie below 3,280 feet (1,000 meters), the northern Persian Gulf and Gulf of Oman, and the Makran coastal plains below 656 feet (200 meters) from 57° E to the Hab River. It also includes the southern Sinai Peninsula and the western coastline of the Red Sea below 656 feet (200 meters).

The Arabian Desert covers 60-65% of the land surface area. It comprises several other deserts, including the Syrian Desert, the Rub al Khali (which includes the Empty Quarter), the Ad Nafud, and the Ad Dahna. The Arabian Desert is protected on its western border by a series of mountain ranges; the Al Hijaz and Asir Mountains extend from the Yemen Highlands to the Sinai Peninsula. The Lebanon and Anti-

Lebanon mountain ranges run from the Sinai to the Taurus Mountains of Southern Turkey. The Arabian Desert slopes from these western mountain ranges toward the Persian Gulf in the east. The desert supports little vegetation. Oases ("oceans in the desert") provide local sources of fresh water and limited agricultural activity (mostly date palms). They are focal points for trade, transportation, and people.

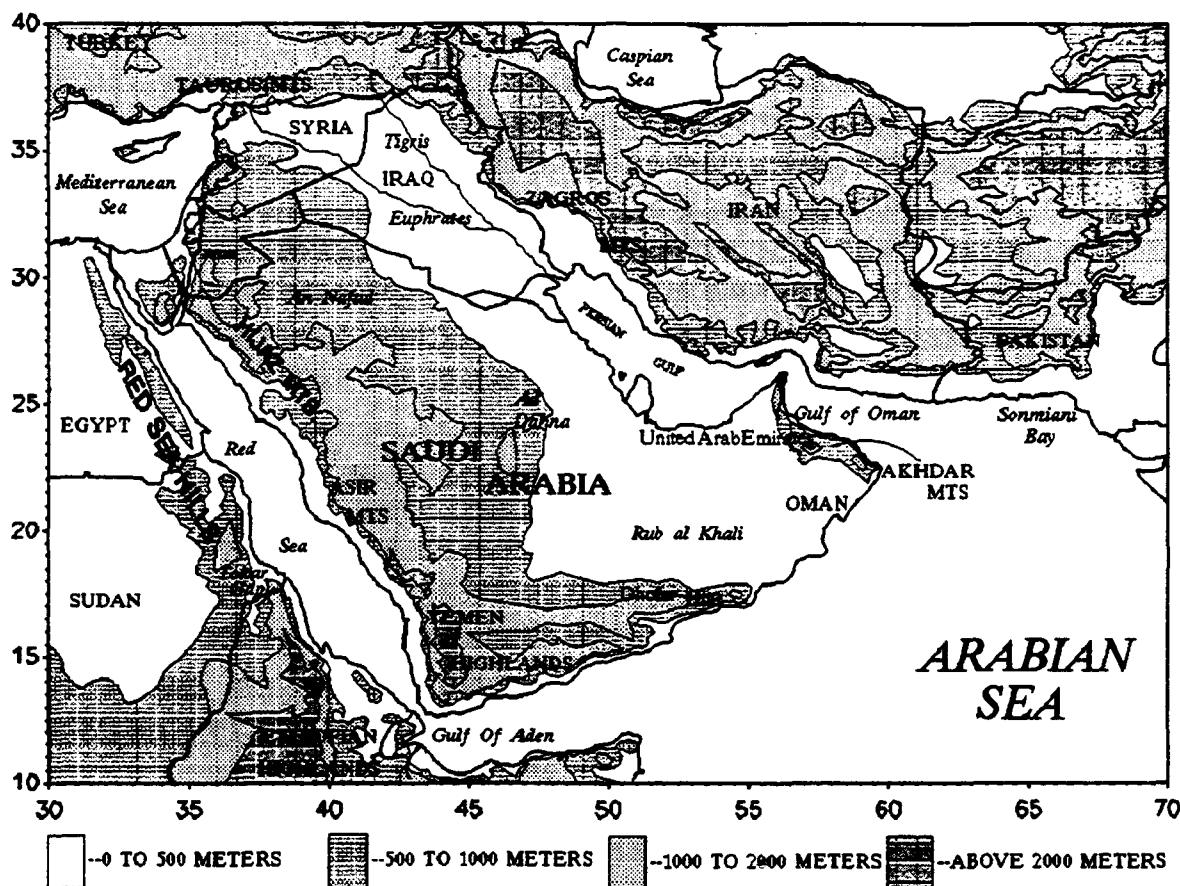


Figure 1-3. Major Topographic and Geopolitical Features of the Middle East Peninsula.

The Dhofar Hills, in western Oman at the southeastern corner of the Middle East Peninsula, form the eastern edge of the Hadhramaut Plateau. Their weathered hills and mountains prevent moisture from entering the Rub al Khali Desert, but their southern slopes are well-watered and extensively cultivated. Elevations do not exceed 5,000 feet (1,524 meters).

The Akhdar (or Hajar) Mountains form an isolated range in northeastern Iran that covers 260 NM (NW to SE) by 87 NM (SW to NW) along the southern edge of the Gulf of Oman. Orographic showers between 5,000 and 9,000 feet (1,524-2,743 meters) MSL dominate the eastern slopes.

The Tigris-Euphrates River Valley, in Iraq and eastern Syria, contains the largest fresh-water basin in the study area. The rivers originate in the Taurus Mountains of Turkey. Irrigation permits extensive agriculture with a wide variety of crops.

Other Features. Several other features have a significant effect on the area's weather even though they lie outside the area; these features include:

The Ethiopian Highlands and Red Sea Hills parallel the western coastline of the Red Sea and the southern coastline of the Gulf of Aden. The Ethiopian Highlands extend northward along the Red Sea coast to the Tokar Gap. The Red Sea Hills extend northward from the Tokar Gap to include the Sinai Peninsula. The break between the Ethiopian Highlands and Red Sea Hills is a significant point of entry for interior African continental air moving into the Red Sea.

The Taurus and Anti-Taurus Mountains form the northern rim of the study area. They effectively block most arctic and polar intrusions and keep them from entering the Middle East Peninsula.

The Zagros Mountains extend 1,000 NM from northwest to southeast across western Iran to the Strait of Hormuz. They channel flow in the northern half of the study area.

STUDY CONTENT. Chapter 2 provides a detailed discussion of the major climatic controls that affect the Middle East Peninsula. These controls range from the macroscale ("semipermanent climatic controls"), through the synoptic ("synoptic disturbances") to the mesoscale ("mesoscale and local features"). The individual treatments of each climatic subregion in subsequent chapters do not include repeated descriptions of these phenomena, but give specifics unique to the individual subregion by focusing on mean distributions and local anomalies of sky cover, winds, precipitation, temperature, and visibility. Meteorologists using this study should read and consider the detailed discussions in Chapter 2 before trying to understand or apply the individual climatic zone discussions in Chapters 3-6. This is particularly

important because the study was designed with two purposes in mind: first, as a master reference to the entire Middle East Peninsula, and second, as a modular reference to the subregions. Chapters 3-5 discuss "situation and relief" and the "general weather" of each subregion by season.

The Red Sea Coastal Plains (Chapter 3) are located between 12° 40' N and 30° N, and 33° E to 43° E. Weather and climate vary greatly from south to north. South of 20° N, weather is controlled by the circulations of the Southwest and Northeast Monsoons. The effects of the land/sea breeze and the Red Sea Convergence Zone (discussed in Chapter 2) are important mesoscale and synoptic weather features, respectively. North of 20° N, mid-latitude features dominate during the Northeast Monsoon, while intense thermal heat lows dominate during the Southwest Monsoon.

The Fertile Crescent (Chapter 4) is the northernmost region in the study area. It extends from 30 to 38° N, and from 36 to 48° E. It is dominated by Mediterranean flow and migratory low-pressure systems. A weak Northeast Monsoon circulation occasionally affects its southeastern corner. Features such as cyclonic activity, and transitory high-pressure cells affect the area. Monsoonal flow also has an influence here, but it is so weak that mid-latitude seasons (winter, spring, summer, and fall) are used. This is the only Middle East Peninsula subregion in which monsoon seasons are not used.

The Arabian Desert (Chapter 5), the largest Middle East Peninsula subregion, includes the Saudi Arabian interior. It lies between 16° N and 34° N and between 35° E and 60° E. The desert is an elevated plateau with a true desert climate. Although the extreme southern portion gets light precipitation with Southwest Monsoon flow, it is still considered desert. Migratory low-pressure systems generate strong winds and frequent duststorms, but seasonal surface pressure patterns are more important weather controls here.

The Persian Gulf Coastal Plains (Chapter 6) lie along the eastern edge of the Middle East Peninsula between 23° N and 31° N and between 48° E and 68° E. They are surrounded by vast deserts to the west (the An Nafud) and south (the Rub al Khali) and by the Zagros Mountains to the north. The coastal plains are split in two by a warm-water barrier formed by the Persian Gulf and the Gulf of Oman. The warm gulf waters control temperature, but prevailing surface wind direction controls seasonal moisture availability and precipitation distributions. A monsoonal circulation dominates east of the Strait of Hormuz, but monsoonal flow has limited influence to the west of the Straits on the Persian Gulf proper.

CLIMATOLOGICAL REGIMES. The southern portion of the Middle East Peninsula is dominated by monsoonal weather, as shown in Figure 1-4; the rest is dominated by the subtropical ridge and, to a lesser extent, by mid-latitude low-pressure systems and Mediterranean weather patterns. The Fertile Crescent, the only subregion with typical mid-latitude seasons, is rarely influenced by monsoonal flow. Subregions influenced by monsoonal circulation normally have a 1- to 2-month transition period between the Southwest and Northeast Monsoons, but monsoon seasons (as well as transition periods) vary by year and location.

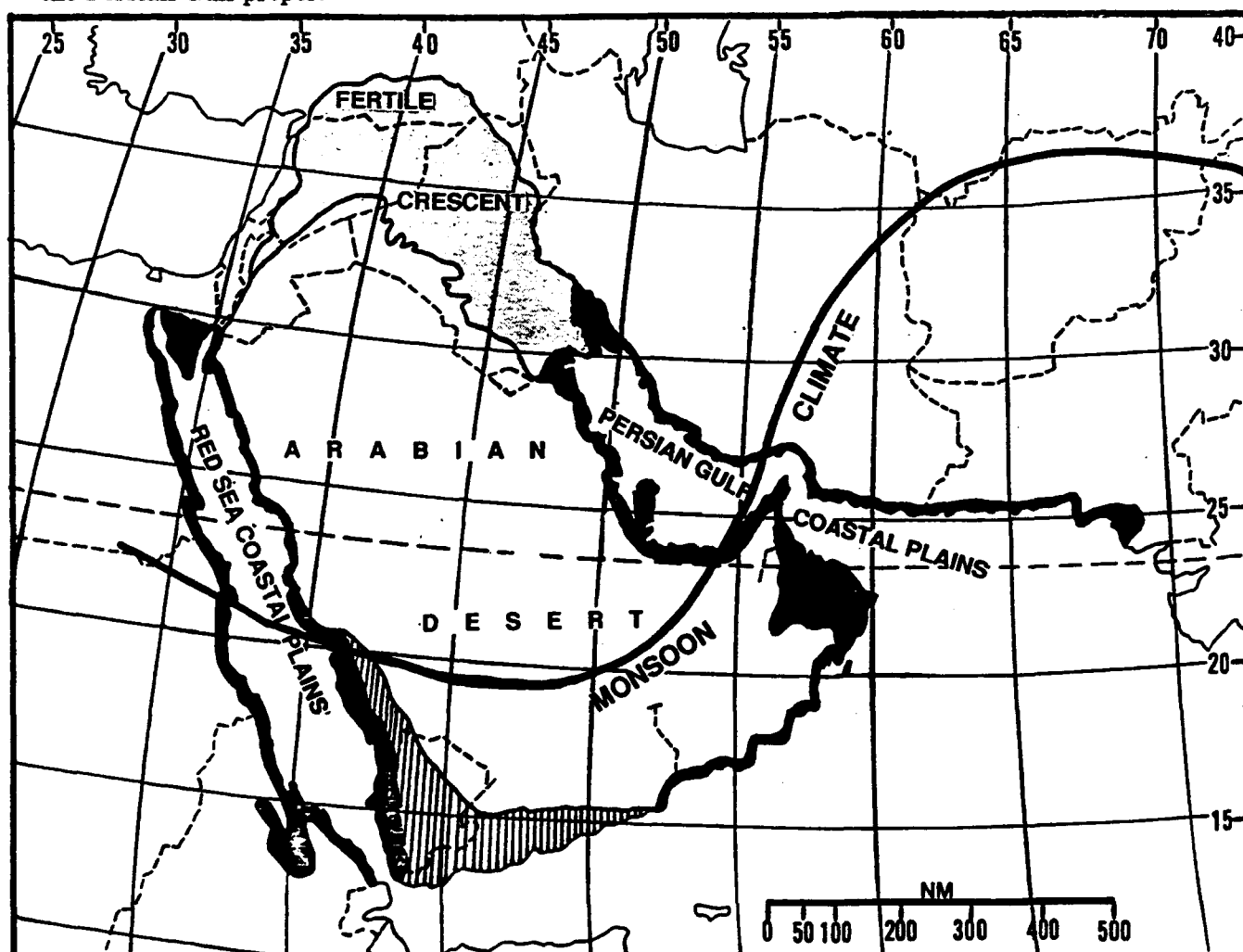


Figure 1-4. The Monsoon Climate with Respect to the Middle East Peninsula. The dark line shows the northernmost limit of monsoon conditions according to Ramage (1971). A more detailed discussion of Ramage's criteria for monsoon climate is provided in Chapter 2.

CONVENTIONS. The spellings of cities and geographical features are those used by the United States Defense Mapping and Aerospace Center (DMAAC). Distances are in nautical miles (NM), except for visibilities, which are in statute miles. Cloud bases and ceilings are in feet/meters above ground level (AGL) but cloud tops are above mean sea level (MSL). Note, however, that the AGL cloud bases given in this study are generalized over large areas; readers must consider terrain in applying these generalized values. AGL cloud bases, for example, are normally representative of valley reporting stations, but not of locations in surrounding mountains where ceilings and cloud bases would be lower and where, in fact, many locations would be obscured. Elevations are in feet with a meter or kilometer (km) equivalent immediately following. Temperatures are in Fahrenheit (° F) with a Celsius (° C) conversion following. Wind speeds are in knots. Precipitation amounts are in inches with a millimeter (mm) conversion following. When synoptic charts are not provided, local time (L) is used.

DATA SOURCES. Most of the information used in preparing this study came from three sources:

- Terminal forecast reference notebooks prepared by deployed units during Operation DESERT SHIELD at selected hard sites.
- Studies, books, atlases, and so on were supplied, with rare exceptions, by the Air

Weather Service Technical Library (AWSTL), the only dedicated atmospheric sciences library in the Department of Defense and the largest such library in the United States.

- Climatological data came direct from the Air Weather Service Climatic Database or through Operating Location A, USAFETAC--the branch of USAFETAC responsible for maintaining and managing this database.

RELATED REFERENCES. This study, while more than ordinarily comprehensive, is certainly not the only source of meteorological and climatological information for the meteorologist concerned with the Middle East Peninsula. USAFETAC/TN-92/003, *Gulf War Weather*, is a day-by-day description of weather in the Middle East Peninsula during Operations DESERT SHIELD, DESERT STORM, and PROVIDE COMFORT; it contains excellent satellite imagery that should be referred to while reading this volume. The United States Navy has published several comprehensive Naval Tactical Applications Handbooks for the Indian Ocean, Gulf of Aden, Red Sea, and Persian Gulf. Station Climatic Summaries for Africa and Asia provide summarized meteorological observational data for many airports on the Middle East Peninsula. Staff weather officers/NCOs and forecasters are urged to contact the Air Weather Service Technical Library for as much data on the region as is currently available.

Chapter 2

MAJOR METEOROLOGICAL FEATURES OF THE MIDDLE EAST PENINSULA

The "major meteorological features" of the Middle East Peninsula are listed below as they appear and are described in this chapter. These features affect the weather and climate of the Middle East Peninsula the year-round. The same features may be discussed in more detail in subsequent chapters as they relate to individual subregions of the study area.

Semipermanent Climatic Controls	2-3
Sea Surface Temperatures (SSTs)	2-3
Sea Surface Currents	2-5
The Monsoon Climate	2-7
The Southwest Monsoon	2-7
Tibetan 200-mb Anticyclone	2-8
Tropical Easterly Jet Stream (TEJ)	2-10
The South Indian Ocean (Mascarene) High	2-10
The Somali Jet	2-13
The Onset Vortex	2-15
The Azores High	2-17
Seasonal Thermal Lows	2-17
The Pakistani Heat Low	2-17
The Saharan Heat Low	2-17
The Saudi Arabian Heat Low	2-18
Monsoon Trough	2-18
The Low Level Persian Gulf Jet (LLPGJ)	2-24
The Northeast Monsoon	2-25
The Persian Gulf Trough	2-25
The Asiatic High	2-25
The Azores High	2-27
The Saharan High	2-28
The Sudanese Heat Low	2-28
The Saudi Arabian High	2-28
The Red Sea Convergence Zone (RSCZ)	2-30
Mid-and Upper-Level Flow Patterns	2-32
The Subtropical Ridge	2-43
Synoptic Disturbances	2-44
Jet Streams	2-44
Storm Tracks	2-47
Cyclonic Activity	2-48
The Atlas Low	2-50
The Cyprus Low	2-56
The Black Sea Low	2-61
The Caspian Sea Low	2-64
Significant Low-Level Persian Gulf Synoptic Effects	2-65
The Omani Convergence Zone (OCZ)	2-66
The Desert Front	2-67
Tropical Disturbances/Cyclones	2-70
Subtropical Cyclones	2-72

Regional Winds	2-73
Etesian	2-73
Sharav	2-74
Khamsin	2-75
Shamal	2-77
Kaus	2-78
Haboob	2-78
Mesoscale and Local Effects	2-79
Duststorms	2-79
Synoptic Conditions	2-80
Local Surface Conditions	2-80
Seasonal Considerations	2-81
Diurnal Considerations	2-81
Dust Devils	2-81
Haze	2-81
Mountain/Valley Winds	2-81
Mesoscale Mountain/Valley Winds	2-81
Microscale Slope Winds	2-82
Mountain Waves	2-85
Inversion Downburst Winds	2-86
Sand Streets	2-87
Land/Sea Breeze	2-88
"Common" land/sea breezes	2-88
"Frontal" land/sea breezes	2-88
Wet-bulb Globe Temperature Index (WBGT)	2-90

SEMIPERMANENT CLIMATIC CONTROLS

SEA-SURFACE TEMPERATURES (SSTs). Figures 2-1a-d provide mean SSTs ($^{\circ}$ F) for the Arabian Sea, Gulf of Aden, Red Sea, Persian Gulf, and eastern Mediterranean Sea. Warm water moderates the Middle East Peninsula's climate along its immediate coastline throughout the year, but the marine boundary layer (with relative humidities averaging 40%) rarely extends more than 20 NM inland or above 3,000 feet (915 meters) MSL. The light grey shading

along the region's coastlines represents the mean distance for marine boundary layer air (sea-breeze) penetration (see "Mesoscale and Local Effects" for more on the land/sea breeze). The diurnal temperature range along the coast is small ($10\text{-}20^{\circ}$ F/ $5\text{-}10^{\circ}$ C), but larger ($20\text{-}35^{\circ}$ F/ $10\text{-}20^{\circ}$ C) beyond the marine boundary layer's influence. Figures 2-1a-d show the mean SST distribution along the region's coastal waters.

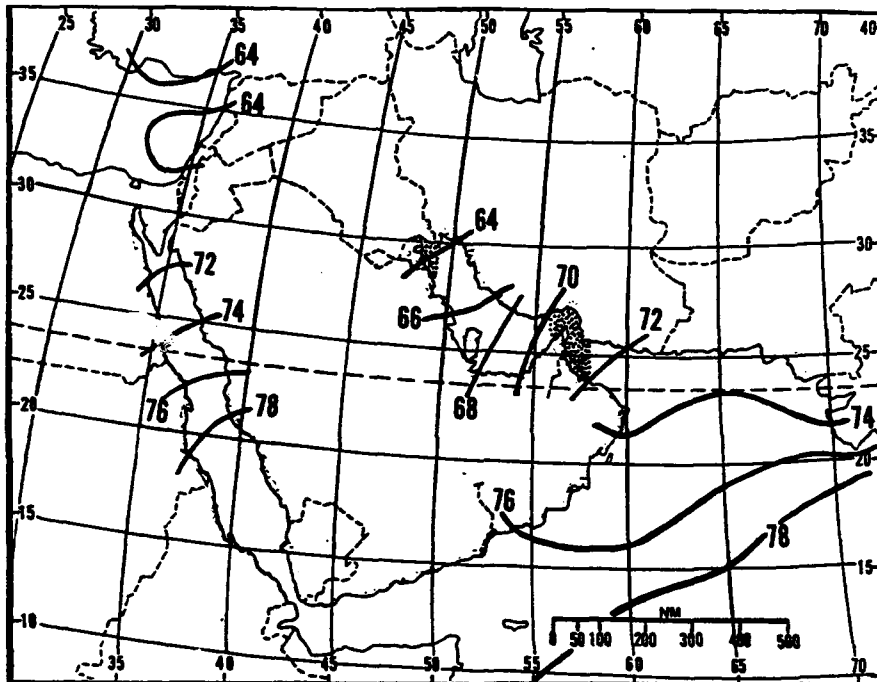


Figure 2-1a. Mean January-February Sea-Surface Temperatures ($^{\circ}$ F). The stippling shows where SST is higher than air temperature. SSTs range from 63 to 78° F ($17\text{-}26^{\circ}$ C), increasing from northwest to southeast. The coolest waters are in the eastern Mediterranean Sea ($63\text{-}64^{\circ}$ F/ $17\text{-}18^{\circ}$ C), the northern Red Sea (72° F/ 22° C), and the Persian Gulf ($64\text{-}70^{\circ}$ F/ $18\text{-}21^{\circ}$ C) from 48 to 55° E. Cool and moist westerly flow, migratory low-pressure systems, and cloud cover keep SSTs lower in these areas.

SEMIPERMANENT CLIMATIC CONTROLS

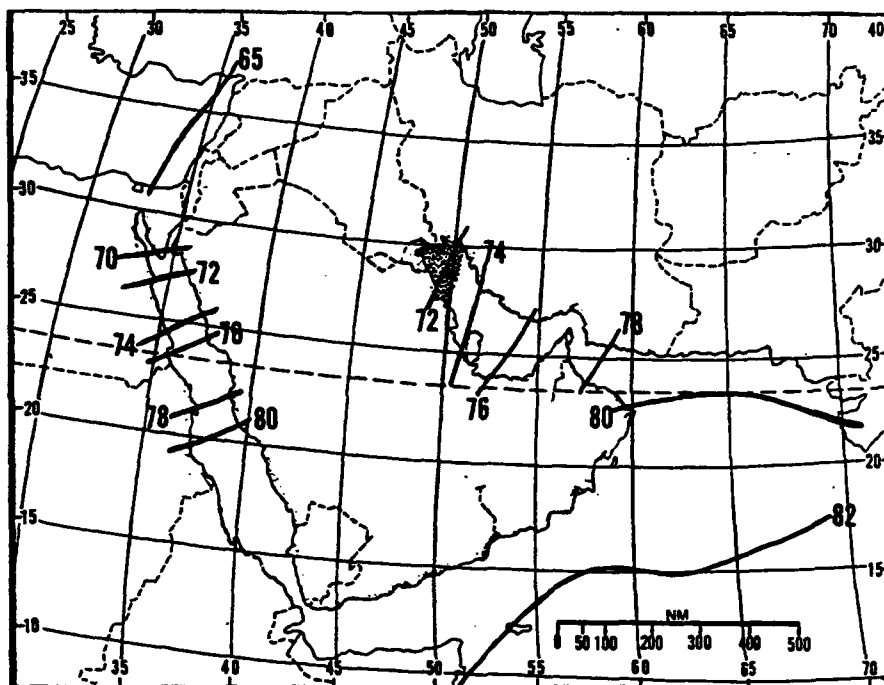


Figure 2-1b. Mean April Sea-Surface Temperatures (° F). SSTs range from 65 to 81° F (18-27° C) with a northwest-to-southeast gradient similar to that of January and February. Temperatures have increased everywhere except for a 2° F (1° C) cooling in the relatively shallow extreme northern Red Sea. Stippling shows where SST is cooler than air temperature.

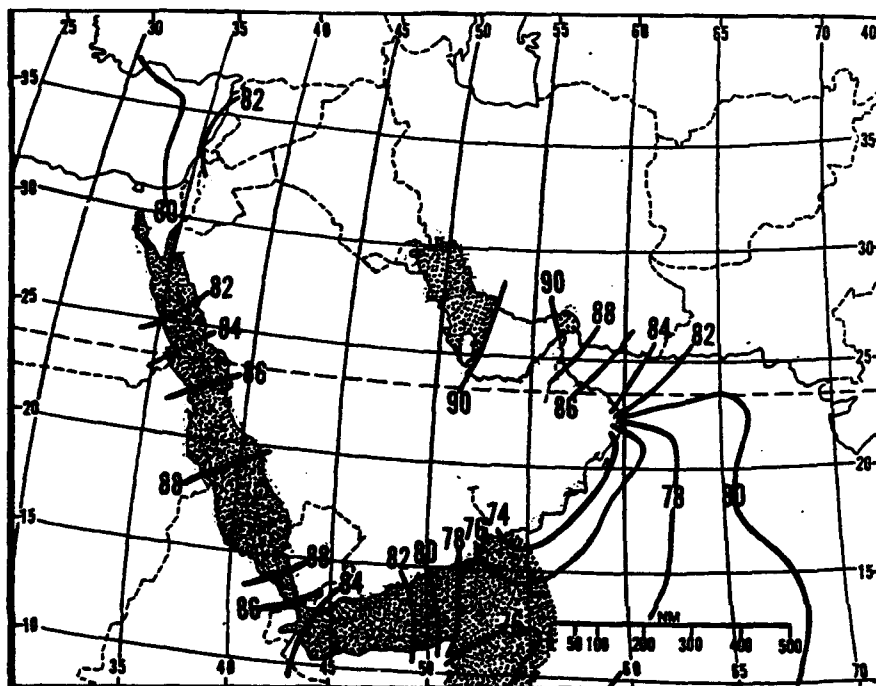


Figure 2-1c. Mean July-August Sea-Surface Temperatures (° F). SSTs range from 74° F (23° C) along the region's southeastern coast to slightly above 90° F (32° C) in the western and eastern Persian Gulf. Southeastern coastal waters are cool because the Somali Jet produces strong upwelling. The Persian Gulf and southern Red Sea are very warm (86-88° F/30-31° C) because of strong insolation and weak synoptic flow. Stippling shows where SST is cooler than air temperature.

SEMIPERMANENT CLIMATIC CONTROLS

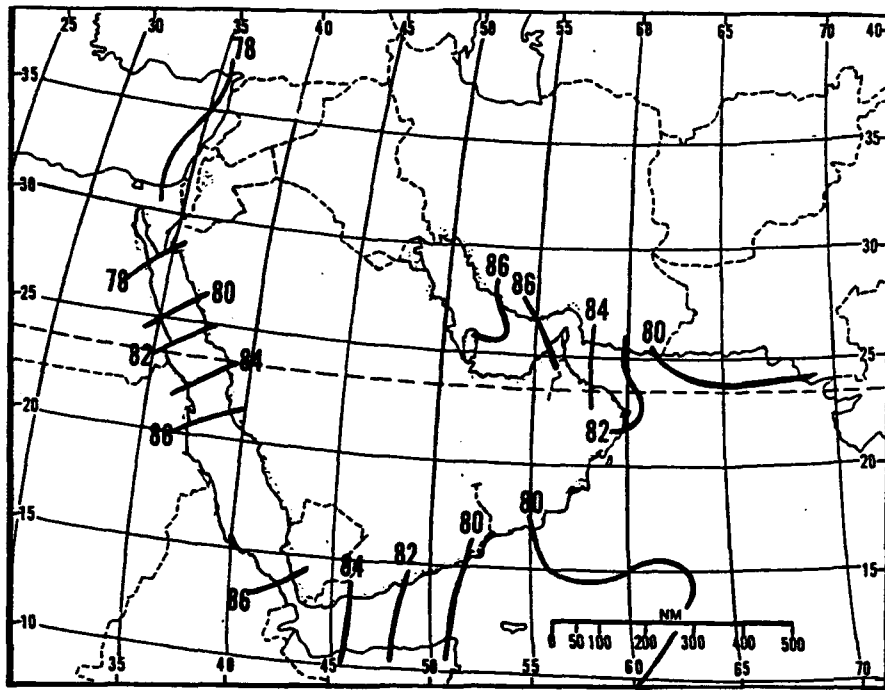


Figure 2-1d. Mean October Sea-Surface Temperatures ($^{\circ}$ F). SSTs range from 78° F (26° C) in the eastern Mediterranean and extreme northern Red Sea to slightly above 86° F (30° C) in the southern Red Sea ($13-21^{\circ}$ N) and the Persian Gulf (west of 56° E).

SEA-SURFACE CURRENTS in the adjacent seas of the Middle East Peninsula do not maintain a constant direction, except for the Persian Gulf and the Gulf of Oman; both flow counter clockwise throughout the year.

Red Sea surface currents are very wind-dependent due to its shallow depth. Gulf of Aden and Arabian Sea surface currents shift with the monsoons. The speed of all the sea-surface currents is about 1 knot.

SEMIPERMANENT CLIMATIC CONTROLS



Figure 2-2a. January Sea-Surface Currents.



Figure 2-2b. July Sea-Surface Currents.

SEMI-PERMANENT CLIMATIC CONTROLS

THE MONSOON CLIMATE. The term "monsoon" is generally applied to areas where there is a seasonal reversal of the prevailing surface winds. The generally accepted definition of a monsoon climate follows four criteria (after Ramage, 1971):

- Prevailing seasonal wind directions between summer and winter must change by at least 120 degrees.
- Both summer and winter mean wind speeds must equal or exceed 10 knots (5 meters/sec).
- Wind directions and speeds must exhibit high degrees of steadiness, and
- No more than one cyclone/anticyclone couplet occurs during January or July in any 2-year period within any 5 degree grid square.

Figure 1-4 (Chapter 1) showed the northern limit of monsoon climate (the dark line) across the Middle East Peninsula based on all four criteria established by Ramage. The monsoon climate occurs in the extreme southern and eastern sections of the region. Climatic controls associated with the Southwest Monsoon are discussed first.

THE SOUTHWEST MONSOON produces southerly flow over the southeastern Middle East Peninsula. Several features maintain, control, and regulate the low, middle, and upper monsoon circulations. Each feature will be discussed separately even though they interact in a cause-effect relationship.

Three mechanisms trigger the large-scale monsoon (Hamilton, 1987): *differential heating, coriolis force, and condensation or evaporation of water vapor.* The Southwest Monsoon reaches full strength from June to September and ends in October. In Chapters 3, 5, and 6, the Southwest Monsoon season is defined for each subregion. The resulting weather (rainfall, cloud cover, prevailing wind direction) will also be covered.

Figure 2-3 shows Southwest Monsoon circulation over the Middle East Peninsula by providing a three-dimensional view of the low (dark portion of the arrow), middle (hatched portion of the arrow), and upper (unshaded portion of the arrow) Southwest Monsoon circulation between 40 and 100° E, and between 10° S and 40° N. The Somali Jet, the Saudi Arabian Heat Low, the Pakistani Heat Low, and the Tropical Easterly Jet (TEJ) are also shown.

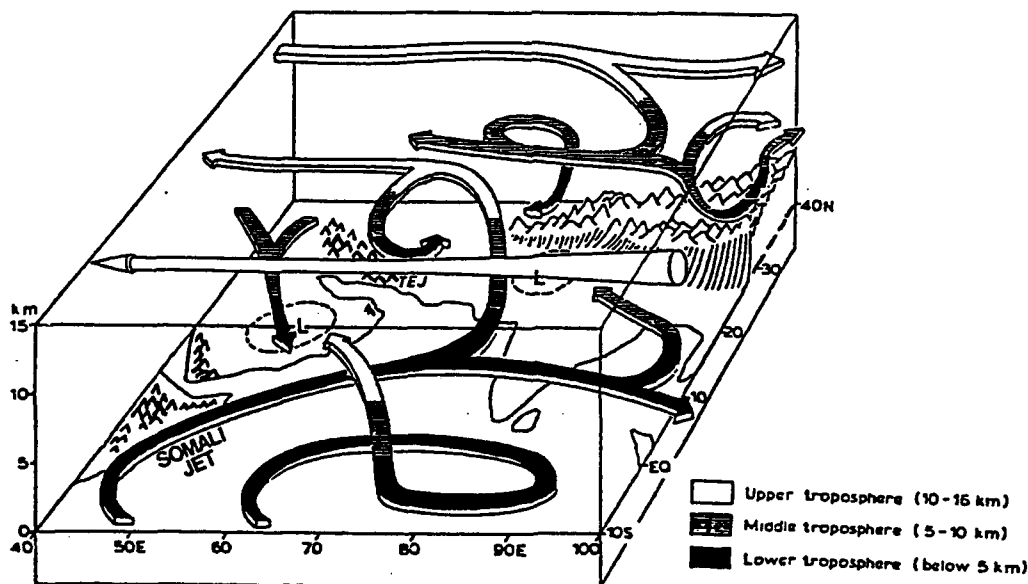


Figure 2-3. Southwest Monsoon Circulation Over Southern Asia and the Indian Ocean (from Hamilton, 1987).

SEMIPERMANENT CLIMATIC CONTROLS

Tibetan 200-mb Anticyclone. This semipermanent upper-air cell acts not only as an upper-level heat source, but as an outflow mechanism for sustaining surface monsoon trough convection between May and October. Latent heat of condensation from widespread convection over Burma warms the troposphere and begins the formation of the anticyclone in

late April to early May (see Figure 2-4a). Strong surface heating on the Tibetan Plateau, with a mean elevation at about 500 mb, shifts this massive upper-level high to Tibet in late May to June (see Figure 2-4b). The mean July 200-mb flow pattern over south-central Asia (Figure 2-4c) shows the large-scale anticyclone anchored over the Tibetan Plateau.

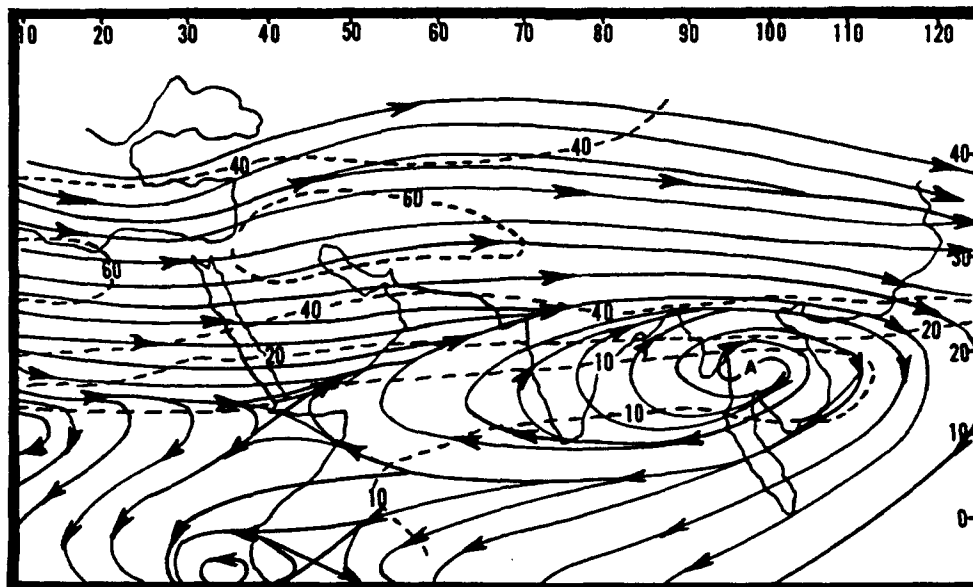


Figure 2-4a. Mean May 200-mb Flow Showing the Tibetan Anticyclone. The "A" represents the Tibetan Anticyclone's position. Dashed lines are isotachs (kts).

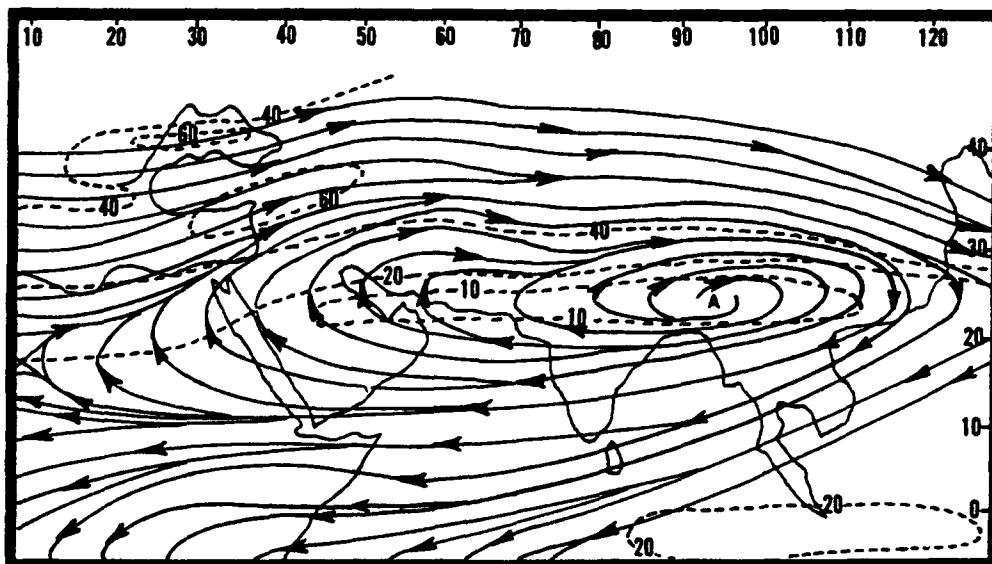


Figure 2-4b. Mean June 200-mb Flow Showing the Tibetan Anticyclone. The "A" represents the Tibetan Anticyclone's position. Dashed lines are isotachs (kts).

SEMIPERMANENT CLIMATIC CONTROLS

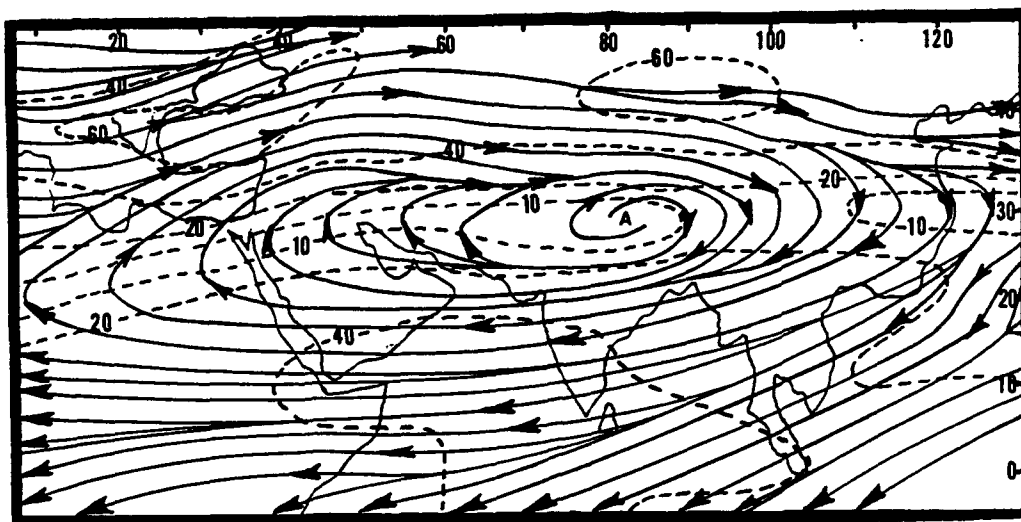


Figure 2-4c. Mean July 200-mb Flow Showing the Tibetan Anticyclone. The "A" represents the Tibetan Anticyclone's position. Dashed lines are isotachs (kts).

By August, moderate snow cover produced by strong Southwest Monsoon convection begins to lower surface temperatures and increase the surface albedo by reflecting more radiation away from the surface. The large amount of heat energy that would normally have been used for surface heating is now used to melt the snowfall and evaporate the runoff. Surface temperatures are affected immediately, but cooling aloft is

gradual. Typically, it takes 1 to 2 months for surface effects to affect the upper levels. Satellite research (Flohn, 1968) showed that the Tibetan Plateau is snow-free 80% of the time during the early Southwest Monsoon. The upper-level anticyclone weakens by October because the surface "trigger" is eliminated; upper-level westerlies move southward over the Plateau.

SEMI-PERMANENT CLIMATIC CONTROLS

Tropical Easterly Jet Stream (TEJ). Found only in summer (Figure 2-5), the TEJ provides an outflow mechanism along the southern edge of the Tibetan 200-mb circulation and sustains the heavy Southwest Monsoon convection. Its mean

position is at about 11° N, but it oscillates between $7^{\circ} 30'$ N and 18° N from May through October. The TEJ is generally found between 100 and 200 mb. Mean speeds average 50-60 knots, but 100-knot speeds are not uncommon.

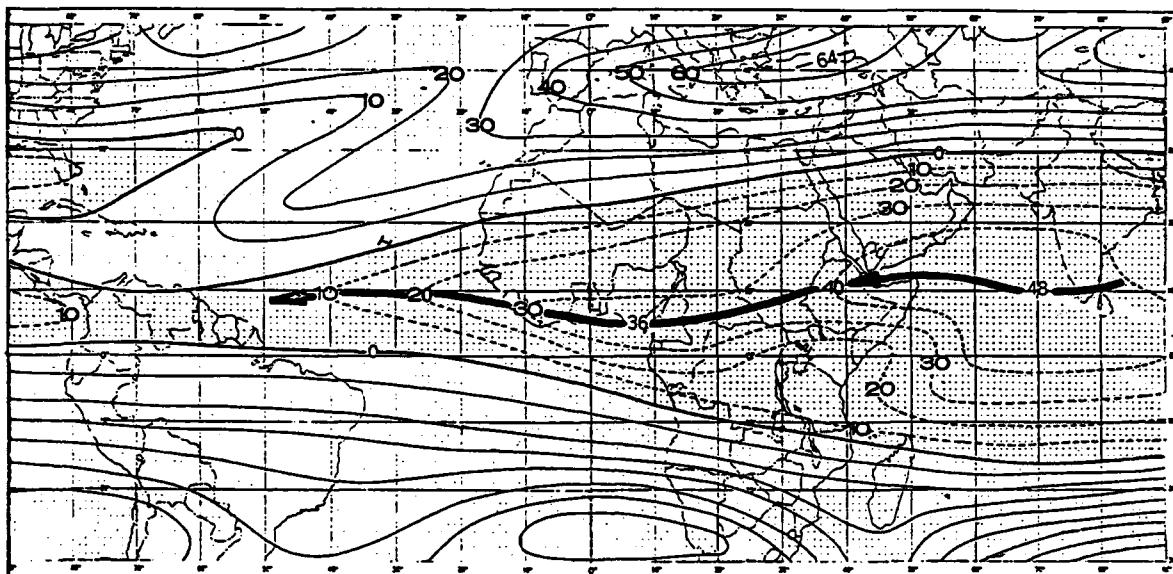


Figure 2-5. Mean July 200-mb Zonal Flow Showing the Tropical Easterly Jet (TEJ). The dark arrow is the TEJ. The stippled area represents easterly flow. Dashed lines are isotachs (kts) of *easterly* flow—solid lines are isotachs (kts) of *westerly* flow.

The South Indian Ocean (Mascarene) High. This semipermanent, Southern Hemisphere high-pressure cell provides cross-equatorial flow (through the Somali Jet) from April through October. It is not a factor on Middle East weather during the Northeast Monsoon. Figures 2-6a-d show mean large-scale surface pressure patterns over the Indian Ocean during the Southwest Monsoon. Note that mean surface pressure patterns (like the ones shown in these figures) do not reflect actual surface flow in the tropics; wind data and streamline analyses

are required to extract the Somali Jet from the broad-scale flow pattern.

The cross-equatorial flow generated by the Mascarene High affects the Middle East Peninsula in two ways: first, the flow surges the surface Monsoon Trough northward over the southeastern and eastern sections of the region, and second, it produces strong cold-water upwelling along the Omani coastline (see "Sea Surface Temperatures").

SEMPERMANENT CLIMATIC CONTROLS

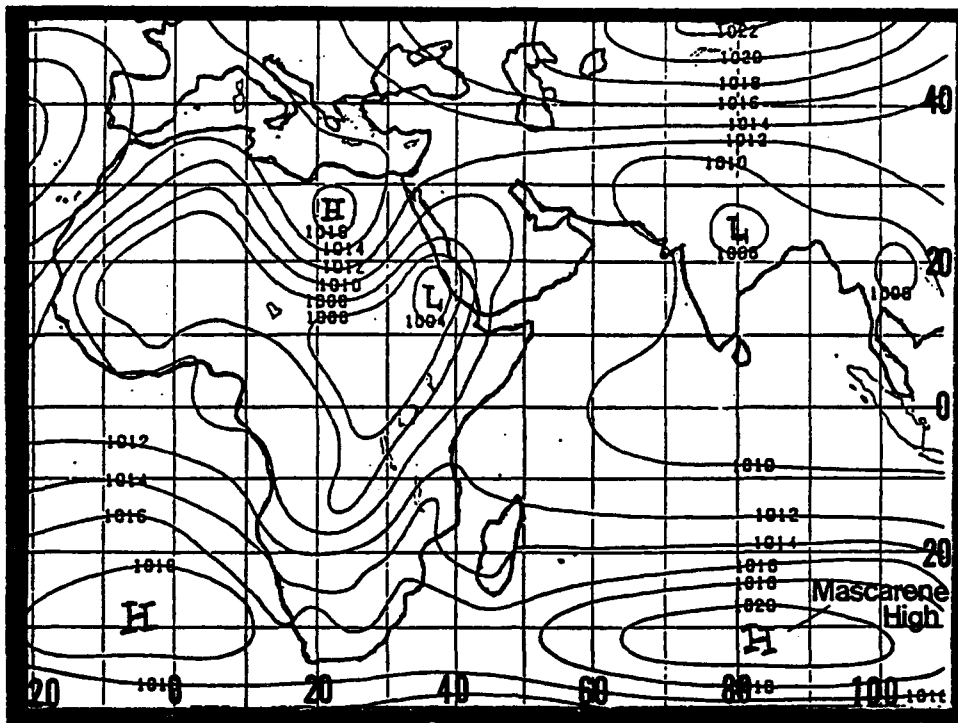


Figure 2-6a. Mean April Position of the Mascarene High. The Mascarene High's mean April position (Figure 2-6a) is 32° S, 83° E, with a central pressure of 1021 mb.

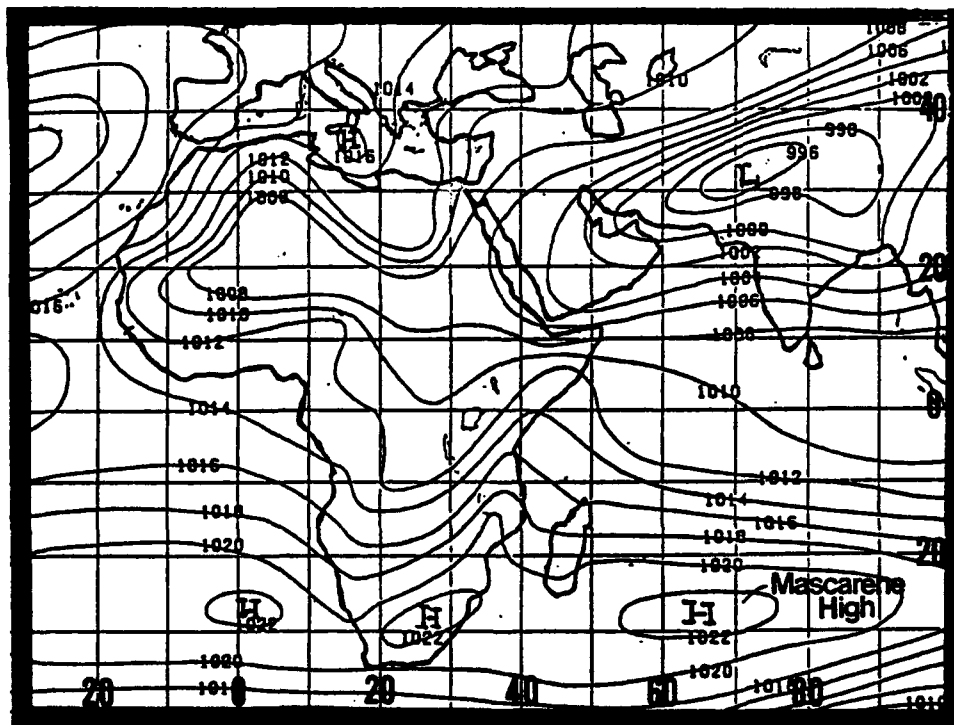


Figure 2-6b. Mean July Position of the Mascarene High. By July, the high strengthens to 1023 mb and shifts northwest to a mean position near 28° S, 65° E.

SEMI-PERMANENT CLIMATIC CONTROLS

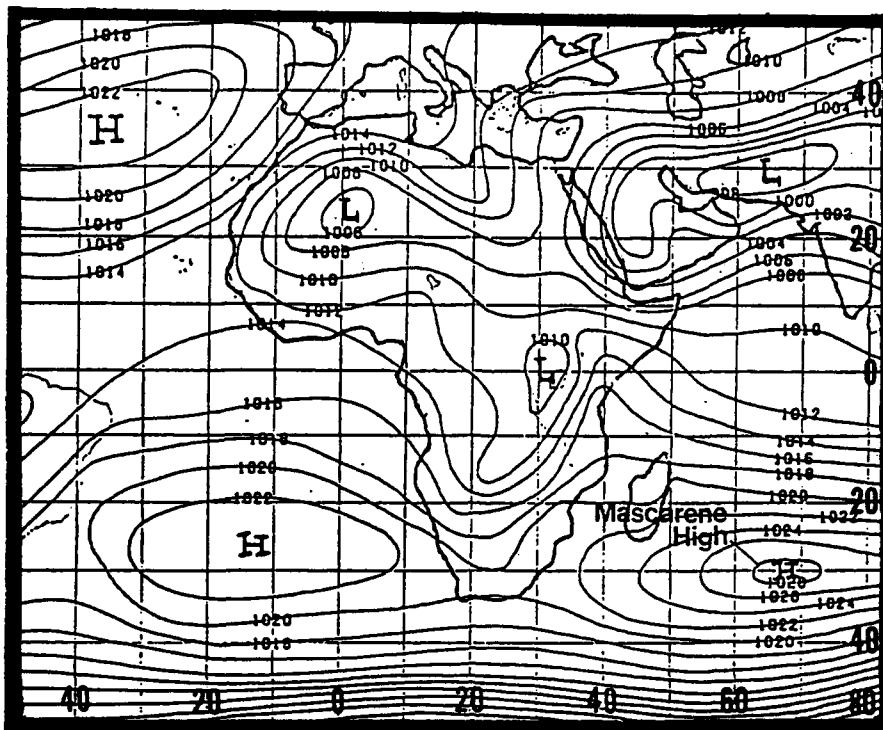


Figure 2-6c. Mean August Position of the Mascarene High. Mean central pressures peak at 1028 mb as the High migrates southeastward to 30° S, 68° E. Maximum low-level cross-equatorial flow peaks in July and August.

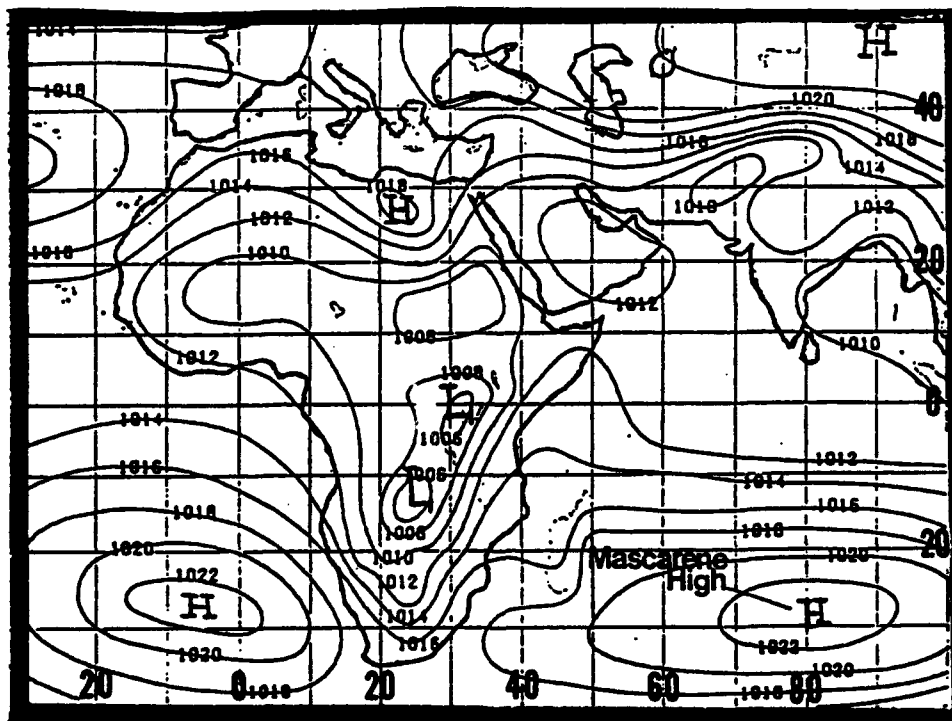


Figure 2-6d. Mean October Position of the Mascarene High. The High migrates farther eastward to 29° S, 80° E; central pressure weakens to 1023 mb.

SEMI-PERMANENT CLIMATIC CONTROLS

The Somali Jet. From April to late October, the Somali Jet enters the Northern Hemisphere between 4,000 and 7,000 feet (1,220-2,134 meters) MSL near the Kenya-Somalia border (39-43° E). Mascarene High outflow is compressed along the eastern edge of equatorial east Africa's mountain ranges to form this jet. Large-scale forcing causes mean monthly jet core wind speeds to oscillate northward from April to July (see Figure 2-7), then back south between August and October. Cyclonic activity in the Southern Hemisphere can create wind "surges" through the Mozambique Channel that intensify the Somali Jet and affect the Middle East Peninsula by causing oscillations of the surface Monsoon Trough. In June, the Somali Jet splits into two distinct branches. The northern branch skirts the southeastern Middle East Peninsula. Little is known about the Jet's characteristics

along the Arabian Sea (north of 12° N), except that dry air from the Saudi Arabian interior caps any cloud development resulting from the Somali Jet over water. Low-level wind speeds along the northern branch may exceed 60 knots, but mean wind speeds at 3,000 feet (915 meters) MSL are 25 to 35 knots over the Arabian Sea. These persistent low-level winds generate intense cold-water upwelling along the Arabian Peninsula's immediate coastline between 52 and 58° E (see "Sea Surface Temperatures"). Frequently, both branches of the Jet may display more than one wind speed maxima; however, it is unclear to what extent these multiple-core jets affect synoptic conditions over open water. Although not shown in the figure, the Somali Jet Stream shifts south of 12° N by late August. The split-branch flow disappears by late September.

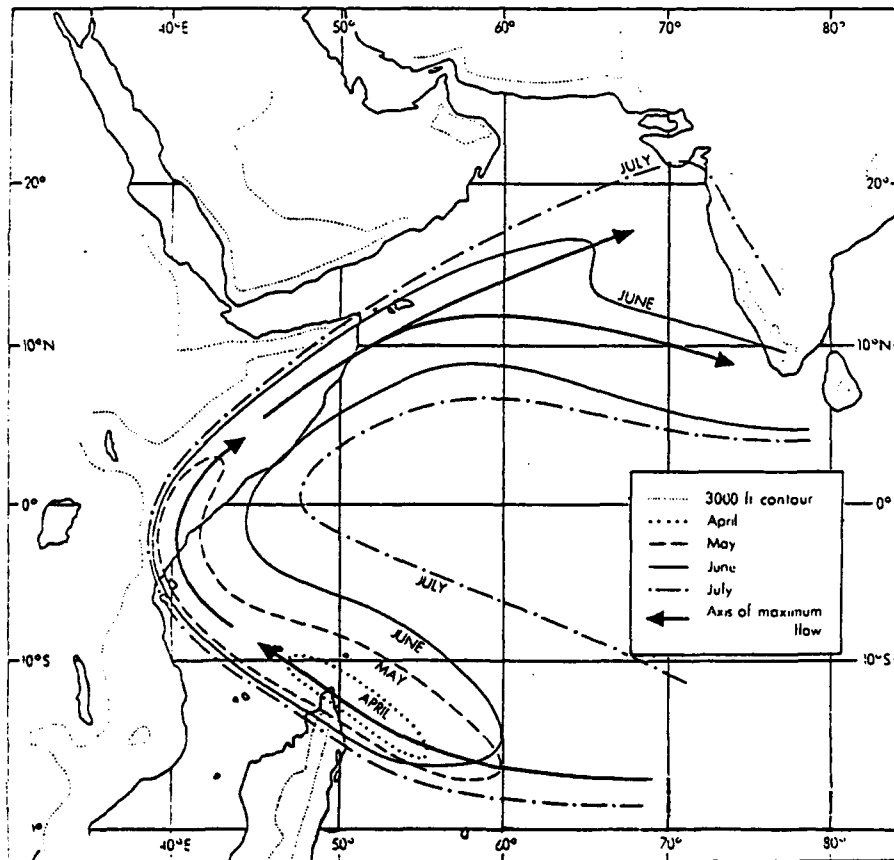


Figure 2-7. Successive Positions of the 20-Knot Isotach at 3,000 Feet (915 meters) AGL Between April and July (from Findlater, 1971). August-October positions are not shown.

SEMIPERMANENT CLIMATIC CONTROLS

Figure 2-8 shows the height and speed variations in a single jet-stream core. Maximum wind speed fluctuates with height over time. Rao (1976) and others have confirmed that surges in cross-equatorial flow are related to Southern Hemispheric low-pressure systems,

with the surge lagging frontal passage across southeast Africa by 1 to 1 1/2 days. Several researchers imply that fluctuations in the Somali Jet affect the entire Southwest Monsoon rainfall mechanism over India.

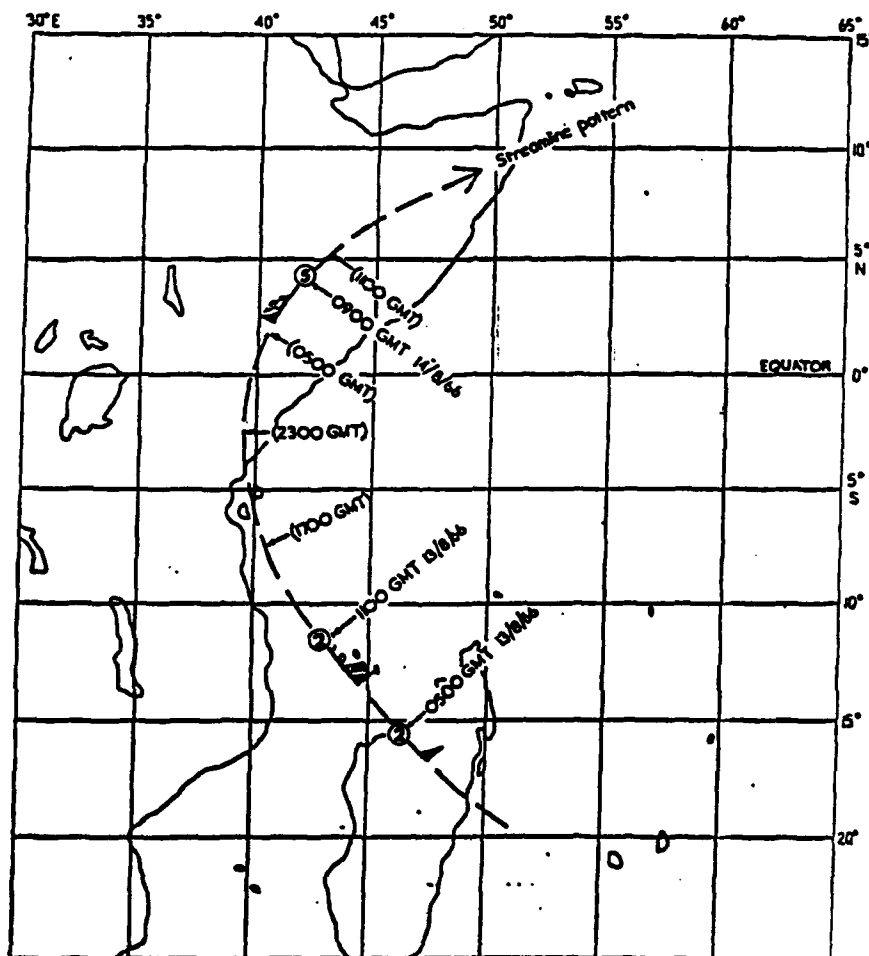


Figure 2-8. Movement of the Somali Jet Core, 13-14 August 1966 (from Findlater, 1969). Note the maximum wind-speed fluctuation with height (numbered circles at point of wind arrow in thousands of feet MSL) between 0500Z on 13 August 1966 and 0900Z on the 14th.

Ardanuy (1979) notes that diurnal variations in the Somali Jet's intensity and height are due to convection and turbulence over Ethiopia and Somalia. However, no information is currently available on possible diurnal variations over the Gulf of Aden. Because wind data over the Arabian Sea is limited, preliminary studies

(MONEX 79) suggest that the Somali Jet's role during the Southwest Monsoon is poorly understood. Krishnamurti (1981) and others believe that the Somali Jet assists the development of the Onset Vortex--an observed precursor to the Southwest Monsoon's onset over India.

SEMIPERMANENT CLIMATIC CONTROLS

The Onset Vortex. The "onset vortex" is a cyclone associated with the arrival of the Southwest Monsoon flow over the Indian Ocean-Arabian Sea area. It normally develops between mid-May and mid-June in the eastern Arabian Sea or the Bay of Bengal. The disturbance resembles, and can become, a tropical cyclone. Formation begins at mid-tropospheric levels (usually at 700 mb), then intensifies down to 850 mb with strong low-level convergence. Strong zonal flow (westerlies produced by the low-level Somali Jet) develop before the onset vortex. These disturbances are 200-500 NM in diameter with a lifespan of 3-10 days. Surface winds near the storm's eye sustain 50 knots or more.

Poor outflow aloft often destroys the disturbance before it reaches the Middle East Peninsula, but intensification west of 60° E longitude is not unknown.

Researchers differ on the relationship between the onset vortex and the Southwest Monsoon. Some believe the vortex is a trigger for the Southwest Monsoon, while others believe it forms in response to the Southwest Monsoon's movement toward the Asian landmass. Figures 2-9a-c show the 850-mb flow *before* (2-9a), *during* (2-9b), and *after* (2-9c) the "onset vortex" of 1979.

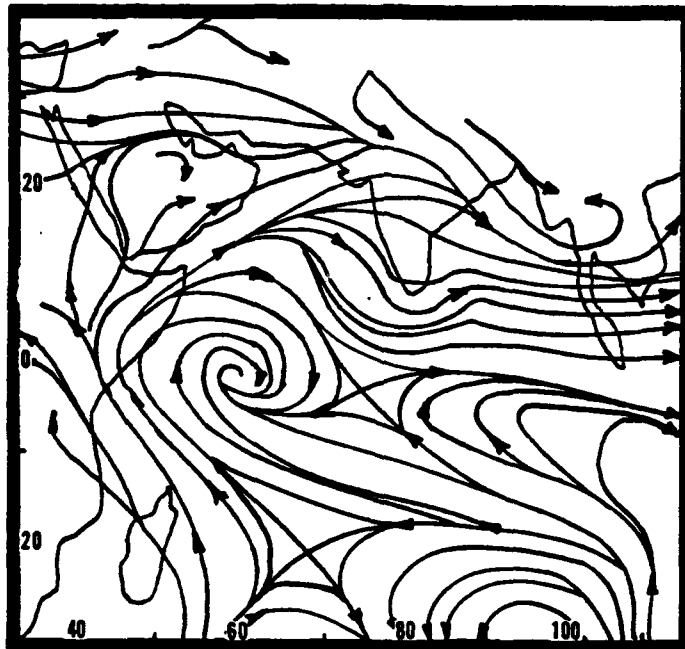


Figure 2-9a. 850-mb Streamline Chart (1200Z) for 23 May 1979 *Prior to Onset Vortex.*

SEMI-PERMANENT CLIMATIC CONTROLS



Figure 2-9b. 850-mb Streamline Chart (1200Z) for 17 June 1979 *During Onset Vortex*. The "C" shows the vortex position.

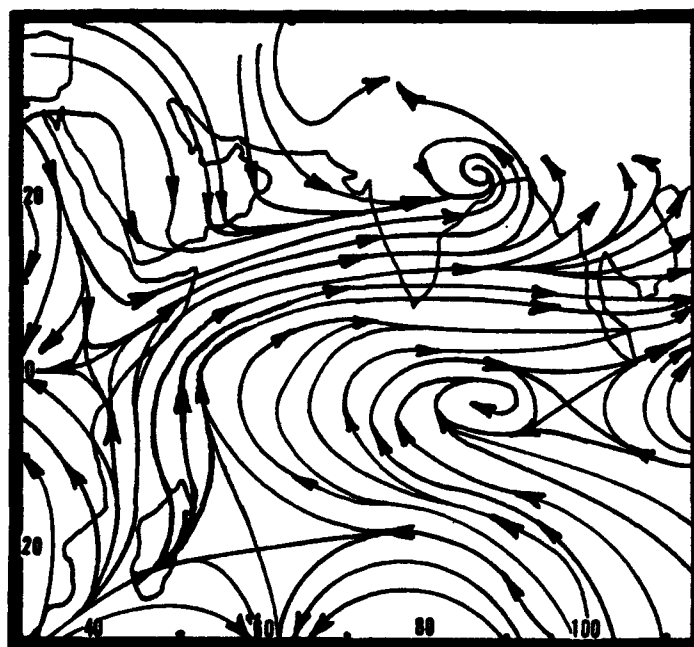


Figure 2-9c. 850-mb Streamline Chart (1200Z) for 27 June 1979 *After Onset Vortex*.

SEMI-PERMANENT CLIMATIC CONTROLS

The **Azores High**, with a mean surface position of 37° N, 37° W, and a central pressure of 1025 mb in July (as shown in Figure 2-10), helps to produce weak northwesterly flow over the northern half of the Middle East Peninsula.

This semipermanent high-pressure cell also effectively blocks any significant mid-latitude cyclonic activity from entering the region during the southwest monsoon.

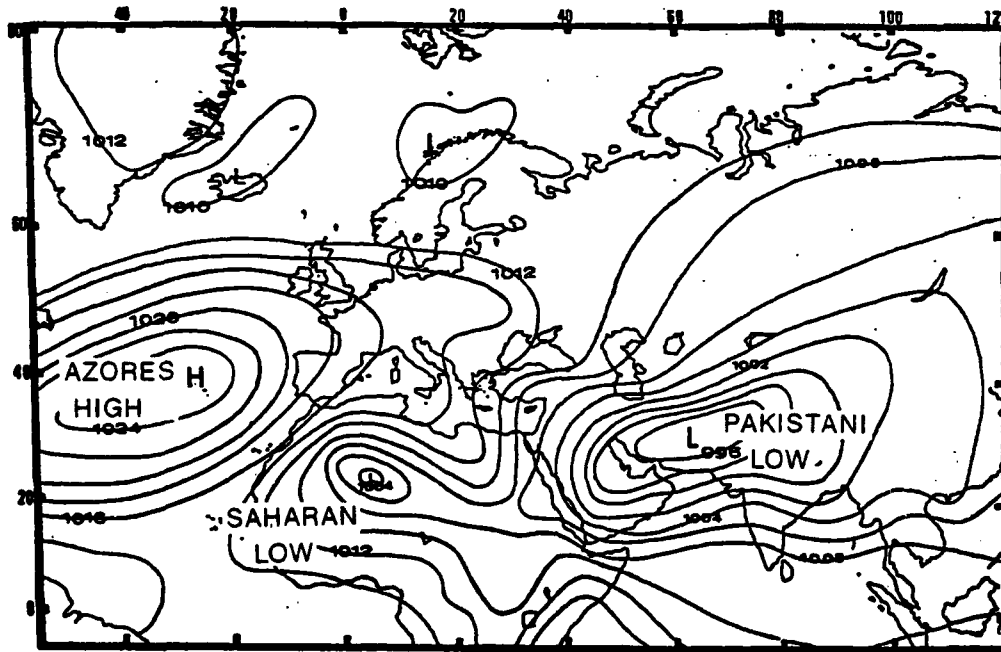


Figure 2-10. Mean July Surface Positions of Azores High, Saharan Low, and Pakistani Low.

Seasonal Thermal Lows. Three well-defined thermal low circulations directly or indirectly affect the Middle East Peninsula during the Southwest Monsoon; two of these (the Pakistani Low and the Saharan Low) are shown in Figure 2-10, above. A fourth (the Sudanese Low) will be discussed in the "Northeast Monsoon" section.

The Pakistani Heat Low. This low-level feature is present over northwestern India and southern Pakistan from May to early October, when it usually breaks down as insolation decreases and the Asiatic High becomes established over south-central Asia. Intensification of the Pakistani Low forces the mean Somali Jet core position (the 20-knot isotach) to oscillate northward and southward between May and October (see "Somali Jet"). As shown in Figure 2-10, the low

anchors the eastern edge of the larger scale trough extending from India to the Sahara during Northern Hemisphere summer. Central pressure ranges from 992 to 996 mb by late June. It is normally cloud-free.

The Saharan Heat Low develops in late March or early April over the Sahara near 25° N, 3° E. This low-level cyclone anchors the western end of the surface Monsoon Trough over the African interior and draws equatorial moisture into the southern Red Sea. In March and April, it is the source of hot, dust-laden air masses. The intensification of southerly winds in the Saharan Heat Low also assists Atlas Low surface development. By July, the semipermanent Saharan Low has a mean surface pressure of 1004 mb--see Figure 2-10.

SEMIPERMANENT CLIMATIC CONTROLS

The Saudi Arabian Heat Low is present from April to late October. It can extend to 650 mb. Its summer position and strength is regulated by intense surface heating over the Rub al Khali Desert. Its mean position (20° N, 48° E) varies little, but its vertical persistence and strength varies diurnally because of an extensive dust

layer aloft. The low weakens at night; descending flow produces northeasterly surface flow at 5-15 knots along the southern Arabian Desert. Since the low does not appear on mean surface pressure charts for July, gradient-level streamline flow over the Middle East Peninsula is provided (Figure 2-11).

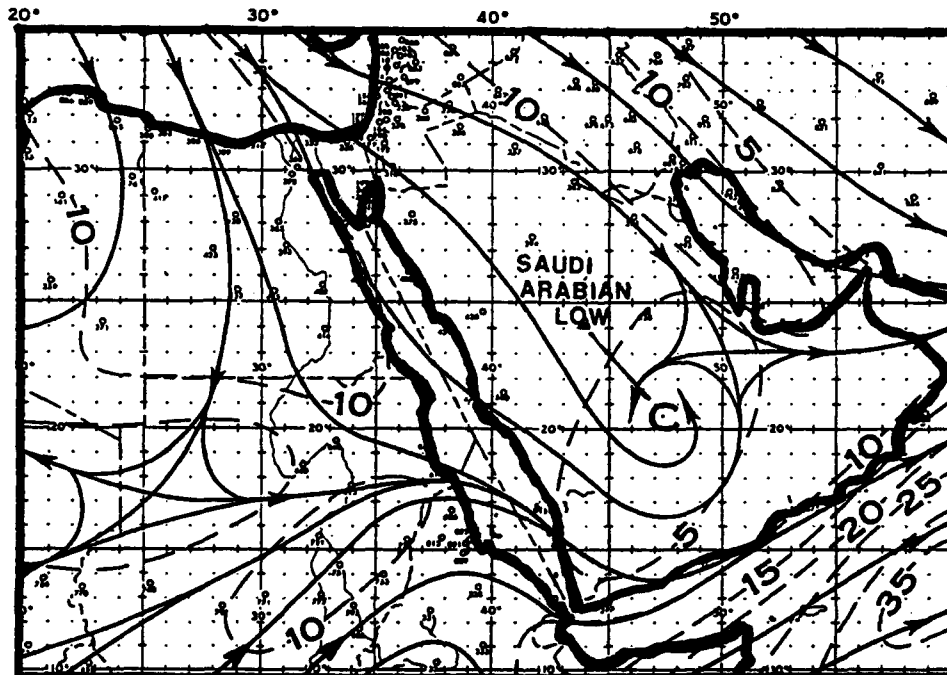


Figure 2-11. Mean July Gradient-Level Flow Showing the Position of the Saudi Arabian Heat Low. Isotachs (dashed lines) in knots.

Monsoon Trough. Movement of the surface Monsoon Trough is extremely complex because of topography. The Ethiopian Highlands form a natural barrier to airflow from the surface to 850 millibars; they split the surface Monsoon Trough into two distinctly separate axes. West of the Ethiopian Highlands, the convergent wind fields producing the surface Monsoon Trough originate in the equatorial South Atlantic, equatorial Africa, and the Sahara. East of the Highlands, cross-equatorial outflow from the Mascarene High is the only factor in surface

Monsoon Trough movement and position. Figure 2-12, opposite, shows the surface Monsoon Trough's mean position over the region from April through November. The dotted lines in this figure show the Monsoon Trough to be normally fragmented and discontinuous across the Middle East. Local land/sea-breeze convergence can appear to be part of the Monsoon Trough in the Red Sea and Gulf of Aden, but they seldom generate extensive convection without support from the Monsoon Trough.

SEMI-PERMANENT CLIMATIC CONTROLS

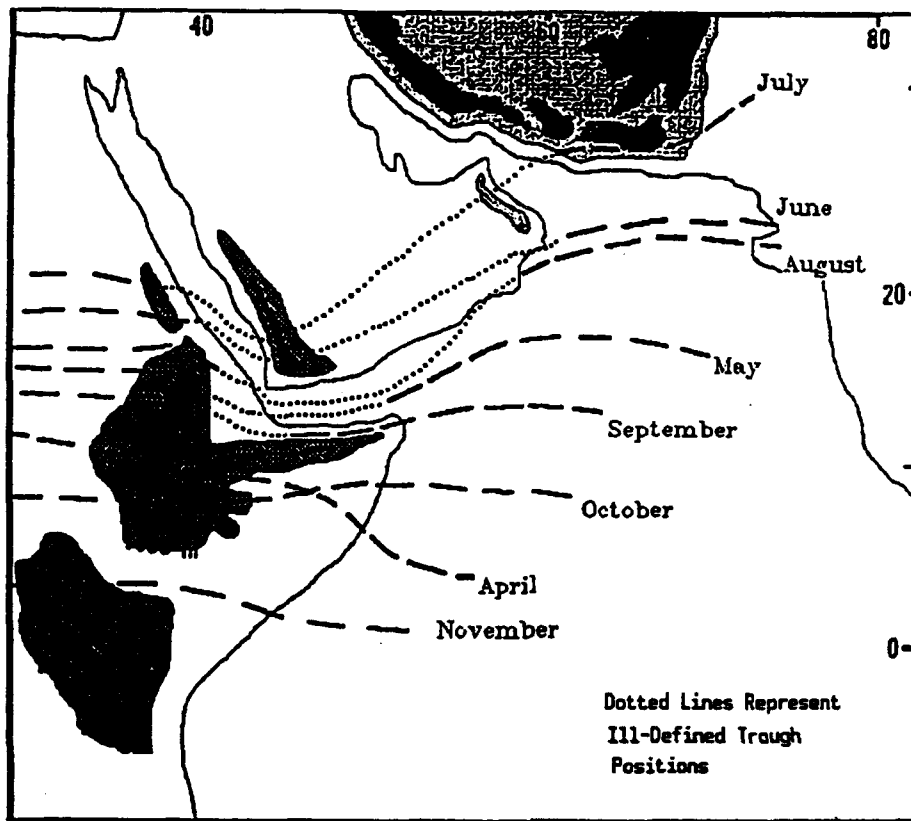


Figure 2-12. Mean Surface Monsoon Trough Positions: April through November. Grey shading represents elevations above 3,000 feet (915 meters); dark shading, elevations above 6,560 feet (2,000 meters). Dotted lines over the Red Sea/Gulf of Aden corridor represent fragmented or discontinuous surface Monsoon Trough positions.

Over the African interior, cloudiness and rainfall rarely surge north of 16° N until the surface Monsoon Trough merges with the "Indian Ocean" surface Monsoon Trough in July and August over the Red Sea and Gulf of Aden. This can occur through the Tokar Gap on the north side of the Ethiopian Highlands.

On satellite imagery, the Monsoon Trough isn't commonly observed across the Tokar Gap and Red Sea; however, in Figures 2-13a (enlarged view) and 2-13b (inset), strong "Africa Interior" low-level flow streams through the Tokar Gap as shown by the dust layer in these infrared photos. The imagery illustrates the recurved low-level

flow's path across the Red Sea and subsequent orographic lift that produces convection on the eastern coastal mountains. The flow moves across the Red Sea toward the eastern coastline south of 22° N, reinforcing the sea breeze and fueling orographic convection along the Asirs and Yemen Mountains. An extensive cluster of convection is visible in Figure 2-13a over the south and south-central edge of the rectangle. The convection typically occurs several hundred nautical miles south of the African Interior Monsoon Trough position. The surface Monsoon Trough axis is assumed to be near the Tokar Gap because suspended dust is moving northeastward into the Red Sea.

SEMIPERMANENT CLIMATIC CONTROLS

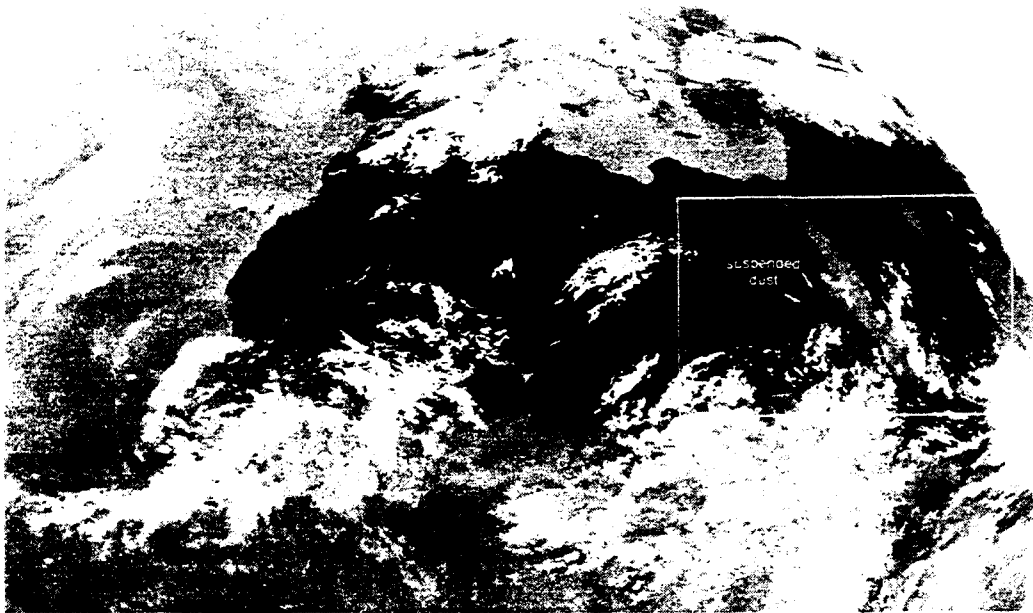


Figure 2-13a. METEOSAT IR Imagery (14 June 1979, 1155Z) of Subtropical Africa and the Middle East Peninsula (from NEPRF, 1980). The inset shows areas of suspended dust.

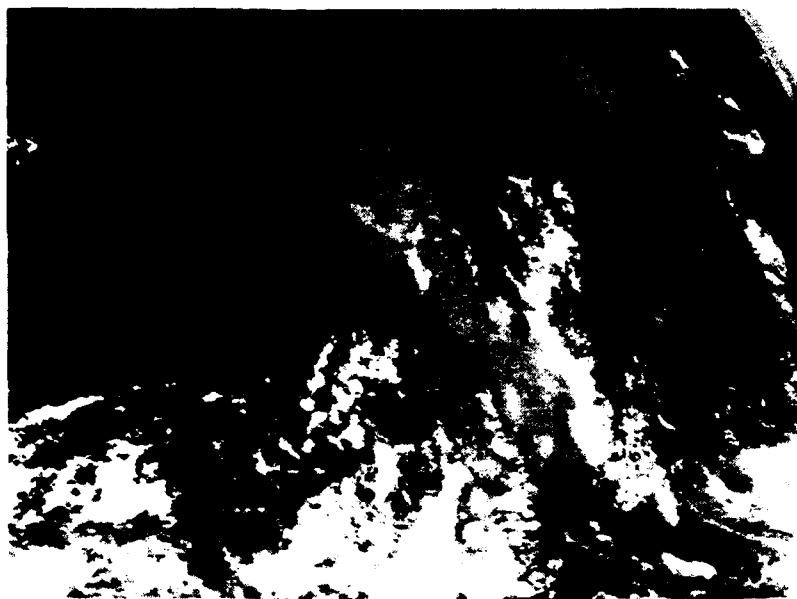


Figure 2-13b. Enlarged View of the Inset in Photo Above. The suspended dust is clearly visible.

SEMPERMANENT CLIMATIC CONTROLS

The surface Monsoon Trough position over the western Indian Ocean is controlled entirely by the Somali Jet. Dry Saharan air doesn't penetrate eastward across the Ethiopian Highlands. A broad-scale subsidence layer, however, is present over the Indian Ocean and Middle East Peninsula. In summer, there are two trough axis lines in the western Indian Ocean; these are referred to by some meteorologists as the "Northern Equatorial Trough" (NET) and the "Southern Equatorial Trough" (SET).

- The NET (the Indian Ocean surface Monsoon Trough) oscillates across 30 degrees of latitude over the Indian Ocean during the Southwest Monsoon. The Somali Jet (southerly low-level

flow) controls the position of the NET axis. By late June, the NET is positioned over the northern Arabian Sea.

- The SET axis oscillates over only 11 degrees of latitude between 7° S and 4° N. Weak large-scale cross-equatorial flow occurs over the equatorial Indian Ocean between 50 and 75° E.

Figures 2-14a-c show NET and SET positions during June, July and August. Note that the surface Monsoon Trough positions shown in Figure 2-12 do not differ significantly from these NET positions. The Indian Ocean Monsoon Trough is generally inactive over the study area and produces little convection.

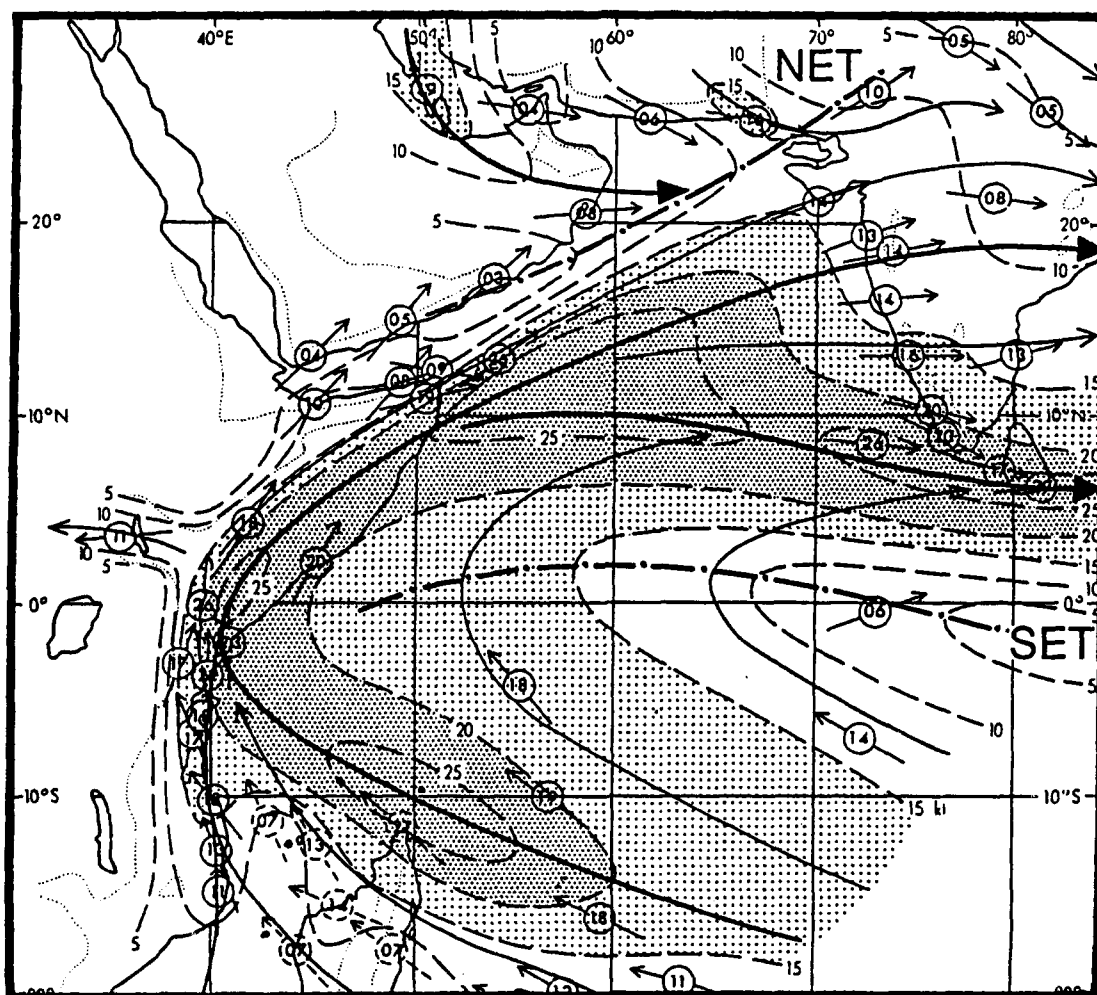


Figure 2-14a. Mean June Positions for the 3,000-Foot Monsoon Trough (NET) and the Southern Equatorial Trough (SET) (from Findlater, 1971).

SEMI-PERMANENT CLIMATIC CONTROLS

Normally, a band of weak low-level equatorial westerlies associated with broad cross-equatorial flow over the equatorial Indian Ocean (not with the Somali Jet) oscillates along and north of the equator between June and August. These equatorial westerlies lie between the NET and SET. Cloud bands frequently develop along the

SET where cyclonic vorticity and convergence is present. A double cloud band has been observed on satellite imagery during some Southwest Monsoons between June and August. SET cloudiness may propagate westward over Somalia when the SET cloud cover organizes into a significant synoptic weather system.

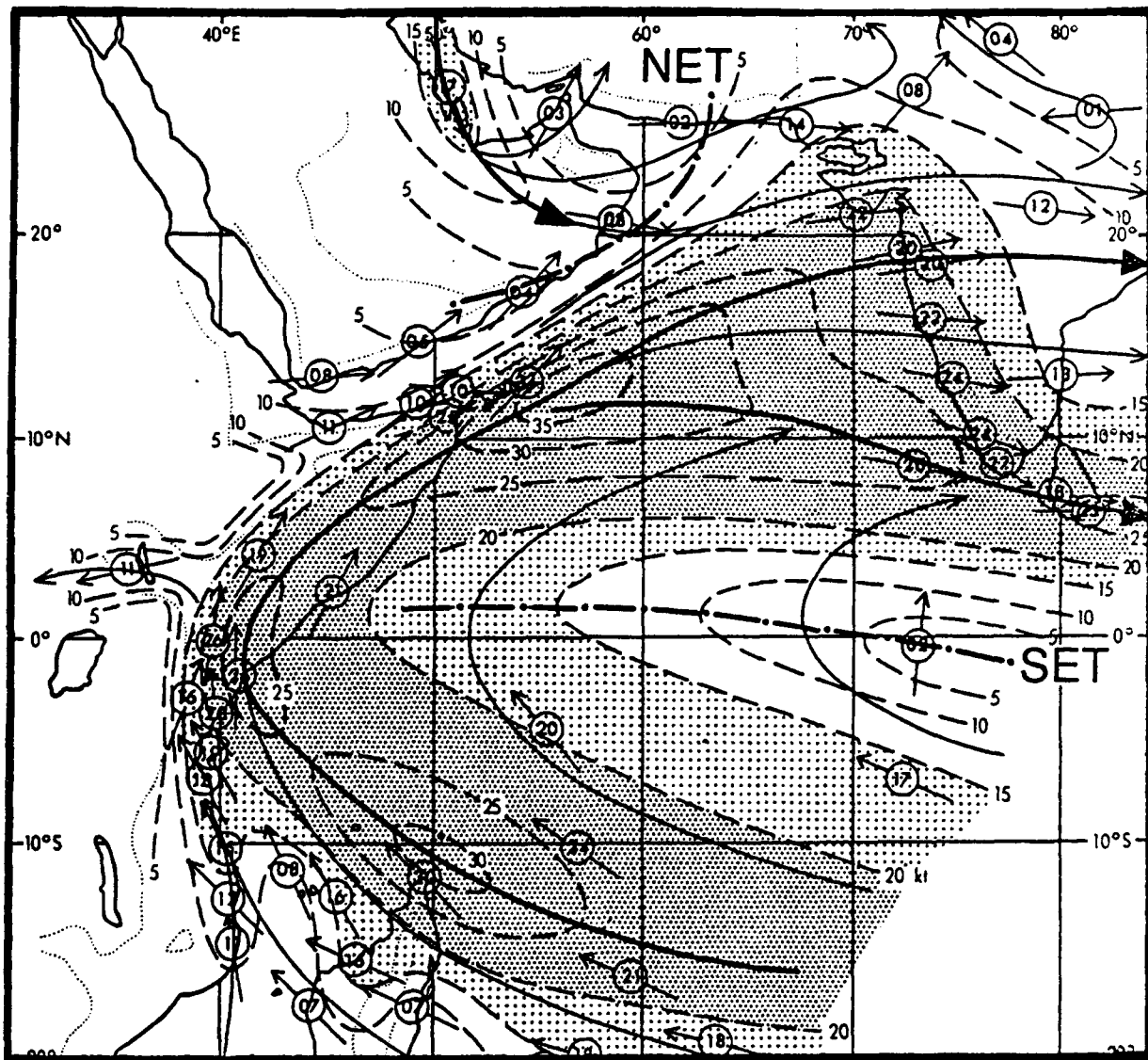


Figure 2-14b. Mean July Positions for the 3,000-Foot Monsoon Trough (NET) and the Southern Equatorial Trough (SET) (from Findlater, 1971).

SEMIPERMANENT CLIMATIC CONTROLS

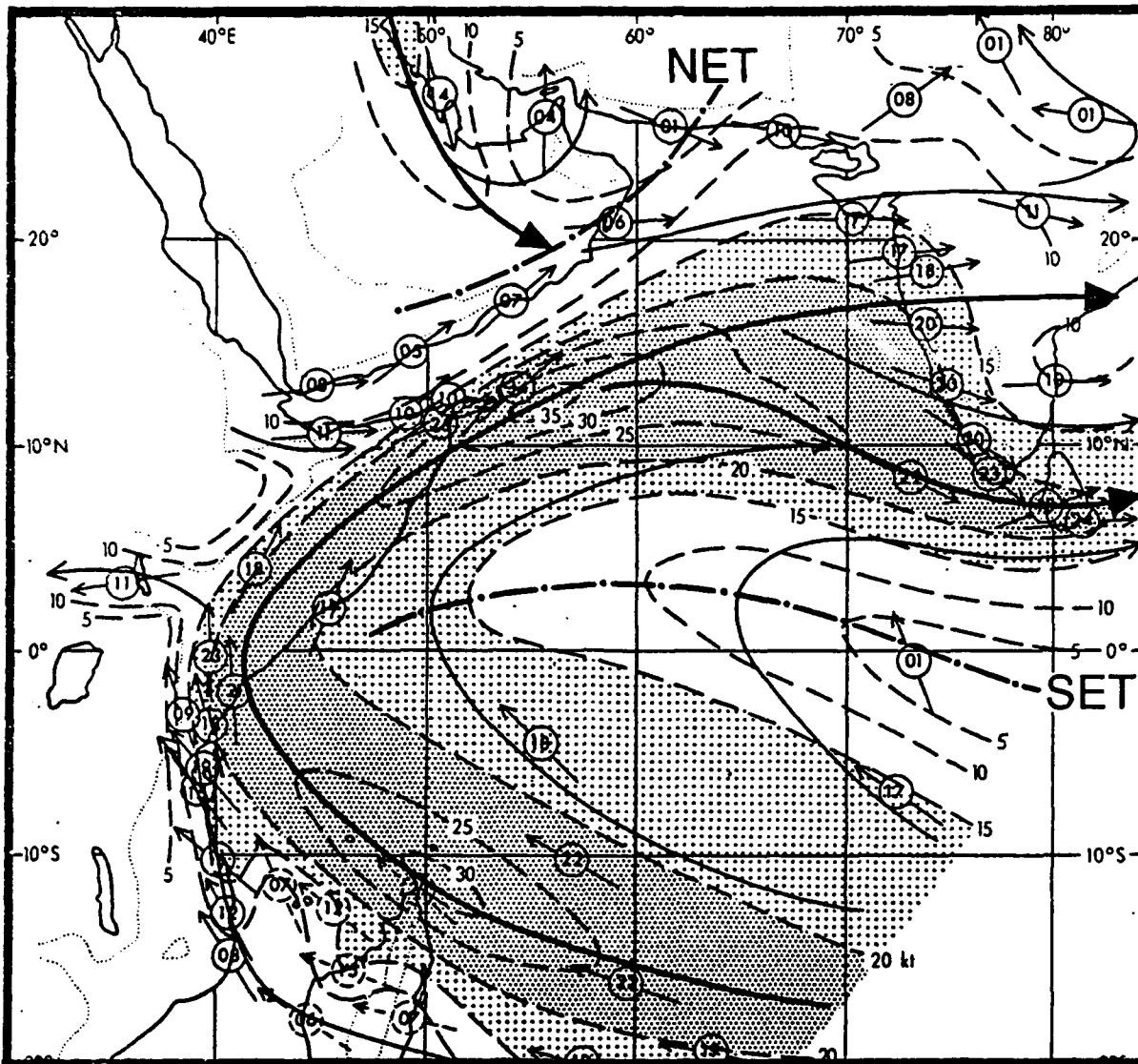


Figure 2-14c. Mean August Positions for the 3,000-Foot Monsoon Trough (NET) and the Southern Equatorial Trough (SET) (from Findlater, 1971).

SEMI-PERMANENT CLIMATIC CONTROLS

The Low-Level Persian Gulf Jet (LLPGJ) is the result of a strong subsidence inversion, terrain, and strong gradient flow during the Southwest Monsoon (June through September). Winds exceed 50 knots from 800 to 1,500 feet (244-457 meters) MSL along the immediate western coast of the Persian Gulf between 24 and 28° N (Figure 2-15). Altitudes and core speeds are

subject to diurnal variations. Maximum wind speeds and lowest altitude of the wind maximum occur near dawn. The LLPGJ is a contributor to the duststorms that occur over the northern Persian Gulf during the Southwest Monsoon. Figure 2-16 shows a vertical wind profile over Bahrain with the Persian Gulf Jet.

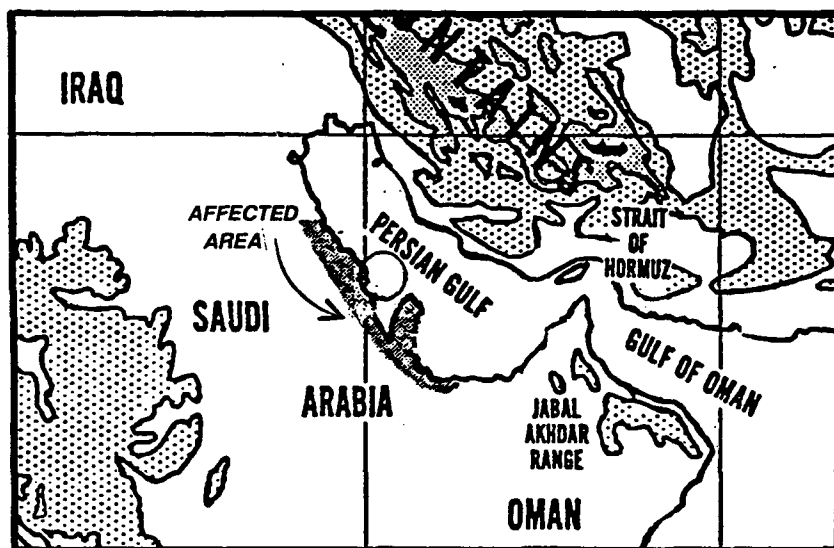


Figure 2-15. Location of the Low-Level Persian Gulf Jet During the Southwest Monsoon (Jun-Sep). The circle near Bahrain identifies the location used in Figure 2-16. The shaded region indicates the approximate area where the low-level jet may be found along the coastline, but does not show the inland extent of this jet.

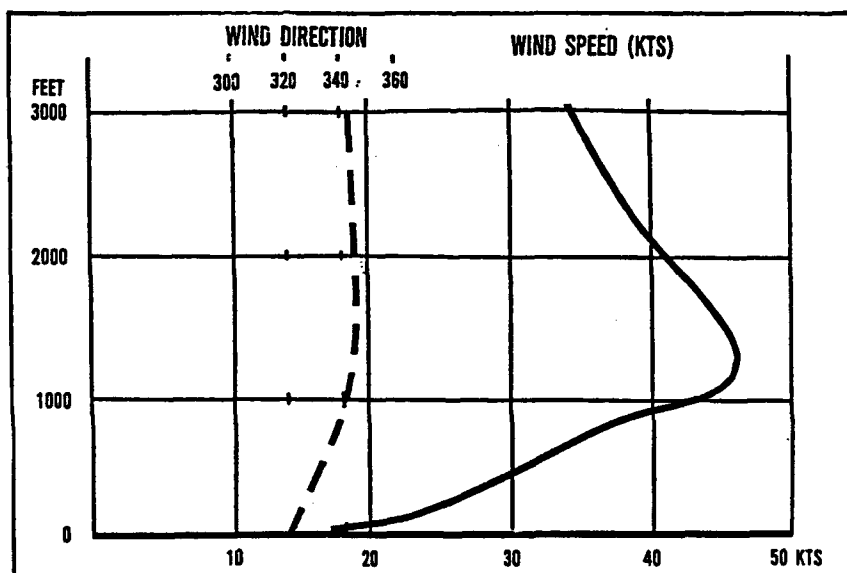


Figure 2-16. Low-Level Vertical Wind Profile of Persian Gulf Jet Over Bahrain.

SEMI-PERMANENT CLIMATIC CONTROLS

THE NORTHEAST MONSOON (winter) occurs from December to March over the southeastern half of the Middle East Peninsula; the northwestern half is seldom affected. This is normally the "dry" season; the Southwest Monsoon (summer) is the "wet" season. However, complex terrain features can result in "wet" Northeast Monsoon conditions along the Red Sea/Gulf of Aden corridor. Northeast Monsoon flow is not mentioned in Chapter 4, but it is referred to by name in Chapters 3, 5, and 6. Readers should review the "General Weather" sections in these chapters with care, since Northeast Monsoon flow affects both transition periods (October-November and April-May).

Any discussion of the Northeast Monsoon must include the Asiatic High, the Saharan High, the Saudi Arabian High, and the Sudanese Low. Surface outflow from these cells combines with topography along the Red Sea/Gulf of Aden corridor to produce orographic lifting and the Red Sea Convergence Zone (RSCZ). The Persian Gulf Trough should also be included in discussions of the Northeast Monsoon.

The Persian Gulf Trough. This weak semipermanent trough forms due to leeside troughing as Northeast Monsoon flow comes out of the mountainous regions of Iran, as well as from heating over the Persian Gulf. It creates a natural path for cyclonic storms moving east and southeast across Syria and Iraq. This is a low-level feature and does not normally exceed 850 mb. Increased ridging over Iran ahead of the polar trough intensifies the Persian Gulf Trough, while redevelopment of the Saudi Arabian High behind the cold front weakens it.

The Asiatic High. This strong but very shallow system dominates much of the Asian continent from late September to late April. Radiation cooling is the primary mechanism for its formation and intensification. Migratory Arctic air masses moving southward into central Asia temporarily reinforce and intensify the high. Centered over western Mongolia, mean central pressure is strongest (1035 mb) in January and February (Figure 2-17a). Vertical extent rarely exceeds 850 mb.

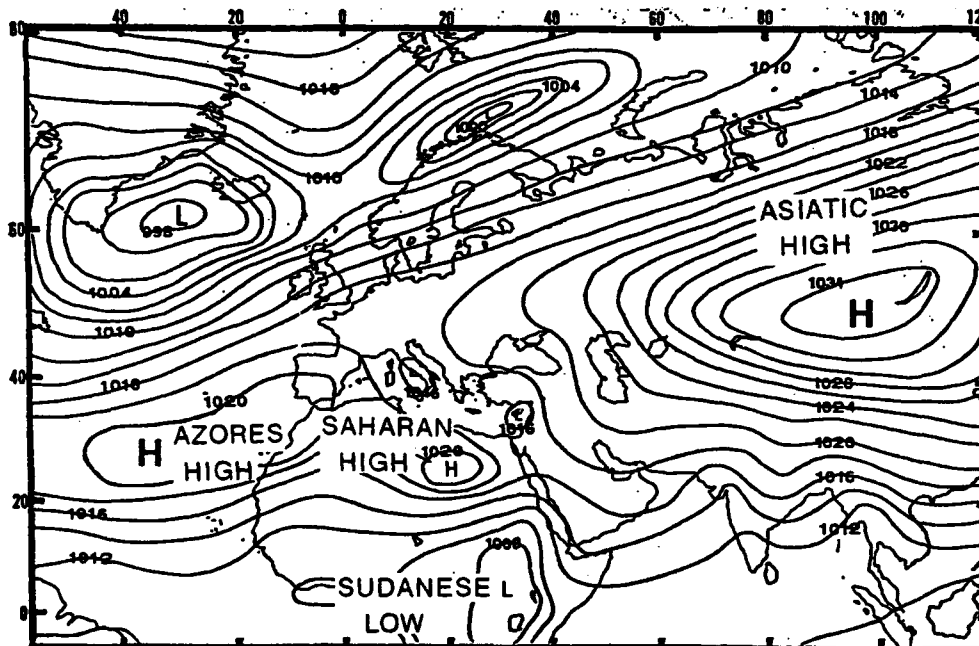


Figure 2-17a. Mean January Surface Positions of Pressure Cells. The Asiatic High is shown at its mean peak strength (1035 mb) near 49° N, 97° E. Maximum low-level northeasterly flow is in January and February because south-central Asia is extremely cold. The Asiatic High may exceed 1050 mb for 1-3 day periods; the highest recorded surface pressure is 1083 mb. Extremely strong highs may intensify northeasterly flow despite the blocking effects of the Himalayas.

SEMIPERMANENT CLIMATIC CONTROLS

Figure 2-17b shows the Asiatic High's mean October position. Its mean central pressure (1023 mb) is near 48° N, 90° E. Note that the Pakistani Heat Low (1010 mb) still anchors the broad-scale thermal trough extending back into Africa, the trough will weaken as insolation decreases.

Radiation cooling strengthens the Asiatic High over south-central Asia. The transition from Southwest-to-Northeast Monsoon flow follows as the Asiatic High establishes flow first into the Arabian Sea, then into the Gulf of Oman, and finally into the Red Sea/Gulf of Aden corridor.

The Middle East Peninsula is so large that the Northeast Monsoon circulation often takes several months (October and November) to become established throughout the region. But by the end of this transition, the broad thermal

trough that anchors the surface Monsoon Trough is no longer present.

At the beginning of spring (March), the Asiatic High migrates northward and weakens. The Northeast Monsoon first retreats along the Red Sea/Gulf of Aden corridor. By the end of March, northeasterly flow penetrates southward to only 10-11°N and the April-May transition from Northeast to Southwest Monsoon circulation begins.

By April, increasing solar radiation weakens the Asiatic High's mean central pressure to 1022 mb (see Figure 2-17c). The broad-scale thermal trough reappears over India, Saudi Arabia, and northeastern Sudan. Northeasterly flow is very weak or non-existent along the Red Sea/Gulf of Aden corridor, and poorly organized in the Arabian Sea and Gulf of Oman.

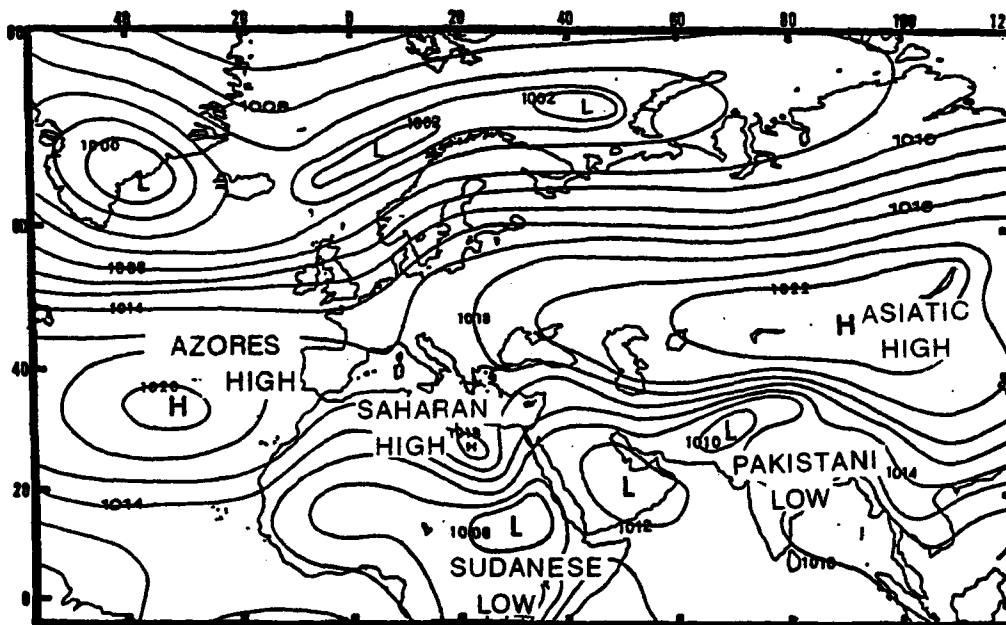


Figure 2-17b. Mean October Surface Positions of Pressure Cells.

SEMI-PERMANENT CLIMATIC CONTROLS

The Azores High. The Azores High is a distant, but important, part of the subtropical circulation pattern. This semipermanent high-pressure cell's mean position is 29° N, 29° W with a mean sea-level pressure of 1021 mb in January. From November to April, it regulates cyclonic activity into the region.

Between October and late November, the Azores High moves to a mean position of 35° N, 30° W and weakens, as shown in Figure 2-17b. Between December and February (as shown in Figure 2-17a), it extends eastward. During fair weather, the weak surface ridge joins with the Saudi Arabian High. As a result, weak high pressure (westerlies to the ridge's north and easterlies to its south) dominates the Middle East Peninsula. Mean westerly (west to north at 3-5 knots) surface flow affects locations north of a line from Port Sudan east-northeastward to the Straits of Hormuz. South of this line, Northeast Monsoon flow dominates surface flow.

In winter and early spring, Azores High ridging northward over the coastal waters of western Europe sometimes establishes a blocking pattern that allows the Polar Jet to slide south or southeastward along the east side of the Azores High into the north-central Sahara. Such a southward displacement produces cold weather outbreaks and severe duststorms in the Sahara, Red Sea, eastern Mediterranean Basin, and sometimes even the Fertile Crescent.

Between March and May, the Azores High moves slowly west-northwestward to near 30° N, 32° W (see Figure 2-17c). Its westerly spring migration away from the African continent weakens the mean high-pressure ridge over north Africa. Cyclonic activity and its main storm track (see "Storm Tracks") dips southward over the western Mediterranean Sea and Atlas Mountains. Intense duststorms are common (see "khamsin conditions") as strong winds sweep across the dry Sahara.

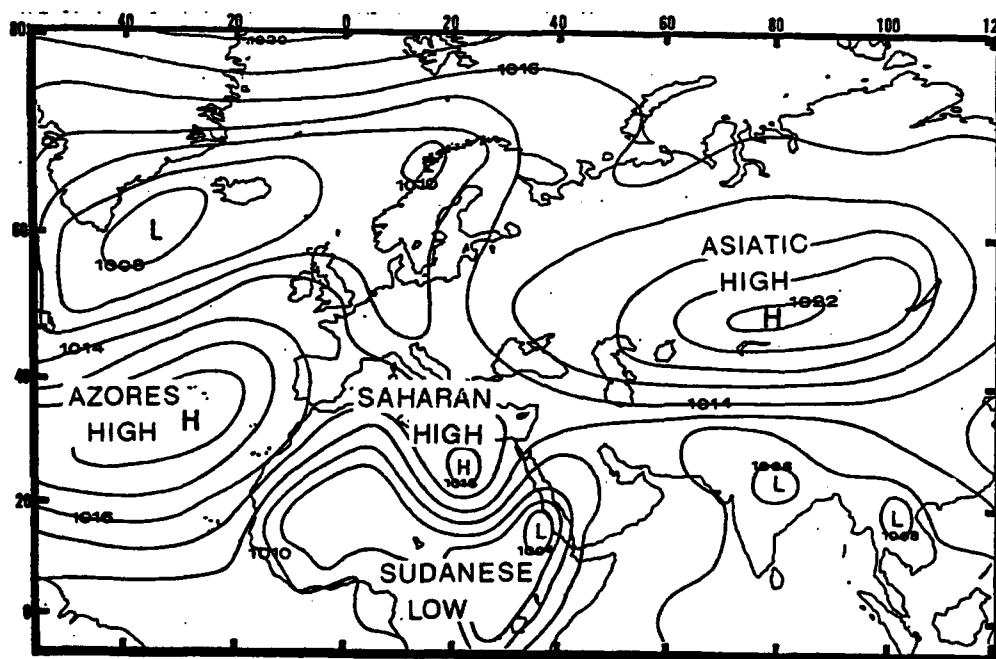


Figure 2-17c. Mean April Surface Positions of Pressure Cells.

SEMIPERMANENT CLIMATIC CONTROLS

The **Saharan High** is present from November to April, reinforcing weak west-northwesterly surface flow into the north Red Sea Coastal Plains, Arabian Desert, Fertile Crescent, and extreme western Persian Gulf Coastal Plains. Mean global sea-level pressure charts typically show the Saharan High extending eastward from the Azores High. Undisturbed synoptic weather patterns in the Sahara often produce an extensive high-pressure ridge over northern Libya and west-central Egypt, but the Saharan High is actually a transitory cold-core high-pressure cell. Its transitory nature is most evident between late January and early April when deep polar troughs enter north Africa. The Saharan High generally moves eastward ahead of disturbances or disappears from synoptic charts entirely. It usually reforms at the surface within 12-24 hours after a frontal passage. From December to early March, the dry desert air, along with radiation cooling, intensifies the High and makes it a mean surface feature. Its mean January position (26° N, 20° E) is shown in Figure 2-17a; central pressure is 1021 mb. The mean April position (25° N, 22° E) is shown in Figure 2-17c; mean central pressure drops to 1018 mb. Because moisture advection and cyclonic activity rarely affect the north and central Sahara, Saharan High outflow is dry and cool.

In rare cases, northwesterlies penetrate southward to 4° N over the African continent when a cold transitory high-pressure cell supports a deep mid-latitude trough passage across the central Red Sea basin. Strong northerly flow may cause severe duststorms and widespread low visibility (less than 3 miles) in the north and central Red Sea Coastal Plains, extreme western Arabian Desert, and western Fertile Crescent subregions.

Typically, Saharan High outflow is a persistent low-level circulation feature of the north and central Red Sea Coastal Plain. Mean surface wind speeds associated with Saharan High outflow average below 6 knots during fair weather periods.

The Sudanese Heat Low. Varying from 1004 to 1012 mb, this low often marks the eastern edge

of large-scale equatorial African low pressure in winter. The Sudanese Low is responsible for advecting moist, warm-sector southwesterlies ahead of low-pressure systems from interior Africa into the Red Sea basin. Southerly flow on the east side of the low, combined with outflow from the Saudi Arabian High, help produce the Red Sea Convergence Zone. The Sudanese Low lies over the high plateaus of southwestern Ethiopia and southeastern Sudan (7° N, 32° E) between December and March (Figure 2-17a), but it migrates northward to $15\text{--}20^{\circ}$ N in April and May (Figure 2-17c). Between June and September, it becomes a broad, poorly defined low-pressure area in southern Sudan, but reappears in October as the closed circulation shown in Figure 2-17b.

The Saudi Arabian High, centered over northwestern Saudi Arabia, is the eastward extension of the Azores-Saharan High pressure ridge in undisturbed synoptic conditions. It becomes well-defined over the Saudi Arabian peninsula during extended fair-weather periods. Its surface and mid-level anticyclonic circulation is common throughout the December-March Northeast Monsoon.

Westerly outflow on the cell's north side steers Mediterranean low-pressure systems and their trailing cold fronts into the northern Red Sea and north central Saudi Arabia. East-northeasterly flow south of the cell helps regulate Northeast Monsoon flow into the Gulf of Aden and the eastern Yemen Highlands. In November, it strengthens northeasterly flow into the western Gulf of Aden, through the Straits of Bab al Mandab, and into the southern Red Sea. Figure 2-18 shows a typical situation in January.

Typically, the Saudi Arabian High "disappears" over the Arabian Desert during frontal passages, reforming after the passage. Initiated and maintained by radiation cooling over the large desert surface, it is actually depicted more frequently than the Saharan High on 6-hour synoptic charts because cyclonic activity penetrates the Arabian Desert less often than the Sahara.

SEMI-PERMANENT CLIMATIC CONTROLS

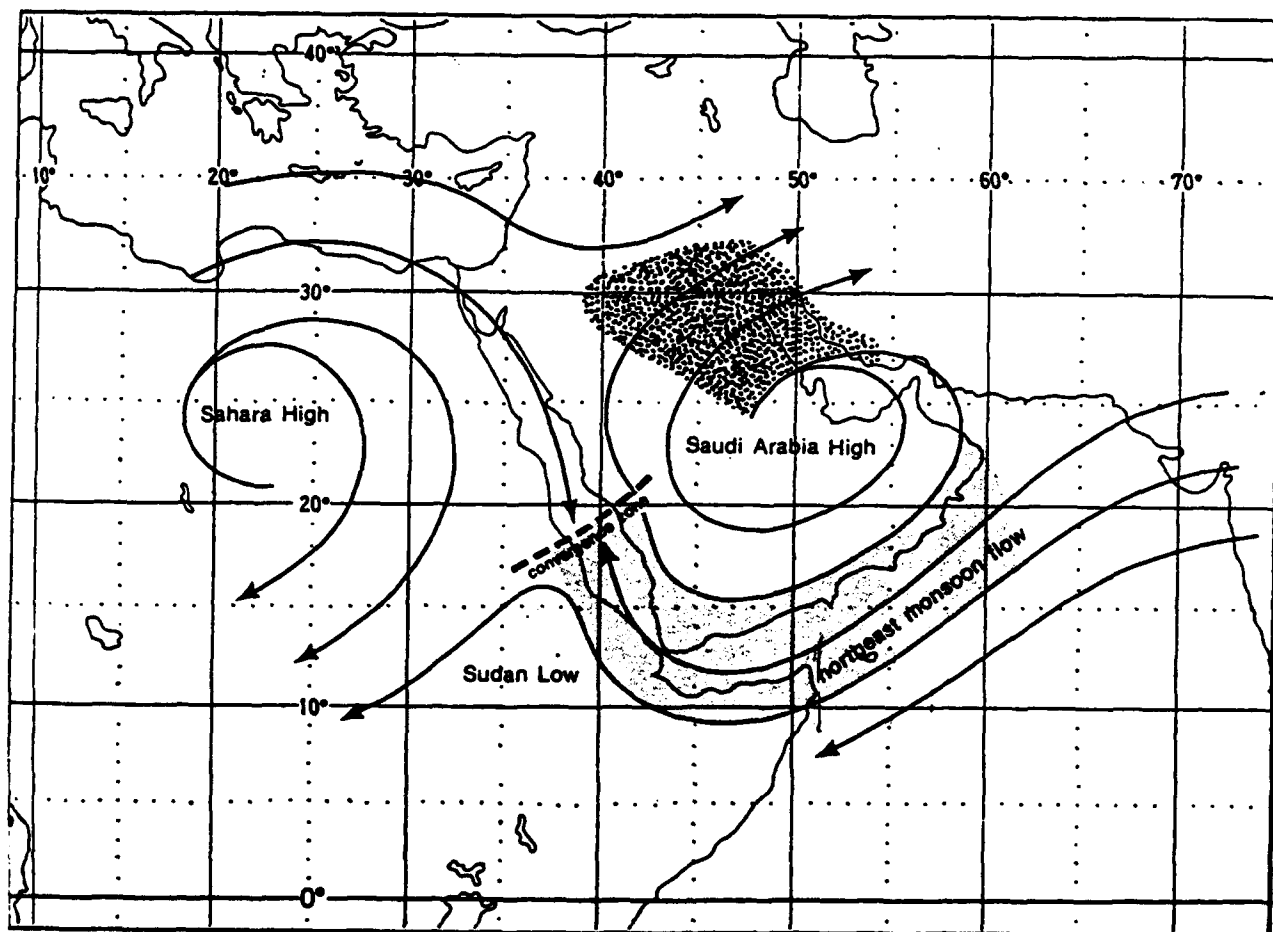


Figure 2-18. Typical January Surface Streamline Flow Pattern Showing the Saudi Arabian High. Stippling shows the westerly outflow component. The gray shaded region denotes outflow support to the Northeast Monsoon circulation. The dashed line is known as the "Red Sea Convergence Zone," or "RSCZ."

SEMIPERMANENT CLIMATIC CONTROLS

The Red Sea Convergence Zone (RSCZ). Terrain along the Gulf of Aden channels Saudi Arabian High outflow and Northeast Monsoon flow into the Red Sea, where they converge with weak northerly flow from the Saharan High to produce the RSCZ, an example of which is shown

in Figure 2-19. A continuous band of stratocumulus (oriented WSW-ENE) forms over open water, but mountains in the Yemen and Ethiopian Highlands break up the feature over land.

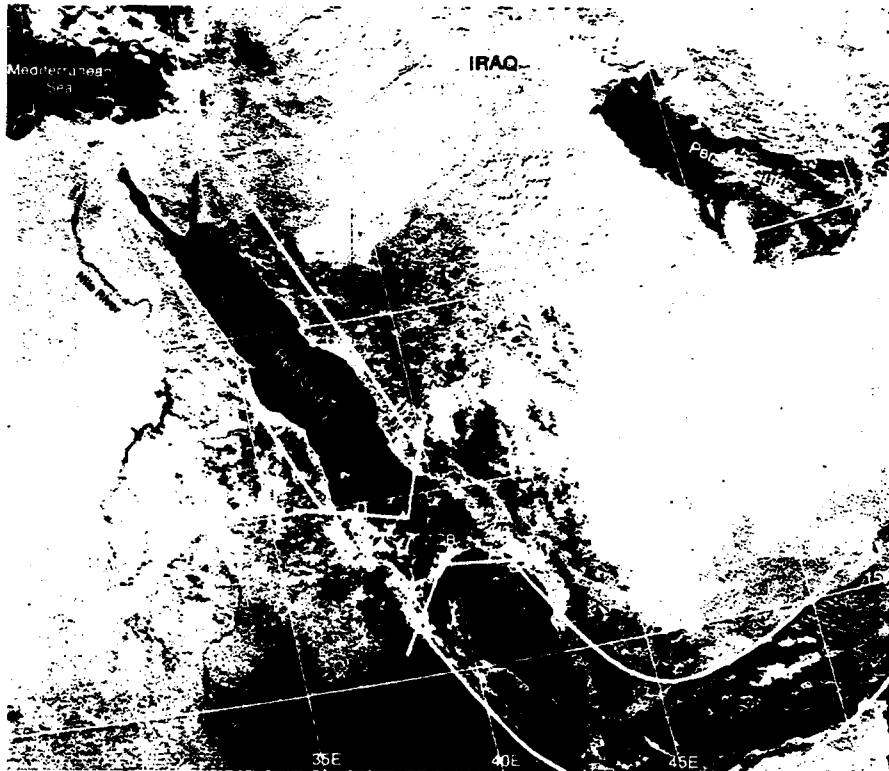


Figure 2-19. Satellite View of Red Sea Convergence Zone (from NEPRF, 1980). This cloud pattern is also referred to as a "Convergence Zone Cloud Band" (CZCB).

The trough oscillates little during undisturbed weather periods because of weak winds. The RSCZ, however, oscillates under three conditions:

- When a southward displacement--on the order of 1-3 days--occurs as short-wave troughs pass over the Red Sea. These short waves, with strong northwesterly flow, move the RSCZ to between 13 and 15° N.
- When warm air advection from interior Africa produces northward movements in the RSCZ. Typically, deep upper-level troughs penetrate low latitudes in January and February. Warm equatorial air and southerly flow (ahead of the cold front) surges northeastward into the central Red Sea. Low-level flow lifts orographically

along the north Yemen Highlands. Convergence between the warm front and RSCZ also occurs. The RSCZ may shift to 25° N with strong southerly flow, but often recovers to its normal position within 24 hours of the trough's passage.

- When there is an increase in Northeast Monsoon flow through the Straits of Bab al Mandab (possible during extended fair weather periods). Southerly flow, deflected through the Straits, may increase with a strengthening Saudi Arabian or Asiatic High.

Figure 2-20 shows the October-April cycle of the RSCZ. Figure 2-21 gives a vertical cross-section of a typical RSCZ along the Red Sea Coastal Plains.

SEMIPERMANENT CLIMATIC CONTROLS

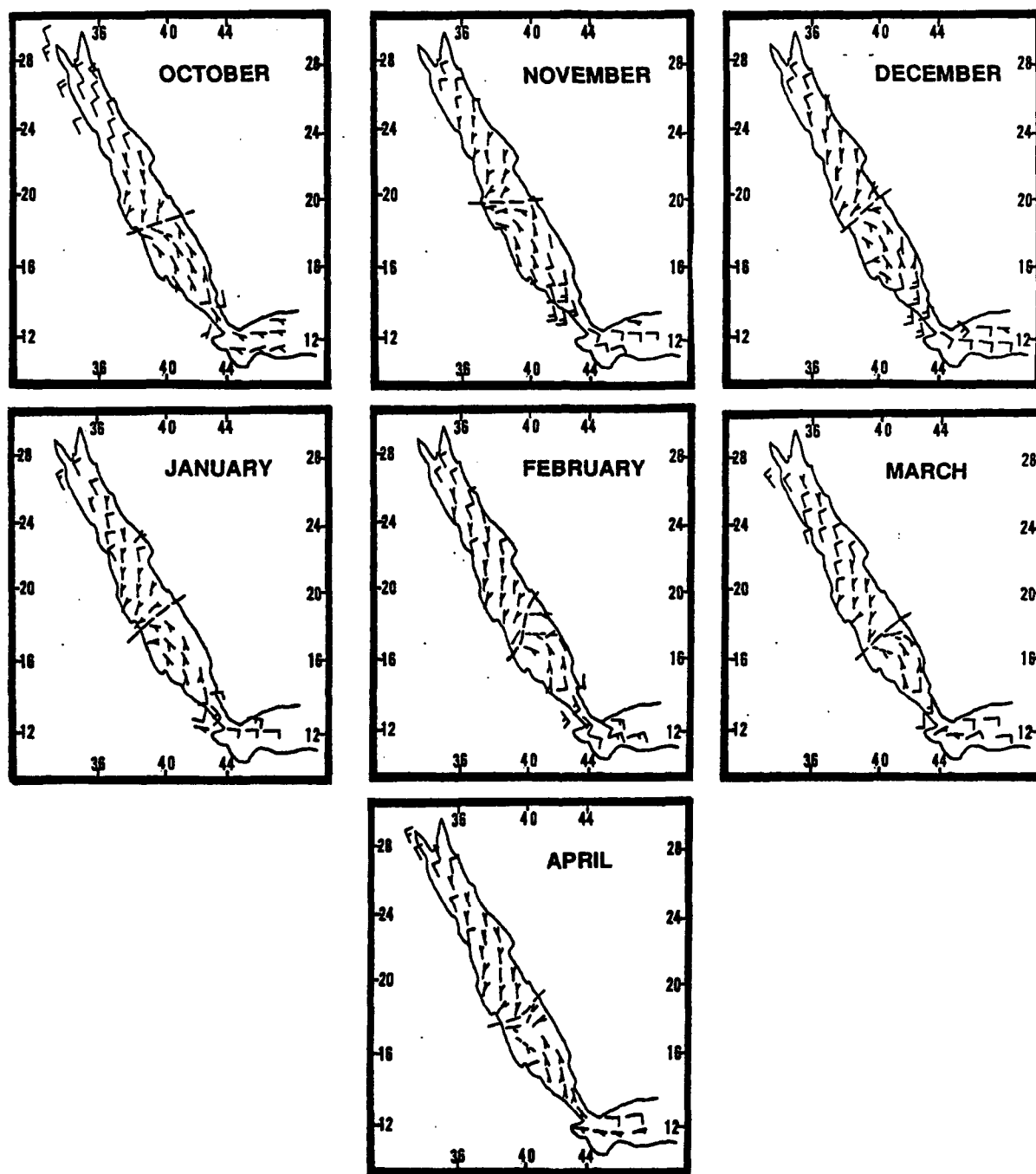


Figure 2-20. RSCZ Positions: October–April. The RSCZ's mean monthly position is denoted by the thick dashed lines. Weak surface convergence first appears as a trough line between 18 and 20° N in early October. Note the increased wind speeds in November north of the Straits of Bab al Mandab. Between October and April, the Saharan and Saudi Arabian Highs usually set up weak convergent flow; Northeast Monsoon circulation supports daily and monthly oscillations in the trough axis position.

SEMIPERMANENT CLIMATIC CONTROLS

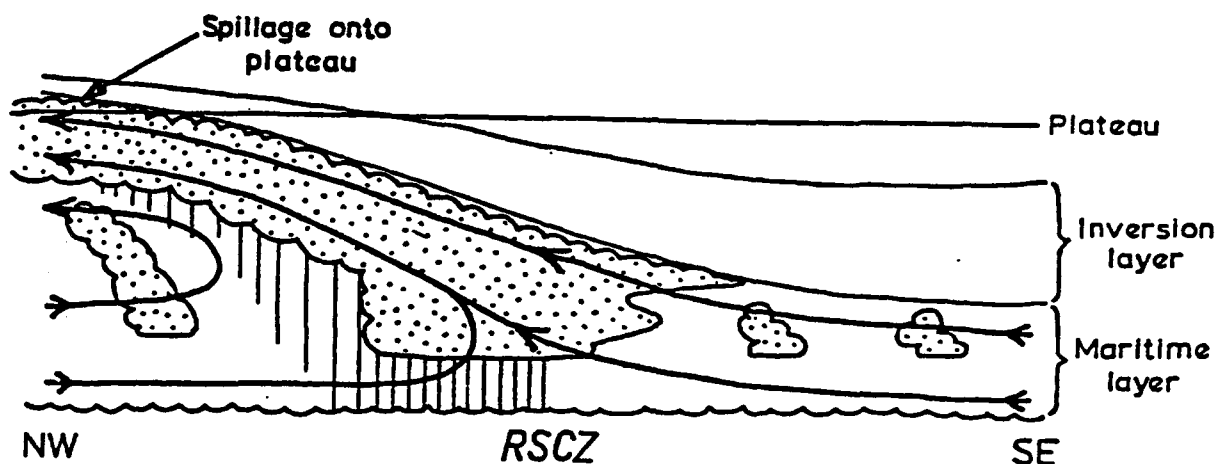


Figure 2-21. Cross-Section View of Stratocumulus Cloud Cover Distributions Along the RSCZ (from Pedgley, 1966). Arrows indicate the mesoscale circulation pattern, while vertical lines represent the rainfall zone.

MID-AND UPPER-LEVEL FLOW PATTERNS.
Figures 2-22 through 2-25 show January, April, July, and October streamline flow at 850,

700, 500, 300, and 200 millibars over the entire SWANEA study area.

SEMI-PERMANENT CLIMATIC CONTROLS

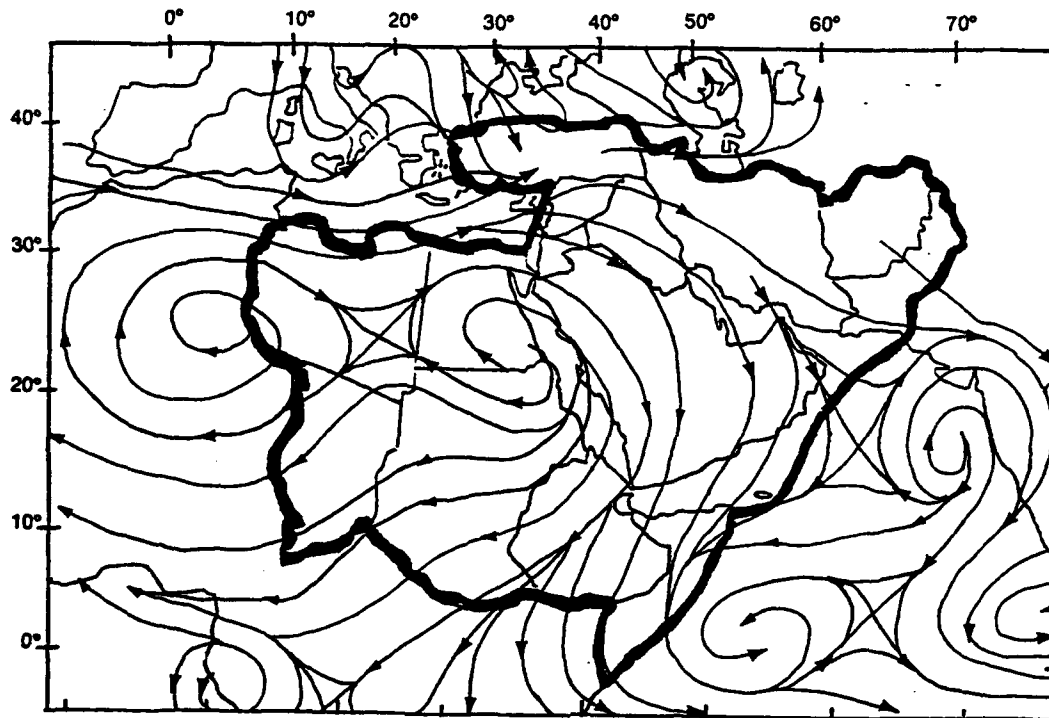


Figure 2-22a. Mean January Upper-Air Flow Pattern, 850 mb.

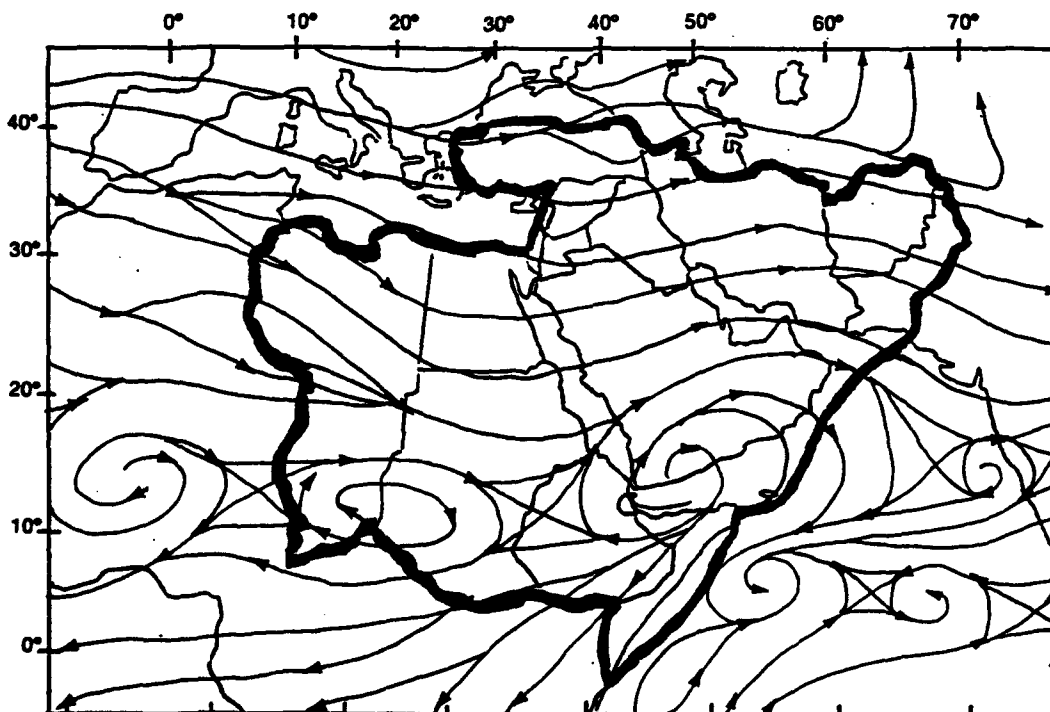


Figure 2-22b. Mean January Upper-Air Flow Pattern, 700 mb.

SEMIPERMANENT CLIMATIC CONTROLS

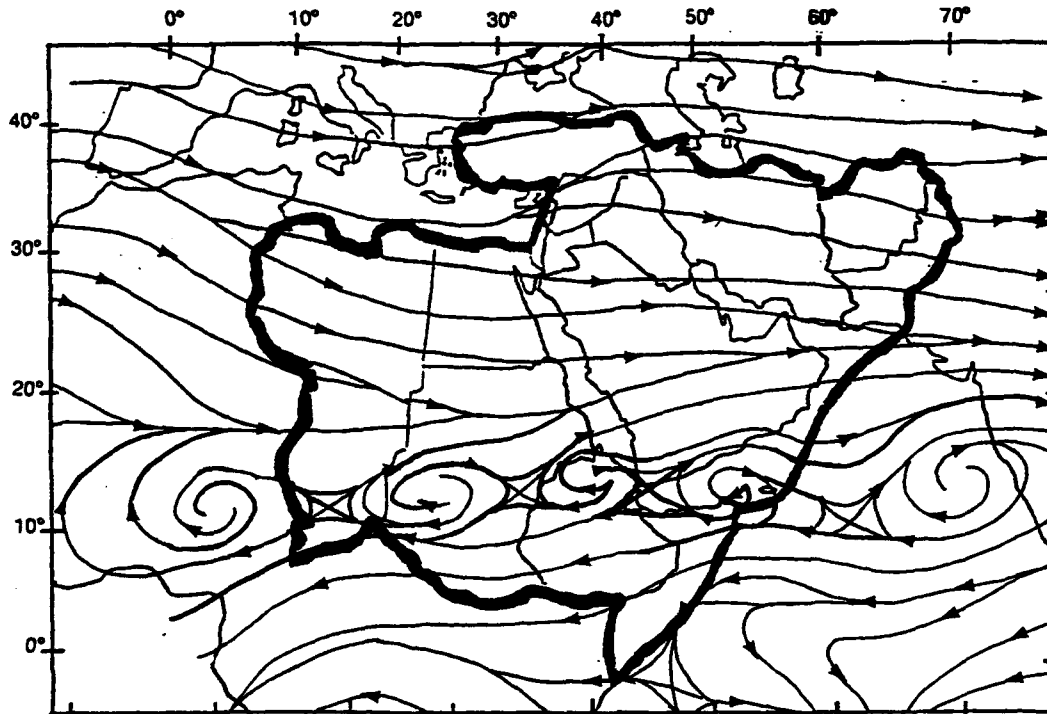


Figure 2-22c. Mean January Upper-Air Flow Pattern, 500 mb.

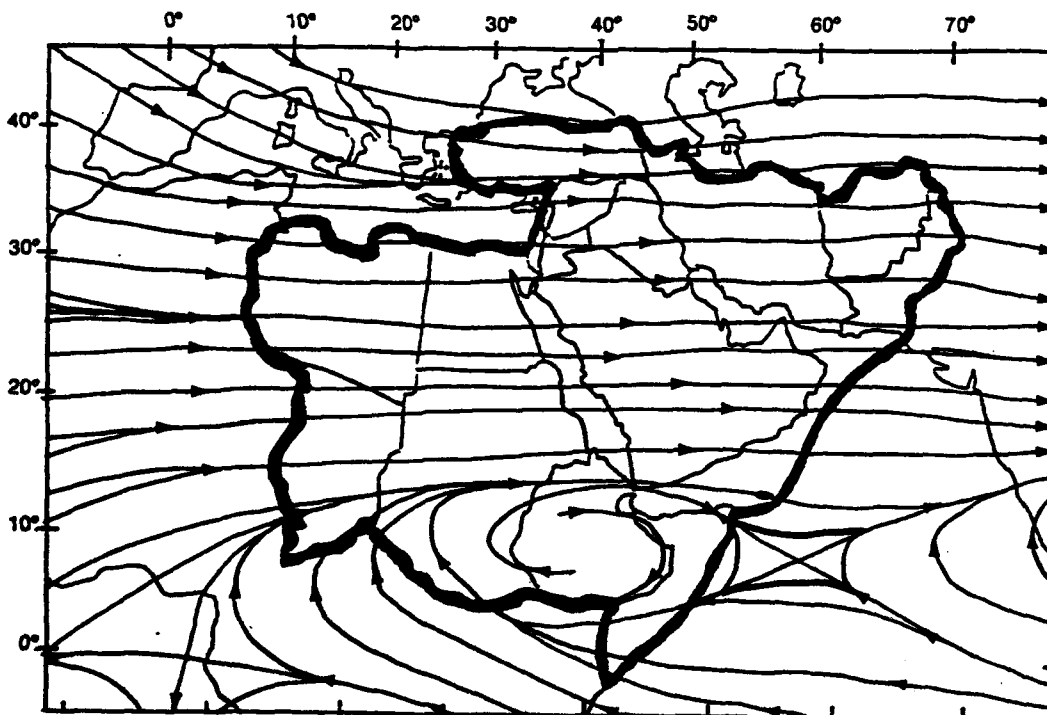


Figure 2-22d. Mean January Upper-Air Flow Pattern, 300 mb.

SEMIPERMANENT CLIMATIC CONTROLS

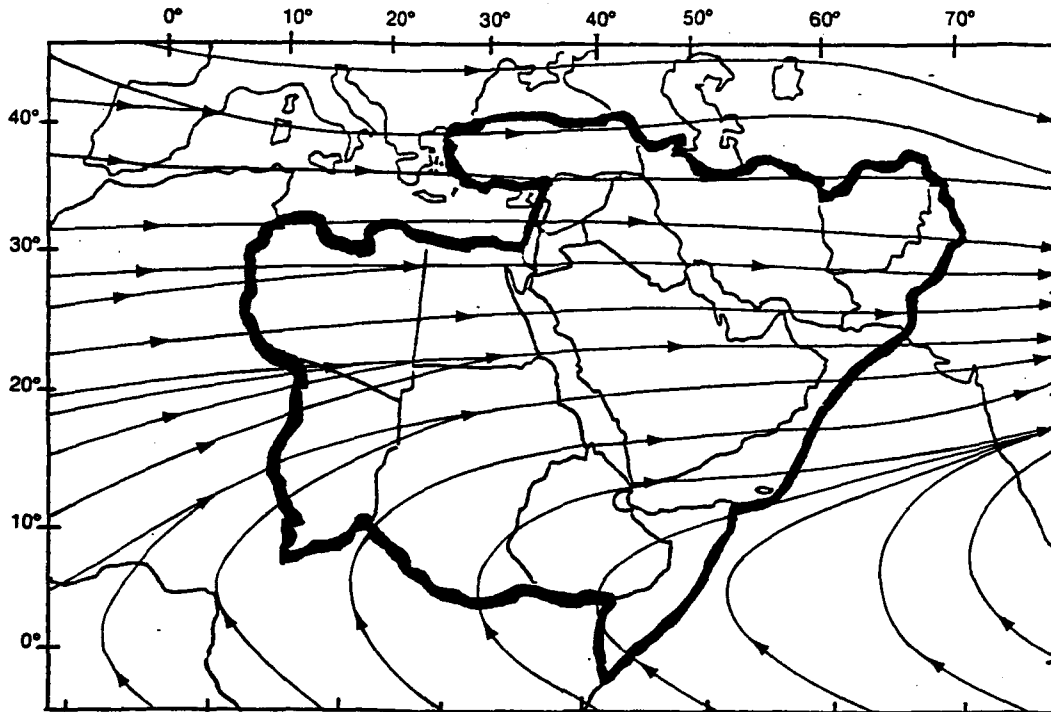


Figure 2-22e. Mean January Upper-Air Flow Pattern, 200 mb.

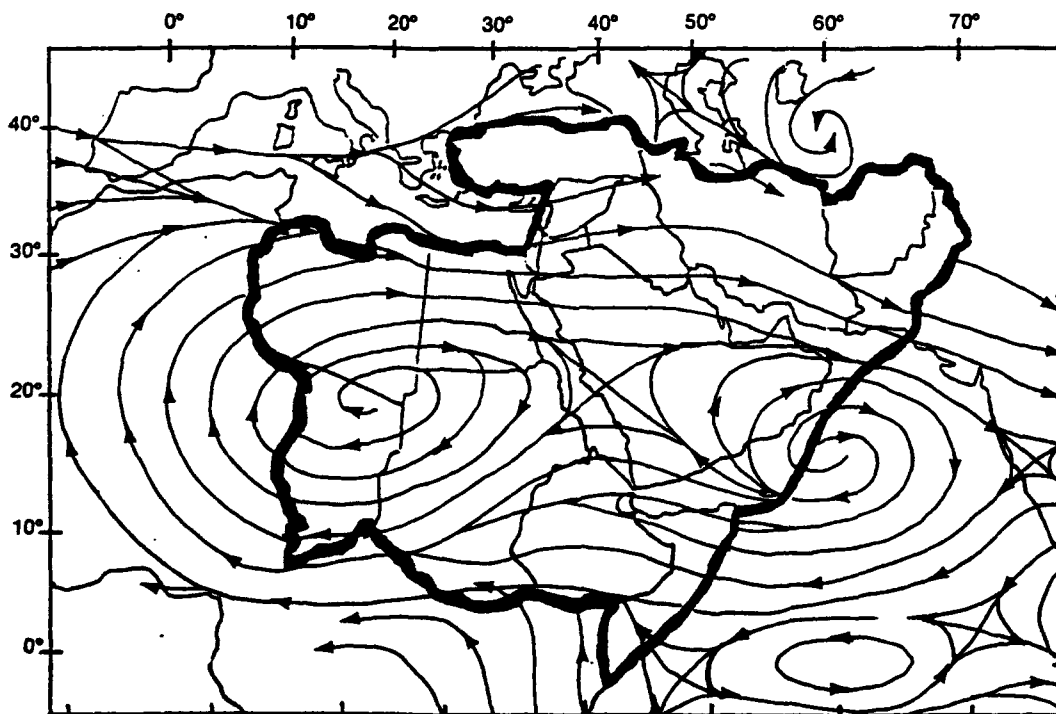


Figure 2-23a. Mean April Upper-Air Flow Pattern, 850 mb.

SEMIPERMANENT CLIMATIC CONTROLS

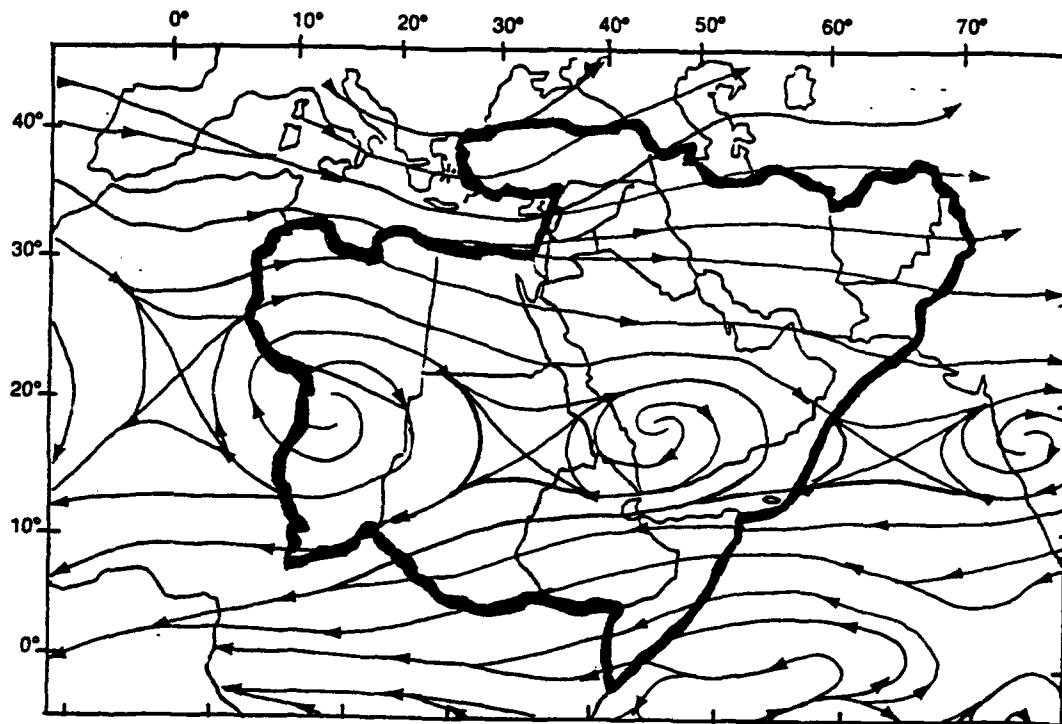


Figure 2-23b. Mean April Upper-Air Flow Pattern, 700 mb.

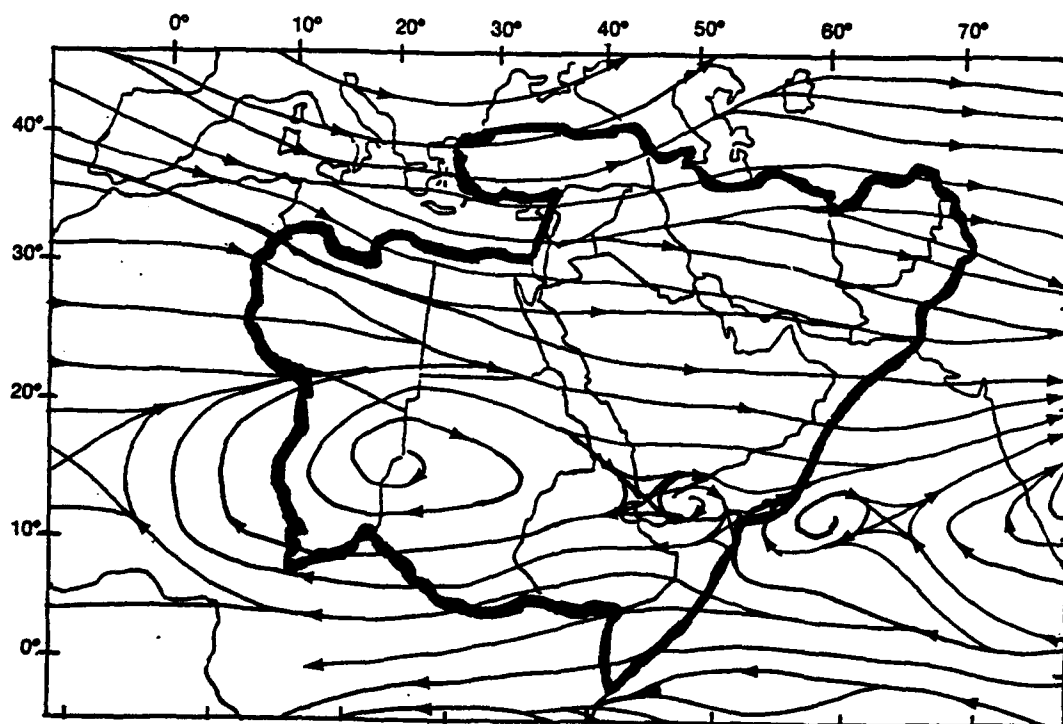


Figure 2-23c. Mean April Upper-Air Flow Pattern, 500 mb.

SEMPERMANENT CLIMATIC CONTROLS

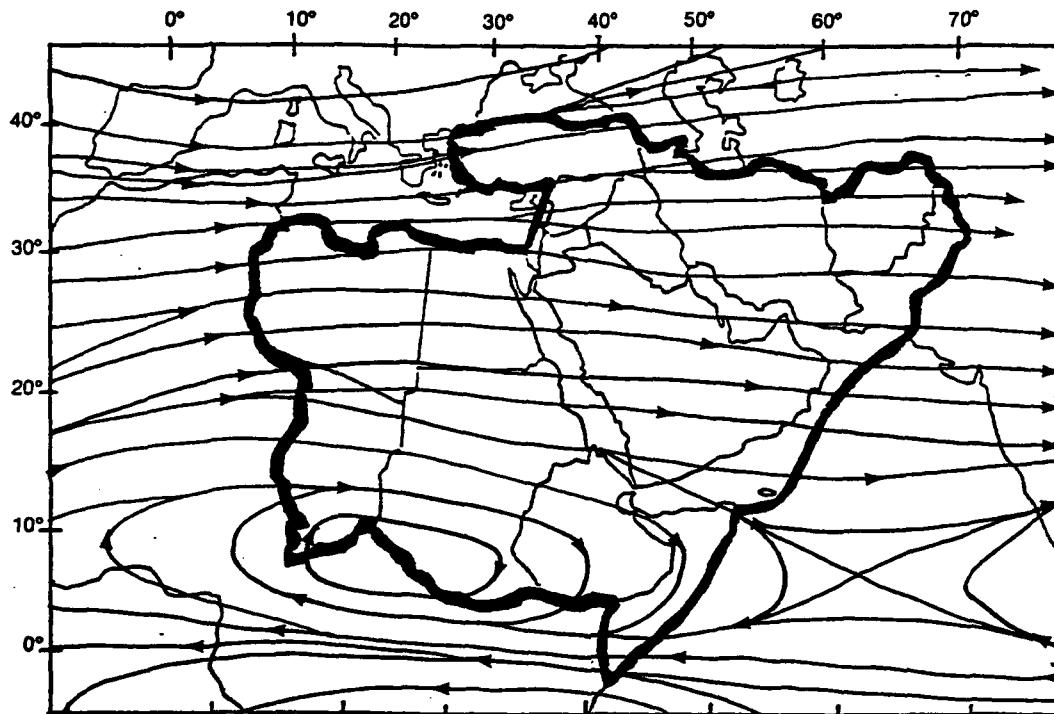


Figure 2-23d. Mean April Upper-Air Flow Pattern, 300 mb.

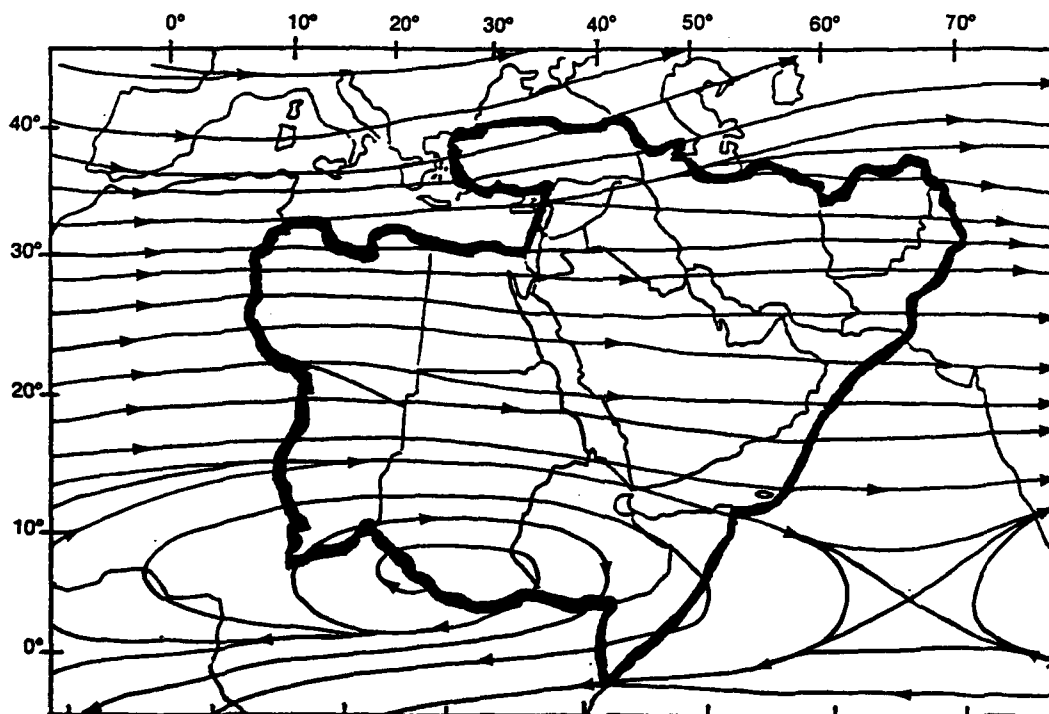


Figure 2-23e. Mean April Upper-Air Flow Pattern, 200 mb.

SEMI-PERMANENT CLIMATIC CONTROLS

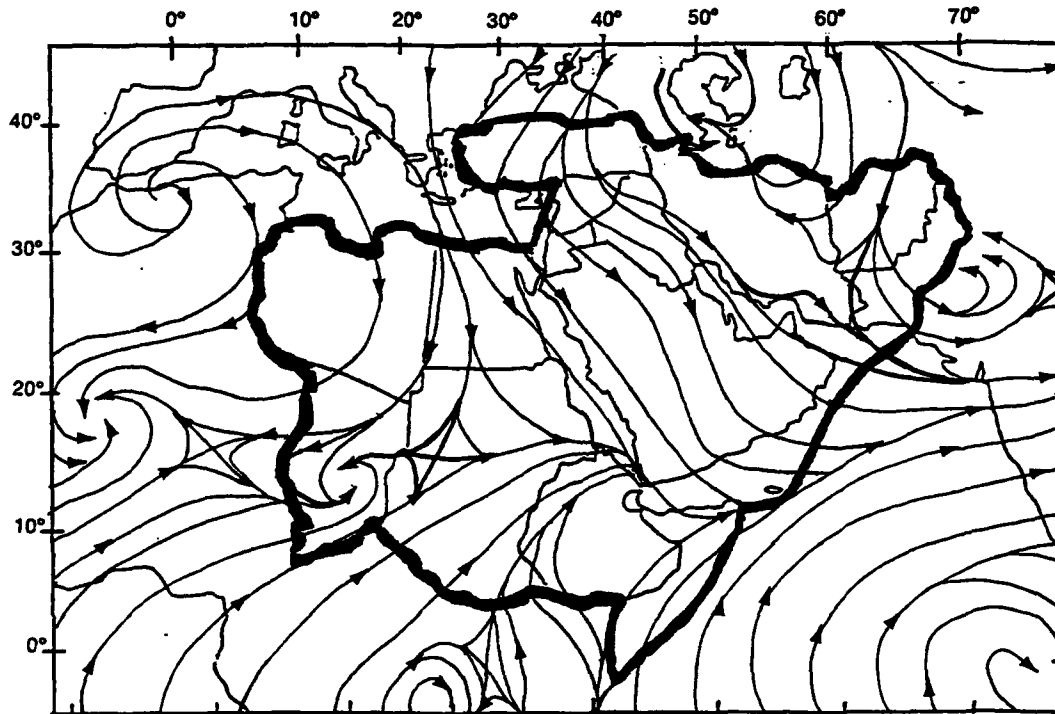


Figure 2-24a. Mean July Upper-Air Flow Pattern, 850 mb.

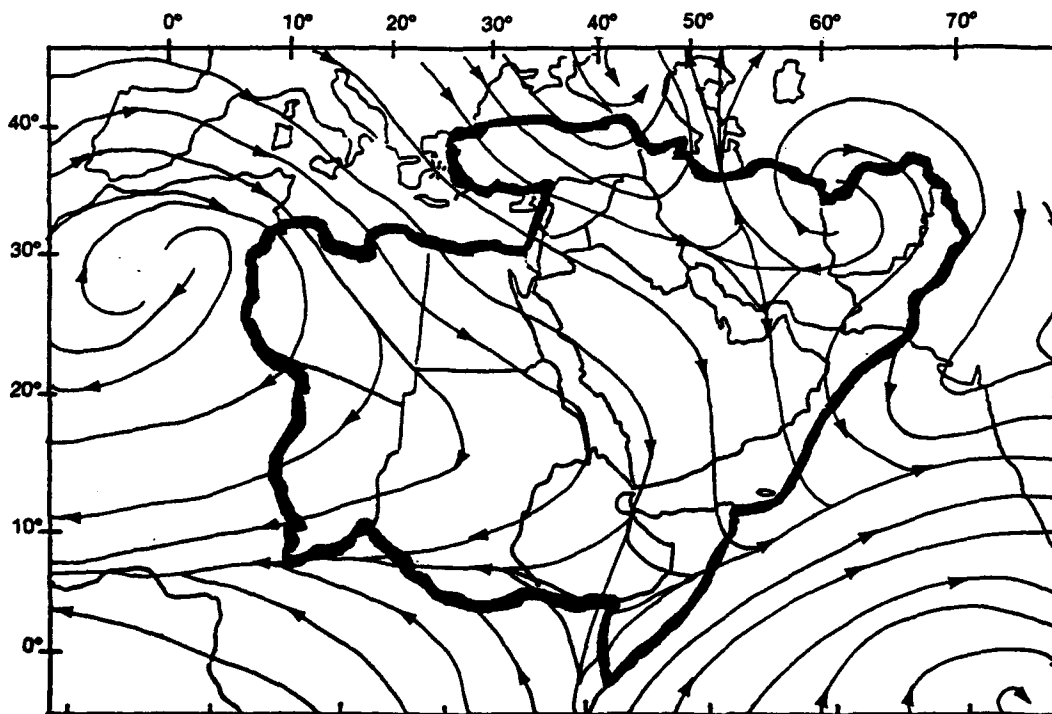


Figure 2-24b. Mean July Upper-Air Flow Pattern, 700 mb.

SEMI-PERMANENT CLIMATIC CONTROLS

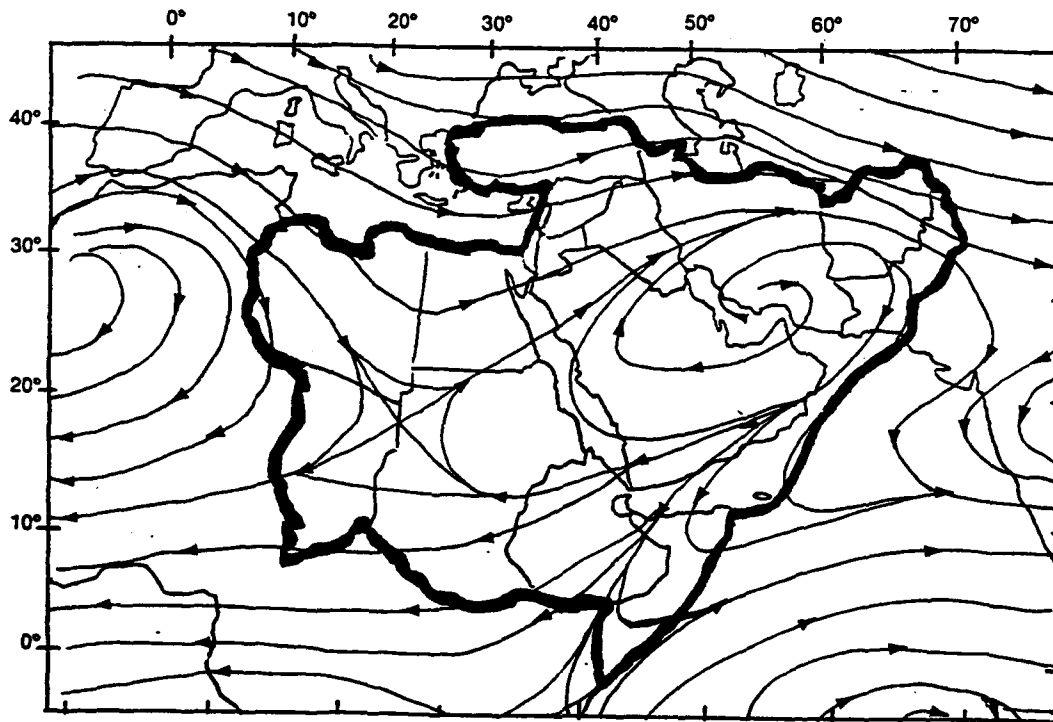


Figure 2-24c. Mean July Upper-Air Flow Pattern, 500 mb.

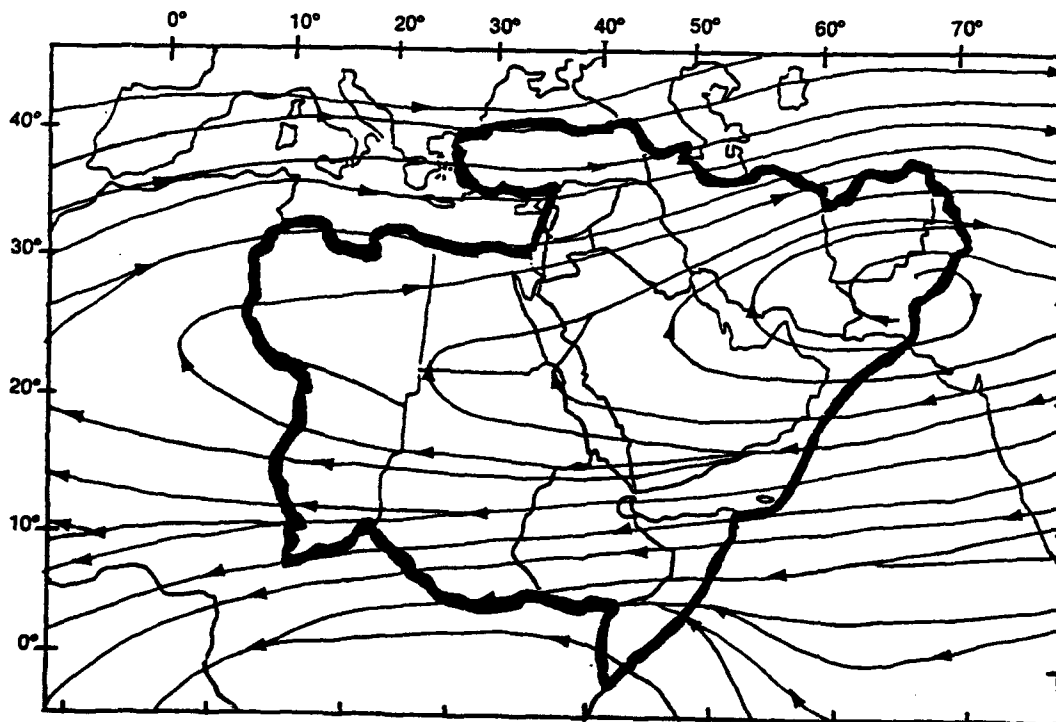


Figure 2-24d. Mean July Upper-Air Flow Pattern, 300 mb.

SEMIPERMANENT CLIMATIC CONTROLS

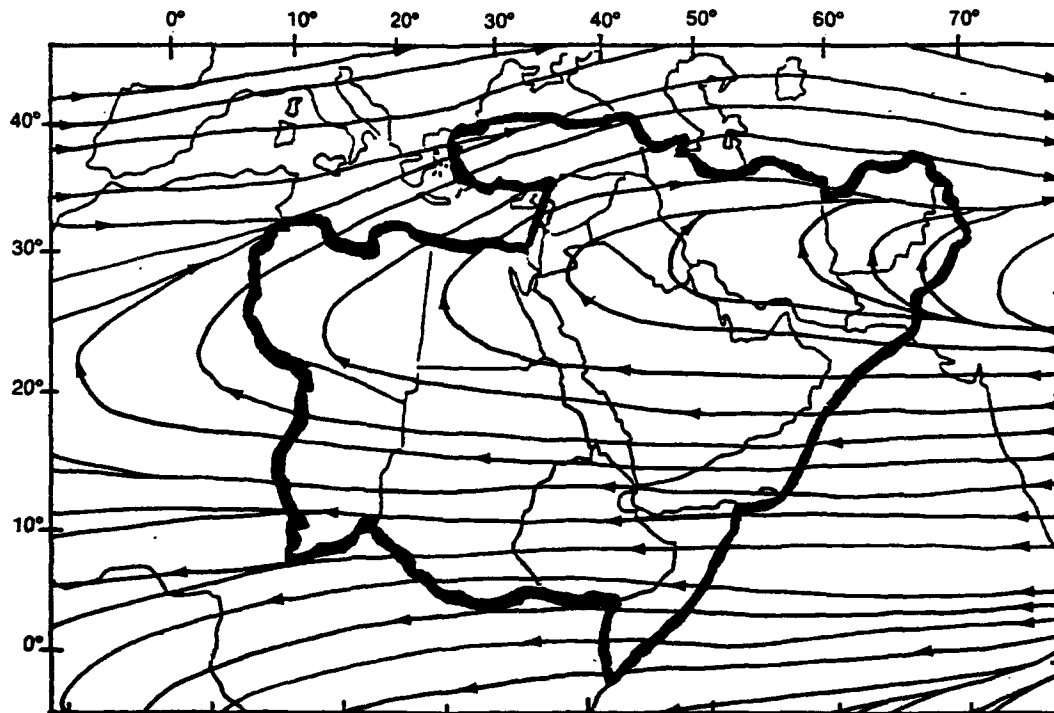


Figure 2-24e. Mean July Upper-Air Flow Pattern, 200 mb.

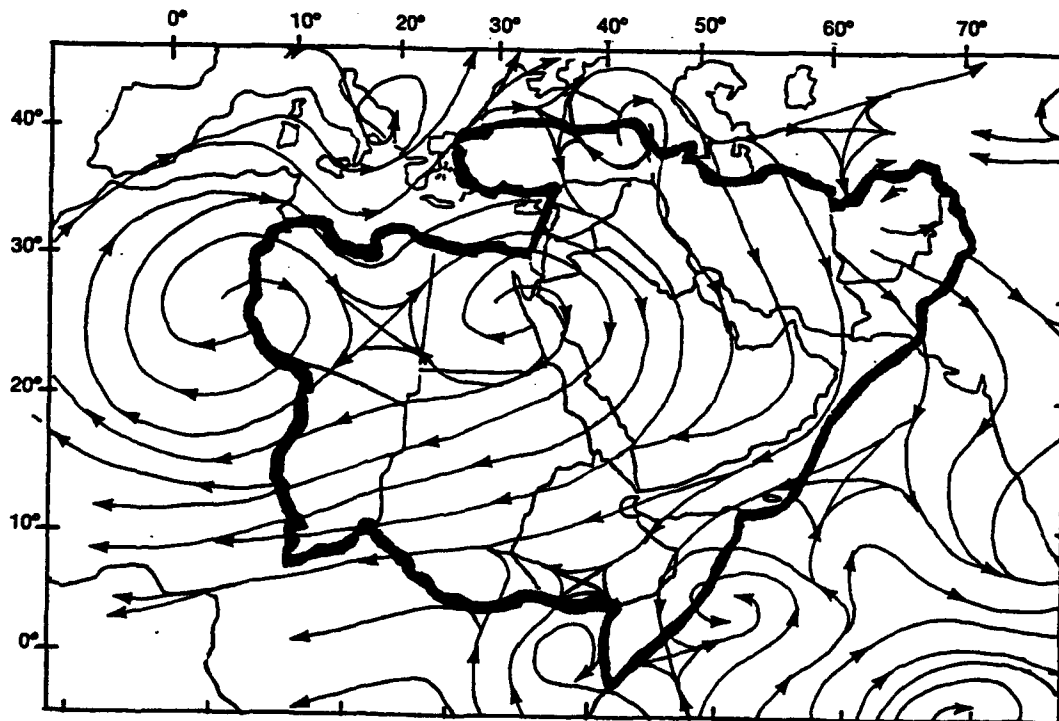


Figure 2-25a. Mean October Upper-Air Flow Pattern, 850 mb.

SEMIPERMANENT CLIMATIC CONTROLS

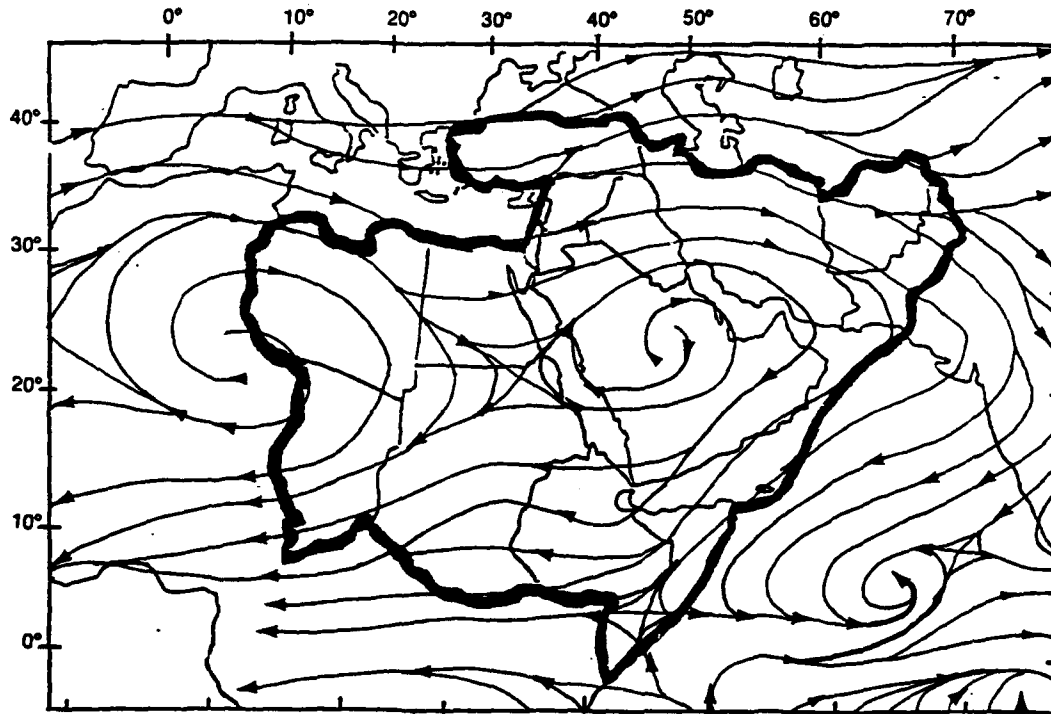


Figure 2-25b. Mean October Upper-Air Flow Pattern, 700 mb.

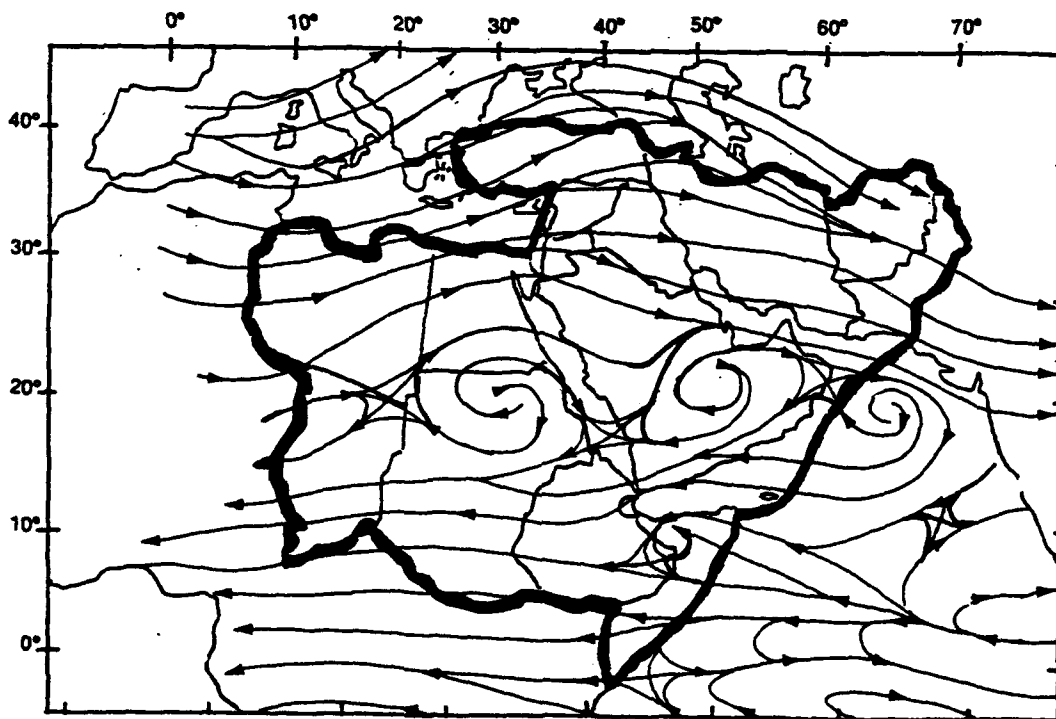


Figure 2-25c. Mean October Upper-Air Flow Pattern, 500 mb.

SEMIPERMANENT CLIMATIC CONTROLS

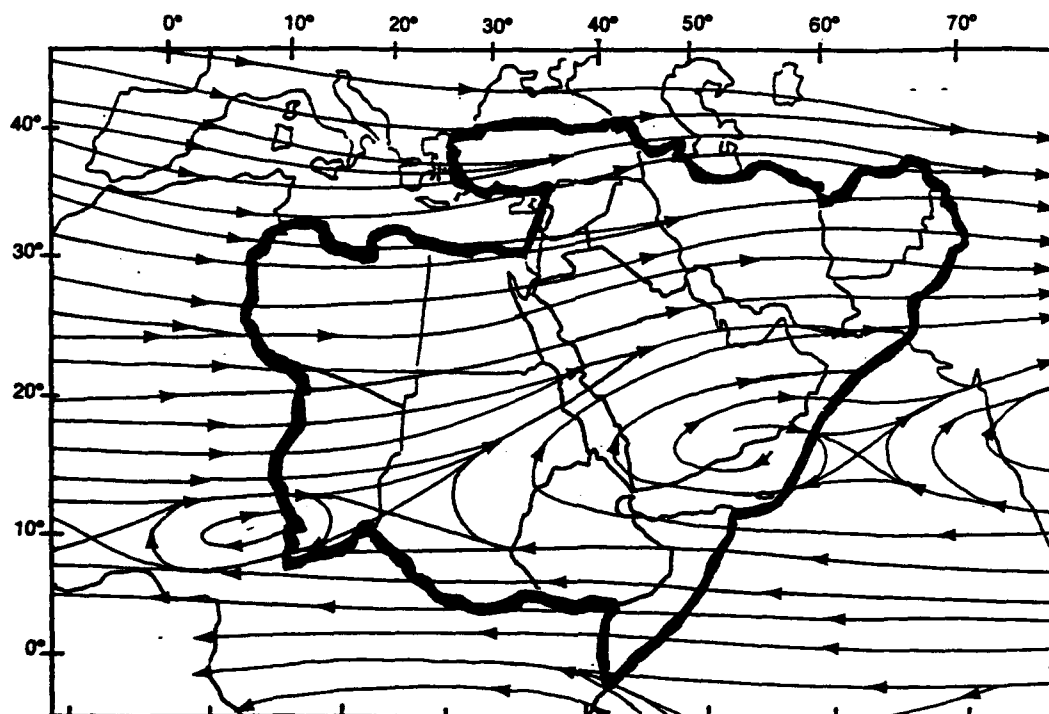


Figure 2-25d. Mean October Upper-Air Flow Pattern, 300 mb.

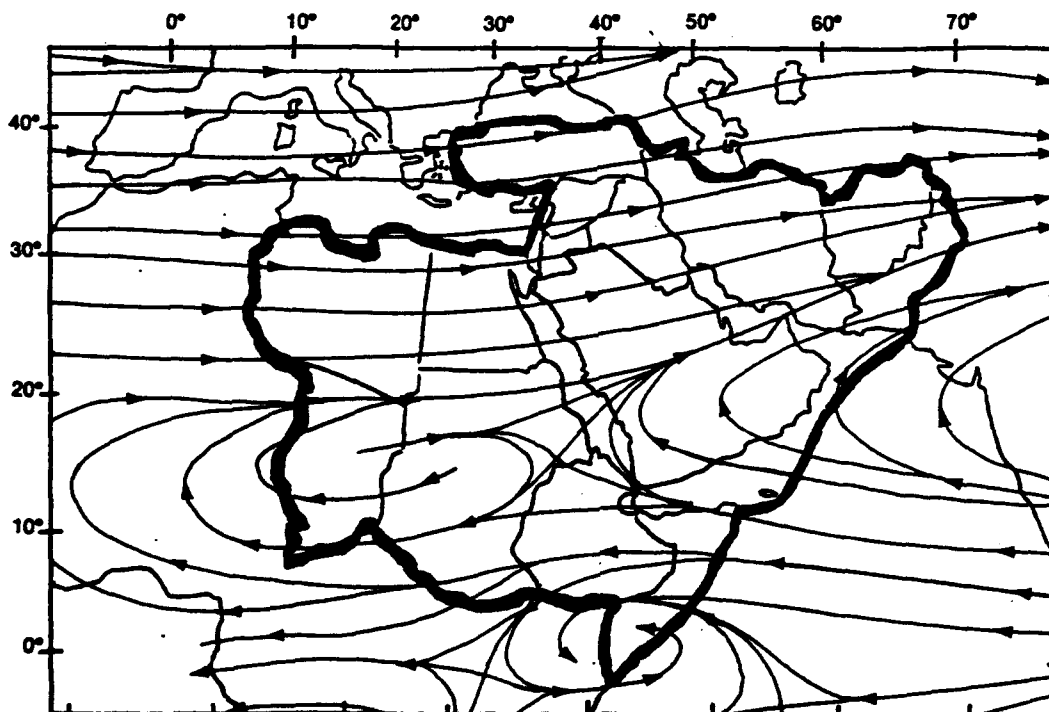


Figure 2-25e. Mean October Upper-Air Flow Pattern, 200 mb.

SEMI-PERMANENT CLIMATIC CONTROLS

THE SUBTROPICAL RIDGE. This upper-level feature, represented graphically by the 200-mb anticyclonic ridge axis line, is the division between upper-level westerly and easterly flow. It oscillates from 6° N in January (Figure 2-26) to 24-27° N in July. This oscillation provides the region with alternating periods of westerly and

easterly upper-level flow. North of 30° N, flow is westerly throughout the year. From May to October, easterlies dominate south of 30° N. In October, southerly to easterly flow only occurs south of 20° N. April and October positions can be inferred from Figures 2-23e and 2-25e.

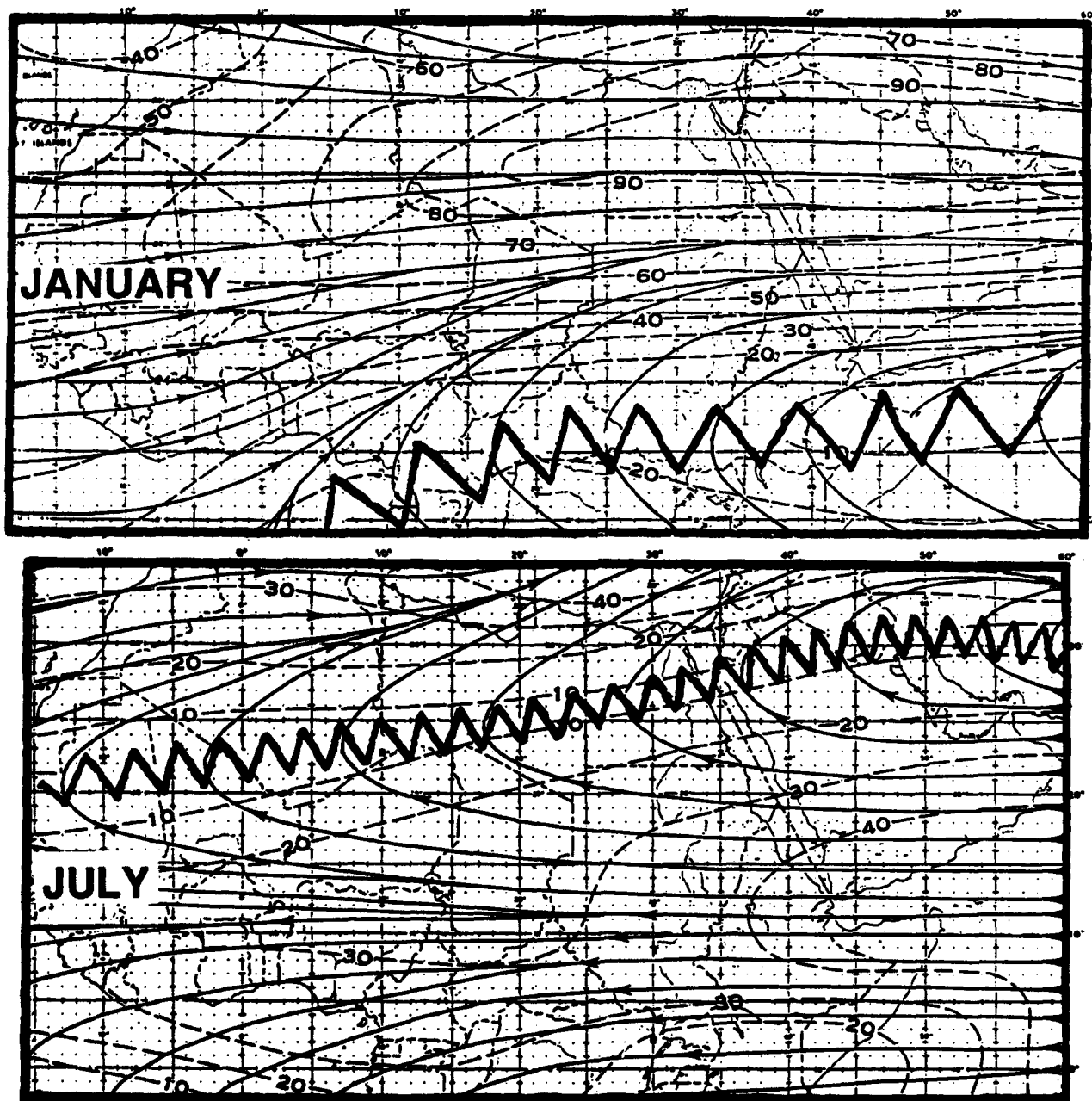


Figure 2-26. Mean January and July Positions of the Subtropical Ridge. The jagged line denotes the mean ridge axis position. Dashed lines are isotachs (kts).

SYNOPTIC DISTURBANCES

JET STREAMS. The Polar Jet (PJ) and Subtropical Jet (STJ) are important to the formation and movement of weather systems that originate over the Mediterranean Basin. The position and movement of the Polar Jet control cold-air advection and mid-level direction

for developing Mediterranean cyclones, while the Subtropical Jet provides steering, shear, and outflow in the upper layers. Figure 2-27 shows the mean positions of these jets in January and July.

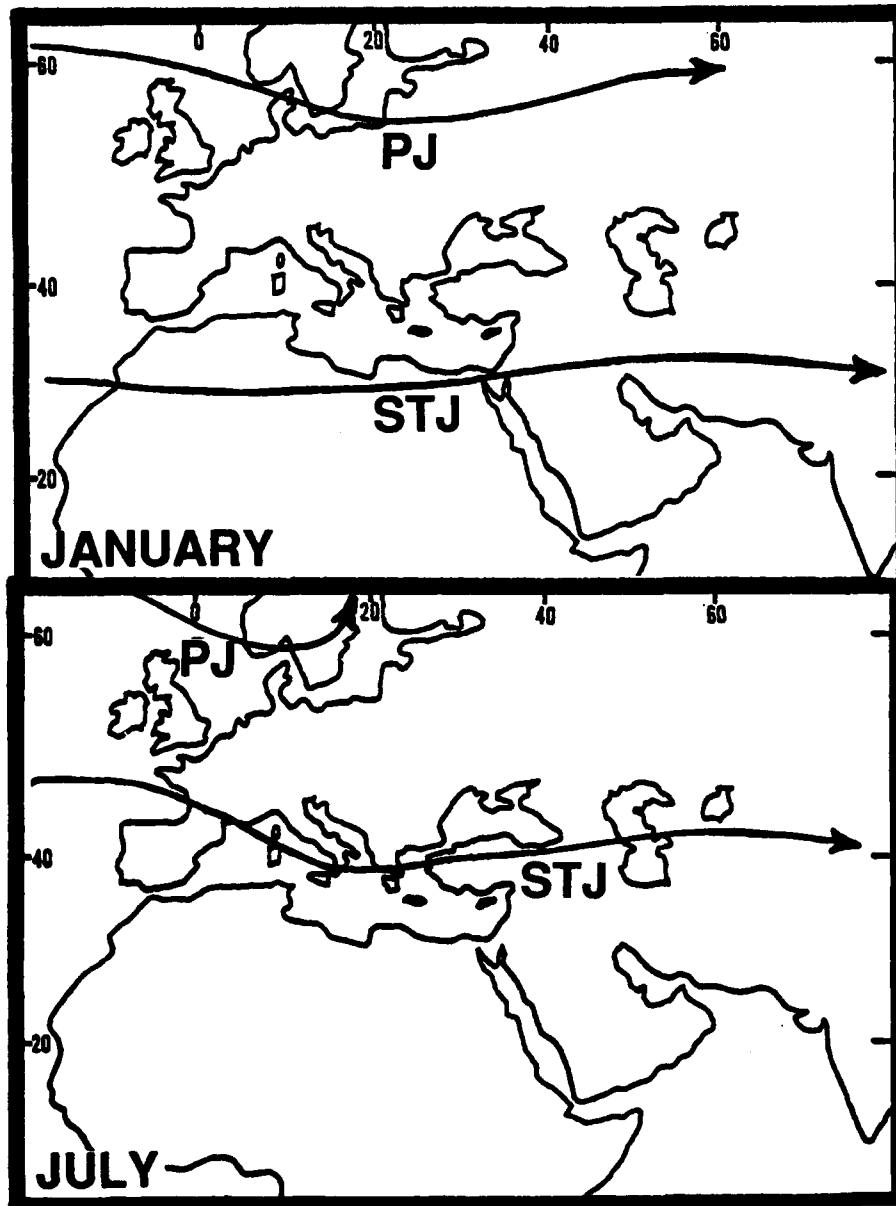


Figure 2-27. Mean January and July Positions of the Polar Jet (PJ) and Subtropical Jet (STJ).

SYNOPTIC DISTURBANCES

Mean PJ positions vary north-south from 100 to 300 NM. Maximum wind speeds from December to March vary from 60 to 160 knots. The PJ is usually found near 30,000 feet (9.2 km) MSL. Southward deviations over the eastern Sahara and the northern Middle East Peninsula are most frequent between December and March, but can occur on rare occasions from April to June. The April-June PJ is found between 30,000 and 34,000 feet (9.2-10.4 km) MSL; maximum wind speeds are between 60 and 140 knots. Although the STJ shows less variability in its daily position, its seasonal variability is greater than that of the PJ. Mean STJ positions

over the subtropics range from 25 to 45° N. Maximum wind speeds between December and April vary between 80 and 180 knots at a mean height of 39,000 feet (12.2 km) MSL. Winds commonly exceed 150 knots in winter and extreme wind speeds have reached 230 knots. Speeds between May and November average between 30 and 60 knots with extremes reaching 100 knots at 39,000-43,000 feet (12.2-13.1 km) MSL.

Figure 2-28 is a vertical cross-section of the STJ. Two cores can develop in this region in December and January.

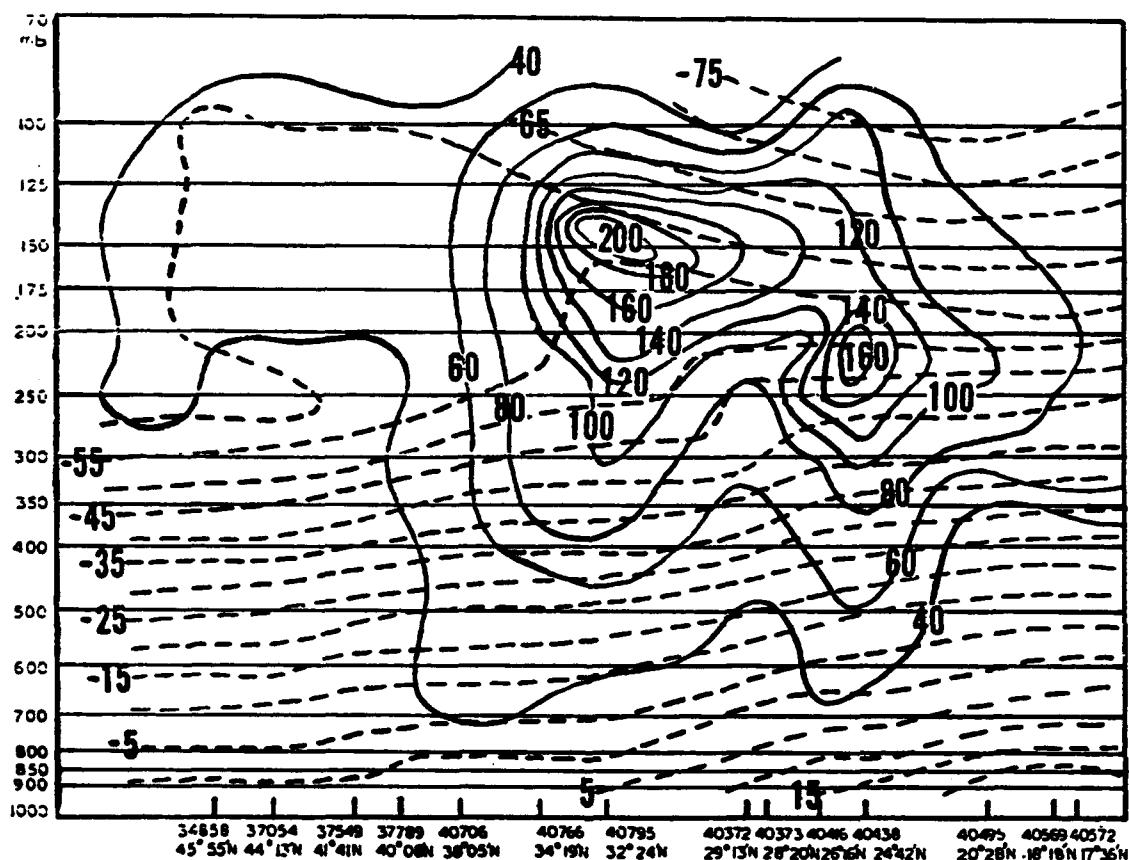


Figure 2-28. Vertical Cross-Section of the Subtropical Jet Along 45° E (5 January 1978, 0000Z). The "Y" axis represents millibar levels, while the "X" axis--from left to right--denotes station identification code (5-digit code number) with the corresponding latitude underneath. Isotachs (solid lines) depict wind speed in knots, and isotherms (dashed lines) depict temperatures aloft (°F).

SYNOPTIC DISTURBANCES

The greatest effects of either jet stream are felt between December and April when cyclonic activity is most common in the eastern Mediterranean Sea, Black Sea, and Caspian Sea basins. Parts of the Middle East Peninsula can experience strong winds, low temperatures, light precipitation, and occasional thunderstorms or light-to-moderate snowfall (above 3,000 feet/915 meters MSL.) Snowfall is extraordinary south of 30° N.

Initially, surface low-pressure cells develop when a strong PJ digs southward of 30° N and forms a deep upper-level trough. Northerly flow often develops on the east side of a blocking high-pressure ridge over the eastern Atlantic. The PJ and upper-level trough may intensify surface lows over the Mediterranean Sea, Black Sea, Caspian Sea, and in the lee of the Atlas Mountains of northwest Africa. Northerly flow ensures that the trough and surface cyclone move eastward into the Middle East Peninsula, but other factors are necessary for strong surface cold fronts to penetrate into the central and southern Red Sea or western Persian Gulf.

The preferred area for low-pressure center intensification during PJ/STJ interaction is often under the southeast quadrant of the upper-level trough. The low often deepens in the area between the two jet streams. Jet stream interaction most frequently occurs with Atlas Low formations because they are generated between 25 and 30° N--nearest the mean position of the STJ. Surface lows that develop in the eastern Mediterranean Sea and move east-southeastward may also receive jet stream support. Figures 2-29a-b illustrate generalized PJ/STJ interaction and low-pressure intensification areas for Atlas and Cyprus Lows.

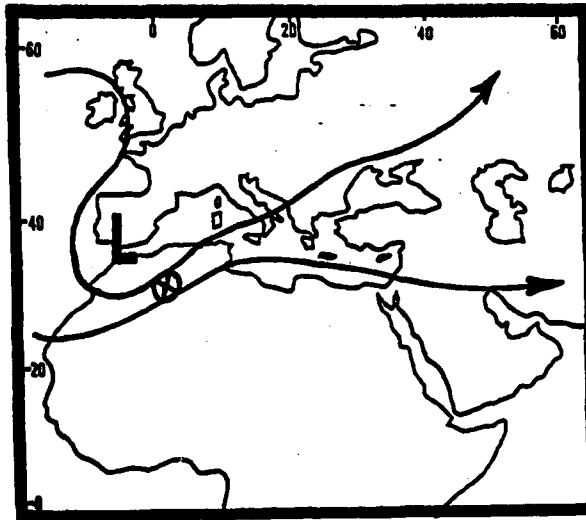


Figure 2-29a. Typical Jet Positions During Formation of Atlas Low. Surface low formation/intensification area is denoted by the circled X.

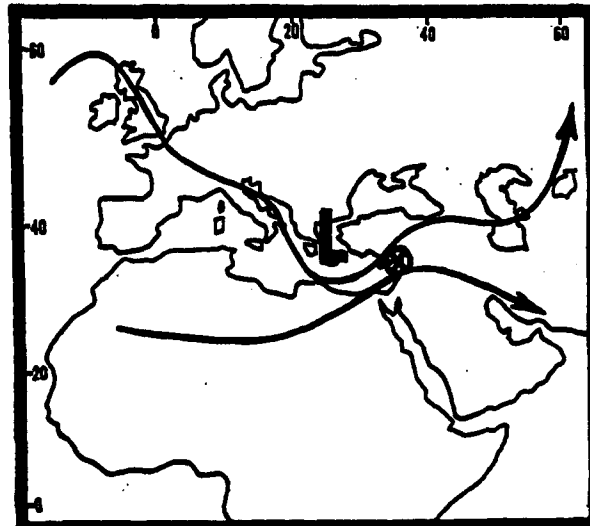


Figure 2-29b. Typical Jet Positions During Formation of Cyprus Low. Surface low formation/intensification area is denoted by the circled X.

SYNOPTIC DISTURBANCES

STORM TRACKS. Figure 2-30a shows typical December-February storm tracks as they affect the Middle East Peninsula. Primary tracks (solid arrow) pass through the eastern Mediterranean Sea basin. Secondary tracks (dashed arrow) generally reflect surface cyclogenesis associated with Cyprus Lows and troughs with southern European cold fronts. This is especially the case for storm tracks through the Persian Gulf (denoted as "A") and the Fertile Crescent (denoted as "B").

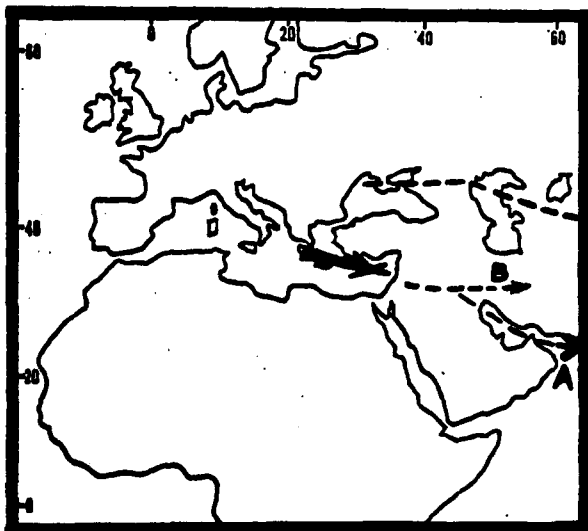


Figure 2-30a. Primary (solid arrow) and Secondary (dashed arrow) Mid-Latitude Storm Tracks, December, January and February. Persian Gulf track (A) and Fertile Crescent track (B).

Figure 2-30b shows the storm tracks that affect the Middle East Peninsula during March, April, and May. Leaside troughing along the Atlas Mountains initiates Atlas Low cyclogenesis inland over northwest Africa. The Atlas Low track produces most mid-latitude frontal-type weather in the region in April and early May. Another cyclogenesis area over the northwest Black Sea may also produce a weak cold front in the Middle East Peninsula. Several secondary storm tracks are possible. An important one is the northern Sahara Desert track (shown with an "X"). This track reflects cyclogenesis along active Atlas Low cold fronts, which remain strong while migrating eastward into the Red

Sea basin. Mid-latitude storms between June and October are very rare. An intense upper-level trough can generate abnormal rainfall in isolated cases.

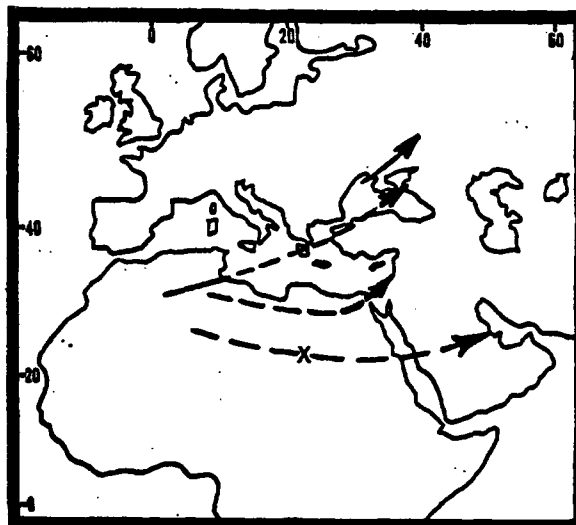


Figure 2-30b. Primary (solid arrow) and Secondary (dashed arrow) Mid-Latitude Storm Tracks, March, April, and May. "X" marks the important Sahara Desert storm track.

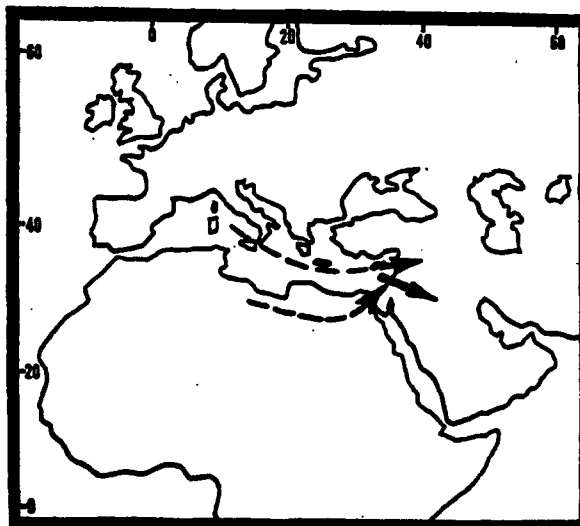


Figure 2-30c. Primary (solid arrow) and Secondary (dashed arrow) Mid-Latitude Storm Tracks, November.

SYNOPTIC DISTURBANCES

The mean November storm tracks shown in Figure 2-30c reflect the southward movement of the Polar Jet. The primary storm track (solid arrow) for November seldom effects the region, but secondary cyclogenesis along the eastern Mediterranean Sea and Sahara Desert are important in November.

The storm track during Operation DESERT STORM, as shown in Figure 2-30d, was more southerly and had more cyclonic curvature over the Middle East Peninsula than usual, causing more extensive weather in the interior and into Kuwait.

CYCLONIC ACTIVITY. Four cyclogenesis areas affect the Middle East Peninsula; their locations and movement are shown in Figure 2-31. These areas are the source regions for (1) Atlas Lows (the northwest African interior), (2) Cyprus Lows (the eastern Mediterranean Sea), (3) Black Sea Lows, and (4) Caspian Sea Lows.



Figure 2-30d. Primary Storm Track during Operation DESERT STORM, January-March 1991.

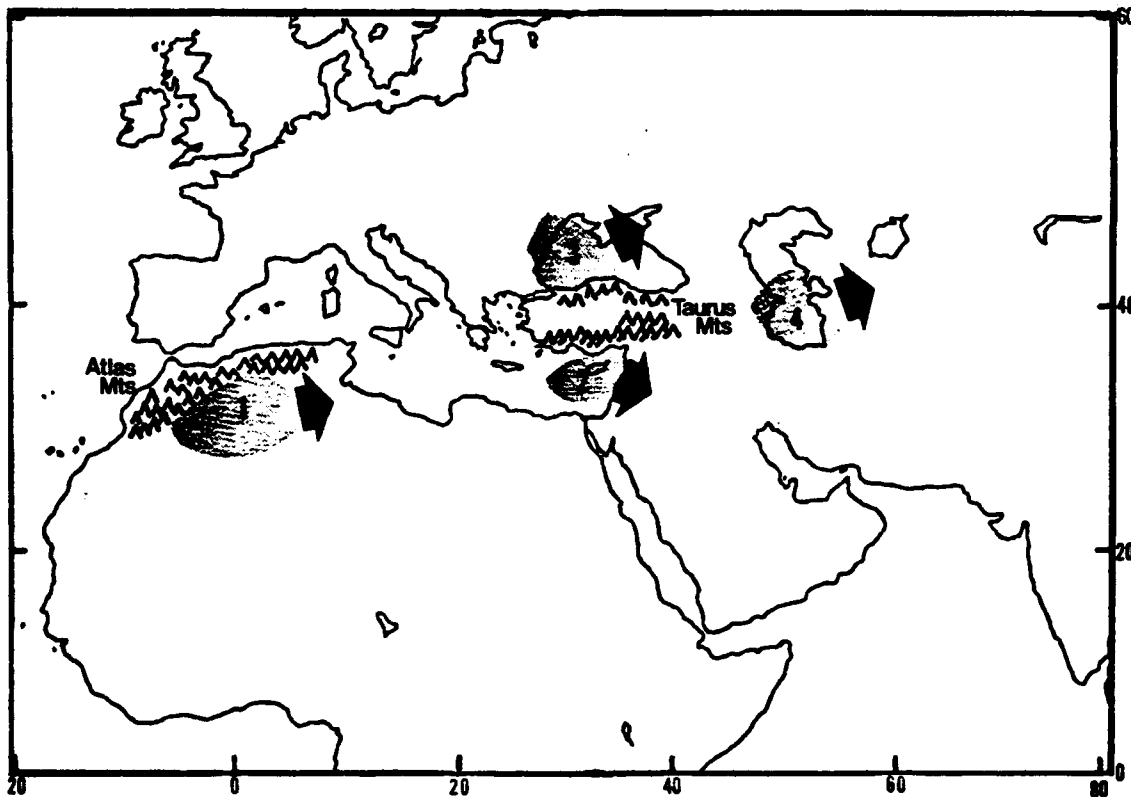


Figure 2-31. Mid-Latitude Cyclogenesis Regions. The four primary areas of cyclogenesis are: (1) for the Atlas Low, (2) for the Cyprus Low, (3) for the Black Sea Low, and (4) for the Caspian Sea Low. Arrows indicate general direction of movement.

SYNOPTIC DISTURBANCES

Although synoptic considerations dictate the specific area for initial low formation and movement, many of the low-pressure systems that affect the Middle East Peninsula develop along an existing cold front. Resultant weather varies significantly with each frontal passage. Surface pressure patterns, short-wave troughs, vorticity advection, and jet-stream positions determine the severity of the system over the Red Sea and northern Middle East Peninsula.

Typically, Cyprus Lows and Atlas Lows extend surface cold fronts into the region; however, very

deep low-pressure systems with upper-level support are necessary for precipitation to occur. On rare occasions, the cold front reaches the Gulf of Aden, as shown in Figure 2-32.

One or two significant cyclonic storms normally pass through the region between December and April. Intense southeastward-moving, upper-level polar troughs support isolated thunderstorms along the north-central Red Sea and strong surface winds that produce duststorms over the Arabian Desert.

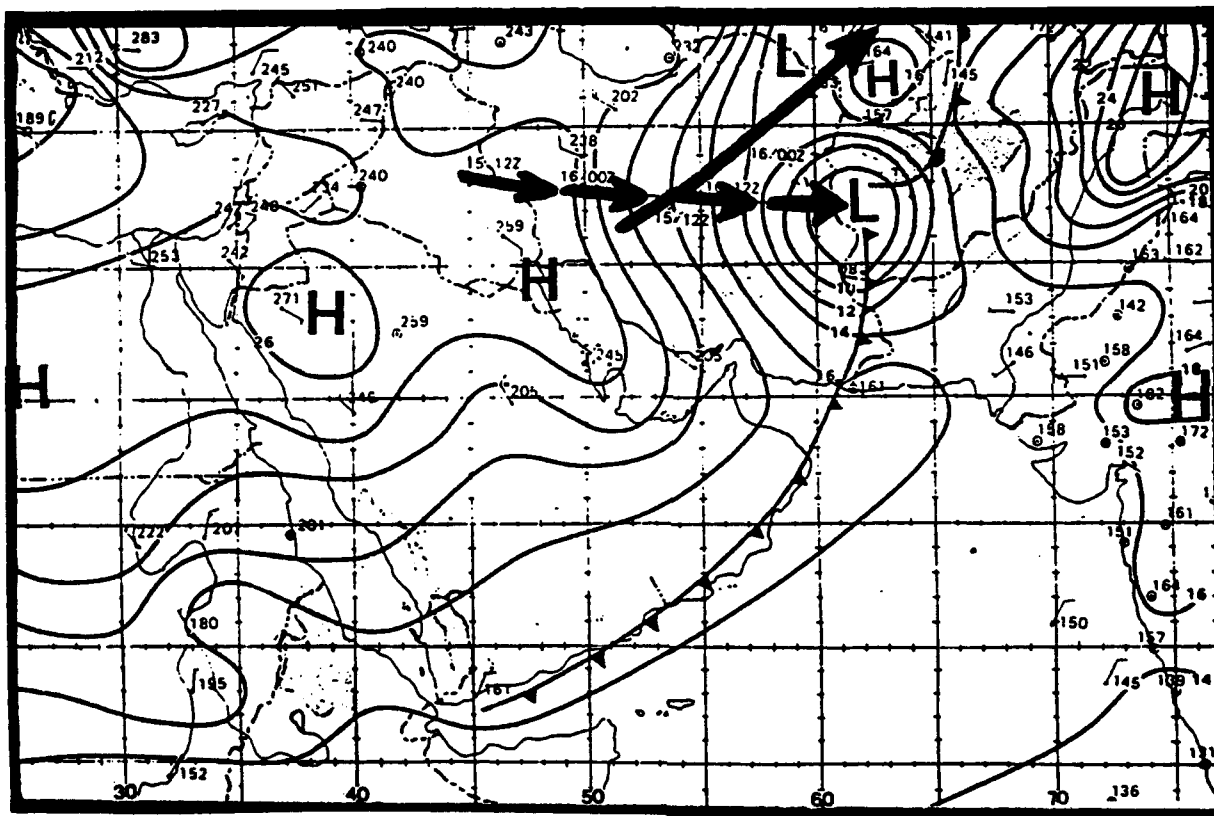


Figure 2-32. Mediterranean-Generated Cyclonic Activity and Trailing Cold Front Entering the Gulf of Aden. The Cyprus Low developed at the surface along a low- and mid-level trough (not shown) associated with a Black Sea Low. The solid arrow shows the path of the Black Sea Low cold front, while the dashed arrow represents Cyprus Low movement. Normally the mountain ranges of Turkey and Iran prevent surface cold fronts from extending southward into the Middle East Peninsula.

SYNOPTIC DISTURBANCES

The Atlas Low. The peak for Atlas (or North African) lows is in March and April, but some form from October to February and in May and June. The average number is 14 a year. They develop in the north-central interior of Algeria southeast of the Atlas Mountains. An Atlas Low generally forms when a mid- or upper-level trough, oriented northeast-southwest over Spain is positioned over a weak surface low or slow-moving cold front. In March and April, the mean Azores High moves northwestward, shifting the mean mid-level flow pattern from zonal to meridional. This can cause a southward movement of transient European disturbances along the Polar Jet, which often digs along the backside of the 500-mb trough. Mid-level cold air and moisture crosses the Atlas range as a cold core "cut-off" low or short wave. These

storms seldom develop or penetrate very far into the eastern Sahara Desert and Red Sea without strong northerly flow and cold mid-level support. If this flow pattern persists for more than 3 days and intense polar air surges south of 30° N, the Polar Jet and the mean Atlas Low storm track temporarily shifts southward into the north-central Sahara. As a result, storms move east across the northern Sahara into the central Red Sea.

Figures 2-33a-e depict a 3-day sequence when Atlas Low cyclogenesis and movement is east-southeastward over the northern Sahara. Figure 2-33a shows the surface conditions over the Mediterranean Sea, north Africa, and Europe on 7 April 1954 (0000Z). Figure 2-33b depicts the 500-mb flow pattern for the same day at 0300Z.

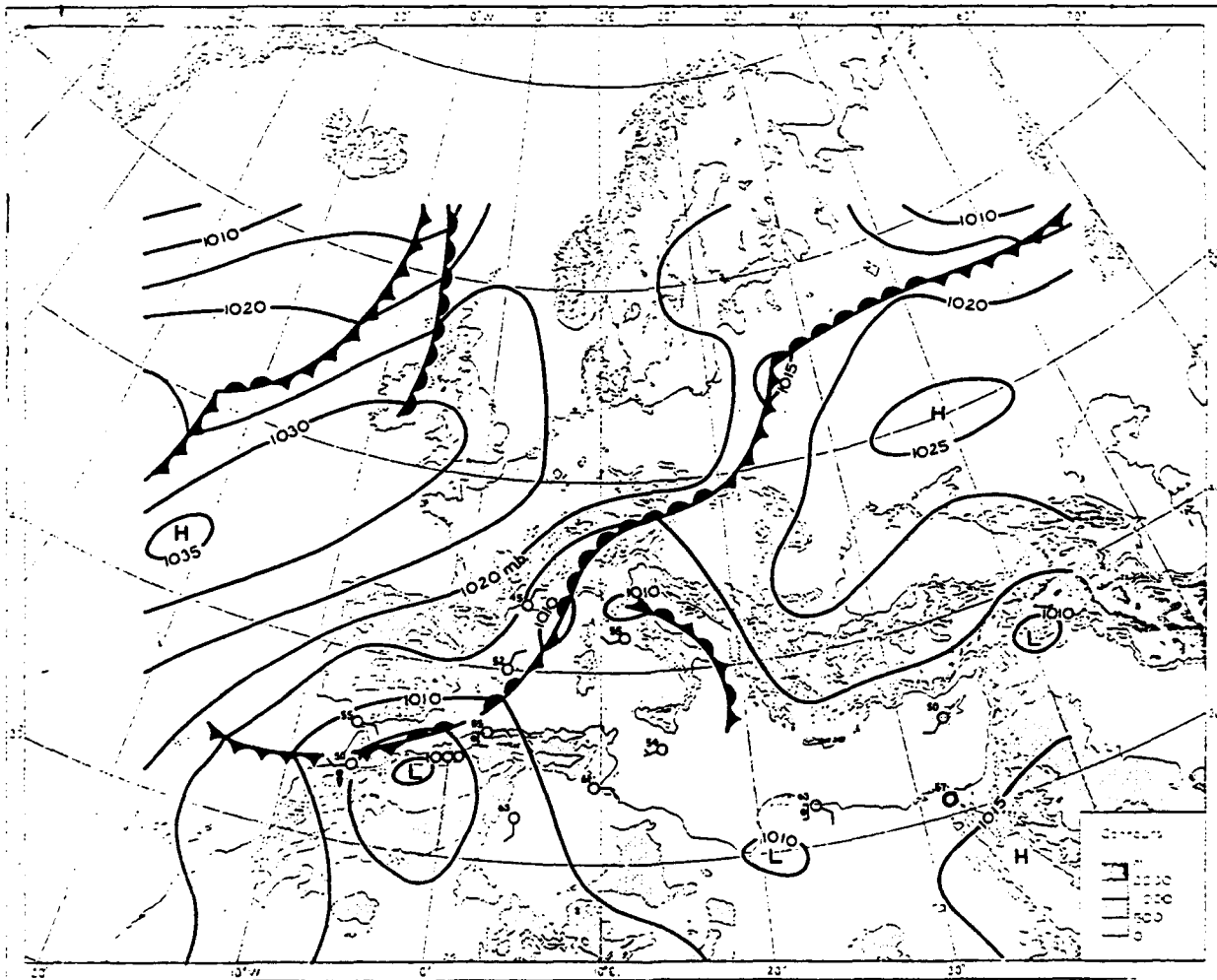


Figure 2-33a. Synoptic Surface Chart (7 Apr 1954, 0000Z), Atlas Low. Pressures in millibars.

SYNOPTIC DISTURBANCES

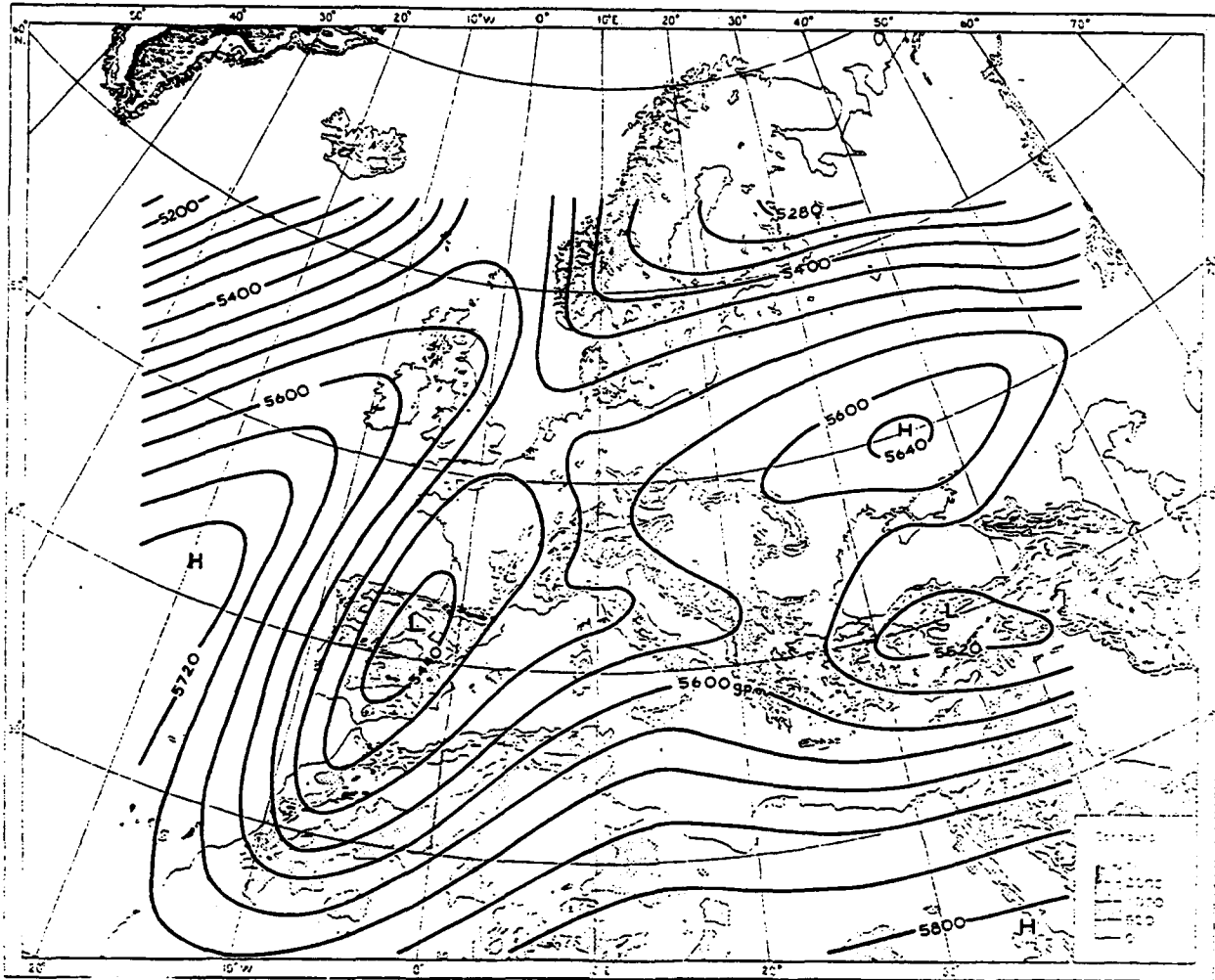


Figure 2-33b. 500-mb Flow (7 April 1954, 0300Z), Atlas Low. Contours represent heights in geopotential meters (gpm).

SYNOPTIC DISTURBANCES

In Figure 2-33c, the 8 April 1954 surface chart (0000Z) shows the Atlas Low developing on the lee side of the Atlas Mountains. Figure 2-33d shows the 500-mb flow pattern on 8 April 1954 (0300Z). The 500-mb trough is moving

southeastward from central Spain into northern, Algeria forming a "cut-off" low at 35° N, 3° E. Figure 2-33e shows the Atlas Low positioned along the Libya-Egypt border approaching the Middle East Peninsula.

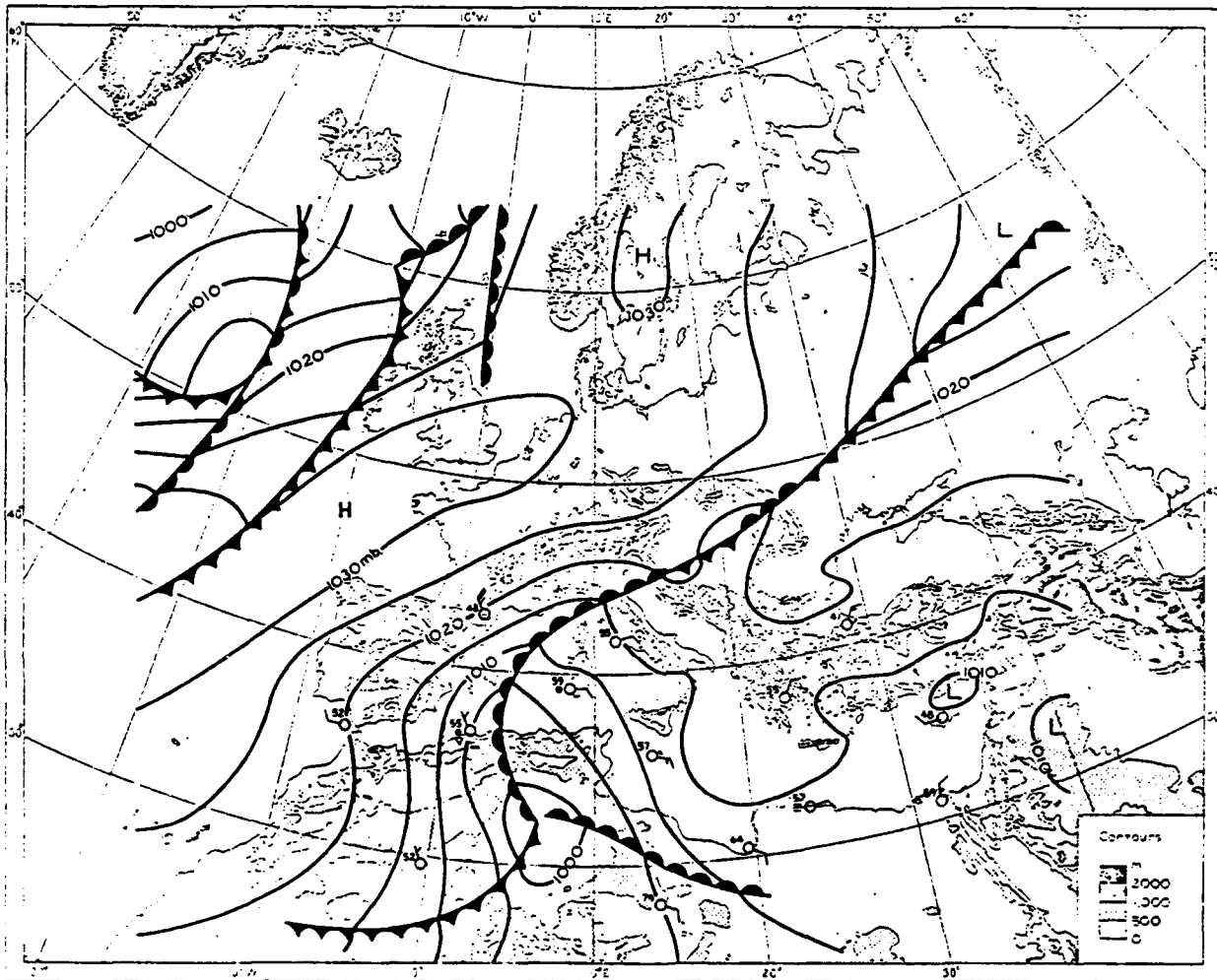


Figure 2-33c. Synoptic Surface Chart (8 April 1954, 0000Z), Atlas Low. Pressures in millibars.

SYNOPTIC DISTURBANCES

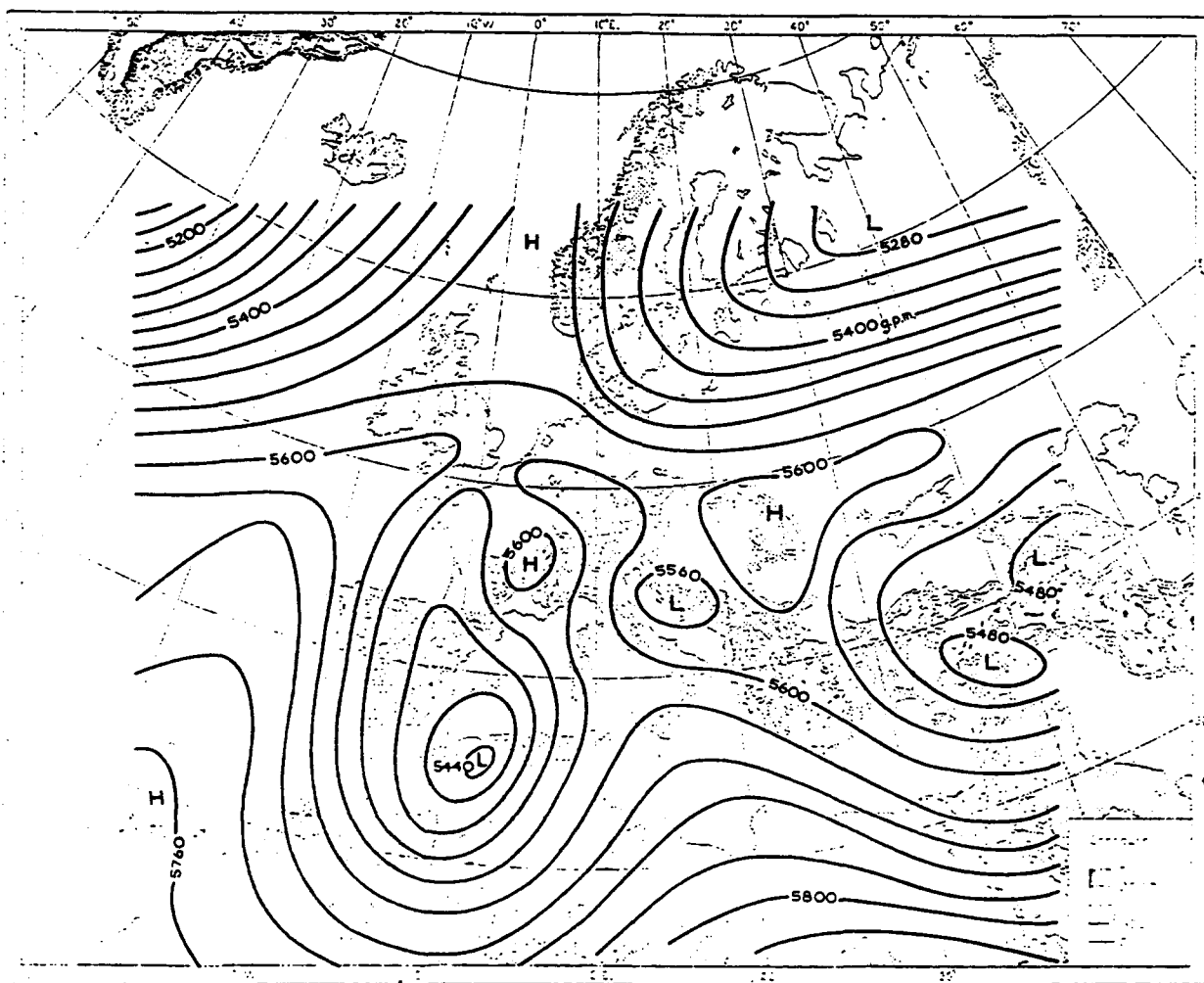


Figure 2-33d. 500-mb Flow (8 April 1954, 0300Z), Atlas Low. Contours represent heights in geopotential meters (gpm).

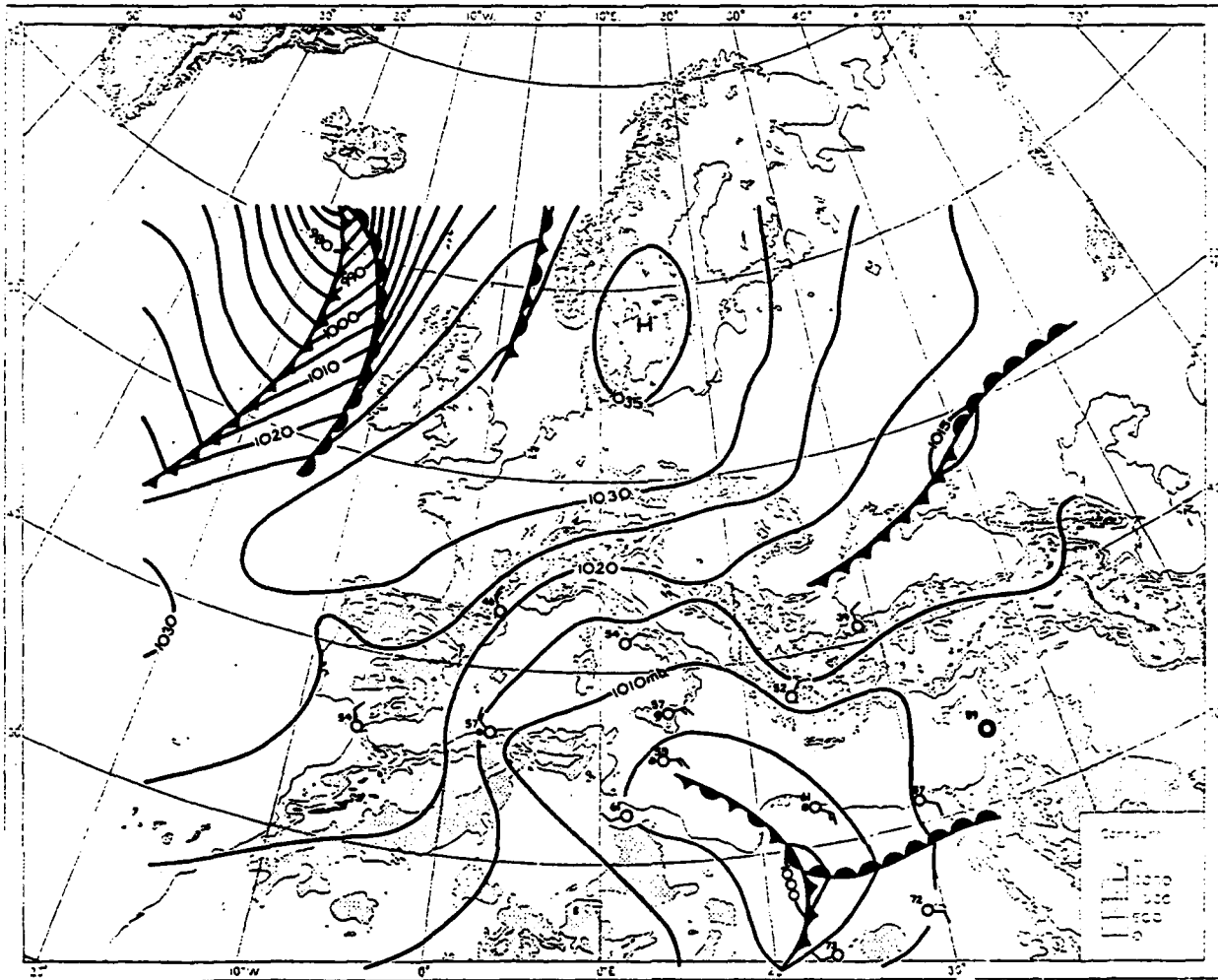


Figure 2-33e. Synoptic Surface Chart (9 April 1954, 0000Z), Atlas Low. Pressures in millibars.

Intense Atlas Lows seldom track eastward across the entire Sahara because many synoptic variables must combine to sustain the storm over the dry Sahara. When they do track eastward, however, Atlas Lows and their trailing cold fronts produce strong surface winds (greater than 25 knots) and widespread dust/sandstorms.

Without sustained northerly flow, Atlas Low movement is northeastward over the south-central Mediterranean. Deep upper-level troughs may produce polar outbreaks over the eastern Sahara, but northerly flow is necessary for the Atlas Low cold front to penetrate deep

into the Middle East Peninsula. The surface trough is often followed by strong surface high pressure that accelerates the frontal boundary southeastward across the central Red Sea. The Atlas Low is responsible for the April "khamsin" wind.

The Subtropical and Polar Jets may intensify a disturbance at mid- and upper levels. A mean wind speed maxima--the Subtropical Jet--occurs over the northern Red Sea in March (110 knots) and April (83 knots). Strong outflow aloft supports isolated thunderstorm activity over the central and northern Red Sea.

SYNOPTIC DISTURBANCES

In Figure 2-34a, the 16 April 1964 (1200Z/1500L) synoptic chart shows an Atlas Low (1001 mb) over west-central Saudi Arabia. To the southeast, the plateaus of western Ethiopia and extreme east-central Sudan have produced a transitory thermal trough, or Sudanese Low, that appears on mean pressure charts as an inverted low-pressure trough.

Although the map (typical for this time of year) shows the inverted trough (solid lines extending to the south and west of the Sudanese Low) looking much like a mid-latitude front, it's only a resemblance. Figure 2-34b shows the synoptic pattern 24 hours later, on 17 April at 1200Z/1500L.

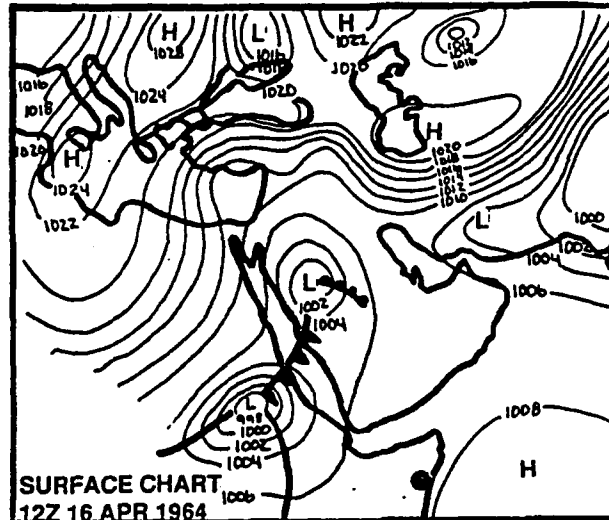


Figure 2-34a. Synoptic Surface Chart (16 April 1964, 1200Z/1500L) Showing an Eastward-Tracking Atlas Low. The surface trough (Atlas Low) extends a well-defined cold front across the central Red Sea. The deeper 998-mb Sudanese thermal low enhances the surface trough.

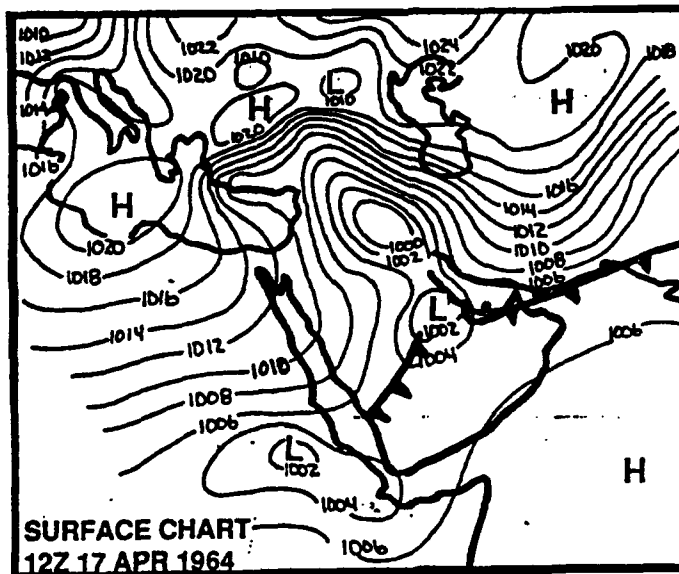


Figure 2-34b. Synoptic Surface Chart (17 April 1964, 1200Z/1500L) Showing Secondary Low Formation Along the Active Cold Front. The Atlas Low has turned northeastward and a secondary low has formed along the cold front. The Mediterranean high-pressure cell pushes the cold front southeastward. The Sudanese Low remains stationary.

SYNOPTIC DISTURBANCES

The Cyprus Low. This migratory low can spawn intense thunderstorm activity over the eastern Sahara, central Red Sea, and northern Arabian Desert between December and March. The two factors contributing to Cyprus Low cyclogenesis are:

- Low-level inflow of northwesterlies from the Aegean Sea (see Figure 2-35) over warm eastern Mediterranean waters (63-65°F/18°C).
- Instability aloft caused by cold slow-moving migratory (mid- and upper-level) polar troughs.

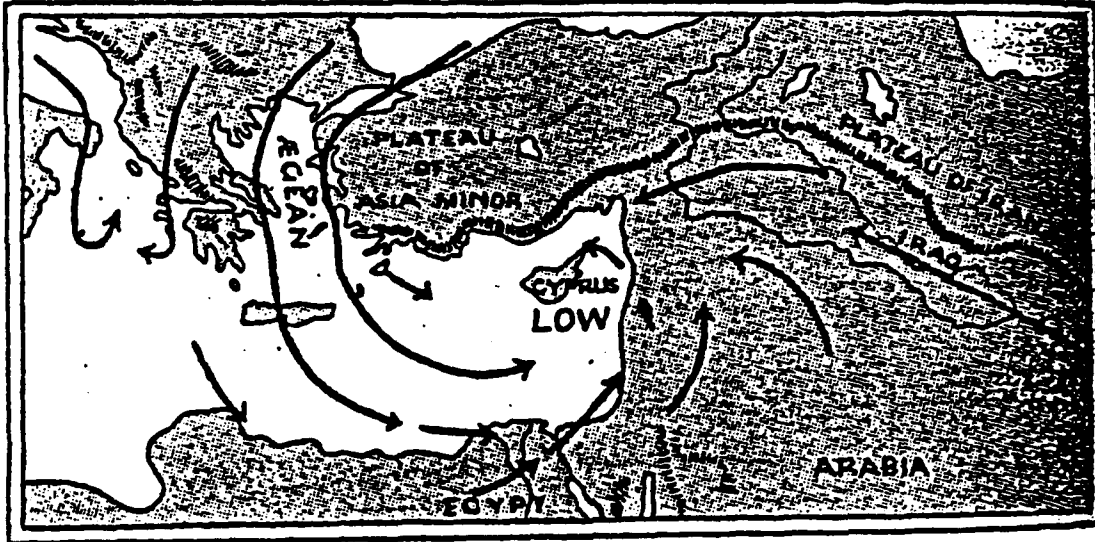


Figure 2-35. Surface Circulation Causing the Development of the Cyprus Low.

The Cyprus Low is generated over a warm water surface. As a result, less instability is needed to sustain lower surface pressures. Furthermore, favorable mid- and upper-level flow (westerlies) occurs frequently throughout December and March, whereas the Atlas Low cyclogenesis area requires a sustained northerly flow pattern, common only during transition seasons.

Cyprus Low formation does not occur exclusively between December and March; Figures 2-36a-d illustrate a mid-November sequence for the phenomenon. Figures 2-36a-c are surface charts showing the 16-18 November 1953 development of the low; 2-36d is the 18 November 500-mb chart.

SYNOPTIC DISTURBANCES

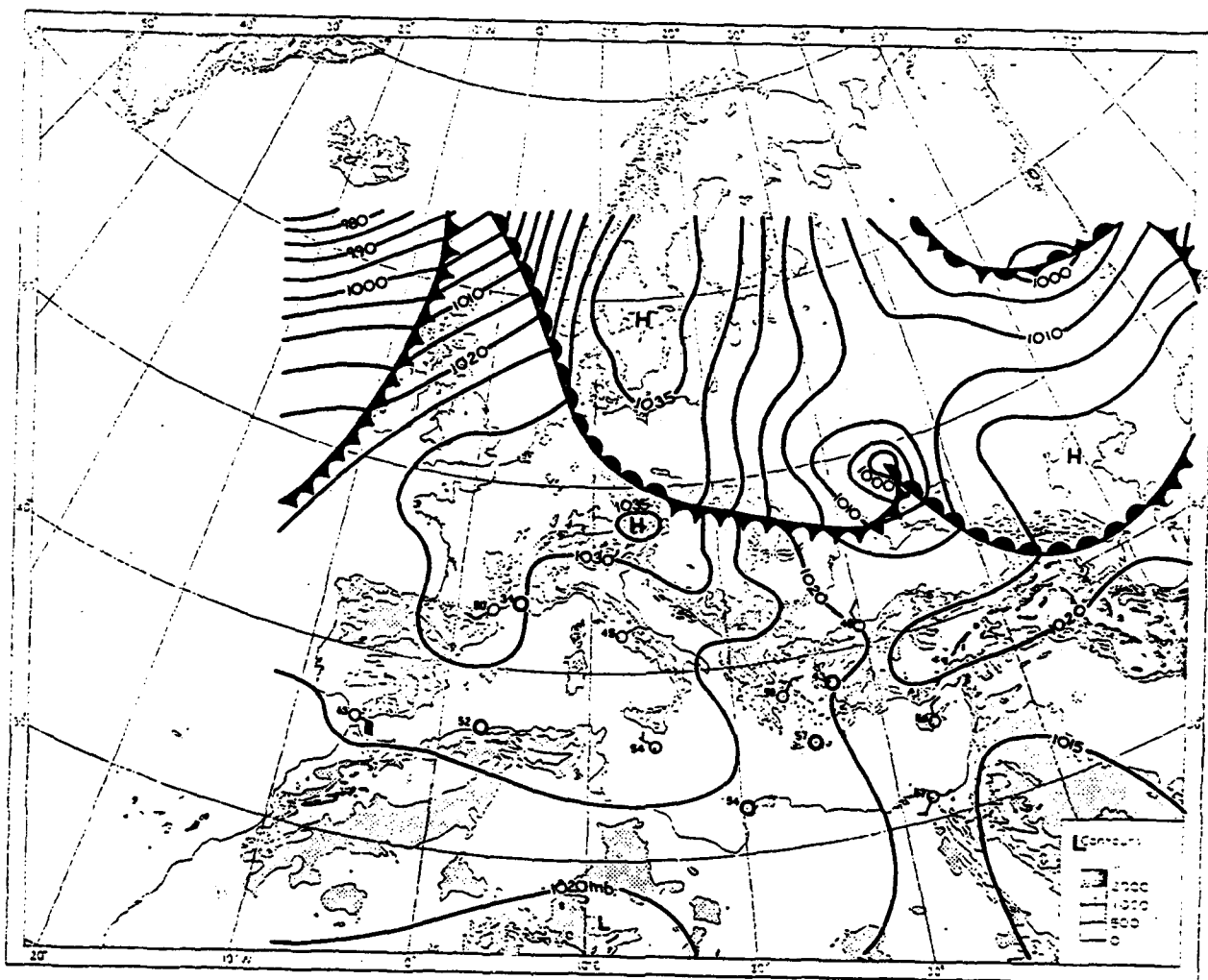


Figure 2-36a. Synoptic Surface Chart (16 November 1953, 0000Z), Cyprus Low.
Pressures in millibars.

SYNOPTIC DISTURBANCES

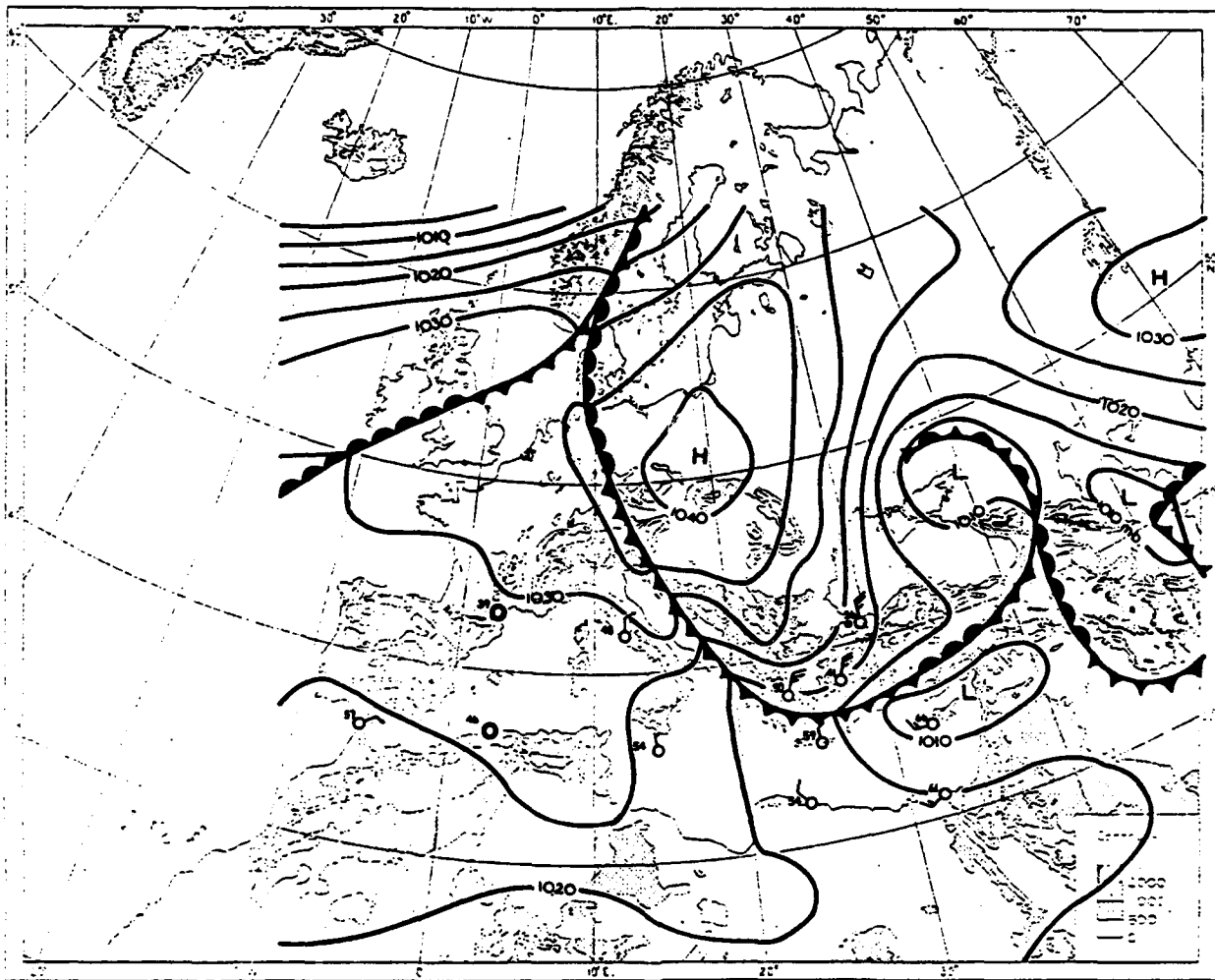


Figure 2-36b. Synoptic Surface Chart (17 November 1953, 0000Z), Cyprus Low.
Pressures in millibars.

SYNOPTIC DISTURBANCES

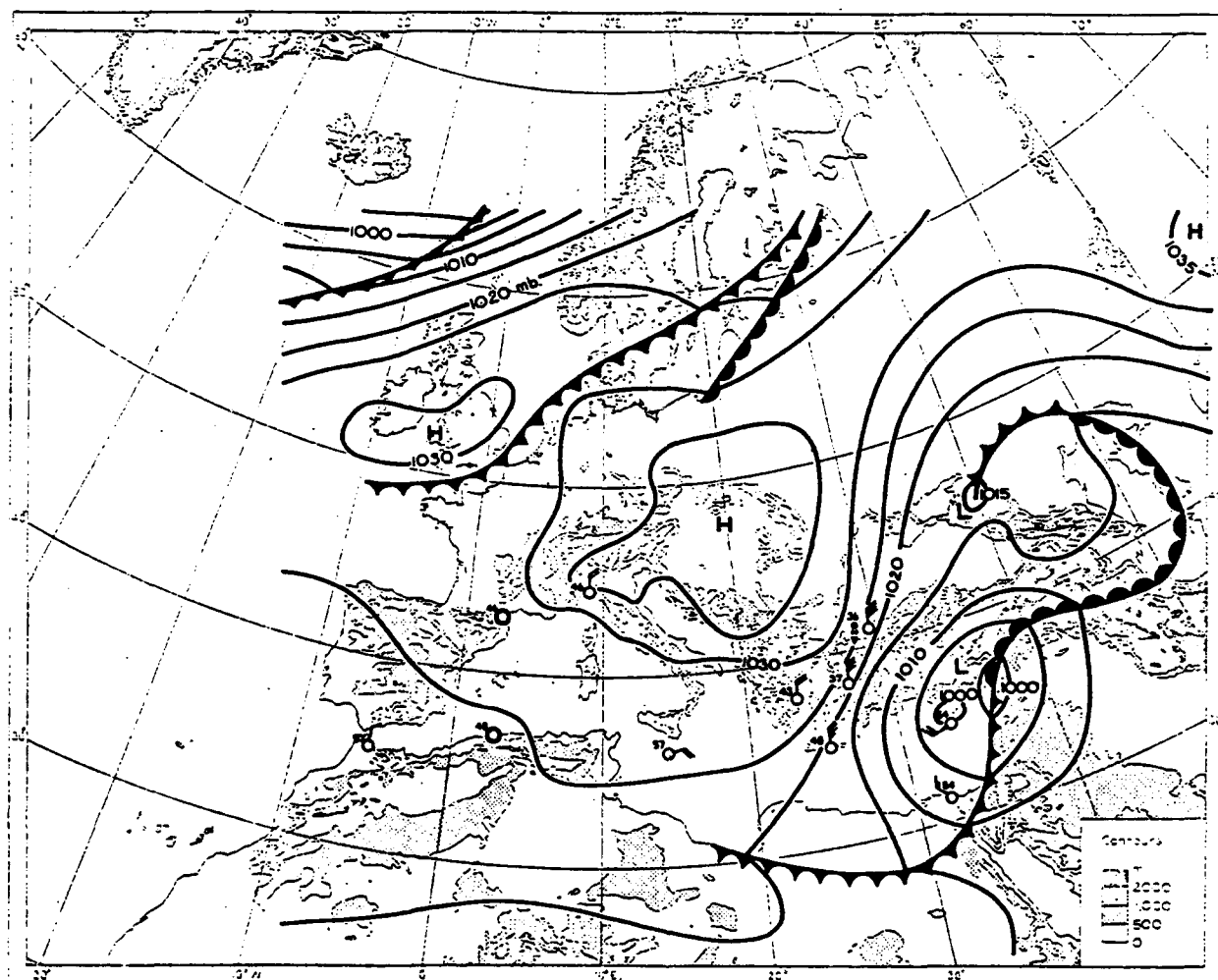


Figure 2-36c. Synoptic Surface Chart (18 November 1953, 0000Z), Cyprus Low. Pressures in millibars.

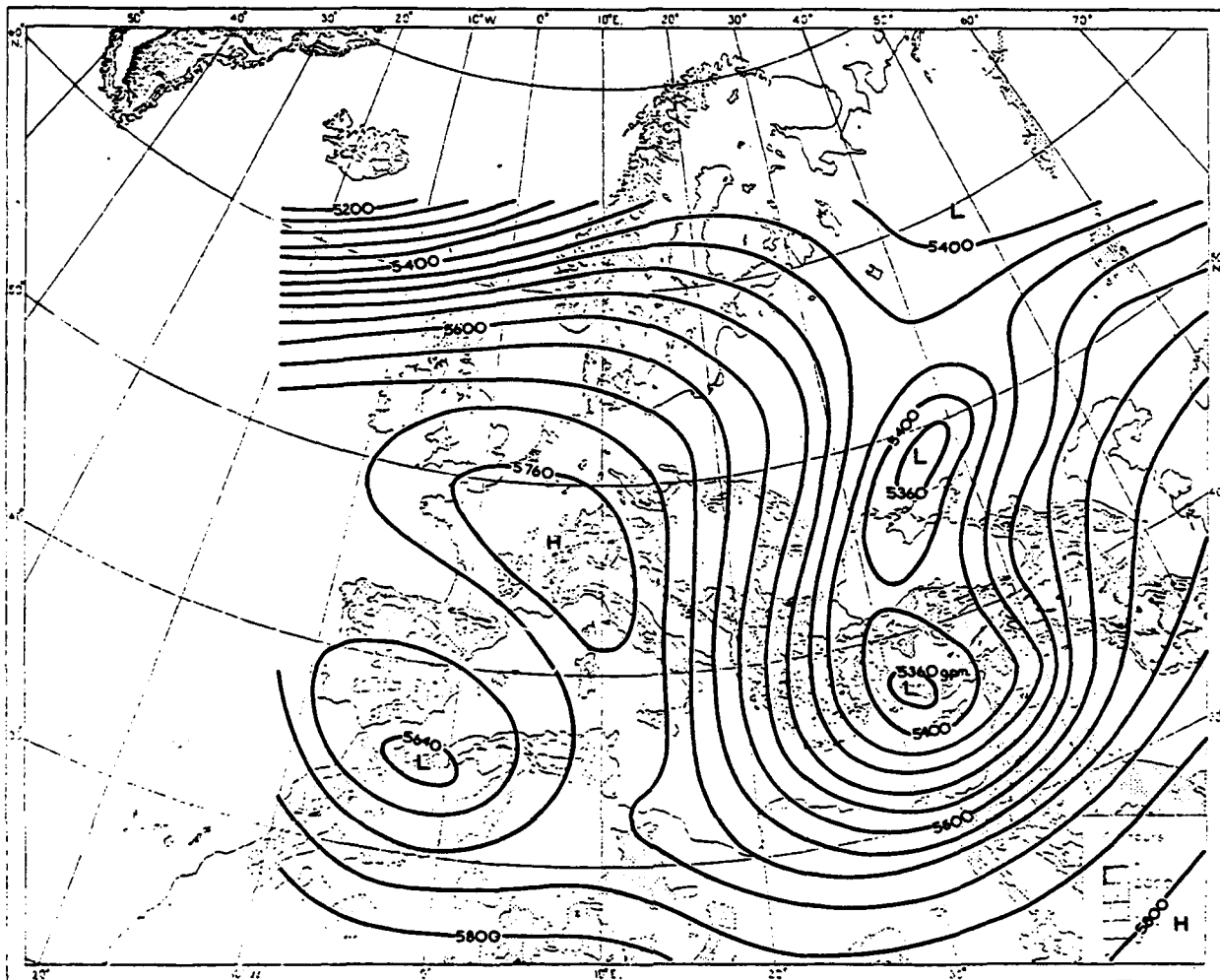


Figure 2-36d. 500-mb Flow (18 November 1953, 0300Z), Cyprus Low. Contours represent heights in geopotential meters (gpm).

A thunderstorm outbreak with significant rainfall requires cold air between 700 and 500 mb, usually 15 to 18° F (8-10° C) lower than the environment. Even lower temperatures are required for the rare snowfall in extreme northwestern Saudi Arabia, western Iraq, Jordan, and Syria. Such conditions occurred in 1991 during Operation DESERT STORM. It happened again in 1992; eastern Jordan got over 20 inches of snow from one such storm.

Occasionally, very cold polar troughs penetrate the eastern Mediterranean Sea with moist low-level support through the Aegean Sea. Warm

Saharan surface air (with Red Sea moisture advected ahead of the surface cold front) creates a favorable environment for severe thunderstorms in the Fertile Crescent and northern Red Sea Coastal Plains. Significant positive vorticity advection is required to trigger their development.

Cyprus Lows most frequently track eastward or southeastward into the Fertile Crescent and western Persian Gulf Coastal Plains. They can produce shamals. On rare occasions, the Cyprus Low moves into the Gulf of Oman.

SYNOPTIC DISTURBANCES

The Black Sea Low. The Black Sea is an important area for cyclogenesis throughout the year. Lows form most frequently during the winter, typically as secondary lows from April through October. The primary surface storms during summer cross central and northern Europe; however, on occasion, a deep mid-latitude trough extends southward over the Black Sea. Figures 2-37a and b are surface charts for 19 and 20 August 1949 at 0000Z. Significant weather features shown are (on the 19th) a developing low-pressure cell near Italy, and (on the 20th) a deepening Black Sea Low with a cold front moving into the Sahara.

Figures 2-37c and d show 0300Z 500-mb flow over North Africa and Europe on 18 and 20 August 1949. A deep 500-mb trough extends from Scandinavia southward to 25° N with a cut-off low forming in support of the surface cyclone over the Black Sea. Although this flow pattern is rare, it produces significant precipitation. The Black Sea's northern fringes freeze over during the winter, but the southern half normally remains ice-free. Cyclogenesis occasionally occurs over the warmer water. Typically, a cold front extends southward into the Fertile Crescent.

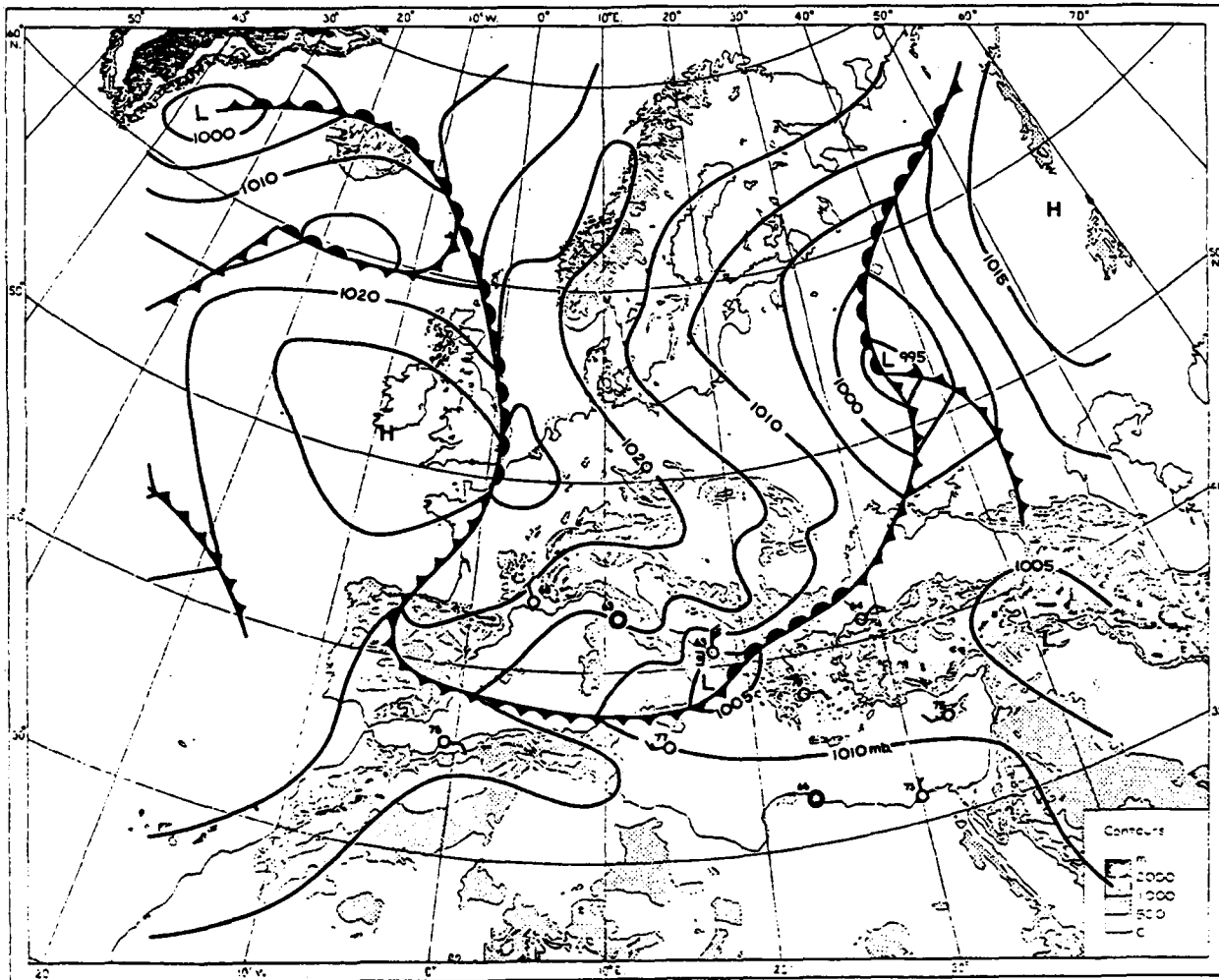


Figure 2-37a. Synoptic Surface Chart (19 August 1949, 0000Z), Black Sea Low. Pressures in millibars.

SYNOPTIC DISTURBANCES

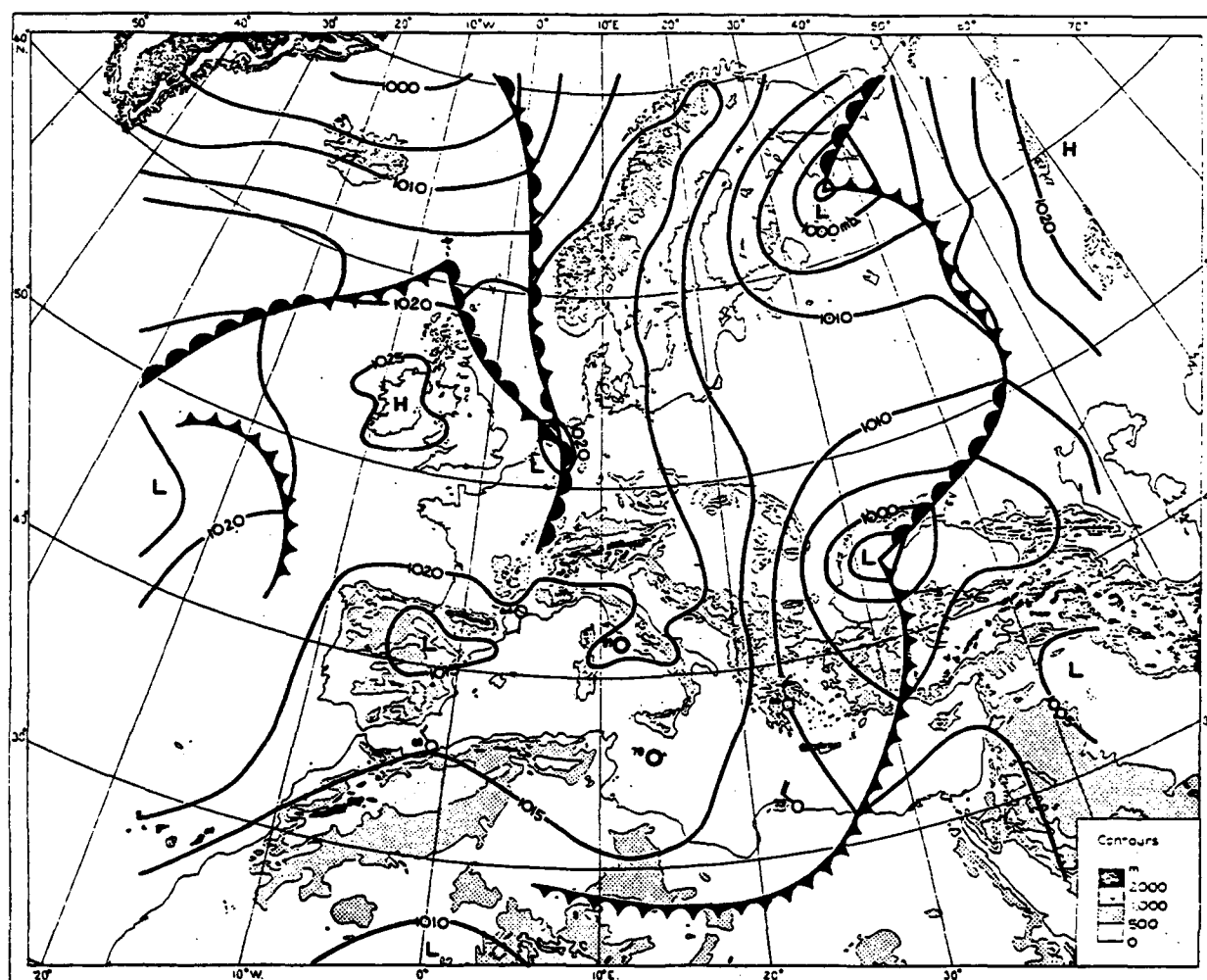


Figure 2-37b. Synoptic Surface Chart (20 August 1949, 0000Z), Black Sea Low. Pressures in millibars.

SYNOPTIC DISTURBANCES

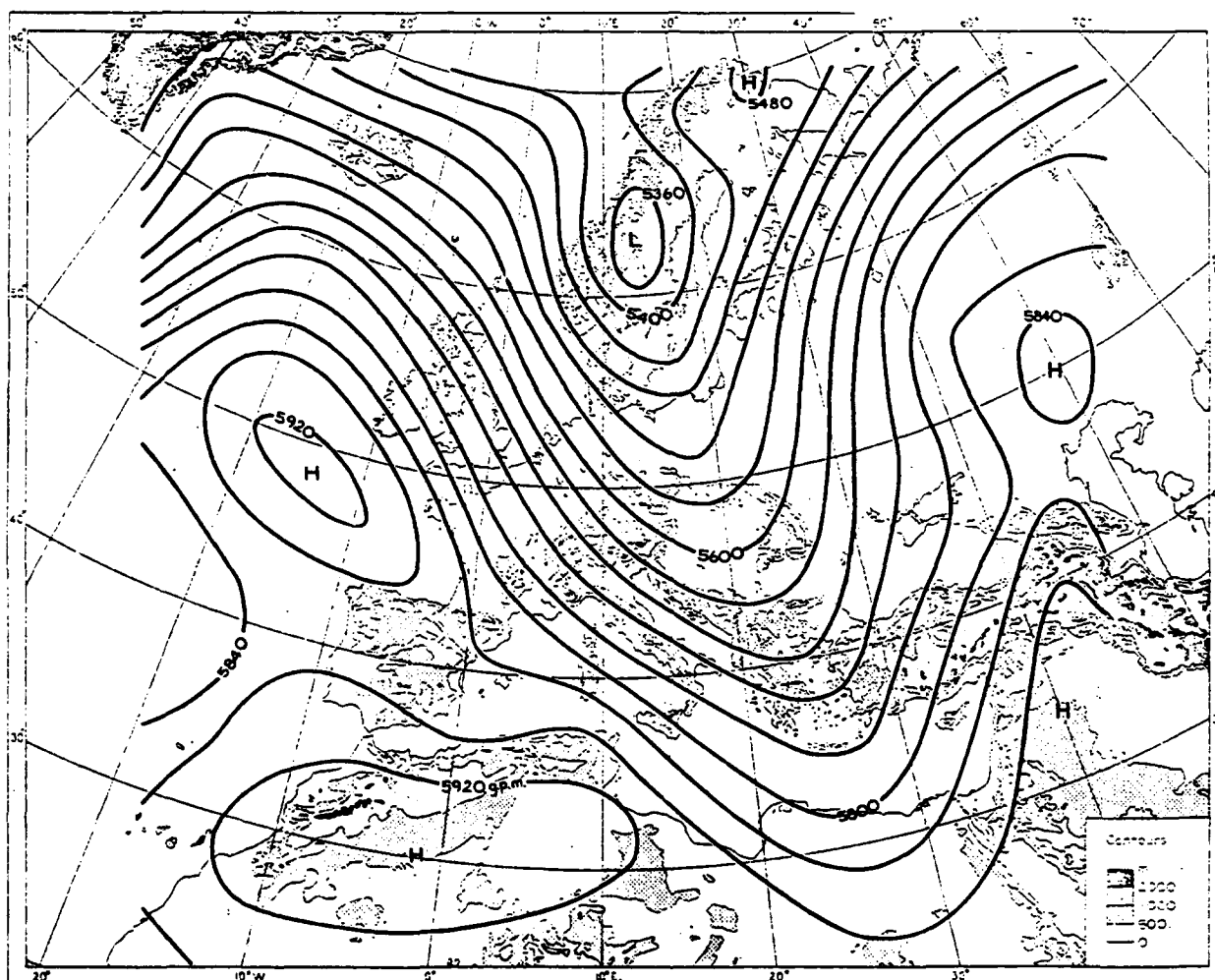


Figure 2-37c. 500-mb Flow (18 August 1949, 0300Z), Black Sea Low. Contours represent height in geopotential meters.

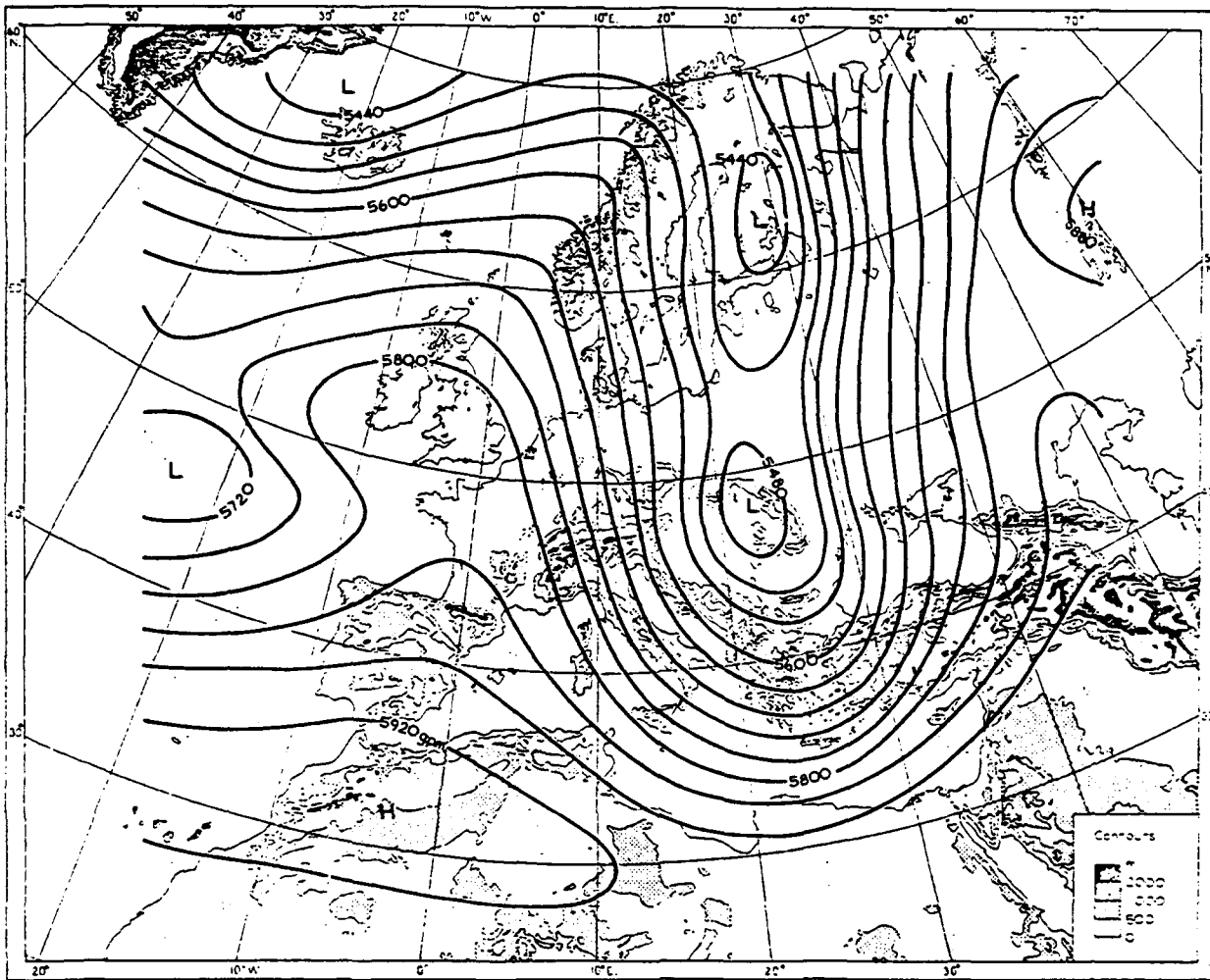


Figure 2-37d. 500-mb Flow (20 August 1949, 0300Z), Black Sea Low. Contours represent height in geopotential meters (gpm).

The Caspian Sea Low. The Caspian Sea provides a low-level moisture source for mid- and upper-level troughs. Surface lows form through lee-side troughing because of the extensive mountain ranges along the southwestern and southern sections of the Caspian Sea coastline. These lows may develop at any time of the year, but their accompanying cold fronts only affect

the Persian Gulf Coastal Plains between December and March. Weak cold fronts reach the area, but they rarely cause more than a weak wind shift and a slight increase in mid-level cloud cover. Between January and February, the northern third of the Caspian Sea becomes ice-covered; lows tend to develop along the southern coast line.

SYNOPTIC DISTURBANCES

Significant Low-Level Persian Gulf Synoptic Effects. As lows move near the northern Persian Gulf, low-level warm and moist air from the Gulf may flow around their northern sides into the northern Arabian Desert and Fertile Crescent. This moist air, enhanced by upslope flow and cooler surface air behind the front, forms fog that can reduce visibilities and ceilings to near zero throughout the northern Arabian Desert and Fertile Crescent Region for up to 72 hours after frontal passage.

Southwesterly moist, low-level flow across the Red Sea associated with migratory synoptic systems can also reach into the interior of the Arabian Desert. This flow can produce 4,000-foot ceilings that extend from the Tokar Gap across the Red Sea to north of Jeddah, then through breaks and passes in the Hijaz Mountains, and ending in the Northern Arabian Desert--see Figure 2-38.

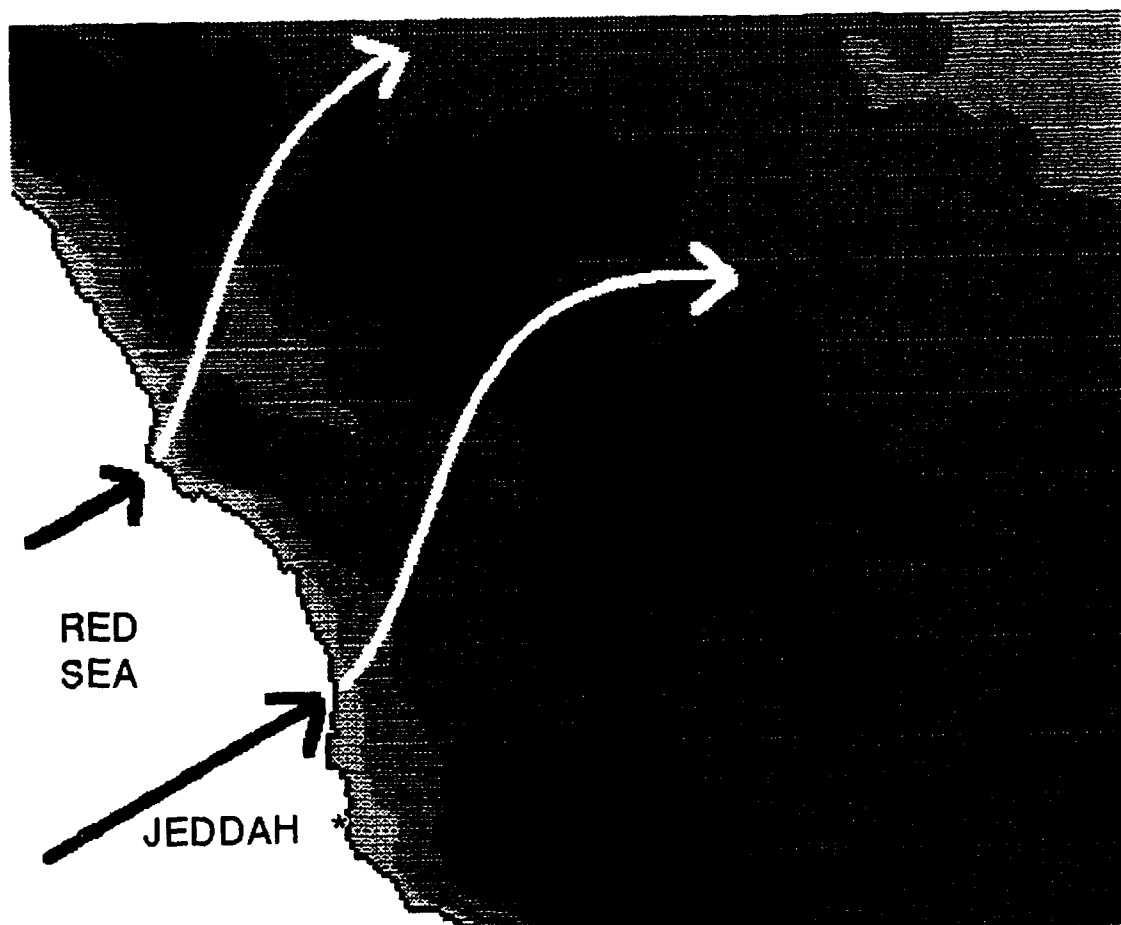


Figure 2-38. Low-Level Southwesterly Flow Across the Red Sea.

Migratory high-pressure cells that become quasi-stationary in the north-central Arabian Desert can cause upslope/advection fog and/or stratus along the Persian Gulf Coastal Region and in the central Arabian Desert as far inland as Riyadh. Low-level flow around the high over the Persian

Gulf comes back onshore, having picked up low-level moisture. The resulting fog and low clouds do not last long after sunrise in the Arabian Desert, but can last throughout the day near the coast.

THE OMANI CONVERGENCE ZONE (OCZ). The OCZ is a low-level boundary where Southwest or Northeast Monsoon flow converges with modified northwesterly flow from the Mediterranean. Surface convergence over the Rub al Khali (Empty Quarter) can extend into the Akhdar (or Hajar) Mountains of northeastern Oman. Figure 2-39 shows the region affected.

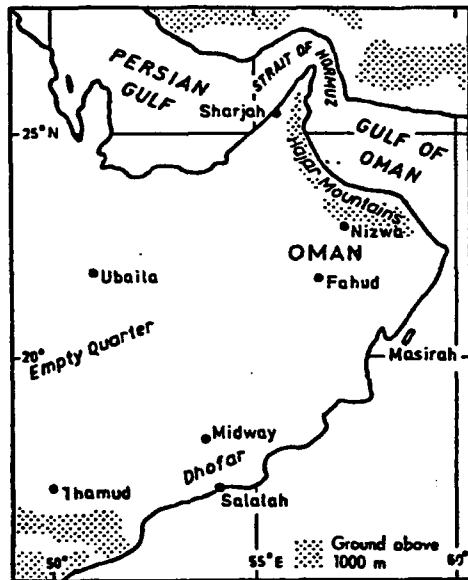


Figure 2-39. Locations Affected by the Omani Convergence Zone (OCZ) (from Pedgley, 1970).

The OCZ is mainly a zone of wind shear. Occasional convective activity can be found over higher terrain. The OCZ is 100 to 150 NM inland from the Omani coast (Figure 2-40a), extending northeast to southwest from 22° N, 57° E to 18° N, 50° E. It normally doesn't form when a cold front is moving through the area. Between February and June, the development of the Southwest Monsoon circulation causes gradual northward movement of the OCZ (Figure 2-40b). After June, the surface Monsoon Trough becomes established and absorbs the OCZ.

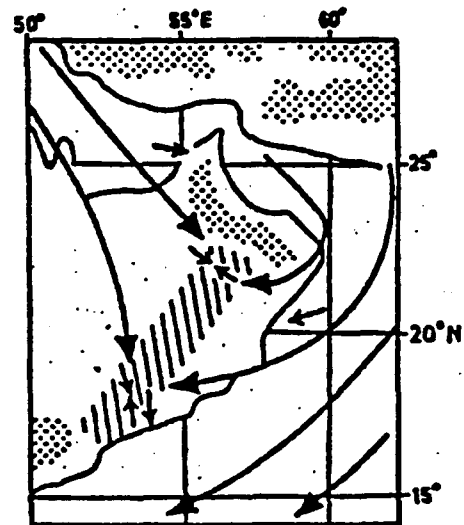


Figure 2-40a. Schematic Patterns of Wind Flow Below 3,000 Feet/915 meters (1000L) Over Oman, January (from Pedgley, 1970). Large arrows represent streamline flow, while short arrows denote prevailing surface wind direction. Hatched areas show the OCZ, and stippled areas represent elevations above 3,280 feet (1,000 meters).

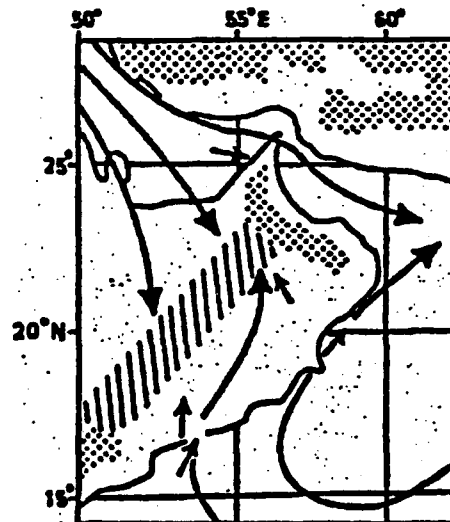


Figure 2-40b. Schematic Patterns of Wind Flow Below 3,000 Feet/915 meters (1000LST) Over Oman, April (from Pedgely, 1970). Large arrows represent streamline flow, while short arrows denote prevailing surface wind direction. Hatched areas show the OCZ, and stippled areas represent elevations above 3,280 feet (1,000 meters).

SYNOPTIC DISTURBANCES

THE DESERT FRONT is the term used to describe the boundary (usually stationary) between Mediterranean air masses and the drier air of the Arabian Desert. Although it can occur throughout the year, it's a rarity in northwestern Saudi Arabia during the Southwest Monsoon. During transitions, both the northern and southern sections of the Middle East Peninsula are affected, but it appears to be confined to the northern half of the peninsula during the Northeast Monsoon.

This boundary can develop in three ways:

- by non-frontal incursions of cooler and moister (Mediterranean) air into the region
- from a stalled cold front during the Northeast Monsoon
- by a northward surge of the Monsoon Trough

Desert fronts are not usually easily located, since little or no sensible weather is associated with them. However, with the right trigger, they can become active weather producers.

Non-frontal cool and moist air masses normally only cause slight cooling of the Arabian Desert. Organized cumulus sometimes develops in the morning in the cool air (Figure 2-41). If the clouds remain long enough, they can be enhanced by upper-air disturbances or sea-breeze development near the coastlines. At other times, only contrasts in air temperature may be noticed. These can range from 18° to 27° F (10-15° C) in extreme cases during the Southwest Monsoon, but differences of 7° F (3° C) are more common.

Desert fronts don't persist for long. A surface low-pressure system passing through the region can produce a noticeable wind shift. Mediterranean air slides southward, with northwesterly flow behind the system moving

beneath the desert air mass. The Mediterranean air mass loses momentum and moisture in this process.

A stationary boundary indicated by a wind-shift line results, with cooler surface air temperatures to the north of the boundary line.

During the Northeast Monsoon, stalled cold fronts usually turn into desert fronts. The boundary is occasionally below the Subtropical Jet. Mid-level impulses passing over the front can cause it to become active and develop surface waves that track across the boundary, producing widespread cloudiness, rain, and thunderstorms. This condition occurred several times during Operation DESERT STORM. During extended fair weather periods, anticyclone development intensifies over North Africa and the south-central Mediterranean. It can increase low-level westerly flow into the area and may cause southeastward penetration by the Mediterranean air mass into the central Arabian Desert. There are pronounced air-mass differences between the Mediterranean and desert air, as reflected in temperatures and dew points.

"Non-frontal" type desert fronts appear during transition seasons over the southeastern Arabian Desert. The Indian Ocean segment of the surface Monsoon Trough migrates up to 300 miles (556 kilometers) through the Arabian Desert, bringing slightly cooler and moister air under the hot, dry desert surface air. Usually, very little cloud cover occurs along the "front" because strong subsidence dominates the mid- and upper-level flow pattern. But as shown in Figure 2-42, cumulus can be present, and there may be a subtle wind shift. This condition may, in fact, be the Omani Convergence Zone (OCZ), but lack of data and research in this sparsely populated region makes the meteorological pattern unclear.



Figure 2-41. Desert Front (dashed line) During October from an Incursion of Mediterranean Air. Note that the cumulus is to the north of the boundary.

SYNOPTIC DISTURBANCES



Figure 2-42. Desert Front (dashed line) During October from a Northward Surge of the Monsoonal Trough. The cumulus is to the south of the boundary.

SYNOPTIC DISTURBANCES

TROPICAL DISTURBANCES/CYCLONES.

Monsoon Trough convection organizes into intense tropical disturbances over the Arabian Sea and northern Indian Ocean, primarily during the transition months of May, October, and November. On rare occasions from June to September, a tropical disturbance propagates westward into the eastern Gulf of Aden and southeastern coasts of the Middle East Peninsula. One storm may provide the only summer rainfall for one or more successive seasons. Organized tropical squall lines in these waters are extremely rare during any month.

The surface Monsoon Trough is responsible for development of tropical cyclones as it moves north and south during transitions. A major source region for Arabian Sea tropical cyclones is located over the Indian Ocean near 11° N, 71° E. Some tropical cyclones form in the Bay of Bengal and move across southern India into the Arabian Sea.

Few hurricane-strength tropical cyclones make landfall west of 60° E. Most tropical disturbances reaching the region have only tropical storm or depression strength winds as strong coastal upwelling off the Omani coastline, along with vertical shearing, limits their development.

The Arabian Sea has about one tropical cyclone a year, but only one every 3 years makes landfall over the Arabian peninsula. Most cyclones move north into western India or Pakistan. When they move into the eastern Gulf of Aden, they propagate westward along the surface Monsoon Trough at 10-25 knots. Typically, heavy rain and high winds occur over the open Indian Ocean. Isolated showers and gusts to 30-40 knots embedded in a cyclone's cloud bands can affect the coastline. Figures 2-43a-c show tropical cyclone tracks for the Indian Ocean/Arabian Sea from 1891 through 1960.

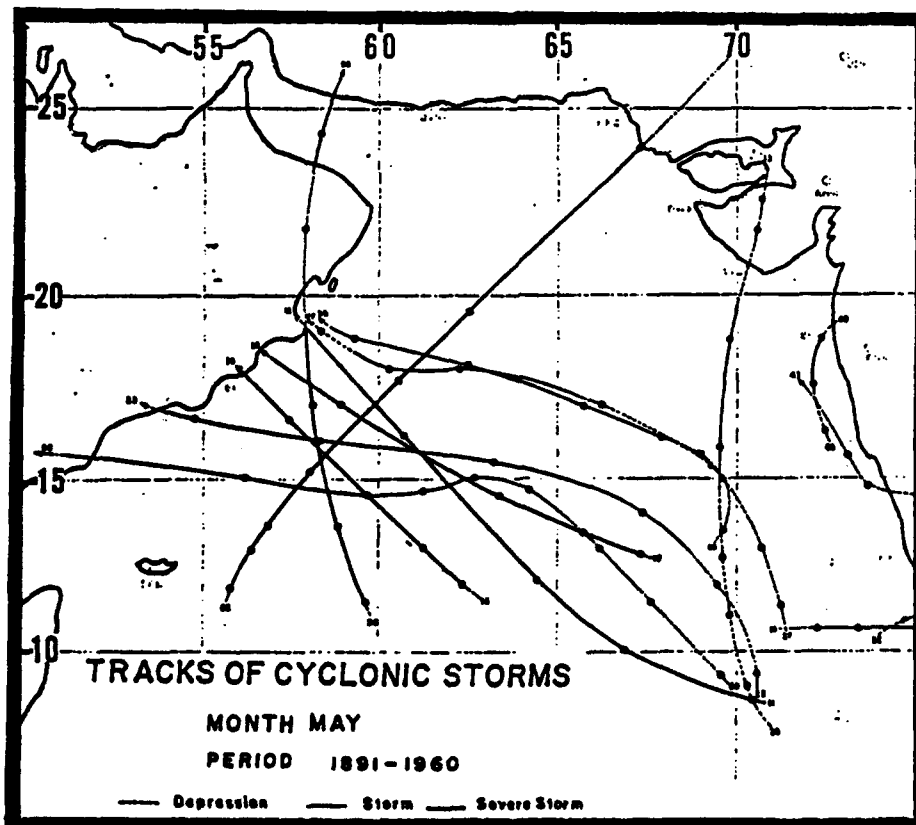


Figure 2-43a. May Tropical Cyclone Tracks, 1891-1960 (from Indian Meteorological Department, 1964).

SYNOPTIC DISTURBANCES

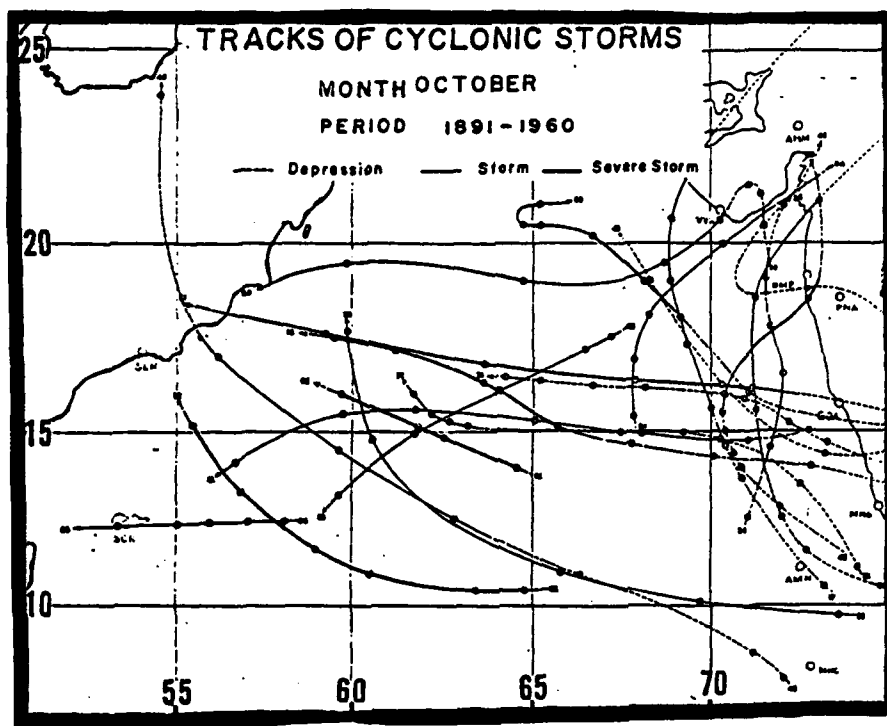


Figure 2-43b. October Tropical Cyclone Tracks, 1891-1960 (from Indian Meteorological Department, 1964).

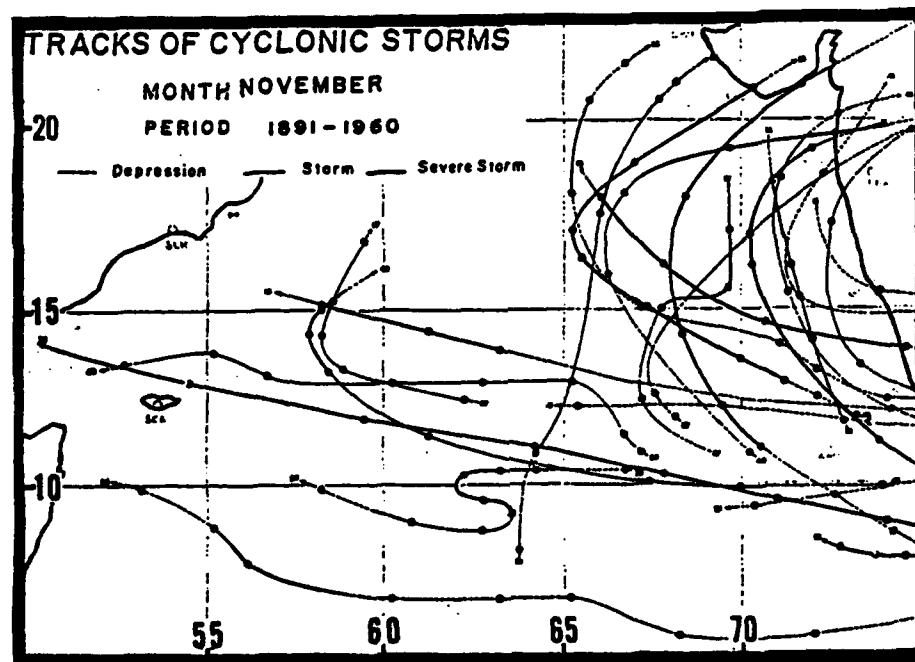


Figure 2-43c. November Tropical Cyclone Tracks, 1891-1960 (from Indian Meteorological Department, 1964).

SYNOPTIC DISTURBANCES

SUBTROPICAL CYCLONES. Also known as the "Monsoon Mid-Tropospheric Low", the subtropical cyclone (Figure 2-44) forms under several conditions at different times of the year in the Arabian Sea. Its circulation is strongest at mid-tropospheric levels. It has a cold core in the middle layers and a warm core aloft (tropical cyclones are warm core throughout). Latent heat release through deep convection may provide sufficient warming to create the appearance of a tropical cyclone circulation, and, given time, can change the low into a tropical cyclone.

The rare subtropical cyclones that develop in the northeast Arabian Sea between June and September are not frontal-type systems. These cyclones develop from downward penetration of a mid- or upper-level low. The pre-existing upper-level low is enhanced by interaction with an advancing upper-level trough in the westerlies. The Somali Jet may assist in initiating cyclonic curvature at 850 mb. These cyclones also occur in the Arabian Sea once or twice a year between November and early March. Deep polar surges may temporarily disrupt Northeast Monsoon flow, causing a subtropical cyclone to form in the wake of a migratory upper-level trough or cut-off low. The

circulation may become self-sustaining as it is gradually surrounded by warmer air. Movement is generally westward with the resumption of normal mid-level flow. Successive polar troughs prevent intensification. Some common characteristics of subtropical cyclones are:

- Subtropical cyclones are self-sustaining. Convection near the center produces a closed circulation. Maximum convergence occurs between 400 mb and 600 mb, the zone of steepest pressure gradients and strongest winds. Upward motion above this zone leads to condensation and deep convection, while descending motion below the convection is cooled by evaporation.
- Tradewinds prevail at the surface away from the center. A subsidence inversion forms over the trade winds. Trade-wind flow is disrupted at the surface closer to the center. The cyclone may or may not actually develop cyclonic circulation at the surface.
- Subtropical cyclones normally do not dissipate; successive upper-level troughs absorb them into the westerlies. Surface friction plays a limited role since they normally don't reach the surface and are normally over water.

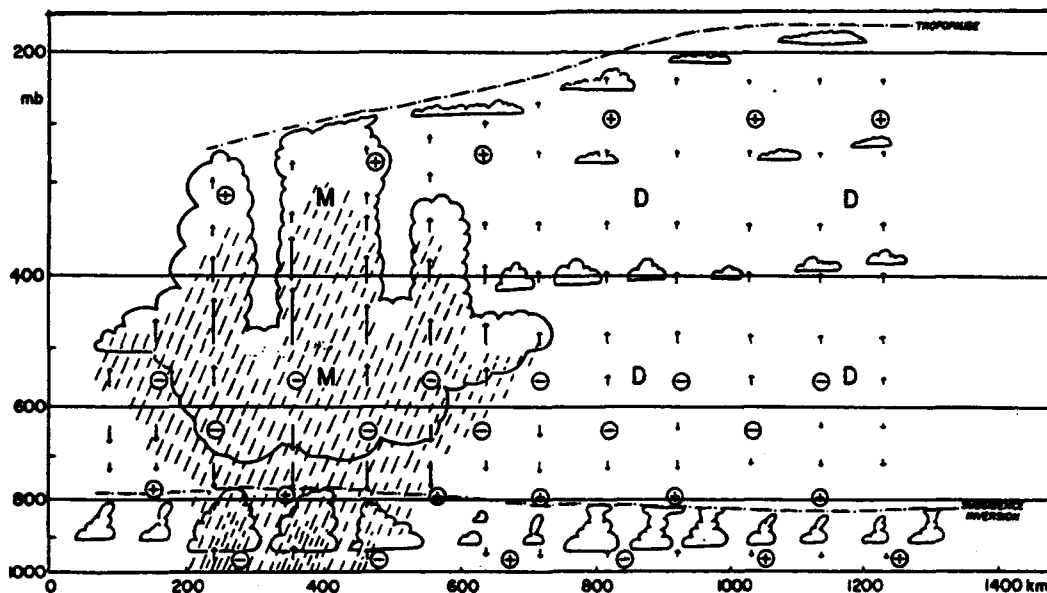


Figure 2-44. Vertical Cross-Section of a Subtropical Cyclone (from Ramage, 1974). Divergence is indicated by plus signs; convergence, by minus signs. Regions of vertically moving air undergoing dry adiabatic temperature changes are denoted by "D", and regions undergoing moist adiabatic temperature changes by "M".

REGIONAL WINDS

Local meteorologists and laymen commonly refer to the winds by their local names rather than by the synoptic conditions causing them. These surface winds produce moderate to severe duststorms, low visibility, and strong gusts over portions of the Middle East Peninsula. They affect areas ranging in size from 500 to 100,000 square NM. The following sections describe the common local winds and their causes. Gradient-level flow and typical synoptic weather patterns (i.e., low-pressure systems) can produce the same conditions.

ETESIAN winds are cool northerlies that cross Turkey and the Aegean Sea from mid-May through mid-September. Northerly flow turns to westerly or west-northwesterly along the southern slopes of the Taurus Mountains. Etesian winds enter the Ansariyeh Mountains, reaching Fertile Crescent locations such as Diyarbakir and Gizantep, Turkey, and Aleppo and Palmyra, Syria. The only distinction

between Etesian and gradient-level flow over the Fertile Crescent is air temperature within the mass surge. It is highly unlikely that true Etesian flow, and its cooler air temperatures, ever reach locations east of Aleppo and Gizantep. However, gradient-level and mean 850-mb flow patterns appear to have similar source regions.

Wind speeds average less than 15 knots, but if Etesian flow undergoes strong adiabatic warming over the Ansariyeh Mountains, speeds can exceed 70 knots. Highest surface wind speed at Palmyra, Syria, was 86 knots in August from the WNW; Aleppo's highest speed was 70 knots in June, also WNW. Severe duststorms accompany persistent Etesian flow. Affected areas include the Syrian Desert and the Tigris-Euphrates River Valley. Etesian flow can intensify gradient-level flow into the extreme western Persian Gulf. Figure 2-45 shows the area affected by the Etesians.

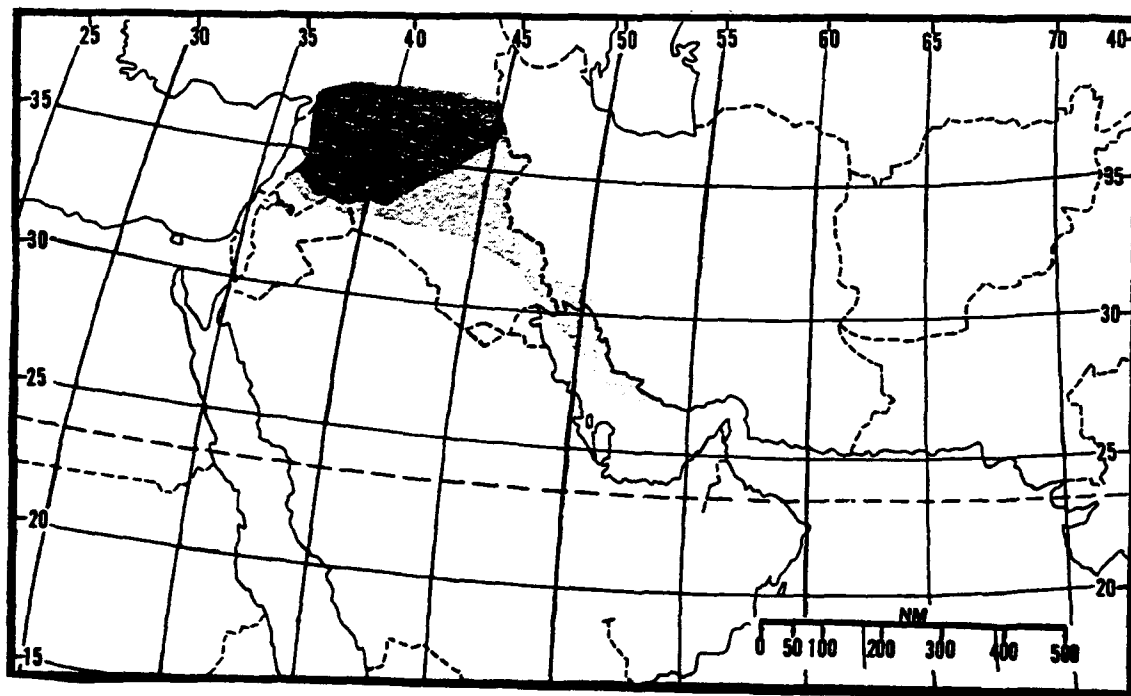


Figure 2-45. Areas Affected by Etesian Winds. The dark grey region represents the area where true Etesian wind flow occurs; the light grey shows areas downwind where Etesian winds can increase winds 10 to 15 knots. Little unmodified Mediterranean air will reach these areas.

REGIONAL WINDS

SHARAVS are hot, dry, dusty winds that occur with lows over the eastern Mediterranean Sea. They result from cyclonic activity, but the areas affected are confined to the southwestern/western Fertile Crescent and northwestern Arabian Desert. Transition periods, primarily May and October, have the highest occurrence of sharavs, which seldom occur from June to September.

The Sharav is not identified by direction--even though it's usually associated with east to southwest winds--but by relative humidity and temperature change. Sharavs are defined by a temperature increase of at least 9° F (5° C) and a relative humidity decrease of at least 25% from the mean of the previous 5 days. In the eastern foothills of the Anti-Lebanon Mountains, strong sharavs drop relative humidity below 20%. Sharav air temperatures often reach 104° F (40° C), and sometimes exceed 121° F (49° C).

Relative humidities can drop into the single digits.

Strong sharav conditions are most common with desert air moving northward in the warm sector of Atlas Lows or stalled Cyprus Lows over land (western Syria). Figure 2-46 depicts a typical track for surface low movement that generates Sharav conditions. The most severe Sharavs occur when the surface low moves due eastward over the Sinai Peninsula, then northeastward over the north Arabian Desert subregion.

Other synoptic conditions can produce sharav winds; for example, stationary highs along the north Arabian Desert subregion produce dry southeasterly desert flow. Severe duststorms at Damascus and Amman are rare, but often occur with Sharav conditions associated with a stagnant synoptic-scale fair weather pattern.

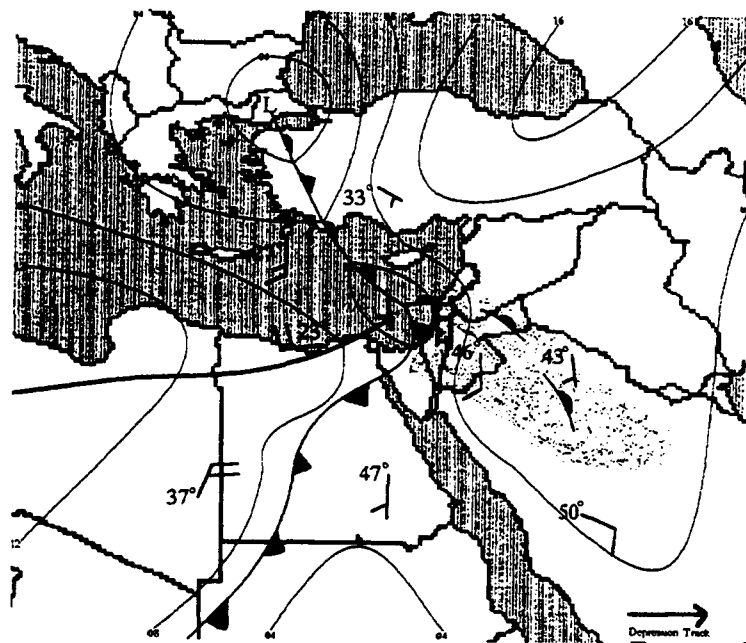


Figure 2-46. Active Storm Track for Sharav Conditions. The storm track is shown by the arrow. The speckled area represents strong southerly flow where the most severe Sharav conditions occur. Temperatures are °C.

REGIONAL WINDS

KHAMSIN. The Arabic term "Khamsin" means "fifty," and refers to the 50 days after Coptic Easter, the period when this hot and dry southerly wind commonly occurs. In Saudi Arabia, the khamsin is called the "Aziab." Although it can occur anytime between February and June, the highest frequency of occurrence is during March and April. Khamsin conditions (hot, extremely dry, southerly surface winds, low visibility, and thick dust) develop when Atlas Lows move eastward over the dry Sahara. The Red Sea Coastal Plains and extreme western Arabian Desert subregions are most often affected.

During intense khamsin conditions, winds average 20-30 knots ahead of the front, and 15-30 knots behind. Air temperature can drop 20° F (8° C) behind the cold front; relative humidities rise from 10-15% to 25-30%. Khamsins last 1 to 3 days, but slow-moving Atlas Lows may produce widespread dust that persists for up to 10 days.

Visibilities are from 1/4 to 3 miles, varying diurnally and seasonally. Turbulent mixing keeps visibilities low in the daytime. Several hours after sunset, rapid cooling at the surface normally stabilizes the lower atmosphere, forming a radiation inversion and capping off the airborne dust; visibilities improve to 3-6 miles. Extremely strong frontal boundaries, with wind speeds greater than 30 knots, prevent the formation of a strong radiation inversion. Winter khamsin duststorms are less severe than in the spring or early summer.

"True" khamsin conditions occur within an elongated oval area located parallel to the cold front (the shaded area under the low in Figure 2-47a). Egyptian meteorologists define a "true" khamsin condition as "any low-pressure system that approaches Cairo from the west to southwest, producing 15 to 25 knot southeasterly surface winds."

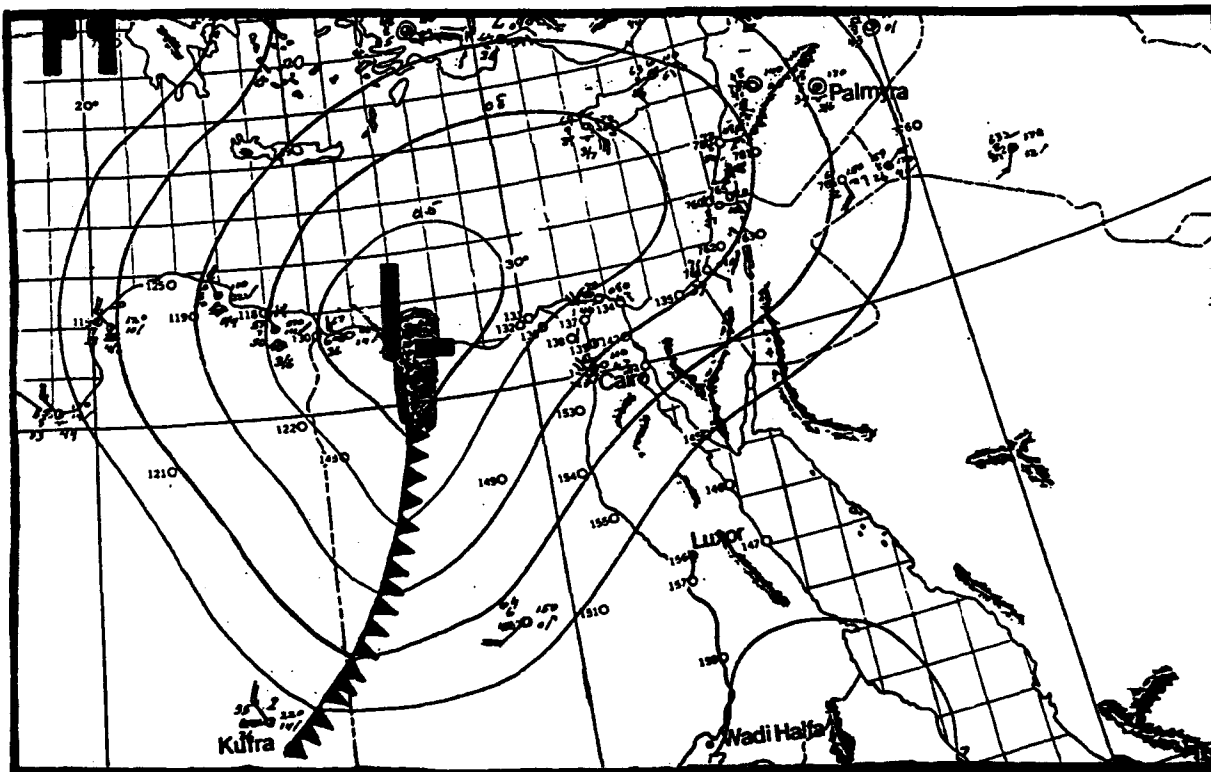


Figure 2-47a. Typical Low Pressure System Storm Track Producing Khamsin Conditions. The area of "true" khamsin conditions is shown by the shaded oval under the low.

REGIONAL WINDS

The northwesterly flow behind the front produces the widespread duststorm activity shown in Figure 2-47b, but that area is not a

"true" khamsin. Visibilities average 1 to 4 miles in the cold sector of the low pressure system.

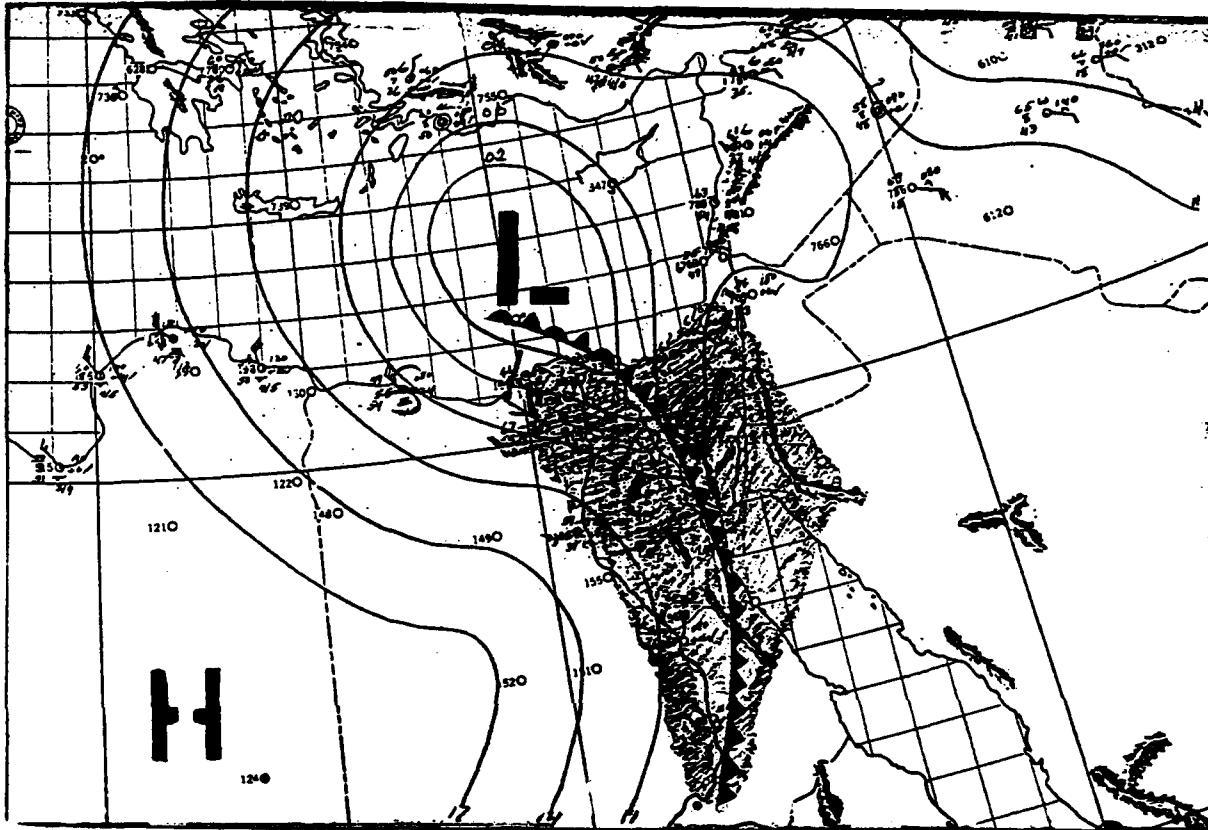


Figure 2-47b. Typical Northeast-Moving Storm Track Producing Widespread Dust. West-northwesterly flow behind the cold front produces widespread dust. This synoptic situation also refers to the Khamsin, but cool northwesterly flow behind the front is not the "true" Khamsin condition.

Deep, slow-moving Atlas Lows moving eastward over the central Sahara (Figure 2-48) produce "embedded" khamsin conditions. The shaded areas are those with widespread dust and 3- to 6-mile visibilities. Soil conditions determine the

actual size of this area. Typically, lowered visibility in dust is less severe to the north of the low. If the Atlas Low turns northeastward at 30° E, southeasterlies concentrate and intensify the khamsin conditions along the Tokar Gap.

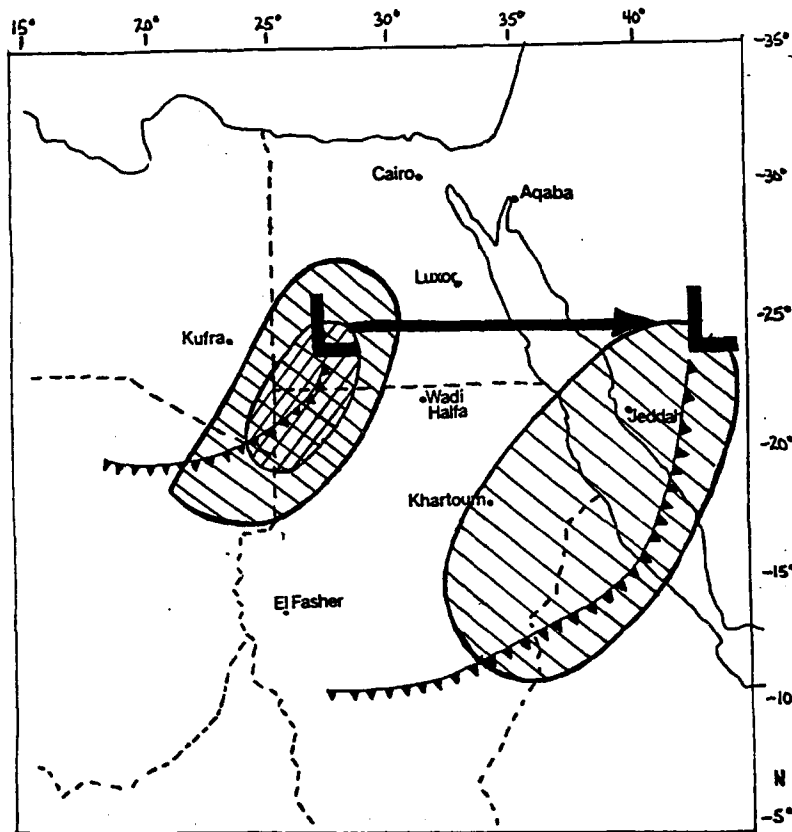


Figure 2-48. Khamsin-Type Conditions Associated With a Rare Eastward-Moving Atlas Low. Cross-hatched zone represents "true" Khamsin conditions (greater than 15-knot winds) and hatched areas denotes widespread duststorm activity.

SHAMAL means "north" in Arabic. It refers to any northerly wind in the Persian Gulf Coastal Plains, Fertile Crescent, and Arabian Desert subregions. Shamal winds may occur at any time of the year, but highest frequencies of strong northwesterly flow occur between October and February.

The **40-day Shamal** is a summertime phenomenon that routinely occurs from early June to mid-July. It is rarely interrupted. Winds average 10-15 knots, but sustained 30-knot winds may last 3-7 days. This wind can be intensified by a mass "surge" in Etesian surface flow, probably caused by the combination of weak leeside troughing in the Persian Gulf and changes in the synoptic-scale, gradient-level flow. The 40-day Shamal normally develops

along the north rim of the Persian Gulf Coastal Plains, the southern Tigris-Euphrates River Valley, and is much less frequent in the extreme western Gulf of Oman and Makran Coastline (see Figure 6-1). Dust and sand may reduce visibilities along the northern rim of the Persian Gulf Coastal Plains to less than 1 mile.

The **3- to 5-day Shamal** normally occurs from December-to-April and is caused by strong northwesterly flow due to a stagnating 500-mb shortwave or an established longwave trough.

The **24- to 36-Hour Shamal** commonly occurs between November and April with fast-moving cold fronts and superimposed shortwave troughs. After the frontal passage, northwesterlies occasionally reach 35-40 knots.

REGIONAL WINDS

KAUS is the name given to a southerly or southwesterly wind that sometimes occurs ahead of a shamal. The Kaus is usually associated with a surface low. Speeds can reach up to 30 knots with this wind. Southerly flow can raise temperatures and intensify the effect of approaching Shamals.

HABOOBS are strong winds with sandstorms or duststorms produced by individual thunderstorms or squall lines. The name is from the Arabic "habb" meaning "wind." Convective downbursts, microbursts, and outflow boundaries produce walls of dust and debris in advance of the storm cell and precipitation. These walls may be several hundred feet high and 1-2 NM across.

Haboobs mainly occur in the Arabian Desert during the late Northeast Monsoon and April-May transition period when outbreaks of thunderstorms are most likely.

Weather in a haboob is severe. Visibilities are usually less than 1/8 NM within the wall of dust. Winds average 25 to 50 knots, with higher gusts. Suspended dust has been observed at over 15,000 feet (4,570 meters). Normal thunderstorm hazards are present. Rainfall actually improves visibility as heavy rain removes the dust.

MESOSCALE AND LOCAL EFFECTS

DUSTSTORMS. Given the right conditions, duststorms dominate terrain below 4,000 feet (1,220 meters) MSL. They occur in the Syrian Desert, the An Nafud Desert, and the Tigris-Euphrates River Valley more frequently than in other locations. During Operations DESERT SHIELD and DESERT STORM, most storms originated in the salt and sand basins along the Tigris-Euphrates River Valley, but they can occur anywhere in the region because of the extremely dry conditions throughout the Middle East Peninsula. Figure 2-49 shows the primary duststorm sources in the study area.

Duststorms carry suspended particles over large distances, often reducing visibility to less than

30 feet (10 meters). Season of occurrence, wind direction, amount of particulate matter, and duration vary by locality. A February 1991 observation reported blowing rocks.

Large-scale duststorms often persist for 1 or 2 days before a frontal passage (such as with an Atlas or Cyprus Low) or with synoptic scale squall lines. Mesoscale squall lines may reduce visibility to less than 1/2 mile for several minutes to an hour along sandy coastlines or in the interior desert regions. Sandstorms differ from duststorms only in the size of the suspended particles. Since sand is heavier, it is seldom raised to more than 3-6 feet (1-2 meters) above the ground; particles settle quickly.

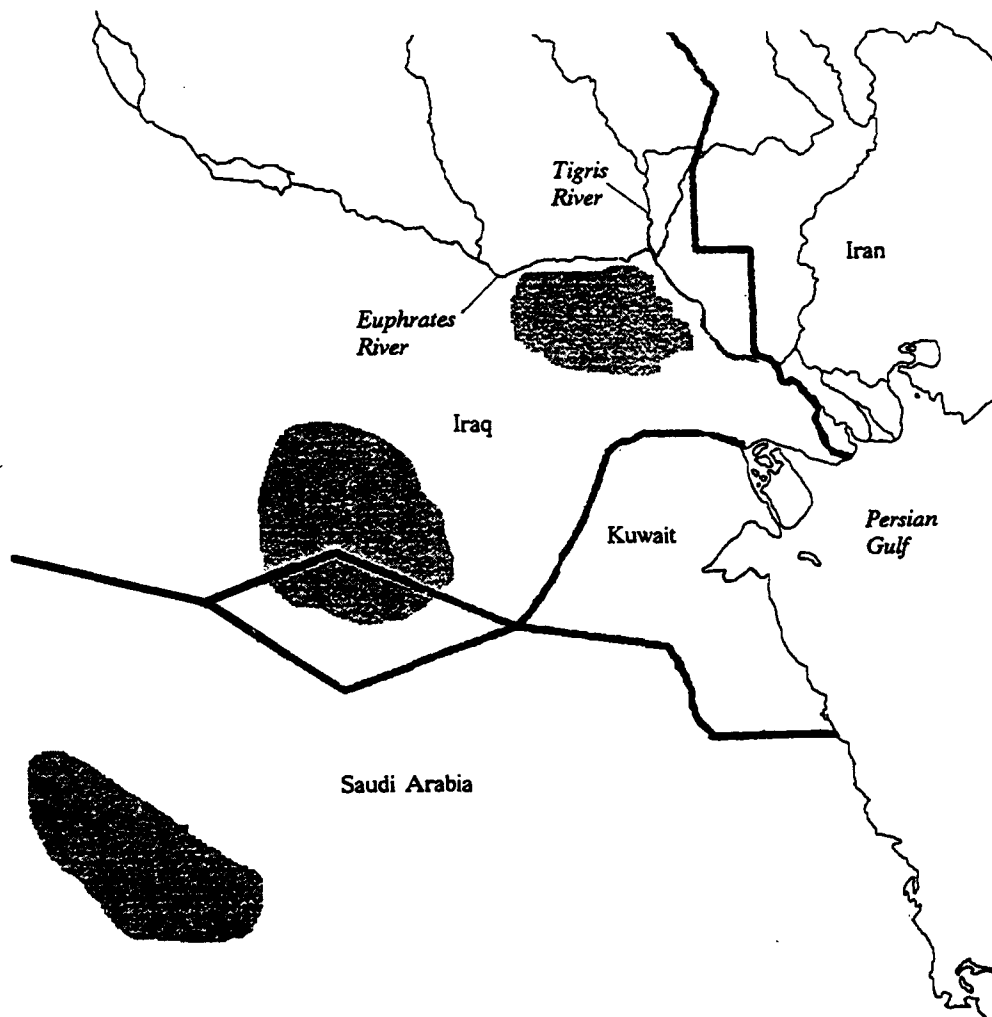


Figure 2-49. Primary Duststorm Source Areas. The three shaded areas are primary source regions for duststorm development.

MESOSCALE AND LOCAL EFFECTS

Surface temperature inversions tend to dampen turbulent mixing in the lowest layers and reduce the effects of duststorms from day to day. Inversions usually break down several hours after sunrise, allowing turbulent mixing in the lowest layers; however, large-scale synoptic disturbances may override the nocturnal duststorm minima. Winds of 15-20 knots are normally sufficient to lift dust, but speeds as low as 10 knots can produce duststorms.

The origin and nature of duststorms depend on general synoptic conditions, local surface conditions, and diurnal/seasonal considerations, as shown below. Figure 2-49 shows the areas of primary duststorm sources.

Synoptic Conditions.

Active cold fronts. Between November and April, duststorms may develop with frontal passages. Wind gusts of 15-20 knots are enough to lift dust. It's not uncommon for Atlas Lows to carry Saharan dust into the Arabian Desert and Fertile Crescent subregions. Severe duststorms occur with shamal winds.

Convective activity. Convection produces local cumulus downdrafts up to 30 knots. Squall lines organize over a larger area, producing cloud bands up to 100 NM long and from 10 to 20 NM wide. Visibilities can be greatly reduced within minutes. Convective activity and duststorms most frequently occur together along the southern Red Sea Coastal Plains and Fertile Crescent subregions.

Northward oscillation in the surface Monsoon Trough. Between mid-June and early September, strong southwesterly flow through the Tokar Gap funnels large amounts of dust into the Red Sea Coastal Plains and western Arabian Desert subregions. Sustained periods (12-36 hours) of strong southwesterly flow reduce visibilities to less than 3 miles between Port

Sudan and Assab. When southwesterlies weaken to 10-15 knots (normal levels), a thin dust haze with 4-7 mile visibility may persist for several weeks.

Stagnant transitory high surface pressure. The Saharan and Saudi Arabian Highs normally strengthen over the subtropics during extended fair-weather periods between November and March. Only a 4-6 mb/10 degrees of latitude surface pressure gradient is necessary to generate a dust-laden surface wind. These can produce severe and widespread duststorm activity and are the most difficult to forecast. Although the situation is easy to recognize, the precise location (timing/areal extent) and severity of occurrence is difficult due to a lack of data. Stagnant air aloft provides little ventilation to remove the dust.

Local Surface Conditions.

Soil type and condition control the amount of particulate matter that can be raised into the atmosphere. Dry sand or silt, for example, is easily lifted by a 10-15 knot wind. Thin haze is a persistent feature of the Middle East Peninsula between April and October as weak winds aloft provide poor ventilation. Large areas of loose silt or sand from the Tigris-Euphrates River Valley, Makran Coast and the entire Red Sea Coastal Plains subregion can be suspended by a strong sea breeze or synoptic flow and last for several hours to several days. Salt and moisture haze is very common in the Persian Gulf because of stagnant synoptic conditions and poor ventilation; visibility is frequently between 4 and 7 miles. Large soil particles quickly settle to the surface, while finer particles remain suspended in the atmosphere for days at a time. Fine dust, sand, salt, or silt may travel hundreds of miles from its source. Distant, large-scale sources of material provide most of the air borne debris over the Red Sea.

MESOSCALE AND LOCAL EFFECTS

Seasonal Considerations.

November to March. Thin dust and haze are the most frequently observed restrictions to visibility. Several weeks of fair weather allows surface heating and sea breezes to accumulate fine silt into the air. Duststorms associated with frontal boundaries are uncommon, but severe; visibility can be 1-3 miles over large areas. Atlas and Cyprus Lows with khamsin and shamal winds cause sustained 20-knot surface winds for 3- to 9-hour periods. Low visibilities may occur with abnormally strong Northeast Monsoon flow (15-25 kt) in the Rub al Khali Desert or southern Red Sea, as well.

April to October. Atlas Lows in late April produce most of severe synoptic-scale duststorms. Sea breezes and daytime thermal heating are the usual causes for meso- and micro-scale duststorm activity during this period.

Diurnal Considerations.

Daytime. Hot and dry surface conditions in June, July, and August across the region produce localized dust and haze. Persistent dryness raises dust to 10,000 feet (3,050 meters) MSL; it can remain suspended for days or weeks. The lowest visibilities occur in mid-morning after the inversion and turbulent mixing raises the dust. They can remain low through the afternoon.

Nighttime. Cooler surface temperatures result in stability; turbulent mixing is minimized. Dust settles beneath the inversion layer throughout the night; visibilities improve to 4-7 miles and are best between 2000 and 0600L.

DUST DEVILS are, in effect, cloudless miniature tornadoes set off by intense summer heating. Diameters range from 10 to 300 feet (3-91 meters); heights can extend to 2,000 feet (610 meters). Dust devils may last for 1 to 15 minutes. They occur most frequently along the sandy coastal zones of the Red Sea and the interior deserts of Saudi Arabia. Wind speeds

are normally between 10 and 25 knots, but some are strong enough to flatten huts.

HAZE is widespread throughout the Middle East Peninsula. During August and September of Operation DESERT SHIELD, pilot reports consistently included remarks of a haze layer in the Arabian Desert that extended to 17,000 feet and had a "boiling" appearance. Both horizontal and slant-range visibilities were reduced. British pilots have reported similar conditions northeast of Aden. The boiling appearance was thought to be caused from thermal updrafts produced by intense surface heating.

MOUNTAIN/VALLEY WINDS develop with fair skies and light and variable synoptic flow. They are a site-specific mesoscale phenomena, common in the Ethiopian and, Yemen Highlands, as well as the Anti Lebanon (Lebanon), Ansariyeh (Syria), Hajar (Oman), Taurus (Turkey), and Zagros (Iran) mountain ranges. Typically, mid- and upper-level subsidence limits regular diurnal convection over these ranges; however, shallow diurnal convection may occur at the mesoscale due to the mountain/valley circulation. There are two types of terrain-induced winds, the mesoscale mountain/valley wind and the localized, microscale "slope" (upslope/downslope) wind. The key differences lie in their temporal and spatial scales.

Mesoscale Mountain/Valley Winds average 6-12 knots. Daytime valley winds (Figure 2-50a) are strongest, averaging 10-15 knots between 650 and 1,300 feet (200 and 400 meters) AGL. Nighttime mountain winds (Figure 2-50b) average only 3-7 knots at the same level. Deep valleys develop more nocturnal cloud cover than shallow valleys because nocturnal air flow convergence is stronger. The mesoscale mountain/valley circulation has a maximum vertical extent of 6,560 feet (2,000 meters) AGL, depending on valley depth and width, the strength of prevailing winds in the mid-troposphere, and the breadth of microscale slope winds.

MESOSCALE AND LOCAL EFFECTS

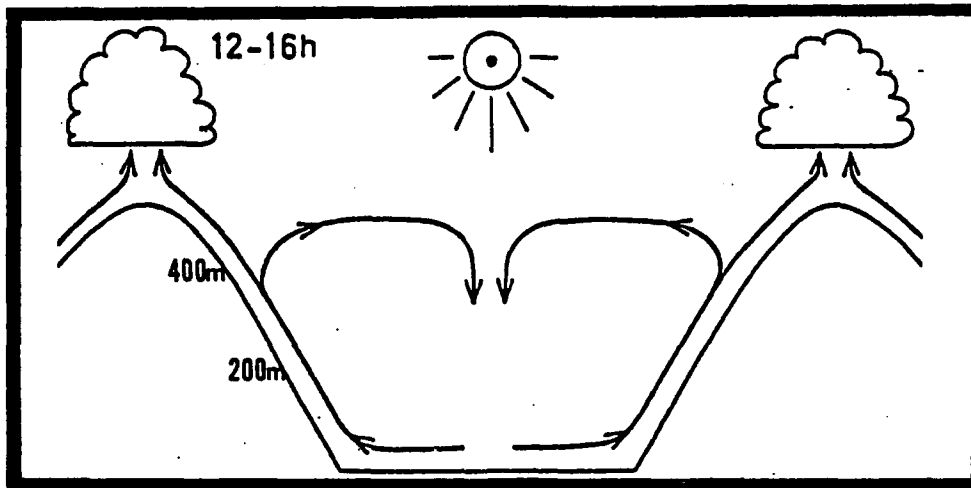


Figure 2-50a. Typical Daytime Mountain/Valley Circulation (from Flohn, 1969).

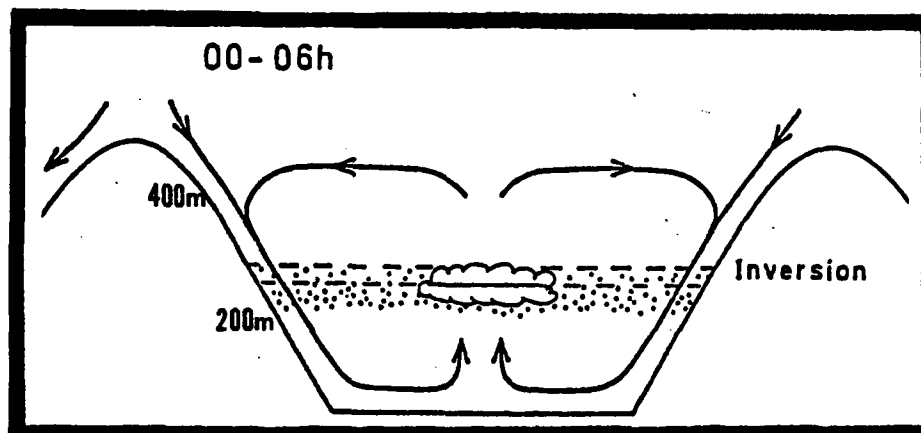


Figure 2-50b. Typical Nighttime Mountain/Valley Circulation (from Flohn, 1969).

Microscale Slope Winds develop along the surface boundary layer (0-500 feet/0-152 meters AGL) of mountains and large hills. Mean daytime upslope wind speeds are 6-8 knots; mean nighttime downslope speeds are 4-6 knots. These speeds are found at elevations no higher than 130 feet (40 meters) AGL. Downslope mountain winds are strongest between

November and March; upslope valley winds are strongest between April and October. Upslope winds are strongest on slopes with southern exposures. Figures 2-51a-h (from Geiger, 1961) show the life cycle of a typical mountain/valley wind circulation. The light arrows represent microscale circulation; the dark arrows, mesoscale circulation.

MESOSCALE AND LOCAL EFFECTS

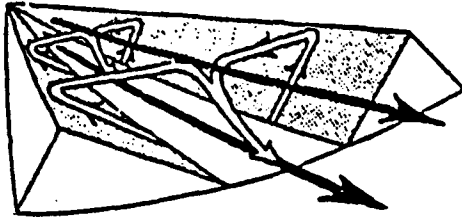


Figure 2-51a. Mountain/Valley Circulation—SUNRISE. Sunshine almost immediately generates upslope wind development, but the downslope mountain wind persists because mesoscale flow overrides microscale flow. Generally, the transition between Figures 2-51a and b is 0700-1000L, but local terrain determines how soon sunlight can start the microscale upslope wind, which is not fully developed until the entire valley surface is heated enough to stop the mesoscale downslope mountain wind.

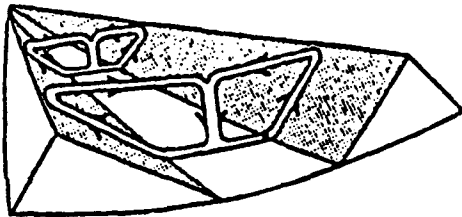


Figure 2-51b. Mountain/Valley Circulation—LATE MORNING. Widespread surface heating continues to generate microscale upslope flow, cutting off any downslope mountain circulation.

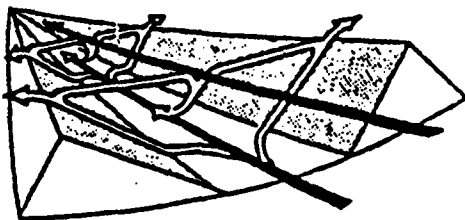


Figure 2-51c. Mountain/Valley Circulation—MIDDAY. Sunshine covers the entire valley floor; upslope flow feeds valley circulation.

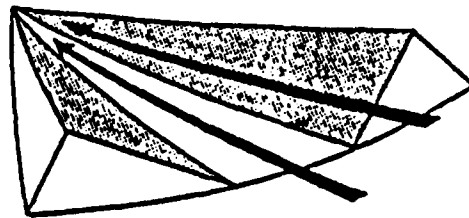


Figure 2-51d. Mountain/Valley Circulation—LATE AFTERNOON. East-facing slopes begin to cool; upslope flow weakens.

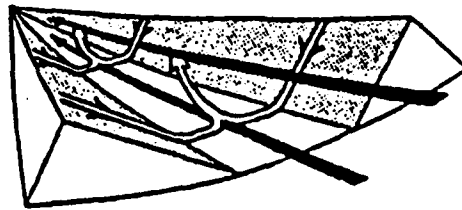


Figure 2-51e. Mountain/Valley Circulation—SUNSET. Although microscale downslope wind components dominate the surface boundary layer, mesoscale upslope valley flow retains weak momentum.

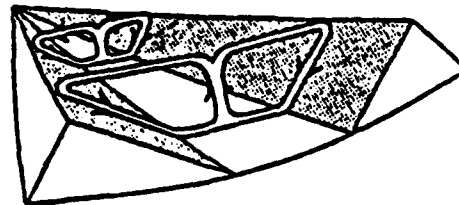


Figure 2-51f. Mountain/Valley Circulation—LATE EVENING. Downslope winds dominate.

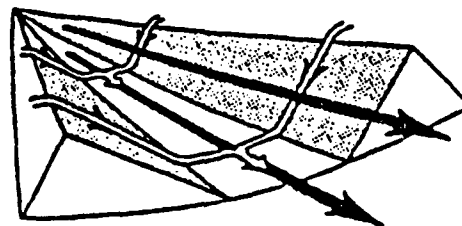


Figure 2-51g. Mountain/Valley Circulation—MIDNIGHT. Downslope winds feed the mountain circulation.

MESOSCALE AND LOCAL EFFECTS

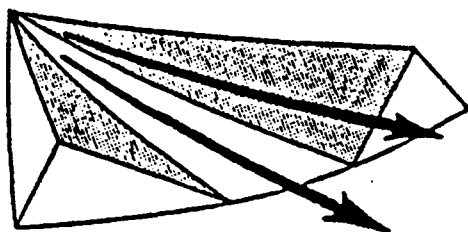


Figure 2-51h. Mountain/Valley Circulation--PRE-DAWN. Winds are calm just before surface heating begins at the microscale; the mesoscale downslope mountain circulation retains its momentum. Microscale downslope winds end just before sunrise; upslope winds begin again at first light.

Orographic lifting may accentuate mesoscale mountain/valley convergence above 6,000 to 7,000 feet (1,830-2,134 meters), producing short-lived convective cells. A mountain/valley circulation supported by the Monsoon Trough occurs between Port Sudan and Assab (see Figure 3-1). The orographic lifting produces heavy convection every day between June and August above 8,000 feet (2,439 meters) MSL; convection and light precipitation occasionally move over the coastal plains. The Taurus and Zagros Mountains produce extensive lifting, cloud cover, and heavy precipitation between November and April. In the Persian Gulf, terrain-induced leeside troughing is common between June and September. Downslope winds from the Zagros help form the feature. On rare

occasion, downslope winds are greater than 70 knots.

The most evident example of mountain/valley circulation, land/sea breeze, and synoptic flow interaction in the Middle East Peninsula occurs along the Persian Gulf Coastal Plains during the Northeast Monsoon. Winds shift with respect to time of day and mountain/valley circulation because synoptic flow is weak. East of the Strait of Hormuz, north or northwesterly airflow descending the Zagros Mountains dominates. Surface winds from the Strait of Hormuz to Ras Hadd are occasionally southwesterly because of Akhdar Mountain winds. However, the transition from light and variable winds, to gusty northeasterly winds south of Ras Hadd can be abrupt.

Mountain inversions develop when cold air builds up along wide valley floors where nighttime downslope wind convergence is weak. The cold air descends from the slopes above the valley at 8-12 knots, but loses momentum when it spreads out over the valley floor. By the time the downslope flow from both slopes can converge, wind speeds average only 2-4 knots. The cold air replaces warm, moist valley air at the surface and produces a thin smoke and fog layer near the base of the inversion. First light initiates upslope winds by warming the cold air trapped on the valley floor. Warming of the entire boundary layer commences near the 500-foot (152-meter) level AGL.

MESOSCALE AND LOCAL EFFECTS

MOUNTAIN WAVES. Between December and March, occasional mid-and upper-level troughs in the westerlies may produce mountain-waves over and in the vicinity of the Taurus, Anti Lebanon, and Zagros Mountains; and the Ethiopian and Yemen Highlands. Mountain-wave turbulence is usually moderate to severe. Criteria for mountain wave formation includes sustained winds of 15-25 knots with wind flow oriented within 30 degrees of perpendicular to the ridge. Waves develop when air at lower levels is forced up over the windward side of the ridge.

Wavelength amplitude is dependent on wind speed and lapse rate above the ridge. Light

winds follow the contour of the ridge with little displacement above and rapid damping beyond. Stronger winds displace air above the stable inversion layer; upward displacement of air can reach the tropopause. Downstream, the wave propagates for an average distance of 50 times the ridge height. Rotor clouds form when a core of strong wind moves over the ridge, but does not exceed 1.5 times the ridge height. Rotor clouds indicate the strongest turbulence, and are more common in the Zagros and Taurus Mountains. These clouds, which warn of mountain waves, may not form in dry regions. Figure 2-52 shows a fully developed lee wave system.

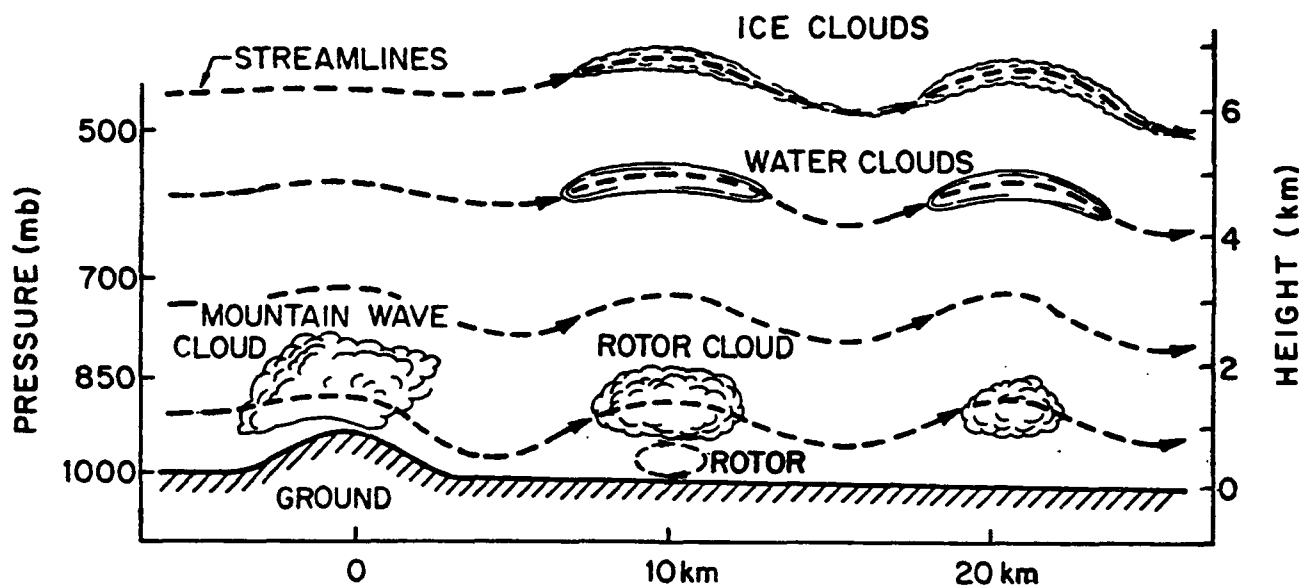


Figure 2-52. Fully Developed Lee Wave System (from Wallace and Hobbs, 1977).

MESOSCALE AND LOCAL EFFECTS

INVERSION DOWNBURST WINDS form in coastal terrain with a 20-foot/mile or greater slope when a sea breeze exceeds 15 knots and there is an inversion aloft. Figure 2-53 shows a typical cycle for downburst winds. Arrows represent direction of airflow. As the sea breeze becomes trapped between the base of the inversion and the sloping terrain, the air begins to "bulge" the inversion base. A sufficiently large "bulge" breaks down the inversion layer allowing the downward flow. Downburst wind

last 15-45 minutes, and reach speeds of 90% of the gradient flow immediately above the inversion. The descending air produces roll vortices and potentially severe local dust/sandstorms along the coast. Visibility may be reduced to less than 1 NM, depending on local surface soil conditions. Downburst winds end when the inversion is reestablished. They are common along the Persian Gulf and southern Red Sea.

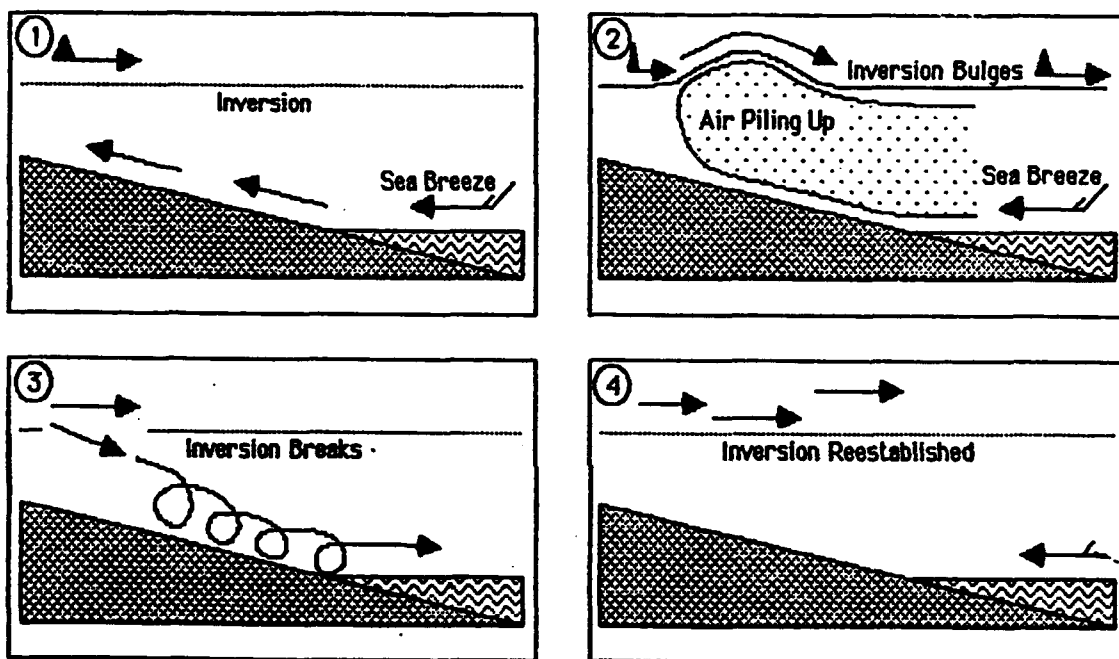


Figure 2-53. Downburst Inversion Sequence. Discussion and figures are provided through the courtesy of MSgt Melody Higdon, 7th Weather Wing, 1989.

MESOSCALE AND LOCAL EFFECTS

SAND STREETS. Vast longitudinal dune formations create localized wind circulations on the Middle East Peninsula. The average longitudinal dune in the Arabian Desert measures 60 to 160 feet (20-50 meters) high and 330 feet (100 meters) wide dunes vary from 1,000 feet (305 meters) to 100 NM in length, and are roughly 1 1/4 NM apart. The sand street develops along the dune crest. The three-dimensional circulation pattern is depicted in Figure 2-54. The roll vortex diameter

approximates the thickness of the boundary layer. Figure 2-55 is a cross-sectional view of airflow over successive dunes. For sand streets to form, there should be little variation of wind direction with height, above average wind speeds, unstable lapse rates near the surface, and an inversion above the convective layer. Roll vortices parallel the prevailing airflow and converge over the dune crests. They normally don't produce clouds because the air is extremely dry.

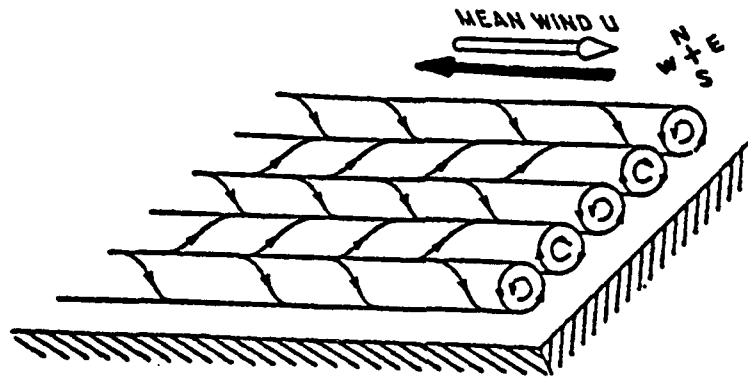


Figure 2-54. Three Dimension View of Longitudinal Vortices in the Boundary Layer (from Hanna, 1969). Southeast winds (DARK ARROW) may also develop roll vortices but northwest flow (LIGHT ARROW) is more common.

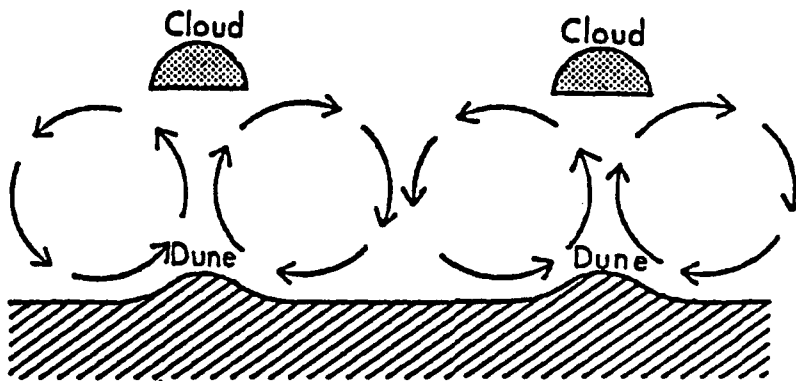


Figure 2-55. Cross-Sectional View of Dune and Cloud Formation Mechanism (from Hanna, 1969). Cloud formation is unlikely because boundary layer air is normally extremely dry.

MESOSCALE AND LOCAL EFFECTS

LAND/SEA BREEZE. Differential surface heating along the coasts generates this diurnal phenomenon. The marine boundary layer rarely extends above 3,000 feet (915 meters) AGL or 15 NM inland unless modified by synoptic flow. Two types of land/sea breezes are found in the Middle East Peninsula: *common* and *frontal*.

"Common" land/sea breezes affect all coastal areas of the Middle East Peninsula. Prevailing local sea breeze wind directions along the western Gulf of Oman, northern Gulf of Aden, and southern Red Sea can vary from the monsoonal wind direction by 45 degrees or more. Figure 2-56 illustrates the "common" or land/sea breeze circulation under calm conditions with no topographic influences and a uniform coastline. Onshore (A) and offshore (B) flow intensifies in proportion to daily heat exchanges between land and water. Common land/sea breezes normally reverse at dawn and dusk.

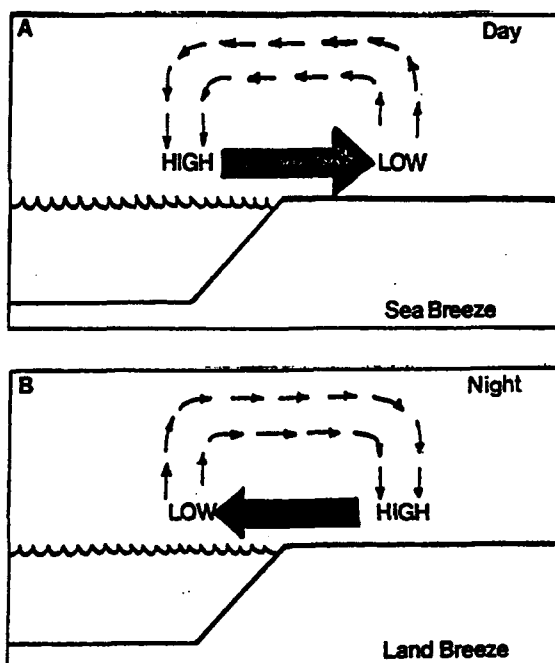


Figure 2-56. The "Common" Daytime Sea Breeze (A) and Nighttime Land Breeze (B). Thick arrows represent pressure gradient and direction of flow.

"Frontal" land/sea breezes are the product of the "front" between the land and sea air masses. The transition for wind reversal is delayed by 1 to 4 hours because gradient flow prevents the sea breeze boundary layer or "front" from moving ashore. Figure 2-57a-f shows a typical "frontal" land/sea breeze sequence. Solid blocks denote the land surface, while dashed lines represent water. Vertical lines show the sea-breeze boundary layer and arrows represent wind circulation.



Figure 2-57a. Gradient Flow With Offshore Wind Component Slopes Gently Over Dense, Cooler Marine Boundary Layer. Shearing action along the "front", or land/sea air mass interface, compacts the layer. Gradient flow strength determines the magnitude of compacting.



Figure 2-57b. Increased Compacting Tightens Pressure Gradient Along Land/Sea Interface. If the gradient is weak, land surfaces heat rapidly. As a result, the surface-pressure gradient and winds resemble those in Figure 2-57a.



Figure 2-57c. Maximum Compacting of the Marine Boundary Layer. At this instant, the surface winds inside the marine boundary layer shown onshore direction. The marine layer surface flow may take several hours to reach the coast. Momentum accelerates wind speed with time.



Figure 2-57d. Frontal Sea Breeze Accelerates Towards Shore. Initial "frontal" sea breezes may sustain 20-knot winds for 15-45 minutes.

MESOSCALE AND LOCAL EFFECTS



Figure 2-57e. Sea Breeze "Front" Reaches the Coast. Note the increased depth of onshore flow in the marine boundary layer. Compare with Figure 2-57c.



Figure 2-57f. Land/Sea Breeze Mechanism in Full Swing. Offshore flow aloft, onshore flow at surface.

Topography that lies perpendicular to coastlines modifies the land/sea breeze in several ways. Orographic lifting induces sea-breeze stratiform/cumuliform cloudiness and deflects surface winds. The mesoscale mountain circulation accelerates the land breeze over open water. Elevated coastal topography produces steep nocturnal temperature gradients. Strong offshore gradient flow produces the frontal land/sea breeze. The north Ethiopian Highlands and the Yemen Mountains modify the land/sea breeze. On a smaller scale, Northeast Monsoon flow through the Strait of Bab al Mandab modifies the land/sea breezes.

Coastal configuration also has an effect on land/sea breezes. Coastlines perpendicular or parallel to synoptic flow maximize and minimize sea breeze penetration, respectively. Hot, dry land surfaces along the coastlines of the Middle East Peninsula significantly modify the moist onshore flow within 20 NM of the coast. Without significant orographic lifting, sea breeze cumulus rarely develops beyond the immediate coastline.

MESOSCALE AND LOCAL EFFECTS

WET-BULB GLOBE TEMPERATURE (WBGT) HEAT STRESS INDEX. The WBGT heat stress index provides values that can be used to calculate the effects of heat stress on individuals. WBGT is computed by using the formula:

$$\text{WBGT} = 0.7\text{WB} + 0.2\text{BG} + 0.1\text{DB}$$

where: WB = wet-bulb temperature
BG = Vernon black-globe temperature
DB = dry-bulb temperature

A complete description of the WBGT heat stress index and the apparatus used to derive it is given in Appendix A of TB MED 507, *Prevention, Treatment and Control of Heat Injury*, July 1980, published by the Army, Navy, and Air Force. The physical activity guidelines shown in Figure 2-58 are based on those used by the three services. Note that the wear of body armor or NBC gear adds 10° F to the WBGT; activity should be adjusted accordingly.

WBGT (°F)	WATER REQUIREMENT	WORK/REST INTERVAL	ACTIVITY RESTRICTIONS
90-up	2 quarts/hour	20/40	Suspend all strenuous exercise.
88-90	1.5-2 quarts/hour	30/30	No heavy exercise for troops with less than 12 weeks hot weather training.
85-88	1-1.5 quarts/hour	45/15	No heavy exercise for unacclimated troops, no classes in sun, continue moderate training 3rd week.
82-85	.5-1 quart/hour	50/10	Use discretion in planning heavy exercise for unacclimated personnel.
75-82	.5 quart/hour	50/10	Caution: Extremely intense exertion may cause heat injury.

Figure 2-58. WBGT Heat Stress Index Activity Guidelines.

Figures 2-59a-d give average maximum WBGTs for January, April, July, and October. They were traced from the full-color WBGT charts in *Global Climatology for the Wet-Bulb Globe Temperature (WBGT) Heat Stress Index*, U.S.

Army Research Institute of Environmental Medicine Natick MA 01760-5007. See also USAFETAC TN--90/005, *Wet-Bulb Globe Temperature, A Global Climatology*, AD-A229028.

MESOSCALE AND LOCAL EFFECTS

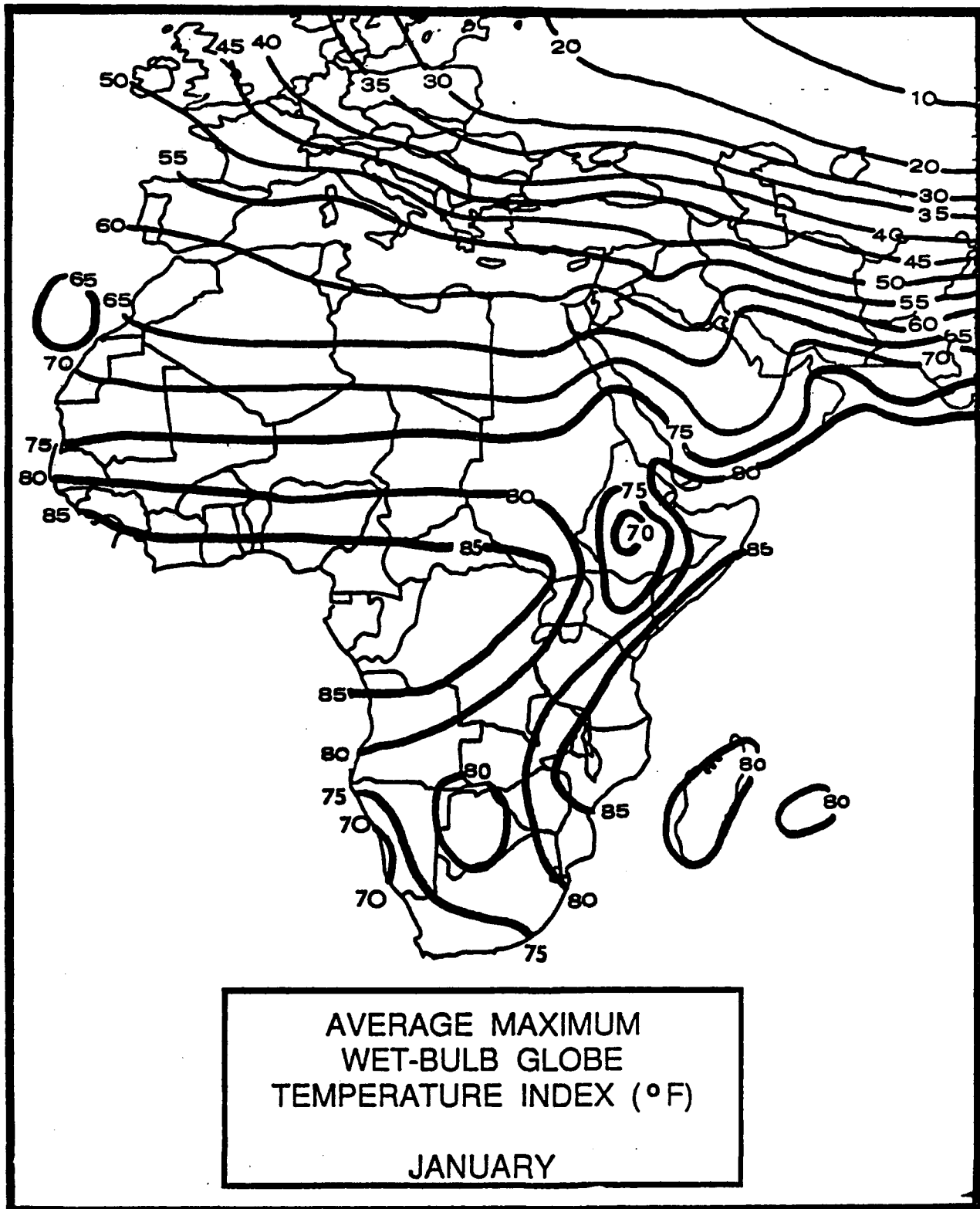


Figure 2-59a. Average Maximum WBGT—January.

MESOSCALE AND LOCAL EFFECTS

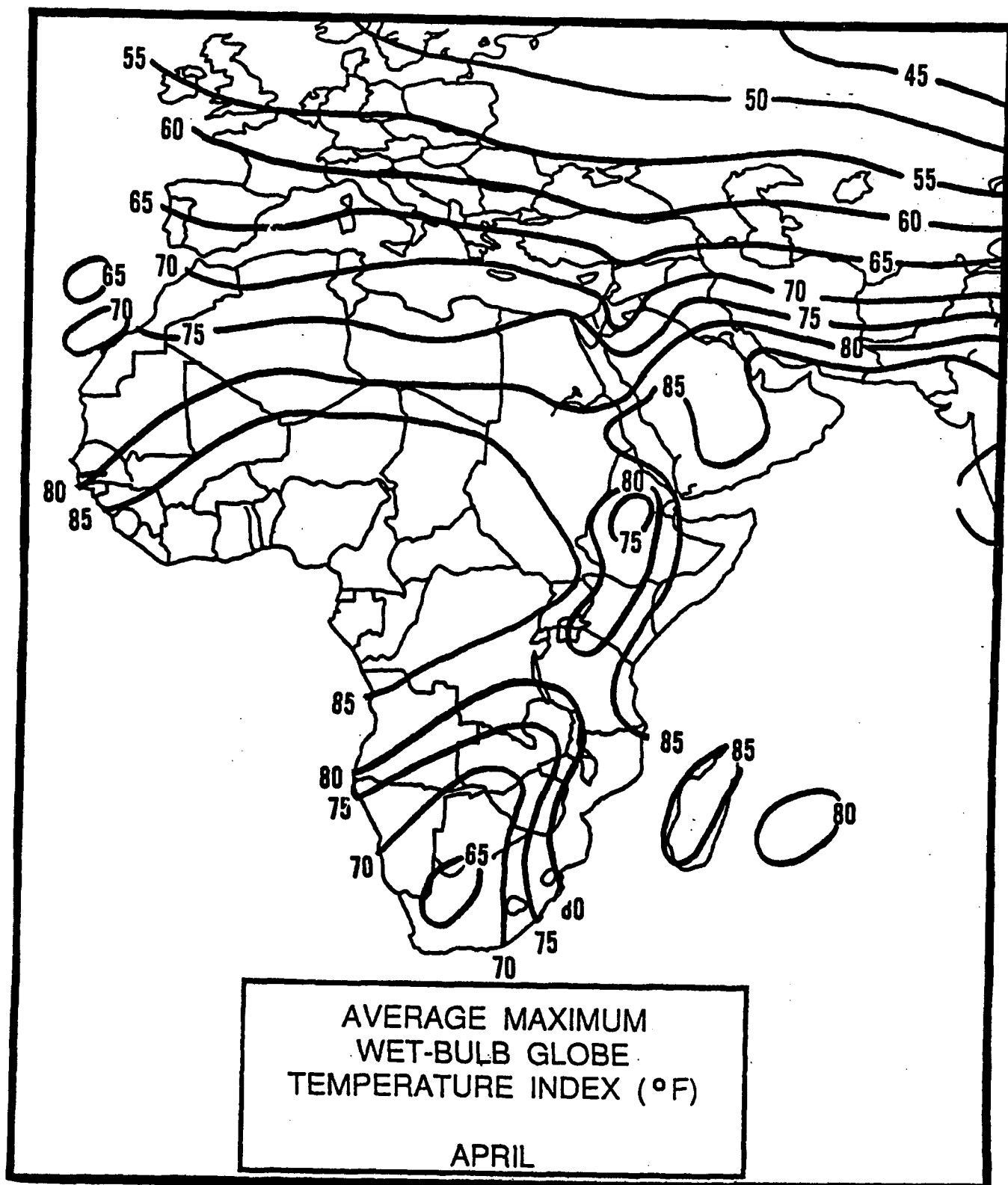


Figure 2-59b. Average Maximum WBGT-April.

MESOSCALE AND LOCAL EFFECTS

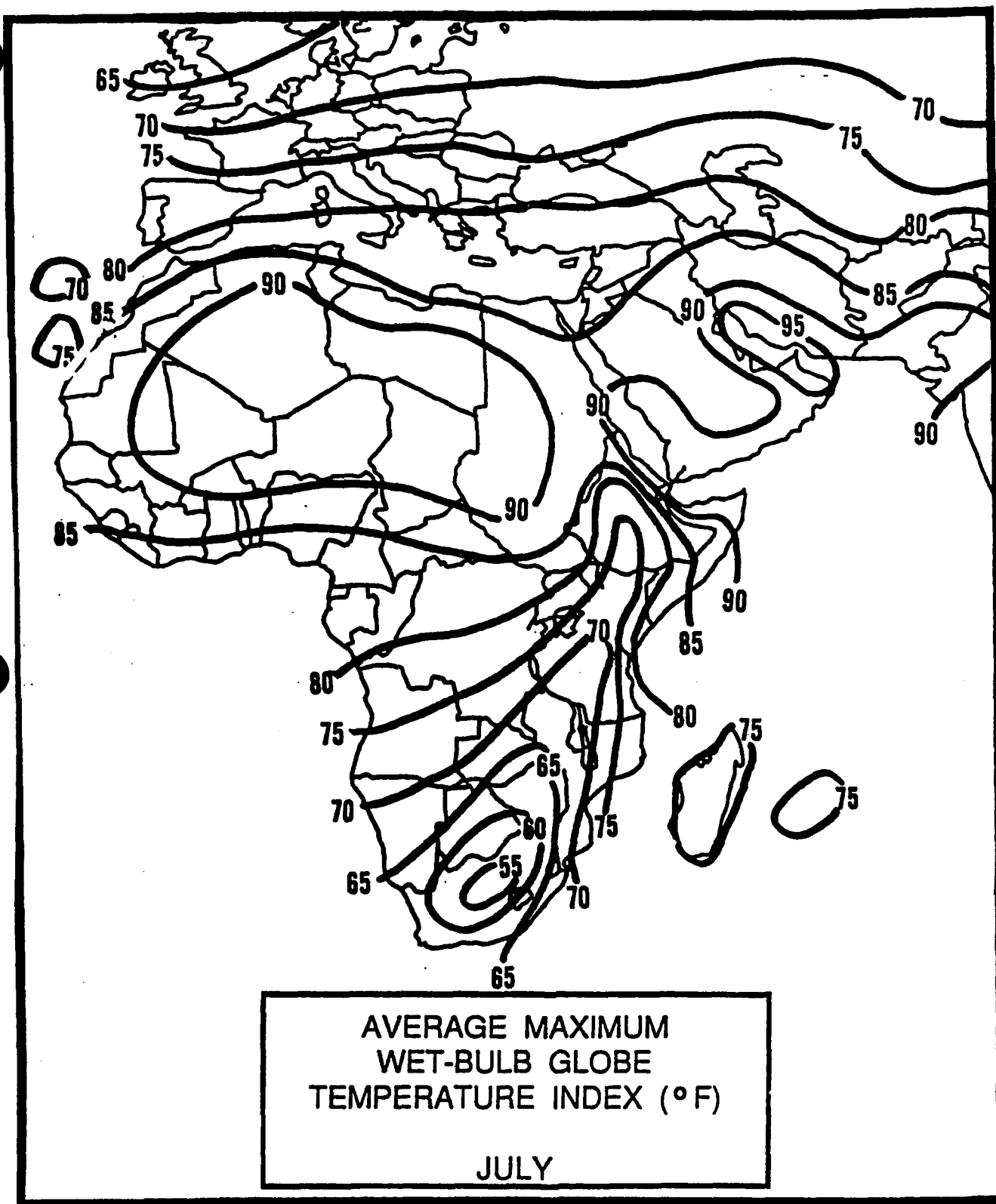


Figure 2-59c. Average Maximum WBGT—July.

MESOSCALE AND LOCAL EFFECTS

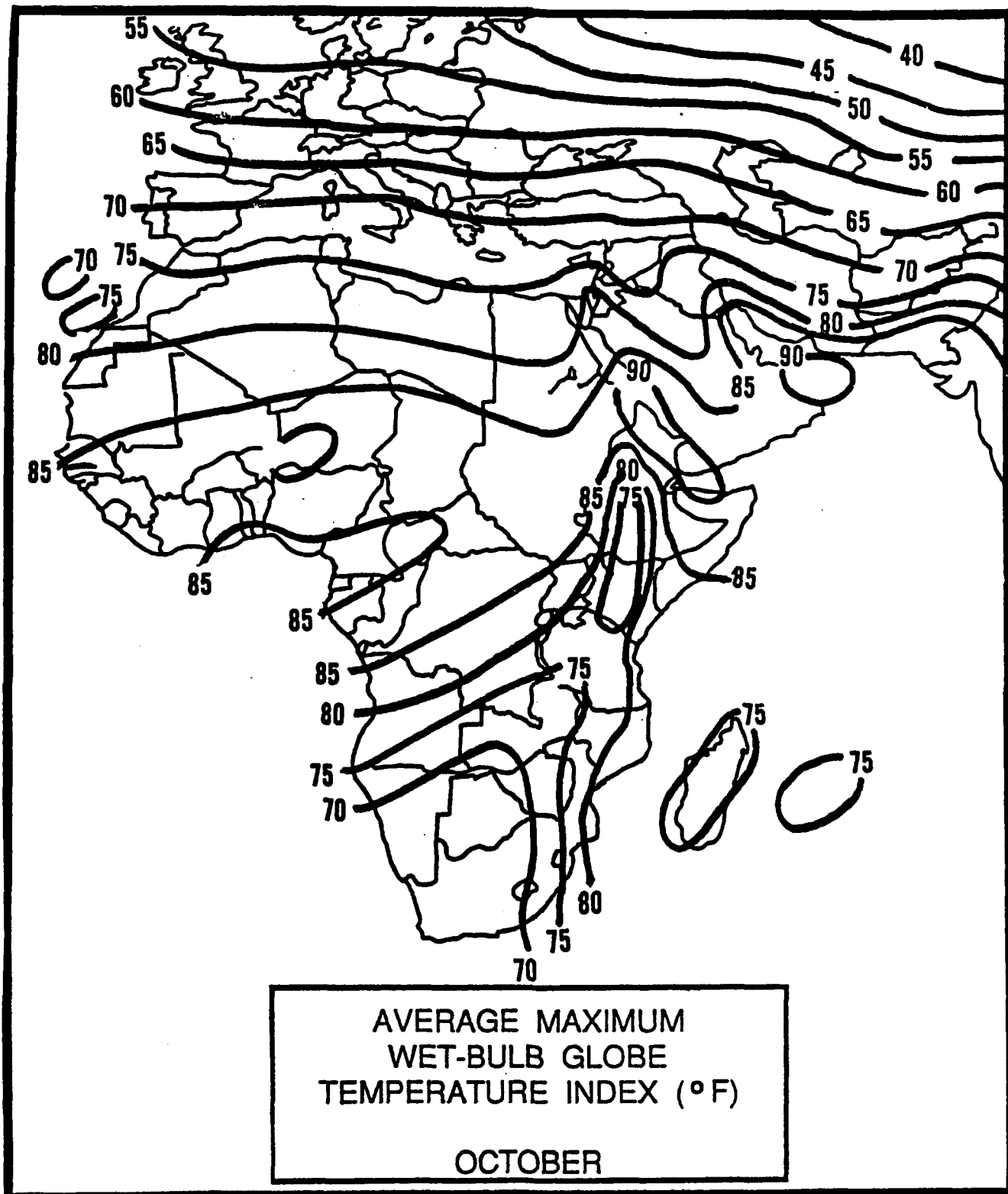


Figure 2-59d. Average Maximum WBGT—October.

Chapter 3

RED SEA COASTAL PLAINS

The Red Sea Coastal Plains contain coastal portions of Egypt, Saudi Arabia, Sudan, Ethiopia, Djibouti, and Yemen. After describing this area's situation and relief, this chapter discusses "general weather conditions" by season.

Situation and Relief	3-2
The Southwest Monsoon--June-September	3-5
General Weather	3-5
Sky Cover	3-5
Visibility	3-7
Winds	3-8
Precipitation	3-10
Temperature	3-11
The Southwest-to-Northeast Monsoon Transition--October-November ...	3-12
General Weather	3-12
Sky Cover	3-12
Visibility	3-14
Winds	3-15
Precipitation	3-15
Temperature	3-17
The Northeast Monsoon--December-March	3-18
General Weather	3-18
Sky Cover	3-18
Visibility	3-20
Winds	3-21
Precipitation	3-22
Temperature	3-26
Northeast-to-Southwest Monsoon Transition--April-May	3-27
General Weather	3-27
Sky Cover	3-27
Visibility	3-28
Winds	3-29
Precipitation	3-30
Temperature	3-31

RED SEA COASTAL PLAINS

SITUATION AND RELIEF

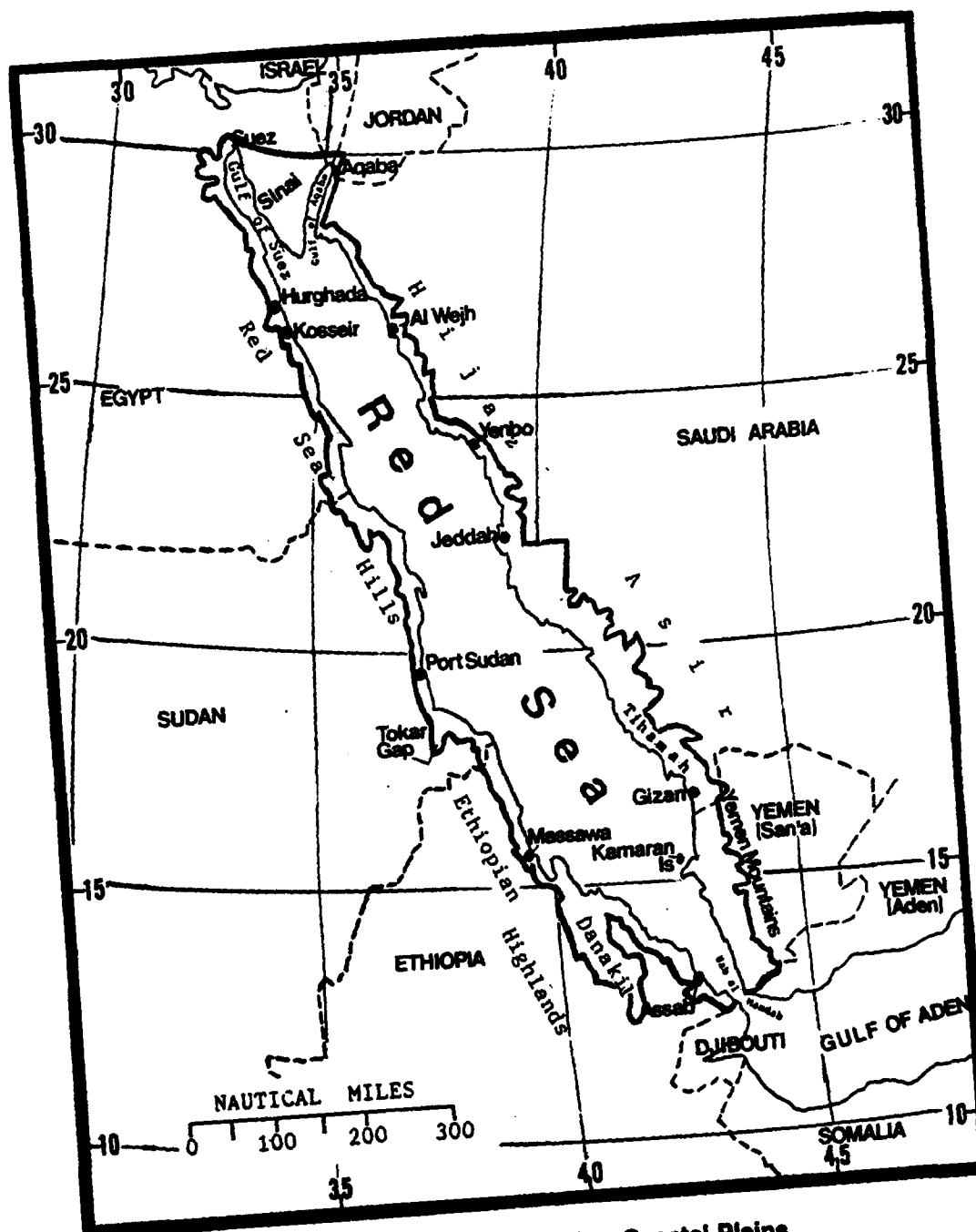


Figure 3-1a. The Red Sea Coastal Plains.

RED SEA COASTAL PLAINS

SITUATION AND RELIEF

STATION: JEDDAH SAUDI ARABIA													
LAT/LON: 21 30 N 39 12 E ELEV: 50 FT													
ELEMENTS	JAN	FEB	MAR	APR	MAY	JUN	JUL	AUG	SEP	OCT	NOV	DEC	ANN
XTRN MAX	95	95	101	104	114	120	111	108	112	105	105	94	120
AVG MAX	83	85	88	93	98	102	101	100	98	96	92	89	94
AVG MIN	67	66	67	72	76	79	81	82	79	75	73	70	74
XTRM MIN	49	52	55	54	63	67	70	72	66	63	61	50	49
AVG PRCP	0.2	0.0	*	0.0	*	*	0.0	0.0	0.0	0.0	0.9	0.6	1.7
MAX MON	0.3	*	2.3	0.0	*	*	*	*	0.1	0.3	6.3	2.1	6.3
FOG DAYS	1	1	1	*	3	5	4	2	4	3	1	*	26
TS DAYS	0	0	0	0	0	0	0	0	0	0	2	0	2
DUST DAYS	3	3	4	4	3	6	4	3	3	*	1	3	37

* = LESS THAN 0.05 INCHES OR LESS THAN 0.5 DAYS

STATION: MASSAWA-IN-ERITREA													
LAT/LON: 15 37 N 39 27 E ELEV: 33 FT													
ELEMENTS	JAN	FEB	MAR	APR	MAY	JUN	JUL	AUG	SEP	OCT	NOV	DEC	ANN
EXT MAX	97	100	102	104	106	111	115	115	111	106	104	97	115
AVG MAX	85	85	89	92	95	102	104	102	98	94	90	87	94
AVG MIN	73	72	74	77	80	84	88	87	85	81	78	73	79
EXT MIN	52	55	55	60	64	65	68	68	66	70	62	61	52
AVG PRCP	1.2	1.2	0.7	0.6	0.2	0.0	0.2	0.3	0.1	0.6	0.7	1.4	7.2
MAX DAY	3.0	1.2	0.9	0.9	0.5	*	2.4	0.1	0.1	2.7	1.4	3.5	3.5
TS DAYS	*	0	*	*	0	0	1	1	0	1	0	1	4

* = LESS THAN 0.05 INCHES OR LESS THAN 0.5 DAYS

STATION: ASSAB-IN-ERITREA													
LAT/LON: 13 04 N 42 23 E ELEV: 46 FT													
ELEMENTS	JAN	FEB	MAR	APR	MAY	JUN	JUL	AUG	SEP	OCT	NOV	DEC	ANN
EXT MAX	91	97	102	104	108	109	109	109	106	104	100	97	109
AVG MAX	85	86	89	94	98	99	102	100	98	94	88	86	93
AVG MIN	72	73	75	78	80	84	86	87	85	79	75	71	79
EXT MIN	50	52	52	57	64	64	70	68	66	64	54	54	50
AVG PRCP	*	*	*	*	*	0.0	0.2	*	*	*	0.2	0.6	1.1
MAX DAY	0.1	0.2	*	*	*	0.0	0.8	*	*	*	0.2	0.9	0.9
TS DAYS	0	0	*	0	*	*	*	0	*	*	*	0	2

Figure 3-1b. Climatological Summaries for Selected Stations in the Red Sea Coastal Plains.

RED SEA COASTAL PLAINS

GEOGRAPHY. The southern boundary of the Red Sea Coastal Plains extends from its southernmost point on the Djibouti-Ethiopia border (12° 45' N, 42° 55' E) directly across the Strait of Bab al Mandab to the Republic of Yemen border. The eastern boundary follows the 3,280-foot (1,000-meter) contour northward along the foothills of the Yemen and Asir Mountains to 21°40' N. From there it goes west over to the 656-foot (200-meter) contour and follows it northward to Aqaba, Jordan. The northern boundary is a line from Aqaba to just south of Suez, Egypt. The western boundary follows the 656-foot (200-meter) contour southward along the western Red Sea coastline to the Djibouti-Ethiopia border. The Danakil Desert plain of northeastern Ethiopia below 656 feet (200 meters) is included.

The western Red Sea Coastal Plain is dominated by red sand and gravel, except for the desolate Danakil Desert, a barren salt flat that extends 70 NM inland from the coast at the subregion's lowest elevation (-512 feet/-156 meters). The rest of the western coastal plain is backed by two extensive mountain ranges from Massawa, Ethiopia, to Hurghada, Egypt. These ranges rise abruptly from the coastal plain, which is less than 25 NM wide. The Ethiopian Highlands and the Red Sea Hills are separated by the Tokar Gap--a natural break and an entry point for westerly surface flow from interior Africa. The Ethiopian Highlands rise abruptly to elevations of 13,000 feet (3,962 meters). The Red Sea Hills are weathered mountains along the coasts of Sudan and Egypt. Most peaks are below 4,800 feet (1,463 meters), but several peaks rise above 6,600 feet (2,010 meters).

SITUATION AND RELIEF

The eastern shoreline includes the foothills of the Yemen Highlands and Asirs. The Yemen coastal plain, called the Tihamah lowlands, is a tidal plain averaging 35 NM in width, but is much narrower in Saudi Arabia. The rugged Hijaz Mountains average less than 5,000 feet (1,524 meters) but they extend down to the sea. There are few natural harbors anywhere along the entire eastern Red Sea Coastal Plain.

The southern half of the Sinai Peninsula, a limestone plateau that separates the Gulfs of Suez and Aqaba, is an extension of the Red Sea Hills. Its highest peak rises above 8,650 feet (2,637 meters).

DRAINAGE AND RIVER SYSTEMS. The Red Sea Coastal Plains are extremely dry. There are no permanent rivers or streams, but deep canyons may temporarily fill with runoff.

LAKES AND RESERVOIRS. The Red Sea and the Gulfs of Suez and Aqaba, are the dominant water bodies. The Red Sea is 1,220 NM long and averages 130 NM in width. North of 20° N, its depth is greater than 1,200 feet (366 m). South of 20° N, it averages only 600 feet (183 meters) deep.

VEGETATION The Red Sea Coastal Plains lack significant vegetation. Except for local agriculture on the Tihamah, the plains are barren, with isolated desert or semi-steppe vegetation. The Tihamah has extensive mangrove swamps and coral shelves along the water's edge.

RED SEA COASTAL PLAINS SOUTHWEST MONSOON

June-September

GENERAL WEATHER. The Monsoon Trough is the most important weather producer during the period. Southwest Monsoon flow originates as early as mid-June and persists until early September. When the Monsoon Trough is at its northernmost position in late July, southwesterly flow penetrates into the central and southern Red Sea, primarily through the Tokar Gap. The orientation of the Red Sea funnels this flow to the southeast, producing low-level convergence, orographic cumulus, and strong northwesterly winds between Port Sudan and Assab. The flow picks up moisture over the Red Sea and assists the sea breeze on the eastern coastline from Jeddah to south of Gizan. Isolated orographic showers occur every afternoon along the Yemen and northern Asir mountain ranges. The areas north of a line between Port Sudan and Jeddah do not get any of the "monsoon" flow through the Tokar Gap and are therefore extremely dry.

SKY COVER. Mean cloudiness is greatest in the southeast (40%) and lowest in the northwest (less than 10%). The Southwest Monsoon is a low point for mean cloudiness in the north; Mean frequencies (Figure 3-2) for Hurghada (5%), Kosseir (5%), and Aqaba (4%) contrast sharply with the mean cloudiness at Massawa (32%) and Assab (39%). The transition zone extends from Port Sudan (30%) northeastward to Jeddah (20%).

Cloudiness distributions are controlled by low-level southwesterly flow through the Tokar Gap. This flow is strongest between mid-July and early September. Most low-level flow turns

southeastward toward the Strait of Bab al Mandab and converges with land/sea breezes along the coastline between Port Sudan and Assab. Weak west-southwesterly flow can reach Jeddah at its northernmost extent. The reinforced sea breeze forms bands of shallow cumulus along the Asirs. Northwesterly flow south of 20° N produces greater amounts of orographic cumulus along the eastern coastline. A continuous band of heavy cumulus often stretches from 14° N to 20° N along the southwestern Asirs and western Yemen Mountains.

Early morning (0500-0900 LST) is the cloudiest on the southwestern coastline between Port Sudan and Assab, and on the eastern coast at Jeddah. Stratocumulus with bases at or below 3,000 feet (915 meters) AGL, however, occur less than 3% of the time at these locations. Stratocumulus dissipates by late morning, leaving scattered altostratus and cirrostratus. Isolated cumulus with bases at or above 6,000 feet (1,829 meters) AGL develops in the afternoon with the sea breeze. Scattered cumulus is typical of the mid-afternoons between Massawa and Assab.

The highest frequencies of ceilings below 3,000 feet (915 meters) AGL are at Port Sudan and Gizan (4%) between 1400 and 1500 LST. Most low ceilings south of Jeddah and Port Sudan occur between mid-July and early September along higher terrain. Isolated thunderstorm bases average 4,000 feet (1,220 meters) AGL with tops to 40,000 feet (12,000 meters) MSL.

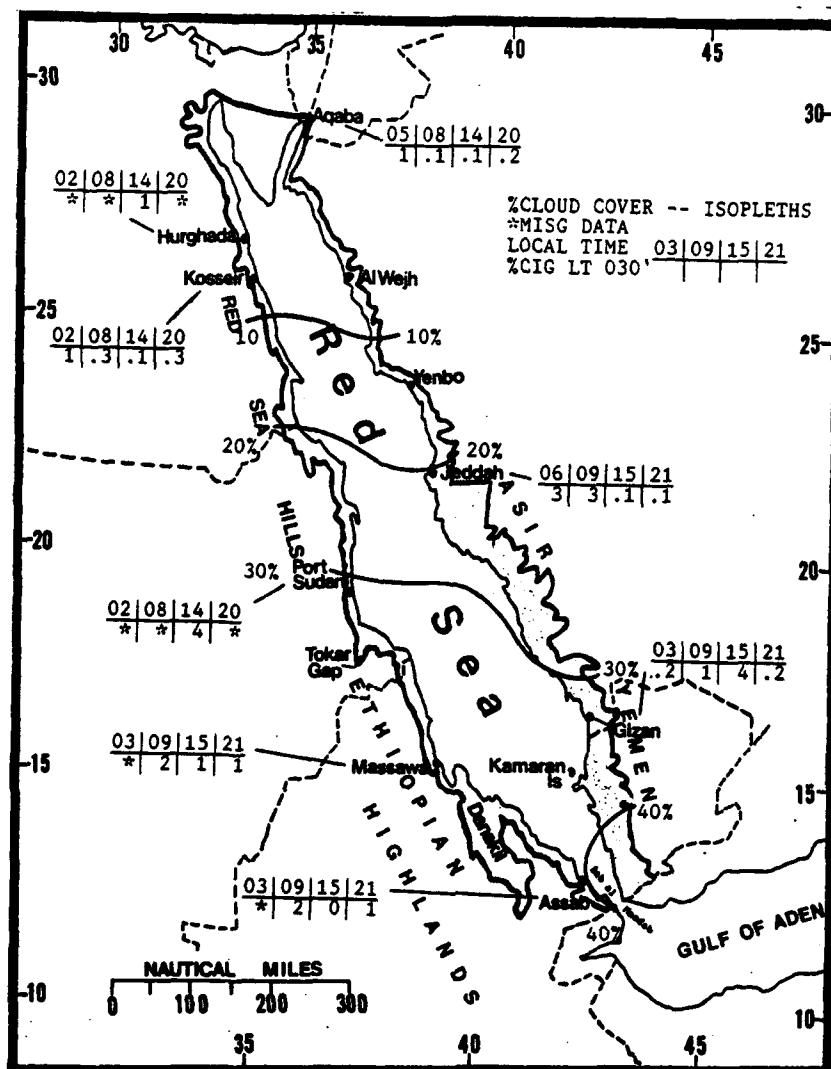


Figure 3-2. Mean Southwest Monsoon Cloudiness (Isolines) and Frequencies of Ceilings Below 3,000 Feet (915 meters), Red Sea Coastal Plains.

RED SEA COASTAL PLAINS SOUTHWEST MONSOON

June-September

VISIBILITY. Blowing dust, sand, and moisture haze are the main restrictions to visibility. The greatest frequency of visibilities below 3 miles occurs during the Southwest Monsoon, especially in July and August when flow from the African interior comes through the Tokar Gap. Visibilities are below 3 miles at Port Sudan 18% and 14% of the time at 0900 and 1500 LST, respectively (see Figure 3-3).

During Operation DESERT SHIELD, visibility at Jeddah was reduced most often in September when a low-level moisture advection pattern off the Red Sea sets up. This surface wind pattern (southwesterly through northwesterly) increases low-level moisture through a 48-hour period

prior to fog formation. Light fog begins to form at 0000L and would lower to 3 miles (4800 meters) by 0300L; if winds became calm, there is a good chance visibility will lower to 1 mile (1600 meters). It was also noted that a nocturnal drainage wind from the Hijaz Mountains would prevent fog formation at Jeddah.

Duststorms/sandstorms can reduce visibility to 100 feet (33 meters) for periods of less than 30 minutes. Reductions in nighttime visibilities are produced by haze since land breezes bring in Red Sea moisture. Nighttime visibilities range from 4 to 7 miles.

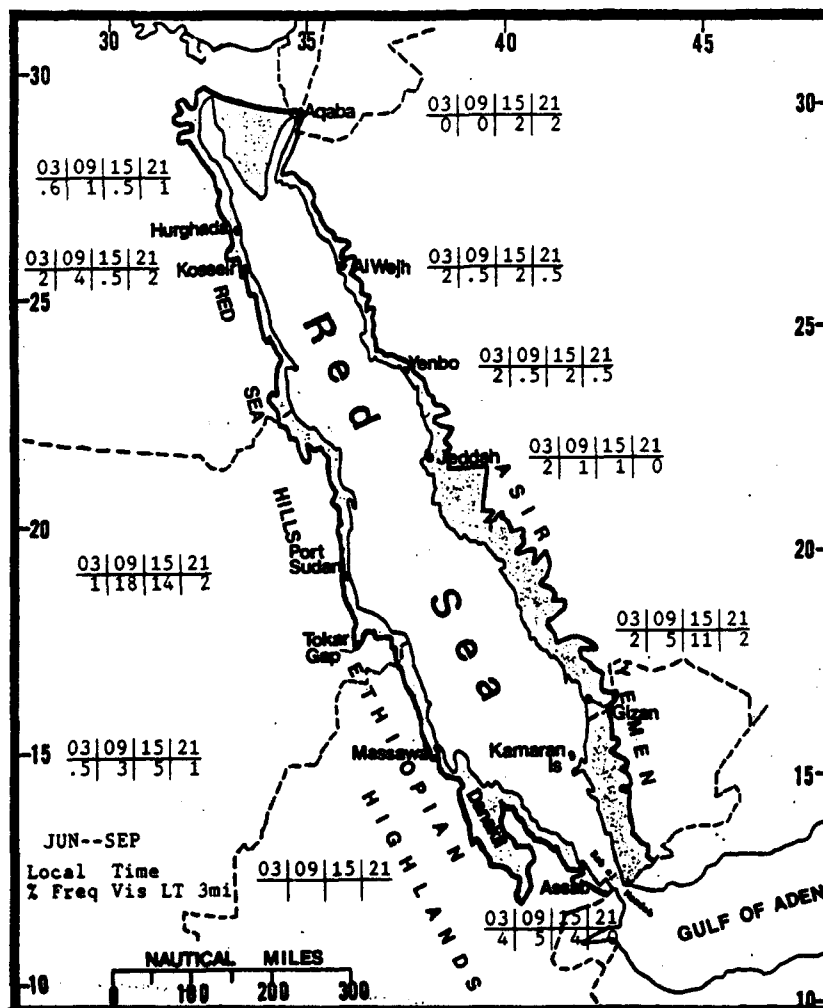


Figure 3-3. Southwest Monsoon Frequencies of Visibilities Below 3 Miles, Red Sea Coastal Plains.

RED SEA COASTAL PLAINS SOUTHWEST MONSOON

June-September

WINDS. During fair weather, Mediterranean air brings light westerly to northerly winds at 6-9 knots north of 22° N. A localized drainage wind out of eastern Israel produces a northerly nighttime breeze at Aqaba. South of 22° N, light land/sea breezes at 5 to 9 knots dominate the coastal fringes until mid-July, when flow from the African interior portion of the surface Monsoon Trough brings stronger winds through the Tokar Gap; speeds increase to 10-13 knots along the southwestern coast between Massawa and Assab.

Figure 3-4 shows mean surface wind speed and prevailing surface wind direction for seven Red Sea Coastal Plain sites. Note that the mean surface wind speed increases at Assab, Jeddah, and Gizan with the flow through the Tokar Gap in July that reinforces the sea breeze from Jeddah southward along the southeastern

coastline. By September, easterly surface winds prevail at Assab, showing the sea-breeze influence that overrides the Tokar Gap flow into the area.

Highest sustained surface wind speeds north of 18° N are caused by early and late season cyclonic activity. The highest recorded wind speeds in June were at Kosseir (from the north at 78 knots) and Al Wejh (from the west at 78 knots), while Yenbo and Port Sudan's highest recorded speed (WNW at 88 knots) was in September.

Highest sustained winds south of 18° N occur with the "African Interior" surface Monsoon Trough and tropical cyclones. The 84-knot wind from the ESE at Assab was probably due to a rare tropical cyclone entering the Gulf of Aden.

		JUN	JUL	AUG	SEP
N	Kosseir	8.50	7.20	7.80	9.00
W	Gizan	6.40	7.10	6.80	6.10
N	Jeddah	6.90	7.20	6.80	6.30
NE-E	Port Sudan	6.10	5.40	5.20	5.40
W	Yenbo	9.40	9.00	9.00	8.30
WNW-W	Al Wejh	9.10	8.60	8.50	9.10
N/E	Assab	9.90	12.60	11.50	10.80

Figure 3-4. Mean Southwest Monsoon Surface Wind Speed (kts) and Prevailing Direction, Red Sea Coastal Plains. Assab's prevailing wind direction is northerly in June, becoming westerly by September.

RED SEA COASTAL PLAINS SOUTHWEST MONSOON

June-September

From Jeddah to Port Sudan and southward, weak 10- to 14-knot easterly winds dominate the mid- and upper-levels. North of this line, weak westerlies at 10-15 knots prevail. Figure 3-5a and b show mean annual wind directions at Giza and Al Wejh, respectively. Between June

and September, the 10,000-foot (3,050-meter) MSL and 15,000-foot (4,573-meter) MSL wind directions are northeasterly at Giza, southwesterly at Al Wejh. Winds at 5,000 feet (1,524 meters) MSL are west-northwest at Al Wejh, but northerly at Giza.

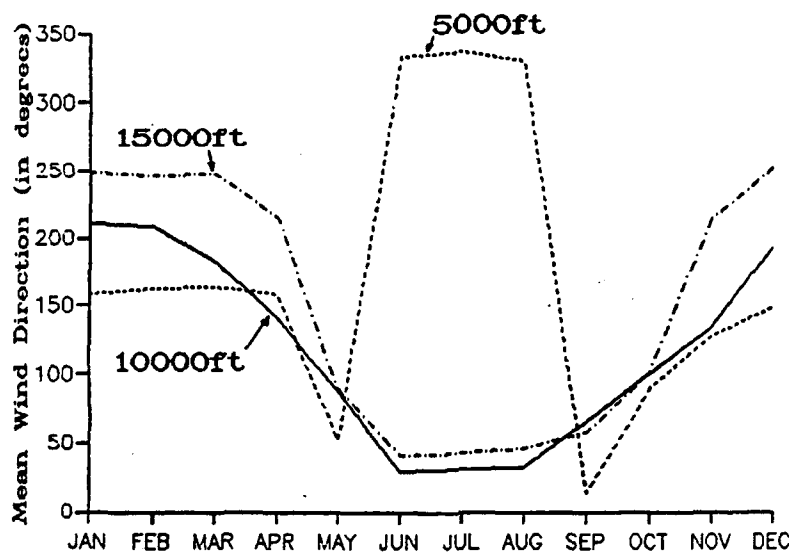


Figure 3-5a. Mean Annual Wind Direction, Giza, Saudi Arabia.

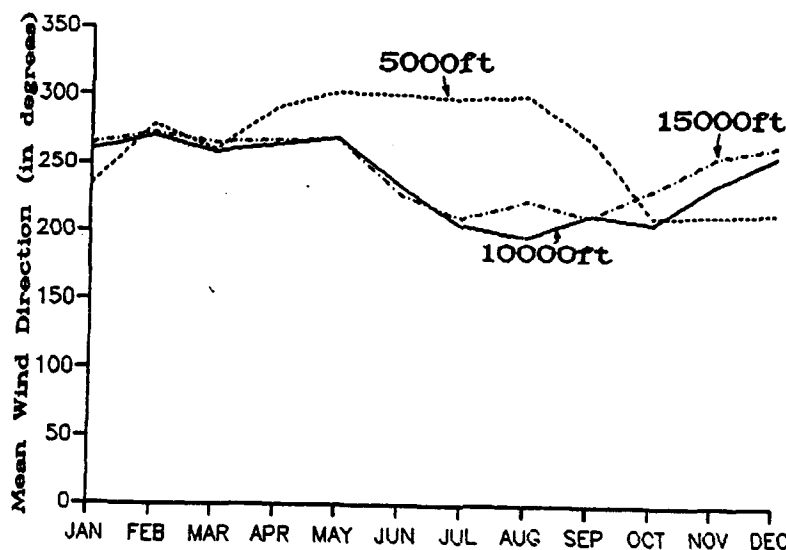


Figure 3-5b. Mean Annual Wind Direction, Al Wejh, Saudi Arabia.

RED SEA COASTAL PLAINS SOUTHWEST MONSOON

June-September

PRECIPITATION. All rainfall during the Southwest Monsoon is from thunderstorms or rainshowers. Precipitation is particularly rare north of 22° N because the surface Monsoon Trough has no affect there. Figure 3-6 shows mean monthly rainfall totals and 24-hour maximums. Rainfall at Port Sudan, Massawa, Gizan, and Assab results from orographic showers and isolated thunderstorms. Precipitation normally increases in July when flow through the Tokar Gap increases. Although not shown in Figure 3-6, July and August rainfall is scant in the Danakil Desert; showers do develop in the mountains surrounding the desert plain, however.

Thunderstorm days range from 5 to 11 a season. Kamaran Island has four thunderstorms in

August, the highest number for any location south of 22° N. Convective activity often originates along the northern Ethiopian Highlands or Yemen Mountains, and spreads out over the coastal plains. Thunderstorms also develop along the northeast Tokar Gap near Port Sudan in July and August between 1400 and 1800L when strong southwesterly flow converges with the sea breeze. The isolated convection and precipitation rarely lasts longer than an hour as strong subsidence aloft minimizes vertical development.

Heavy dew is common along southern coasts; it contributes to the seasonal precipitation total. Salt haze and high relative humidities (above 75%) are also common.

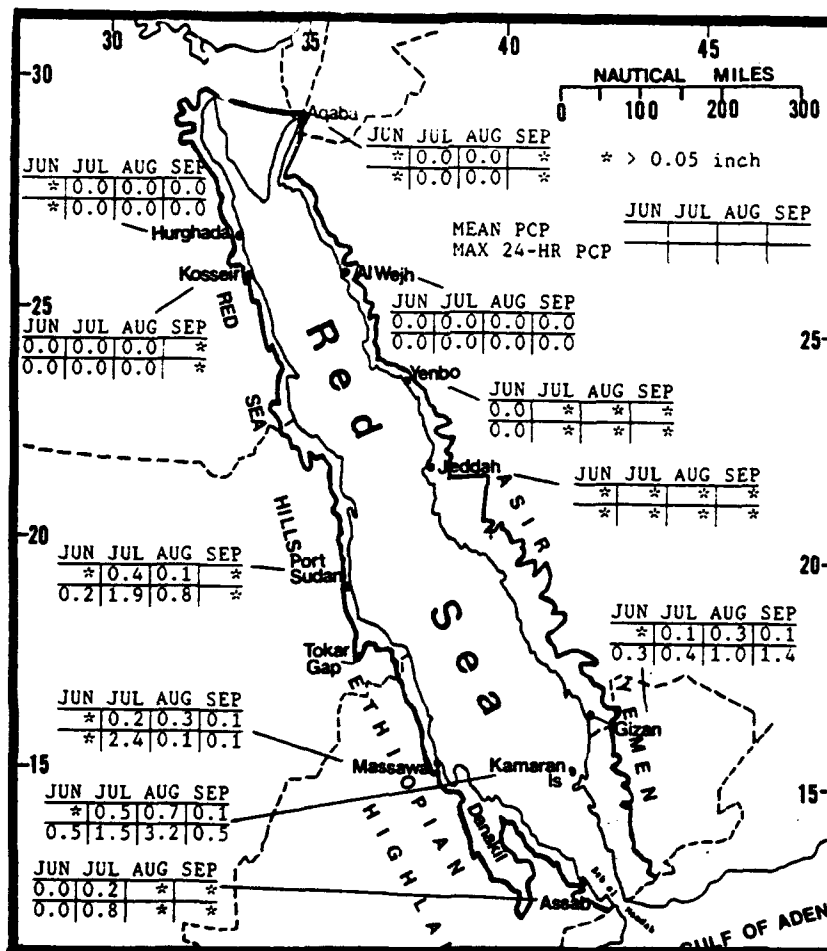


Figure 3-6. Mean Southwest Monsoon Monthly/Maximum 24-hour Precipitation, Red Sea Coastal Plains.

RED SEA COASTAL PLAINS SOUTHWEST MONSOON

June-September

TEMPERATURE. The Southwest Monsoon is very warm along the coast, despite Red Sea surface temperatures of 86-88° F (30-31° C) in the central and southern portions. Mean daily highs range from 84° F (29° C) at Kosseir, to 106° F (41° C) at Port Sudan (see Figure 3-7).

Mean daily lows range from 73° F (23° C) at Kosseir to 87° F (31° C) at Massawa and Assab. The record high for the Southwest Monsoon is 118° F (48° C) in August at Port Sudan. The record low is 54° F (12° C) in September at Aqaba, where cool drainage winds occur.

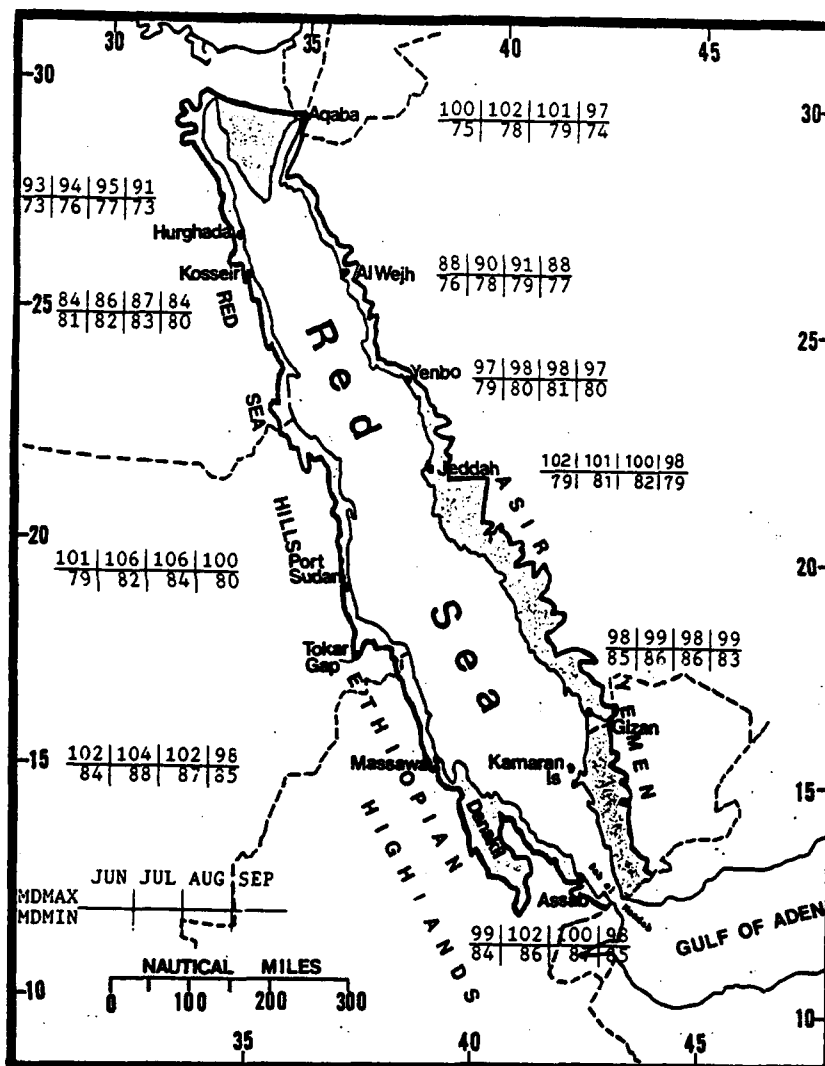


Figure 3-7. Mean Southwest Monsoon Daily Maximum/Minimum Temperatures (° F), Red Sea Coastal Plains.

RED SEA COASTAL PLAINS SOUTHWEST-TO-NORTHEAST MONSOON TRANSITION

October-November

GENERAL WEATHER. The Red Sea Convergence Zone (RSCZ) dominates the transition weather pattern. The RSCZ forms between 18 and 20° N; stratocumulus, shallow isolated cumulus, and scattered light rainshowers are present within 50 NM either side of the RSCZ. Dry and weak northwesterly flow to the north of the cloud and precipitation zone, and moist, moderate flow to the south, are common.

Subsidence aloft is considerably weaker during October and November than during the Southwest Monsoon, but mid- and upper-levels remain very dry and stratocumulus and cumulus cloud development is shallow. Thunderstorms are extremely rare, but they can be produced by strong mid- and upper-level troughs.

SKY COVER. Most cloud cover forms along the RSCZ. Mean cloud cover (see Figure 3-8) is less than 40% across the entire region. The highest mean is 30-34% in an area that extends 100 NM north and south of the Tokar Gap. The transition shows a dramatic decrease in "monsoon" flow through the Tokar Gap. As a result, weak and dry northwesterly surface flow migrates southward to 18° N in October. The northwesterlies converge with strong southeasterlies channelled into the southern Red

Sea through the Strait of Bab al Mandab, producing very widely scattered orographic cumulus and stratocumulus in the Yemen Mountains up to 100 NM north of Gizan, as well as on the eastern slopes of the northern Ethiopian Highlands from Port Sudan to Assab.

In the north, mean cloudiness increases by 10 to 20% because shallow diurnal cumulus development is more frequent. The sea breeze produces isolated cumulus since subsidence aloft is considerably weaker. During the early morning, stratocumulus develops along the coast north of a line between Kosseir and Al Wejh where the land breeze pushes cool nighttime surface air over warmer water (78° F/26° C) in the northern Red Sea.

Morning stratocumulus with bases at 3,000 feet (915 meters) AGL or below occur slightly more often at Gizan and Massawa (4%) than at Kosseir and Aqaba (3%) because the coastal waters are warmer. The terrain surrounding Hurghada and Port Sudan produces afternoon cumulus with bases below 3,000 feet (915 meters) AGL 13 and 11% of the time, respectively. Diurnal cumulus bases range from 5,000 feet to 6,000 feet (1,524-1,829 meter) AGL, but tops rarely exceed 7,000 feet (2,134 meters) MSL.

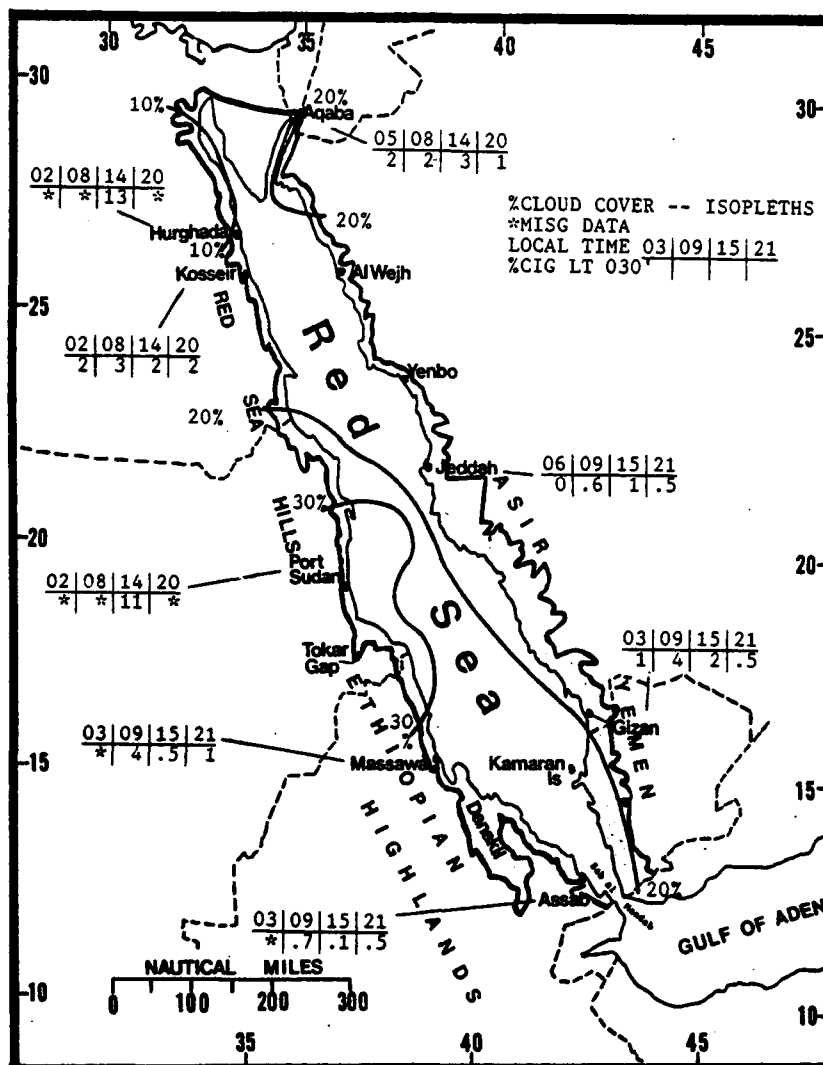


Figure 3-8. Mean SW-NE Monsoon Transition Cloudiness (Isolines) and Frequencies of Ceilings Below 3,000 Feet (915 meters), Red Sea Coastal Plains.

RED SEA COASTAL PLAINS SOUTHWEST-TO-NORTHEAST MONSOON TRANSITION

October-November

VISIBILITY. October and November have the best visibilities of the entire year. Duststorms and sandstorms occur with frontal passages and strong surface winds, but fair weather and light winds prevail through most of the transition. Visibilities below 3 miles (Figure 3-9) are uncommon. Early-morning haze may lower

visibilities below 6 miles, but haze rarely lingers past 0900L. No distinct diurnal change is evident, but the southwest-coast from Port Sudan to Assab shows a slight midday peak. Dust/sand haze and occasional smoke develops on rare occasions with strong southeasterlies that funnel through the Strait of Bab al Mandab.

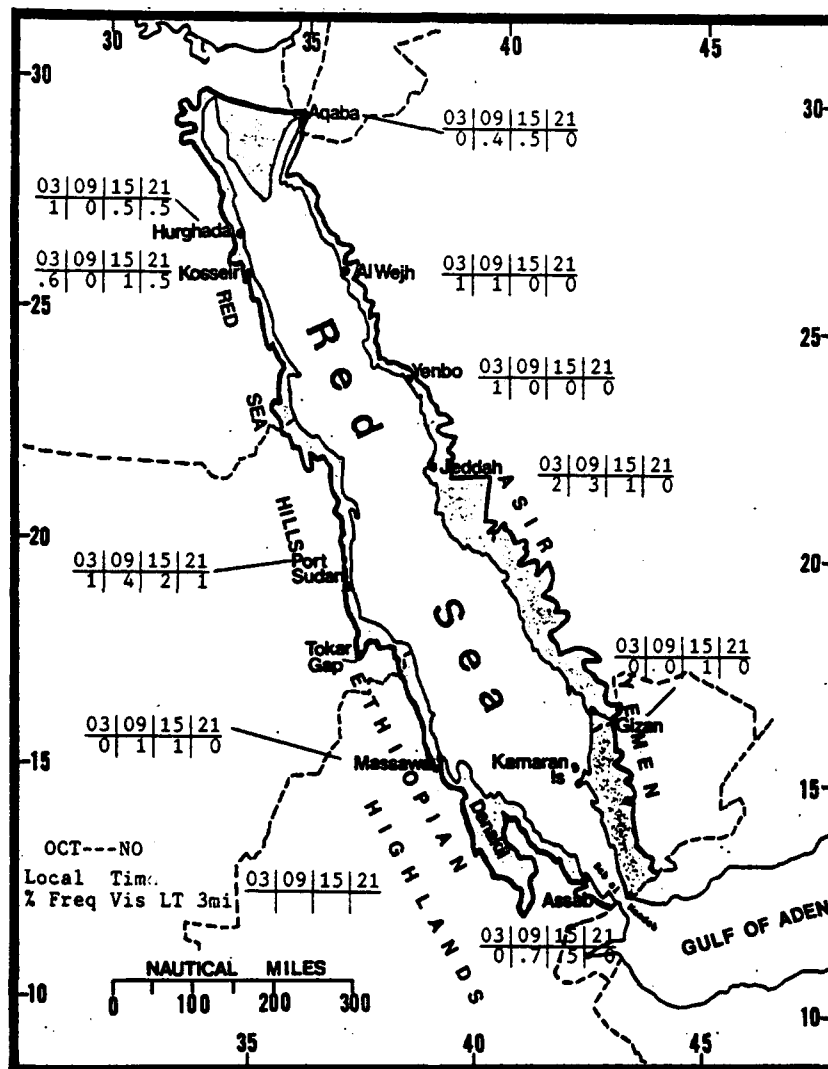


Figure 3-9. SW-NE Monsoon Transition Frequencies of Visibilities Below 3 Miles, Red Sea Coastal Plains.

RED SEA COASTAL PLAINS SOUTHWEST-TO-NORTHEAST MONSOON TRANSITION

October-November

WINDS. Figure 3-10 gives mean surface wind speeds and prevailing direction for several Red Sea Coastal Plain sites. Southeasterlies penetrate northwestward over the Red Sea to an average of 18° N in October and 20° N in November. Variable winds at 5-9 knots are concentrated along the RSCZ. Winds are strong at Assab (14-19 knots) because of its proximity to the Strait of Bab al Mandab, where Northeast Monsoon flow funnels into the Red Sea. Yenbo recorded the highest transition season wind speeds--southerly at 96 knots in October, and easterly at 68 knots in November.

		OCT	NOV
N	Kosseir	8.40	8.90
E	Gizan	5.80	5.80
N	Jeddah	5.30	5.60
N	Port Sudan	5.20	9.10
W	Yenbo	6.80	6.40
W/NNE	Al Wejh	7.80	7.60
E-SE	Assab	13.70	18.90

Figure 3-10. Mean SW-NE Monsoon Transition Wind Speed (kts) and Prevailing Direction, Red Sea Coastal Plains. Al Wejh prevailing winds in October are westerly, changing to north-northeasterly in November.

At Gizan (refer to Figure 3-5a), wind directions at 10,000 feet (3,050 meters) are easterly. Winds at 15,000 feet (4,573 meters) MSL are easterly in October, veering to southwesterly in November. Southwesterly winds frequently occur at 30,000 feet (9,134 meters) MSL, but the mean wind speed is only 20 knots.

At Wejh (see Figure 3-5b), the 15,000-foot (4,573-meter) MSL wind in October is southwesterly at

16 knots, changing to west-southwesterly at 23 knots in November. Mean wind speed at 30,000 feet (9,146 meters) MSL increases from 40 knots in October to 60 knots in November, both from the west-southwest.

PRECIPITATION. November is the wettest month of the year for Yenbo, Jeddah, and the western coastline from 18° N to Hurghada (Figure 3-11). At Hurghada and Kosseir, 0.1 inches (2.5 mm) is the highest mean monthly rainfall total for the year, even though their maximum 24-hour rainfall amounts are 1.6 inches (41 mm) and 1.3 inches (33 mm), respectively. Port Sudan is the wettest location, averaging 2 inches (51 mm) in November, with 24-hour maximum rainfall amounts of 3.1 inches (79 mm) and 4.4 inches (112 mm) during October and November, respectively. The rare episodes of heavy thunderstorms that produce these precipitation totals result from strong low-level convergence of southwesterly flow through the Tokar Gap with the RSCZ. Thunderstorm bases average 5,000 feet (1,500 meters) AGL with tops to 35,000 feet (10,700 meters) MSL.

When a rare Northeast Monsoon surges into the Gulf of Aden and converges with a weak land breeze circulation off the eastern slopes of the north Ethiopian Highlands, warm/moist air enters the Strait of Bab al Mandab, producing nocturnal thunderstorm activity from Assab to Massawa. Although such activity can produce isolated heavy downpours between 0300 and 0600 LST, widespread heavy rain, lightning, and/or squalls do not accompany these storms.

Widespread thunderstorm activity occurs with strong divergence aloft. A surge of low-level southwesterly flow through the Tokar Gap, combined with an upper-level trough creating speed divergence aloft, can trigger convective activity.

RED SEA COASTAL PLAINS
SOUTHWEST-TO-NORTHEAST MONSOON TRANSITION

October-November

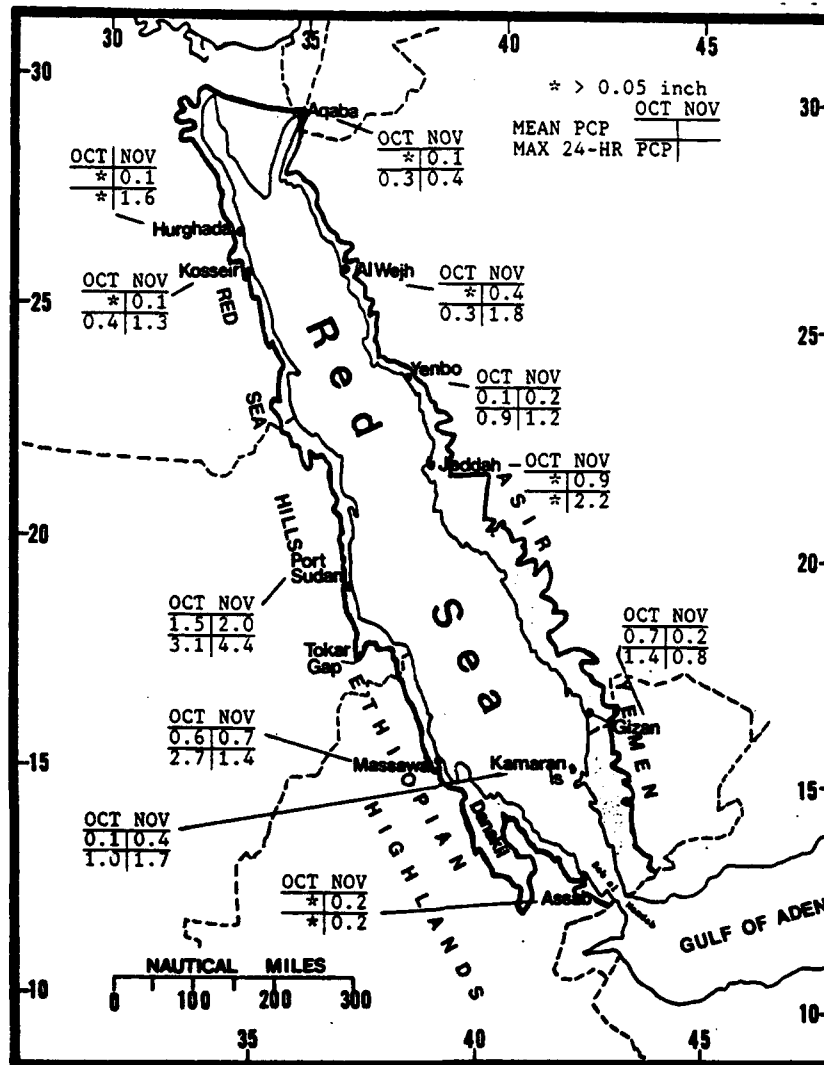


Figure 3-11. Mean SW-NE Monsoon Transition Monthly/Maximum 24-hour Precipitation, Red Sea Coastal Plains.

RED SEA COASTAL PLAINS SOUTHWEST-TO-NORTHEAST MONSOON TRANSITION

October-November

TEMPERATURE. Mean daily highs (Figure 3-12) range from 84 to 97° F (29-36° C) in October, and from 78 to 91° F (26-33° C) in November. The record high in October is 117° F (47° C) at Port Sudan; November's is 107° F (42° C) at Assab.

Mean daily lows range from 67 to 81° F (19-27° C) in October, and from 60 to 78° F (16-26° C) in November. The record lows are 46° F (8° C) at Al Wejh in October, and 15° F (-9° C) at Yenbo in November.

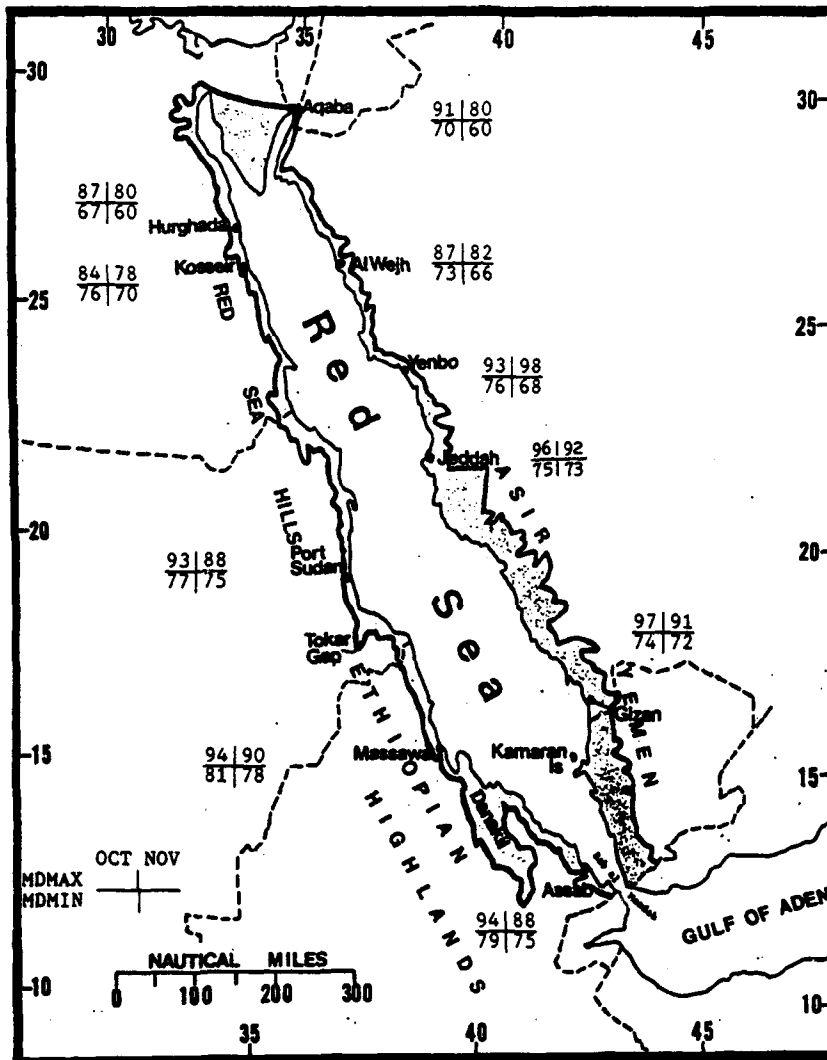


Figure 3-12. Mean SW-NE Monsoon Transition Daily Maximum/Minimum Temperatures (° F), Red Sea Coastal Plains.

RED SEA COASTAL PLAINS NORTHEAST MONSOON

December-March

GENERAL WEATHER. Northeast Monsoon cloud cover and rainfall distributions are dominated by the Red Sea Convergence Zone (RSCZ). Outflow from the Saharan High results in northwesterly flow in the northern half of the Red Sea; flow in the southern half is southeasterly. Low-level convergence produces a stratocumulus cloud band extending 50 to 75 NM either side of the trough.

SKY COVER. The Northeast Monsoon is the cloudiest season of the year. The RSCZ produces stratocumulus and isolated cumulus, that increases mean cloudiness over most of the southwestern coast to more than 40% (Figure 3-13). Massawa has the highest cloud cover frequency; low ceilings there result from persistent surface flow through the Strait of Bab al Mandab that produces scattered stratocumulus. Abnormally strong southeasterly flow may increase cumulus cloud cover (with 3,000-5,000 foot/915-1524 meter bases) along the northern Ethiopian Highlands; this cover can build eastward to the coastline.

Increased mid-latitude cyclonic activity brings mostly altostratus and cirrus across the Sinai Peninsula. Cirrus dominates a broad zone between Jeddah and Aqaba on the east coast (and between Port Sudan and Kosseir on the west coast), due to the presence of the Subtropical Jet.

Although there is no regular sea-breeze cumulus, low-ceiling data in Figure 3-13 indicates localized development at Hurghada.

Morning stratocumulus is scattered to broken at 2,000 feet (610 meters) AGL from Port Sudan to Assab--the area with 40% mean cloudiness in Figure 3-13. When the RSCZ produces a continuous band of stratocumulus, the layer can extend northeastward to the opposite coastline at about 18° N. Through the afternoon hours, scattered-to-broken stratocumulus and isolated cumulus lie along the southwestern shoreline at 4,000 feet (1,220 meters) AGL. Cloud cover dissipates along the eastern coastline. Stratus with bases at or below 2,000 feet (610 meters) occur, about three times during any given Northeast Monsoon; stratus ceilings are at or below 1,000 feet (305 meters) less than 1 day a season. Stratus and stratocumulus may develop with an approaching surface cold front or with localized convergence.

The RSCZ produces more low cloud cover with a southeastward-moving cold front, surging northward to about 25° N in the southwesterly flow ahead of the front. On occasion, a deep low- or mid-level trough moves over the Red Sea to 20-25° N, inducing strong southwesterly surface flow into central Red Sea. These troughs provide light-to-moderate showers, but isolated thunderstorms are possible. Cloud bases average 5,000 feet (1,500 meters) AGL with tops to 35,000 feet (10,700 meters) MSL.

In the southern Sinai, Gulf of Suez, and Gulf of Aqaba, troughs and the Subtropical Jet produce most of the cloud cover. A weak sea breeze produces additional low clouds.

**RED SEA COASTAL PLAINS
NORTHEAST MONSOON**

December-March

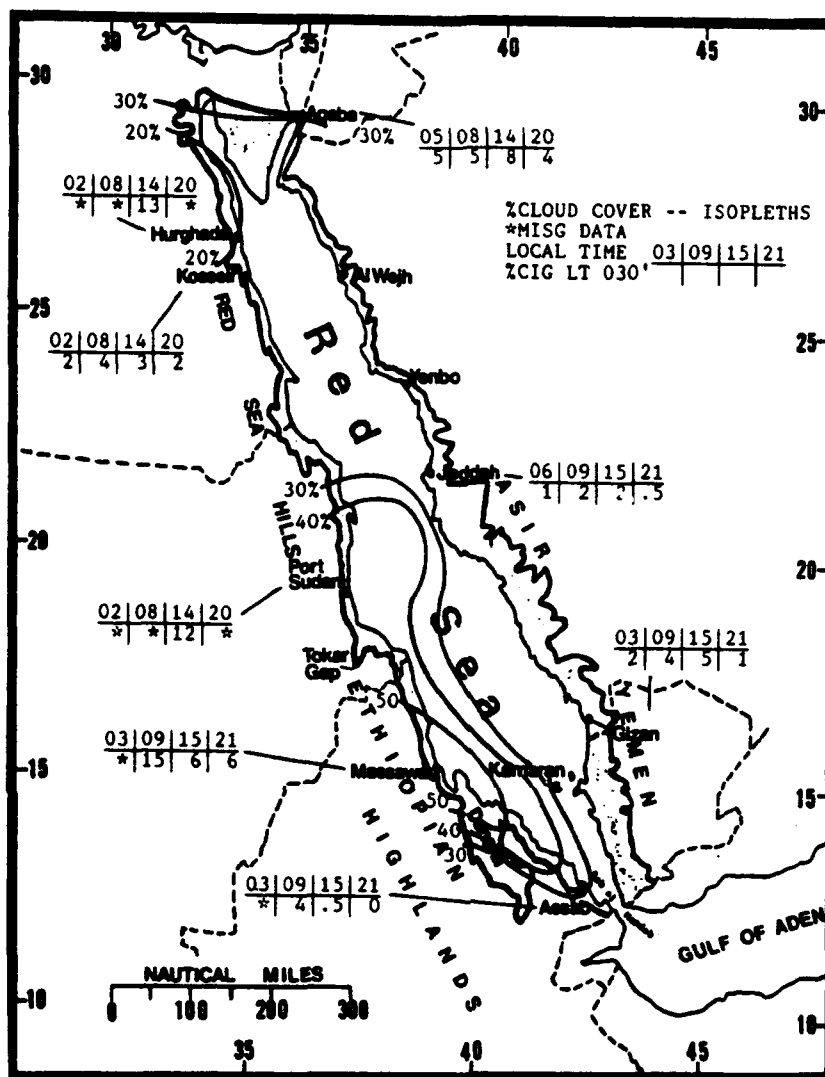


Figure 3-13. Mean Northeast Monsoon Cloudiness (Isolines) and Frequencies of Ceilings Below 3,000 Feet (915 meters), Red Sea Coastal Plain.

RED SEA COASTAL PLAINS NORTHEAST MONSOON

December-March

VISIBILITY. As shown in Figure 3-14, Port Sudan (6-9% between 0900 and 1500 LST) and Jeddah (2-3% between 0300 and 0900 LST) see the greatest frequencies of low visibility. The primary obstructions to vision across the Red Sea Coastal Plains are dust, sand, and moisture haze. Fog is rare. Low visibilities along the RSCZ are due to dust, low rain clouds, and moisture haze.

Fair weather prevails north of the RSCZ axis; visibilities are rarely below 6 miles. However, frontal passages greatly reduce visibility with strong southwesterly surface flow along a warm front that brings in dust and sand from the Sahara. Low visibilities also occur along the immediate cold front when wind speeds are above 15 knots.

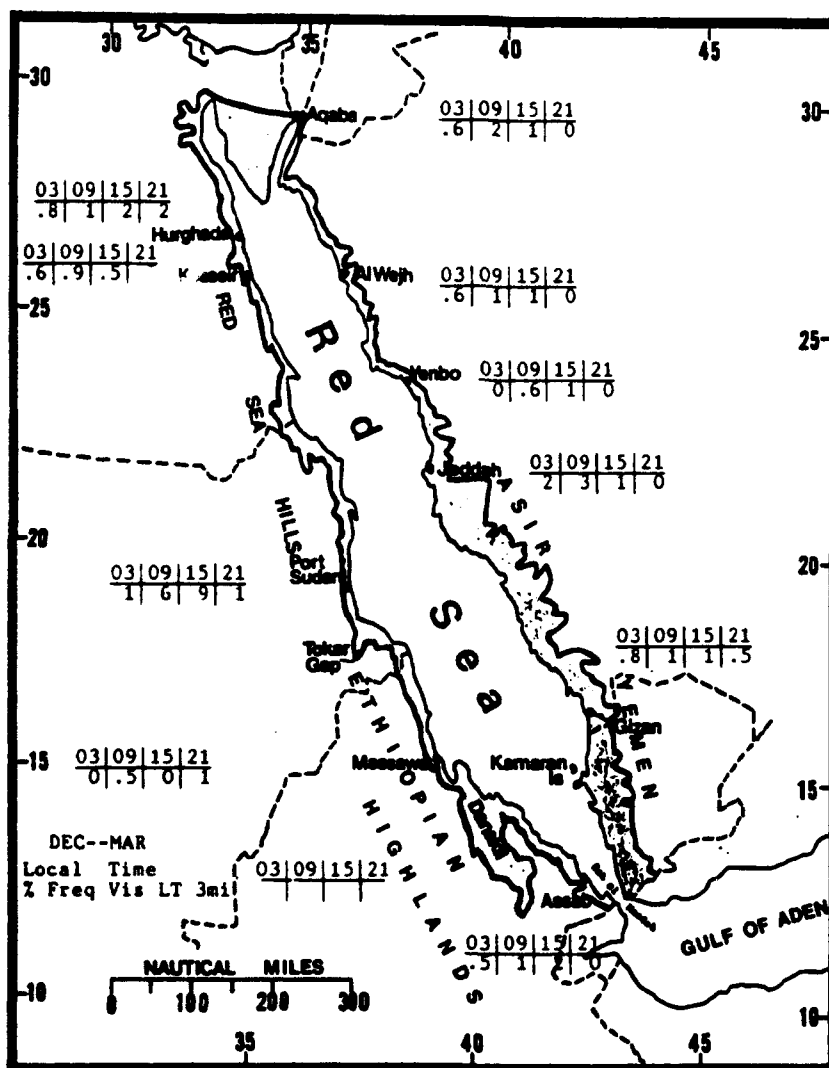


Figure 3-14. Mean Northeast Monsoon Frequencies of Visibilities Below 3 Miles, Red Sea Coastal Plains.

RED SEA COASTAL PLAINS NORTHEAST MONSOON

December-March

WINDS. Figure 3-15 gives mean Northeast Monsoon surface wind speed and prevailing direction for seven locations. Only Assab and Gizan remain south of the RSCZ axis, as indicated by the prevailing southerly surface winds. Note that the mean wind direction at Gizan (Figure 3-5a) for 5,000-feet (1,524-meter)

MSL is steady at south-southeast from December through March. Figure 3-16 shows mean Northeast Monsoon wind speeds between 30,000 and 45,000 feet (9.1-13.7 km) and mean monthly wind directions at Al Wejh. The strong westerly upper-level flow is due to the Subtropical Jet Stream.

		DEC	JAN	FEB	MAR
N	Kosseir	8.50	9.10	9.20	9.10
E/SSW-W	Gizan	5.70	6.00	5.90	5.90
NNE-N	Jeddah	6.60	6.50	7.00	6.60
N	Port Sudan	9.10	9.80	8.20	8.60
WNW-W	Yenbo	6.20	6.90	7.00	7.90
NNE-W	Al Wejh	7.70	8.20	8.70	9.30
SSE	Assab	18.70	17.20	17.40	18.00

Figure 3-15. Mean Northeast Monsoon Surface Wind Speed (kts) and Prevailing Direction, Red Sea Coastal Plains. The wind direction at Gizan changes from easterly to south-southwesterly to westerly from December to March.

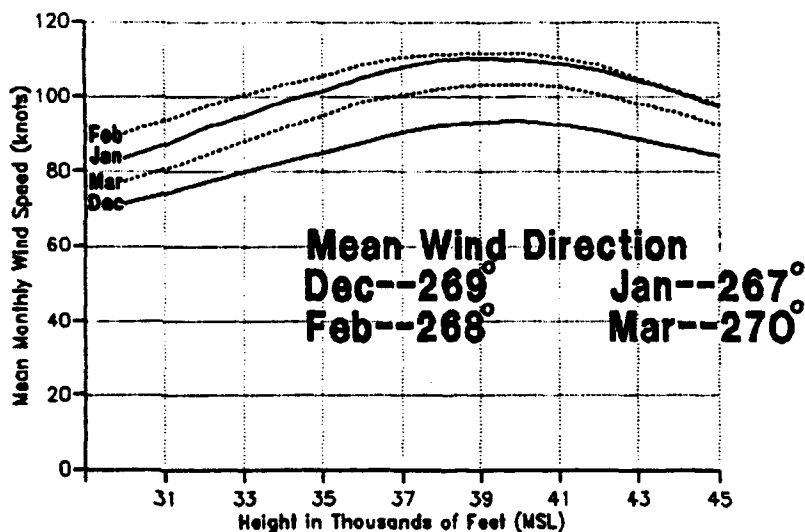


Figure 3-16. Mean Wind Speeds (30,000-45,000 Feet/9,1-13,7 km) MSL at Al Wejh, Saudi Arabia.

RED SEA COASTAL PLAINS NORTHEAST MONSOON

December-March

PRECIPITATION. The RSCZ produces stratocumulus clouds with embedded light rain showers during the Northeast Monsoon. Isolated showers occur two or three times a month, normally in the afternoon or early evening in conjunction with the sea breeze. Fair weather prevails north of the RSCZ. Surface cold fronts bring some cloudiness, but seldom produce rainfall.

Mean monthly precipitation (Figure 3-17) shows a north-to-south increase in rainfall toward the RSCZ trough axis. Massawa receives the most rainfall for the period by far, with 4.5 inches/114

mm. The sharp contrasts between stations show the affect of the RSCZ.

Egyptian stations in the northwest Red Sea Coastal Plains get less than 0.1 inches (2.5 mm) of rain during the entire Northeast Monsoon, while Aqaba averages 0.9 inches (23 mm). Although mean monthly precipitation totals are low north of Yenbo, a deep Cyprus Low can produce significant precipitation if a deep mid-level trough supports the surface trough. Al Wejh, for example, once got 3.6 inches (91 mm) on 1 day in February. Such events, however, are extremely rare.

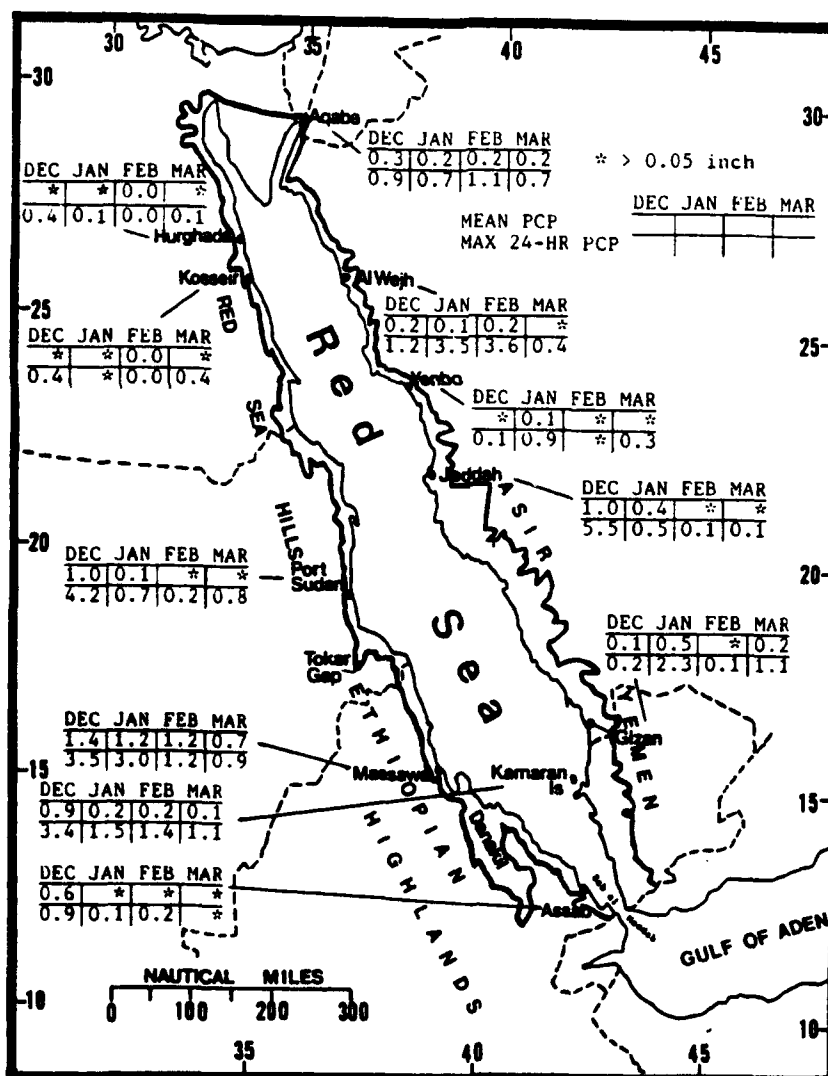


Figure 3-17. Mean Northeast Monsoon Monthly/Maximum 24-hour Precipitation, Red Sea Coastal Plains.

RED SEA COASTAL PLAINS NORTHEAST MONSOON

December-March

For the rare heavy rainfall event to occur, strong mid-and upper-level troughs must accompany the surface low. Figures 3-18 and 3-19 show two different Cyprus Lows in the eastern

Mediterranean Sea; heavy rainfall is only produced by the synoptic pattern in Figures 3-19a and b.

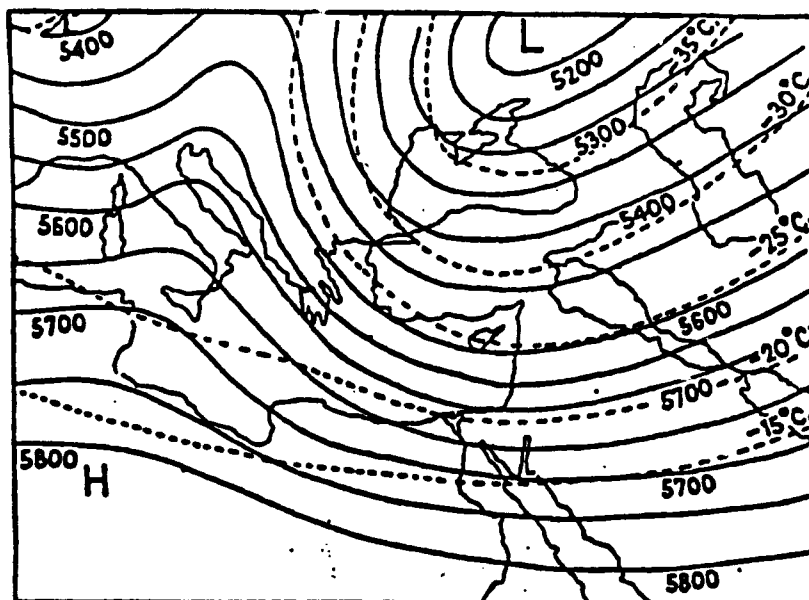


Figure 3-18a. 500-mb Contour Chart Over an Intense Surface Low With No Precipitation. Dashed lines represent isotherms ($^{\circ}\text{C}$) at 5-degree intervals, while solid lines represent geopotential height (gpm) at 50-meter intervals.

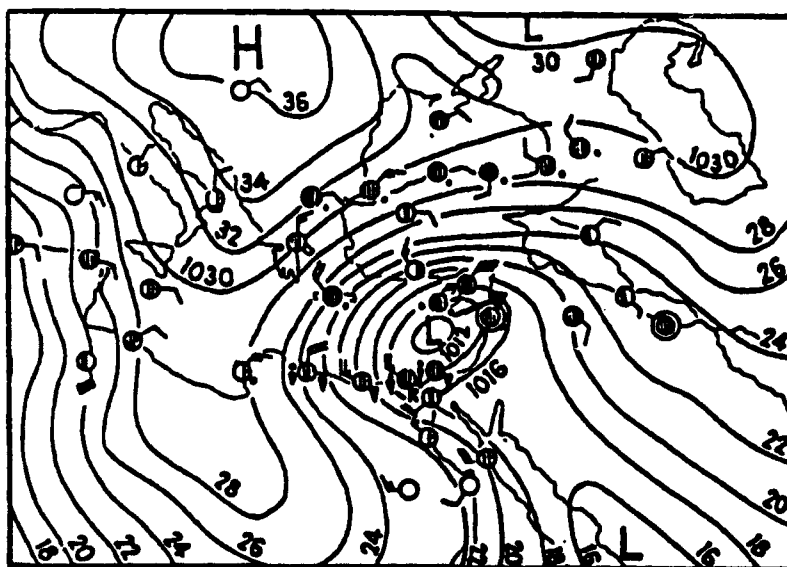


Figure 3-18b. Surface Chart Depicting Cyprus Low Position Beneath a Shallow Mid-Level Trough With No Precipitation. Solid lines denote surface pressure in millibars at 2-mb intervals. Arrow shows movement of the surface low pressure system.

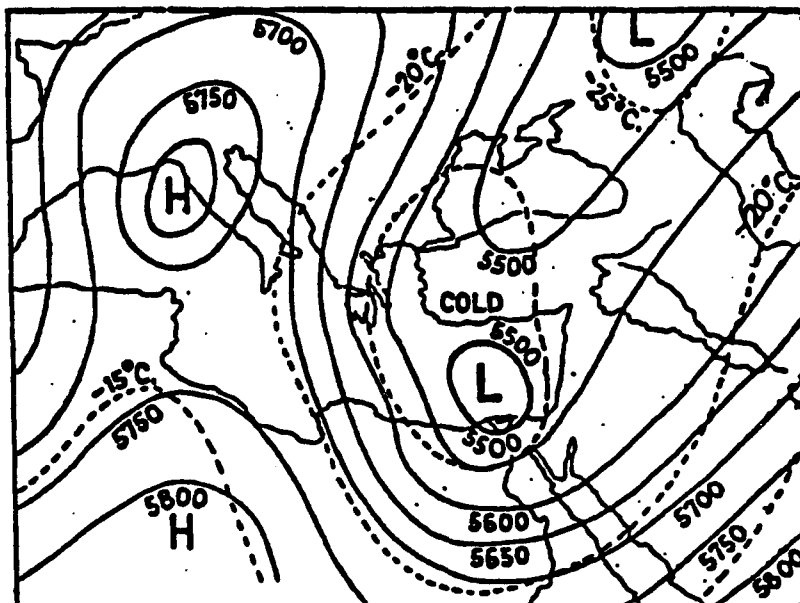


Figure 3-19a. 500-mb Contour Chart Over an Intense Surface Low That Produced Significant Rainfall In The Northern Red Sea Coastal Plains. Dashed lines represent isotherms (°C) at 5-degree intervals, while solid lines denote geopotential height (gpm) at 50-meter intervals.

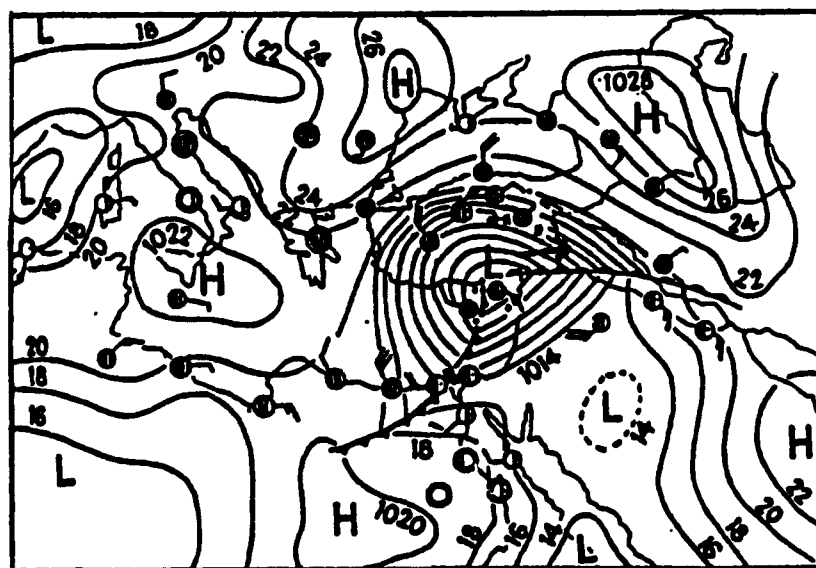


Figure 3-19b. Surface Chart Depicting Cyprus Low Position Beneath a Deep Mid-Level Trough That Produced Significant Rainfall. Solid lines denote surface pressure in millibars at 2-mb intervals. Arrow shows movement of the surface low pressure system.

RED SEA COASTAL PLAINS NORTHEAST MONSOON

December-March

Heavy precipitation can occur over the Sinai Peninsula when the slope of the Subtropical Jet (at 200 to 400 mb) reverses its normal pattern, as shown in Figure 3-20. In the reversed pattern, ridging creates the upper-level divergence needed for producing showers and thunderstorms. Single-day rainfall totals over the Sinai Peninsula may exceed 1 inch (25 mm). Heavy rainfall may also occur along the RSCZ when the Subtropical Jet and the Polar Jet are both over the Red Sea. The two jet streams

"share energy" and produce isolated thunderstorm activity. Intense thunderstorm outbreaks may occur with prolonged instability.

During the early days of Operation DESERT STORM, a combination of convergence of the Subtropical and Polar Jets, cyclogenesis over the northern Red Sea, and orographic lifting from the Hijaz Mountains produced widespread precipitation in the eastern Red Sea Coastal Plains and on into the interior of the peninsula.

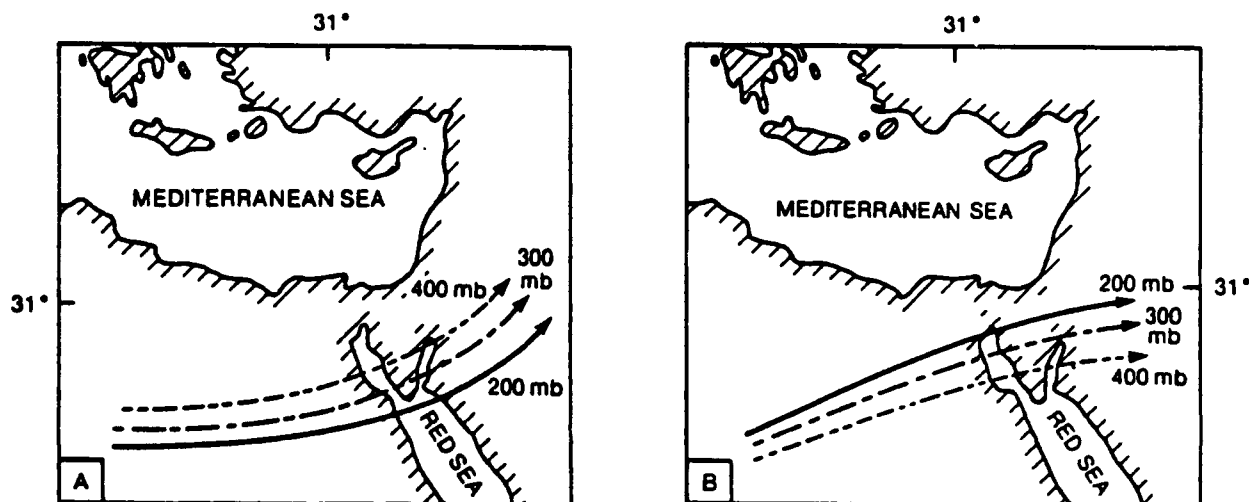


Figure 3-20. A Normal (A) and Reversed (B) Slope of the Upper-Level Wind Flow Pattern. Notice the 200-mb jet core is located to the north of the 400-mb maximum in (b).

Locations along and immediately south of the RSCZ are at their wettest during the Northeast Monsoon; between Massawa and Assab, 60 to 80% of the annual rainfall falls during this

season. Drizzle and light rain showers dominate the southwestern Red Sea Coastal Plains, but thunderstorms may develop over the coastal mountains and drift back over the coast.

RED SEA COASTAL PLAINS NORTHEAST MONSOON

December-March

TEMPERATURE. As shown in Figure 3-21, mean daily lows range from 49 to 75° F (09-24° C); mean daily highs, from 68 to 89° F (20-32° C). The southern Red Sea Coastal Plains south of Jeddah and Port Sudan remain warm throughout the season. The area between 24 and 26° N is a transition zone that marks the southernmost penetration of Mediterranean air masses and the northernmost extent of Northeast Monsoon flow. The Mediterranean air

mass behind a cold front causes a wind shift and, occasionally, rapid decreases in surface air temperature with northwesterly to northerly winds. Within the warm sector of intense systems, southwesterly to southerly flow may rapidly increase surface air temperature. Record lows and highs for the coastal plains are 39° F (04° C) at Hurghada and 102° F (39° C) at Massawa and Assab.

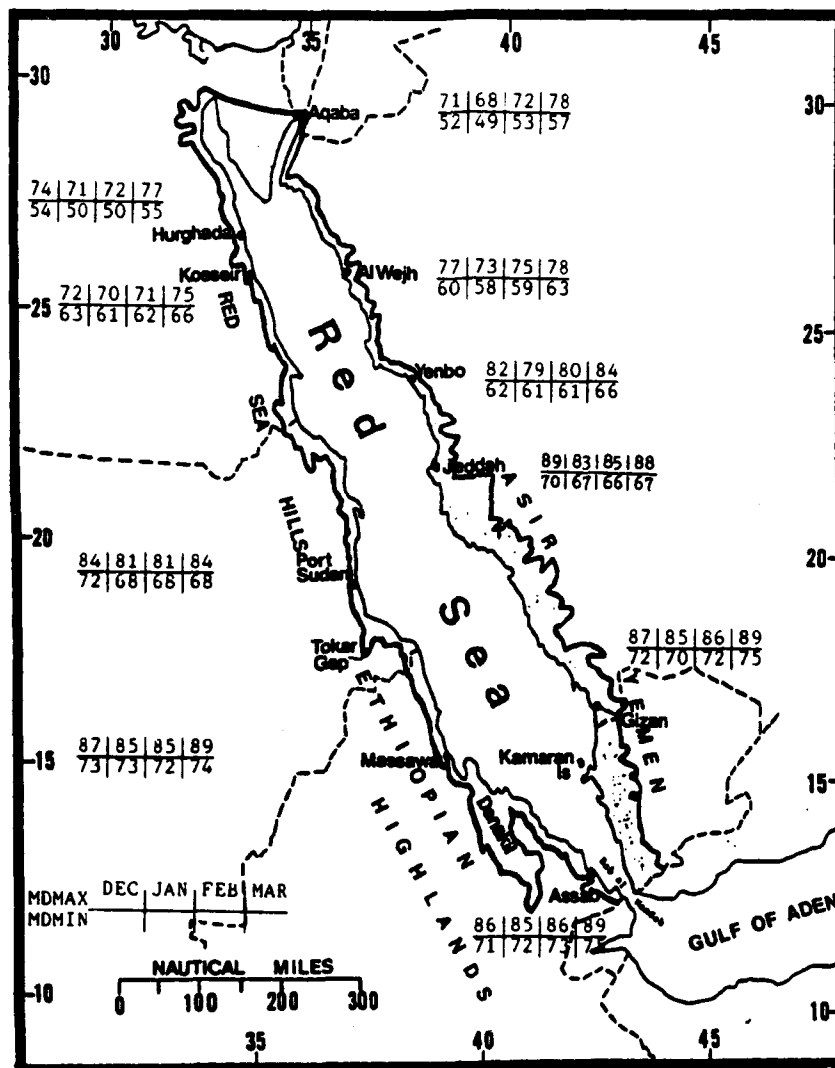


Figure 3-21. Mean Northeast Monsoon Daily Maximum/Minimum Temperatures (° F), Red Sea Coastal Plains.

RED SEA COASTAL PLAINS NORTHEAST-TO-SOUTHWEST MONSOON TRANSITION

April-May

GENERAL WEATHER. April and May are hot and dry, with fair weather and only shallow, sea breeze-induced cumulus convection. The Red Sea Convergence Zone (RSCZ) deteriorates rapidly during April as Northeast Monsoon flow weakens. Rare but intense Atlas Lows can produce severe duststorms with strong southerly-to-southwesterly surface winds and extremely high air temperatures. In extreme cases, isolated thunderstorm activity occurs north of 25° N within the warm sector of an Atlas Low. For a thunderstorm to occur, however, a southward surge of cold mid- or upper-level air and a Polar-Subtropical Jet interaction must accompany the surface disturbance. This may occur once or twice a season, but it may be 3 to 4 years before

another. Thunderstorm bases average 4,000 feet (1,200 meters) AGL with tops to 40,000 feet (12,2 km) MSL.

SKY COVER. Temperature differences between land and sea become more of a factor now as shallow sea-breeze cumulus develops along elevated coastal ranges south of 20° N between 1000 and 1500 LST. Mean transition cloudiness averages 10 to 20% north of 20° N, and 20 to 30% south of 20° N (Figure 3-22). The southwest coastline from Massawa south to the Straits of Bab al Mandab has the highest mean cloudiness, with Massawa at 30% and Assab at 31%. Ceilings below 3,000 feet (915 meters) AGL do not exceed 10%.

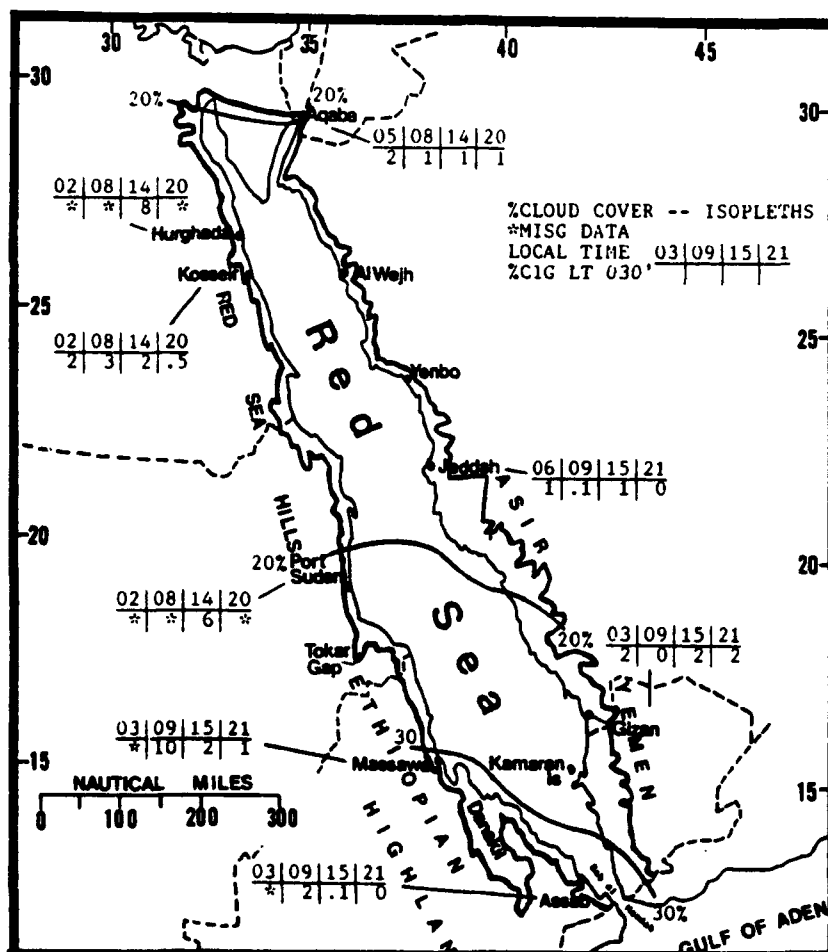


Figure 3-22. Mean SW-NE Monsoon Transition Cloudiness (Isolines) and Frequencies of Ceilings Below 3,000 feet (915 meters), Red Sea Coastal Plains.

RED SEA COASTAL PLAINS NORTHEAST-TO-SOUTHWEST MONSOON TRANSITION

April-May

VISIBILITY. Although visibilities are above 6 miles 90% of the time, the "Khamsin" produces severe dust/sandstorm activity north of 20° N in April. Khamsin conditions persist from an hour to 4 days depending upon the strength, location, and movement of the Atlas Low.

Dust/sandstorm intensity peaks from 1200 to 1500 LST and may lower visibility to 300 feet (91 meters). Highest occurrence of visibilities below 3 miles is at Port Sudan, with 7 to 8% from 0900 to 1500 LST (Figure 3-23).

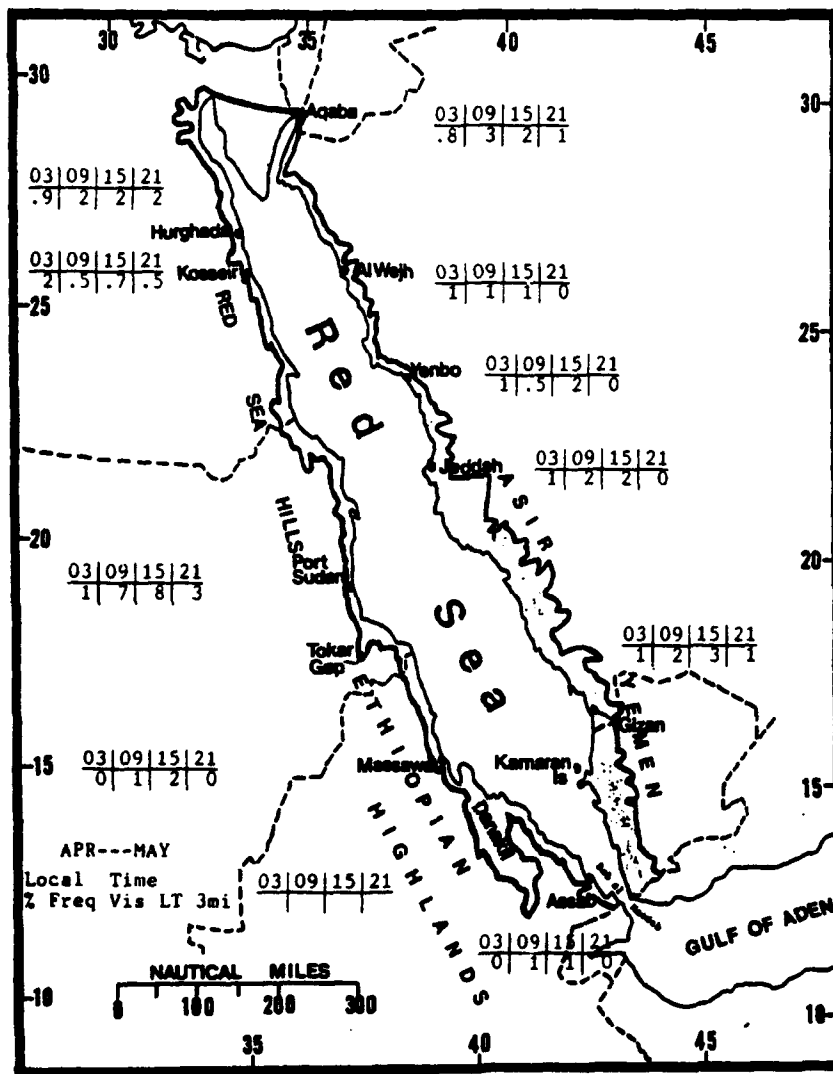


Figure 3-23. Mean NE-SW Monsoon Transition Frequencies of Visibilities Below 3 Miles, Red Sea Coastal Plains.

RED SEA COASTAL PLAINS **NORTHEAST-TO-SOUTHWEST MONSOON TRANSITION**

April-May

WINDS. Mean northwesterly surface flow averages 6 to 9 knots along the Red Sea to about 17° N, where Assab and the Strait of Bab al Mandab get strong east-to-south flow at 13 to 18 knots--see Figure 3-24. The highest maximum sustained surface wind (west at 60 knots) was at Al Wejh in April. Mean April upper-level wind direction at Al Wejh is westerly; speeds are 26

knots at 15,000 feet (4573 meters) MSL, 61 knots at 30,000 feet (9.1 km) MSL, and 83 knots at 39,000 feet (11.9 km) MSL. In May, speeds decrease to 21, 40, and 56 knots, respectively. At Gizan, mean mid-level direction changes from westerly to east-northeasterly by May; mean April-May speeds are 6 to 10 knots. See Figures 3-5a and b for additional data.

		APR	MAY
N	Kasseir	8.40	8.00
W	Gizan	6.00	6.50
N	Jeddah	7.30	6.80
N	Port Sudan	7.30	6.80
W	Yenbo	8.20	8.80
W-NW	Al Wejh	9.20	9.10
SE-E	Assab	18.20	13.20

Figure 3-24. Mean NE-SW Monsoon Transition Wind Speed (kts) and Prevailing Direction, Red Sea Coastal Plains.

RED SEA COASTAL PLAINS NORTHEAST-TO-SOUTHWEST MONSOON TRANSITION

April-May

PRECIPITATION. During April, the RSCZ dissipates as Northeast Monsoon circulation weakens. RSCZ precipitation is light, but sea breeze-induced cumulus may create short-lived, isolated rain showers at Massawa, Kamaran Island, and Gizan. An occasional thunderstorm may develop, providing larger rainfall amounts (0.5-1.0 inch/13-25 mm).

North of 20° N, Aqaba (in April) and Al Wejh receive measurable mean monthly rainfall--see Figure 3-25. Less than 0.05 inches (1.3 mm) is normal throughout the northern area, where

rainfall rarely occurs. A late April or early May frontal passage, however, may provide the total seasonal rainfall for several years. Rainfall occurs about 1 day a season every third or fourth year, even though Atlas Low activity peaks in April. Reasons for the scant rainfall are:

- the air mass has dry, Saharan origins, and
- sustained cold-air support at the mid- and upper-levels is seldom associated with intense Atlas Lows.

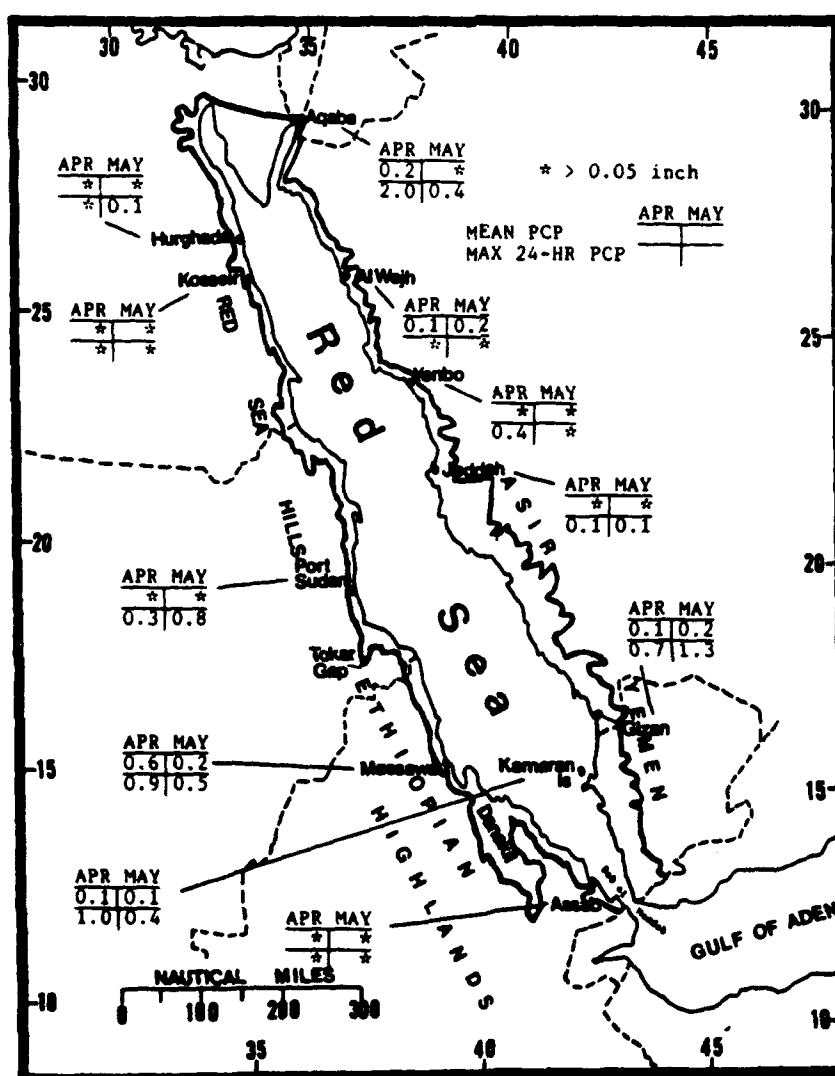


Figure 3-25. Mean NE-SW Monsoon Transition Monthly/Maximum 24-hour Precipitation, Red Sea Coastal Plains.

RED SEA COASTAL PLAINS NORTHEAST-TO-SOUTHWEST MONSOON TRANSITION

April-May

TEMPERATURE. In April and May, intense daytime heating and nocturnal radiation cooling at the surface produces large mean diurnal temperature ranges (Figure 3-26). The largest such range in April (23° F/13° C) is at Jeddah; The largest May range is 24° F (14° C) at Aqaba.

Mean daily highs range from 80° F (27° C) at Kosseir in April to 98° F (37° C) at Assab in May. Record highs in April range from 102° F (39° C) at Port Sudan to 108° F (42° C) at

Kosseir. Record highs in May range from 102° F (39° C) at Kosseir to 114° F (46° C) at Yenbo and Jeddah.

Mean daily lows range from 61° F (16° C) in the north at Hurghada, to 82° F (28° C) in the south at Gizan. Record lows for April range from 36° F (2° C) at Port Sudan to 61° F (16° C) at Gizan. Record lows in May range from 32° F (0° C) at Al Wejh, to 73° F (22° C) at Gizan.

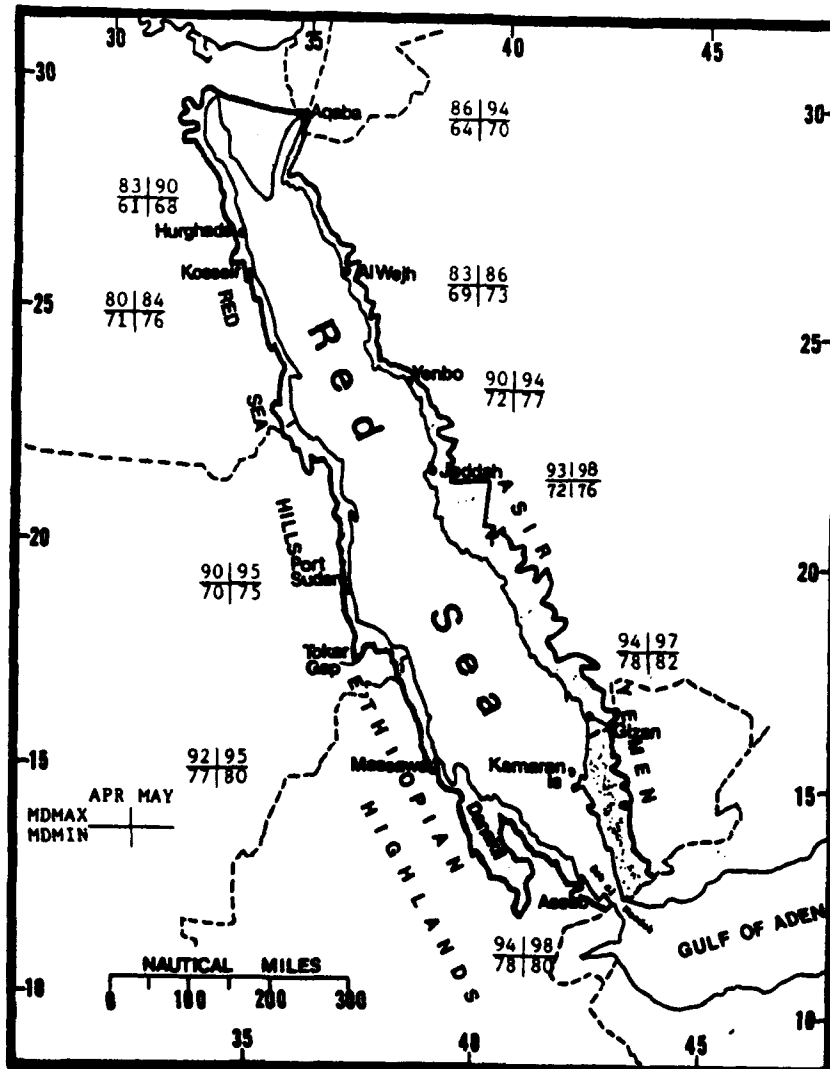


Figure 3-26. Mean NE-SW Monsoon Transition Daily Maximum/Minimum Temperatures (° F), Red Sea Coastal Plains.

Chapter 4

THE FERTILE CRESCENT

The Fertile Crescent comprises most of Iraq, Syria, and small portions of south central Turkey, southwestern Iran below 1,620 feet (500 meters), and northeastern Jordan. After describing the area's situation and relief, this chapter discusses "general weather conditions" by season.

Situation and Relief	4-2
Winter—December-March	4-7
General Weather	4-7
Sky Cover	4-7
Visibility	4-9
Winds	4-10
Precipitation	4-13
Temperature	4-18
Spring—April-May	4-19
General Weather	4-19
Sky Cover	4-19
Visibility	4-21
Winds	4-22
Precipitation	4-22
Temperature	4-25
Summer—June-September	4-26
General Weather	4-26
Sky Cover	4-26
Visibility	4-28
Winds	4-29
Precipitation	4-30
Temperature	4-31
Fall—October-November	4-32
General Weather	4-32
Sky Cover	4-32
Visibility	4-34
Winds	4-35
Precipitation	4-36
Temperature	4-38

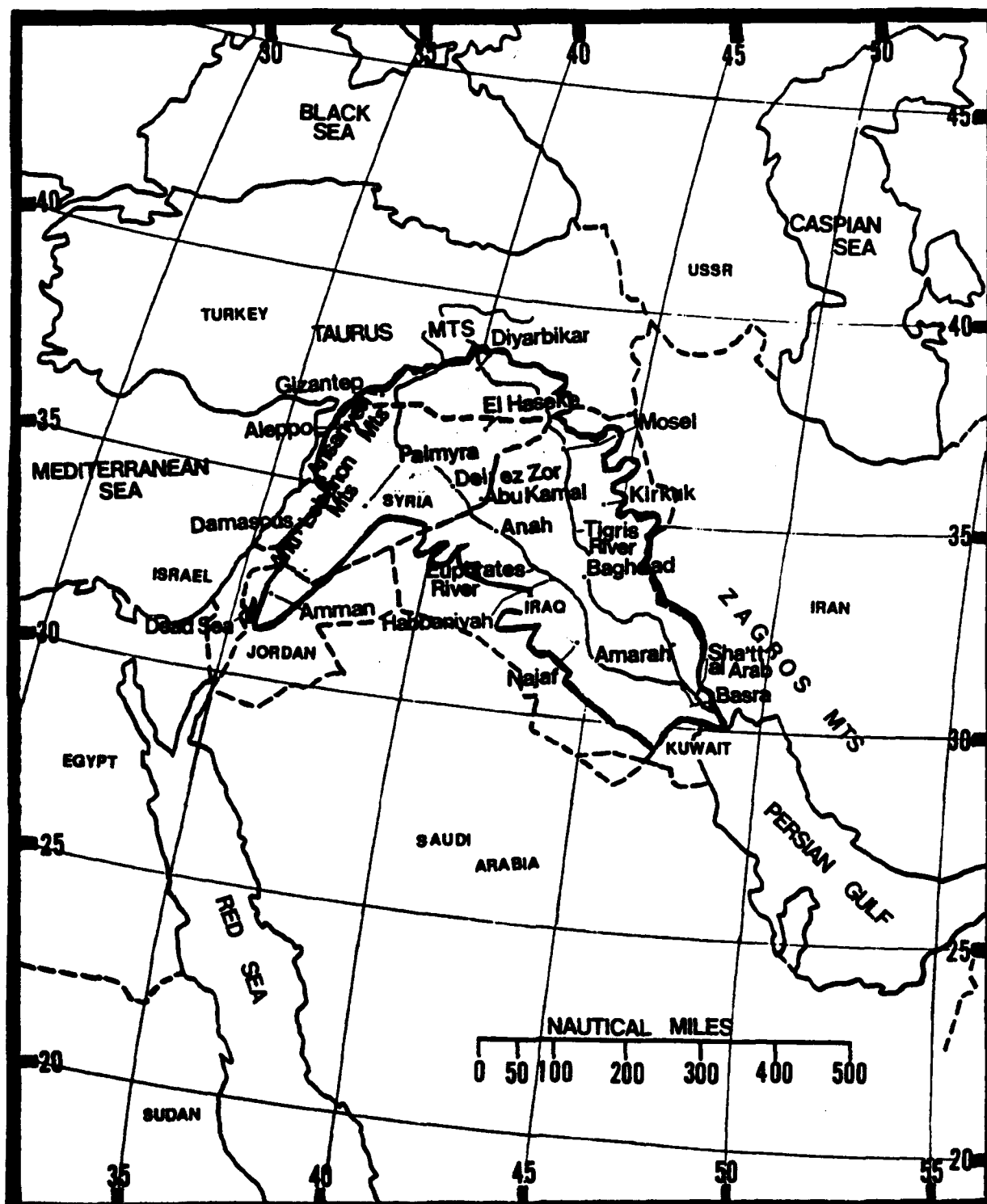


Figure 4-1a. The Fertile Crescent. The Fertile Crescent comprises 80% of the Tigris/Euphrates drainage system. It extends northwestward from the northwestern edge of the Persian Gulf through Iraq and includes extreme southern and southeastern Turkey, eastern and southern Syria, and west-central Jordan. Data summaries for selected stations in the Fertile Crescent are given in Figure 4-1b.

THE FERTILE CRESCENT

SITUATION AND RELIEF

STATION: AMMAN/KING ABDULLAH JORDAN												
LAT/LON: 31 57 N 35 57 E ELEV: 2530 FT												
ELEMENTS	JAN	FEB	MAR	APR	MAY	JUN	JUL	AUG	SEP	OCT	NOV	DEC
XTN MAX	81	86	90	103	108	109	108	108	108	99	91	77
AVG MAX	84	88	92	103	108	109	108	108	108	99	91	77
AVG MIN	39	40	43	49	57	61	65	65	62	57	50	42
XTN MIN	21	19	26	34	38	48	54	54	48	41	27	25
AVG PRCP	2.7	2.9	1.2	0.6	0.2	0.0	0.0	0.0	0.2	1.3	1.8	10.9
MAX MON	4.8	7.5	2.8	2.2	1.0	0.0	0.0	0.0	0.8	1.8	5.0	4.3
MAX DLY	2.4	3.1	1.4	1.6	0.8	0.0	0.0	0.0	0.6	1.8	3.1	3.1
TS DAYS	1	1	1	1	1	1	1	1	1	1	1	1
DUST DAYS	1	1	1	2	1	1	1	1	1	1	1	1
FOG DAYS	2	1	1	0	0	0	0	0	0	0	1	1

* = LESS THAN 0.05 INCHES OR LESS THAN 0.5 DAYS

STATION: HANAN/IRAC												
LAT/LON: 33 20 N 44 24 E ELEV: 112 FT												
ELEMENTS	JAN	FEB	MAR	APR	MAY	JUN	JUL	AUG	SEP	OCT	NOV	DEC
XTN MAX	80	85	89	108	113	110	123	121	117	108	85	81
AVG MAX	81	85	89	108	113	110	123	121	117	108	85	81
AVG MIN	39	43	49	58	68	74	78	77	71	62	51	43
XTN MIN	21	23	27	39	50	61	68	68	58	44	27	19
AVG PRCP	1.1	1.4	1.2	0.7	0.2	0.0	0.0	0.0	0.1	0.8	1.1	6.7
MAX MON	5.1	7.8	5.1	3.2	1.3	0.5	0.1	1.1	0.2	0.7	6.2	4.5
MAX DLY	12	8	4	3	3	2	3	2	1	2	5	14
TS DAYS	1	1	2	3	3	0	0	0	0	1	2	1
DUST DAYS	3	4	5	6	6	5	8	6	3	4	2	2
APP TEMP												

* = LESS THAN 0.05 INCHES OR LESS THAN 0.5 DAYS

STATION: BASRA/IRAC												
LAT/LON: 30 30 N 47 50 E ELEV: 7 FT												
ELEMENTS	JAN	FEB	MAR	APR	MAY	JUN	JUL	AUG	SEP	OCT	NOV	DEC
XTN MAX	80	87	93	109	118	119	122	121	117	108	94	81
AVG MAX	80	86	94	104	108	104	105	101	91	77	64	55
AVG MIN	44	48	56	65	74	80	81	80	74	68	58	48
XTN MIN	24	31	39	51	59	68	68	68	68	49	38	30
AVG PRCP	1.8	1.0	0.9	0.8	0.8	0.0	0.0	0.0	0.1	1.1	1.1	0.9
MAX MON	7.5	3.4	4.2	5.8	3.2	0.1	0.1	1.3	0.8	5.9	4.1	13.9
MAX DLY	14	12	10	10	9	10	10	6	6	7	14	118
TS DAYS	0	0	1	2	0	0	0	0	0	0	0	3
DUST DAYS	2	3	3	4	8	7	8	4	3	1	1	48
APP TEMP												

* = LESS THAN 0.05 INCHES OR LESS THAN 0.5 DAYS

STATION: HARBANIYAH/IRAC												
LAT/LON: 33 22 N 43 34 E ELEV: 1430 FT												
ELEMENTS	JAN	FEB	MAR	APR	MAY	JUN	JUL	AUG	SEP	OCT	NOV	DEC
XTN MAX	79	87	97	108	116	120	123	122	119	108	97	79
AVG MAX	80	85	93	108	116	120	123	122	119	108	97	79
AVG MIN	39	42	48	58	68	73	78	77	70	60	51	42
XTN MIN	18	23	27	38	50	60	70	67	62	41	28	20
AVG PRCP	0.8	0.7	1.0	0.8	0.3	0.0	0.0	0.0	0.1	0.8	0.8	4.8
MAX MON	2.4	2.1	3.3	4.2	3.2	0.0	0.0	0.3	0.8	1.8	3.1	10.0
MAX DLY	10	3	1	1	1	0	0	1	2	0	1	10
TS DAYS	1	1	2	3	1	0	0	0	0	0	2	1
DUST DAYS	3	5	7	8	8	7	7	3	3	2	3	4
APP TEMP												

* = LESS THAN 0.05 INCHES OR LESS THAN 0.5 DAYS
- = INSUFFICIENT DATA FOR CLIMATOLOGICAL SUMMARIZATION

STATION: KIRKUK/IRAC												
LAT/LON: 33 28 N 44 24 E ELEV: 331 FT												
ELEMENTS	JAN	FEB	MAR	APR	MAY	JUN	JUL	AUG	SEP	OCT	NOV	DEC
XTN MAX	72	80	88	98	110	116	118	116	108	91	79	118
AVG MAX	58	68	78	88	103	109	108	101	90	74	61	83
AVG MIN	38	40	45	54	65	74	78	79	71	62	52	43
XTN MIN	20	20	22	34	47	57	68	67	49	34	24	20
AVG PRCP	2.5	2.8	3.2	1.9	0.8	0.0	0.0	0.0	0.0	0.2	1.7	2.4
MAX MON	5.4	6.2	9.8	5.6	4.4	0.1	0.0	0.1	1.5	6.1	6.4	30.3
MAX DLY	2	1	1	2	2	0	0	1	0	1	2	13
TS DAYS	1	2	3	4	4	1	0	0	1	2	1	19
DUST DAYS	2	1	3	3	4	5	5	3	3	1	1	37
APP TEMP												

* = LESS THAN 0.05 INCHES OR LESS THAN 0.5 DAYS

Figure 4-1b. Climatological Summaries for Selected Stations in the Fertile Crescent.

THE FERTILE CRESCENT

GEOGRAPHY. The Fertile Crescent's northern boundary begins at the Persian Gulf at the Sha'tt Al Arab River--the confluence of the Tigris and Euphrates Rivers--near 30° N, 48° 30' E. It extends northward along the Iran/Iraq border to 35° N, then follows the 1,620-foot (500-meter) contour through northeastern Iraq to the Turkey-Iraq-Syria border at 37° 05' N, 42° 25' E. From there, it follows the 3,280-foot (1,000-meter) contour through Turkey to the Syrian border at 37° 45' N, 36° 40' E. It then extends north to south from the Turkey-Syria border to the Ansariyeh Mountains above 3,280 feet (1,000 meters) in Syria, and then along the Syrian border with Lebanon and Israel. At the Syria-Israel-Jordan border, it follows the 1,620-foot (500-meter) contour southward to 31° N, 35° 40' E.

The southern boundary extends from 31° N, 35° 40' E, north-northeast to the 1,620-foot (500-meter) contour west of Palmyra, Syria at 36° N, 38° E. It follows this contour through Syria and western Iraq to 33° N. The boundary then extends eastward along 33° N for 70 NM to 42° 35' E and the 656-foot (200-meter) contour line. The 656-foot (200-meter) contour is followed southeastward to the Iraq-Kuwait border to the Persian Gulf coast and the Sha'tt al Arab River.

The Fertile Crescent is dominated by the Tigris and Euphrates Rivers and their tributaries. Both rivers originate in Turkey and flow southeastward into the Persian Gulf. The Euphrates flows through northeastern Syria before entering Iraq. The Tigris forms the northeast border of Syria and Turkey. Both come together 100 NM upstream from the Persian Gulf to form the Sha'tt al Arab River, which marks the Iraq-Iran border 50 NM from the Gulf.

The Tigris and Euphrates flow in very narrow, but steep channels through Turkey, northeastern Syria, and northern Iraq. North of Baghdad,

SITUATION AND RELIEF

they form wide, well-defined flood plains, the outer edges of which form natural levees. Southeast of Baghdad, the river valleys are level. The river channels are actually elevated above the valley floor in places because the rivers flood, change course, and periodically return to older channels. Common features along the Tigris-Euphrates River Valley are marshes, dry oxbow lake beds, and sandbars.

The Zagros Mountains and their foothills rim the Fertile Crescent on the east. The Arabian Desert plateau dominates the area southwest of the river valley. The northern fringe of the Fertile Crescent includes the foothills of the Taurus Mountains.

DRAINAGE AND RIVER SYSTEMS. The Tigris River is 1,000 NM long with an extensive system of tributaries. The Great Zab, the Lesser Zab, and the Diyala Rivers feed the Tigris from lakes near the Turkish and Iranian borders. The Luristan province of western Iran is the source of many smaller rivers and streams (or wadis) that feed into the Tigris when sufficient rainfall fills the dry streambeds.

The Euphrates River is 1,480 NM long with a few large tributaries; the Khabir River in eastern Syria is the only one of any size. A number of small streams feed the Euphrates in Turkey and northern Syria, but isolated wadis are the only tributaries of the Euphrates in Iraq.

The Orontes River is 209 NM long. It originates in the Bekaa Valley of Lebanon and flows northward through Syria into Turkey. The Orontes River valley is 20-30 NM wide with extensive marshlands immediately east of the Ansariyeh Mountains. The Yarmuk in southern Syria and the Zarqa in northeast Jordan are the only rivers in the extreme southwestern portions of the Fertile Crescent. Figure 4-2 shows the most important rivers, streams, and lakes in the subregion.

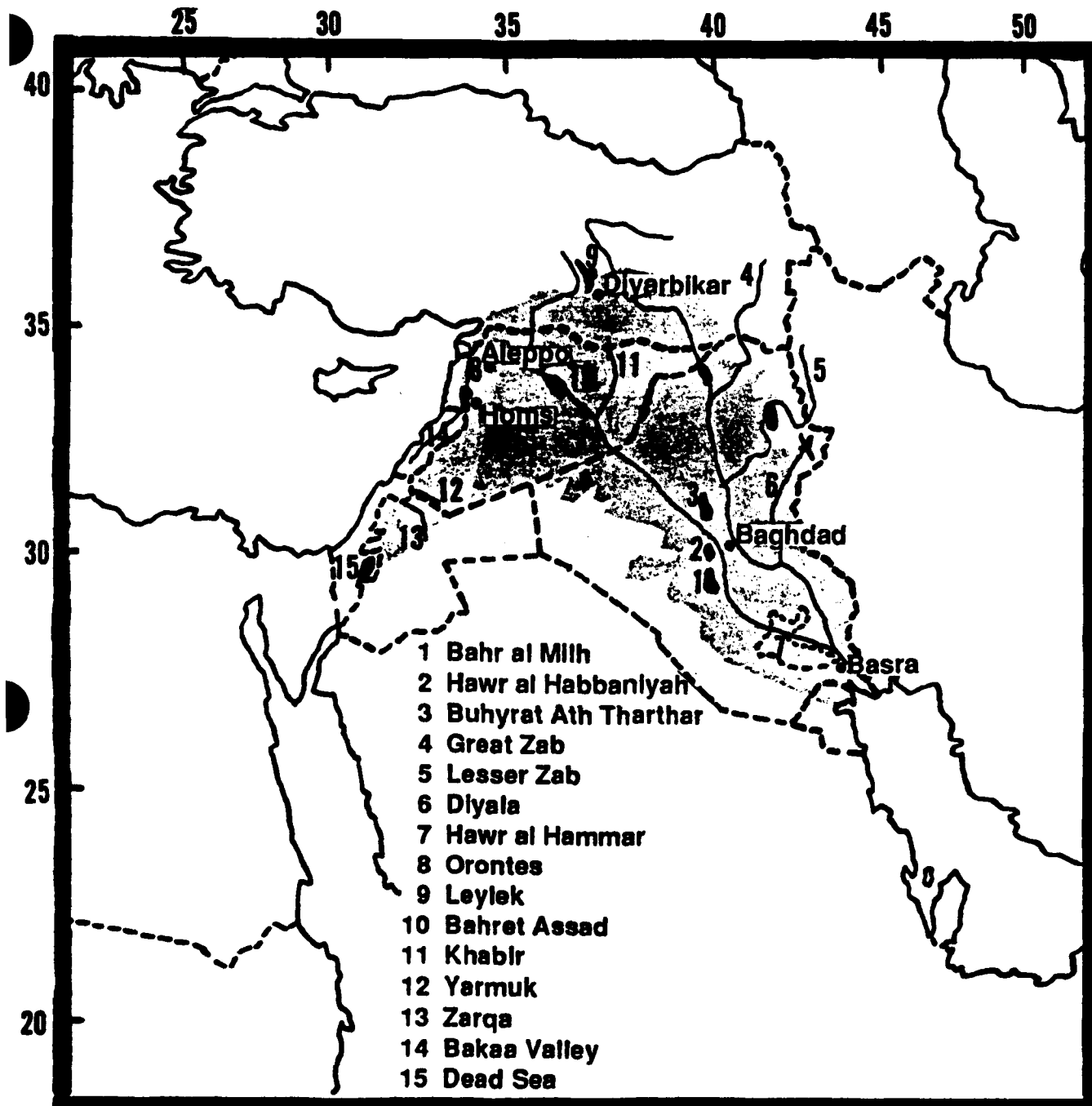


Figure 4-2. The Fertile Crescent's Important Rivers, Streams, and Lakes.

LAKES AND RESERVOIRS. There are three large freshwater lakes near Baghdad. The Buhyat Ath Tharthar, a flood control reservoir 48 NM northwest of Baghdad, is 17 by 39 NM.

The Hawr al Habbaniyah, 17 NM south of BuhyatAth Tharthar, is 7 by 13 NM. The Bahr al Milh, 5 NM south of Hawr al Habbaniyah is about the same size as Buhyat Ath Tharthar.

THE FERTILE CRESCENT

A number of oxbow lakes and shallow ponds lie along the Euphrates/Tigris flood plain between Baghdad and the Persian Gulf. They all vary in size with seasonal flooding. The largest is the brackish and shallow Hawr al Hammar; after heavy flooding, it can take 2 months to return to normal.

The largest lake in Turkey is the Leylek, 13 NM long and 2-4 wide. In Syria, the Bahret Assad, 20 NM east of Aleppo, is 43 NM long and 7-13 NM wide. The Bahret Homs lake, 6 NM southwest of Homs, Syria, is 9 NM long and 2-4 NM wide. There are several other shallow, semipermanent lakes in central and southwestern Syria.

SITUATION AND RELIEF

VEGETATION. The most fertile area lies between Buhyat Ath Tharthar and the Persian Gulf. Dates and cotton are the primary crops, but irrigation sustains several others. Besides the fertile valley vegetation, scattered date palms and aquatic grasses flourish in isolated pockets along the Tigris and Euphrates. Some sections of eastern Syria and western Iraq contain sparse grasses and mixed forest. Alpine vegetation flourishes in southeastern Turkey. Isolated evergreen and mountain shrubs are found in narrow bands along the eastern Anti-Lebanon and Ansariyeh Mountains.

THE FERTILE CRESCENT WINTER

December-March

GENERAL WEATHER. Winter weather in the Fertile Crescent generally features fair skies, but migratory low, middle, or upper troughs may affect the subregion every 3 to 5 days. These systems bring short periods of rainshowers, multilayered clouds, and an occasional duststorm.

The origin of these troughs is very important. Cyprus Lows consistently produce more rain, cloudiness, and thunderstorms across the Fertile Crescent than any other surface low because they contain more low-level moisture. If supported by a mid- and upper-level trough, the Cyprus Low can produce clouds and precipitation over a wide area.

Very cold mid-level troughs bring occasional snowfall in elevations above 2,000 feet (610 meters). One inch (25 mm) or more of snow falls at Diyarbikar on 1 or 2 days every 3 years.

The 24- to 36-hour or 3- to 5-day Shamals can occur with deep polar air surges. Deep Black Sea Lows may contain enough polar air aloft to extend a well-defined surface cold front into the Fertile Crescent. During Operations DESERT SHIELD/STORM, systems that affected the region were more frequent and caused extensive cloudiness, rain, and fog.

SKY COVER. Winter is the cloudiest season; mean values range from 33% at Baghdad to 61% at Aleppo (see Figure 4-3). Aleppo's average reaches a peak of 70% in the morning and the early afternoon hours during December and January. Cloud cover decreases from the

northwest to the southeast since the Mediterranean moisture is lost while crossing the Anti-Lebanon/Ansariyeh Mountains.

Most winter cloud cover is from cyclonic activity, but cirrus occurs with the Subtropical Jet. Cumulus and cumulonimbus development is common with mid-level and surface troughs. Cool and moist Mediterranean air enters the Fertile Crescent every 3 to 5 days; cold fronts bring clear skies or widely-scattered altocumulus. Weak mid- or upper-level troughs without surface fronts may produce scattered cumulus. Thunderstorms produce cloud tops to 40,000 feet (12,915 meters); bases are between 4,000 and 5,000 feet (1,220-1,524 meters) AGL.

Low clouds with surface troughs have bases between 2,000 and 3,000 feet (610-915 meters) AGL. Typically, low cloud cover is cumulus embedded within a thin stratus deck. Stratus and stratocumulus commonly form along the Ansariyeh's and Anti-Lebanon's eastern slopes, but it seldom accompanies surface troughs south of 35° N or east of 35° E. Ceilings are below 2,000 feet (610 meters) AGL on 2 or 3 days a month in December and January along the Tigris-Euphrates River Valley between Baghdad and Basra. Ceilings less than 1,000 feet (305 meters) AGL, are thin-layered stratus along a warm front when southeasterlies are 10 knots or better; this is rare, but it can occur when a strong surface low tracks into the Persian Gulf and brings low-level Gulf moisture. Stratus and fog usually dissipate quickly after the cold front passes.

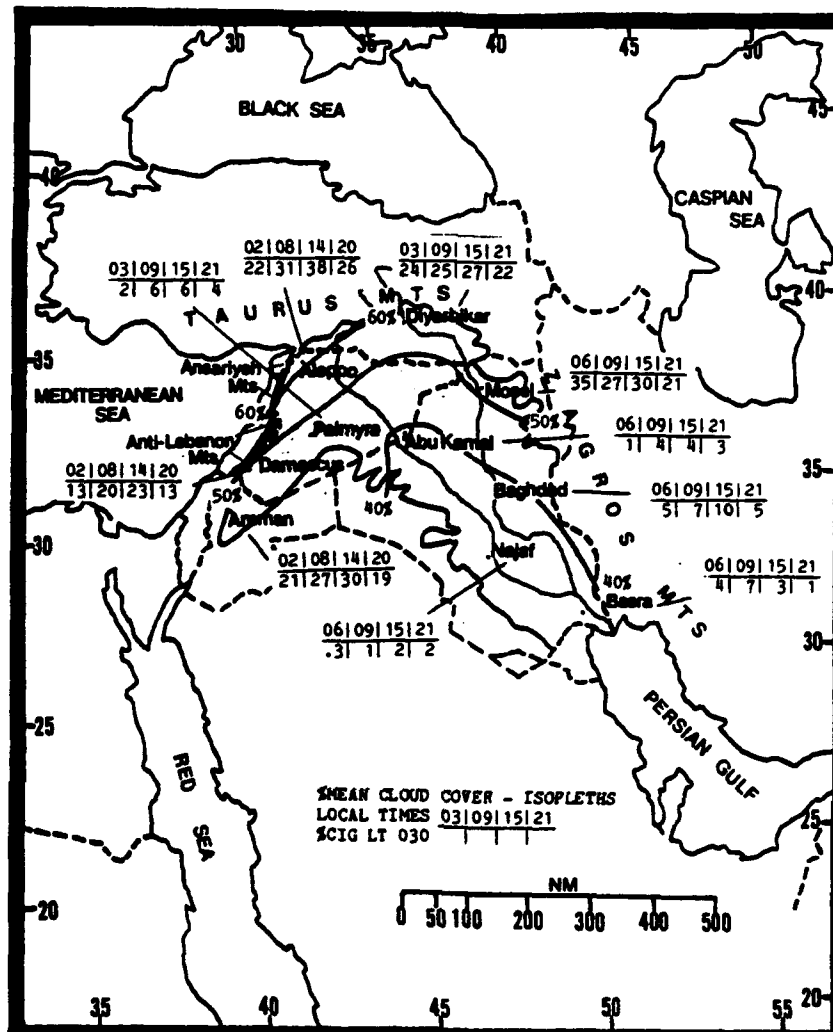


Figure 4-3. Mean Winter Cloudiness (Isolines) and Frequencies of Ceilings Below 3,000 Feet (915 meters), Fertile Crescent.

THE FERTILE CRESCENT WINTER

December-March

VISIBILITY. Fog, haze, smoke, dust, and blowing sand restrict winter visibilities, but fog is the primary cause of low visibilities in the northeastern part of the Fertile Crescent from Diyarbikar to Damascus. Radiation fog occurs between 2200 and 0600 LST with fair weather, cold nights and light winds, but usually burns off before 1100 LST (Figure 4-4).

Around Baghdad and Basra, fog or moisture haze may form on calm evenings after moderate rainfall, sometimes persisting for long periods of time if cold and stable regime sets in and passage of a surface low has brought in moist air off the Gulf. Dust, haze, and smoke are

concentrated over large industrial and manufacturing areas. Strong winds with migratory lows can produce blowing dust or sand. In fact, shamals produce more duststorms/sandstorms in the winter months than in any other season. Severe and unpredictable duststorms/sandstorms may also occur with an intensifying Saudi Arabian High during extended fair weather.

Visibilities below 3 miles are most common during the winter months. Low visibility during the 2100 to 0300 LST period are mostly fog and/or haze-related events, while blowing dust and sand is more common during the day.

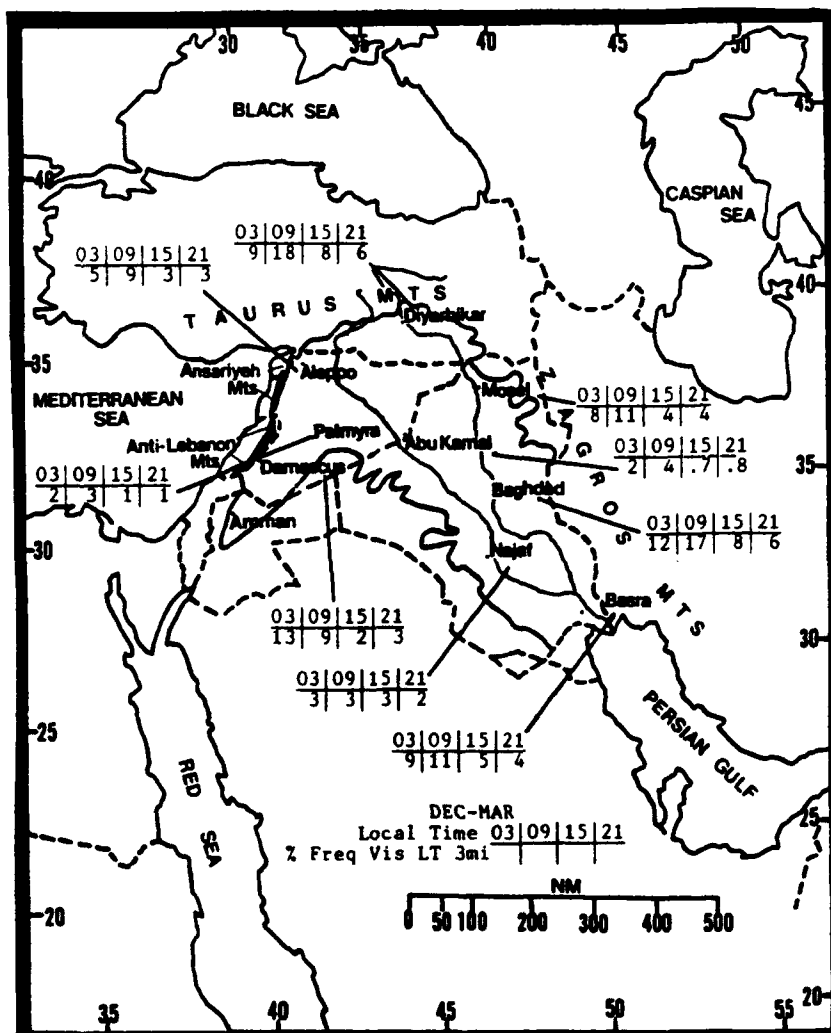


Figure 4-4. Mean Winter Frequencies of Visibilities Below 3 Miles, Fertile Crescent.

THE FERTILE CRESCENT WINTER

December-March

WINDS. Winter surface winds are normally light and variable except during cyclonic activity. Typically, fair weather westerlies or weak northwesterlies occur with weak transitory Saharan and Saudi Arabian Highs. Lowest mean surface wind speeds are along the foothills of the Taurus and Zagros Mountains, which offer a natural wind break from Siberian air masses. The mountains prevent cold northerly and northwesterly synoptic flow penetration except on rare occasions when the entire interior plateau of Turkey is snow-covered. Northerly flow may slip southward along the Taurus Mountain foothills because cold air piles up on the plateau and drains through the narrow Euphrates River Valley. Strong northerlies may funnel to Aleppo across northern Syria.

As shown in Figure 4-5, easterly winds prevail at Aleppo, Damascus, and Mosel in December; easterly flow persists at Aleppo and Mosel into January and February. The easterly wind components may be the result of calm synoptic conditions that allow local mesoscale winds (such as nocturnal drainage) to dominate.

Maximum winter surface winds vary widely. The highest recorded sustained gust at Aleppo was northerly at 51 knots in December. Palmyra recorded 90 knots from the south-southwest, also in December. In contrast, Najaf's peak was northeast at 50 knots in March. At Basra, the maximum was from the west-southwest at 43 knots, in February.

Figure 4-6a shows a mean westerly wind from 5,000 feet (1,524 meters) to 15,000 feet (4,573 meters) MSL at Baghdad, while Aleppo (Figure 4-6b) and Damascus (Figure 4-6c) vary from south-southwest to westerly. At all three stations, mean 5,000-foot (1,524-meter) speeds range from 11 to 14 knots; 10,000-foot (3,050-meter) wind speeds average from 16 to 23 knots. Wind speeds at 15,000 feet (4,573 meters) MSL average from 28 to 32 knots at Damascus and Baghdad, but only from 20 to 26 knots at Aleppo. Mean monthly 39,000-foot (11,890-meter) wind speeds for all three upper-air stations are shown in Figure 4-7.

		DEC	JAN	FEB	MAR
E/W	Aleppo	4.30	5.00	5.60	6.30
NNE/SW	Damascus	5.30	6.20	7.00	7.20
W-NNW	Najaf	4.50	5.00	5.60	6.30
WNW-NNW	Basra	5.40	6.00	6.20	6.40
W	Palmyra	4.30	4.10	5.40	6.40
E/W	Mosel	1.10	1.60	1.80	2.20
NW-N	Diyarbikar	3.50	3.60	4.30	4.50
W-N	Baghdad	4.70	5.70	6.30	7.10

Figure 4-5. Mean Winter Surface Wind Speed (kts) and Prevailing Direction, Fertile Crescent. The slash that separates wind directions illustrate differences between the beginning and the end of the winter season.

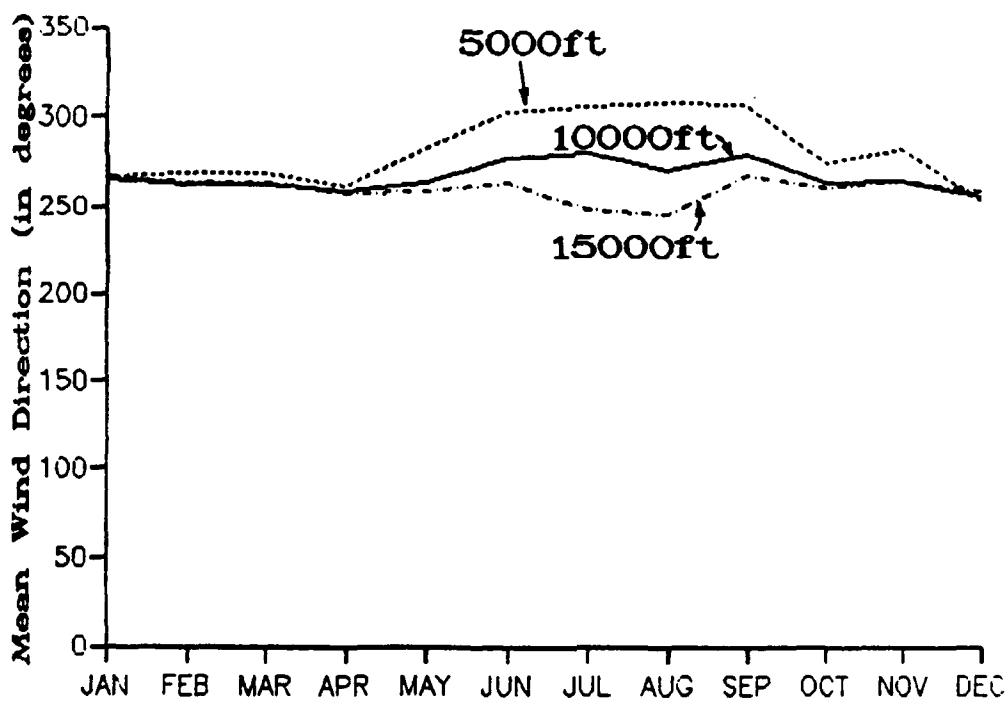


Figure 4-6a. Mean Annual Wind Direction, Baghdad, Iraq.

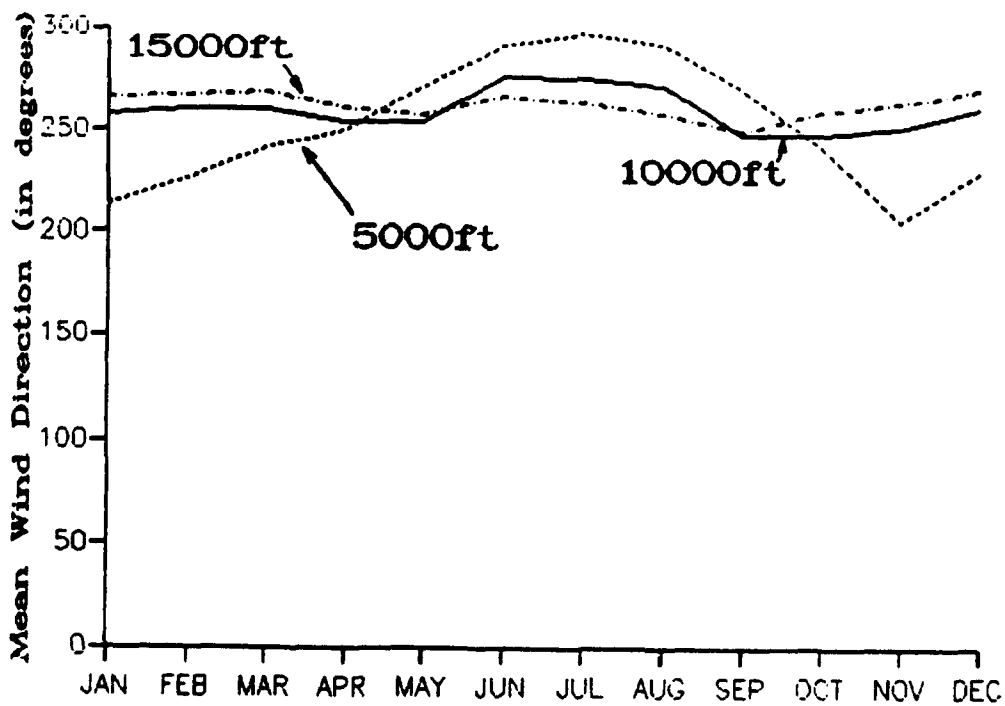


Figure 4-6b. Mean Annual Wind Direction, Aleppo, Syria.

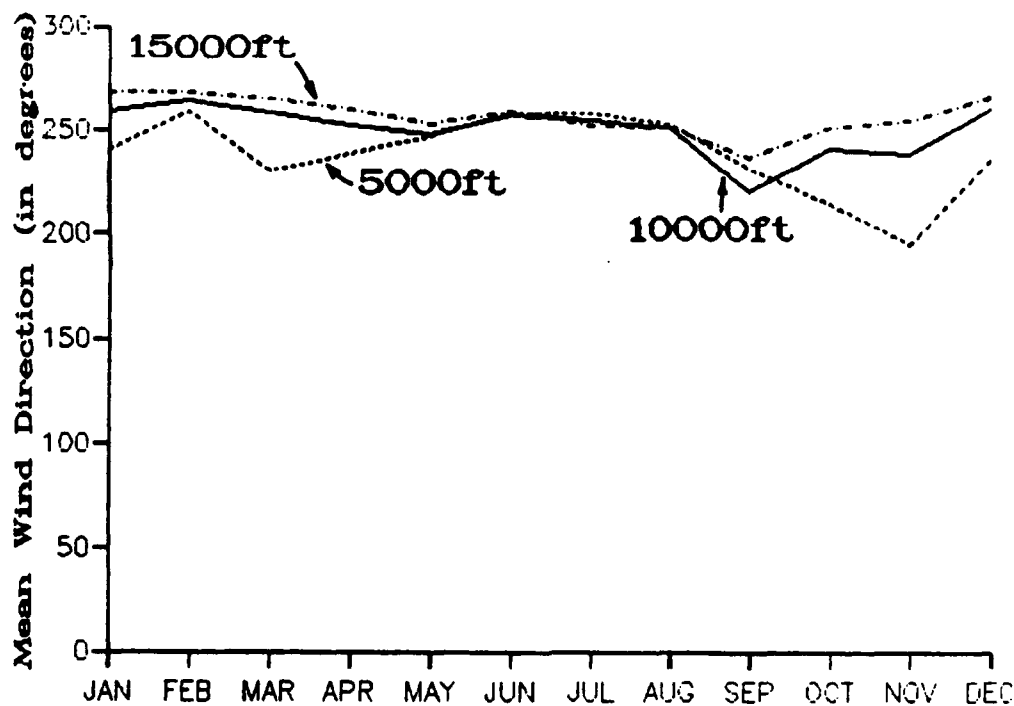


Figure 4-6c. Mean Annual Wind Direction, Damascus, Syria.

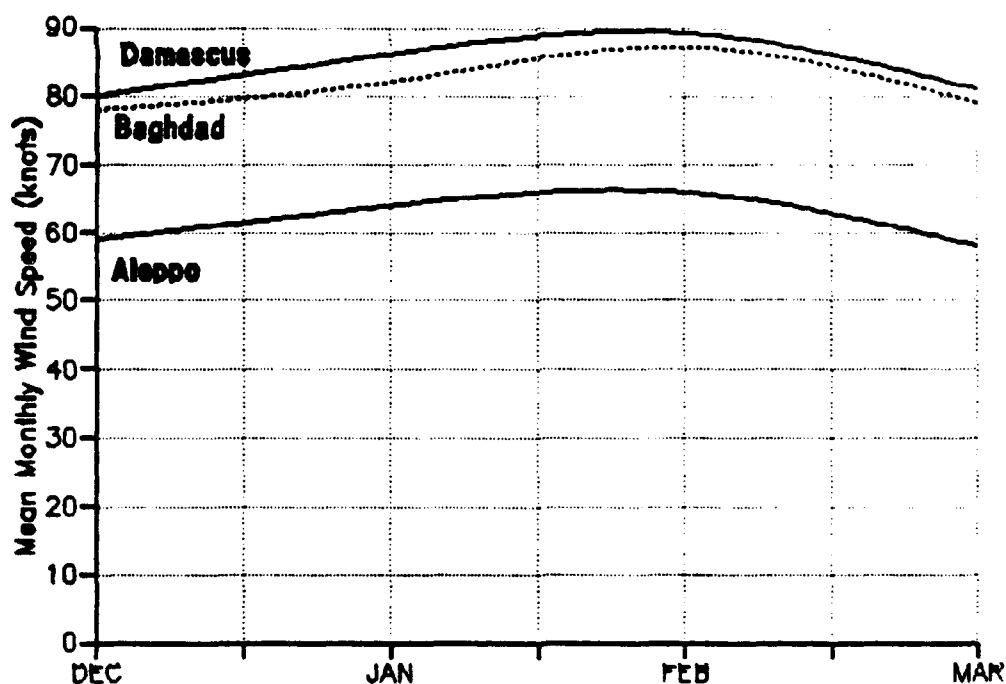


Figure 4-7. Mean Monthly (Winter) 39,000-Foot (11,900-meter) MSL Wind Speeds (kts), Fertile Crescent Upper-Air Data Network. This level is the approximate height of the Subtropical Jet. Wind direction is westerly during all months.

THE FERTILE CRESCENT WINTER

December-March

PRECIPITATION. Mediterranean systems regularly produce rainfall; more than 80% of the annual precipitation occurs during the winter at many Fertile Crescent locations. Nearly all precipitation is from rainshowers or thunderstorms associated with surface cold fronts and transitory lows. Cold fronts cross the subregion every 3 to 5 days. Light rain showers or drizzle due to warm-front overrunning are rare, but warm-front precipitation may be induced by orographic lifting along the Taurus Mountains when a Cyprus Low intensifies over the Ansariyeh Mountains.

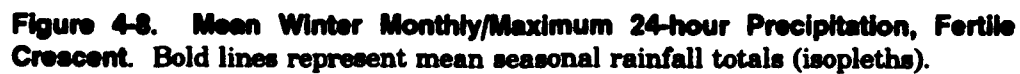
Winter rainfall is extremely variable in duration and intensity. Even though it may rain only 1 or 2 days in a given month, 1-day rainfalls may exceed the monthly mean (Figure 4-8). The heaviest 24-hour maximum rainfall in winter was at Najaf in February, but the observing stations are so sparse here that higher amounts may have gone undetected. The Anti-Lebanon, Ansariyeh, and Taurus Mountains produce heavy precipitation occasionally from severe thunderstorms. Continuous rainfall for more than 3 hours is uncommon, but stations in the foothills of the Taurus Mountains between Diyarbikar and Gizantep have recorded 12-hour rainfalls. These rare events occur when a Cyprus Low stalls and intensifies over the Ansariyeh Mountains, causing continuous orographic lifting.

Strong thunderstorms (see Figure 4-9) can cause localized flooding. Knowledge of surface drainage is vital for forecasting flash floods. Thunderstorms form when there is cold air aloft over a low- or mid-level trough. Figure 4-10a-d shows the difference between a Cyprus Low with and without the cold-air support needed to produce severe thunderstorms and heavy precipitation. Severe thunderstorms may produce hail once or twice during a winter month. Hail is normally small, but can reach marble-size.

Thunderstorms and rainshowers occasionally develop along a wind shift line preceding a cold front. Thunderstorms may also occur when a pre-frontal vortex forms along the lee side of the southern Anti-Lebanon Mountains near Damascus. This "meso low" can generate bands of showers with embedded cumulonimbus in advance of the surface front with southeasterly or southerly surface winds.

Snow is a rare in the Fertile Crescent, but can occur in the foothills of the Taurus/Zagros Mountains of southeastern Turkey and northeast Iraq. Snow rarely stays on the ground more than a few days, but several inches (51 mm) once remained for 8 days near Diyarbikar. Snow has been well documented along the southern Anti-Lebanon Mountains between Damascus and Amman. In March 1980, Amman received over 23 inches (600 mm) from an intense Cyprus Low.

December-March



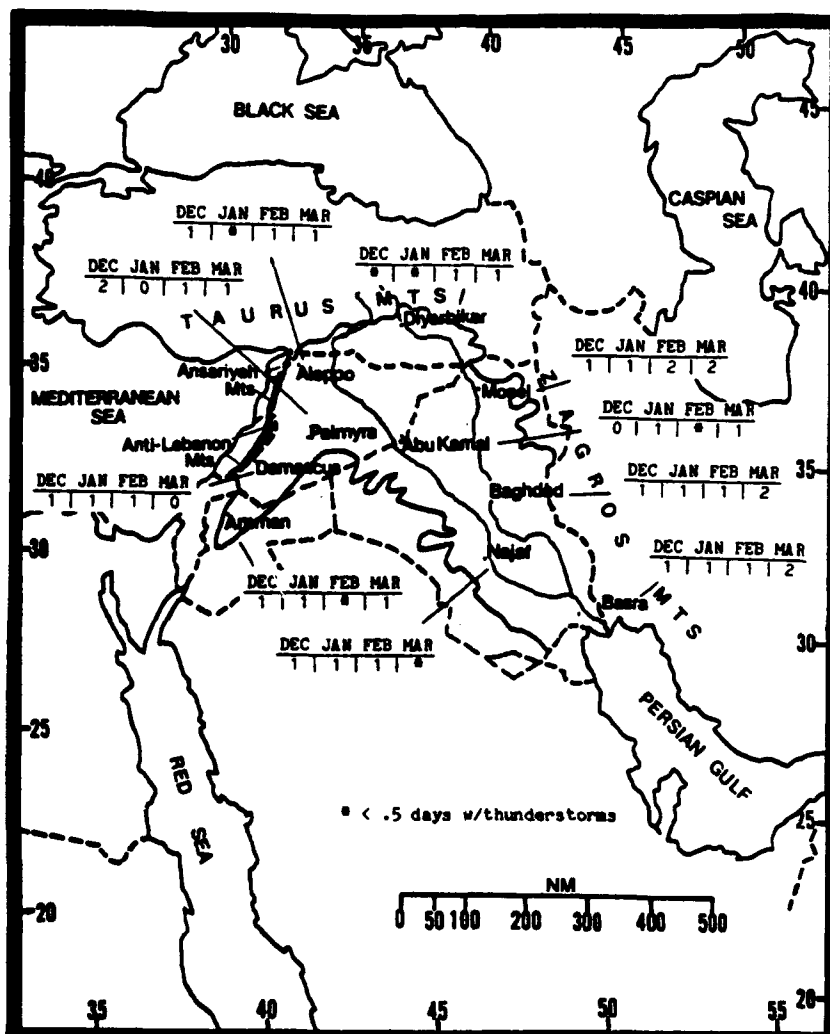


Figure 4-9. Mean Winter Frequencies of Thunderstorms, Fertile Crescent.

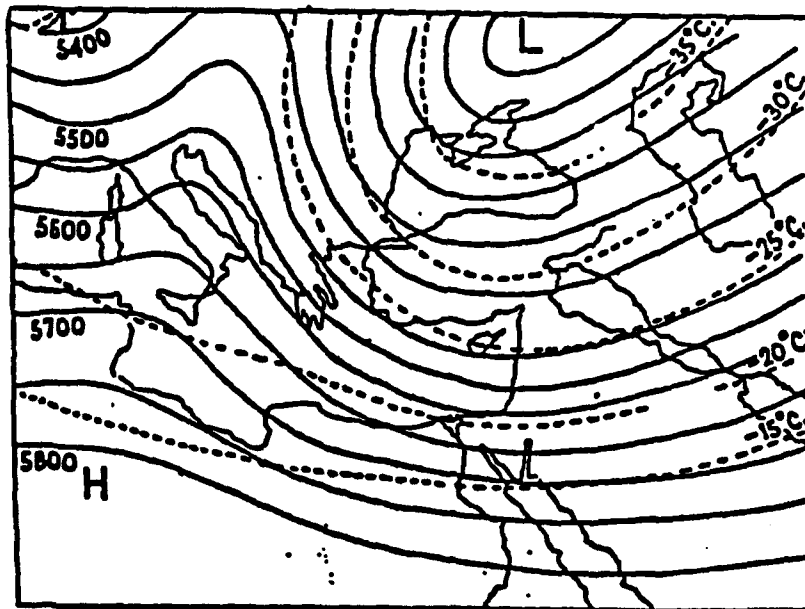


Figure 4-10a. 500-mb Contour Chart Over a Cyprus Low With No Severe Thunderstorms Or Heavy Precipitation. Dashed lines represent isotherms (° C) at 5-degree intervals, while solid lines represent geopotential height (gpm) at 50-meter intervals.

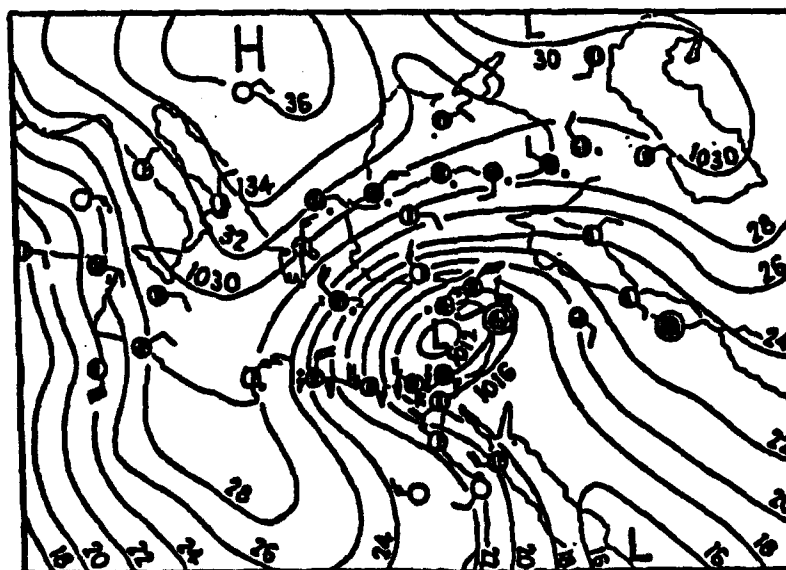


Figure 4-10b. Surface Chart Depicting Cyprus Low Position Beneath a Weak Mid-Level Trough With No Severe Thunderstorms or Heavy Precipitation. Solid lines represent surface pressure in millibars at 2-millibar intervals. Arrow shows movement of the system.

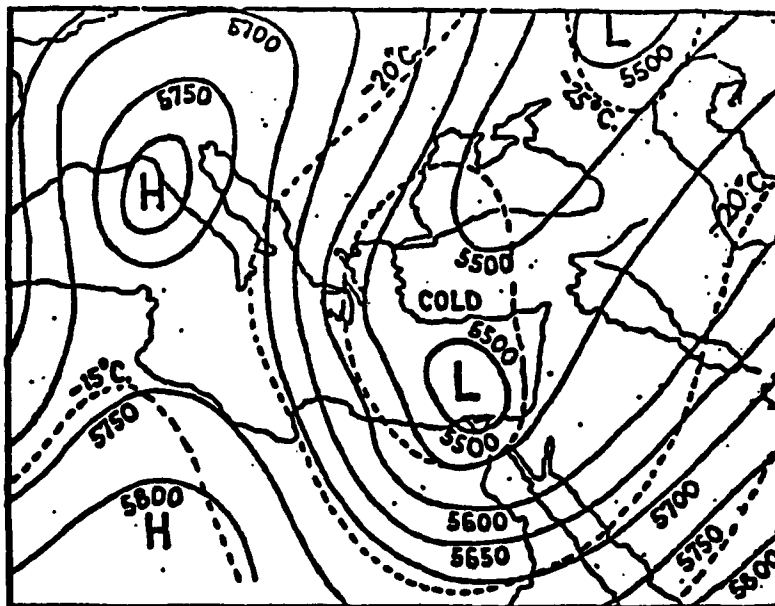


Figure 4-10c. 500-mb Contour Chart Over an Intense Cyprus Low With Severe Thunderstorms and Heavy Precipitation. Dashed lines represent isotherms (°C) at 5-degree intervals, while solid lines represent geopotential height (gpm) at 50-meter intervals.

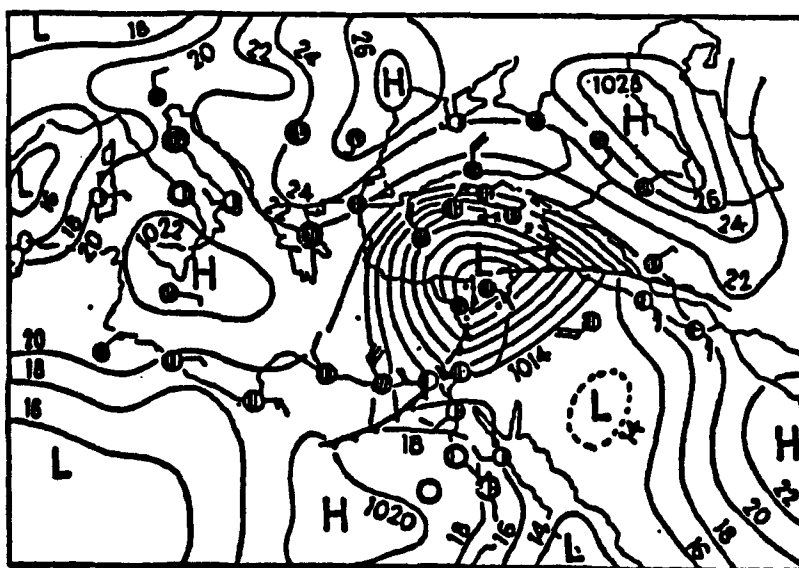


Figure 4-10d. Surface Chart Depicting Cyprus Low Position Beneath a Strong Mid-Level Trough With Severe Thunderstorms and Heavy Precipitation. Solid lines represent surface pressure in millibars at 2-millibar intervals. Arrow shows movement of the system.

THE FERTILE CRESCENT WINTER

December-March

TEMPERATURE. Mean daily January highs are the lowest of the year at most locations in the Fertile Crescent (Figure 4-11). They range from 42° F (5° C) at Diyarbikar to 60° F (16° C) at Basra. Mean daily lows are also lowest in January; they range from 28° F (-02° C) at Diyarbikar to 44° F (6° C) at Basra. At 2,120 feet (646 meters), Diyarbikar is in the foothills of the Taurus Mountains. If the interior plateau of Turkey is entirely snow-covered, abnormally cold air may drain southward into the Taurus foothills. The record low, -5° F (-21° C), was set in Diyarbikar in January. The record high, also at Basra, was 96° F (36° C) in March.

Mediterranean air mass penetrations warm adiabatically along the leeward side of the Ansariyeh and Anti-Lebanon Mountains, producing strong winds and large temperature increases (18-21°

F/10-11° C). Amman, Damascus, and Aleppo are affected.

Strong surface fronts associated with Cyprus Lows normally lower surface temperatures by about 10° F (5° C) in Syria and south-central Turkey. Intense Cyprus Lows with cold air support moving east-southeast across the Fertile Crescent may raise temperatures to 90-95° F (29-32° C) in late March (see the Sharav). Temperatures usually drop 20-25° F (12-14° C) within an hour after frontal passage.

Mean relative humidity along the Sha'tt al Arab River is 60% at midday and 90% at night. Early morning temperature inversions are common during December and January; they may extend from the surface to 2,000 feet (610 meters) AGL, and persist until 1200 LST.

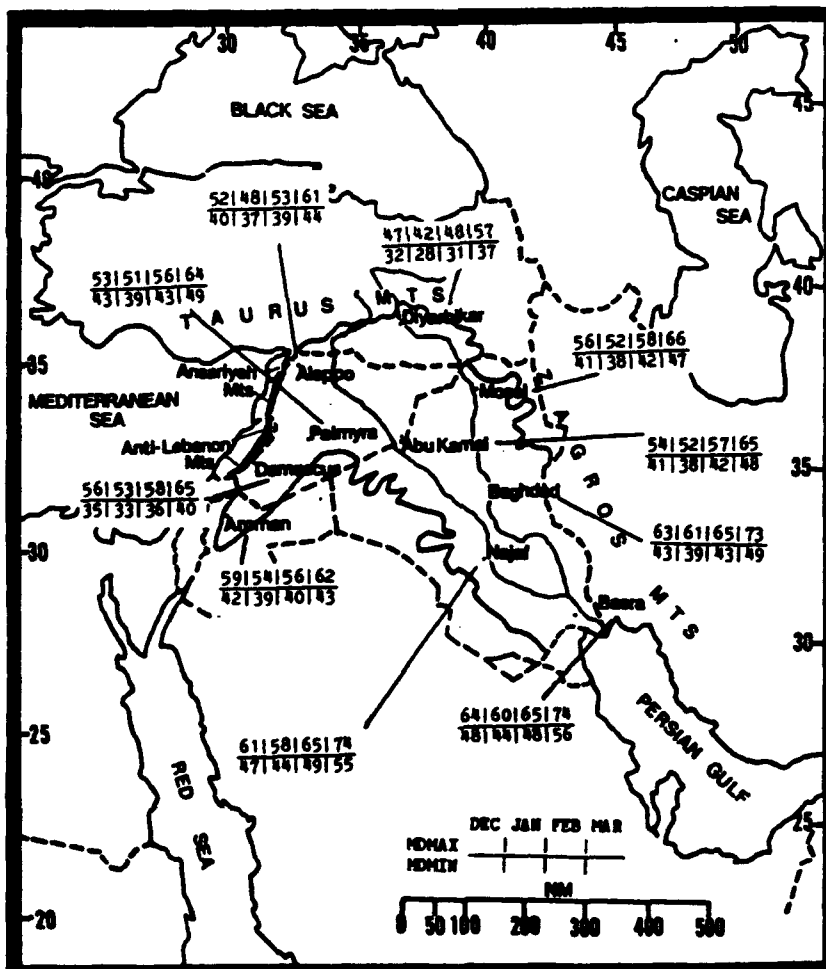


Figure 4-11. Mean Winter Daily Maximum/Minimum Temperature (° F), Fertile Crescent.

THE FERTILE CRESCENT SPRING

April-May

GENERAL WEATHER. Cyclonic activity affects the Fertile Crescent every 3-5 days in the spring. Major surface lows are the Cyprus, Atlas, and Black Sea Lows. Each has a distinctly different storm track, air-mass type, and weather pattern that depends on the magnitude of mid- and upper-level support.

Fair-weather periods are dominated by transitory high-pressure cells, thin cirrus, and warm temperatures. Extended fair-weather periods of 7 to 14 days produce a stagnant atmosphere, abnormally high temperatures, and/or rapid-developing, but localized, severe duststorm activity.

SKY COVER. Mean April-May cloudiness (Figure 4-12) ranges from 29% at Basra to 50% at Diyarbikar. Cirrus is common with the Subtropical Jet. Altocumulus and altostratus may develop with a 500- or 700-mb trough. Maximum mid-level cloudiness occurs when these troughs are associated with a surface cold front. Stratocumulus and cumulus develop with 850-mb troughs and surface cold fronts. Cumulus is dominant during fair weather periods.

By mid-May, most cloud cover is from weak mid-level troughs and/or the Subtropical Jet. As fewer migratory lows enter the subregion, conditions improve south of 35° N.

Strong surface heating produces shallow daytime cumulus. On rare occasions, strong heating in front of a mid-level trough produces a severe thunderstorm with hail between Baghdad and Basra. One-inch (127-mm) hail fell near Basra on 29-30 April 1957. Thunderstorm tops may exceed 40,000 feet (12.2 km) MSL throughout the region.

Altocumulus and altostratus bases are normally between 10,000 and 14,000 feet (3,050-4,268 meters) AGL; they average 5,000 feet (1,524 meters) in thickness. Stratocumulus and cumulus bases with 850-mb and surface troughs average 4,000-5,000 feet (1,220-1,524 meters) AGL, with tops of 6,000-8,000 feet (1,829-2,439 meters) MSL. A rare stratus deck with ceilings below 1,000 feet (305 meters) AGL can develop ahead of a stagnant low-pressure system in the eastern Mediterranean. Thin stratus is a typical low-cloud type at Diyarbikar, Baghdad, and Basra, but it rarely constitutes a ceiling.

Ceilings are at or below 3,000 feet (915 meters) AGL more frequently in the afternoon. Higher frequencies of low ceilings (Figure 4-12) occur at Mosel, Diyarbikar, Amman, and Aleppo; Aleppo has a peak frequency of 26% at 1400L. Rare afternoon thunderstorms can also produce ceilings below 3,000 feet (915 meters) AGL in the southern Tigris-Euphrates River Valley.

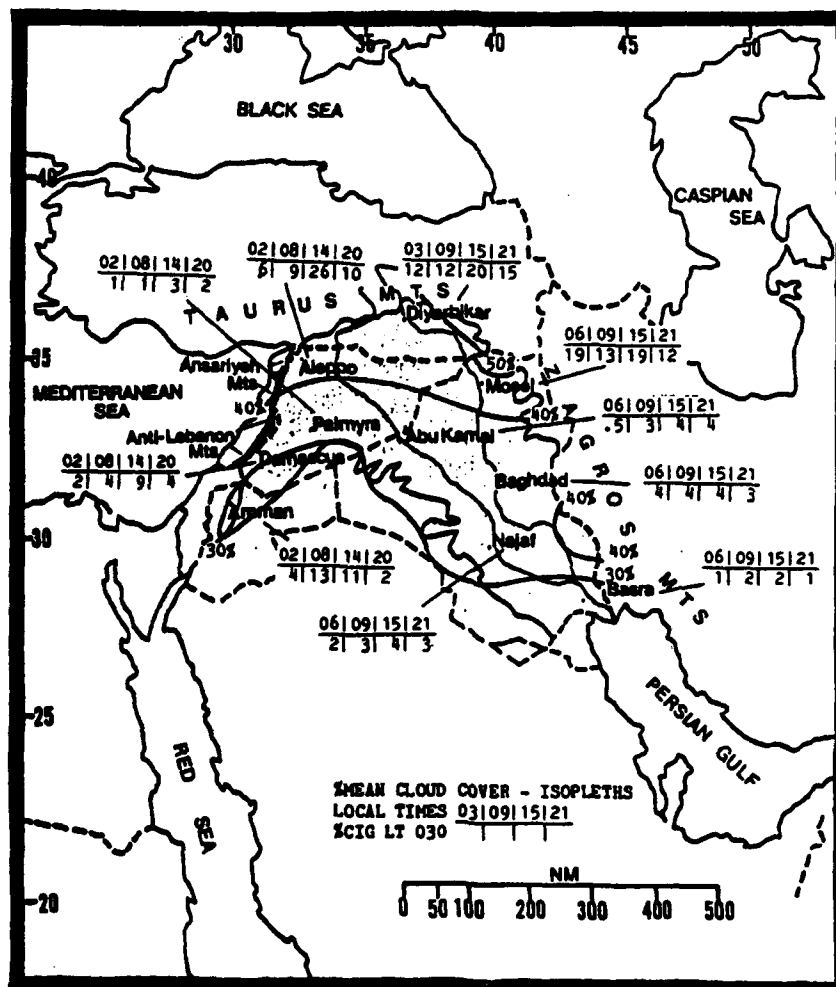


Figure 4-12. Mean Spring Cloudiness (isolines) and Frequencies of Ceilings Below 3,000 Feet (915 meters), Fertile Crescent.

THE FERTILE CRESCENT SPRING

April-May

VISIBILITY. Most reduced visibilities (see Figure 4-13) are caused by fog, or by thunderstorms with heavy rain or blowing dust. Fog, however, rarely reduces visibility below 3 miles; the frequency is only 0.2 to 4.0% of the time. Low visibilities with advection fog, heavy rain, and low stratus decks occur with cyclonic activity. Radiation fog forms most frequently between 0000 and 0800L during April. Low visibility at

Palmyra, at Damascus, and in the Tigris-Euphrates River Valley is due more to blowing dust than fog. The fine silt and sand in the flood plain between Baghdad and Basra is easily lifted with a 10-knot wind. Thunderstorms, migratory lows, or intense surface heating creating turbulent mixing can all generate enough winds. Thunderstorms with blowing dust occur most often between 1400 and 2200L.

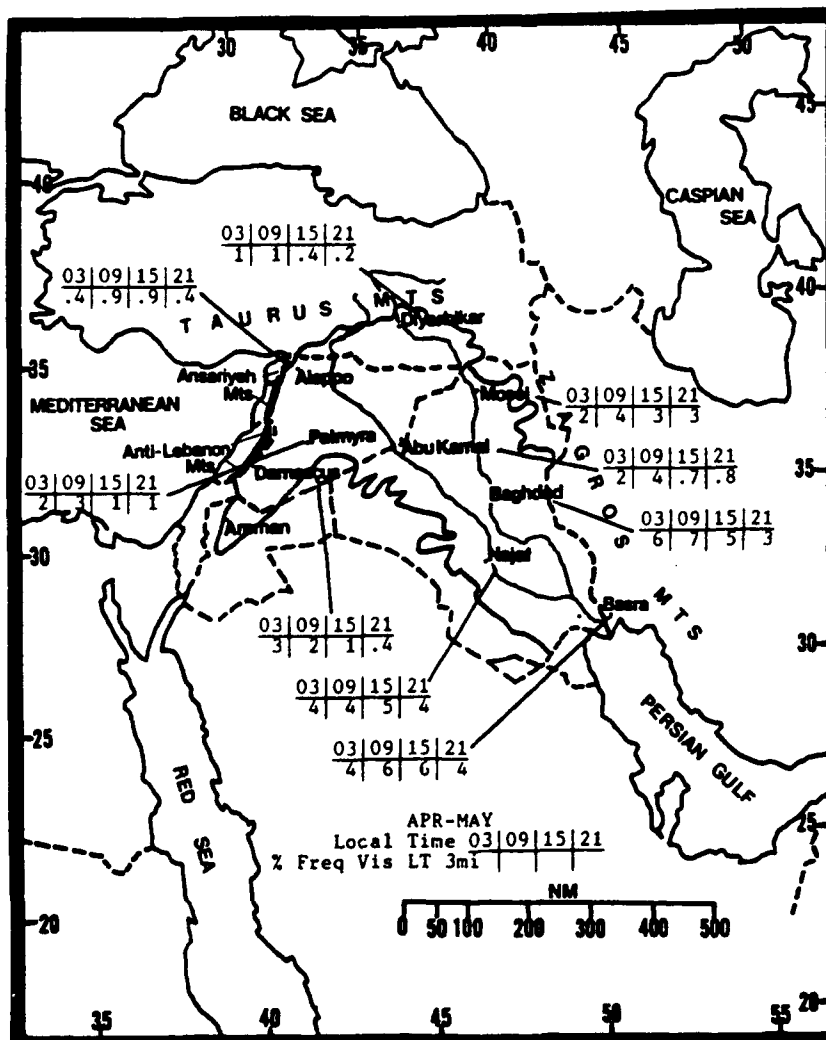


Figure 4-13. Mean Spring Frequencies of Visibilities Below 3 Miles, Fertile Crescent.

THE FERTILE CRESCENT SPRING

April-May

WINDS. Westerlies dominate across the Fertile Crescent during the spring. Weak southwest-to-northwest surface flow originates from the Mediterranean Sea and the northern Sahara. Westerly flow is turned by the Taurus and Zagros Mountains to northerly and northwesterly in the southern Tigris-Euphrates River valley. Mean surface wind speeds and prevailing directions are shown for April and May in Figure 4-14. Strong surface winds are normally due to intense migratory lows. Atlas Lows produce most sustained wind speeds above 30 knots. The Fertile Crescent's highest recorded wind speed during the spring was southwesterly at 61 knots at Aleppo. Severe localized duststorms are common with the strong winds generated by intense Atlas Lows.

		APR	MAY
W	Aleppo	6.30	6.50
SW	Damascus	8.10	7.30
NNW	Najaf	6.70	6.20
N	Basra	6.70	6.40
W	Palmyra	7.30	8.10
W	Mosel	2.70	3.00
W-NW	Diyarbikar	4.40	4.40
WNW	Baghdad	7.50	7.10

Figure 4-14. Mean Spring Surface Wind Speed (kts) and Prevailing Direction, Fertile Crescent.

Surface flow is southerly ahead of the surface low more than 85% of the time. An occluded system can produce weak easterlies preceding the cold front (but less than 15% of the time), as the cold front itself produces southwesterly surface flow.

Mid- and upper-level winds are westerly to west-southwesterly across the Fertile Crescent. Mean April-May wind speed at Damascus is 20 knots at 10,000 feet (3,050 meters), 27 knots at 15,000 feet (4,573 meters), 54 knots at 30,000 feet (9,146 meters), and 66 knots at 39,000 feet (11,890 meters). Baghdad's mid- and upper-level wind profile is nearly the same as that for Damascus.

PRECIPITATION. Mean spring rainfall (Figure 4-15) increases from southwest to northeast across the Fertile Crescent. Highest mean monthly and seasonal precipitation totals occur north of Mosel and Aleppo (36° N). The least falls in southern Syria (Palmyra and Damascus), northern Jordan (Amman), and northwestern Iraq.

The air ahead of an Atlas Low is extremely dry, warm, and dust-laden. The warm front is usually marked by a wind shift at the surface with little cloud cover or precipitation except along the foothills of the upper Zagros Mountains. Significant weather includes thin mid- and upper-level cloudiness, isolated short-duration drizzle, and strong southwesterly flow near the low. The Atlas Low normally tracks eastward so that the only possible low-level moisture sources available are the Red Sea, the Persian Gulf, and the Dead Sea. A mid-level trough must support the Atlas Low to create isolated thunderstorm activity along the cold front. Strong mid-level troughs may bring in moisture from the Persian Gulf and intensify the Atlas Low over Baghdad or Basra, causing rainfall and occasional thunderstorms with hail along the mid-level trough axis.

Cyprus Lows produce a different weather pattern than Atlas Lows; they have more low-level moisture and typically track east-southeastward through the Fertile Crescent. On rare occasions, the Cyprus Low remains an active weather-producer into the Persian Gulf. Most Cyprus Lows generate southerly flow ahead of the cold front. The warm sector is usually cloudless, but orographic lifting against the Taurus and Zagros Mountains may produce scattered cumulus, stratocumulus, and short-lived rainshowers. Precipitation amounts vary widely, and rely on colder and moister air aloft over Turkey. Steady rains occur most often when the Cyprus Low forms as a secondary surface low under a mid-level trough extending southward from Turkey.

Cyprus Low cold fronts produce heavy orographic convection, thunderstorms, and moderate precipitation along the Ansariyeh Mountains. The deep low-level moisture is often

THE FERTILE CRESCENT SPRING

April-May

squeezed out before reaching Aleppo, but mean April (1.9 inches/48 mm) and May (1.1 inches/28 mm) precipitation totals suggest that at least some moisture is able to cross the mountains. Orographic lifting along the Taurus and Zagros Mountains produces higher precipitation totals along these ranges. Mean seasonal precipitation distributions (see the 1.6 inch/41 mm isohyet in Figure 4-15) effectively illustrate the typical Mediterranean air mass and moisture boundary limits during active Cyprus Low storm tracks.

Mid-level troughs associated with Black Sea Lows initiate orographic showers at Diyarbikar and Mosel when a mid-level cold pocket is positioned over Turkey.

Spring thunderstorms (Figure 4-16) in the southeastern Tigris-Euphrates River Valley are produced by instabilities associated with troughs and the Subtropical Jet. They develop with a weak inflow of Persian Gulf moisture and strong surface heating between Basra and Baghdad. Although thunderstorms normally last less than 30 minutes, they may persist for 1 or 2 hours with continued strong upper-level divergence. On very rare occasions, a well-defined cold front sets off isolated thunderstorms between Baghdad and Basra, but frontal thunderstorms are primarily concentrated north of 35° N.

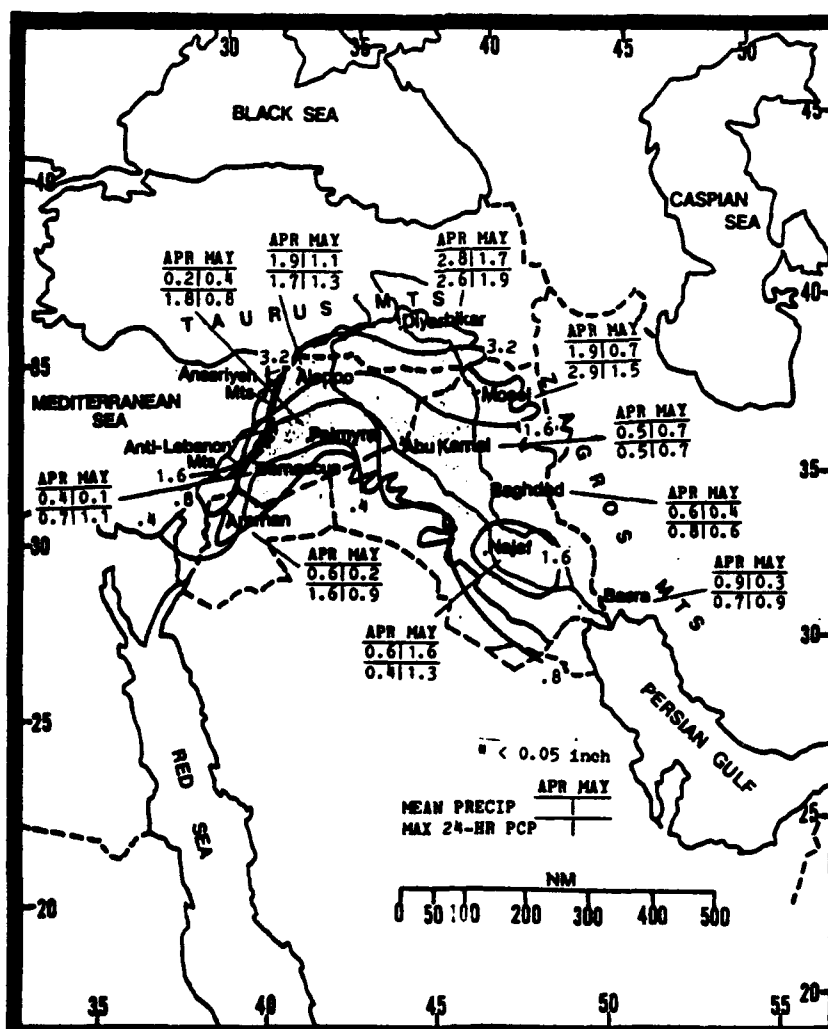


Figure 4-15. Mean Spring Monthly/Maximum 24-hour Precipitation, Fertile Crescent. Bold lines represent mean seasonal rainfall totals (isopleths).

THE FERTILE CRESCENT SPRING

April-May

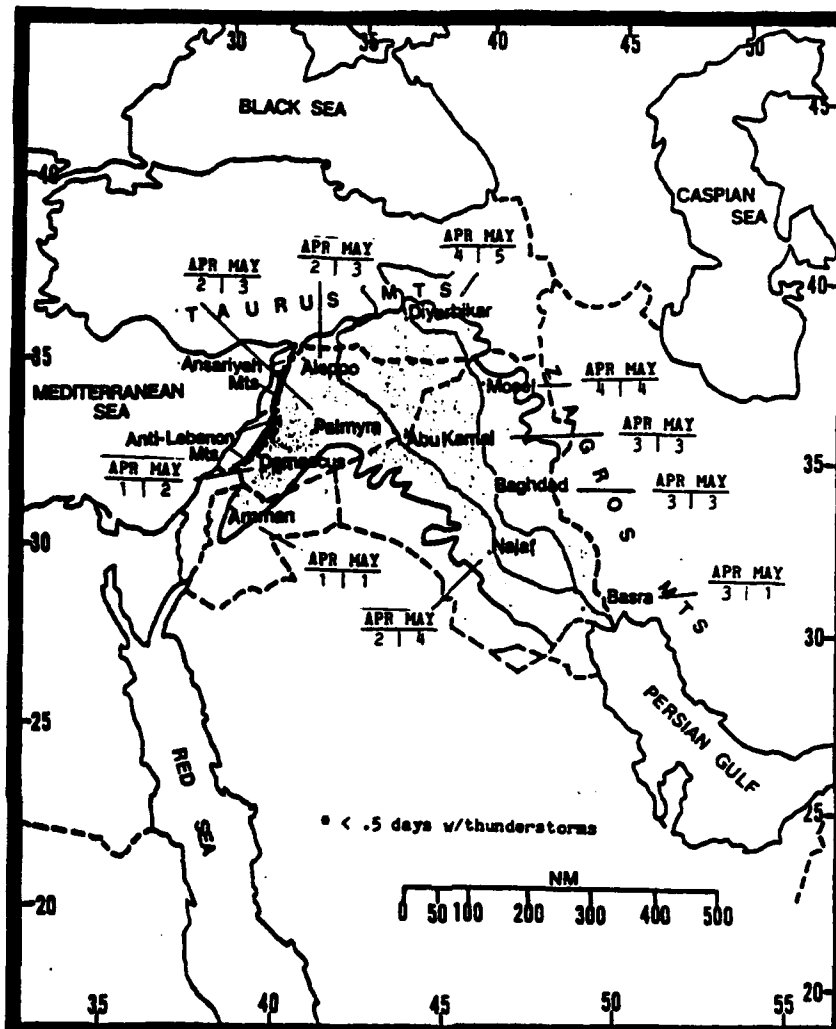


Figure 4-16. Mean Spring Frequencies of Thunderstorms, Fertile Crescent.

THE FERTILE CRESCENT SPRING

April-May

TEMPERATURE. Mean daily highs and lows in April and May increase quickly between 9 and 14° F (5 and 0° C) at each station. April mean daily highs range from 67° F (19° C) at Diyarbikar to 88° F (31° C) at Basra. May mean daily highs range from 79° F (26° C) at

Diyarbikar to 98° F (37° C) at Basra. Mean daily lows range from 45° F (7° C) at Damascus in April, to 75° F (24° C) at Basra in May. The record low during spring is 27° F (-3° C) at Diyarbikar in April; the record high, 117° F (47° C) at Basra in May.

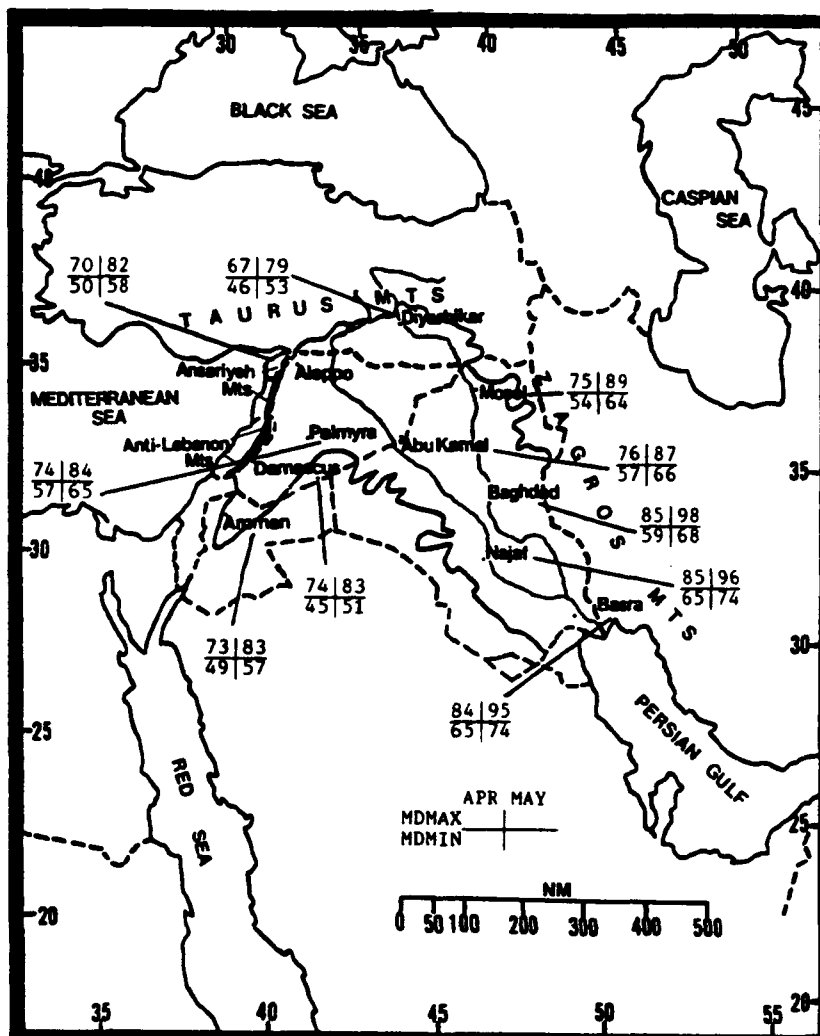


Figure 4-17. Mean Spring Daily Maximum/Minimum Temperatures (° F), Fertile Crescent.

THE FERTILE CRESCENT SUMMER

June-September

GENERAL WEATHER. Between June and September, a dry northwest surface flow prevails over the Fertile Crescent. Extremely arid conditions, clear skies, and light 11- to 20-knot mid-level winds (5,000-15,000 feet/1,524-4,573 meters) MSL persist. The Etesian winds produce moderate 10- to 15-knot westerlies across the northern Fertile Crescent in June and July. The north and central Ansariyeh Mountains are the entry points for the Etesian flow. Aleppo is the most likely place to be affected, but mass surges in Etesian flow may push into the central Tigris-Euphrates River Valley. Weak upper-level troughs can produce rainfall, but very little precipitation occurs during the summer, especially in June or July.

SKY COVER. Summer skies are often clear. In July and August, thin bands of Subtropical Jet cirrus (from west-southwest to east-northeast) provide the only significant cloud cover in the entire Fertile Crescent. Mean cloudiness (Figure 4-18) is extremely low. Diyarbakir has the highest mean cloudiness (12%) but there are no

clouds at all on 23-28 days a month during July and August.

Middle and high cloud cover may occur in June with extremely rare upper-level troughs that produce scattered altocumulus bases at or above 14,000 feet (4,268 meters) AGL; tops are usually below 18,000 feet (5,487 meters) MSL.

Intense surface heating or strong sea breezes can result in isolated clusters of afternoon cumulus with ceilings between 3,000 and 5,000 feet (915-1,524 meters) AGL near the Taurus, Anti-Lebanon, Ansariyeh, and Zagros mountains. This short-lived cumulus is less than 2,000 feet (610 meters) thick.

Ceilings are seldom below 3,000 feet (915 meters) AGL (Figure 4-18) in the summer, but those ceilings that do occur peak around mid-day and vary with topography. Ceilings at or below 1,000 feet (305 meters) AGL are normally due to early morning stratus that drift inland from the Persian Gulf but disperses quickly after sunrise.

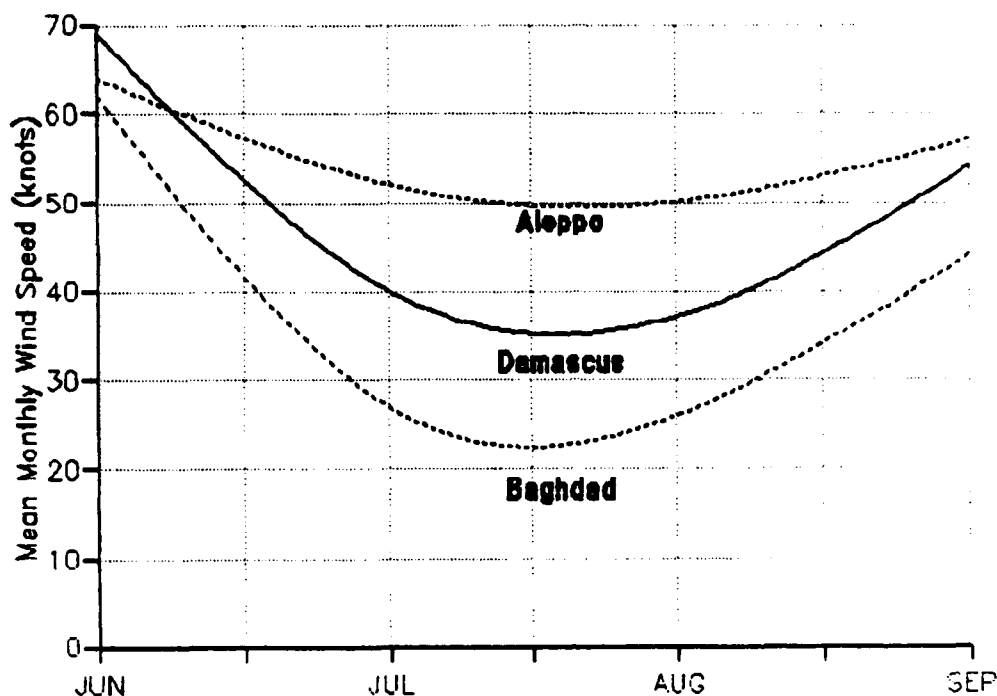


Figure 4-21. Mean Monthly (Summer) 39,000-Foot (11,900-meter) MSL Wind Speeds (kts), Fertile Crescent Upper-Air Network. This level is roughly the height of the Subtropical Jet.

PRECIPITATION. Summers are extremely dry; many locations record no measureable precipitation. Several stations in the foothills of the Taurus Mountains (Diyarbakir, Aleppo, and Gizantop) average 0.3-0.4 inches (8-10 mm) for the season, but none in July and August. The foothills' isolated rainfall develops from shallow diurnal convection and rare mid-level troughs moving over the rugged terrain.

A rare thunderstorm may occur anytime during the summer, but it is usually an isolated convective cell that produces only virga. No 24-hour maximum rainfall totals exceed 2 inches (51 mm), and many locations have never

exceeded 0.5 inches (13 mm) in a 24-hour period. Summer thunderstorm days average less than 1 a month; locations in southern Turkey average slightly more than 1 a month in June and September only. One thunderstorm, resulting from a rare mid- or upper-level trough, may provide the only measureable summer precipitation for 4 or 5 years. As a result, many Fertile Crescent locations have a mean monthly precipitation total of less than 0.05 inches (1.3 mm) because one isolated shower occurred in a 10- to 20-year period. No precipitation or thunderstorm day figures are included in the summer season discussion because so few locations receive significant rainfall'

June-September



THE FERTILE CRESCENT SUMMER

June-September

VISIBILITY. Haze and suspended dust are the main summer restrictions to visibility. Localized duststorms and sandstorms occur in every month--forecasting their development and duration is difficult.

During Operation DESERT SHIELD in August and September, it was common for northerly winds to blow sand from the dried-up salt marshes along the Tigris-Euphrates River Valley into Basra and the Persian Gulf.

Haze that lowers visibilities to 4-7 miles is common. Thicker dust haze builds through July

and August as winds in the lower 15,000 feet (4,573 meters) MSL become stagnant at less than 20 knots. Localized dust and sandstorms worsen haze conditions aloft. Visibilities often go below 3 miles in duststorms and sandstorms, but thick haze (with visibilities of 1-3 miles) can persist for up to 2 weeks.

Baghdad, Mosel, and Basra have the highest frequencies of low visibility in the Fertile Crescent (Figure 4-19). Moisture haze consisting of salt and dust particles is common at Basra.

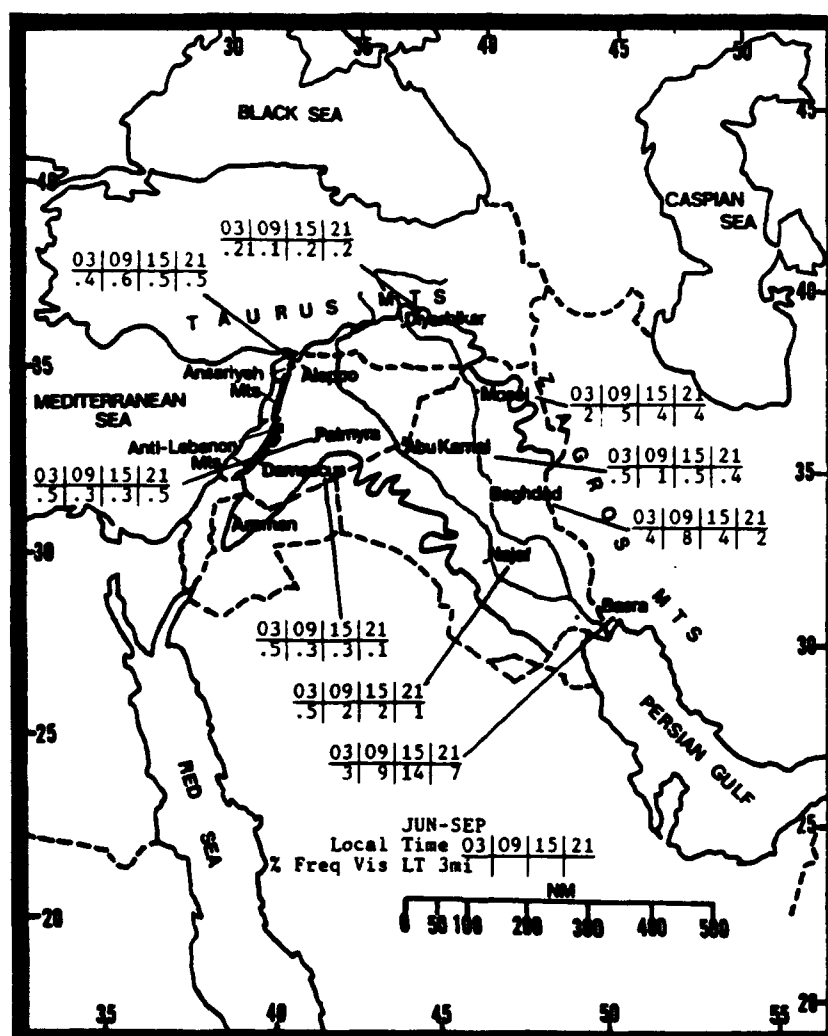


Figure 4-19. Mean Summer Frequencies of Visibilities Below 3 Miles, Fertile Crescent.

THE FERTILE CRESCENT SUMMER

June-September

WINDS. In Figure 4-20, the mean summer surface wind speeds and prevailing wind directions are given for several Fertile Crescent locations. Except for local terrain variations, most locations have westerly flow caused by the large-scale pressure gradient (higher surface pressures in the Mediterranean region vs. the Monsoon Trough. Mean summer surface winds are stronger than the other seasons due to the

intense surface heating that creates a large pressure gradient. At times, the Etesian winds funnel into Syria along the Taurus-Zagros Mountain chain. Etesian flow and the 40-day Shamal may exceed 25 knots. Aleppo and Gizantep are affected by Etesian winds, while Baghdad, Mosel, and Basra get the 40-day Shamals.

		JUN	JUL	AUG	SEP
W	Aleppo	8.70	9.80	9.00	6.40
SW	Damascus	8.50	9.70	9.00	6.10
N-W	Najaf	8.90	10.10	8.30	5.50
NW	Basra	8.50	8.40	7.50	6.30
W	Palmyra	9.90	11.30	10.40	6.90
W	Mosel	3.30	3.20	2.90	2.20
W-NW	Diyarbikar	5.80	6.10	5.40	4.50
W-NW	Baghdad	9.00	9.50	8.70	6.50

Figure 4-20. Mean Summer Surface Wind Speed (kts) and Prevailing Direction, Fertile Crescent.

Maximum recorded wind speeds during summer include 86 knots from the west-northwest at Palmyra in August; 70 knots from the west-northwest at Aleppo in June; 53 knots from the south at Basra in September; and 41 knots from the north-northwest at Baghdad in September. All these winds were associated with a rare thunderstorm.

Refer to Figure 4-6a-c for mean annual 5,000-foot (1,524-meter), 10,000-foot (3,050-meter), and

15,000-foot (4,573-meter) level wind directions for Baghdad (4-6a), Aleppo (4-6b), and Damascus (4-6c). Winds are generally west-southwesterly and below 20 knots in the summer at these levels.

Figure 4-21 shows mean monthly 39,000-foot (11,900-meter) wind speeds for the Fertile Crescent's upper-air network. The mean summer wind direction at all three locations is southwesterly to west-southwesterly.

THE FERTILE CRESCENT SUMMER

June-September

TEMPERATURE. The extremely arid surface conditions and clear skies allow temperatures to reach 100° F (38° C) frequently. In July and August, temperatures reach 100° F (38° C) in the Tigris-Euphrates River Valley south of 35° N almost every day. Mean daily highs range from 90° F (32° C) at Aleppo in September to 111° F (44° C) at Baghdad in June (Figure 4-22). The record high is 122° F (50° C) in July at Baghdad, but it's likely that 130° F (54° C) temperatures have occurred in remote locations to the west of Baghdad and Najaf. Mean daily lows range

from 57° F (14° C) at Damascus in September to 85° F (29° C) at Najaf in July and August. The record low during the summer is 37° F (3° C) at Damascus in September.

Diurnal temperature ranges are large in the summer as clear skies bring intense daytime surface heating and rapid radiation cooling at night. At most locations, the range is 30 to 40° F (12-23° C). High humidity along the northwestern Persian Gulf causes unbearable daytime living conditions at Basra.

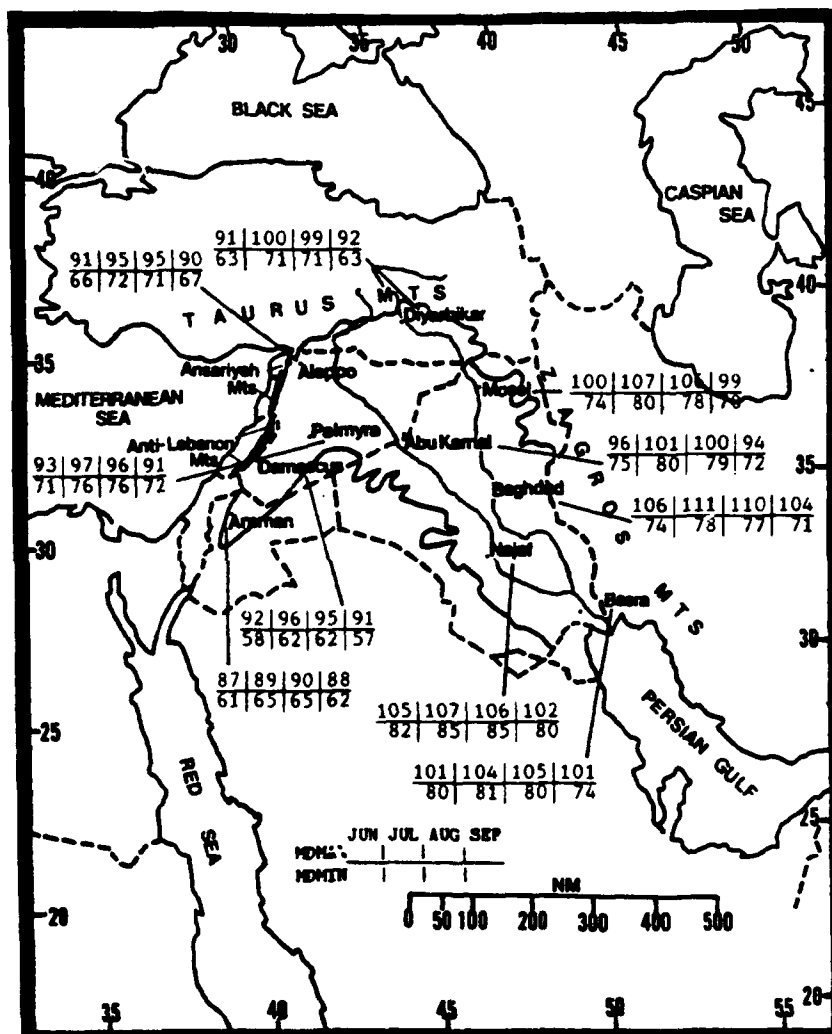


Figure 4-22. Mean Summer Daily Maximum/Minimum Temperatures (° F), Fertile Crescent.

THE FERTILE CRESCENT FALL

October-November

GENERAL WEATHER. Frontal systems return to the Fertile Crescent by early November; they bring multi-layered cloud decks and precipitation. The greatest cloud cover, heaviest rainfall, and highest frequencies of lows occur north of a line extending from Aleppo to Mosel. Orographic showers and occasional thunderstorms (only 1-3 days a season) develop. South of the Aleppo-Mosel line, frontal systems produce only widely scattered showers, most lasting for no more than 15 minutes.

SKY COVER. Mean cloudiness increases from between 3 and 12% in the summer to between 24 and 40% during the fall (Figure 4-23), because frontal systems increase in November. October sky cover is dominated by Subtropical Jet cirrus and scattered mid-level altocumulus and altostratus associated with weak 500-mb troughs. These cloud types are most prevalent north of 35° N. Shallow and isolated fair weather cumulus develops throughout the northern Tigris-Euphrates River Valley and

Taurus-Zagros foothills, but it rarely exceeds 2/8ths coverage.

The average cloud base for fair weather cumulus is 5,000 feet (1,524 meters) AGL; tops rarely exceed 8,000 feet (2,439 meters) MSL. Cirrus shields commonly form between 30,000 and 39,000 feet (9,146-11,890 meters) MSL. Mid-level altocumulus/ altostratus ceilings normally develop between 12,000 and 14,000 feet (3,658-4,268 meter) AGL with moderate 500-mb and weak 700-mb troughs.

Frequencies of ceilings below 3,000 feet (915 meters) AGL are greatest at Mosel, with 13% at 0600L (Figure 4-23). Most low ceilings are caused by troughs or isolated thunderstorms. That can produce 1,500-foot (457-meter) AGL ceilings. Ceilings below 1,000 feet (305 meters) AGL are extremely rare.

Thunderstorm tops can exceed 40,000 feet (12,195 meters) MSL, but seldom occur outside of the Taurus-Zagros foothills.

October-November



THE FERTILE CRESCENT FALL

October-November

VISIBILITY. Blowing dust and sand are the main restrictions to visibility. In October and November, 24- to 36-hour Shamals may produce 1- to 2-mile visibilities over wide areas along the surface trough axis. Shamals occur 1 to 4 times in a typical fall.

Radiation fog may develop on any fall evening between 2200 and 0600L when clear skies and calm winds prevail, but it rarely lowers visibility below 3 miles. The highest frequency of visibility below 3 miles (Figure 4-24) is 9% at Basra at 0900L.

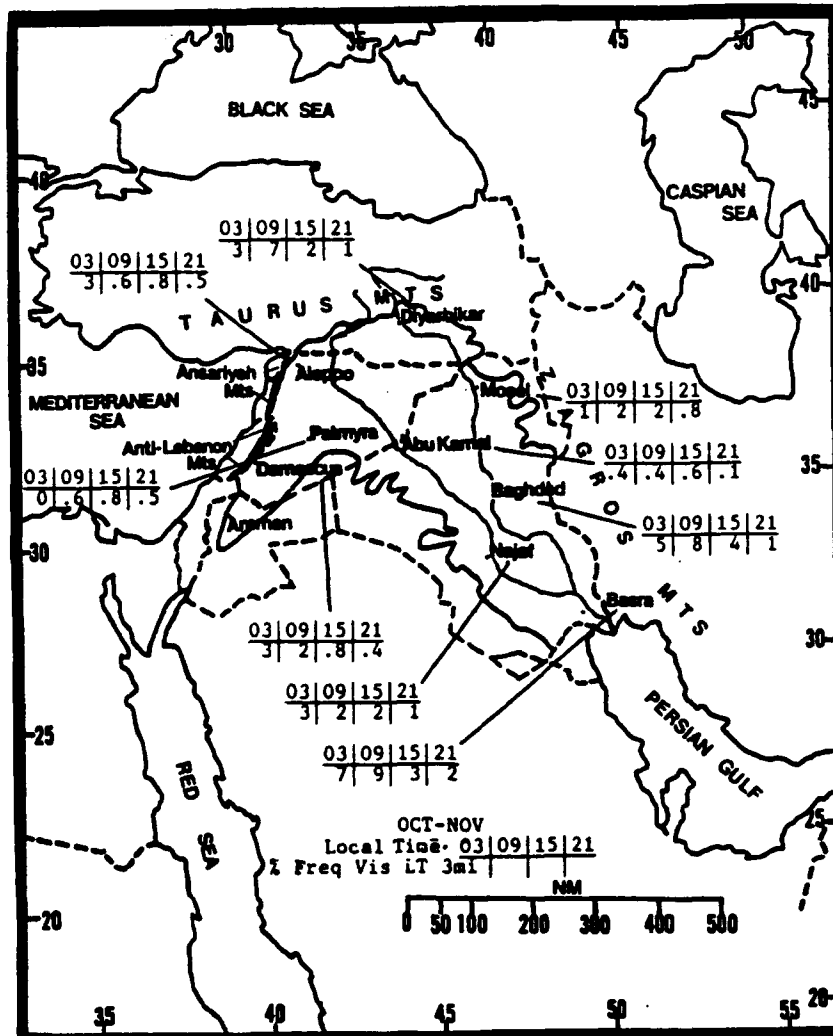


Figure 4-24. Fall Frequencies of Visibilities Below 3 Miles, Fertile Crescent.

THE FERTILE CRESCENT FALL

WINDS. Figure 4-25 shows mean fall surface wind speeds and prevailing wind direction for several Fertile Crescent locations. Westerly-to-northerly surface winds dominate. Aleppo's 180-degree wind shift from October to November is misleading. Surface winds are light and variable, but the highest frequency of November surface observations (less than 20%) are easterly. Mean wind speeds at all locations average 6 knots or less.

Refer to Figures 4-6a-c for mean wind directions at 5,000 feet (1,524 meters), 10,000 feet (3,050 meters), and 15,000 feet (4,573 meters MSL at Baghdad, Aleppo, and Damascus. At 5,000 feet (1,524 meters) MSL, the 30° wind shift at Aleppo and Damascus between October and November indicates that the eastern cell of the anticyclone over the northern Red Sea quickly moves 200-300 NM east-northeastward.

Rapid changes in 850-mb flow patterns (as well as at other levels) illustrate the subtle but dramatic effects that distant large-scale thermal

features have on circulation and transition weather patterns in the Middle East Peninsula.

October-November

		OCT	NOV
W/E	Aleppo	4.00	3.60
N	Damascus	4.90	5.00
N-W	Najaf	4.80	4.90
NW	Basra	5.00	5.90
W	Palmyra	5.20	4.00
W	Mosel	1.40	0.90
NW	Diyarbikar	3.60	3.00
N	Baghdad	5.20	4.90

Figure 4-25. Mean Fall Surface Wind Speeds (kts) and Prevailing Direction, Fertile Crescent. The slash drawn between prevailing wind directions at Aleppo indicate wind direction in October/November.

THE FERTILE CRESCENT FALL

October-November

PRECIPITATION. Mean fall rainfall amounts (Figure 4-26) increase steadily, reflecting subtle shifts in low- and mid-level circulation patterns and increased cyclonic activity. For most

southern locations, deep mid- and upper-level troughs produce isolated showers and thunderstorms that usually produce less than 0.25 inches (6 mm) of rain.

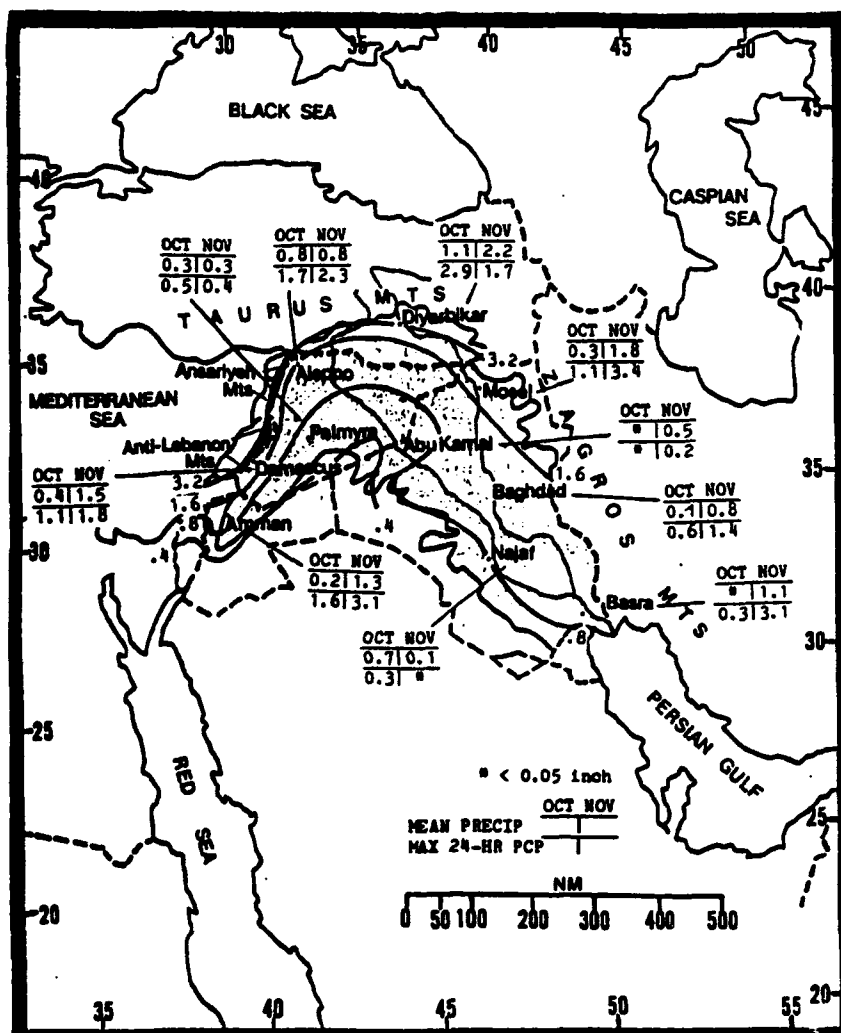


Figure 4-26. Mean Fall Monthly/Maximum 24-hour Precipitation, Fertile Crescent. Bold lines are mean seasonal rainfall totals.

THE FERTILE CRESCENT FALL

October-November

Thunderstorm duration is normally less than 30 minutes. A slow-moving cold front supported by a cold mid-level trough can produce severe thunderstorms with small hail near Baghdad and Basra, but they are rare. Figure 4-27 shows the mean distribution of thunderstorm days during the fall. The highest number of

thunderstorm days (3) is in October at Najaf, with only 1 in November; the Najaf data is questionable, however, since the POR is only 4-6 years. Most other locations along the Tigris-Euphrates River Valley see an increase in thunderstorm days in November.

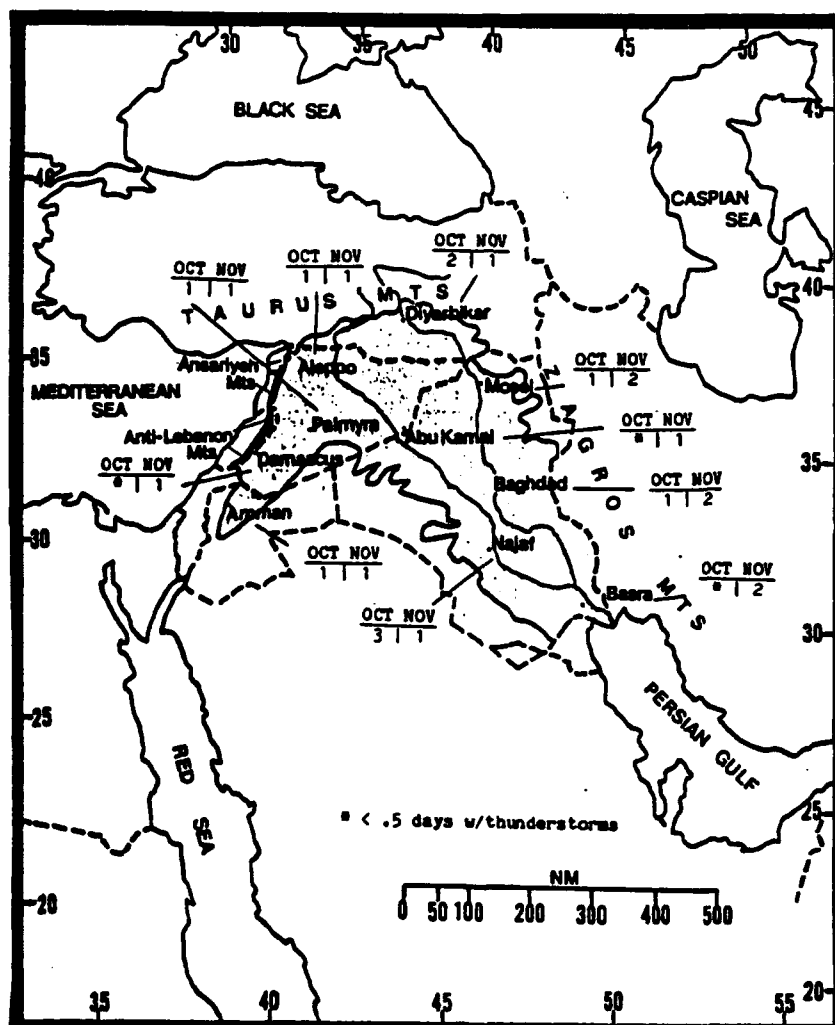


Figure 4-27. Mean Fall Frequencies of Thunderstorms, Fertile Crescent. Najaf thunderstorm days are questionable.

THE FERTILE CRESCENT FALL

October-November

TEMPERATURE. Mean daily highs in October range from 93° F (34° C) at Baghdad to 77° F (25° C) at Diyarbikar (Figure 4-28). There is an appreciable November decrease; mean daily highs range from 77° F (25° C) at Basra to 59° F (16° C) at Diyarbikar. Mean daily lows in

October range from 69° F (20° C) at Najaf to 51° F (11° C) at Diyarbikar. In November, mean daily lows range from 56° F (14° C) at Basra to 39° F (4° C) at Diyarbikar. Record lows and highs are 19° F (-7° C) at Aleppo in November and 113° F (45° C) at Basra in October.

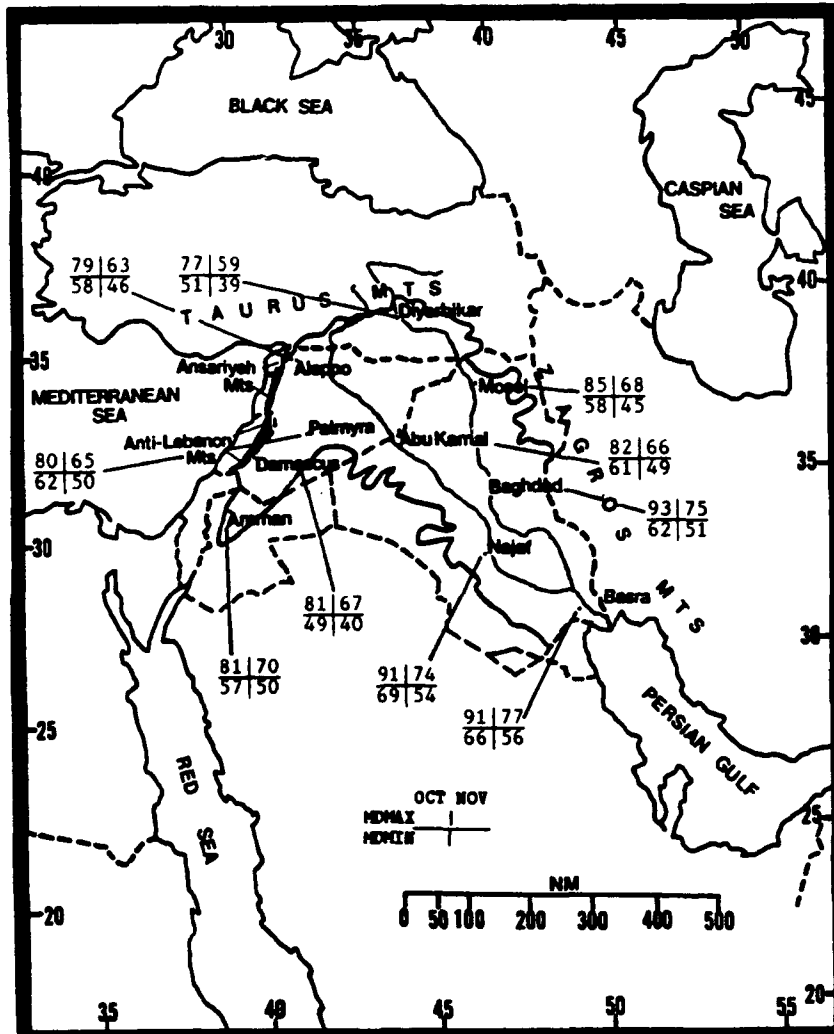


Figure 4-28. Mean Fall Daily Maximum/Minimum Temperatures (° F), Fertile Crescent.

Chapter 5

ARABIAN DESERT

The Arabian Desert subregion comprises large portions of Saudi Arabia and Oman as well as smaller sections of Iraq, Syria, Jordan, Republic of Yemen, and the United Arab Emirates. After describing the area situation and relief, this chapter discusses "general weather conditions" by season.

Situation and Relief	5-2
The Southwest Monsoon—June-September	5-6
General Weather	5-6
Sky Cover	5-6
Visibility	5-8
Winds	5-9
Precipitation	5-12
Temperature	5-13
The Southwest-to-Northeast Monsoon Transition—October-November . . .	5-14
General Weather	5-14
Sky Cover	5-14
Visibility	5-15
Winds	5-16
Precipitation	5-17
Temperature	5-18
The Northeast Monsoon—December-March	5-19
General Weather	5-19
Sky Cover	5-19
Visibility	5-21
Winds	5-22
Precipitation	5-23
Temperature	5-25
The Northeast-to-Southwest Monsoon Transition—April-May	5-27
General Weather	5-27
Sky Cover	5-27
Visibility	5-29
Winds	5-30
Precipitation	5-31
Temperature	5-34

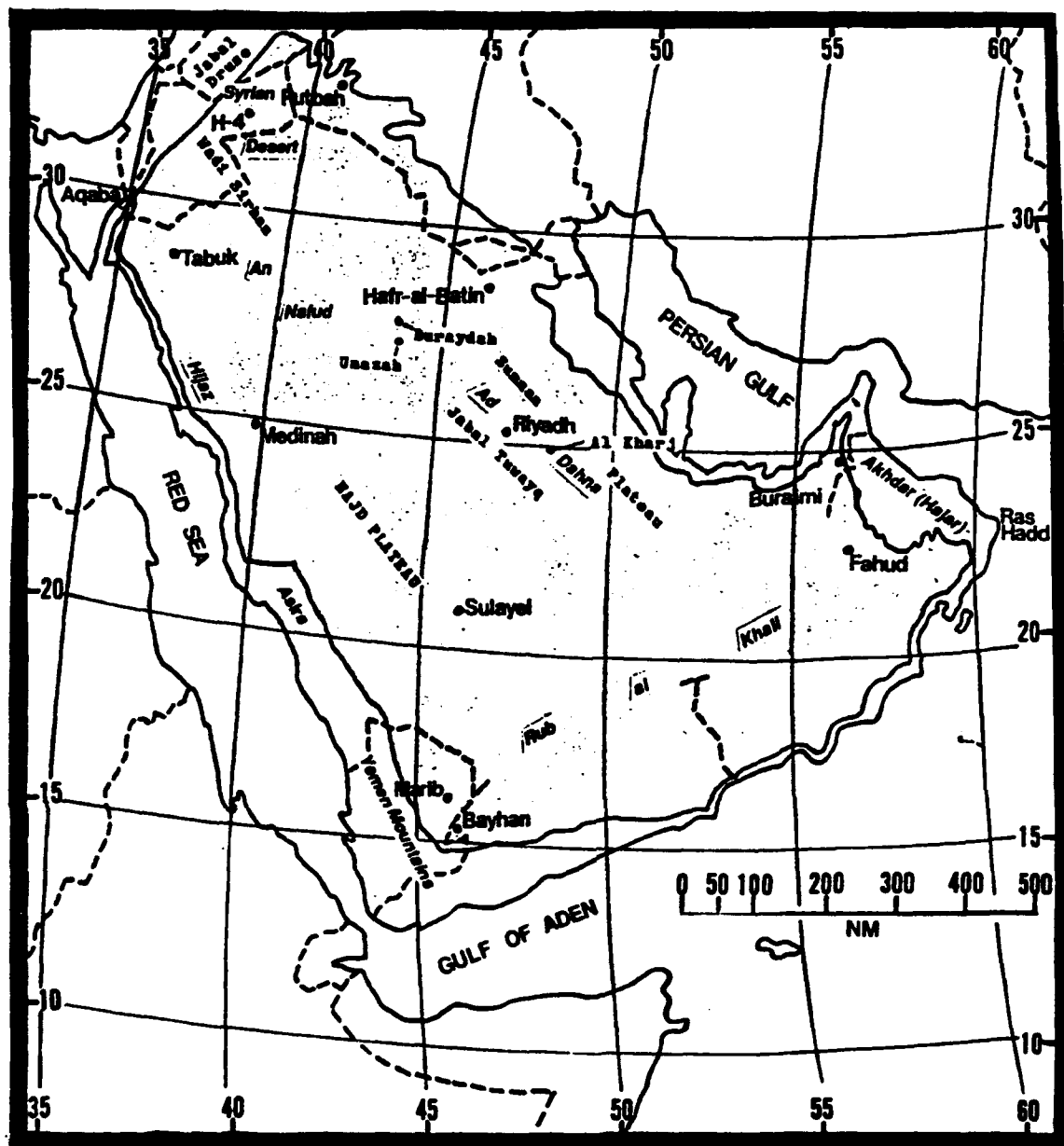


Figure 5-1a. The Arabian Desert. The Arabian Desert subregion comprises most of Saudi Arabia and small portions of Jordan, Syria, and Iraq. Data summaries for selected stations in the study area are provided in Figure 5-1b.

THE ARABIAN DESERT

SITUATION AND RELIEF

STATION: MEDINA SAUDI ARABIA													
LAT/LON: 24 39 N 39 39 E ELEV: 1950 FT													
ELEMENTS	JAN	FEB	MAR	APR	MAY	JUN	JUL	AUG	SEP	OCT	NOV	DEC	ANN
XTREM MAX	86	93	104	108	113	117	117	117	113	104	95	89	117
AVG MAX	75	79	87	94	100	108	108	107	108	96	84	76	93
AVG MIN	55	58	63	71	76	84	84	84	80	72	63	55	70
XTREM MIN	34	45	38	57	62	74	72	77	70	59	50	37	34
AVG PRCP	*	*	0.3	0.1	0.3	*	0.2	0	*	*	0.2	0.3	1.6
MAX MON	0.8	-	1.8	0.8	0.8	-	*	-	-	-	0.8	1.0	3.3
FOG/HAZE	2	3	5	4	6	3	2	*	1	1	2	1	29
TS DAYS	0	0	1	1	1	0	0	0	0	0	0	0	3
DUST DAYS	3	2	2	1	2	2	1	0	1	1	0	0	14
AFT TEMP	72	77	84	91	97	103	101	103	102	92	83	73	

* = LESS THAN 0.05 INCHES OR LESS THAN 0.5 DAYS

STATION: RIYADH SAUDI ARABIA													
LAT/LON: 24 43 N 48 43 E ELEV: 1922 FT													
ELEMENTS	JAN	FEB	MAR	APR	MAY	JUN	JUL	AUG	SEP	OCT	NOV	DEC	ANN
XTREM MAX	88	95	100	108	113	117	120	120	113	108	93	86	120
AVG MAX	70	74	82	93	102	107	109	107	104	94	81	71	91
AVG MIN	46	50	57	68	77	81	83	81	77	68	57	50	66
XTREM MIN	19	29	32	36	59	67	67	62	62	50	35	31	19
AVG PRCP	0.8	0.6	0.4	0.3	0.3	0	0	0	0	0	0.4	0.6	3.4
MAX MON	2.3	5.2	2.4	2.0	1.5	*	*	*	0	0	1.9	1.7	9.5
FOG DAYS	1	0	0	0	0	0	0	0	0	0	0	1	2
TS DAYS	0	0	1	4	*	*	0	0	0	0	0	0	6
DUST DAYS	3	5	4	5	6	7	8	4	3	2	3	2	50
AFT TEMP	70	74	79	90	100	106	108	106	102	93	80	71	

* = LESS THAN 0.05 INCHES OR LESS THAN 0.5 DAYS

STATION: RUTBAH IRAQ													
LAT/LON: 33 02 N 40 17 E ELEV:													
ELEMENTS	JAN	FEB	MAR	APR	MAY	JUN	JUL	AUG	SEP	OCT	NOV	DEC	ANN
XTREM MAX	77	89	95	101	108	112	115	114	113	100	95	76	115
AVG MAX	55	60	68	78	89	97	101	102	97	86	72	58	80
AVG MIN	34	36	37	50	59	65	70	70	63	55	45	37	52
XTREM MIN	6	10	7	21	32	42	54	58	59	48	33	23	6
AVG PRCP	0.7	0.8	0.7	0.7	0.6	0.0	0.0	0.0	*	0.2	0.6	0.8	4.9
MAX MON	2.7	2.3	5.1	3.4	2.7	0.1	*	*	0.7	2.6	2.5	2.5	10.6
MAX DAY	0.8	1.3	0.7	1.7	0.9	*	*	*	0.2	1.2	1.0	1.8	1.8
TS DAYS	*	*	1	3	2	0	0	0	*	1	1	1	9
DUST DAYS	2	1	4	4	4	4	2	3	2	3	1	2	32
AFT TEMP													

* = LESS THAN 0.05 INCHES OR LESS THAN 0.5 DAYS

Figure 5-1b. Climatological Summaries for Selected Stations in the Arabian Desert.

THE ARABIAN DESERT

GEOGRAPHY. The Arabian Desert is a sand-covered, rocky plateau that slopes gradually from west to east toward the Persian Gulf and the Arabian Sea. The irregular boundary that defines this subregion encloses an area not normally affected by the marine boundary layer.

The southern boundary begins in the southwest at the border of the Republic of Yemen at 14° 50' N, 46° E at the 3,280-foot (1,000-meter) MSL contour. The southern border follows this contour eastward to 50°E, then extends east-northeastward to the 656-foot (200-meter) contour, which it follows to 18° 10' N, 56° 25' E.

The eastern boundary begins at 18° 10' N, 56° 25' E and parallels the coastline, 20 NM inland, to the Akhdar (Hajar) Mountains and Ras Hadd at about 60° E. At this point, it reaches the 1,620-foot (500-meter) MSL contour on the western side of the Akhdar Mountains, which it follows to 25° N. The boundary then parallels the Persian Gulf (again about 20 NM inland) northwestward across the United Arab Emirates to 26° N. From there, it follows the 305-foot (100-meter) contour northwestward to the Kuwait-Saudi Arabia-Iraq border at 29° 30' N.

The northern boundary follows the 656-foot (200-meter) MSL contour northwestward to 33° N. It then parallels 33° N westward to the 1,620-foot (500-meter) contour and extends into Syria to 34° N, 38° E.

The western boundary starts at 34° N, 38° E. After running southwest to the intersection of 37° E and the Jordan border, it continues to 29° 40' N, 36° 10' E. From there, it follows the 1,620-foot (500-meter) contour around Aqaba to the 656-foot (200-meter) MSL contour, continuing southward along the Red Sea to 21° 40' N where it moves a short distance westward to the 4,920-foot (1,500-meter) MSL contour. From here, it runs south to the Republic of Yemen border at 14° 50' N, 46° E.

The Arabian Desert is a collection of several large deserts, as shown in Figure 5-1a. In the north, the Syrian Desert extends across southeastern Syria, eastern Jordan, southwestern Iraq, and northern Saudi Arabia.

SITUATION AND RELIEF

The Jebel Druse in southern Syria is a barren mountain range that extends only 5 NM in the Syrian Desert.

The An Nafud Desert covers most of northwestern Saudi Arabia. The desert surface is dark rock and gravel covered by sand and isolated clumps of short grasses. The southern portion has sand dunes that range in height from 395 to 590 feet (120-180 meters). Both the An Nafud and Syrian Deserts are bordered on the north and east by a semiarid steppe with numerous wadis, or semipermanent stream beds; the largest of these is Wadi Sirhan, which drops 985 feet (300 meters) below the Syrian Desert plateau.

The Hijaz Mountains, oriented NNW to SSE along the Red Sea from 24 to 28° N, separate the humid northern Red Sea Coast from the Arabian Desert. Elevations rarely exceed 6,900 feet (2,100 meters) MSL. Two significant breaks near 21°40' N and 24° N allow low-level flow into the desert. The western slopes of the Hijaz are rugged and barren with numerous volcanic peaks. Their eastern slopes have numerous wadis draining eastward towards isolated oases, the largest of which is Medinah. The eastern foothills form barren lava beds known as "harras."

The Asir and Yemen Mountains rise in elevation and extend southward while continuing to separate the Arabian Desert from the Red Sea. The eastern foothills are barren and gravel-covered, with isolated wadis cutting shallow valleys. The Arabian Desert begins below 4,930 feet (1,500 meters) MSL along the eastern foothills.

The Najd Plateau lies immediately east of the Hijaz and northern Asirs. It slopes gently from southeastern Jordan (4,500 feet/1,370 meters MSL) to south-central Saudi Arabia (2,460 feet/750 meters MSL). The plateau contains level, sand-covered plains and large, elongated sand dunes, along with hills and rocky ridges. Dunes reach 50 feet (15 meters) in height. Lava, cinder cones, haystack-shaped knobs, and boulders are common in the western Najd. Several wadis extend from the central Najd towards the Persian Gulf.

THE ARABIAN DESERT

The Jabal Tuwayq lies along the eastern edge of the Najd. This steep, dust-covered, rocky slope extends 530 NM from northwest to southeast across east-central Saudi Arabia, often rising 690 to 820 feet (180-250 meters) above level ground. Because it contains several important wadis and oases, this is the most populated area of Saudi Arabia. The city of Riyadh, along with the settlements of Buraydah, Unayzah, and Al Kharj are located here, near the largest oasis.

The Ad Dahna Desert and Summan Plateau lie east of the Jabal Tuwayq. Both are barren desert with the terrain sloping 2,300 feet (700 meters) MSL in the west to only 800 feet (244 meters) MSL in the east. There are wadis, isolated cinder cones, and sand dunes throughout the Ad Dahna. Sebkhahs (level sand, silt, clay, and salt pans with a thin hard crust) are found in all desert areas of Saudi Arabia, but most often in the lower elevations, where underground water is closer to the surface. Sebkhahs have quicksand-type soils beneath the thin crust.

The Rub al Khali Desert, also called "The Empty Quarter," is the second largest sand desert in the world. It covers most of the southern Arabian Desert subregion--an area of about 300 by 650 NM. Sand dunes in the western and central portions of the desert form continuous crescent-

SITUATION AND RELIEF

shaped northeast-to-southwest formations. Dune heights can reach 656 feet (200 meters). Surface winds keep the dunes in constant motion. The Rub al Khali extends to within 20 NM of the Arabian Sea along the Omani coastline. There are numerous large sebkhahs in Oman.

RIVERS AND DRAINAGE SYSTEMS. There are no permanent rivers in the Arabian Desert. The wadis drain the runoff when rainfall occurs, usually toward the Persian Gulf. Surface water seeps into the subterranean water table, but enough occasionally remains at the surface for an hour or two to drain into the sebkhahs or oases.

LAKES AND RESERVOIRS. There are no lakes or reservoirs in the desert, but there are important oases at Medinah and Riyadh. Numerous smaller oases support large populations in the Jabal Tuwayq. Oases also support nomadic herdsmen throughout the Hijaz.

VEGETATION. Most of the Arabian Desert is barren or sparsely covered with grass clumps. Wadi valleys and oases are the only sources of date palms, fig trees, and other fruit trees. Date palms provide a fifth of Saudi Arabia's cash crops. Less than 1% of the Arabian Desert surface is considered arable, but this figure is increasing due to extensive irrigation.

THE ARABIAN DESERT SOUTHWEST MONSOON

June-September

GENERAL WEATHER. The Saudi Arabian Heat Low and dry northwesterly surface flow dominate the Arabian Desert between June and September--as might be expected, it is very hot and very dry. Extensive dust haze reduces visibilities to 4 to 7 miles and there are locally severe duststorms.

The persistent Saudi Arabian Heat Low normally lies over the Rub al Khali as part of the Monsoon Trough; it produces northwesterly flow over much of the subregion. By day, the low generates 7- to 12-knot winds that swirl dust and sand into the air. Thick haze spreads gradually throughout the period because mid-level winds are too weak to provide good ventilation. At night, thin haze persists as surface winds weaken to 5-9 knots. Strong radiation cooling lowers temperatures quickly. Daily diurnal temperature ranges of 35 to 50° F (20-28° C) are common in the Rub al Khali and Nafud Deserts.

SKY COVER. Figure 5-2 shows that mean cloudiness incidence is very low except along the southern end of the subregion. The peaks along the Arabian Sea coast are due to moisture

brought in by the Somali Jet and the stratus formed from warm air moving over cooler waters. Mean cloudiness of 20 to 40% along the southwestern fringes of the Arabian Desert is due to sea breeze and orographic lifting along the western Asir and Yemen Mountains.

Cloud bases average 7,000 feet (2,130 meters) MSL; tops of isolated thunderstorms over the western Asir and Yemen Mountains reach 40,000 feet (12.2 km) MSL. Since the interior Arabian Desert region is not affected by Southwest Monsoon flow but by hot and dry northwesterlies, thin cirrus is often the only cloud type. Cloud bases over the Akhdar Mountains in Oman average 4,000 feet (1,220 meters); thunderstorm tops can exceed 50,000 feet (15.2 km).

About once every 3 years, a tropical depression or tropical storm reaches the southeastern Arabian Peninsula. These systems may produce the only cloud and/or ceiling observed in the Rub al Khali over a 5- to 10-year period. Multilayered cloud bases may form below 3,000 feet (915 meters) AGL, and tops of isolated thunderstorms may reach 45,000 feet (13.7 km).

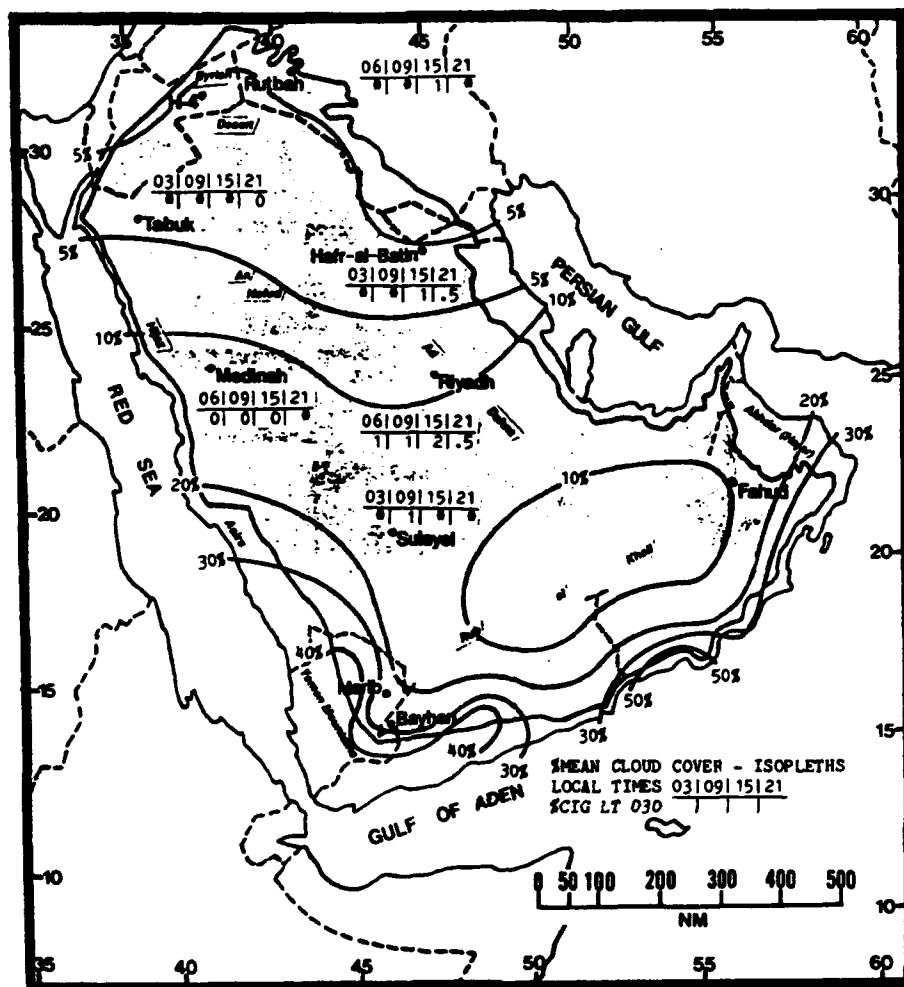


Figure 5-2. Mean Southwest Monsoon Cloudiness (Isolines) and Frequencies of Ceilings Below 3,000 Feet (915 meters), Arabian Desert.

THE ARABIAN DESERT SOUTHWEST MONSOON

June-September

VISIBILITY. Suspended or blowing dust/sand particles are the main restrictions to visibility. The hot and dry weather, with subsidence aloft, provides ideal conditions for persistent haze. Dust haze can exceed 15,000 feet (4,573 meters) MSL. Localized duststorm activity is common when surface heating peaks in late afternoon and during a 40-day Shamal; duststorms continue into early evening hours. The Saudi Arabian Heat Low intensifies surface winds and

increases the already large amounts of dust and sand suspended in the air; visibilities of 4-7 miles are common from July to September.

Early morning radiation fog may form between June and August, but light or calm winds are uncommon. When there is an early morning calm, strong radiation cooling can produce thin ground fog.

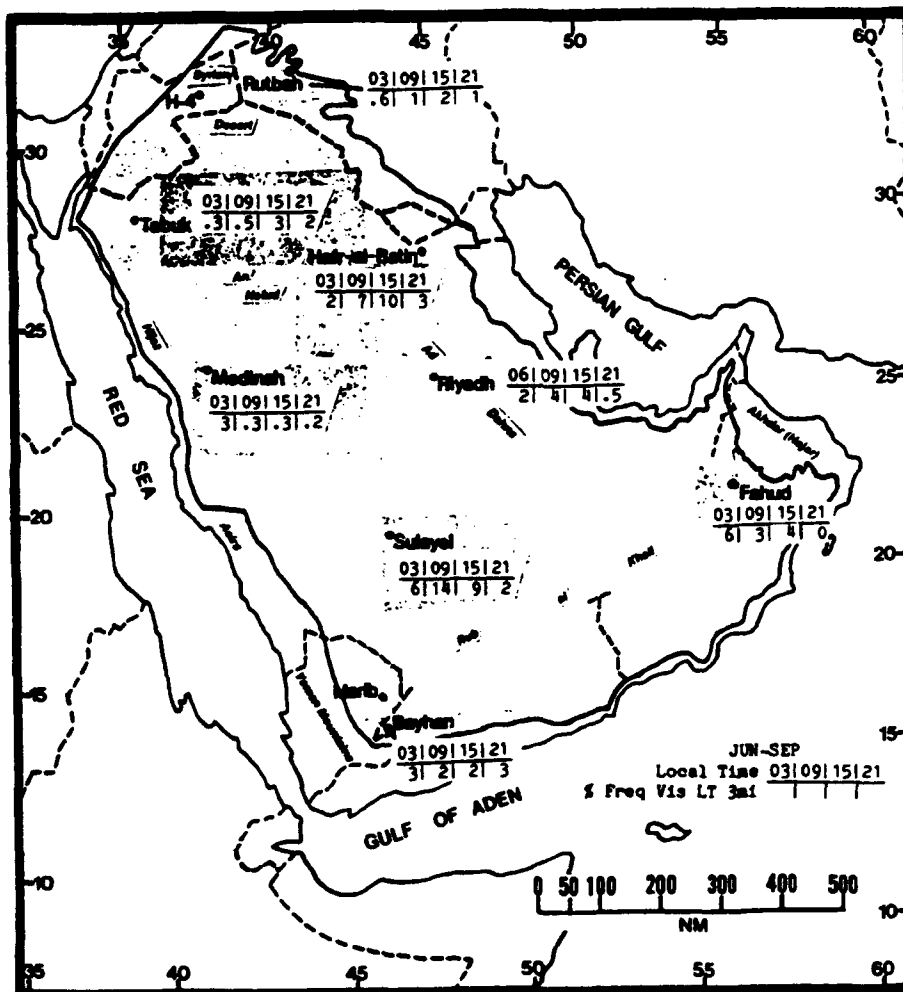


Figure 5-3. Southwest Monsoon Frequencies of Visibilities Below 3 Miles, Arabian Desert.

THE ARABIAN DESERT SOUTHWEST MONSOON

June-September

WINDS. Figure 5-4 shows mean Southwest Monsoon surface wind speed and prevailing direction for eight Arabian Desert stations, most of which have northwesterly flow. The 40-day Shamal occurs in mid-June to mid-July and produces duststorms with 10- to 15-knot northwesterly winds along the northern fringes of the Arabian Desert; typically, Rutbah, H-4, and Hafr-al-Batin are affected. These winds can blow continuously for 5-10 days. Prevailing direction at Buraimi shifts between July and August due to the northward migration of the surface Monsoon Trough and strong mountain breezes. At Marib, deflected low-level northeasterly flow from the Saudi Arabian Heat Low and a strong mountain wind circulation from the Yemen Mountains produce the season-long southerly winds. It's unlikely that the surface Monsoon Trough consistently penetrates this far inland. Maximum recorded wind speeds

across the subregion include 52 knots from the north at Hafr-al-batin in June, and 56 knots from the southwest at Madinah in July.

Figures 5-5a-c show 5,000-foot (1,524-meter), 10,000-foot (3,050-meter), and 15,000 (4,573-meter) MSL mean wind directions at Tabuk, Hafr-al-Batin, and Riyadh. The spikes shown at Riyadh in August and September are actually small shifts in direction that cross 360 degrees. Mean wind speeds are only 9-19 knots at all three levels at all stations shown.

At 39,000 feet (11.9 km), mean wind direction is easterly and southeasterly over the entire region. Mean 39,000-foot wind speed at Hafr-al-Batin is 14 knots, less than the mean speed at the 5,000- and 10,000-foot (1,524 and 3,050-meter) MSL levels in July and August.

		JUN	JUL	AUG	SEP
N	H-4	5.20	4.30	3.60	3.80
NW-N	Hafr'al-Batin	10.00	10.10	9.10	6.80
S	Marib	7.30	8.00	7.30	8.30
WNW/S-SE	Buraimi	8.30	8.50	9.10	8.40
W-N	Sulayel	6.00	6.10	6.00	5.60
WNW-W	Riyadh	7.40	7.90	6.80	4.70
N	Madinah	7.00	7.60	7.10	6.20
NNW-W	Tabuk	6.40	6.10	5.70	5.50

Figure 5-4. Mean Southwest Monsoon Surface Wind Speeds (kts) and Prevailing Direction, Arabian Desert.

**THE ARABIAN DESERT
SOUTHWEST MONSOON**

June-September

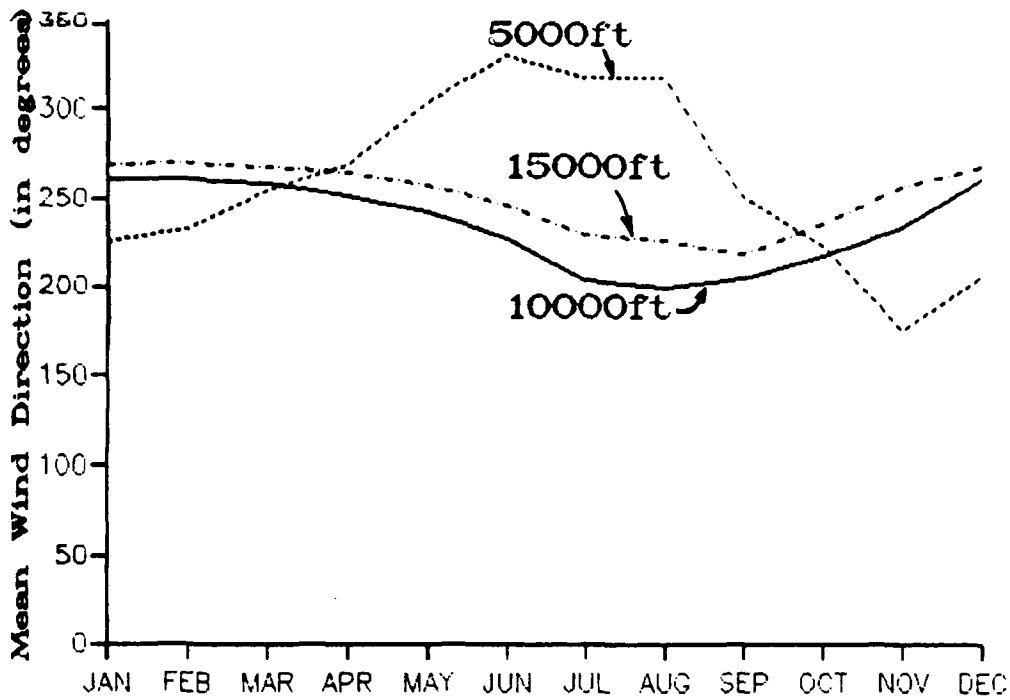


Figure 5-5a. Mean Annual Wind Direction, Tabuk, Saudi Arabia.

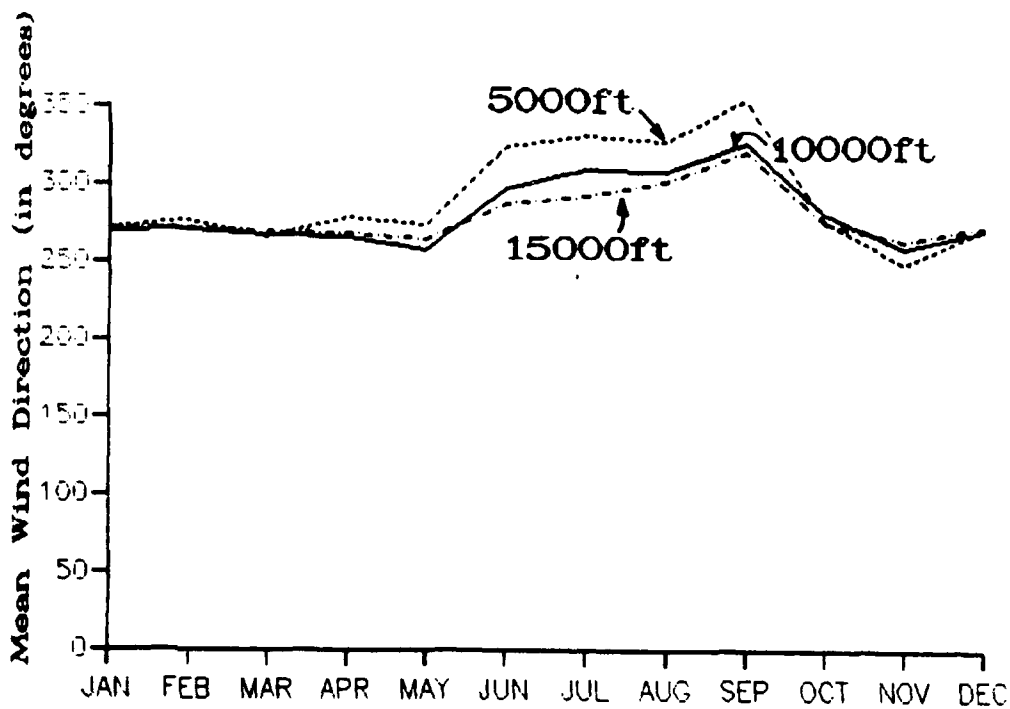


Figure 5-5b. Mean Annual Wind Direction, Hafr-al-Batin, Saudi Arabia.

**THE ARABIAN DESERT
SOUTHWEST MONSOON**

June-September

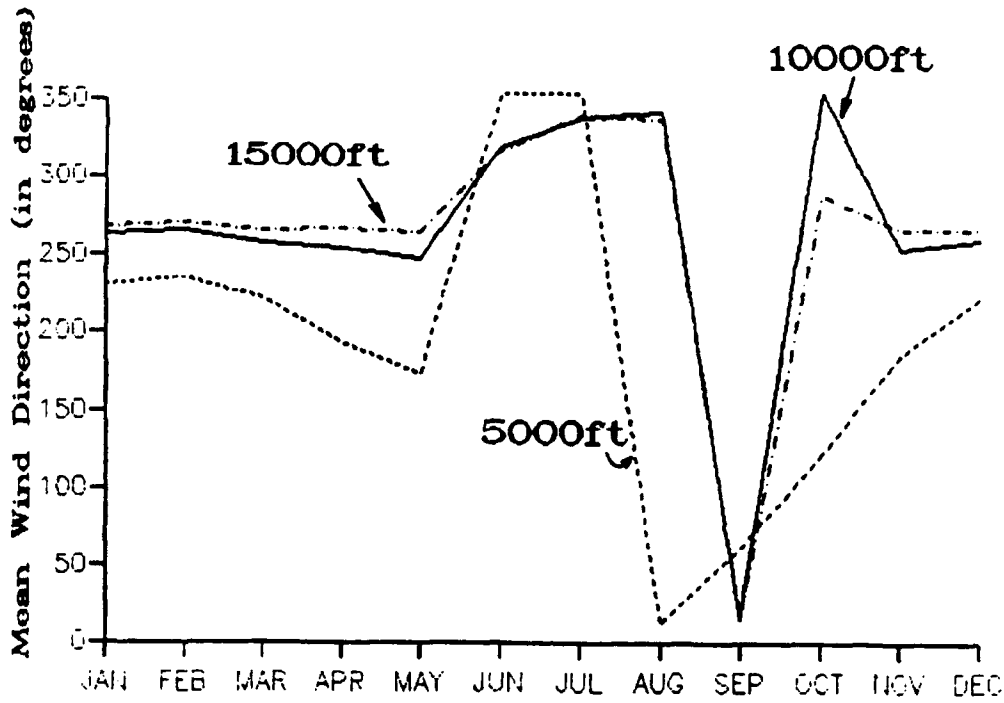


Figure 5-5c. Mean Annual Wind Direction, Riyadh, Saudi Arabia.

THE ARABIAN DESERT SOUTHWEST MONSOON

June-September

PRECIPITATION. North of 18° N, the Southwest Monsoon is rainless during 9 out of 10 years except near Medinah (Figure 5-6), where an occasional light shower develops due to orographic lifting along the Hijaz Mountains. The increase in July precipitation coincides with the time of maximum flow through the Tokar Gap to the eastern shores of the Red Sea. South of 18° N, Southwest Monsoon flow may carry moisture inland, usually producing showers only

along immediate coasts. At Bayhan and Fahud, all seasonal rainfall is the result of downwind convection from a combined sea breeze/surface Monsoon Trough that oscillates over eastern Oman during the Southwest Monsoon. This combination can produce rainshowers and thunderstorms over the Akhdar Mountains; little, if any, rain falls over the eastern Rub al Khali.

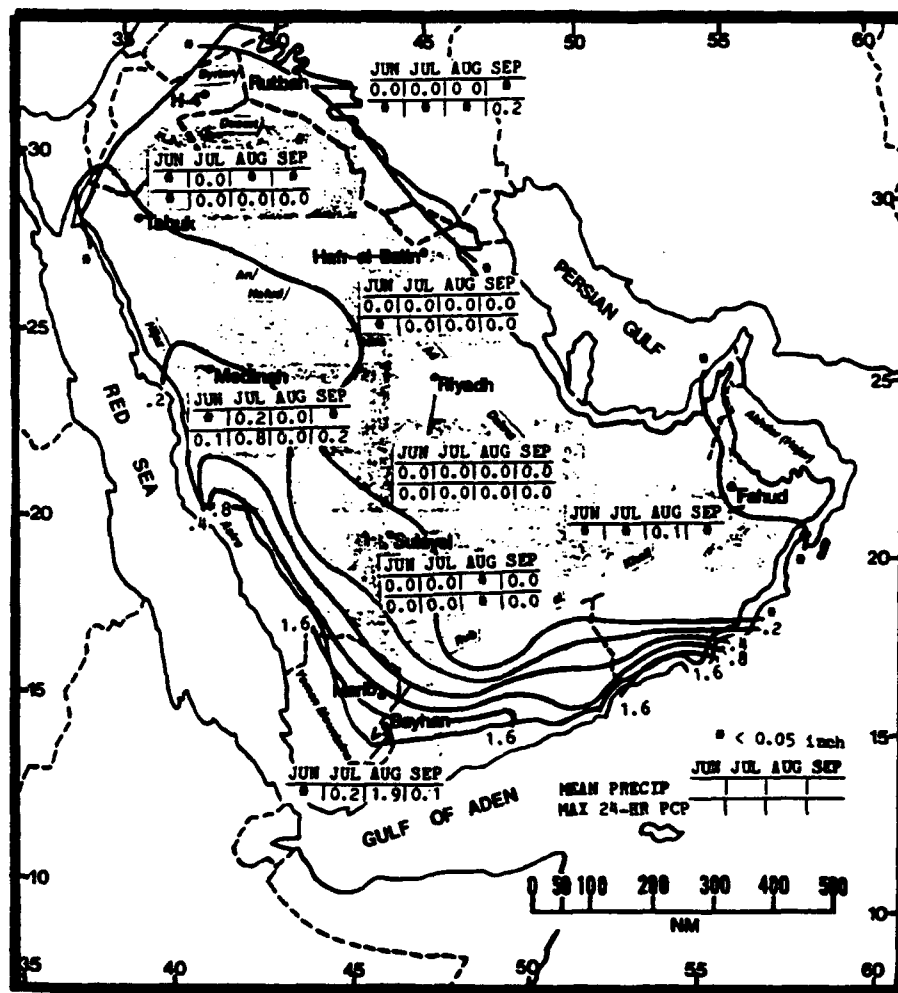


Figure 5-6. Mean Southwest Monsoon Monthly/Maximum 24-hour Precipitation, Arabian Desert. Bold lines represent mean seasonal rainfall totals.

THE ARABIAN DESERT SOUTHWEST MONSOON

June-September

TEMPERATURE. Summers are extremely hot. Many locations have recorded temperatures above 115° F (46° C). The maximum recorded temperature is 122° F (50° C) at Fahud in June, but it's likely that surface temperatures have exceeded 130° F (54° C) in the Rub al Khali and at other desert locations. As shown in Figure 5-7, the dry desert air and clear skies

produce large diurnal variations that average at least 20° F (12° C) at most locations. At Fahud, there is a 36° F (20° C) difference in average June highs and lows. The record low during the Southwest Monsoon was 23° F (-5° C) at Riyadh in September. Mean relative humidity averages 45% near sunrise, but only 10 to 15% by afternoon.

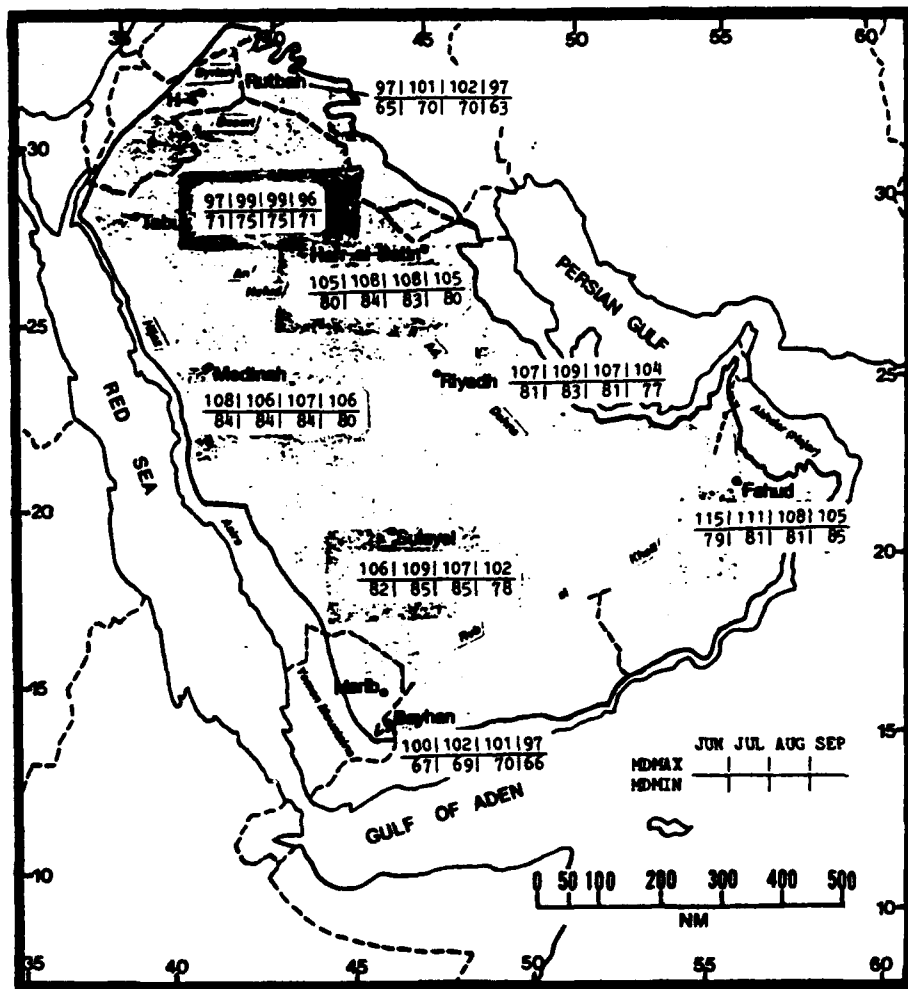


Figure 5-7. Mean Southwest Monsoon Daily Maximum/Minimum Temperatures (° F), Arabian Desert.

THE ARABIAN DESERT SOUTHWEST-TO-NORTHEAST MONSOON TRANSITION

October-November

GENERAL WEATHER. The transition is marked by the weakening of the Saudi Arabian Heat Low, which slowly contracts during the 3- to 4-week period in mid-October to mid-November as the Northeast Monsoon develops and the surface Monsoon Trough moves south. Over time, the strong radiative cooling induces a weak anticyclonic surface circulation (the Saudi Arabian High) even during daylight hours. By mid- to late-November, the Saudi Arabian High replaces the thermal heat low's circulation.

SKY COVER. Mean cloudiness remains low from the Rub al Khali northward across the Arabian Desert (Figure 5-8). Frequency is higher across the northern edge of the subregion due to a November increase in mid-latitude frontal systems; these increase mid-and upper-level cloud amounts over Rutbah, Tabuk, Medinah,

and Riyadh. Shallow altocumulus and altostratus form with deep 500- and 700-mb troughs, but cloud-cover distributions decrease from north to south. Mid-level clouds average 14,000 to 18,000 feet (4,268-5,487 meters) AGL, but few cloud tops extend above 20,000 feet (6,097 meters) MSL. Thin cirrus accompanies most disturbances and, with weak troughing, is often the only cloud.

Shallow diurnal cumulus begins to develop in October as excursions of Mediterranean air into the northwestern Arabian Desert become more frequent. On occasion, scattered cumulus and a rare thunderstorm form southward to 22° N along a deep mid-level trough axis. Cumulus bases average 5,000-7,000 feet (1,524-2,134 meters) AGL, but tops rarely extend above 8,000-9,000 feet (2,439-2,743 meters) MSL.

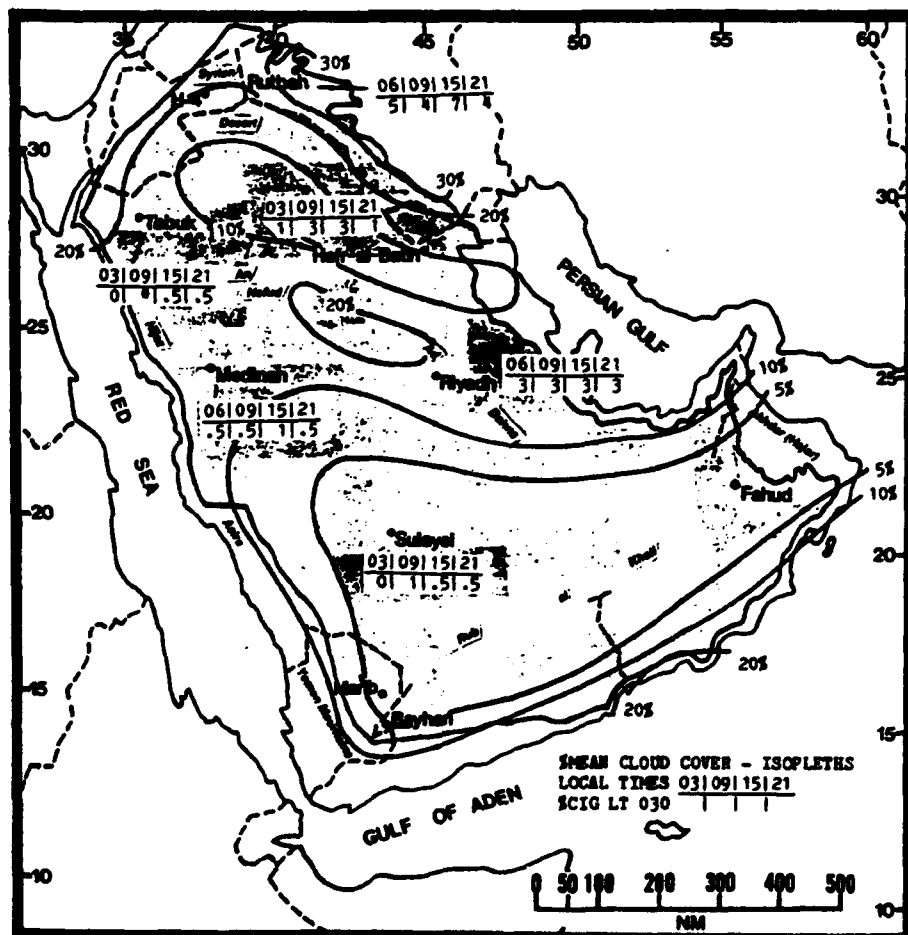


Figure 5-8. Mean SW-NE Monsoon Transition Cloudiness (isolines) and Frequencies of Ceiling Below 3,000 Feet (915 meters), Arabian Desert.

THE ARABIAN DESERT **SOUTHWEST-TO-NORTHEAST MONSOON TRANSITION**

October-November

VISIBILITY. Weakening of the Saudi Arabian Heat Low decreases the amount of suspended dust and sand particles in the air, but surface wind speeds above 12 knots can still produce widespread blowing dust/sand; local visibilities are less than a mile.

In November, weak cold fronts (north of 21° N) and mid-level troughs produce moderate-to-severe duststorms once or twice each transition, but the overall frequency of visibilities below 3 miles is no more than 6% during any 3-hour reporting period (Figure 5-9).

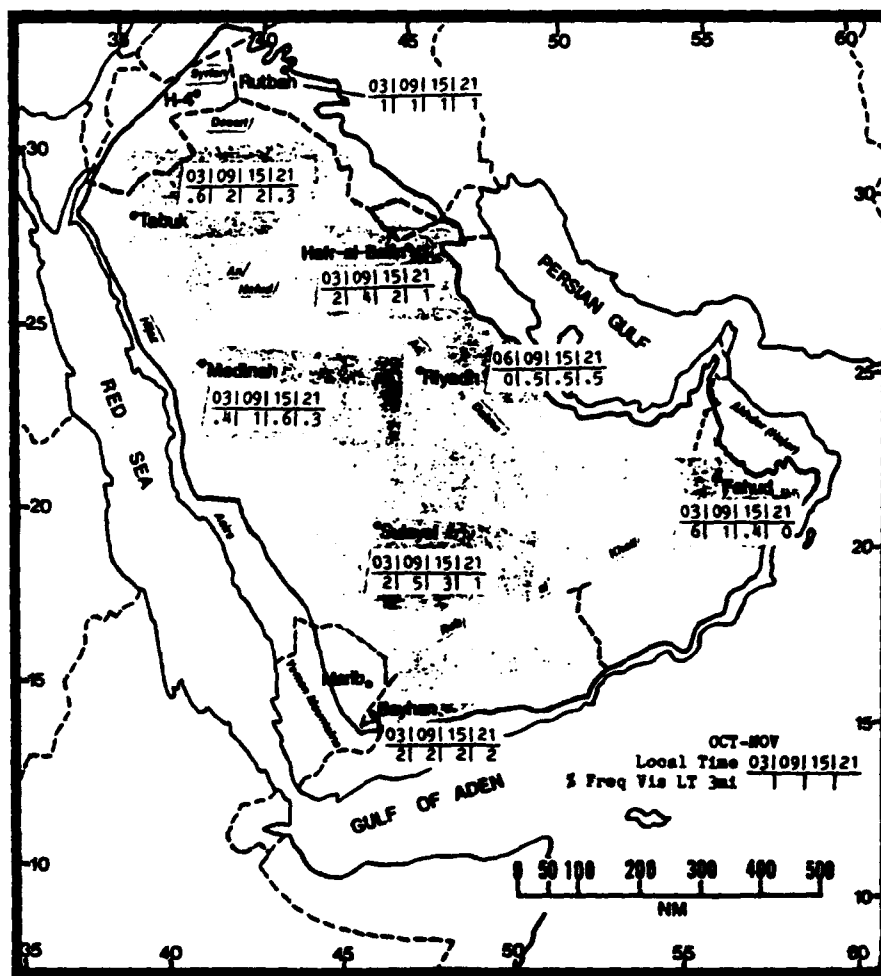


Figure 5-9. SW-NE Monsoon Transition Frequencies of Visibilities Below 3 Miles, Arabian Desert.

THE ARABIAN DESERT SOUTHWEST-TO-NORTHEAST MONSOON TRANSITION

October-November

WINDS. Figure 5-10 shows mean surface wind speeds and prevailing wind directions at several Arabian Desert locations during the transition. Wind directions across the subregion are very different as the Saudi Arabian Heat Low weakens and the Saudi Arabian High develops. The prevailing winds at Buraimi become northwesterly as the Monsoon Trough weakens and moves to the south.

Day-to-day variations in surface heating produce variations in the position and magnitude of the Saudi Arabian Heat Low. Several thermally-induced mesolows, rather than one individual low, seem to form over the interior; these were noted on local area work charts prepared by the DESERT SHIELD Forecast Unit.

By early November, the Northeast Monsoon is established over the Gulf of Oman and eastern Gulf of Aden; it produces a northeasterly surface flow that pushes the Monsoon Trough away from the Rub al Khali Desert. Local drainage winds contribute to prevailing wind directions at Riyadh, Sulayel, Medinah, and Tabuk until, as November progresses, enough radiation cooling occurs at night in the Rub al Khali to develop a weak high pressure area (anticyclone) over the Arabian Desert. Higher surface wind speeds are occasionally produced by weak cold fronts (north of 21° N) and mid-level troughs that begin to enter the subregion in November.

Refer again to Figures 5-5a and c for mean annual wind directions at Tabuk and Riyadh at

5,000 feet (1,524 meters), 10,000 feet (3,050 meters), and 15,000 feet (4,573 meters) MSL. At Tabuk (Figure 5-5a), the change is reflected at 5,000 feet, with winds shifting from southwesterly to southerly. Winds at 10,000 and 15,000 feet are more westerly due to the influence of mid-latitude systems. At Riyadh (5-5c), the mean direction at 5,000 feet shifts from east-southeasterly to southerly. At 10,000 feet, the direction shifts from northerly to west-southwesterly.

The mean wind speed at 39,000 feet (11.9 km) MSL at Tabuk increases from 61 to 79 knots from October to November, while Riyadh's 39,000-foot wind speed increases from 41 to 62 knots. The mean direction remains westerly at both stations.

		OCT	NOV
W	H-4	4.20	4.50
N	Harf'Batin	6.80	7.10
W	Marib	11.30	11.70
NW	Buraimi	7.40	6.00
E	Sulayel	4.60	6.10
S	Riyadh	4.20	4.60
E	Medinah	5.80	6.30
W/E	Tabuk	4.90	4.20

Figure 5-10. Mean SW-NE Monsoon Transition Surface Wind Speeds (kts) and Prevailing Direction, Arabian Desert.

THE ARABIAN DESERT SOUTHWEST-TO-NORTHEAST MONSOON TRANSITION

October-November

PRECIPITATION. Mean precipitation (Figure 5-11) increases significantly from October to November across the northern half of the region, but amounts still remain small; 0.6 inches (15 mm) at Rutbah is the largest. South of 21° N, little precipitation falls during the transition. Although Fahud shows no measurable precipitation in either month, locations to the east can see local rainshowers from disturbances moving in from the Arabian Sea. These showers usually remain over the Akhdar Mountains and do not move across the peninsula. Frontal systems reach the subregion north of 21° N as early as mid-October, but most troughs are weak at this time; virga, rather than rainfall, is common. Maximum 24-hour rainfall amounts of 1.2 inches (30.5 mm) have occurred, but are extremely rare.

By mid-November, strong polar lows occasionally move through the eastern Mediterranean. Weak cold fronts may extend southward to Riyadh and set off light rainshowers along the frontal boundary. Over half the November rainfall at Riyadh occurs with a deep mid- or upper-level trough that causes widely scattered showers and produces locally heavy rainfall. As a result, only one storm could be responsible for all the rainfall in an entire season at Riyadh or Medinah. November rainfall is more frequent at Hafr-al-Batin (at the extreme southern end of the surface low track) as weak fronts bring rainshowers and isolated thunderstorms. Mean thunderstorm frequency at Hafr-al-Batin is 2 in October and 1 in November. There are none in the south, and only one in November at Tabuk.

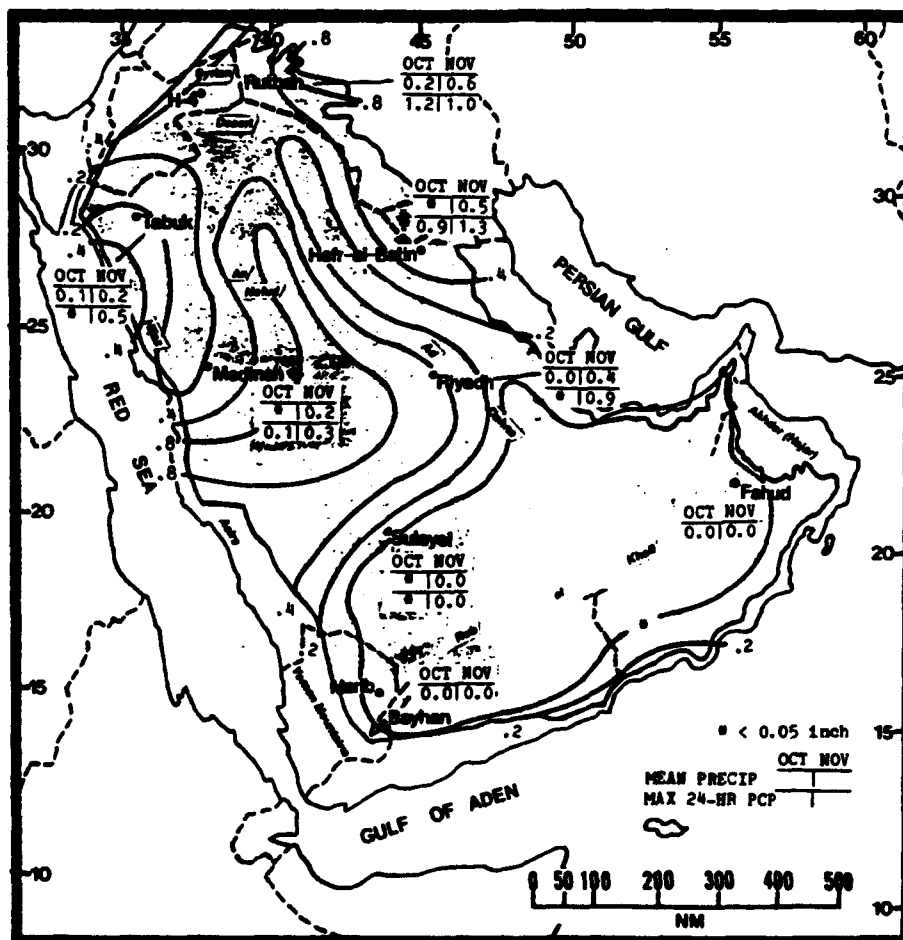


Figure 5-11 Mean SW-NE Monsoon Transition Monthly/Maximum 24-hour Precipitation, Arabian Desert. Bold line represent mean seasonal rainfalls totals.

THE ARABIAN DESERT **SOUTHWEST-TO-NORTHEAST MONSOON TRANSITION**

October-November

TEMPERATURE. Mean daily highs range from 98° F (37° C) to 72° F (17° C) and average 7-16° F (4-9° C) lower in November than October (Figure 5-13). Mean daily lows during the 2-month transition range from 72° F (22° C) at

Medinah in October to 45° F (7° C) at Rutbah in November. The record high was 108° F (42° C) at Hafr-al-Batin in October. The record low was 32° F (0° C) at Tabuk in November.

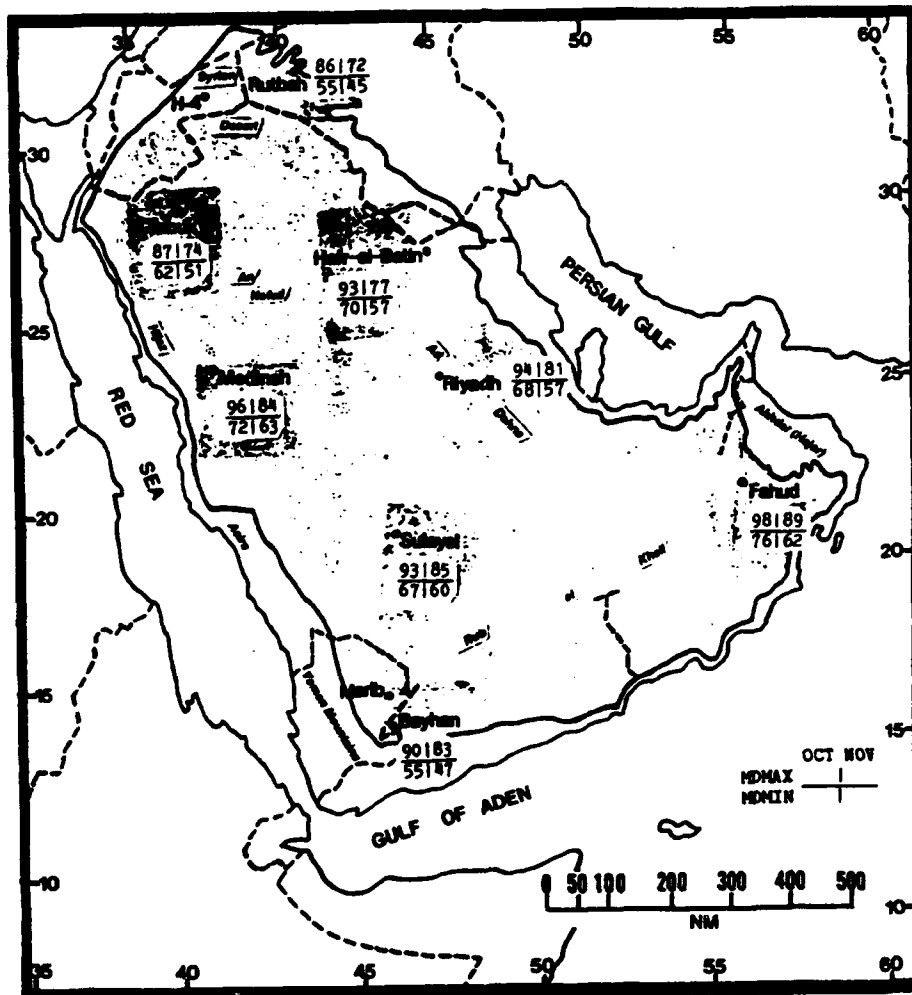


Figure 5-12. Mean SW-NE Monsoon Transition Daily Maximum/Minimum Temperatures (° F), Arabian Desert.

THE ABABIAN DESERT NORTHEAST MONSOON

December-March

GENERAL WEATHER. Mid-latitude lows usually affect the northern portion of the subregion every 3-5 days during the Northeast Monsoon, but they affect the southern portion only once or twice a month. With strong cold fronts, shamal conditions produce low visibility and high winds over widespread areas. Strong thunderstorms often develop along narrow zones of upper-level divergence. Although only one or two thunderstorms occur at a given location in a season, heavy rainfall may approach or exceed mean annual precipitation totals. Without upper-level support, only light-to-moderate rainshowers occur along cold fronts. Snow can be seen in the northern Arabian Desert, but it usually melts immediately upon reaching the ground.

SKY COVER. Cloud cover, at 9-40%, is moderate. Subtropical Jet cirrus is the main cloud type during fair weather; it often precedes mid- and upper-level troughs into the Arabian Desert. The lowest mean cloudiness (Figure 5-13) is over the An Nafud and Rub al Khali Deserts; the highest is along the northern edge where frontal activity is most frequent. December and March usually have the most cloud cover and cyclonic activity. Ceilings below 3,000 feet (915 meters) AGL are most frequent at Rutbah, where 8-12% frequencies are high for the desert; this is probably due to Rutbah's proximity to the source region for Cyprus Lows. Most low cloud observed in the desert is morning stratocumulus or diurnal/frontal cumulus.

Surface lows with polar jet support normally track north of the subregion. Weak cold fronts normally produce altocumulus and altostratus with bases at 12,000 feet (3,658 meters) AGL and tops to 20,000 feet (6.1 km); some cumulus or stratocumulus may be present. Stronger cold

fronts can generate cumulus or stratocumulus with bases from 6,000 to 10,000 feet (1,829-3,050 meters) AGL, as some middle cloud. Cold fronts with abundant mid-level moisture and upper-level divergence can produce cumulus with ceilings at 2,000 to 3,000 feet (610-915 meters) AGL, layered to 25,000 feet (7.6 km) with embedded thunderstorm tops to 40,000 feet (12.2 km) MSL.

As a general rule, if a front is oriented north to south, skies clear rapidly behind. However, if the orientation is northeast to southwest, altocumulus may continue to form after the front passes to the east.

If significant rain falls with frontal passage, scattered stratocumulus can form on the next few mornings. On rare occasions, stratus ceilings may form at 100-300 feet (30-90 meters) after frontal passage, on the north side of the low. This occurs in the northern end of the subregion where Persian Gulf moisture can be brought in, but may extend westward as far as Tabuk. It can last up to 72 hours after frontal passage, as occurred during Operation DESERT STORM.

Sea-breeze cumulus develops along most coastal regions, but only small amounts reach the desert interior. Along the Akhdar and Yemen Mountains, sea-breeze cumulus increases due to orographic lifting; this can, on occasion, effect Fahud, Buraimi, or Bayhan.

Upslope/advection stratus from the Persian Gulf can affect the eastern Arabian Desert up to 300 NM inland. Usually the stratus comes in during the early morning hours and dissipates rapidly after sunrise, but it can persist longer with lower air temperatures.

**THE ABABIAN DESERT
NORTHEAST MONSOON**

December-March

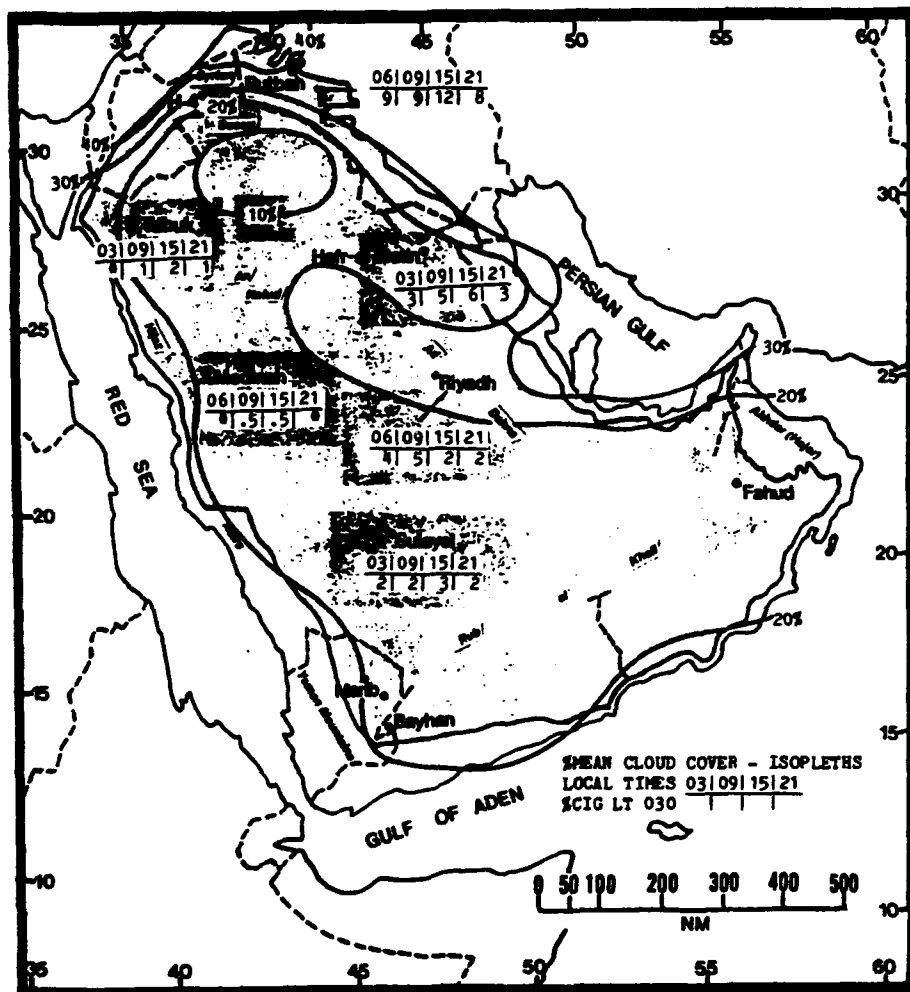


Figure 5-13. Mean Northeast Monsoon Cloudiness (Isolines) and Frequencies of Ceilings Below 3,000 Feet (915 meters, Arabian Desert.

THE ABABIAN DESERT NORTHEAST MONSOON

December-March

VISIBILITY. Dust and haze are the main visibility restrictions during the Northeast Monsoon, but fog and rain are occasional problems. Cyclonic activity can produce 24- to 36-hour or 3- to 5-day Shamals. Northwesterly winds at 12 to 20 knots generate localized duststorms and reduce visibility below 3 miles for up to 24 hours, about 3 days a season. If fair weather persists for 5 to 10 days after a 3- to 5-day Shamal, thick haze aloft will persist. Ground fog can develop at some locations between 2100 and 0300L. Strong radiation

cooling with calm winds produces light fog for 2 to 4 days a season, but visibilities rarely go below 3 miles unless heavy residual moisture and cold, stable conditions are present.

Stations in the Rub al Khali (Sulayel, Fahud, and Bayhan) are affected by blowing dust and sand nearly every afternoon during the Northeast Monsoon as extremely dry conditions let dust accumulate in the boundary layer. Visibility is usually 4-7 miles, but at Sulayel, 0900L visibility is below 3 miles 12% of the time.

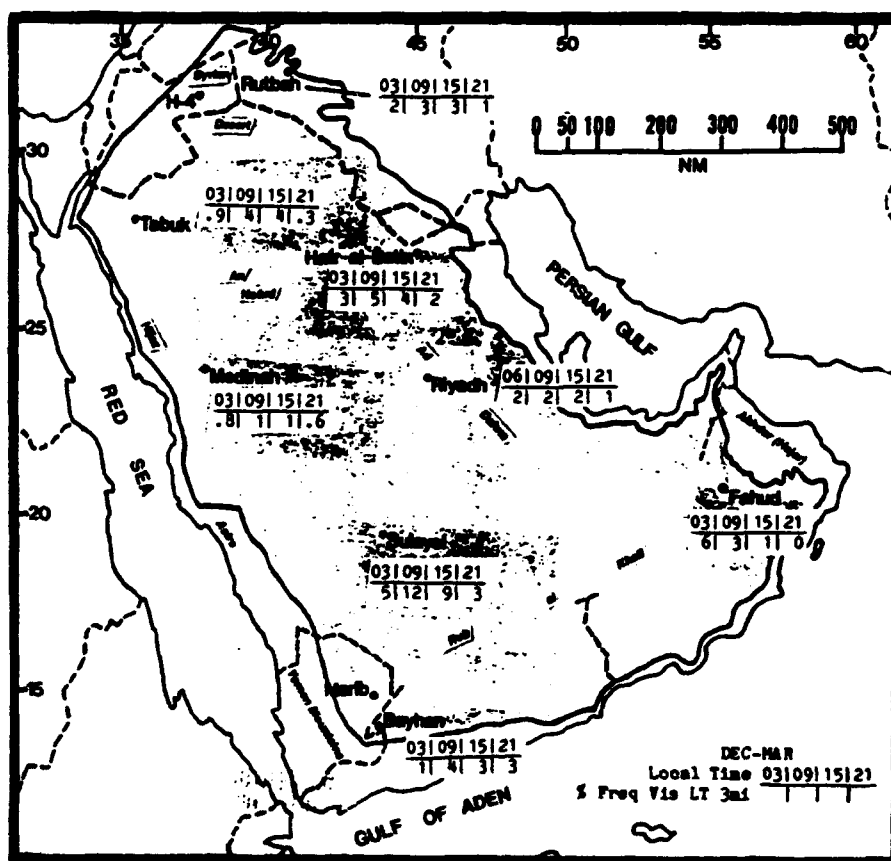


Figure 5-14. Northeast Monsoon Frequencies of Visibilities Below 3 Miles, Arabian Desert.

THE ABABIAN DESERT NORTHEAST MONSOON

December-March

WINDS. Figure 5-15 shows mean Northeast Monsoon surface wind speeds and prevailing wind directions across the Arabian Desert. Mean speeds are less than 10 knots throughout the season, but directions, controlled by the Northeast Monsoon, the Saudi Arabian High, and the location of nearby mountains, vary considerably across the subregion.

Mean wind directions at 5,000 feet (1,524 meters) MSL reflect surface circulation around the Saudi Arabian High. At Tabuk and Riyadh, directions vary between 210 and 240 degrees,

but westerlies predominate at Hafr-al-Batin (refer to Figures 5-5a-c). Mean wind speeds at 5,000 feet average 11 to 15 knots. At 10,000 and 15,000 feet (3,050-4,573 meters) MSL, directions are westerly at all three locations. At 30-38 knots, mean wind speed is strongest at 15,000 feet. The Subtropical Jet is a significant feature of the upper-level pattern. Mean speeds at 39,000 feet (11.9 km) MSL--the level at which the jet is typically found--are shown in Figure 5-16. Highest wind speeds occur between 25 and 30° N.

		DEC	JAN	FEB	MAR
SW-W	H-4	5.20	5.90	7.10	7.10
W-N	Hafr'al-Batin	7.30	7.60	8.40	8.70
W-N	Marib	8.10	7.90	6.70	6.10
W-NW/SE	Buraimi	6.50	6.80	7.80	9.60
E-NE	Sulayel	6.60	6.90	7.30	9.00
S-SE	Riyadh	5.10	6.00	6.60	6.90
E/W	Medinah	6.00	6.30	6.70	7.80
E	Tabuk	4.00	4.90	5.70	6.40

Figure 5-15. Mean Northeast Monsoon Surface Wind Speeds (kts) and Prevailing Direction, Arabian Desert. Slashes separating prevailing wind direction at Medinah and Buraimi denote wind shifts between February and March.

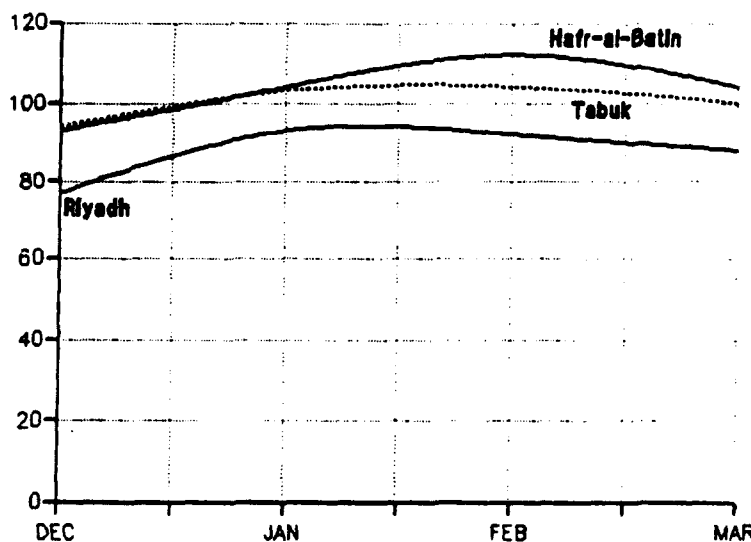


Figure 5-16. Mean Monthly (Northeast Monsoon) 39,000-Foot (11.9-km) MSL Wind Speed (kts), Upper-Air Network, Arabian Desert.

THE ABABIAN DESERT NORTHEAST MONSOON

December-March

PRECIPITATION. The Northeast Monsoon is the wettest part of the year at most locations, except at Bayhan and Fahud on the southern end of the peninsula. Even though this is the "wet" season, most months average less than 1 inch (25mm). Measurable rainfall occurs on only 1-3 days a month. Hafr-al-Batin averages 1.4 inches (35.6 mm) in January, but this is based on only a 6-year period of record.

Northeast Monsoon precipitation develops along fronts, with sea breezes, and under strong upper-level divergence. Figure 5-17 shows the results of precipitation produced by fronts that reach Riyadh and the Persian Gulf coast; this activity doesn't penetrate much farther south. Figure 5-17 also shows that 24-hour rainfall often exceeds monthly totals and lends emphasis to the fact that such extreme conditions might well occur only once over a 10- to 20-year period during the Northeast Monsoon. A single desert thunderstorm may yield rainfall that exceeds the mean annual precipitation total; it may then be several years until the next measurable rainfall.

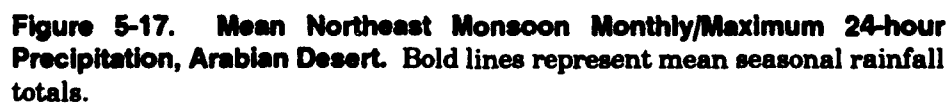
Although snow is rare, it falls over the northern An Nafud and Syrian Deserts about once a season with the passage of an abnormally cold polar air mass; it usually melts immediately.

Rain can fall between Tabuk and Rutbah when a secondary surface low forms over northwest Saudi Arabia or eastern Jordan. Northern Red Sea moisture fuels the surface low, but upper-level divergence is necessary for a widespread thunderstorm outbreak to occur.

Most rainshowers and thunderstorms occur with Cyprus Lows, but moisture in these systems is limited south of 21° N. As a result, the Rub al Khali remains very dry during the Northeast Monsoon except in March, when polar air masses penetrate south of 21° N more than in other months. A rare March thunderstorm with heavy rain may occur with a deep upper-level trough. Most rainfall precedes the trough under a zone of upper-level divergence when there is persistent moist southwesterly flow in the middle levels.

Northeast Monsoon flow brings moisture and orographic showers to the eastern slopes of the eastern Rub al Khali, which lies in the rain shadow of the Akhdar Mountains in Oman. When convection is well-established, cloud canopies may move over the lee side. These orographic showers may be responsible for the exceptional March rainfall at Fahud and nearby locations, but the Omani Convergence Zone (OCZ) may also be the cause.

December-March



THE ABABIAN DESERT NORTHEAST MONSOON

December-March

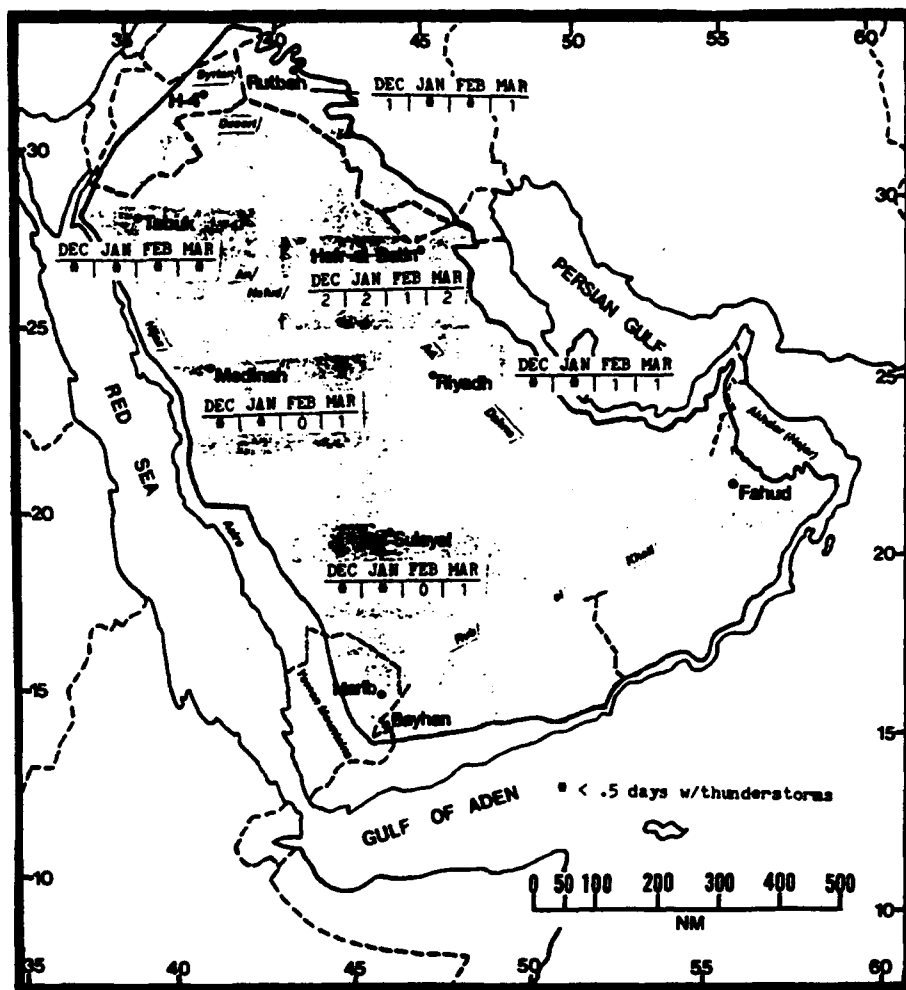


Figure 5-18. Mean Northeast Monsoon Frequencies of Thunderstorms, Arabian Desert.

THE ABABIAN DESERT NORTHEAST MONSOON

December-March

TEMPERATURE. Northeast Monsoon temperatures (Figure 5-19) are the lowest of the year. Mean daily highs range from 55° F (13° C) at Rutbah in January to 93° F (34° C) at Fahud in March. Mean daily lows range from 34° F

(1° C) at Rutbah in January to 63° F (17° C) at Medinah and Fahud in March. The record low was 14° F (-10° C) at Tabuk in March, while the record high is 107° F (42° C) at Hafr-al-Batin in February.

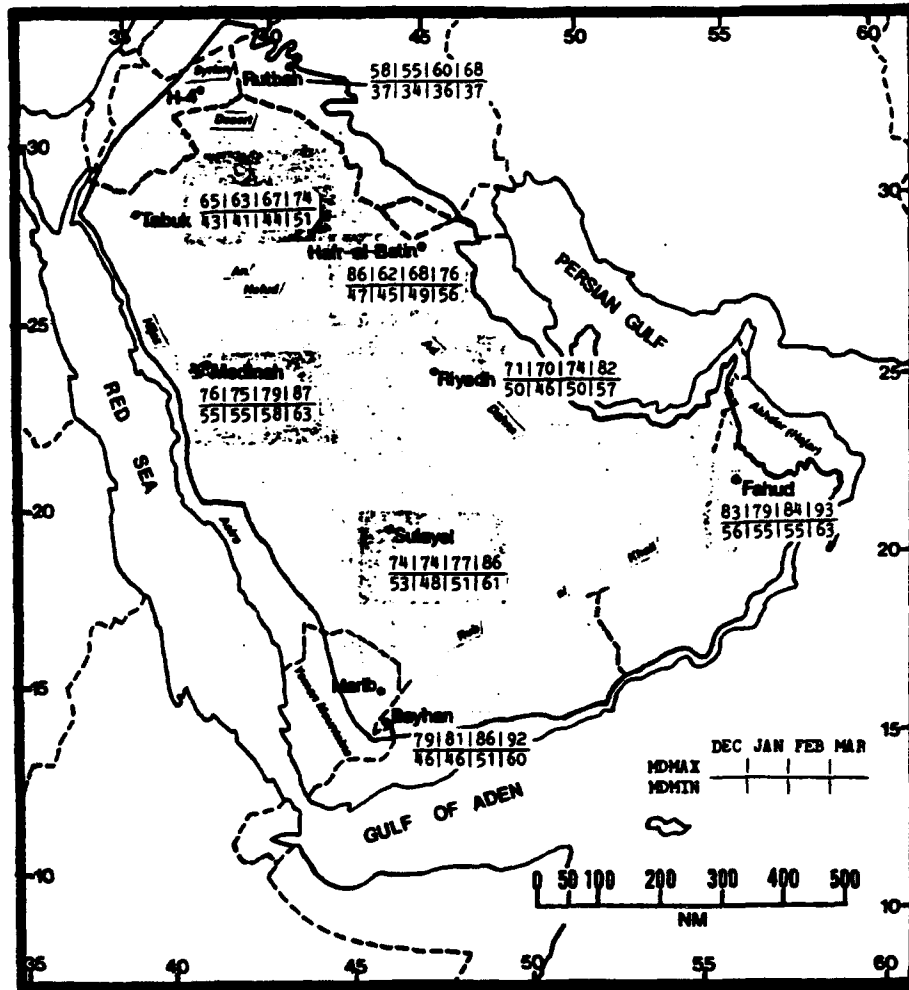


Figure 5-19. Mean Northeast Monsoon Daily Maximum/Minimum Temperatures (° F), Arabian Desert.

THE ARABIAN DESERT NORTHEAST-TO-SOUTHWEST MONSOON TRANSITION

April-May

GENERAL WEATHER. Strong surface heating, frontal systems, and mid- and upper-level troughs are important weather features of the NE-SW Monsoon transition. Solar radiation increases in April and May, causing instability and formation of the Saudi Arabian Heat Low. Cyprus Lows from the eastern Mediterranean Sea track across the northern fringe of the Arabian Desert every 3-7 days. When a cold front is supported by troughing at the mid- and upper-levels, widespread rainfall and isolated thunderstorms can develop. Thunderstorm severity is determined by the strength of the cold air aloft. On rare occasions, an Atlas Low tracks eastward across the central Red Sea toward the Persian Gulf. These systems generate strong winds along with widespread dust and low visibility, but they are often rainless. Heavy rain and thunderstorms can occur if upper-level divergence and low-level moisture are present.

SKY COVER. Mean cloudiness (isolines in Figure 5-20) is similar to that of the Northeast Monsoon. In April, frontal systems continue to be the primary source of low and middle clouds. Low clouds with bases between 2,000 and 3,000 feet (610-915 meters) AGL form along the cold front. The intense solar radiation modifies the

cold air behind the cold front before it reaches the Arabian Desert. More often than not, cold fronts become desert fronts or trough lines between 20 and 30° N, where they may cause scattered mid- and upper-level cloud cover.

The frequency of ceilings below 3,000 feet (915 meters) AGL is less than 5% everywhere except Rutbah at 1500 and 2100L (Figure 5-20). Rutbah's extreme northern position puts it nearest the storm track in April, when lows still affect the Persian Gulf. Increased low-ceiling frequencies at other locations at 1500 and 2100L are caused by diurnal cumulus and stratocumulus. Low ceilings at 0300 and 0900L are due to ground fog and shallow stratocumulus.

Cirrus is common with the Subtropical Jet Stream. Diurnal fair-weather cumulus, early morning stratocumulus, and patchy ground fog are typical post-frontal conditions north of 25° N. By May, cloud cover is mainly cirrus and altocumulus, with bases at or above 7,000 feet (2,134 meters) AGL. Migratory lows are very infrequent by early May. By mid- to late-May, mornings are clear.

April-May



THE ARABIAN DESERT NORTHEAST-TO-SOUTHWEST MONSOON TRANSITION

April-May

VISIBILITY. Blowing dust and sand are the primary causes of reduced visibilities. Strong surface heating causes localized low-level turbulence. There are brief periods with visibilities below 3 miles. Haze and 4- to 7-mile visibilities are common during fair weather. Mid- and upper-level troughs and surface cold fronts may cause 24- to 36-hour (or 3- to 5-day) shamals that result in widespread dust/sandstorm activity once or twice in each transition. On rare occasions, visibility can be reduced to near zero for several minutes to several hours.

Frontal systems may produce isolated areas of heavy rain and 2- to 4-mile visibilities once or twice a transition at Rutbah and Hafr-al-Batin. Post-frontal visibilities are normally greater than 7 miles.

Figure 5-21 shows frequencies of visibilities below 3 miles across the subregion. Nearly all are caused by blowing dust and sand. The highest occurrence is at Sulayel, where intense surface heating during the day produces swirling winds. At night, surface winds are weak, but the suspended particles produce persistent haze.

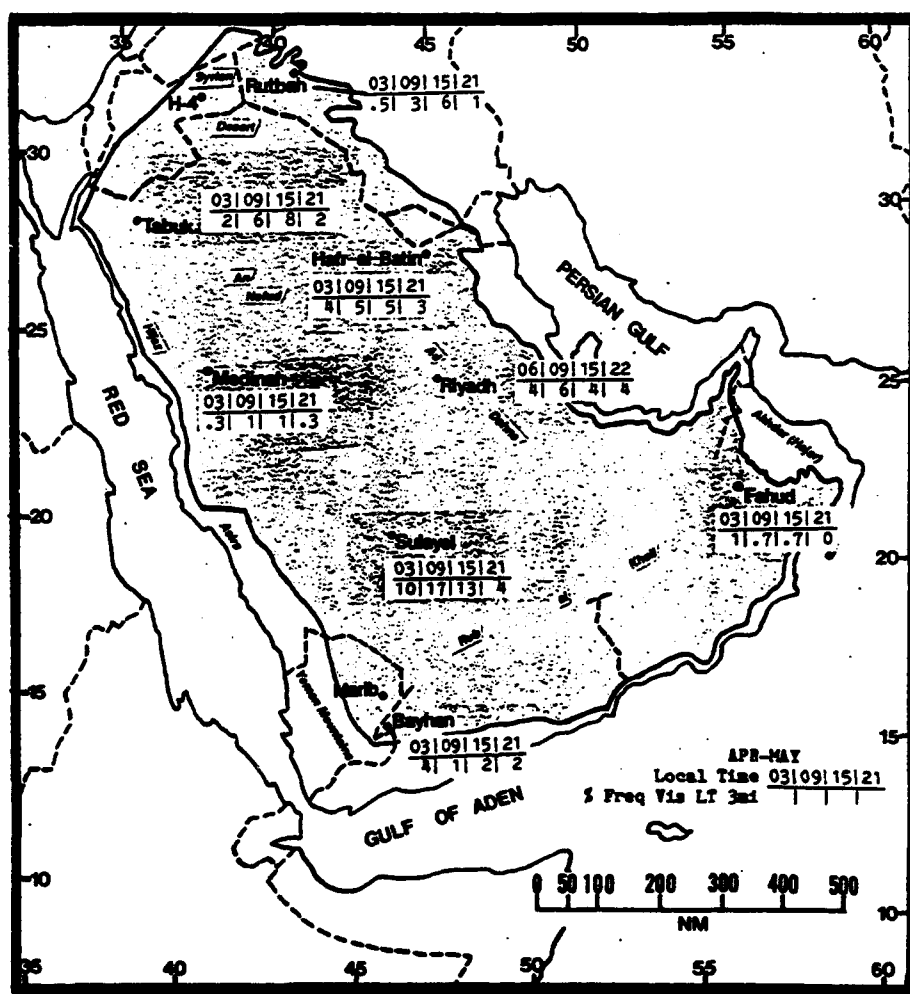


Figure 5-21. NE-SW Monsoon Transition Frequencies of Visibilities Below 3 Miles, Arabian Desert.

THE ARABIAN DESERT **NORTHEAST-TO-SOUTHWEST MONSOON TRANSITION**

April-May

WINDS. Intense surface heating in April and May gradually causes the Saudi Arabian Heat Low to redevelop in the Rub al Khali. By mid-May, northwesterly gradient flow into the low is well established. Figure 5-22 gives mean NE-SW Monsoon transition surface wind speeds and prevailing wind directions at various Arabian Desert locations.

The highest surface wind speeds in April include 75 knots at H-4, 65 knots from the NNE at Sulayel, and 51 knots from the WNW at Medinah. The highest May wind speeds include 45 knots from the NNE at Riyadh, 60 knots from the WNW at Hafr-al-Batin, and 87 knots from the north at Marib. These high-speed surface winds produce zero visibilities in dust and sand. Surface heating can generate intense mesoscale thermal-low circulations, dust devils, or simple thermal turbulence.

		APR	MAY
W	H-4	7.40	6.20
N	Harf'Batin	8.40	8.70
W/S	Marib	11.10	8.50
WNW	Buraimi	8.50	9.70
E	Sulayel	8.10	7.20
N	Riyadh	6.50	6.20
W	Medinah	7.30	7.20
N/W	Tabuk	7.10	6.80

Figure 5-22. Mean NE-SW Monsoon Transition Surface Wind Speeds (kts) and Prevailing Direction, Arabian Desert. Slashes separating prevailing wind direction at Marib and Tabuk denote wind shifts between April and May.

THE ARABIAN DESERT NORTHEAST-TO-SOUTHWEST MONSOON TRANSITION

April-May

PRECIPITATION. As shown in Figure 5-23, all reporting stations (except Sulayel) see at least 0.1 inch (2.5 mm) of precipitation a month in May. Overall averages remain small. Rutbah, Hafr-al-Batin, and Tabuk get precipitation from frontal systems, while rainfall at other locations is from isolated, non-frontal type thunderstorms. Although surface cold fronts seldom initiate thunderstorms south of 25° N, mid- and upper-level troughs do. Trough passages, coupled with instability from surface heating produce nearly all the rainfall south of 25° N. Thunderstorm bases here average 4,000 feet (1,220 meters) AGL and tops can exceed 45,000 feet (13.7 km) MSL.

April and May are conducive to thunderstorm development in the Arabian Desert; the increase in activity is shown in Figure 5-24.

Increasing solar radiation creates convective instability, and there is little subsidence aloft to cap it. The Polar Jet brings in moisture and cooler mid-level air while the Subtropical Jet provides outflow and upper-level moisture. Diurnal surface heating may cause isolated cumulus but the mid- or upper-level support (divergence, cold air aloft, and troughing) intensifies convection more often in April and May than at any other time of the year. Most of these conditions disappear when the Southwest Monsoon sets in.

In the southwestern Arabian Desert (from Medinah south to Bayhan), moist Red Sea low-level flow produces orographic showers and thunderstorms along the western slopes of the Yemen Asir mountain ranges. Heavy convection can be carried downwind along the lee sides.

THE ARABIAN DESERT
NORTHEAST-TO-SOUTHWEST MONSOON TRANSITION

April-May

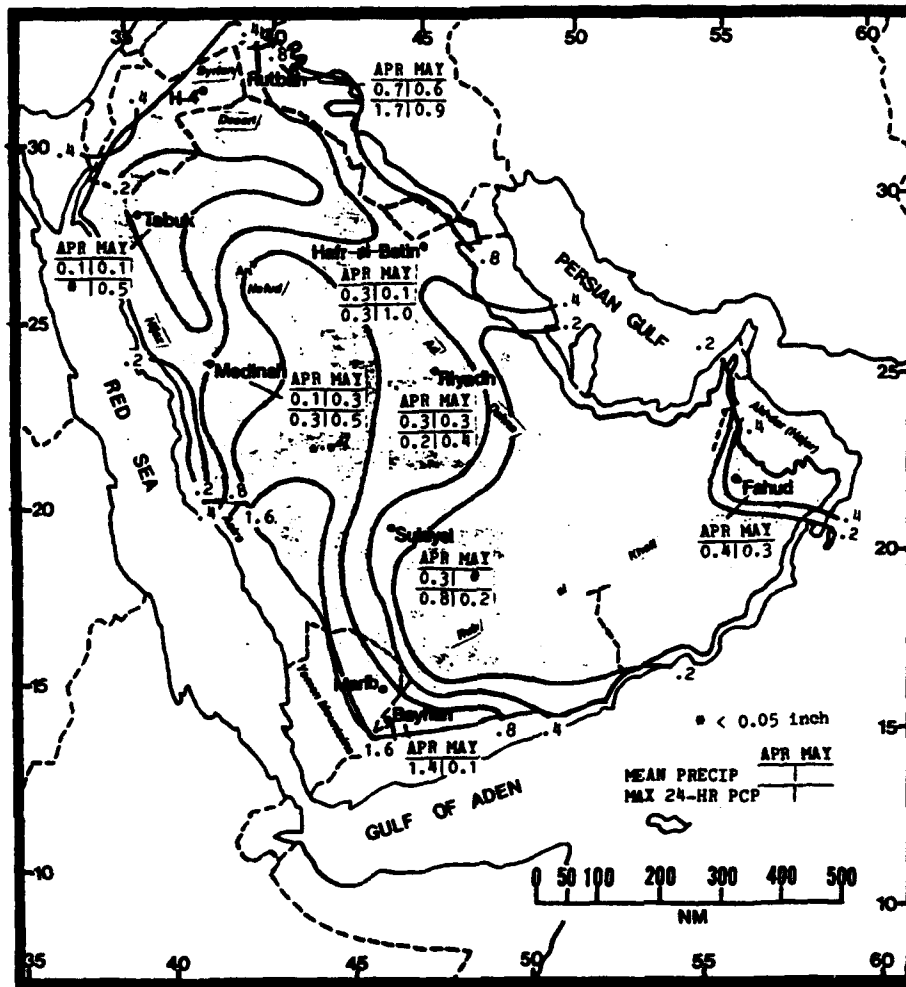


Figure 5-23. Mean NE-SW Monsoon Transition Monthly/Maximum 24-hour Precipitation, Arabian Desert. Bold lines represent mean seasonal rainfall totals.

**THE ARABIAN DESERT
NORTHEAST-TO-SOUTHWEST MONSOON TRANSITION**

April-May

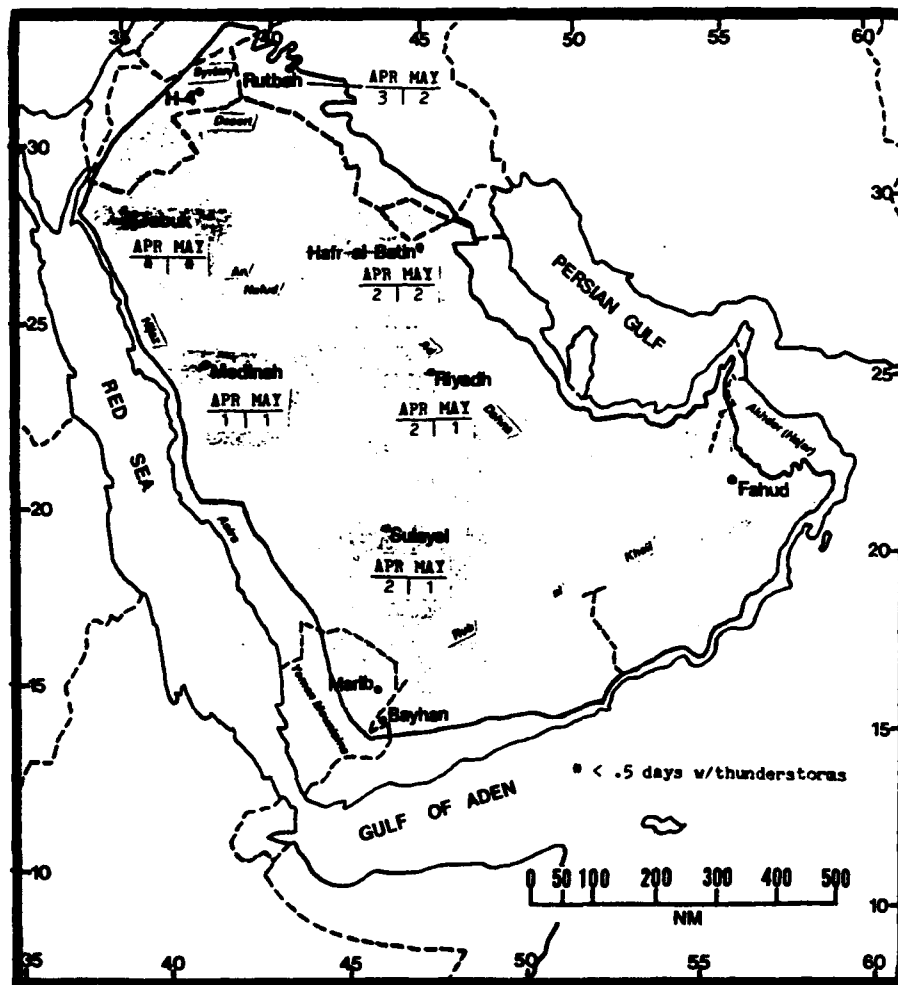


Figure 5-24. Mean NE-SW Monsoon Transition Frequencies of Thunderstorms, Arabian Desert.

THE ARABIAN DESERT **NORTHEAST-TO-SOUTHWEST MONSOON TRANSITION**

April-May

TEMPERATURE. Mean daily highs for April range from 78° F (26° C) at Rutbah to 95° F (35° C) at Fahud (Figure 5-25). Mean daily lows for April range from 50° F (10° C) at Rutbah to 71° F (22° C) at Medinah. Mean daily highs in May range from 89° F (32° C) at Rutbah to

107° F (42° C) at Fahud. Mean daily lows in May range from 59° F (15° C) at Rutbah to 80° F (27° C) at Sulayel. Record lows and highs for the season are 32° F (0° C) at Hafr-al-Batin in April, and 118° F (48° C) at Riyadh in May.

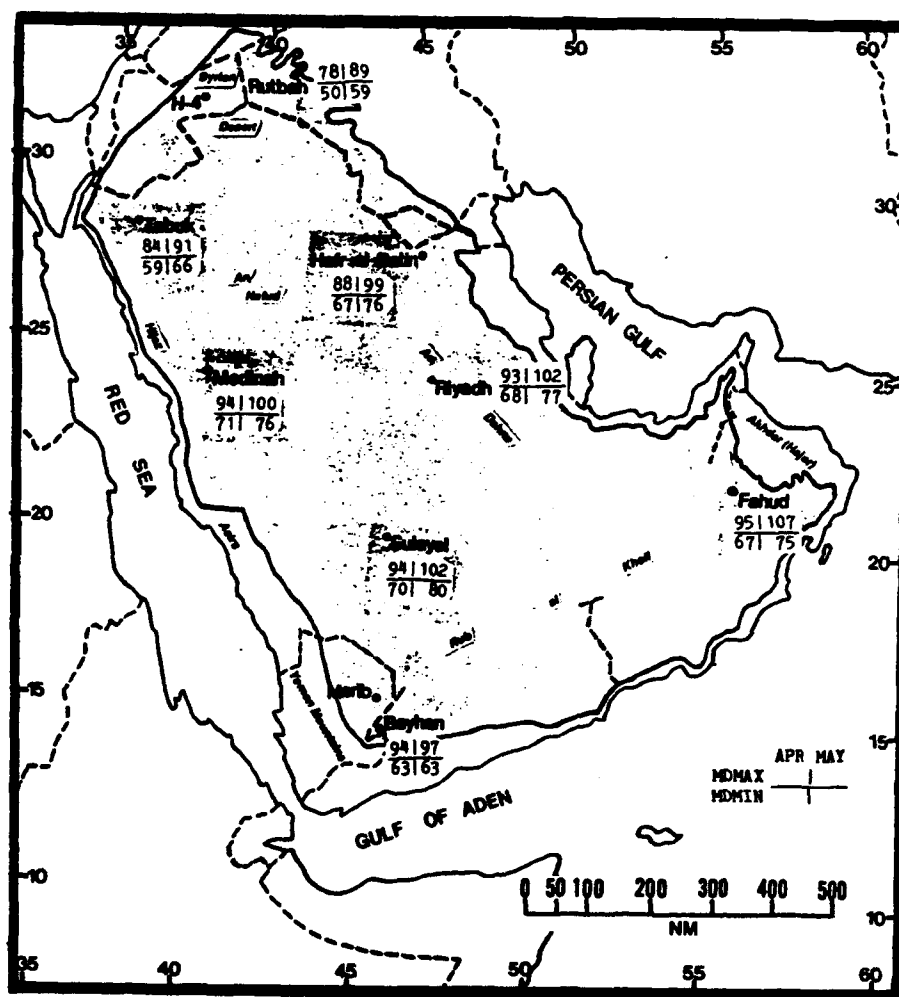


Figure 5-25. Mean NE-SW Monsoon Transition Daily Maximum/Minimum Temperatures (F), Arabian Desert.

Chapter 6

PERSIAN GULF COASTAL PLAINS

The Persian Gulf Coastal Plains comprise the coastal fringes surrounding the Persian Gulf, Gulf of Oman, and western Arabian Sea. The study area includes Kuwait, Bahrain, Qatar, and small coastal portions of Yemen, Oman, Iraq, Iran, and Pakistan. After describing the area's situation and relief, this chapter discusses its "general weather" by season, as shown below.

Situation and Relief	6-2
The Southwest Monsoon--June-September	6-6
General Weather	6-6
Sky Cover	6-6
Visibility	6-9
Winds	6-11
Precipitation	6-14
Temperature	6-16
The Southwest-to-Northeast Monsoon Transition--October-November ..	6-17
General Weather	6-17
Sky Cover	6-17
Visibility	6-19
Winds	6-20
Precipitation	6-21
Temperature	6-23
The Northeast Monsoon--December-March	6-24
General Weather	6-24
Sky Cover	6-24
Visibility	6-26
Winds	6-27
Precipitation	6-28
Temperature	6-30
The Northeast-to-Southwest Monsoon Transition--April-May	6-31
General Weather	6-31
Sky Cover	6-31
Visibility	6-33
Winds	6-35
Precipitation	6-36
Temperature	6-37

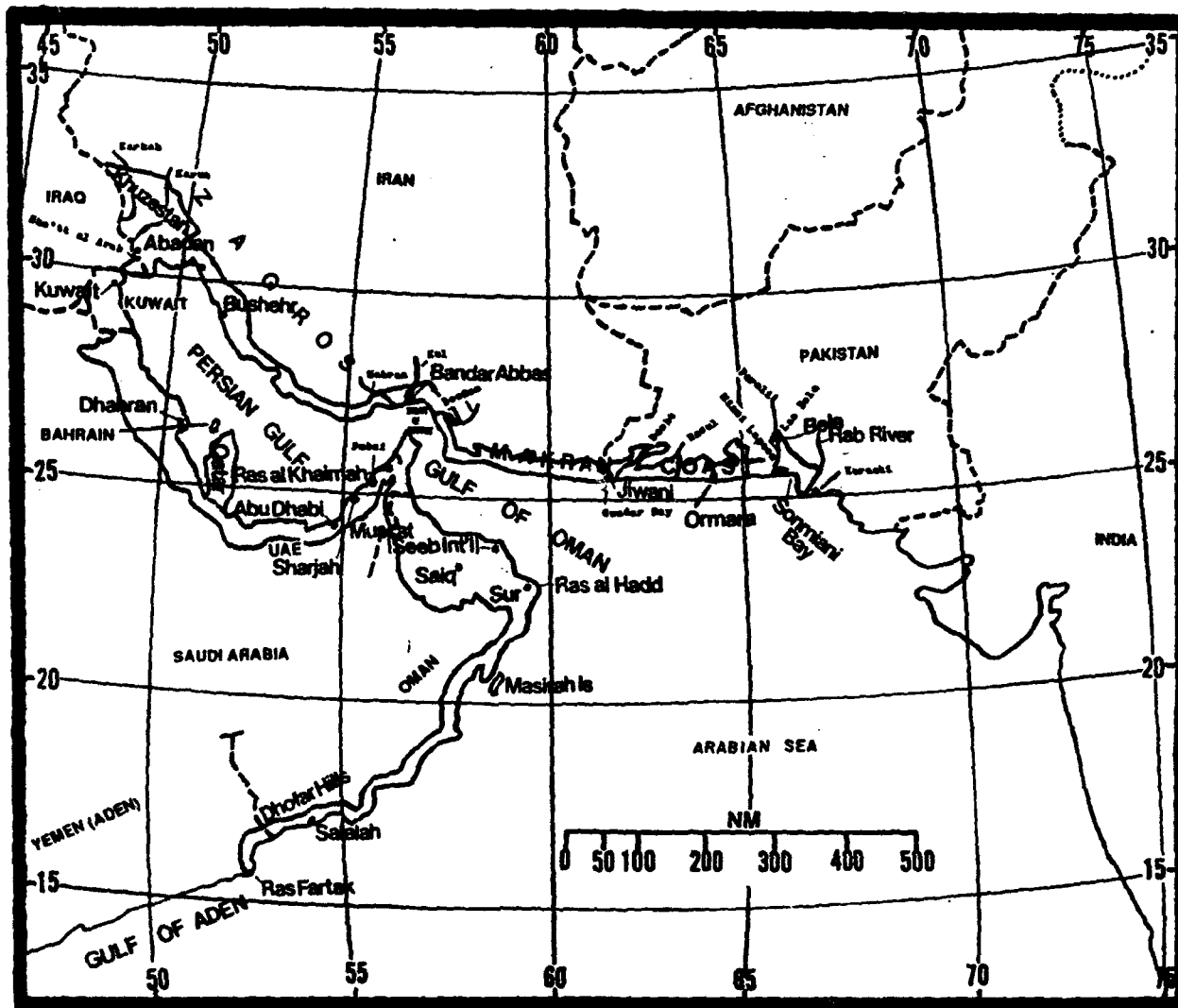


Figure 6-1a. The Persian Gulf Coastal Plains. As shown, this area includes coastal regions of the Persian Gulf, Gulf of Oman, Sonmiani Bay, and Oman. Figure 6-1b provides climatological summaries for Dhahran and Kuwait.

PERSIAN GULF COASTAL PLAINS

SITUATION AND RELIEF

STATION: <u>DHAHRAN SAUDI ARABIA</u>													
LAT/LON: <u>26 26 N</u> <u>50 10 E</u> ELEV: <u>75 FT</u>													
ELEMENTS	JAN	FEB	MAR	APR	MAY	JUN	JUL	AUG	SEP	OCT	NOV	DEC	ANN
XTREM MAX	96	97	100	113	118	120	120	124	118	112	99	90	124
AVG MAX	69	71	79	89	99	107	108	108	103	95	84	73	80
AVG MIN	53	55	61	69	77	83	86	85	80	73	65	57	70
XTREM MIN	31	34	41	50	63	67	70	72	69	54	46	38	31
AVG PRCP	0.9	0.5	0.5	0.1	0.0	0.0	0.0	0.0	0.0	0.0	0.2	0.8	3.0
MAX MON	5.0	3.2	1.9	0.6	0.7	0.0	0.0	0.0	0.0	0.0	0.6	4.3	6.1
FOG DAYS	2	2	1	*	*	*	*	1	2	2	1	2	13
TS DAYS	*	*	2	1	0	0	0	0	0	0	1	*	5
DUST DAYS	5	6	8	8	12	16	14	9	8	3	3	3	96
APP TEMP													

* = LESS THAN 0.05 INCHES OR LESS THAN 0.5 DAYS

STATION: <u>KUWAIT INTL KU</u>													
LAT/LON: <u>29 14 N</u> <u>47 59 E</u> ELEV: <u>156 FT</u>													
ELEMENTS	JAN	FEB	MAR	APR	MAY	JUN	JUL	AUG	SEP	OCT	NOV	DEC	ANN
XTREM MAX	86	96	106	112	120	122	121	120	116	113	97	87	122
AVG MAX	65	69	79	88	101	110	113	112	107	96	80	68	90
AVG MIN	46	48	56	65	74	80	84	82	75	67	57	47	65
XTREM MIN	24	30	38	49	59	68	74	69	62	52	33	29	24
AVG PRCP	1.0	0.6	0.4	0.8	0.2	*	0	0	0	*	0.6	0.7	4.5
MAX MON	2.9	3.8	2.0	2.6	0.7	*	0	0	0	0.5	4.2	2.3	9.5
FOG DAYS	3	1	1	*	*	0	*	*	1	1	1	1	10
TS DAYS	1	1	1	4	2	0	*	0	0	*	2	1	12
DUST DAYS	5	8	11	11	14	11	11	12	12	10	6	7	118
APP TEMP	65	69	77	88	105	111	120	115	110	98	80	68	

* = LESS THAN 0.05 INCHES OR LESS THAN 0.5 DAYS

Figure 6-1b. Climatological Summaries for Dhahran and Kuwait International.

PERSIAN GULF COASTAL PLAINS

GEOGRAPHY. The northern coastal boundary of the Persian Gulf Coastal Plains begins at the northern end of the Persian Gulf at Iran's Karun River plain (where elevations are below 1,620 feet/500 meters MSL), south to 30° N. The boundary then follows the coastal plains of southern Iran and Pakistan southeastward to the Hab River in Pakistan. The southern boundary extends along the western Persian Gulf coastline to include all of Kuwait, from the Sha'tt al Arab southwards to the Strait of Hormuz. The Persian Gulf Coastal Plains also include the Akhdar (Hajar) Mountains to the 1,620 foot (500 meter) MSL contour on their western side, south to 22° N. The rest of the boundary is marked by the 656-foot (200-meter) MSL contour that extends southwestward to Ras Fartak at 15° 40' N, 52° 20' E.

The Persian Gulf, 530 NM long, extends from the Sha'tt Arab (Tigris-Euphrates River) delta to the Strait of Hormuz. Width averages 140 NM before narrowing at the Strait of Hormuz. At 65 to 200 feet (20-60 meters), the Persian Gulf is relatively shallow, except on the immediate western side of the Strait of Hormuz where depths reach 300 feet (90 meters). The Strait of Hormuz averages 50 NM in width, but the narrowest part is slightly less than 30 NM. Depth is 130 to 260 feet (40-80 meters).

The Gulf of Oman extends from the Strait of Hormuz to the Arabian Sea. The generally accepted boundary between the Gulf of Oman and the Arabian Sea is an arbitrary line drawn from Jiwni (25° 02' N, 61° 50' E) south-southwest to Ras al Hadd (22° 31' N, 59° 45' E). Width increases from 130 NM at the Strait of Hormuz to 200 NM at the Arabian Sea.

Sonmiani Bay lies just northeast of Karachi, Pakistan; it is 26 NM wide along its northeastern shore and 59 NM wide as it merges with the Arabian Sea. Maximum depth is 240 feet (73 meters), but most depths are less than 120 feet (37 meters).

The Karun River Plain, also known as the "Khuzestan," extends 87 NM northeast from the Persian Gulf to the foothills of the Zagros Mountains of Iran. Salt marshes dominate the

SITUATION AND RELIEF

Khuzestan. A network of small rivers descends from the Zagros to the Persian Gulf coast. The terrain from the Khuzestan to the Strait of Hormuz along the Iranian coast is in sharp contrast to the west coast. Numerous mountain ranges parallel the Persian Gulf, with a narrow (20- to 40-NM) coastal plain extending southeastward to 20 NM southeast of Bushehr. From Bushehr to the Strait of Hormuz, the mountains rise almost immediately at the coast. Average elevations are 11,000 feet (3,355 meters) MSL. The highest peak is 14,465 feet (4,410 meters) MSL near 30° 07' N, 51° 26' E.

The narrow (10-15 miles) Makran Coast extends from the Strait of Hormuz to Pakistan's Hab River. The surface is sand and gravel with a thin salt crust. Salt marshes, sand dunes, and lagoonal flats are common. River deltas at Gwadar Bay and Las Bela widen the coastline to 45 NM. Elevations exceed 5,000 feet (1,524 meters) MSL only 40 NM from the coastline, and 10,000 feet (3,050 meters) MSL just 90 NM inland.

Western and southern Persian Gulf coastlines are flat from the Sha'tt Arab River to the Strait of Hormuz. Except for the 100-NM wide Qatar Peninsula, the coastal plains extend 20 NM inland. Bahrain is one of several sand-covered islands located 20 NM east of the peninsula. The main island is about 25 NM long and 10 NM wide, with a peak elevation of 370 feet (113 meters), it is connected to the mainland at Dhahran by a man-made causeway.

The southern Gulf of Oman coastline is extremely narrow (10-17 NM wide) from the Strait of Hormuz to Ras al Hadd, located on the most southeastern point of the peninsula. The Akhdar Mountains parallel the coastline; peak elevation is 10,100 feet (3,079 meters) MSL near 23° 14' N, 57° 17' E.

The coastline is 7-20 NM wide from Ras al Hadd southwest to Ras Fartak along the northern Gulf of Aden. The Dhofar Hills (with a peak elevation over 5,000 feet (1,524 meters) MSL 7 NM inland) parallel the coastline from 52° E to 55° E. The narrow coastal plain is sandy, but monsoon rains support extensive cultivation.

PERSIAN GULF COASTAL PLAINS

RIVERS AND DRAINAGE SYSTEMS. There are no permanent rivers along the southern Persian Gulf and Gulf of Oman, but numerous wadis drain the Dhofar Hills and Akhdar Mountains. On the northern Persian Gulf coast, several rivers drain from the Zagros Mountains. The Karkeh River (300 NM long) and the Karun River (435 NM long) flow through the Khuzestan. The Karkeh flows through the marshlands to the Tigris. The Sha'tt al Arab empties large quantities of fresh water into the northwest end of the Persian Gulf. Along the Makran coast, small rivers that cut wide and level floodplains enter the Gulf of Oman every 25 to 35 NM. The Dasht River drains in Gwadar Bay. The Porali River drains in the Miani Lagoon just inland of Sonmiani Bay. The Hab River flows to the Arabian Sea just west of Karachi at the eastern end of the subregion.

LAKES AND RESERVOIRS. Siranda Lake in Pakistan, east of Miani Lagoon, is 7 NM long and 1-2 NM wide. It is the only lake in the Persian Gulf Coastal Plains.

SITUATION AND RELIEF

VEGETATION. With few exceptions, desert vegetation is common across the entire coastline. The southern slopes of the Dhofar Hills support a variety of palm and date trees. Elephant grasses and other lush growth forms in isolated areas near Salalah. Cash crops are grown in wadi valleys. In the Akhdar Mountains, small acacia and frankincense trees grow between 1,620 and 3,280 feet (500-1,000 meters) MSL. A wide variety of small bushes, shrubs, grasses, and herbs are also found in the Akhdar Mountains. Scattered juniper and walnut trees grow above 3,280 feet (1,000 meters) in the north, and mountain vegetation grows on the eastern slopes.

In the Khuzestan, prairie-type short grasses dominate. Irrigation is used extensively for agriculture; cotton and date palms are the chief crops. Along the Makran Coast, mangroves, citrus trees, palm trees, tamarix shrubs, and taller grasses grow only along river banks.

PERSIAN GULF COASTAL PLAINS THE SOUTHWEST MONSOON

June-September

GENERAL WEATHER. The surface Monsoon Trough divides the Persian Gulf Coastal Plains subregion into two distinctly different weather patterns. North of the Trough, a hot, dry, stagnant air mass dominates, and the Southwest Monsoon is rainless. Dust or salt haze produces 4- to 7-mile visibilities. Daytime highs along the coastlines can exceed 93° F (34° C). At night, thin radiation fog and salt or moisture haze mixed with the dust is common. South of the surface Monsoon Trough axis, isolated rainfall, diurnal cumulus, and early morning stratus or stratocumulus occurs with moist southwesterly low-level flow. Tropical cyclones occasionally affect the eastern Makran and Omani coasts. Most develop during transitions, but some can occasionally form near the beginning or end of the Southwest Monsoon.

SKY COVER. Mean cloudiness (Figure 6-2) is highest along the Makran coast and the western Arabian Sea between Masirah and Salalah. Mean cloudiness is 60-75% at Salalah, and 40-67% along the Makran coast eastward from Jiwani to the Hab River. Early morning fog and stratus influence mean cloudiness in the southern end of the Persian Gulf from Dhahran to Abu Dhabi (10-16%). Mean cloudiness decreases to less than 6% in the northern Persian Gulf where thin cirrus is the rule.

Mean cloud cover on the western Gulf of Oman coastline averages less than 20%. Cloud bases average 8,000 feet (2,439 meters) AGL near the coastline. Orographic lifting forms daytime cumulus, accounting for increased cloudiness (20-38%) along the Akhdar Mountains, where heavy afternoon convection may form and move westward in easterly flow aloft towards Sharjah. Thunderstorms form along higher

ridge crests; bases average 2,000-3,000 feet (610-915 meters) AGL and tops can exceed 50,000 feet (15.2 km) MSL.

East of Jiwani along the Makran coast, moist Southwest Monsoon flow is lifted by the mountain ranges. In July and August, 4/8 to 6/8ths of morning stratus and stratocumulus form, with bases between 1,500 and 3,000 feet (457-915 meters) MSL. Heavy convection (and the occasional thunderstorm) is confined to 30-50 NM inland over the mountains. The cumulus may combine with pre-existing monsoon convection over northwest India and central Pakistan. These infrequent occurrences can produce heavy rainshowers near the Hab River Delta. Convection seldom travels west of Jiwani.

Figure 6-3 shows the common coastal stratus between Salalah and Masirah Island; mean cloud cover there averages 40-75% during the Southwest Monsoon. The stratus extends 50 NM southwest and northeast of Salalah and, in extreme cases, to Ras al Hadd. Although the precise cause is not known, it is probably formed by upwelling and topography. Bases average 600 feet (183 meters) AGL between 0400 and 0800L. Dew point depression is usually less than 6° F (3° C). Between 0800 and 1500L, bases lift to 1,000 feet (305 meters) AGL, but they rarely go above 2,000 feet (610 meters). Tops range from 3,000 to 5,000 feet (915-1,524 meters) MSL, as confirmed by PIREPs during Operation DESERT SHIELD. Bases are lowest at Salalah, but can be 500-1,000 feet (152-305 meters) higher over Masirah Island. The stratus dissipates on those rare occasions when a tropical disturbance (usually a subtropical cyclone) temporarily disrupts the southwesterly low-level flow.

PERSIAN GULF COASTAL PLAINS THE SOUTHWEST MONSOON

June-September

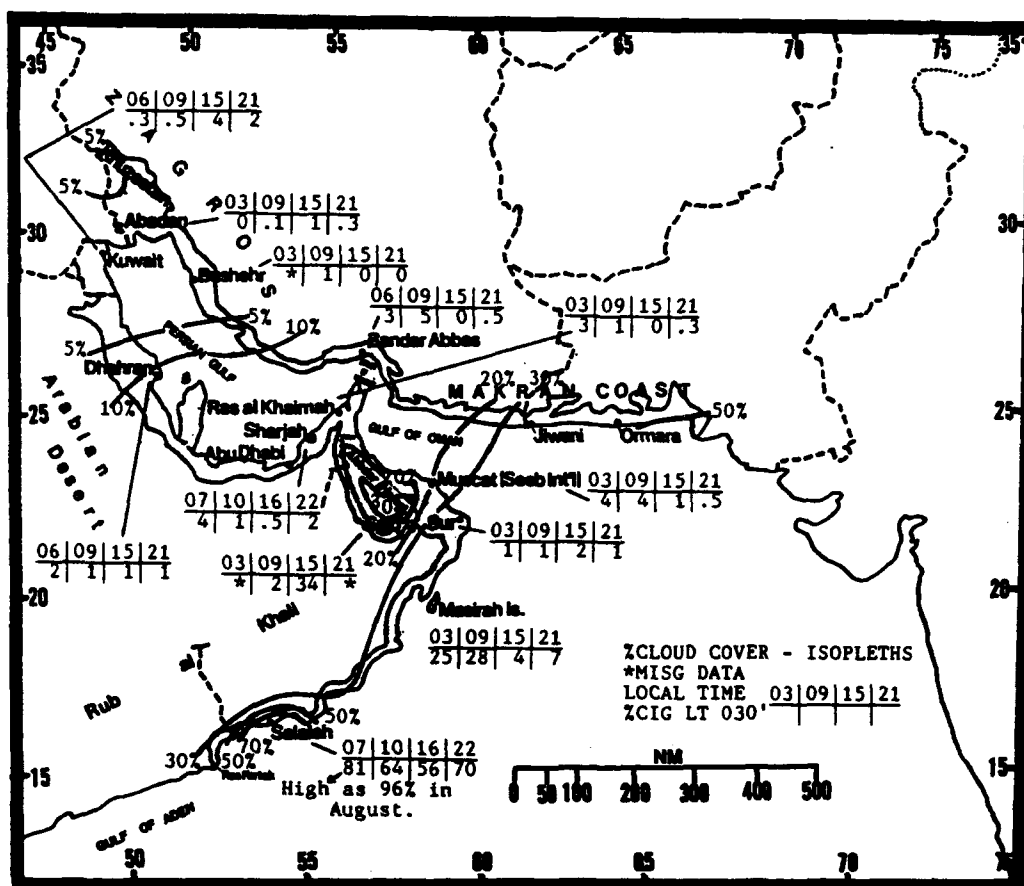


Figure 6-2. Mean Southwest Monsoon Cloudiness (Isolines) and Frequencies of Ceiling Below 3,000 Feet (915 meters), Persian Gulf Coastal Plains.



Figure 6-3. DMSP LS Low Enhancement Photo of Stratus Deck Near Salalah, Oman on 30 June 1979 (0750Z). The stratus layer (black arrow) is clearly visible at 17° N between 52 and 55° E.

PERSIAN GULF COASTAL PLAINS THE SOUTHWEST MONSOON

June-September

VISIBILITY. Blowing dust, dust haze, and salt haze are the main obstructions to vision. Dust haze persists throughout the Southwest Monsoon under the subsidence inversion layer at 10,000 feet (3,050 meters) MSL. Northwesterlies over the northern Arabian Desert combine with the Saudi Arabian Heat Low to generate strong daytime winds that produce blowing dust. The dust rises into the middle layers and remains suspended there for weeks at a time, causing 4- to 7-mile visibilities over the Persian Gulf and western Gulf of Oman.

Weak winds and warm sea-surface temperatures in the Persian Gulf produce intense surface inversions up to 3,280 feet (1,000 meters) MSL. High concentrations of salt and moisture help lower local visibilities to 2 miles. At most locations along the Persian Gulf, the highest frequencies of visibility below 3 miles (Figure 6-4) are between 0900 and 1500L. Visibilities remain low at night as light surface winds maintain the persistent dust and salt haze. During a 40-day Shamal, prevailing northwesterly winds advect sand and dust from their primary source regions in Iraq and

northwestern Saudi Arabia. They combine with the low-level Persian Gulf Jet that extends from 75 NM southeast of Kuwait to 100 NM southeast of Abu Dhabi to raise still more dust throughout the western Persian Gulf. Fog and/or mist caused by salt haze may occur in the early morning when surface winds are very light.

Fog and stratus at Salalah and Masirah Island are responsible for the high incidence of visibilities below 3 miles between night and early morning. Visibilities are better along the Akhdar Mountains, Gulf of Oman, and Makran Coast. Persistent southwesterly flow from the ocean, nocturnal mountain winds, and a weakening low-level subsidence inversion normally keep visibilities good. Mountain winds prevent thick low-level dust and salt haze from accumulating, but haze aloft at Sur and Saiq may produce 4- to 7-mile visibilities at midday. At Seeb International, salt/moisture haze may be present if daytime surface winds are less than 5 knots. When the nocturnal mountain breeze is light, radiation fog and thick moisture haze may form along the coast and the marshlands.

**PERSIAN GULF COASTAL PLAINS
THE SOUTHWEST MONSOON**

June-September

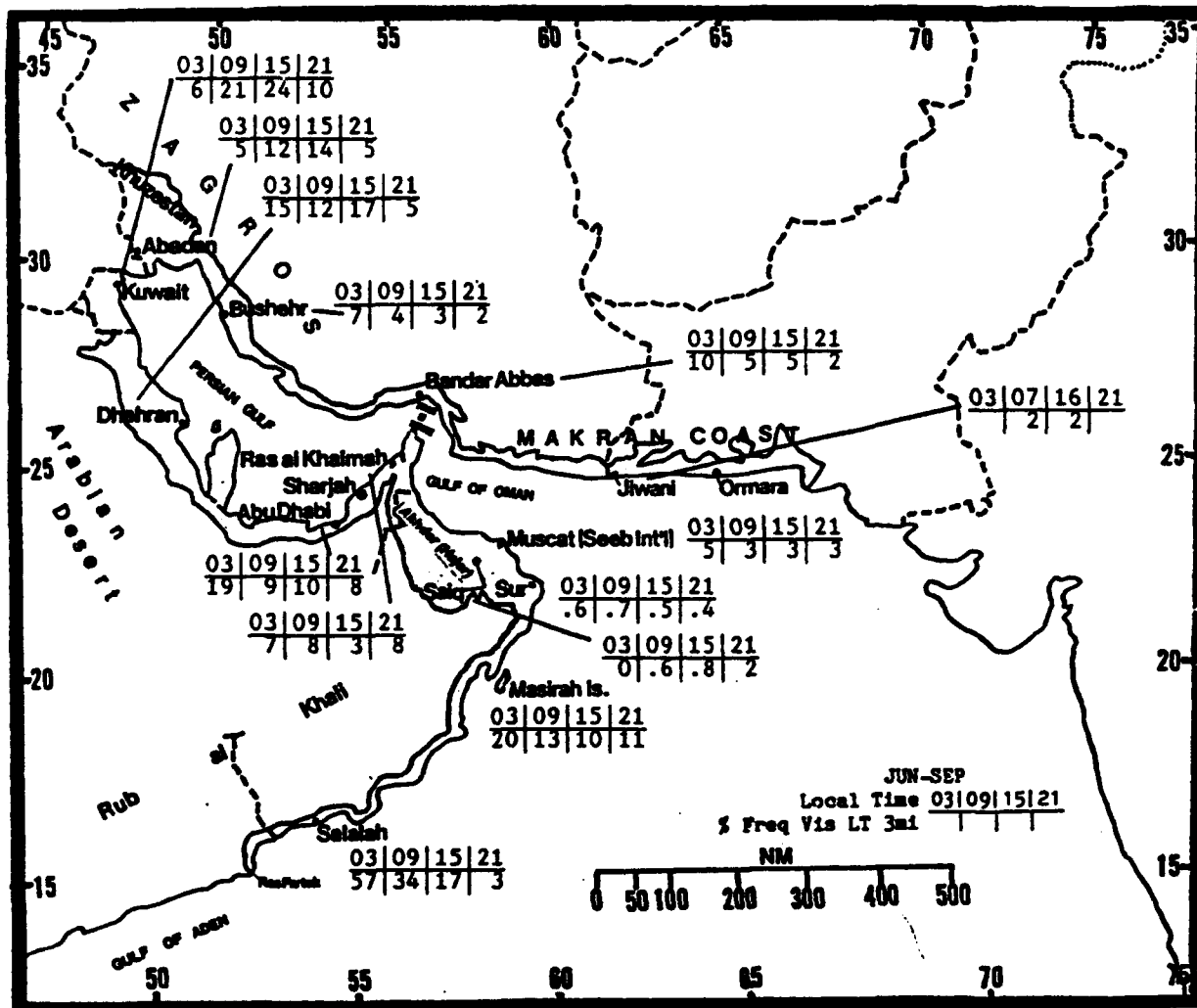


Figure 6-4. Southwest Monsoon Frequencies of Visibilities Below 3 Miles, Persian Gulf Coastal Plains. NOTE: Jiwani does not report between 2100 and 0300L.

PERSIAN GULF COASTAL PLAINS **THE SOUTHWEST MONSOON**

June-September

WINDS. Figure 6-5 gives mean surface wind speeds and prevailing wind directions for selected Persian Gulf Coastal Plains locations. The slash in the prevailing wind direction shows the change that occurs during the season. Winds at Doha Int'l and Abu Dhabi are easterly only during September; winds at Ras al Khaimah are southerly only during June. The strongest mean surface winds occur at Masirah (10-16 knots) due to the Somali Jet.

In general, southwesterly surface flow is due to the Monsoon Trough position which, in July, can cross the Strait of Hormuz. Weak easterly or southerly flow usually marks the position of the Monsoon Trough axis, but land/sea breeze convergence can be mistaken for surface Monsoon Trough winds in the Strait of Hormuz. On occasion, easterlies at 15-25 knots funnel through the Strait of Hormuz.

The low level Persian Gulf Jet occurs along the immediate western shoreline from 28° to 24° N. Maximum speeds are just before dawn. Mean low- and mid-level wind directions shown in Figures 6-6a-d for Salalah, Seeb International, Kuwait International, and Jiwani show the variability of winds over the subregion. In

Figure 6-6a, for example, the mean direction at Salalah at 5,000 feet (1,524 meters) is WSW, except in September, when flow is ENE. The wind shift represents the southward movement of the monsoon circulation and the Somali Jet. Mean wind speed averages 12-14 knots during this period. The mean 5,000-foot wind direction at Seeb Int'l (Figure 6-6b), Kuwait Int'l (Figure 6-6c), and Jiwani (Figure 6-6d) is northwesterly during the Southwest Monsoon. Mean speeds average 7-10 knots at Jiwani and Seeb, but 18-21 knots at Kuwait (June through August). Winds at 10,000 feet (3,050-meters) and 15,000 feet (4,573-meters) at Seeb, Jiwani, and Salalah are north to northeast, but over Kuwait, they are west to northwest. Mean speeds are lightest at Seeb and Jiwani at 10-12 knots, increasing over Kuwait to 16-19 knots.

Mean seasonal winds at 39,000 feet (11.9 km) MSL are easterly at 26-43 knots over Salalah, easterly to southeasterly at 15-20 knots over Seeb, southeasterly to southwesterly at 13-32 knots over Kuwait, and easterly at 12-25 knots over Jiwani. The lightest mean wind speeds over Kuwait occur with southerly upper-level flow in July and August as the position of the Subtropical Ridge axis shifts.

		JUN	JUL	AUG	SEP
S/NNW	Ras'Khaimah	5.70	5.30	6.00	4.00
NW-N/E	Abu Dhabi	8.30	7.60	8.50	7.40
W-N	Saiq	8.00	7.80	7.00	7.50
NE	Seeb Int'l	4.90	5.70	5.80	5.10
SSW	Masirah	13.70	16.30	13.90	10.90
N	Dhahran	10.80	8.90	8.20	6.70
NW	Kuwait	12.10	10.30	9.00	6.70
WNW	Abadan	10.40	9.80	8.60	6.00
W	Bushehr	8.40	7.40	6.90	5.80
S	Ban'r Abbas	8.30	9.20	9.10	8.00
SSW	Sur	8.20	9.10	8.40	9.20
SE-S	Jiwani	6.60	7.50	6.90	5.30
NNW/E	Doha Int'l	11.30	8.40	8.20	6.40
E	Ban'r L'ngheh	6.20	7.60	9.20	8.50
S-SW	Salalah	7.00	6.40	5.40	5.80

Figure 6-5. Mean Southwest Monsoon Surface Wind Speeds (kts) and Prevailing Direction, Persian Gulf Coastal Plains.

**PERSIAN GULF COASTAL PLAINS
THE SOUTHWEST MONSOON**

June-September

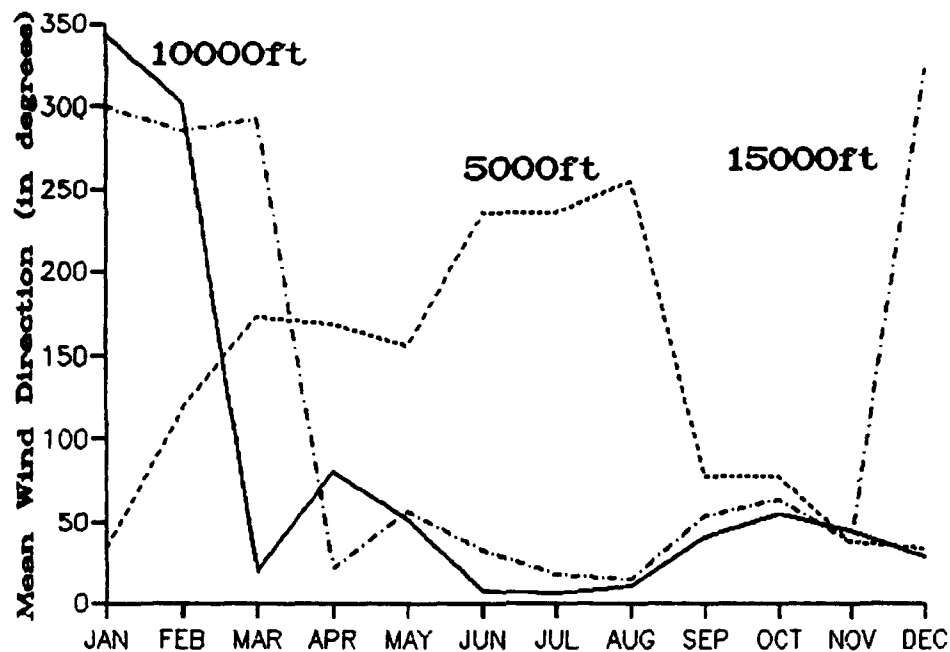


Figure 6-6a. Mean Annual Wind Direction, Salalah, Oman.

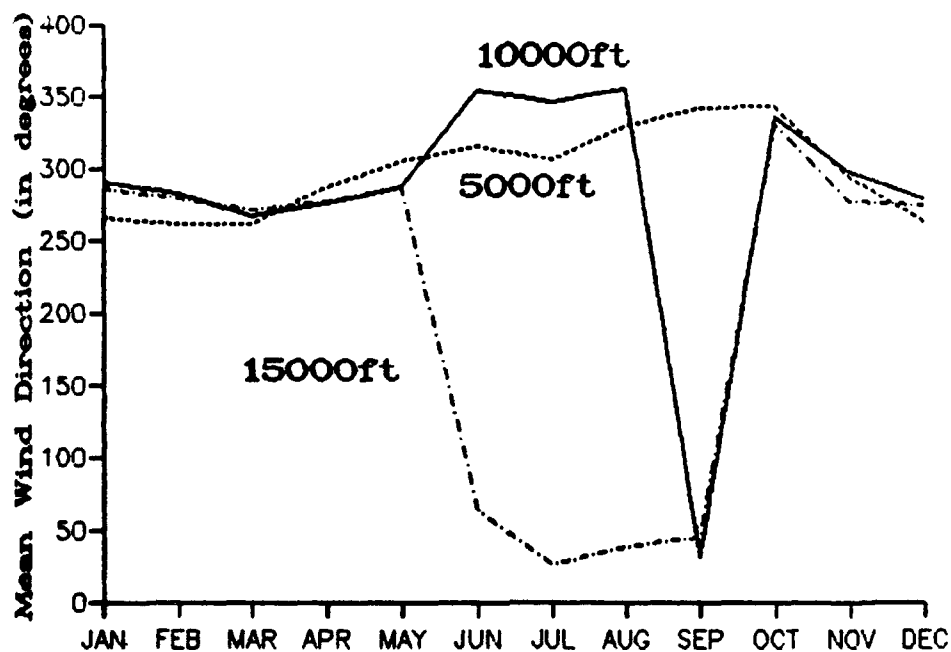


Figure 6-6b. Mean Annual Wind Direction, Seeb IAP (Muscat, Oman).

**PERSIAN GULF COASTAL PLAINS
THE SOUTHWEST MONSOON**

June-September

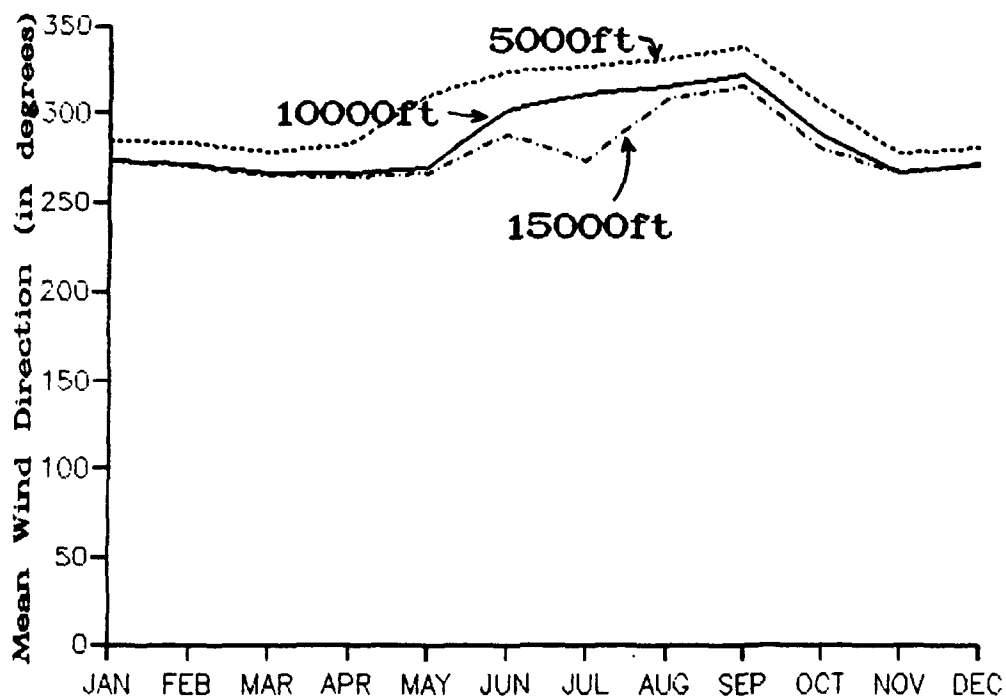


Figure 6-6c. Mean Annual Wind Direction, Kuwait IAP, Kuwait.

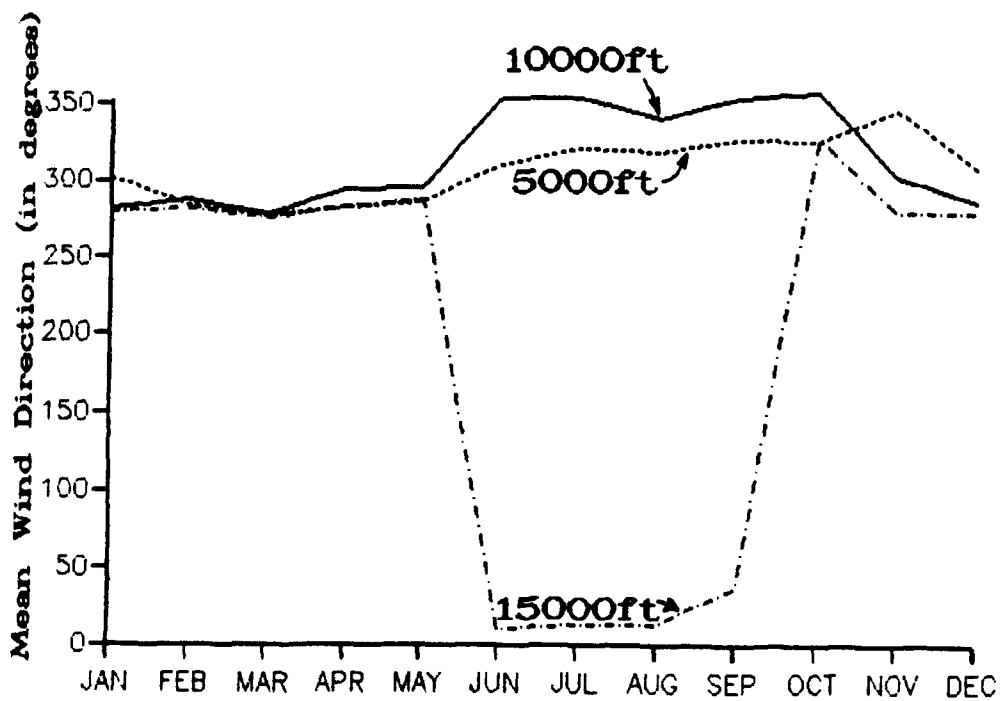


Figure 6-6d. Mean Annual Wind Direction, Jiwani, Pakistan.

PERSIAN GULF COASTAL PLAINS **THE SOUTHWEST MONSOON**

June-September

PRECIPITATION. Very little precipitation falls in and around the Persian Gulf from June to September, but locations south of the Monsoon Trough get most of it.

The frequent stratus at Salalah results in intermittent drizzle and occasional rainshowers at any time of day, but there is a weak diurnal precipitation maximum between 0400 and 0800L.

Maximum 24-hour precipitation amounts (Figure 6-7) result from tropical disturbances or heavy monsoon convection. Strong monsoon convection

produces 0.25- to 0.75-inch (6-19 mm) rainfalls along extreme eastern Makran coastal ranges. The Omani coastline maximums are due to tropical disturbances. A tropical cyclone or "onset vortex" produced 11 inches (279 mm) of rain in a 24-hour period at Muscat in June 1890. Rare heavy rainfall in July and August can occur when a subtropical cyclone forms in the Arabian Sea. Quarter-inch (6 mm) rains may occur at Masirah and Salalah, but 1-inch (25 mm) rainfalls are possible inland over the Akhdar Mountains. Storms dissipate rapidly after moving onshore.

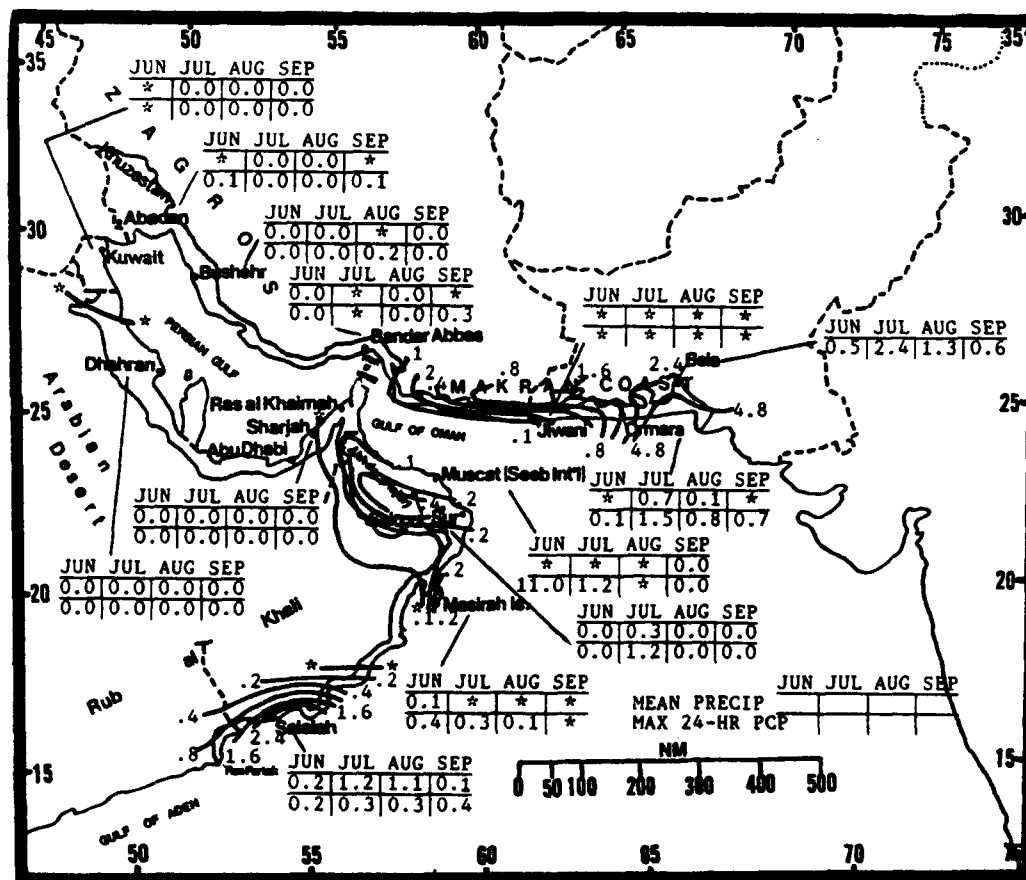


Figure 6-7. Mean Southwest Monsoon Monthly/Maximum 24-hour Precipitation, Persian Gulf Coastal Plains. Bold lines represent mean seasonal rainfall totals. Asterisks (*) represent <0.05 inches (1.3 mm).

PERSIAN GULF COASTAL PLAINS THE SOUTHWEST MONSOON

June-September

Thunderstorms are extremely rare from June to September except in the Akhdar Mountains. Daytime cumulus buildups result from sea-breeze convergence, orographic lifting, and the surface Monsoon Trough. The most severe and widespread thunderstorm activity occurs when a rare upper-level trough or short wave migrates eastward over the Gulf of Oman and Arabian Sea. Thunderstorm activity is concentrated along the highest ridge crests of the Akhdar Mountains and the Makran coastal ranges. Cloud bases are estimated to be above 4,000-5,000 feet (1,220-1,524 meters) AGL, with tops 50,000 feet (15.2 km) MSL over the Makran coastal ranges. Concorde aircrews, however, have reported tops exceeding 63,000 feet (19.2 km). Such heavy convection is the result of upper-level trough interaction with pre-existing monsoon convection. A sea breeze can combine with these other factors to intensify convection.

Light-to-moderate thunderstorms can form over the northern Persian Gulf with upper-level troughs, but precipitation falls mostly on the higher ridges of the Zagros Mountains. Thunderstorm "blow-off" can spread over the Khuzestan area, normally producing only virga. Thunderstorms may produce gusty downslope winds at Bushehr and Bandar Abbas in western Iran.

On rare occasions, the Makran coast receives moderate-to-heavy precipitation from tropical cyclones that track westward across India. In Figure 6-8, the solid arrow shows the cyclone's typical track, while the dashed arrow shows a secondary track that produces heavy rain and thunderstorms along the southern slopes of the Makran coastal ranges as it taps warm moisture from the Arabian Sea.

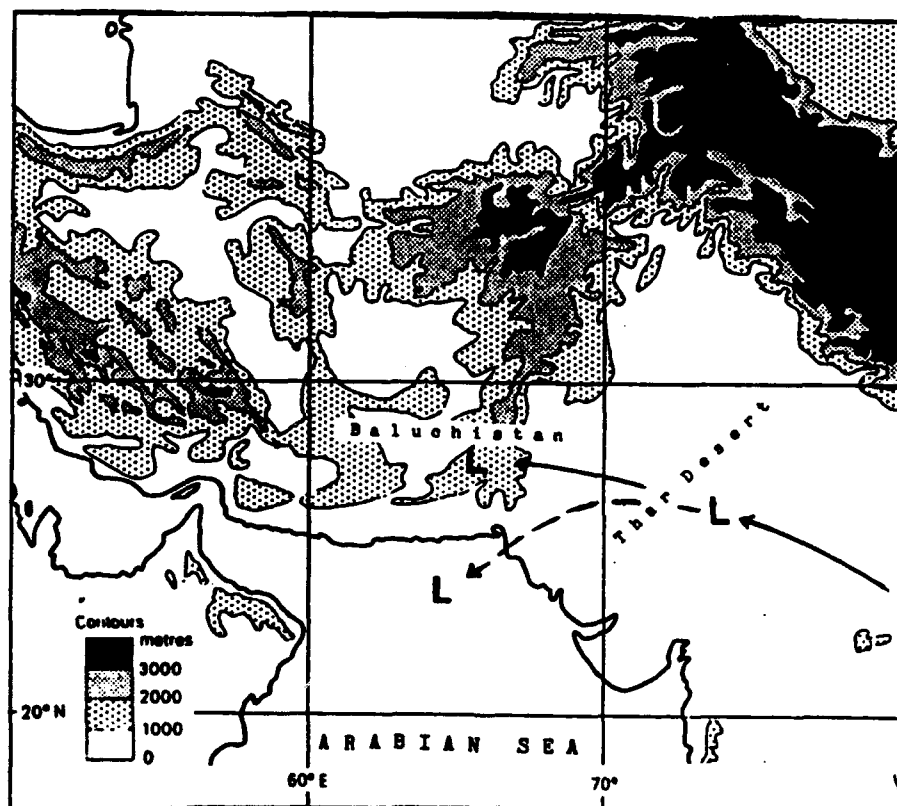


Figure 6-8. A Tropical Disturbance Over the Northwest India-Central Pakistan Area Which May Produce Heavy 24-hour Rainfall Along the Makran Coast. The dashed arrow represents storm movement that provides heavy rainfall.

PERSIAN GULF COASTAL PLAINS **THE SOUTHWEST MONSOON**

June-September

TEMPERATURE. Extremely hot air masses dominate most of the subregion. North of the surface Monsoon Trough, dry northwesterly gradient flow from the Arabian Desert dominates. Since heated desert air spreads eastward to the coast, daytime air temperatures are moderated only along a very narrow 1-10 NM strip of coastline, but conditions are still uncomfortable due to high relative humidities.

All 4 months of the Southwest Monsoon have mean daily highs of 93° F (34° C) or better along the Persian Gulf (Figure 6-9). The highest daily high is 113° F (45° C) at Kuwait in July. Hot Persian Gulf waters keep mean daily minimums

up to 75° F (24° C) at Kuwait in September and 90° F (32° C) at Bandar Abbas in July and August.

The Gulf of Oman and Arabian Sea coasts are slightly cooler as Southwest Monsoon flow is moderated by ocean waters. Mean daily highs range from 81° F (27° C) at Salalah in August to 102° F (39° C) at Seeb in June. Mean daily lows range from 72° F (22° C) at Saiq in September to 88° F (31° C) at Seeb in June. The record high is 124° F (51° C) at Dhahran in August. The record low is 57° F (14° C) at Ras Khaimah in June.

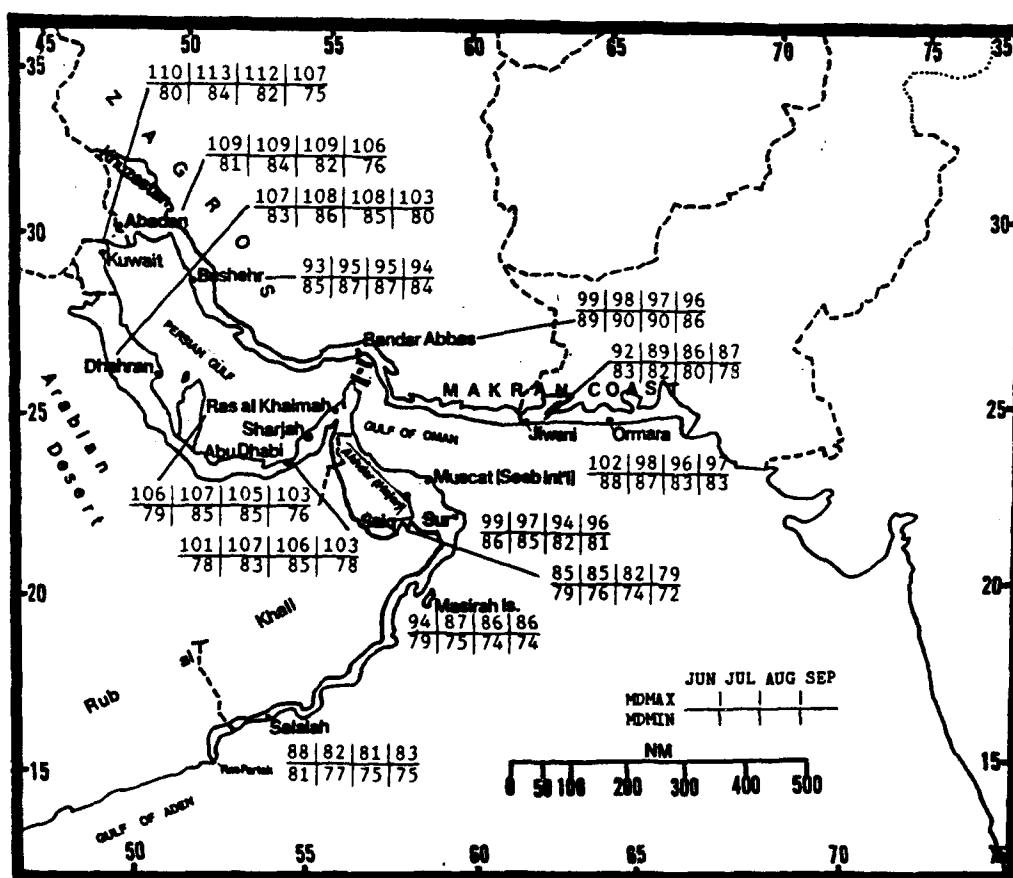


Figure 6-9. Mean Southwest Monsoon Daily Maximum/Minimum Temperatures (° F), Persian Gulf Coastal Plains.

PERSIAN GULF COASTAL PLAINS SOUTHWEST-TO-NORTHEAST MONSOON TRANSITION

October-November

GENERAL WEATHER. The transition from the Southwest to the Northeast Monsoon is a period of light and variable surface winds, some frontal systems, early morning stratus and stratocumulus (with calm conditions), and scattered afternoon sea-breeze cumulus. The surface Monsoon Trough recedes southward, the Saudi Arabian Heat Low dissipates, and mid-level subsidence weakens. Fronts are normally limited to the northern Persian Gulf, but on rare occasions, a system crosses the Gulf of Oman in November.

SKY COVER. Mean cloudiness (Figure 6-10) is highest along the extreme northwest end of the Persian Gulf because of increasing cold fronts that produce multilayered clouds. There is a secondary cloudiness peak of 20% in the south near Salalah due to coastal stratus and stratocumulus.

Along the Makran coast, ceilings are below 3,000 feet (915 meters) AGL (Figure 6-10) less than 1% of the time. There are very few low ceiling between 1000 and 1600L.

At Saiq, the highest frequency of low ceilings is at 1500L (9%) when shallow diurnal

cumulus, the dominant cloud type, results from orographic lifting of the sea breeze along the Akhdar Mountains' eastern slopes. Some locations in the Akhdar Mountains receive little or no precipitation unless an orographic thunderstorm develops. Most cumulus bases are between 2,000 and 3,500 feet (610-1,067 meters); tops can reach to 20,000 feet (6,097 meters) with towering cumulus and 40,000 feet (12.2 km) with thunderstorms.

Shallow altocumulus with mid-level troughs occurs only once or twice a month, usually with bases at 12,000 to 14,000 feet (3,659-4,268 meters) AGL. Subtropical Jet cirrus is common.

When more intense migratory lows enter the northwest Persian Gulf, multilayered clouds with bases at 2,000-3,000 feet (610-915 meters) may develop. Ceilings behind slow-moving fronts or north of developing surface lows may lower to 300 feet (90 meters) for up to 6 hours after frontal passage and up to 100 NM north of the low-pressure center. A system sometimes tracks into the Gulf of Oman, but this is rare since it requires strong upper-level support more characteristic of the Northeast Monsoon.

October-November



PERSIAN GULF COASTAL PLAINS **SOUTHWEST-TO-NORTHEAST MONSOON TRANSITION**

October-November

VISIBILITY. Figure 6-11 gives frequencies of visibility below 3 miles across the Persian Gulf Coastal Plains. Low visibility is more common at night than during the day at most stations; Abu Dhabi has the most occurrences (12%). Visibility never drops below 3 miles at Salalah, and does so only on rare occasions at Masirah, Sur, and Seeb. The sea breeze/valley breeze at Saiq causes some dust haze and low stratocumulus between 0900 and 1500L, but visibility rarely drops below 3 miles.

In October and November, light winds and cooler land surfaces produce radiation fog and moisture haze. The rare migratory low can reduce visibilities over widespread areas with blowing

dust and sand. Precipitation seldom lowers visibility significantly.

Early morning mist or fog can occur anywhere along the coastlines during calm conditions. The cooler land/mountain breeze over the Makran coast often spreads over the moist marine boundary layer; thin fog forms over water and pushes inland when the land breeze subsides at about 0600 or 0700L. The warm, moist coastal environment and light surface winds combine to produce thick salt haze along the northwestern Persian Gulf at Abadan, Bushehr, and Kuwait; the haze may persist for 1-3 weeks during extended fair weather.

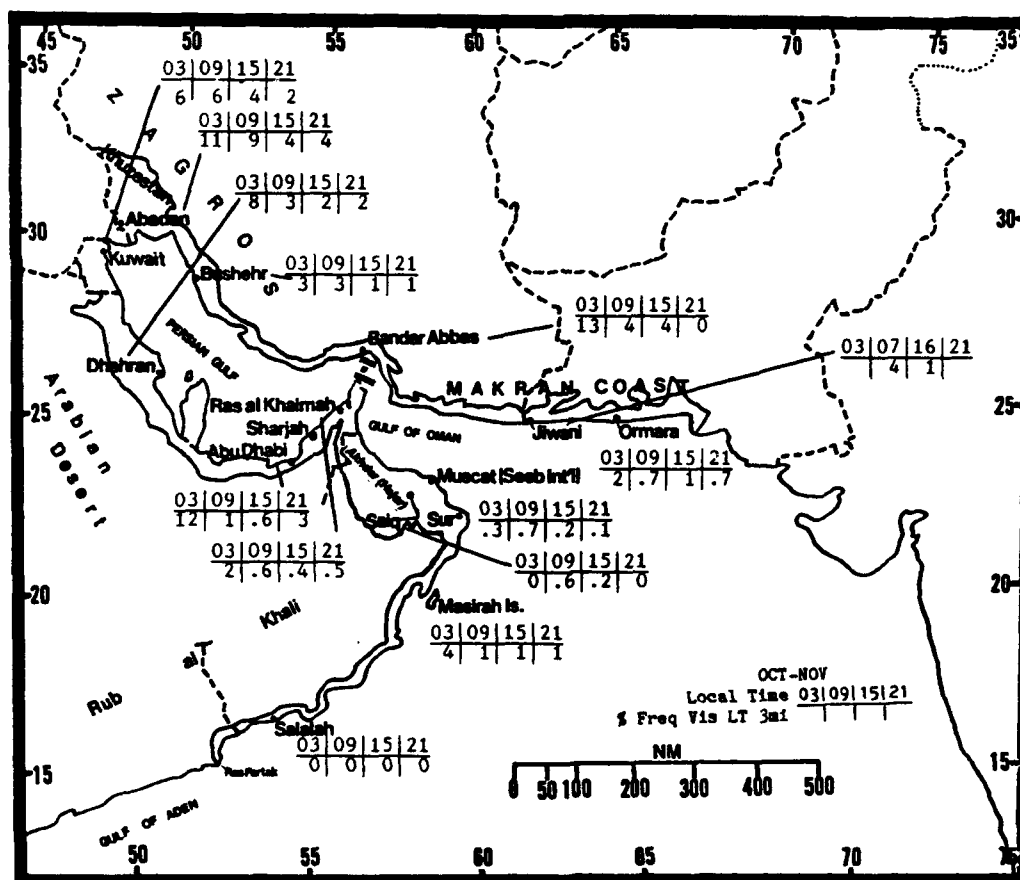


Figure 6-11. SW-NE Monsoon Transition Frequencies of Visibilities Below 3 Miles, Persian Gulf Coastal Plains. Note that Jiwani does not report between 2100 and 0300L.

PERSIAN GULF COASTAL PLAINS **SOUTHWEST-TO-NORTHEAST MONSOON TRANSITION**

October-November

WINDS. Figure 6-12 shows mean SW-NE Monsoon Transition surface wind speeds and prevailing directions for several stations. The slash between mean wind direction at Ras al Khaimah, Seeb, and Sur indicates a change that takes place in November. The November south to southwesterly flow is terrain-induced along the Akhdar Mountain range. The strongest transition surface winds occur in the northern Persian Gulf. The highest recorded wind speeds are southerly at 88 knots at Bandar Lengeh, easterly at 83 knots at Bushehr, and northerly at 83 knots at Bandar Abbas. Although the exact causes are not well known, these maximum speeds may result from isolated thunderstorm microbursts.

October-November flow is northwesterly at mid- and upper-levels at Seeb, Kuwait, and Jiwani. At Salalah, low- to mid-level flow is northeasterly. The Monsoon Trough lies south of Salalah, but the mid-level subtropical ridge axis is still to the north, where it produces northeasterlies.

From October to November, upper-level (39,000 feet/11.9 km MSL) mean winds increase from 59 to 76 knots at Kuwait, from 29 to 60 knots at Seeb, and from 32 to 68 knots at Jiwani. Mean direction is westerly. Mean speed at Salalah increases from 21 to 28 knots--mean direction changes from 202° to 252°.

		OCT	NOV
WNW/S	Ras'Khaimah	3.80	3.30
E	Abu Dhabi	6.70	6.20
N-E	Saiq	7.00	6.10
N/SSW	Seeb Int'l	4.60	4.40
SSW-E	Masirah	7.40	6.10
N	Dhahran	6.60	7.10
NNW	Kuwait	7.00	7.20
WNW	Abadan	4.10	5.40
NNW	Bushehr	6.70	6.20
S	Ban'r Abbas	7.60	7.30
N/SSW	Sur	6.60	5.10
S-W	Jiwani	5.00	4.80
NNW	Doha	6.70	6.70
E	Ban'r L'engeh	7.30	7.40
N	Salalah	4.70	4.90

Figure 6-12. Mean SW-NE Monsoon Transition Surface Wind Speeds (kts) and Prevailing Direction, Persian Gulf Coastal Plains. The slashes between prevailing wind directions at Doha Int'l, Abu Dhabi, and Ras Khaimah denote October to November wind shifts.

PERSIAN GULF COASTAL PLAINS SOUTHWEST-TO-NORTHEAST MONSOON TRANSITION

October-November

PRECIPITATION. Mean precipitation (0-0.4 inches/0-10 mm) is light and widely scattered across the subregion during October. Any troughs entering the area in October are weak. In November, locations close to the Persian Gulf proper average at least 0.2 inches (5 mm); the higher amounts result from the increased strength and frequency of systems across the northern sections. Salalah's October precipitation is light drizzle and scattered rainshowers from stratus and stratocumulus along the coast.

Maximum 24-hour rainfalls at Kuwait, Abadan, and Bushehr (Figure 6-13) occur with strong systems that produce strong northwesterly winds (shamals) and heavy rainshowers or isolated thunderstorms. These events, however, are too infrequent to affect mean statistics. In November, maximum rainfall totals range from 0.5 inches (13mm) in Dhahran to 5.9 inches (150 mm) at Bushehr. The Zagros and Akhdar Mountains provide additional lift that results in significantly increased precipitation at nearby locations. An average of three strong surface troughs enter the Persian Gulf proper every November, but there is less than one in October.

In November, thunderstorms with tops to 40,000 feet (12.2 km) MSL produce isolated downpours

and small hailstones along the eastern slopes of the Akhdar Mountains. These storms can be produced in two ways. Most often, a strong Northeast Monsoon flow "surge" accelerates the sea breeze up the mountain slopes. A secondary cause is strong surface or mid-level troughing; the trough axis is often inactive, but strong northwesterly flow may converge with the sea breeze on the eastern slopes. If conditions are right during the day, a convergence line of active thunderstorms may stretch from 23 to 26° N on eastern slopes.

November thunderstorms are most severe along the mountain ridge immediately east of Ras al Khaimah, where the terrain extends northward towards the Strait of Hormuz. Small hailstones have been observed there.

Tropical disturbances can develop in the Arabian Sea. The 1.5 inch (38 mm) October maximum rainfall at Seeb occurred with one such disturbance. Precise rainfall records for other locations near Seeb were unavailable, but it's likely that maximum 24-hour rainfalls in the Akhdar Mountains have exceeded 2-3 inches (51-56 mm) with a tropical cyclone.

PERSIAN GULF COASTAL PLAINS
SOUTHWEST-TO-NORTHEAST MONSOON TRANSITION

October-November

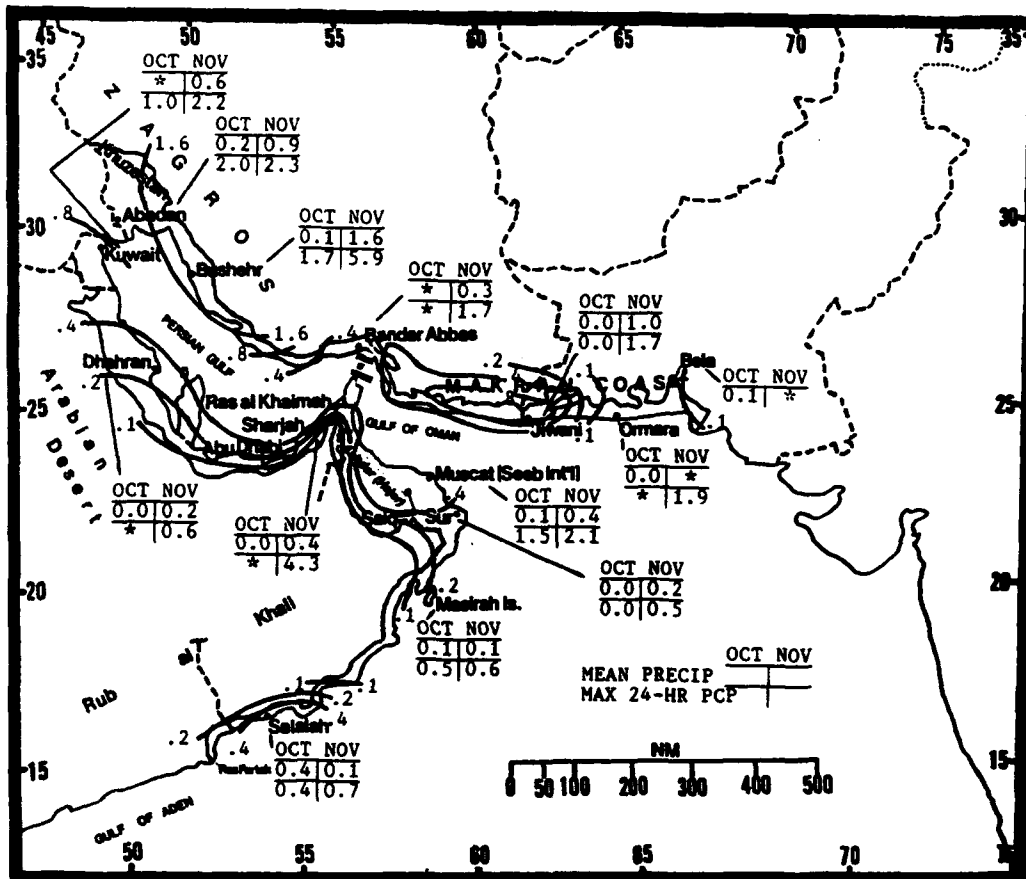


Figure 6-13. Mean SW-NE Monsoon Transition Monthly/Maximum 24-hour Precipitation, Persian Gulf Coastal Plains. Bold lines represent mean seasonal rainfall totals. Asterisks (*) represent rainfall amounts below 0.05 inches (1.3 mm).

PERSIAN GULF COASTAL PLAINS **SOUTHWEST-TO-NORTHEAST MONSOON TRANSITION**

October-November

TEMPERATURE. Figure 6-14 shows mean daily highs and lows for October and November. October highs range from 73° F (23° C) at Saiq to 97° F (36° C) at Ras al Khaimah; mean daily lows range from 66° F (19° C) at Saiq to 81° F (27° C) at Bander Abbas. In November, mean

daily highs range from 66° F (19° C) at Saiq to 88° F (31° C) at Ras al Khaimah. Lows range from 56° F (13° C) at Abadan to 71° F (22° C) at Bandar Abbas, Seeb, and Masirah Island. The record high during the transition was 113° F (45° C); the low, 33° F (1° C), both at Kuwait.

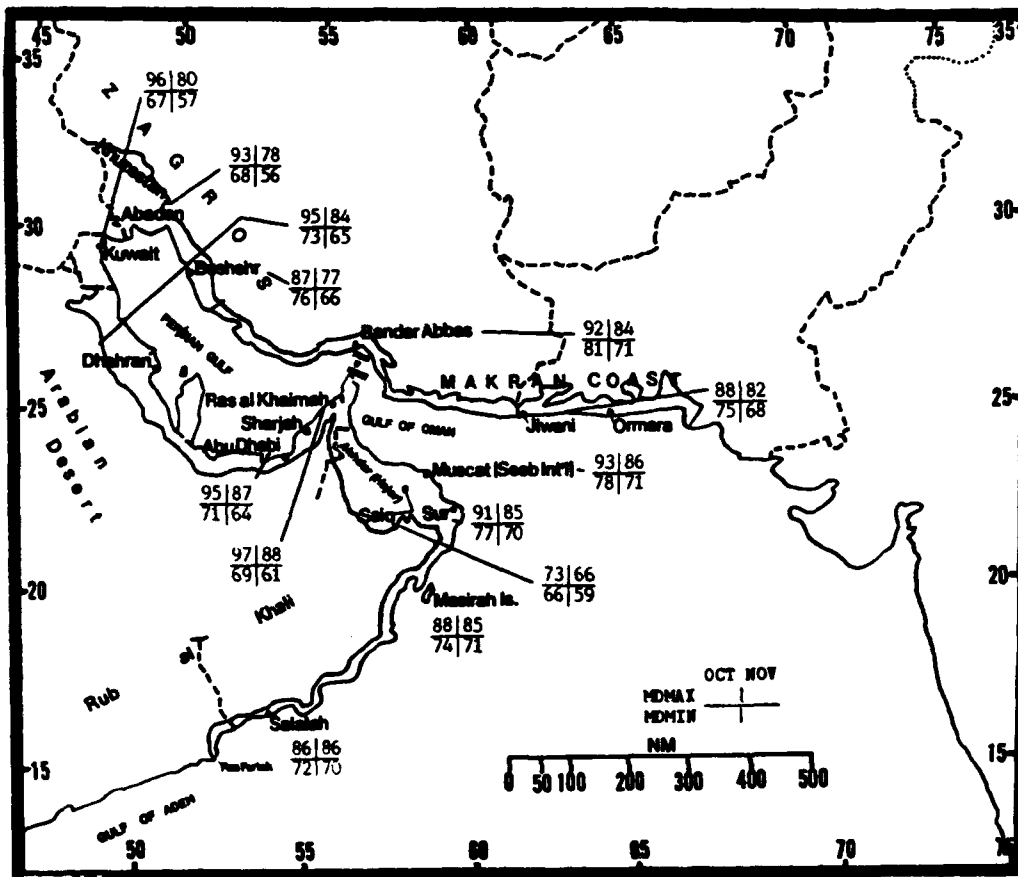


Figure 6-14. Mean SW-NE Monsoon Transition Daily Maximum/Minimum Temperatures (° F), Persian Gulf Coastal Plains.

PERSIAN GULF COASTAL PLAINS NORTHEAST MONSOON

December-March

GENERAL WEATHER. Low-pressure systems are the most important weather-producing feature of the Northeast Monsoon. Strong surface lows move from northwest to southeast across the Persian Gulf and Gulf of Oman, producing orographic showers and thunderstorms, heavy isolated rainfall, and low ceilings one to three times during December and January. Strong cold fronts produce gusty winds (15-25 knots), widespread dust, scattered rainshowers, and on rare occasions, nighttime low temperatures between 25 and 35° F (-4 and 2° C) in the northwestern Persian Gulf. The strong surface lows are supported by deep mid- and upper-level troughs.

SKY COVER. Mean cloudiness (isolines in Figure 6-15) decreases from northwest to southeast. In the northwestern half of the Persian Gulf Coastal Plains, mean cloudiness (30-40%) is dominated by Subtropical Jet cirrus, mid-level altocumulus (500- and 700-mb troughs), and early morning stratus and stratocumulus. The southeastern half of the subregion is dominated by thin cirrus, early morning stratus or stratocumulus, and isolated cumulus produced by the sea breeze.

The warm, southerly flow ahead of strong low-pressure centers causes stratus and

stratocumulus to develop on northern shores from Abadan to Sonmiani Bay; stratus bases average 1,000-1,500 feet (305-457 meters). Mid-latitude systems affect the northern Persian Gulf with frontal systems and surface lows; ceilings can be near zero to the north and west of the low for up to 72 hours after frontal passage. Stratocumulus may develop over the next 1 or 2 days if cold air follows the front, or if there has been significant rainfall (above 0.1 inch/2.5 mm). Stratocumulus bases range from 4,000 to 6,000 feet (1,220 to 1,829 meters) AGL over the Persian Gulf. Stratus can form on the Persian Gulf coastline from Dhahran to Abu Dhabi after frontal passage, when migratory high-pressure cells shift low-level flow to NNE. Stratocumulus over the Gulf of Oman and north Arabian Sea is less pronounced; it lasts for only 6 hours before the warm water surface modifies the cold air.

Sea-breeze cumulus, with 2,000- to 3,000-foot/610-915-meter bases AGL, forms ceilings 13% of the time at Saiq at 1500L from December to March (Figure 6-15). High frequencies of low ceilings in the northern Persian Gulf are due to more frequent low-pressure systems. Stratus along the Omani coastlines form low ceilings at night at Salalah and Masirah Island.

**PERSIAN GULF COASTAL PLAINS
NORTHEAST MONSOON**

December-March

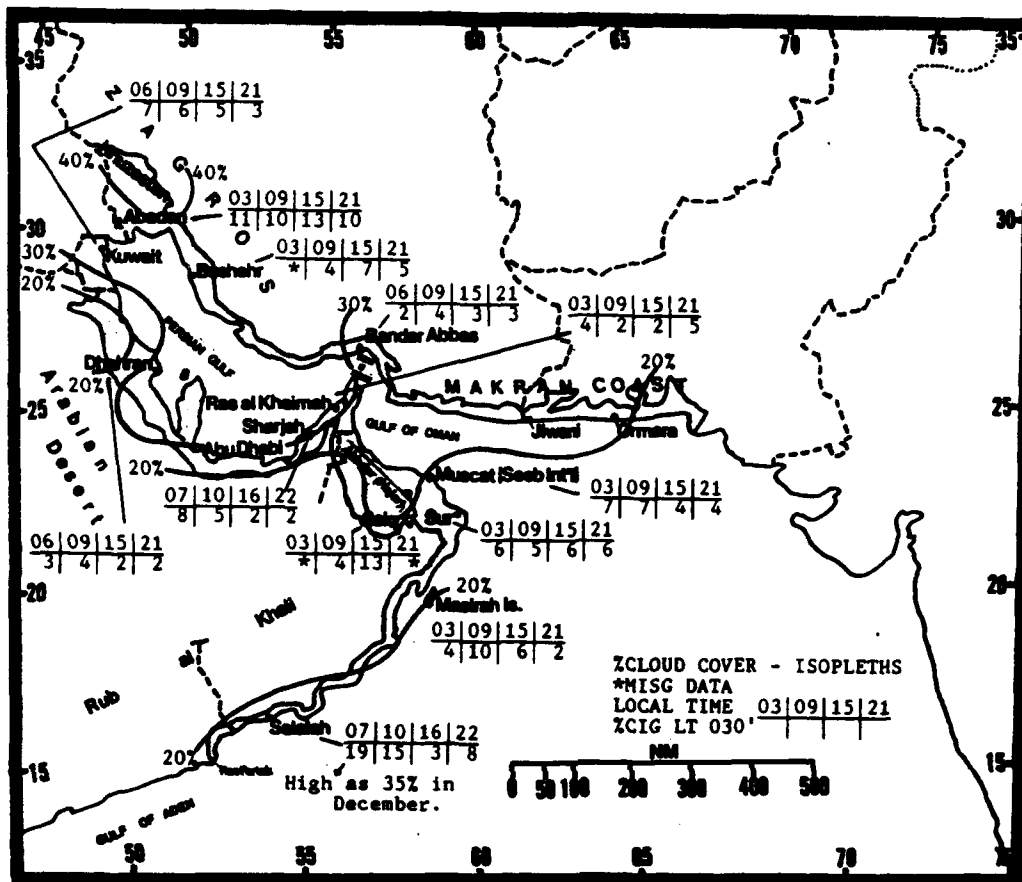


Figure 6-15. Mean Northeast Monsoon Cloudiness (Isolines) and Frequencies of Ceilings Below 3,000 Feet (915 meters), Persian Gulf Coastal Plains.

PERSIAN GULF COASTAL PLAINS NORTHEAST MONSOON

December-March

VISIBILITY. Northeast Monsoon visibilities are dominated by dust, sand, dust haze, and occasional radiation fog. Strong migratory lows track across the Arabian Desert and Persian Gulf one to three times a month. These systems, with strong surface winds in both the warm and cold sectors, cause blowing dust and sand. More intense systems can bring dust from distant sources in the Arabian Desert. If a system is followed by an extended period of fair weather (5-10 days), thick haze can reduce visibility to

4-5 miles from the surface to 10,000 feet (3,050 meters) MSL. Duststorms are common along the Makran coast when migratory lows enter the Strait of Hormuz. Mist, salt haze, or radiation fog can form under calm conditions anytime and anywhere along the coast, but visibility rarely drops below 3 miles except between 2100 and 0600L. Figure 6-16 shows frequencies of visibilities below 3 miles across the subregion; the highest frequency (13% at 0300L) at Abu Dhabi is due to increased onshore flow.

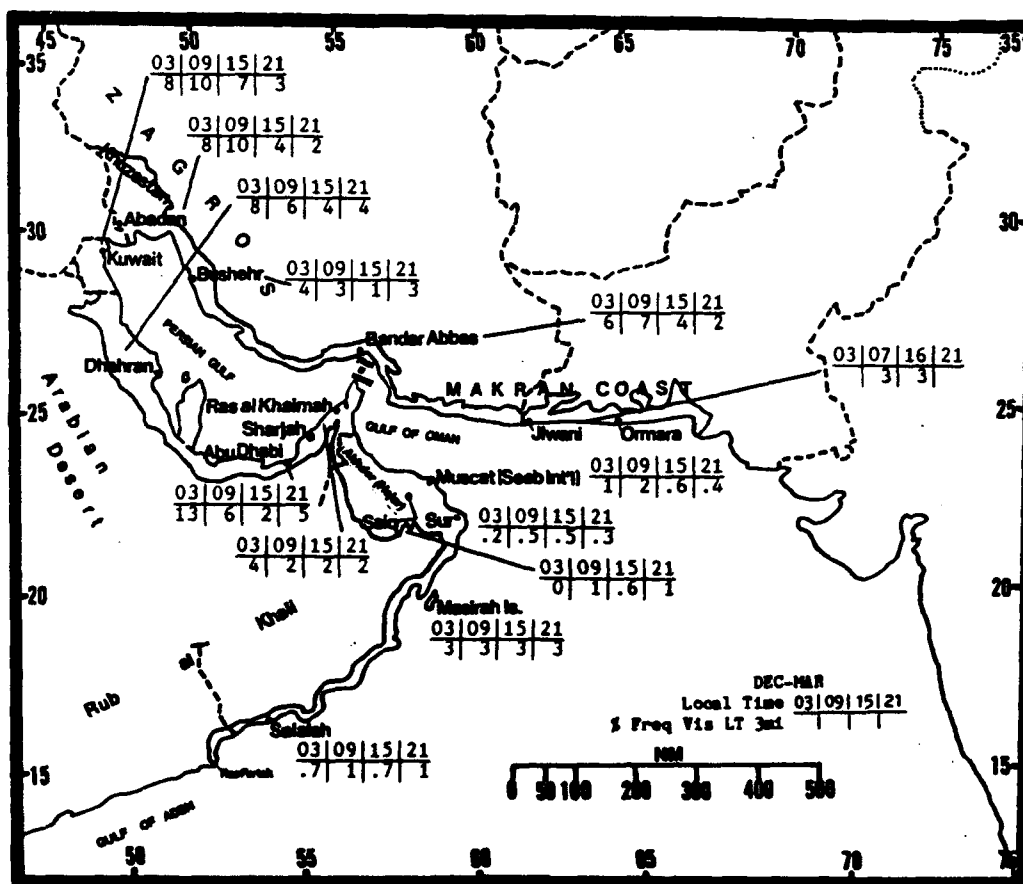


Figure 6-16. Northeast Monsoon Frequencies of Visibilities Below 3 Miles, Persian Gulf Coastal Plains. Note that Jiwani does not report between 2100 and 0300L.

PERSIAN GULF COASTAL PLAINS NORTHEAST MONSOON

December-March

WINDS. Figure 6-17 shows mean Northeast Monsoon surface wind speeds and prevailing direction for selected locations. Although Northeast Monsoon flow dominates, surface winds vary from westerly to northerly.

Prevailing surface wind directions are heavily influenced by local effects. Local sea breezes and mountain/valley circulations control the winds at locations like Salalah, Sur, Seeb Int'l, Masirah, Ras Khaimah, and Saiq. At Bandar Abbas, prevailing wind direction is southerly (onshore flow); at Jiwani, it is northerly to westerly (offshore flow). At Saiq, winds are weak southeasterly at 5-6 knots between December and February, but southwesterly at 8 knots in March. Peak winds observed for the season were 82 knots from the east at Jiwani, 91 knots from the north at Bandar Lengeh, 50 knots from the north at Saiq, and 85 knots from the south at Bandar Abbas.

The mean 5,000-foot (1,524 meter) MSL wind direction at Salalah (refer to Figure 6-6a) shows a gradual shift from northeasterly (December and January) to southeasterly (February), to southerly (March). Mean speeds vary between 11 and 13 knots. At 10,000 feet (3,050 meters) MSL, the mean wind direction shifts from northwesterly (February) to north-northeasterly (March), with mean speeds averaging 14 knots through the period. At 15,000 feet (4,573 meters) MSL, winds are westerly-to-northwesterly from 14 to 19 knots. Figure 6-6c shows the mean wind direction for Kuwait International as westerly at all three levels; mean speed averages only from 11 to 19 knots.

		DEC	JAN	FEB	MAR
S	Ras'Khaimah	3.90	3.90	4.50	4.60
NW	Abu Dhabi	6.30	6.30	8.10	7.80
SE/SW	Saiq	5.00	5.00	6.20	7.80
SW-W	Seeb Int'l	4.90	4.80	5.10	5.70
E-NE/SSW	Masirah	8.40	7.00	8.50	7.30
NW-N	Dhahran	7.40	7.60	7.90	8.10
WNW	Kuwait	7.10	6.60	8.30	8.00
WNW	Abadan	5.60	5.90	6.30	7.00
NNW	Bushehr	6.70	6.90	6.10	7.40
S	Ban'r Abbas	6.10	6.50	6.30	7.00
N/SSW	Sur	7.20	6.60	7.00	7.40
N-W	Jiwani	4.70	5.40	5.50	6.00
NNW	Doha Int'l	7.70	7.10	9.10	9.10
NE-E	Ban'r L'engeh	6.20	6.80	6.80	8.60
N/S	Salalah	7.20	6.70	6.40	5.30

Figure 6-17. Mean Northeast Monsoon Surface Wind Speeds (kts) and Prevailing Direction, Persian Gulf Coastal Plains. The slashes between prevailing wind directions at Saiq, Masirah, Sur, and Salalah denote wind shifts that occur between February and March.

Figure 6-18 gives Northeast Monsoon wind speeds at 39,000 feet (11.9 km) for Jiwani, Kuwait, Seeb, and Salalah. This level is about the height of the Subtropical Jet.

PERSIAN GULF COASTAL PLAINS NORTHEAST MONSOON

December-March

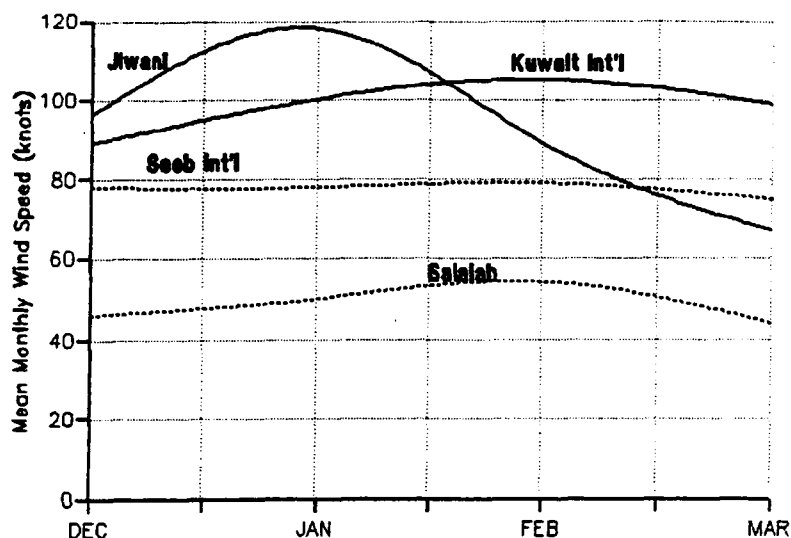


Figure 6-18. Mean Northeast Monsoon Wind Speeds at 39,000 Feet (11.9 km) MSL (kts), Persian Gulf Coastal Plains. This level approximates the height of the Subtropical Jet.

PRECIPITATION. Normally, Northeast Monsoon precipitation (Figure 6-19) results from the migratory low-pressure systems that move from the northwest into the Zagros Mountains or through the Persian Gulf. About twice a month, a weak system or trough continues into the Gulf of Oman and Makran Coast.

Lows tracking into the Zagros Mountains affect the weather at Abadan and Kuwait, and also at Bushehr where orographic lifting can produce heavy showers. Dhahran and Bandar Abbas normally see only a weak wind shift.

Lows that track through the Persian Gulf can produce significant weather throughout the subregion. The surface low normally establishes a moist warm front along the southern Zagros Mountains. Orographic showers can fall at Bushehr, Ras al Khaimah, Bandar Abbas, and Saiq. If the surface low tracks into the Gulf of Oman, warm front showers can develop at Jiwani or Ormara. Orographic showers can also spread downwind over Sur and Seeb. Rainshowers along the cold front are usually scattered. Local meteorologists classify the northwest-to-southeast storm track as a 3- to 5-day Shamal.

Cyprus and Black Sea Lows produce more significant weather across the Persian Gulf Coastal Plains than any other migratory system. The Cyprus Low is an active, moist storm system; its main track lies northwest to southeast through the Persian Gulf proper. An intense Cyprus Low may cause isolated thunderstorms near the surface low-pressure and along the cold front if a mid- or upper-level trough lies over the surface low.

Indirectly, Black Sea Lows produce rainfall, cold air outbreaks, and strong west to northwest winds. They normally have trailing cold fronts that extend southward across the Zagros Mountains. The stronger cold fronts have cold 700-mb and/or 500-mb troughs associated with the surface cyclogenesis over the Black Sea, and potentially severe thunderstorms can develop. A secondary surface low sometimes forms on a Black Sea Low cold front over the warm waters of the Persian Gulf. A rare secondary low may form in the northwestern Gulf of Oman and continue eastward along the Makran Coast. Heavy orographic showers can occur along the warm front. Only one of six frontal passages through the Persian Gulf results in a secondary low-pressure center.

PERSIAN GULF COASTAL PLAINS NORTHEAST MONSOON

December-March

As shown in Figure 6-19, mean monthly precipitation amounts vary significantly across the Persian Gulf Coastal Plains. At many locations, December and January are the peak months for rainfall, but there is rarely enough cold air aloft to produce heavy precipitation east of 55° E. Orographic lift along the coasts can generate heavy rain as the Arabian Sea provides low-level moisture. Bushehr, Bandar Abbas,

Saiq, Jiwani, and Ormara are most often affected by orographic precipitation.

Although the Northeast Monsoon is normally responsible for 80% of yearly rainfall, some years produce little or none. The season is abnormally dry when strong mid- and upper-level ridging prevents significant troughing south of 40° N.

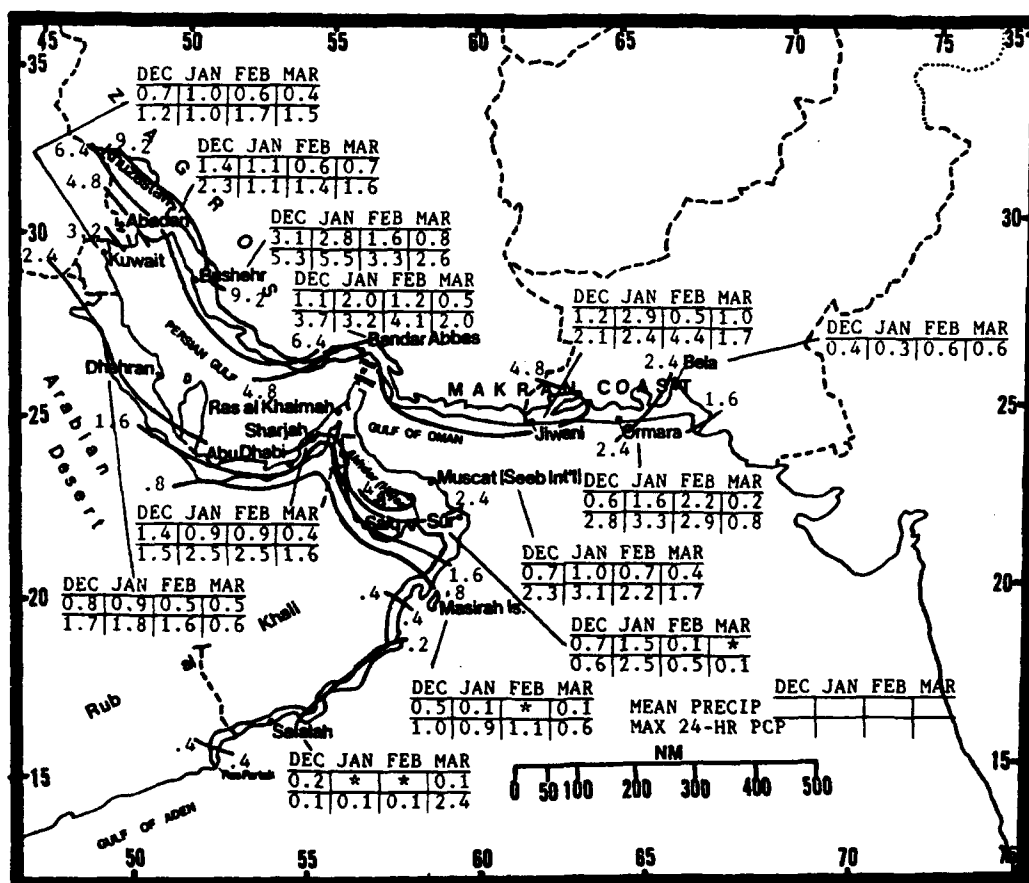


Figure 6-19. Mean Northeast Monsoon Monthly/Maximum 24-hour Precipitation, Persian Gulf Coastal Plains. Bold lines represent mean seasonal rainfall totals. The asterisk (*) represents less than 0.05 inches (1.3 mm) of rainfall.

PERSIAN GULF COASTAL PLAINS NORTHEAST MONSOON

December-March

TEMPERATURE. Mild days and cool evenings are typical between December and March (Figure 6-20). Mean daily highs range from 58° F (14° C) at Saiq in January to 85° F (30° C) at Salalah in March. Mean daily lows range from 45° F (7° C) at Abadan in January to 72° F (22° C) at Sur in March. The season's record

high was 106° F (41° C) at Kuwait in March. Record lows are 24° F (-4° C) at Abadan and Kuwait, 35° F (2° C) at Jiwarei, and 50° F (10° C) at Sur, all in December. Across the subregion, mean relative humidity averages 60% for all hours, 68% during early morning, and 42% by mid-afternoon.

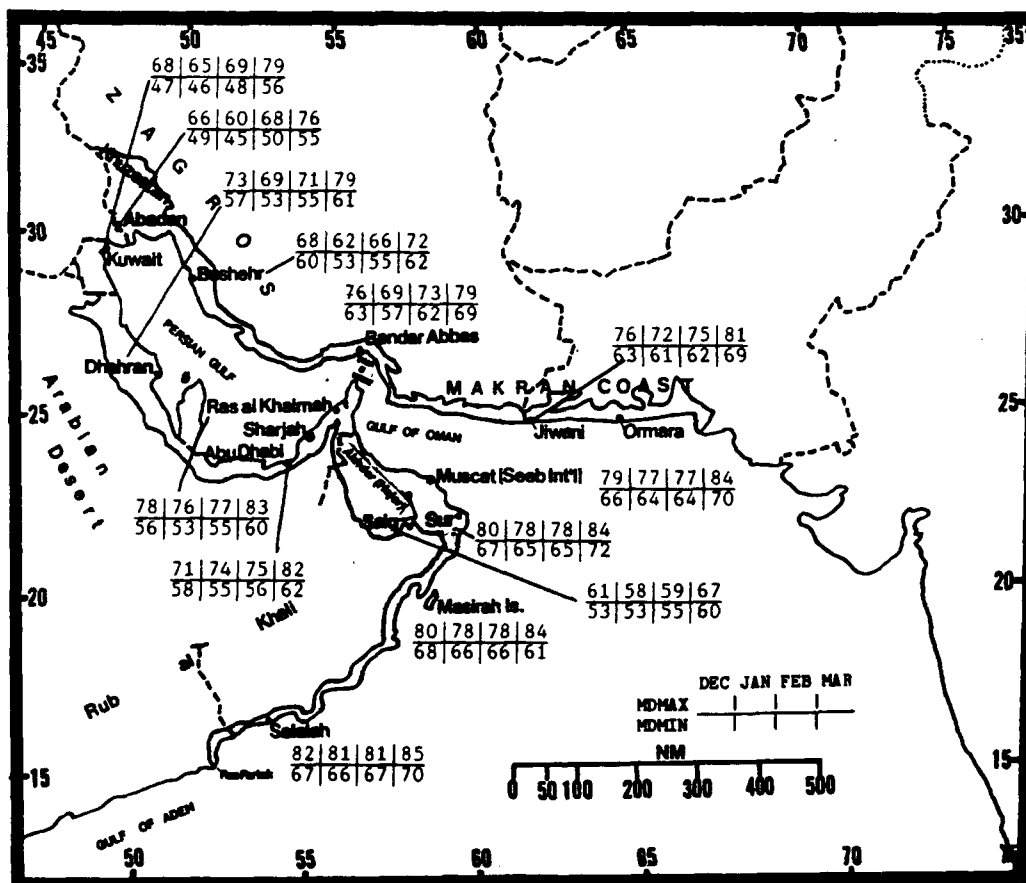


Figure 6-20. Mean Northeast Monsoon Daily Maximum/Minimum Temperatures (° F), Persian Gulf Coastal Plains.

PERSIAN GULF COASTAL PLAINS NORTHEAST-TO-SOUTHWEST MONSOON TRANSITION

April-May

GENERAL WEATHER. Warm days, local sea-breeze convection, thin dust in the air, and salt haze characterize the fair-weather periods of April and May. At night, thin radiation fog develops under calm conditions along coastlines, but visibility is rarely below 3 miles. Active cold fronts, isolated thunderstorms, and severe duststorms occur once or twice during April, all produced by surface lows tracking through the Persian Gulf and Gulf of Oman. The strength of these systems depends on whether or not there is mid- and upper-level troughing, with cold air support, above the surface trough.

SKY COVER. During the NE-SW Monsoon transition, mean cloudiness (see the isolines in Figure 6-21) decreases markedly from northwest to southeast. The most cloudiness (over 40%) is in the extreme northwest corner of the subregion, dropping to 20% near the Strait of Hormuz. The lowest cloud cover (8%) is found near the Omani coast at Seeb International. Slightly higher percentages along the southern Omani coast and the eastern Makran coast are caused by the return of the Somali Jet's southwesterly flow (pre-Southwest Monsoon circulation) over the Arabian Sea and extreme eastern Gulf of Aden.

Most low cloud cover results from frontal systems and early morning coastal stratus. Only extremely rare, very intense surface lows produce multilayered clouds. Ceilings below 5,000 feet (1,524 meters) AGL require instability in the mid- or upper-levels. Mid-level clouds are found near 700- and 500-mb troughs, with bases normally between 10,000 and 14,000 feet (3,050-4,268 meters) MSL.

Surface heating is strong in April and May, causing thunderstorm activity to reach its annual peak, but the average number of occurrences is only 1-4 days. Thunderstorms may be exceptionally strong if they occur along an active cold front. Cloud bases are between 4,000 and 6,000 feet (1,220-1,829 meters) AGL; tops can exceed 40,000 feet (12.2 km).

Stratus or stratocumulus produce the few ceilings below 3,000 feet (915 meters) at most stations except in the Akhdar Mountains near Saiq. With an elevation of 5,756 feet (1,755 meters), Saiq receives diurnal cumulus produced by orographic lifting, causing the only ceilings below 1,000 feet (305 meters) in the subregion.

The coastlines of the Strait of Hormuz are the only other locations where diurnal cumulus is produced. A combination of a strong land-sea breeze and orographic lifting produces bases of 5,000 to 7,000 feet (1,524-2,134 meters) AGL; thickness rarely exceeds 2,000 feet (610 meters).

On rare occasions, an "onset vortex" and/or a tropical cyclone affects the subregion during the transition. Tropical cyclones are more likely to occur in May than April. An onset vortex makes landfall only once every 10 years; typically, they enter the Persian Gulf Coastal Plains between Sur and Masirah Island, but they may hit the coast anywhere between Jiwani and Salalah. Tropical disturbances produce a multilayered cloud shield that can extend 200-300 NM from the system's center.

**PERSIAN GULF COASTAL PLAINS
NORTHEAST-TO-SOUTHWEST MONSOON TRANSITION**

April-May

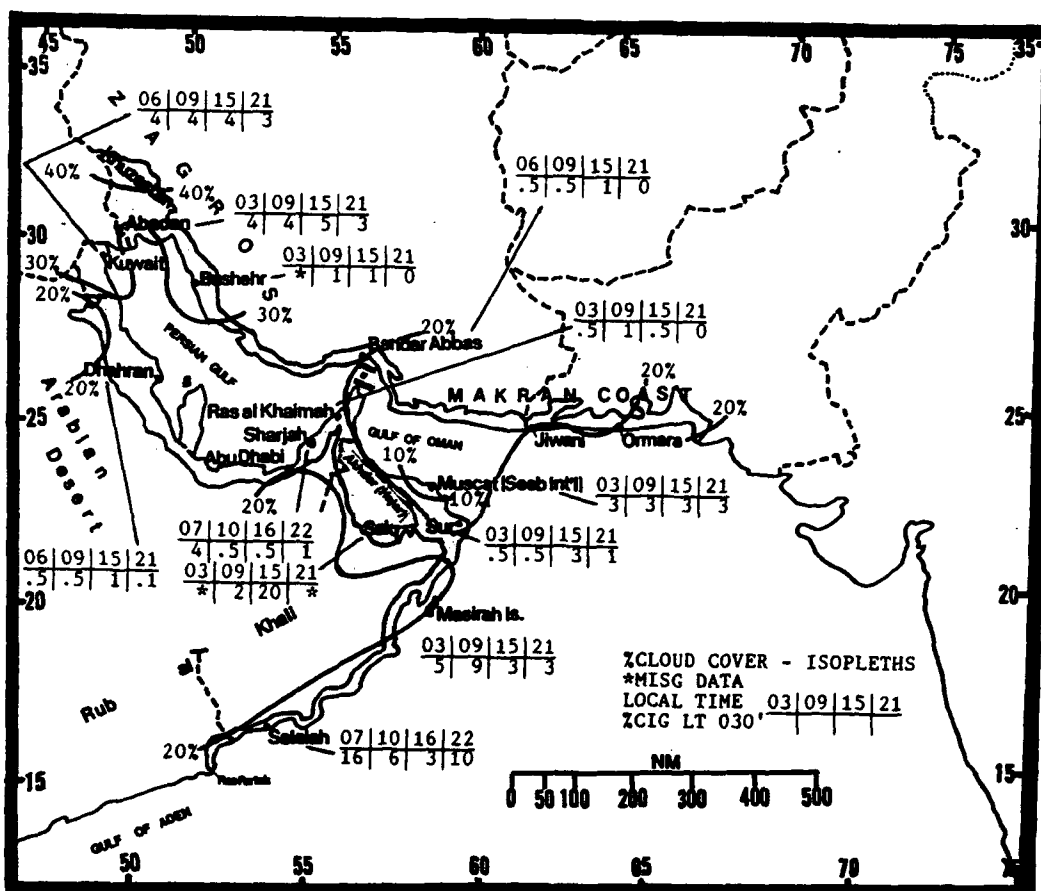


Figure 6-21. Mean NE-SW Monsoon Transition Cloudiness (Isolines) and Frequencies of Ceiling Below 3,000 Feet (915 meters), Persian Gulf Coastal Plains.

PERSIAN GULF COASTAL PLAINS NORTHEAST-TO-SOUTHWEST MONSOON TRANSITION

April-May

VISIBILITY. Early morning mist, salt haze, and fog are the most common nighttime obstructions to vision. During the day, dust haze develops with greater frequency, often reducing visibilities to 4-7 NM. The Saudi Arabian Heat Low begins to raise large amounts of dust into the atmosphere by late April-early May. About half the reporting stations show a daytime peak in visibilities below 3 miles (Figure 6-22). Stations located within the circulation of the thermal heat low are affected by the blowing dust originating in the Arabian Desert. In other cases (Bandar Abbas and Bushehr), the sea breeze can cause local duststorms and low visibility during the daylight hours. Suspended dust can remain airborne and combine with

moisture to produce persistent dust/salt haze lasting for 2 to 7 days.

Kuwait has the highest frequency of visibilities below 3 miles in the subregion, (12% at 0900L). This results from early morning fog, salt haze, and mist mixed with a high concentration of dust and dust haze.

The rare migratory low-pressure system (typically an Atlas Low) can produce severe duststorms and widespread low visibilities that last from 6 to 36 hours; southwesterly to southeasterly winds can exceed 50 knots across the Saudi Arabian Peninsula.

PERSIAN GULF COASTAL PLAINS
NORTHEAST-TO-SOUTHWEST MONSOON TRANSITION

April-May

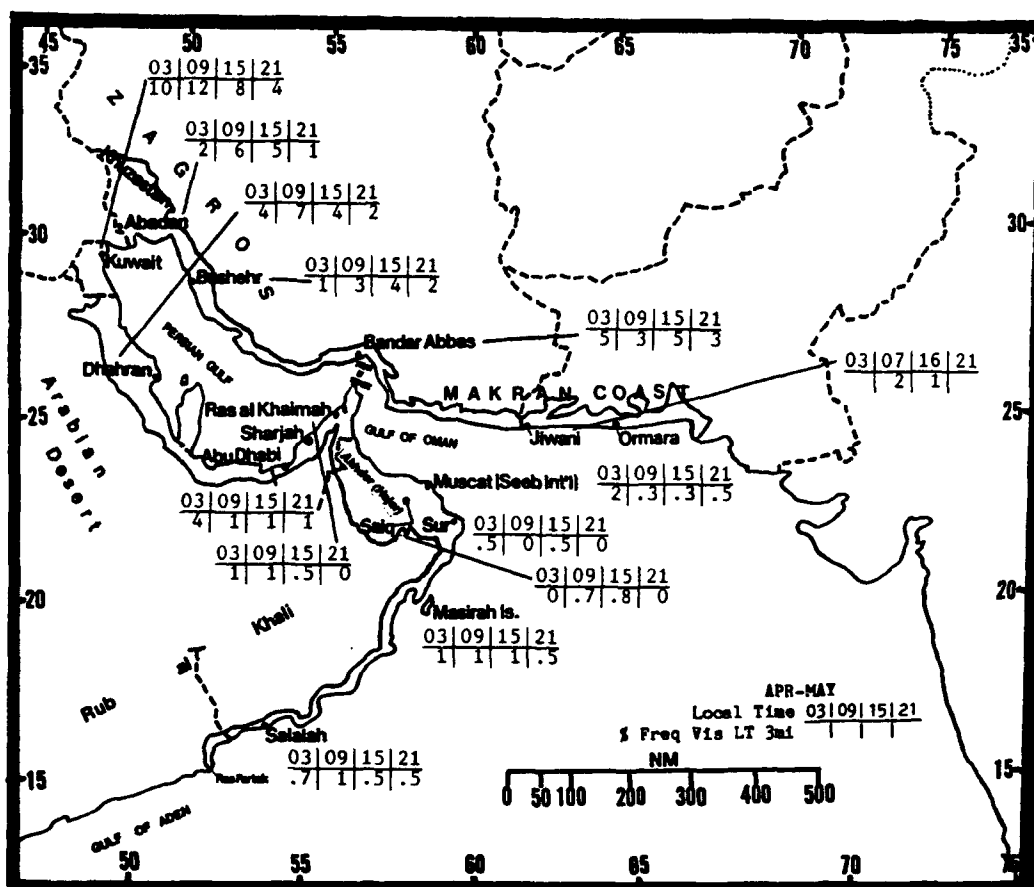


Figure 6-22. NE-SW Monsoon Transition Frequencies of Visibilities Below 3 Miles, Persian Gulf Coastal Plains.

PERSIAN GULF COASTAL PLAINS **NORTHEAST-TO-SOUTHWEST MONSOON TRANSITION**

April-May

WINDS. In response to the pressure gradient, prevailing surface flow is north-to-northwest in the northwestern corner of the subregion. South-to-southwest flow prevails elsewhere as the Saudi Arabian Heat Low develops and produces weak southerly (cyclonic) surface circulation over most of the Persian Gulf Coastal Plains. At Salalah and Masirah, the Somali Jet's development produces a south-southwesterly flow. Figure 6-23 gives mean surface wind speeds and prevailing wind directions for selected stations.

		APR	MAY
S	Ras'Khaimah	5.10	5.30
NW	Abu Dhabi	8.20	8.00
WSW-SSW	Saiq	8.70	7.60
W-SSW	Seeb Int'l	5.50	6.50
SSW	Masirah	9.00	12.30
N	Dhahran	8.10	8.70
NNW	Kuwait	8.00	8.30
NNW	Abadan	7.50	7.20
W-NW	Bushehr	7.50	7.20
S	Ban'r Abbas	8.00	8.50
SSW	Sur	6.20	8.80
W-SW	Jiwani	6.60	6.30
N	Doha Int'l	8.80	9.10
S	Ban'r L'ngah	8.10	8.20
SSW	Salalah	5.10	6.20

Figure 6-23. Mean NE-SW Monsoon Transition Surface Wind Speeds (kts) and Prevailing Direction, Persian Gulf Coastal Plains.

Salalah's mean annual upper-level wind direction (refer to Figure 6-6a) is significantly different from other stations because of its proximity to the surface Monsoon Trough, the Somali Jet, and Southwest Monsoon mid-level circulation. Seeb (Figure 6-6b) is only 500 NM to the northeast of Salalah, but its mean direction profile is very different, and similar to that for Kuwait and Jiwani.

The mean 700-mb flow has a small anticyclone centered over southeastern Saudi Arabia, in response to strong surface heating that also develops the Saudi Arabian Heat Low. At 15,000 feet, mean wind direction is westerly; mean speed is 19 knots in April and 12 knots in May. Wind direction at this level is also the opposite of Salalah's. The anticyclonic flow in the mid-levels forms a strong subsidence inversion over the subregion by late May.

PERSIAN GULF COASTAL PLAINS **NORTHEAST-TO-SOUTHWEST MONSOON TRANSITION**

April-May

PRECIPITATION. The mean precipitation amounts in Figure 6-24 show a marked decrease between April and May, but the degree of decrease varies widely. These differences are most noticeable at Jiwani, Ormara, Kuwait, and Sur. Large variations in mean monthly and maximum 24-hour rainfall are primarily associated with lower frequencies of frontal systems, but thunderstorm activity is also a factor. The May maximum 24-hour rainfall at Salalah (6.7 inches/170mm) occurred during a tropical cyclone. May is one of the peak months for tropical and subtropical cyclone formation in the Arabian Sea.

Thunderstorm frequency is highest at many locations in April due to (1) active cold fronts the

still bring in moisture and instability, (2) intense heating over land, (3) strong sea breezes that lift moist air over coastal mountain ranges, and (4) mid-level instability associated with deep mid- or upper-level troughs.

Mid-level subsidence is another important thunderstorm control. The Saudi Arabian Heat Low immediately west of the subregion is normally unstable below 850 mb. Synoptic-scale anticyclonic circulation (subsidence) develops at the mid-levels, but it takes several weeks to establish itself firmly. On the larger scale, the Sahara, Saudi Arabian interior, interior plateaus of Turkey and Iran, and lowlands of Pakistan regularly develop a well-defined subsidence layer at mid-levels by late May.

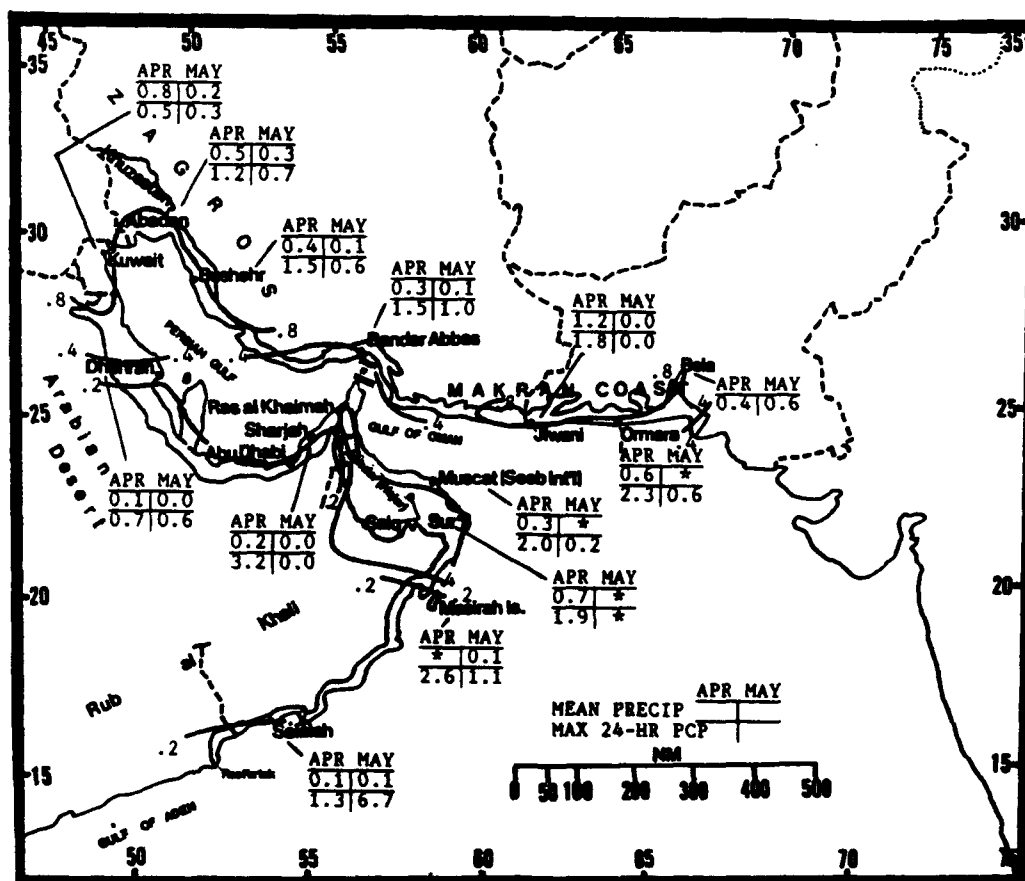


Figure 6-24. Mean NE-SW Monsoon Transition Monthly/Maximum 24-hour Precipitation, Persian Gulf Coastal Plains. Bold lines represent mean seasonal rainfall totals.

PERSIAN GULF COASTAL PLAINS **NORTHEAST-TO-SOUTHWEST MONSOON TRANSITION**

April-May

TEMPERATURE. In April, mean daily highs range from 73° F (23° C) at Saiq to 93° F (34° C) at Seeb (Figure 6-25). Mean daily lows range from 65° F (18° C) at Kuwait and Abadan to 79° F (26° C) at Sur. In May, mean highs range

from 81° F (27° C) at Saiq to 103° F (38° C) at Seeb. Mean May lows range from 73° F (23° C) at Abadan and Saiq to 86° F (30° C) at Seeb. The large differences in temperature are due to elevation.

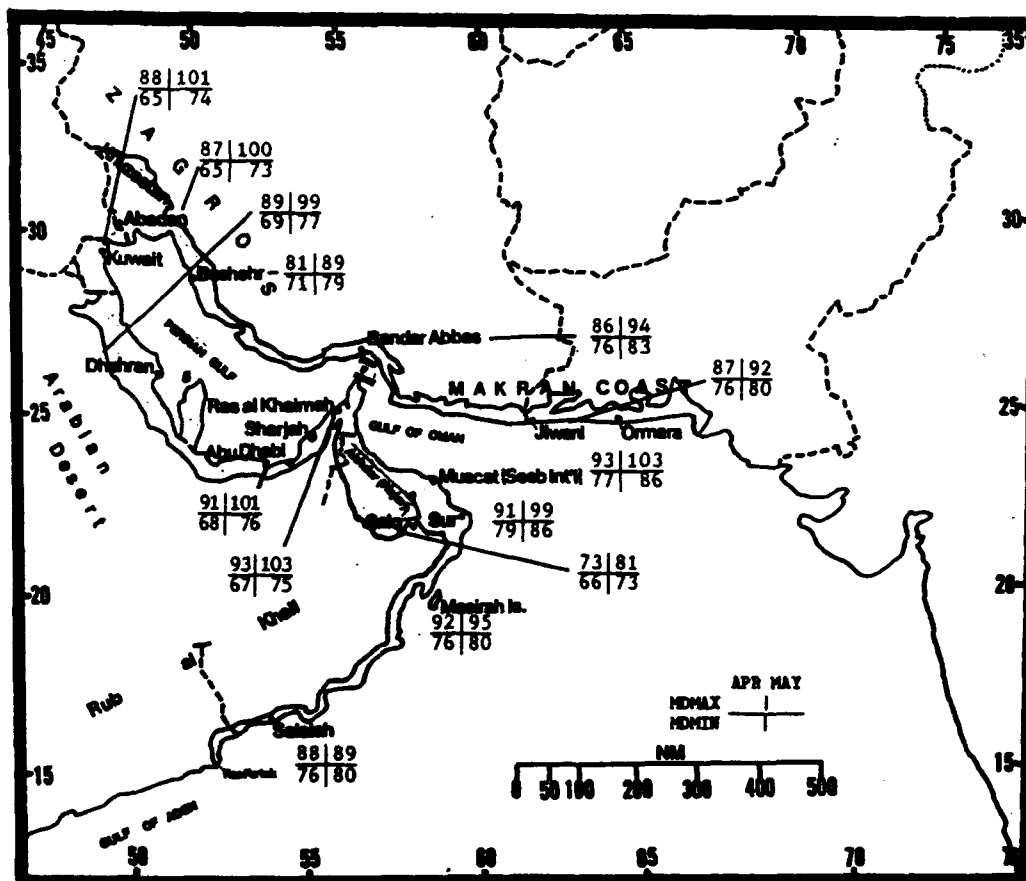


Figure 6-25. Mean NE-SW Monsoon Transition Daily Maximum/Minimum Temperatures (° F), Persian Gulf Coastal Plains.

BIBLIOGRAPHY

- Abdulahad, G., *Thunderstorms and Hailstorms at Baghdad*, Meteorological Memoirs Vol. 1, Republic of Iraq, Ministry of Communications, Directorate General of Civil Aviation, Baghdad, pp. 33-39, 1962.
- Africa*, AWS/FM-100/001, HQ Air Weather Service. Scott AFB, IL, March 1980.
- Aleppo-Baghdad-Karachi Air Route*, Aviation Meteorological Report 3, Meteorological Office, Aviation Services Division, Air Ministry, October 1934.
- Allison, L.J., et al., *A Quasi-Global Presentation Of TIROS III Radiation Data*, NASA SP-53, NASA, 1964.
- Alpert, P., "An Early Winter Subtropical Cyclone In The Eastern Mediterranean," *Israel Journal of Earth-Sciences*, Vol. 33, pp. 151-156, 1984.
- Anderson, D.L.T., "The Low-Level Jet As A Western Boundary Current," *Monthly Weather Review*, Vol. 104, pp. 907-921, 1976.
- Arabia*, United Kingdom Meteorological Office, Investigations Division Climatological Report No. 95, Air Ministry, Bracknell, 1957.
- Ardanuy, P., "On The Observed Diurnal Oscillation Of The Somali Jet," *Monthly Weather Review*, Vol. 107, pp. 1694-1700, 1979.
- Asmara, Eritrea; Africa*, Weather Division, HQ Army Air Forces, 1944.
- Atkinson, G.D., *Forecaster's Guide to Tropical Meteorology*, AWS/TR-240, HQ Air Weather Service. Scott AFB, IL, 1971.
- Atkinson, G.D., and Sadler, J.C., *Mean Cloudiness And Gradient-Level Wind Charts Over The Tropics, Volume 2, Charts*, AWSTR 215, HQ Air Weather Service, Scott AFB, IL, 1970.
- Attlee, Gizaw, *Weather and Climate at Addis Ababa, Dire Dawa, and Jimma*, Imperial Ethiopian Government Civil Aviation Administration Meteorological Service, 1965.
- Attlee, Gizaw, *Weather at Asmara*, Imperial Ethiopian Government Civil Aviation Administration Meteorological Service, 1964.
- Bannon, P.R., "On The Dynamics Of The East African Jet. Part I. Simulation Of Mean Conditions For July," *Journal Of Atmospheric Science*, Vol. 36, pp. 2139-2152, 1979.
- Bannon, P.R., "On The Dynamics Of The East African Jet. Part II. Jet Transients," *Journal Of Atmospheric Science*, Vol. 36, pp. 2153-2168, 1979.
- Bannon, P.R., "On The Dynamics Of The East African Jet. Part III: Arabian Sea Branch," *Journal Of Atmospheric Science*, Vol. 39, pp. 2267-2278, 1982.
- Bhalotra, Y.P.R., *Weather at Port Sudan*, Memoir No. 3, Sudan Meteorological Service, January 1960.
- Bhalotra, Y.P.R., *Meteorology of Sudan*, Memoir No. 6, Sudan Meteorological Service, September 1963.

- Bruce, J.G., "The Wind Field In The Indian Ocean And The Related Ocean Circulation," *Monthly Weather Review*, Vol. 111, pp. 1442-1452, 1983.
- Bryson, R.A., et al., *Normal 500mb Charts For The Northern Hemisphere*, Report No. 8, AF 19 (604)-992, 29pp., 1957.
- Cadet, D., and Desbois, M., "A Case Study Of A Fluctuation Of The Somali Jet During The Indian Summer Monsoon," *Monthly Weather Review*, Vol. 109, pp. 182-187, 1981.
- Charney, J.G., "Dynamics Of Deserts And Drought In The Sahel," *Quarterly Journal Of The Royal Meteorological Society*, Vol. 101, No. 428, pp. 193-202, 1975.
- Climate - British and Italian Somaliland*, AWS Directorate of Climatology, HQ Air Weather Service, Scott AFB, IL, Dec 1955.
- The Climate of Ethiopia*, date & author unknown.
- Climatic Atlas of Asia I, Maps of Mean Temperature and Precipitation*, Goscomgidromet USSR, Vocikov Main Geophysical Observatory, WMO, 1981.
- Climatic Study of the Red Sea South and Gulf of Aden, Near Coastal Zone*, Naval Oceanography Command Detachment, NSTL Station, Bay St Louis, MS, September 1982.
- Climatic Study - Report 4295*, USAF Environmental Technical Applications Center, AWS (MATS), July 1962.
- Climatological Summary For Baghdad Airport*, Directorate Of Civil Aviation, Iraqi Meteorological Department, Baghdad, 1956.
- Climatological Wind Factor Calculator-Mean Isogon-Isotach Charts*, SACM 105-2, Vol. 2, 1960.
- A Contribution to Forecasting In Iraq, Habbaniya, Iraq*, Aviation Meteorological Reports, Meteorological Office, Aviation Services Division, Air Ministry, July 1939.
- Crutcher, H.L., *Selected Meridional Cross Sections Of Heights, Temperatures, And Dew Points Of The Northern Hemisphere*, NCDC-NOAA, NAVAIR 50-1C-59, 1971.
- Dayan, U., and Abramski, R., *Heavy Rains In The Middle East Related To Unusual Jet Stream Properties*, AWS/FM-100/022, HQ Air Weather Service, Scott AFB, IL, April 1984.
- Desai, P.S., "The Summer Atmospheric Circulation Over The Arabian Sea," *Journal of Atmospheric Science*, Vol. 24, pp. 216-220, 1967.
- Dubief, J., *Le Climat du Sahara--Tome II*, L'Institut de Meteorologie et de Physique du Globe de L'Algerie, Alger, 1963.
- The Easterly Jet Stream in the Tropics*, AWS/FM-100/019, HQ Air Weather Service, Scott AFB, IL, September 1980.
- El-Fandy, M.G., "Barometric Lows of Cyprus," *Quarterly Journal Of The Royal Meteorological Society*, Vol. 72, pp. 291-306, 1946.

- El-Fandy, M.G., "The Effect of the Sudan Monsoon Low on the Development of Thundery Conditions in Egypt, Palestine and Syria," *Quarterly Journal Of The Royal Meteorological Society*, Vol. 78, pp. 31-38, 1948.
- El-Fandy, M.G., "Effects of Topography and Other Factors on the Movement of Lows in the Middle East and Sudan," *Bulletin Of The American Meteorological Society*, Vol. 31, pp. 375-381, 1950.
- Ethiopia (Including Eritrea) Parts I and II, and Part III*, United Kingdom Meteorological Office, Investigations Division Climatological Report No. 60, Air Ministry, Bracknell, 1962.
- Farr, G.R., "Seasonal And Global Distribution Of The Jet Stream And Its Kinetic Energies In The Northern Hemisphere," Masters Thesis, Dept of Meteorology, Univ. of Utah, 1964.
- Fett, R.W., *North Atlantic and Mediterranean Weather Analysis and Forecast Applications--Volume 3*, NEPRF Technical Note 80-07, Monterey, CA, 1980.
- Fett, R.W., *Weather Analysis And Forecast Applications; Volume 5--Part 1, The Indian Ocean, Red Sea/Persian Gulf*, NEPRF Technical Report 83-03, Monterey, CA, 1983.
- Findlater, J., "Cross-Equatorial Jet Streams At Low Levels Over Kenya," *Meteorological Magazine*, Vol. 95, pp. 353-364, 1966.
- Findlater, J., "Some Further Evidence Of Cross-Equatorial Jet Streams At Low Level Over Kenya," *Meteorological Magazine*, Vol. 96, pp. 216-219, 1967.
- Findlater, J., "Interhemispheric Transport Of Air In The Lower Troposphere Over The Western Indian Ocean," *Quarterly Journal Of The Royal Meteorological Society*, Vol. 95, pp. 400-403, 1969.
- Findlater, J., "A Major Low-Level Air Current Near The Indian Ocean During The Northern Summer," *Quarterly Journal Of The Royal Meteorological Society*, Vol. 95, pp. 362-380, 1969.
- Findlater, J. "The Strange Winds Of Ras Asir," *Meteorological Magazine*, Vol. 100, pp. 46-54, 1971.
- Findlater, J., "Mean Monthly Airflow At Low Levels Over The Western Indian Ocean," *Geophysical Memoirs*, No. 115, British Meteorological Office, Vol. 16, Number 1, 1971.
- Findlater, J., "Aerial Explorations Of The Low-Level Cross-Equatorial Current Over Eastern Africa," *Quarterly Journal Of The Royal Meteorological Society*, Vol. 98, pp. 274-289, 1972.
- Flight Hazards at Baghdad Airport*, Research Section of the Meteorological Department, Government of Iraq Ministry of Communications and Works, Meteorological Department, Baghdad, 1956.
- Flohn, H., *Studies on the Meteorology of Tropical Africa*, Bon Met Abhund, Heft 5, Bonn, 1965.
- Flohn, H., *Contributions To A Meteorology Of The Tibetan Highlands*, Dept Of Atmospheric Sciences--Colorado State Univ., Research Paper No. 130, 1968.
- General Circulation Of The Atmosphere*, Portuguese Meteorological Service, DIA LN 783-70, 1970.
- Giles, B.D., "Extremely High Atmospheric Pressure," *Weather*, Vol. 25, pp. 19-24, 1970.
- Grant, K., *Vector Mean Winds And Humidities In The Lower Troposphere Over Arabia And Environs In July*, Special Investigations Memorandum No. 3, Meteorological Office, Bracknell, UK, 1983.

- Gupta, M.G., et al., "A Study Of TEJ Current Characteristics From MONEX Data," *MAUSAM*, Vol. 36, No. 2, pp. 221-228, 1985.
- Hamilton, M.G., "Monsoons-An Introduction," *Weather*, Vol. 42, pp. 186-193, 1987.
- Hammer, R.M., "Rainfall Patterns In The Sudan," *Journal Of Tropical Geography*, Vol. 35, pp. 40-50, 1972.
- Hart, J.E., et al., "Aerial Observations Of The East African Low-Level Jet Stream," *Monthly Weather Review*, Vol. 106, pp. 1714-1724, 1978.
- Hastenrath, S., et al., *A Contribution to the Dynamic Climatology of Arabia*, Department of Meteorology, The University of Wisconsin, Madison, Archiv Fur Meteorologie Geophysik Und Bioklimatologie, 1979.
- Hastenrath, S., *Climate And Circulation Of The Tropics*, Reidel Publ Inc., Dordrecht, 1985.
- Huzayyin, S. A., "Notes on Climatic Conditions in Southwest Arabia (Yaman and the Hadhramaut)," *Royal Meteorological Society Quarterly Journal*, Vol. 71, pp. 129-140, 1945.
- Indian Ocean Atlas*, Central Intelligence Agency, 1976.
- Iraq*, United Kingdom Meteorological Office, Investigations Division Climatological Report No. 104, Air Ministry, Bracknell, 1960.
- Joshi, P.C., and Desai, P.S., "The Satellite-Determined Thermal Structure Of Heat Low During Indian Southwest Monsoon Season," *Advanced Space Research*, Vol. 1, pp. 57-60, 1985.
- Karapiperis, L.N., "A Classification Of The Ethesians On The Basis Of The Prevailing Isobaric Conditions," *Meteorologische Rundschau*, Vol. 6, FTD-ID (RS) T-1633-81, 1982.
- Kheder, J., *A Note On Some Climatic Features of Iraq*, Meteorological Memoirs Vol 1, Republic of Iraq, Ministry of Communications, Directorate General of Civil Aviation, Baghdad, 1962.
- Krishnamurti, T.N., et al., "Numerical Simulation Of The Somali Jet," *Journal of Atmospheric Science*, Vol. 33, pp. 2350-2362, 1976.
- Krishnamurti, T.N., et al., "On The Onset Vortex Of The Summer Monsoon," *Monthly Weather Review*, Vol. 109, pp. 344-363, 1981.
- Lahey, J.F., et al., *Atlas Of 300mb Wind Characteristics For The Northern Hemisphere*, Final Report. Part 1., AF 19 (604)-2278, Univ of Wisc Press, 1960.
- Leroux, M., *The Climate Of Tropical Africa-Part B.*, FTD-ID(RS)T-0615-85, Foreign Technology Division translation, Wright-Patterson, OH, pp. 526-566, 1983.
- Leroux, M., *The Climate Of Tropical Africa-Atlas, Volume 2*, 1983.
- Marcil, G., *Meteorology Of The Persian Gulf And Of Several Airports On The Arabian Coast*, FTD-ID-(RS)T-0113-85, 1985.
- Marhoun, H., *Synoptic Study of A Hailstorm At Al Qurna In Southern Iraq*, Meteorological Memoirs Vol 1, Republic of Iraq, Ministry of Communications, Directorate General of Civil Aviation, Baghdad, 1962.

Marshall, T.A., *A Synoptic Meteorology Of The Tropical Oceans*, Ministry Of Defence, British Naval Oceanography And Meteorology, Memorandum No. 1, 1988.

Meteorological Study Of Air Route Between Jeddah And Dar-Es-Salaam, Air France, FTD-ID(RS)T-0114-85, 1985.

Membery, D.A., "A Unique August Cyclonic Storm Crosses Arabia," *Weather*, Vol. 40, pp. 108-114, 1985.

Morth, H.T., *Introduction To The Climate Of Africa-Notes to Support Lectures On Regional Climatology*, East African Meteorological Service, Nairobi Kenya, date unknown.

Mukherjee, A.K., and Bahuguna, A.K., "A Satellite Study Of Stratus Clouds Off Yemen Coast," *MAUSAM*, Vol. 38, pp. 193-196, 1987.

Mukherjee, A.K., and Gurunadham, G., "Stratus Clouds Off Yemen Coast," *MAUSAM*, Vol. 36, pp. 287-290, 1985.

National Intelligence Surveys 25C and 27, Cyprus, Turkey, Section 23, Weather and Climate, U.S. Central Intelligence Agency, 1970.

National Intelligence Survey 55, Ethiopia and the Somalilands, Section 23, Weather and Climate, U.S. Central Intelligence Agency, 1965.

National Intelligence Surveys 30 and 32, Iraq/Arabian Peninsula, Section 23, Weather and Climate, U.S. Central Intelligence Agency, 1970.

National Intelligence Survey 49, Libya, Section 23, Weather and Climate, U.S. Central Intelligence Agency, 1965.

National Intelligence Survey 54, Sudan, Section 23, Weather and Climate, U.S. Central Intelligence Agency, 1965.

National Intelligence Surveys 28A, 28B, 29, and 31, Syria, Lebanon, Jordan, Israel, Section 23, Weather and Climate, U.S. Central Intelligence Agency, 1969.

National Intelligence Survey 53, United Arab Republic, Section 23, Weather and Climate, U.S. Central Intelligence Agency, 1968.

Navy Marine Climatic Atlas of the World, Volume IX, NAVAIR 50-1C-65, Naval Oceanography Command Detachment, Asheville, NC, May 1981.

Ownbey, J.W., *Climatic Summaries For Major 7th Fleet Ports And Waters*, NWSED, NAVAIR 50-1C-62, 1973.

Palmn, E., and Newton, C.W., *Atmospheric Circulation Systems*, Academic Press, New York and London, 1969.

Pant, M.C., "Some Characteristic Features Of The Low-Level Jet Field Over The Arabian Sea During The Indian Summer Monsoon", *MAUSAM*, Vol. 33, pp. 85-90, 1982.

Pedgley, D.E., "The Red Sea Convergence Zone; Part 1 - The Horizontal Pattern Of Winds," *Weather*, Vol. 21, pp. 350-359, 1966.

Pedgley, D.E., "The Red Sea Convergence Zone; Part 2 - Vertical Structure," *Weather*, Vol. 21, pp. 394-405, 1966.

Pedgley, D.E., "Cyclones along the Arabian Coast," *Weather*, Vol. 24, pp. 456-468, 1969.

- Pedgley, D.E., "Diurnal Variation of the Incidence of Monsoon Rainfall over the Sudan," *Meteorological Magazine*, Vol. 98, pp. 97-107 (Part I) and pp. 129-134 (Part II), 1969.
- Pedgley, D.E., "The Climate of Oman," *Meteorological Magazine*, Vol. 99, pp. 29-37, 1970.
- Pedgley, D.E., "Diurnal Incidence Of Rain And Thunder At Asmara And Addis Ababa, Ethiopia," *Meteorological Magazine*, Vol. 100, pp. 67-71, 1971.
- Pruss, W.F., *Climatological Wind Factors Calculator-Charts Of Vector Standard Deviation Of Winds*, 3WWM 105-5, 3WW, Offutt AFB, NE, 1962.
- Rainfall in Ethiopia*, Civil Aviation Department Climatological Institute Addis Ababa, Ethiopia, date unknown.
- Ramage, C.S., "The Subtropical Cyclone," *Journal of Geophysical Research*, Vol. 67, pp. 1401-1411, 1962.
- Ramage, C.S., "The Summer Atmospheric Circulation Over The Arabian Sea," *Journal of Atmospheric Science*, Vol. 23, pp. 145-150, 1966.
- Ramage, C.S., *Monsoon Meteorology*, Academic Press, New York, 1971.
- Rao, G.V., and Haney, J.L., "Kinematic And Thermal Structures Of Two Surges In The Northern Mozambique Channel Area," *Quarterly Journal Of The Royal Meteorological Society*, Vol. 108, pp. 957-974, 1982.
- Rao, G.V., van de Boogaard, H., and Bolhofer, W.C., "Further Calculations Of Sea-Level Air Trajectories Over The Equatorial Indian Ocean," *Monthly Weather Review*, Vol. 106, pp. 1465-1475, 1978.
- Red Sea And Gulf Of Aden-Oceanographical And Meteorological Data, Number 129*, Dutch Meteorological Service, Koninklijk Nederlands Meteorologisch Instituut, Amsterdam, 1949.
- Reed, R.J., "Principal Frontal Zones Of The Northern Hemisphere In Winter And Summer," *Bulletin Of The American Meteorological Society*, Vol. 41, pp. 591-598, 1960.
- Riehl, H., *Jet Streams Of The Atmosphere*, Tech Report No. 32, Dept of Atmospheric Science, Colorado State Univ., 1962.
- Sadler, J.C., *The Mean Winds Of The Upper Troposphere Over The Central And Eastern Pacific*, N62306-69 and N00188-71-M-6783, NEPRF, Monterey, CA, 1972.
- Sadler, J.C., *The Upper Tropospheric Circulation Over The Global Tropics*, UHMET 75-05, NSF Grant No. GA-36301, 1975.
- Sadler, J.C., *The Upper Tropospheric Circulation Over The Global Tropics. Part II-The Statistics*, UHMET 77-02, NSF Grant No. GA-36301, 1977.
- Saha, K., "Air And Water Vapour Transport Across The Equator In Western Indian Ocean During Northern Summer", *Tellus*, Vol. 22, pp. 681-687, 1970.
- Schneider-Carius, K., "The Ethesians," *Meteorologische Rundschau*, Vol. 1, FTD-ID (RS) T-1632-81, 1982.
- Sheikh Othman Airfield, Aden, Yemen*, Weather Division, HQ Army Air Forces, 1944.

- Sikka, D.R., and Gadgil, S., "On The Maximum Cloud Zone And The ITCZ Over Indian Longitudes During The Southwest Monsoon," *Monthly Weather Review*, Vol. 108, pp. 1840-1853, 1980.
- Singh, M.S., "Tropospheric Structure And Jet Streams Over The Middle East In Winter," *MAUSAM*, Vol. 31, pp. 241-246, 1980.
- Singh, R., and Raj, H., "A Satellite Study Of The Tropical Easterly Jet During Monsoon '77," *MAUSAM*, Vol. 33, pp. 113-120, 1982.
- Singh, R., "A Study Of Sea Surface Pressure, Sea Surface Temperature And Cloudiness Patterns Over Indian Ocean Region In Some Years Of Contrasting Southwest Monsoon Rainfall: Part II," *MAUSAM*, Vol. 34, pp. 205-212, 1983.
- Soliman, K.H., *Thunderstorms and Floods In Egypt*, reprinted from Proceedings Vol. II 1946, The Egyptian Academy of Science, Cairo, 1947.
- Soliman, K.H., "Rainfall Over Egypt," *Quarterly Journal Of the Royal Meteorological Society*, Vol. 79, pp. 389-397, 1953.
- Solot, S.B., *The Meteorology Of Central Africa*, AWSTR 105-50, HQ Air Weather Service, Scott AFB, IL, 1950.
- Solot, S.B., "General Circulation Over The Anglo-Egyptian Sudan and Adjacent Regions," *Bulletin Of The American Meteorological Society*, Vol. 31, pp. 85-94, 1950.
- Steadman, R.G., "A Universal Scale Of Apparent Temperature," *Journal Of Climate And Applied Meteorology*, Vol. 23, pp. 1674-1687, 1984.
- Sutton, L.J., *Rainfall In Egypt--Statistics, Storms And Run-Off*, Ministry Of Public Works, Meteorological Department--Cairo, Paper No. 53, 1947.
- Tunnell, G.A., "World Distribution Of Atmospheric Water Vapour Pressure," *Geophysical Memoirs*, British Met Office, Vol. 12, No. 100, 1958.
- Tracks Of Tropical Depressions And Cyclones In The Bay Of Bengal And Arabian Sea--1877-1960*, Indian Meteorological Department, 1964.
- Tropical East Africa*, AWS/FM-100/006, HQ Air Weather Service, Scott AFB, IL, March 1980.
- Tropical Meteorology in Africa--4th Seminar*, East African Met Service, Nairobi, 1965.
- van de Boogaard, H., *The Mean Circulation Of The Tropical And Subtropical Atmosphere-July*, NCAR, NCAR/TN-118+STR, NCAR, Boulder, CO, 1977.
- van de Boogaard, H., and Rao, G.V., "Mesoscale Structure Of The Low-Level Flow Near The Equatorial East African Coast," *Monthly Weather Review*, Vol. 113, pp. 91-107, 1984.
- Walker, J.M., "Some Ideas On Winter Atmospheric Processes Over Southwest Asia," *Meteorological Magazine*, Vol. 96, pp. 161-167, 1967.
- Walker, J.M., "The Monsoon Of Southern Asia: A Review," *Weather*, Vol. 27, pp. 178-189, 1972.

Walters, K.R., *A Descriptive Climatology For Baledogle Somalia*, USAFETAC/TN-88/001, USAF Environmental Technical Applications Center, Scott AFB, IL, 1988.

Walters, K.R., and W.F. Sjoberg, *The Persian Gulf Region--A Climatological Study*, USAFETAC/TN-88/002, USAF Environmental Technical Applications Center, Scott AFB, IL, 1988.

Weather Conditions Suitable For Aerial Photography In Turkey, Air Weather Service, 1947.

Weather Factors Affecting Aerial Photography in Ethiopia, date & author unknown.

Weather in the Indian Ocean to Latitude 30 South and Longitude 95 East including the Red Sea and Persian Gulf. Volume I: General Information, and Volume II: Local Information Part I Red Sea, NAVENVPREDRSCHFAC, NEPRF, April 1980.

Western Indian Ocean, AWS/FM-100/018, HQ Air Weather Service, Scott AFB, IL, August 1980.

World Survey of Climatology Vol 9, Climates of Southern and Western Asia, Elsevier Scientific Publishing Company, Amsterdam-Oxford-New York, 1981.

World Survey of Climatology Vol 10, Climates of Africa, Elsevier Publ. Co., Amsterdam, 1972.

Young, J.A., et al., *Summer Monsoon Winds from Geostationary Satellite Data: Summer MONEX 1 May to 31 July, 1979*, Univ of Wisc Meteorology Dept, NSF Grant No. ATM-78-21873, 1980.

Zohdy, Hussein Mohamed, *Troughs in the Westerlies Related to Winter Rainfall Patterns in Yemen*, Thesis Paper, Cairo University, 1971.

DISTRIBUTION

HQ USAF/XOOOW, Rm BD927, Washington, DC 20330-5054	1	Ctr for Ag Meteorology and Climatology, Chase Hall-East Campus,	
OSAF/SS, Rm 4C1052, Pentagon, Attn: Weather, Washington, DC 20330-6560	1	Univ of Nebraska-Lincoln, Lincoln, NE 68583-0728	1
USTC I3/J4-OW, Scott Dr., Bldg 1900, Scott AFB, IL 62225-7001	2	Dept of Marine, Earth, and Atmospheric Sciences, North Carolina St Univ	
AWS/XTX/DO/DOO, Lowry St., Bldg 1521, Scott AFB, IL 62225-5008	1	Box 8208, Raleigh, NC 27695-8208	1
Det 4, AWS, Bldg 91027, Hurlburt Fld, FL 32544-5000	1	School of Meteorology, Univ of Oklahoma, 200 Felger St.,	
HQ AFGWC/DOM/DOF/SY, MBB39, 106 Peacekeeper Dr., Ste 2N3,		Norman, OK 73019-5000	1
Offutt AFB, NE 86113-4039	1	Dept of Atmospheric Sciences, Stand Agriculture Hall, Oregon St Univ	
AFSC/DON, Stop 82, Bldg 715, Patrick Ave., Falcon AFB, CO 80912-5000	1	Corvallis, OR 97331-2209	1
USAFETAC, Scott AFB, IL 62225-5000	6	Dept of Meteorology, 503 Walker Bldg, Penn St Univ,	
OL-A, USAFETAC, Federal Building, Rm 305, Asheville, NC 28801-2723	1	University Park, PA 16802-5000	1
AFSPACECOM/DOWA, Bldg 1, Stop 7, Peterson Rd., Peterson AFB, CO 80914-5001	1	Dept of Marine Sciences, Univ of Puerto Rico, Mayaguez, PU 00708-5000	1
USAICS, Attn: ATSI-CDW, Ft Huachuca, AZ 85613-6000	1	Dept of Earth and Atmospheric Sciences, Stadium Hall,	
AFMCI/DOW, Bldg 266, Post 108P Chidlaw Rd., Wright-Patterson AFB,		Purdue Univ, West Lafayette, IN 47907-5000	1
OH 45433-5000	1	Library, Rand Corporation, PO Box 2138, Santa Monica, CA 90406-5000	1
FASTC/TAW, Wright-Patterson AFB, OH 45433-6508	1	Dept of Earth and Atmospheric Sciences, St Louis Univ,	
ASD/WE, Bldg 91, 3rd St, Wright-Patterson AFB, OH 45433-6503	1	PO Box 8099-Laclede Station, St Louis, MO 63156-5000	1
AFIT/CIR, Wright-Patterson AFB, OH 45433-6583	1	Dept of Meteorology, Univ of St Thomas, 3812 Montrose Blvd,	
WL/DOW, Wright Patterson AFB, OH 45433-6543	1	Houston, TX 77006-5000	1
PL/WE, Kirtland AFB, NM 87117-5000	1	Dept of Meteorology, San Jose St Univ, One Washington Square,	
RL/WE, Griffiss AFB, NY 13441-5700	1	San Jose, CA 95192-5000	1
AFESC/RDXT, Bldg 1120, Stop 21, Tyndall AFB, FL 32403-5000	1	Dept of Meteorology, Texas A&M Univ, College Station, TX 77843-5000	2
ESD/WE, Vandenberg Dr., Bldg 1624, Hanscom AFB, MA 01731-5000	1	US Military Academy, USMA Library, West Point, NY 10996-5000	1
PL/TSMI, Research Library, Hanscom AFB, MA 01731-5000	1	Dept of Oceanography, Stop 9d, US Naval Academy,	
AFFTC/WE, Edwards AFB, CA 93523-5000	1	Annapolis, MD 21402-5000	1
USCENTCOM/CCI3-W, Bldg 540, MacDill Blvd, MacDill AFB, FL 33608-7001	1	Dept of Meteorology, Univ of Utah, Salt Lake City, UT 84112-5000	1
AFTAC/WS, Patrick AFB, FL 32925-5000	1	Dept of Meteorology, Utah St Univ, UMC 4840, Logan, UT 84322-5000	1
USAFALCENT RA, Pope AFB, NC 28308-5000	1	Dept of Environmental Sciences, Clark Hall, Univ of Virginia,	
AMC/XOWR, Bldg P40 N, Martin Ave, Scott AFB, IL 62225-5000	1	Charlottesville, VA 22903-5000	1
ISOW/OGSW, Attn: Lt Kelly, 150 Bennett, Bldg 90730, Hurlburt Field,		Dept of Meteorology, Univ of Wisconsin, 1225 W Dayton St.,	
FL 32544-5000	1	Madison, WI 53706-5000	1
AFSOC/DOW, Hurlburt AFB, FL 32544-5000	1	USAF/DOW, Unit 3050, Box 15, APO AE 09094-5000	1
ATC/DOTW, Bldg 399, Rm B27, D St., East, Randolph AFB, TX 78150-5000	1	USAF/DOW, Unit 3050, Box 500, APO AE 09094-5000	1
3395TCHTS/TTMV, Keesler AFB, MS 39534-5000	2	17AF/DOW, Unit 4065, APO AE 09136-5000	1
Det 5, HQ AWS, Keesler AFB, MS 39534-5000	1	Det 1, 86 OPS GP, Unit 8495, APO AE 09094-5000	1
CFA, C-2/SWO, APO AP 96258-0210	1	HQ USEUCOM EC13, Unit 30400, Box 1000, APO AE 09128-4209	1
PACAF/DOW, Bldg 1102, Hickam AFB, HI 96853-5000	1	7WS, CINCUSAREUR/AREAWX, APO AE 09403-5000	1
USSTRATCOM, J315, 901 SAC BLVD, STE BA3, Offutt AFB, NE 68113-5000	1	7WS, Unit 29351, APO AE 09014-5000	1
ACC/DOW, Bldg 21, 30 Elm St, Ste 215, Langley AFB, VA 23655-2093	1	48 Weather Flight, APO AE 09464-5000	1
24WS, Unit 0640, APO AA 34001-5000	1	105 Weather Flight, Tennessee Air National Guard, PO Box 17267, Nashville,	
9COS/AOSW, Bldg 1130, Shaw Dr., Shaw AFB, SC 29152-5410	1	TN 37167-2091	1
12AOQ/AOSW, E Ave., Bldg 2900, Bergstrom AFB, TX 78743-5000	1	107 Weather Flight, Selfridge ANGB, MI 48045-5024	1
24WS/CC, APO AA 34001-5000	1	110 Weather Flight, MO ANG, 131TFW, Bridgeton, MO 63044-2371	1
ATSI/CDW, US Army Intel, Ft Huachuca AI, AZ 85613-5000	1	111 Weather Flight, Ellington ANGB, TX 77034-5586	1
USCENTCOM/CCI3-W, MacDill AFB, FL 33608-7001	1	113 Weather Flight, Hulman Fld, Terre Haute, IN 47830-5000	1
USSOCENT/SCJ2-SWO, MacDill AFB, FL 33608-7001	1	116 Weather Flight, WA ANG, Bldg 304, McChord AFB, WA 98433-5000	1
USSOCOM/SOJ3-W, MacDill AFB, FL 33608-6001	1	120 Weather Flight, Buckley ANGB, CO 80011-9999	1
1WG, Bldg 168, Hardoe St., Ft McPherson, GA 30300-5000	1	121 Weather Flight, Stop 28, Andrews AFB, MD 20331-6539	1
OL-A, SWS, AFZJ/SWO, Ft Irwin, CA 92310-3000	1	122 Weather Flight, New Orleans NAS, LA 70143-0200	1
CDR USASOC, Attn: AOIN-ST, Ft Bragg, NC 28307-5200	1	123 Weather Flight, Portland IAP, OR 97218-2797	1
JSOC/Weather, P.O. Box 70239, Ft Bragg, NC 28307-5000	1	125 Weather Flight, PO Box 580340, Tulsa AFS, OK 74158-0340	1
75th RGR (Attn: SWO), Ft Benning, GA 31905-5000	1	126 Weather Flight, WLANG, 350 E College, Milwaukee, WI 53207-6298	1
HQ 5th U.S. Army, AFKB-OP (SWO), Ft Sam Houston, TX 78234-7001	1	127 Weather Flight, Forbes Fld, Topeka, KS 66619-5000	1
Library, USAFA (DFSEL), Colorado Springs, CO 80840-5000	1	130 Weather Flight, Yeager Apt, Charleston, WV 25311-5000	1
USDAO Ndjamena, State Dept Pouch Room, Washington, DC 20521-2410	2	131 Weather Flight, Barnes Map, Westfield, MA 01085-1385	1
USDAO/AIRA, Cairo, Box 9, APO New York 09527-0061	2	140 Weather Flight, Willow Grove NAS, PA 19090-5105	1
USDAO Baghdad, State Dept Pouch Room, Washington, DC 20520	1	146 Weather Flight, GTR Pittsburg ANG AN, PA 15231-0459	1
USDAO/AIRA Tel Aviv, Israel, APO New York 09672-5000	1	154 Weather Flight, Camp Robinson, North Little Rock, AR 72118-2200	1
USDAO/AIRA Amman, APO New York 09892-5000	2	156 Weather Flight, 5225 Morris Fld Dr., Charlotte, NC 28208-5797	1
USDAO Muscat, State Dept Pouch Room, Washington, DC 20520-62220	2	159 Weather Flight, c/o HQ FLANG, State Arsenal, St Augustine, FL 32085-1008	1
USDAO/AIRA Islamabad, PSC Box 32, APO New York 09614-0006	2	164 Weather Flight, Rickenbacker ANGB, OH 43217-5007	1
USDAO/AIRA, Ambassador, APO New York 09038-0001	2	165 Weather Flight, Standford Fld, Louisville, KY 40213-2678	1
USDAO Mogadishu, Somalia, State Dept Pouch Room, Washington, DC 20520	1	181 Weather Flight, 8150 W Jefferson Blv, Dallas, TX 75211-9570	1
USDAO Khartoum, Box 18, Ambassador, APO New York 09668-5000	1	195 Weather Flight, 4146 Naval Air Rd., Port Hueneme, CA 93041-4001	1
USDAO Damascus, State Dept Pouch Room, Washington, DC 20520	1	199 Weather Flight, Wheeler AFB, HI 96854-5000	1
USDAO Sanaa, State Dept Pouch Room, Washington, DC 20521-6330	1	200 Weather Flight, 5680 Beulah Rd., Sandston, VA 23150-6109	1
Dept of Meteorology, Florida State Univ, Tallahassee, FL 32306-5000	1	202 Weather Flight, Otis ANGB, MA 02542-5028	1
Dept of Meteorology, Univ of Hawaii, 2525 Correa Road, Honolulu,		203 Weather Flight, Ft Indiantown GAP, Annville, PA 17003-5002	1
HI 96822-5000	1	204 Weather Flight, McGuire AFB, NJ 08641-6004	1
Dept of Atmospheric and Oceanic Science, Space Research Bldg,		207 Weather Flight, 3556 N. Michigan Rd., Shelbyville, IN 46176-4914	1
Univ of Mich, 2455 Hayward, Ann Arbor, MI 41809-2143	1	208 Weather Flight, 206 Airport DE, St Paul, MN 55107-4098	1
Dept of Meteorology and Physical Oceanography, Univ of Miami,		209 Weather Flight, PO Box 5218, Austin, TX 78763-5218	1
Miami, FL 33149-1098	1	210 Weather Flight, Ontario ANGB, CA 91761-7627	1
Dept of Atmospheric Science, Univ of Missouri, 701 Hitt St.,		COMNAVOCEANCOM (C4pi Brown, Code N332), Stennis Space Ctr,	
Columbia, MO 65211-5000	1	MS 39529-5001	1

NAVOCEANO (Rusty Runum), Bldg 8100, Rm 203D, Stennis Space Ctr,
 MS 39522-5001 2
 Maury Oceanographic Library, Naval Oceanography Office, Stennis Space Ctr,
 MS 39522-5001 1
 Naval Research Laboratory, Monterey, CA 93943-5006 1
 Naval Research Laboratory, Code 4323, Washington, DC 20375 1
 Naval Postgraduate School, Chmn, Dept of Meteorology, Code 63,
 Monterey, CA 93943-5000 1
 Naval Eastern Oceanography Ctr (Clim Section), U117 McCady Bldg, Norfolk NAS,
 Norfolk, VA 23511-5000 1
 Naval Western Oceanography Ctr, Box 113, Attn: Tech Library,
 Pearl Harbor, HI 96860-5000 1
 NAVOCEANCOMFAC, NAS North Island, San Diego, CA 92135-5130 1
 Naval Air Warfare Center-Weapons Division, Geophysical Sciences Branch, Code 3254,
 Attn: Mr. Roger Helvey, Point Mugu, CA 93042-5001 1
 WSO, H & HS Marine Station Wea, MCAS Tustin CA 92710-5000 1
 Armed Forces Medical Intelligence Center, Information Services Division
 Bldg 1607, Ft Detrick, Frederick, MD 21702-5004 1
 TECOM, Dir for Technology, APG Met Team, Bldg 1134, Attn: AMSTE-TC-AM CAB,
 Aberdeen Proving Ground, MD 21005-5001 1
 Atmospheric Sciences Laboratory (SLCAS-AS-1 3 10-2c), White Sands Missile Range,
 NM 88002-5501 1
 TECOM Atmos Sci Div, AMSTE-TC-AA (MacBlain), White Sands Missile Range,
 NM 88002-5504 1
 White Sands Met Team, AMSTE-TC-AM (WS), White Sands Missile Range,
 NM 88002-5501 1

Army Missile Command, ATTN: AMSMI-RD-TE-F, Redstone Arsenal,
 AL 35898-5250 1
 USATECOM, ATTN: AMSTE-TC-AM (RE) TCOM Met Team, Redstone Arsenal,
 AL 35898-8052 1
 USATECOM, ATTN: AMSTE-TC-AM (AB), Aberdeen Proving Ground,
 MD 21005-5001 1
 Director, U.S.A.-CETEC, Attn: GL-AE (Whitmarsh), Fort Belvoir, VA 22060-5546 1
 Technical Library, Dugway Proving Ground, Dugway, UT 84022-5000 1
 OFCM, Attn: Col Dumont, Suite 900, 6010 Executive Blvd, Rockville, MD 20852 1
 HQ NATO Staff Meteorological Officer IMS/OPS APO AE 09724 1
 NOAA/MASC Library MCS, 325 Broadway, Boulder, CO 80303-3328 2
 NOAA Library-EOC4WSC4, Attn: ACQ, 6009 Executive Blvd, Rockville, MD 20852 1
 NOAA/NESDIS (Attn: Nancy Everson, E/RA22), World Weather Bldg, Rm 703,
 Washington, DC 20233 1
 Meteorological Office (Met O 9), London Road, Bracknell, Berks RG12 2SZ, UK 1
 National Meteorological Library, Meteorological Office (Met O 18a),
 London Road, Bracknell, Berks RG12 2SZ, UK 1
 NGDC, NOAA, Mail Code E/GC4, 325 Broadway, Boulder, CO 80333-3328 1
 NWS W/OSD, Bldg SSM C-2 East-West Hwy, Silver Spring, MD 20910 1
 NIST Pubs Production, Rm A635, Admin Bldg, Gaithersburg, MD 20899 1
 DTIC-FDAC, Cameron Station, Alexandria, VA 22304-6145 2
 AUL/LSE, Maxwell AFB, AL 36112-5564 1
 AWSTL, Scott AFB, IL 62225-5438 35